Studies on the metallacyclic chemistry of thiourea monoanion and dianion ligands; synthesis, structures and theoretical investigations

A thesis

submitted in fulfilment

of the requirements for the degree

of

Doctor of Philosophy in Chemistry

at

The University of Waikato

by

Obinna Chibueze Okpareke

THE UNIVERSITY OF
WAIKATO
Te Whare Wānanga o Waikato

2020

Dedication

To my late father Mazi Simeon Nwafor Okpareke (Ebubedike)

Abstract

This thesis presents studies on the metallacyclic chemistry of thiourea dianion and monoanion ligands. The versatility of thioureas and their relatives (thiosemicarbazones and selenoureas) has been attributed to the propensity to functionalise the imine protons with a variety of functional groups. Asymmetrically substituted thioureas have been known to form coordination complexes with a variety of metal precursors including platinum, palladium, nickel, ruthenium rhodium, iridium, technetium and molybdenum. This thesis investigates the effect of varying the functionality or steric properties of the ligands on the physical, chemical, structural, and geometric properties of the resulting complexes.

The thesis is organised into seven chapters. Chapter one is the review of the literature of the chemistry of thioureas, their properties, method of synthesis, applications and reactivity towards metals. A number of coordination complexes of thioureas with various metal precursors are also reviewed and the structural, chemical and biological properties of these complexes are discussed. The coordination chemistry of other related ligands including the selenoureas and thiosemicarbazones are also reviewed.

Chapter two details the synthesis and reactivity of pyridyl substituted thiourea ligands towards *cis*-$[PtCl_2(PPh_3)_2]$ (PPh_3 = triphenylphosphine). In this chapter the synthesis of a series of pyridyl-substituted thiourea dianion and monoanion complexes of the type $[Pt\{SC(=NR^1)NR^2\}(PPh_3)_2]$ and $[Pt\{SC(=NR^1)NHR^2\}(PPh_3)_2]^+$ respectively (where R^1 = phenyl, *p*-nitrophenyl, and *p*-methoxyphenyl; $R^2 = Py(CH_2)_n$ n = 0, 1, 2; Py = 2-pyridyl) was explored. The complexes were characterised by ESI-MS, ^1H NMR, ^{31}P NMR, FTIR and single crystal X-ray crystallography. Initial NMR investigation indicated isomerism in the complexes. Theoretical Gibbs free energy calculations were performed on the DFT optimised geometries of the complexes and the difference in electronic Gibbs free energy ΔG ($GPt_{distal} - GPt_{proximal}$) between the two possible isomers of the dianion complexes were evaluated. A positive difference in Gibbs free energy values predicted a kinetically favoured proximal isomeric configuration for the thiourea dianion complexes (where the pyridyl functional group is bonded to the platinum adjacent nitrogen) The monoanion complex on the other hand gave a negative calculated Gibbs free energy difference, indicating a kinetically favoured distal

isomeric configuration for the complex (where the pyridyl functional group is bonded to the nitrogen remote from the platinum metal). $^{31}P\{^{1}H\}$ NMR investigations revealed the presence of an initial proximal isomer for the dianion complexes, which underwent solution phase isomerisation into the distal isomeric forms of the complexes and/or a mixture of the proximal and distal isomers. The opposite trend was recorded for the monoanionic complex, where the formation of an initial distal isomer and subsequent isomerisation into a 1:3 mixture of the proximal and distal isomeric forms of the complex was observed. Introducing an alkyl spacer between the pyridyl and the thiourea functional group did not have any significant effect on isomerism, however the steric nature and size of the R substituents in the complex affected the isomerisation process. X-ray crystallography was used to establish the NP_2S square planar geometry of the complexes. The dianion complexes are *N,S*-chelating so that each donor atom is opposite a phosphane-P atom; a *trans*-influence is evident on the Pt–P bonds. In the monoanion complex, the anion coordinates in a similar fashion to that established in the neutral analogues and systematic variations in geometric parameters are evident.

Chapter three investigates the coordination chemistry of organo-phosphorus palladium and nickel complexes of these asymmetrically substituted pyridyl thiourea ligands synthesised in Chapter two. The reaction of pyridyl-substituted thiourea ligands of the form $R^1NHC(S)NHR^2$ (where $R^1 = Py(CH_2)_n$; n = 0,1,2, R^2 = Ph, or *p*-$C_6H_4NO_2$) with $[PdCl_2(dppe)]$, $[PdCl_2(PPh_3)_2]$ or $[NiCl_2(dppe)]$ resulted in cationic complexes of the type $[M\{SC(NR^1)HNR^2\}(L_2)]X$, (M = Pd or Ni, L = PPh_3 or L_2 = dppe and X = BF_4 or BPh_4, dppe = bis-diphenylphosphinoethane) and a neutral complex $[Pd\{SC{=}(NPh)NC_6H_4NO_2\}(dppe)]$. The major outcome of this study is the synthesis of the six-membered ring cationic palladium complex **3a**, where the palladium metal is coordinated to the pyridyl nitrogen. $^{31}P\{^{1}H\}$ NMR indicated the possibility of *E/Z* isomerism in the complex. X-ray crystal structures of the complexes showed that introducing an alkyl spacer between the pyridyl and thiourea functionalities resulted in juxtaposition of the pyridyl functional group from the proximal to the distal position.

Chapter four explores the synthesis and structure of half sandwich arene ruthenium, Cp* rhodium and iridium complexes of the pyridyl substituted thioureas (Cp* = pentamethylcyclopentadienyl) The complexes were formed from the metal

dimers $[C_6Me_6/cymene\ RuCl_2]_2$ or $[Cp^*MCl_2]_2$ (M = Rh, Ir) and a set of pyridyl substituted ligands to form complexes. The ruthenium complexes formed mononuclear bisthiourea complexes $[(\eta^6\text{-}C_6Me_6)Ru\{SC(=NPy)NHPh\}\{SC(NHPy)NHPh]$ **4a** and $[(\eta^6\text{-}C_6Me_6)Ru\{SC(=NPy)NHC_6H_4OMe\}\{SC(NHPy)NHC_6H_4OMe]$ **4b** with a three legged piano stool configuration where the C_6Me_6 arene ligand occupies three coordination sites on the ruthenium metal and the remaining three positions are occupied by the two thiourea ligands coordinated in a bidentate and monodentate fashion to a *pseudo*-octahedral geometry. Introduction of the alkyl spacer between the pyridyl and thiourea functional groups resulted in tridentate cationic mono thiourea complexes of the form $[(\eta^6\text{-}C_6Me_6)Ru\{SC(=N(CH_2)_2Py)NHR]PF_6$ **4c - 4d**, (R = Ph, or *p*-$C_6H_4NO_2$). X-ray crystal structures of the complexes showed that the longer arm of the pyridyl functionality allows the ligand to fold around the metal centre resulting in tridentate coordination. Introduction of the bulky PPh_3 ligand into the coordination sphere of the ruthenium complex resulted in mono-cationic bidentate complexes of the form $[(\eta^6\text{-}C_6Me_6)Ru\{SC(=N(CH_2)_nPy)NHR\}PPh_3]X$ (n = 0, 1, 2; R = Ph, *p*-$C_6H_4OCH_3$, *p*-$C_6H_4NO_2$; X = BF_4 or PF_6) **4e-4q**.

The pentamethylcyclopentadienyl rhodium and iridium complexes formed similar *pseudo*-octahedral three legged piano stool complexes with a Cl anion occupying one of the coordination sites along with N,S donor atoms of the cationic thiourea ligand to form neutral complexes of the type $[Cp^*M\{SC(=NPy(CH_2)_n)NR\}Cl]$ **4r-4w**, (where M = Rh or Ir, n = 0, 1, 2 and R = Ph or, *p*-$C_6H_4OCH_3$). The chloride anion in the complexes were later substituted with the bulky PPh_3 to give monocationic complexes $[Cp^*M\{SC(=NPy(CH_2)_n)NR\}PPh_3]$ **4x-4ze** as BF_4 salts.

In Chapter five, a series of asymmetrically substituted thioureas containing phosphonate, hydroxyalkyl and silatrane functional groups were synthesised and characterised. Supramolecular interactions in the crystal structure of the phosphonate substituted thioureas were analysed using the Non-covalent Interaction (NCI) program *Bonder*, a locally developed program, which provides numerically equivalent results to existing NCI codes such as NCIplot, NCImilano or Multifwn. The coordination chemistry of these thiourea ligands were explored by reacting them with platinum and palladium precursor complexes *cis*-$[PtCl_2(PPh_3)_2]$ and $[PdCl_2(dppe)]$. The resulting complexes were characterised by ^1H, ^{31}P NMR, ESI-MS and X-ray crystallography. The results show that the complexes formed mostly cationic complexes of the type

[Pt{SC(NPh)NHR}$(PPh_3)_2$]BF_4 **5a-5e** and [Pd{SC(NPh)NHR}dppe]BF_4 **5h-5k** (R = phosphonate, hydroxyethyl, dihydroxyethyl and silatrane functional groups). The X-ray crystal structure of the complexes confirmed the square planar NP_2S geometry of the compounds.

Chapter six introduces a new set of alkyl bridged bisthiourea ligands and their organo-phosphorus platinum group metal complexes of the type [{(PtSC(NPh)$NHC_6H_5)_2CH_2$}$(PPh_3)_4$] $\cdot 2BPh_4$ **6a**, [M_2{(SC(NPh)$NHC_6H_5)_2CH_2$}$(dppe)_2$]$\cdot 2BPh_4$ **6b-6c** (where M = Pd, Ni), [Pt_2{SC(NPh)NH}$_2(CH_2)_n(PPh_3)_4$]$\cdot 2BPh_4$ **6d-6g** (n = 4, 6, 8, 12), and [M_2{SC(NPh)NH}$_2(CH_2)_4(dppe)_2$]$\cdot 2BPh_4$ **6h-6o** (where M = Pd, Ni). The ESI-mass spectral analysis of the complexes showed the presence of the monochelated and dichelated species. Increasing the molar concentration of the metal precursor complexes and reaction time from 2 to 8 hours resulted in the disappearance of the monochelated species from the ESI-mass spectra of the platinum complexes, but not for the palladium and nickel complexes. $^{31}P\{^1H\}$ NMR characterisation of the methylene bridged bisthiourea complexes **6a-6c**, showed multiplets indicative of isomerism. These peaks however disappeared as the length of the bridging alkyl chain increased. X-ray crystallographic studies were used to confirm the coordination geometry of the complexes.

Acknowledgements

The journey leading to the completion of this PhD was a daunting and humbling one. Thankfully a handful of very talented individuals who were at hand and through their collective effort has greatly improved the final outcome.

First I want to express my gratitude for the privilege of working with two of the best Supervisors in the University of Waikato, Professor Bill Henderson and Associate Professor Joseph Lane. The combination of their experiences and profound understanding of the chemical principles and facts in the work helped in shaping every stage of this project. Apart from their versed knowledge, their dedication and humility made the research a lot easier. I would not have asked for a better supervisory team.

In addition to my supervisors, several other scientists and professionals contributed immeasurable time and knowledge to the success of this research. Special thanks to Emeritus Professor Brian Nicholson and Associate Professor Graham Saunders for sharing their knowledge of X-ray crystallography, Dr Judith Burrows of the Molecular Biology and Genetics research laboratory in the School of Science, University of Waikato for helping to collect all the X-ray crystallographic data and Professor Edward R. T. Tiekink of the Research Centre for Crystalline Materials, School of Science and Technology, Sunway University Malaysia, for contributing his excellent knowledge of X-ray crystallography to my research.

This thesis would not have been possible without the help of the hardworking technical staff in Chemistry; Pat Gread, Annie Barker, John Little, Steve Cameron, Jenny Stockdill. Thanks for the invaluable behind the scene work that you do, including sourcing chemicals, troubleshooting, and maintaining all laboratory equipment.

I am also very grateful to the University of Waikato Science Librarian Cheryl Ward for her dedication, humility and help with a number of different things including finding research articles and books, tutorials on the use of Endnote, Word and Excel and formatting of the final thesis.

I will not forget my very good friend Dylan McQuiston for sharing his knowledge of NMR spectroscopy with me when I first arrived at the University of

Waikato. My co-research students in Laboratory, Raymond Onyekachi, Hamming Tang, Simeon Atiga, Ryland, Hayden, Golf, Stravan, Mohammed whose different but interesting personalities made working in the Laboratory fun.

My family were most supportive during this research. I am very thankful to my wife Uchechi for her understanding and unwavering support and my two lovely daughters, Akunnaya and Chinemerem for being very good girls, especially on occasions that I had to take them to the Library with me.

Finally, I am grateful to the School of Science, and the University of Waikato for Funding and the Tertiary Education Trustfund Nigeria for Academic Staff Training Scholarship.

Table of Contents

List of Figures

List of Tables

List of Schemes

List of Abbreviations

NMR – nuclear magnetic resonance spectroscopy

FTIR – Fourier transform infrared spectroscopy

ESI-MS – electrospray ionisation mass spectrometry

Δ – chemical shift ppm (NMR)

m/z – mass to charge ratio (ESI-MS)

s – singlet (NMR), strong (IR)

d – doublet (NMR)

t – triplet (NMR)

q^t – quintet (NMR)

m – multiplet (NMR), medium (IR)

w – weak (IR)

J – coupling constant in Hz (NMR)

m.p – melting point

DFT – Density Functional Theory

NCI – noncovalent interaction

$CDCl_3$ – deuterated chloroform

COD – 1, 5-cyclooctadiene

DMSO – dimethyl sulfoxide

Py – pyridyl

Ph – phenyl

Cp* – pentamethylcyclopentadienyl (η^5-C_5Me_5)

PPh_3 – triphenylphosphine

Dppe – 1,2-bis(diphenylphosphino)ethane

Dppf – 1,2-bis(diphenylphosphino)ferrocene

HIV – human immunodeficiency virus

HDL – high density lipoprotien

ΔG – The difference in Gibbs free energy

Chapter 1

Metallacyclic chemistry of thiourea monoanion and dianion ligands; synthesis, structure and reactivity

1.1 Introduction to metallacyclic chemistry

The term metallacycle has been used to describe mostly compounds containing two metal-carbon bonds (**1**) as part of a ring system[1]. Many compounds of the type **2** containing metals in rings and usually known as chelates were not formerly classified as metallacycles. Due to constant changes in naming conventions, metallacycles now refer to rings containing a metal centre[2,3]. The ring system can thus be derived from neutral, monoanionic or dianionic ligands. Metallacycles include cyclometallated complexes which often contain chelating donor atoms (usually S, Se, O, N, P, As etc)[1,4]. A vast number of metallacyclic complexes are possible with a diverse class of compounds containing rings of any size and atoms of any element[5]. The chemistry and applications of metallacyclic transition metal complexes in organic and organometallic chemistry has been the subject of a number of reviews [6-8]. The present review will be restricted to the complexes of thiourea ligands and related compounds containing *N*,*S*-donor ligands.

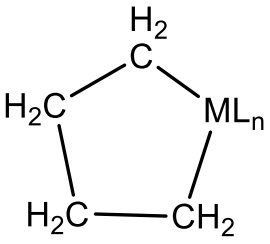

1

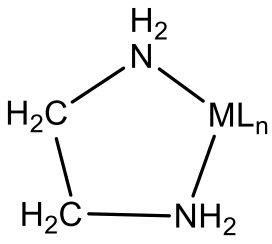

2

1.2 Thioureas

Thioureas are a group of versatile organosulfur compounds of the form **3**. Thioureas have attracted a great deal of interest from chemists and biologists for a very long time. This is not only because of their ease of synthesis but also as a result

of the flexibility of modification of the substituents on the nitrogen with a variety of designer groups giving rise to variability in physical, chemical and biological properties[9]. Thioureas have been applied in pharmacy and medicine as antioxidants[10], antiallergens[11], antibacterial[12,13], antiinflammatory[14], antithyroid[15], antiepileptic[16], antihypertensive[17], and anticancer drugs[18,19]. In agriculture, they have been used as rodenticides[20], insect growth regulators[21] and in seed germination and plant growth control[22,23]. Furthermore, their use as catalysts in the production of a variety of home and industrial products has been well documented[24,25]. Apart from that, many thiourea derivatives have been employed as synthetic precursors in coordination[26], supramolecular[27,28] and materials chemistry [29-31].

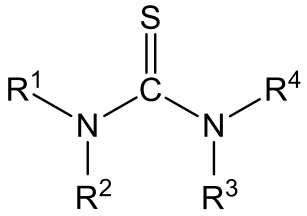

3

1.3 Synthesis and general structure of thioureas

1.3.1 *Synthesis of thiourea ligands*

Different methods have been proposed and used in the synthesis of thioureas including the reaction of amines with carbon disulfide[32], thiophosgene[33] and the acidification of cyanamides in the presence of lithium aluminium hydrogen sulfide[34]. However, the reaction of aryl or alkyl isothiocyanates with primary or secondary amines remains the most straightforward and best method of synthesising thioureas (**Scheme 1.1**). This is due to the ability of this method to generate very pure products in high yields[35]. The reaction is usually carried out in diethyl ether due to the solubility of the reactants and insolubility of the products in ether.

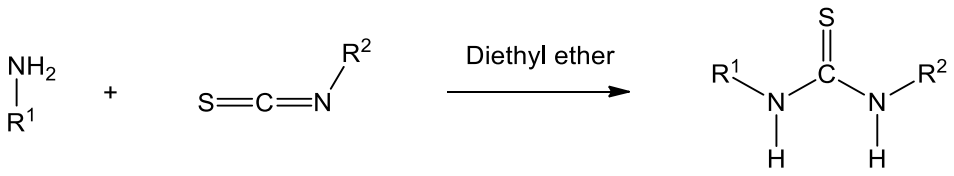

Scheme 1.1: Reaction scheme for the synthesis of thioureas from isothiocyanates.

Despite the success of the above method, an environmentally benign method was recently introduced for the synthesis of symmetrical *N,N'*-disubstituted thioureas in aqueous solution[36]. This method involves the microwave irradiation of a mixture of a primary aromatic amine and unsubstituted thiourea in water using polyethylene glycol PEG-400 as catalyst (**Scheme 1.2**). The advantage of this method is that it eliminates the use of flammable and volatile organic solvents, harsh reaction conditions, poor yields and many side reactions common with other methods.

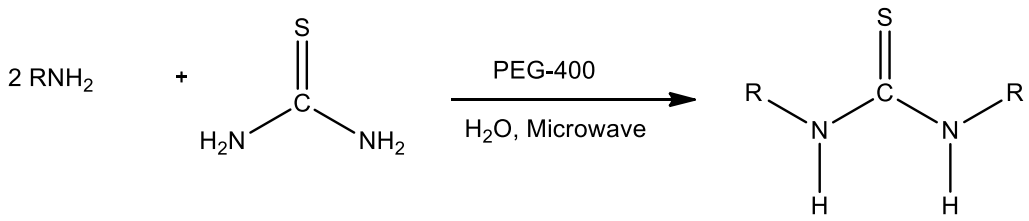

Scheme 1.2: Microwave synthesis of symmetrically di-substituted thioureas in aqueous solution.

1.3.2 *Structure of thiourea ligands*

The possibility of modification of the substituents on the nitrogen of the thiourea with a variety of alkyl or aryl functional groups results in fascinating structural, physical and chemical properties. Several symmetrically and unsymmetrically substituted thiourea ligands have been reported in the literature containing alkyl and aryl functionalities including methyl[37] **4**, phenyl **5,6**[38-40], morpholine **7**, and a range of pyridyl functionalities **8**,**9**,**10,11**[39,41,42]. Many acyl thiourea derivatives of the type in **12** and **13** have also been reported in the literature[43-47]. Only a small selection of the large number of thioureas available in the literature have been presented here as representative examples.

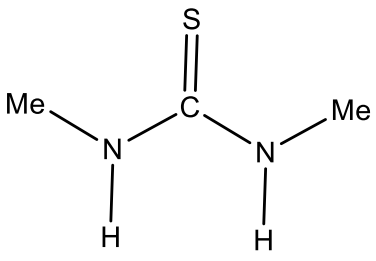

4

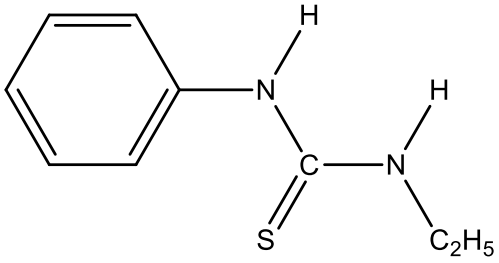

5

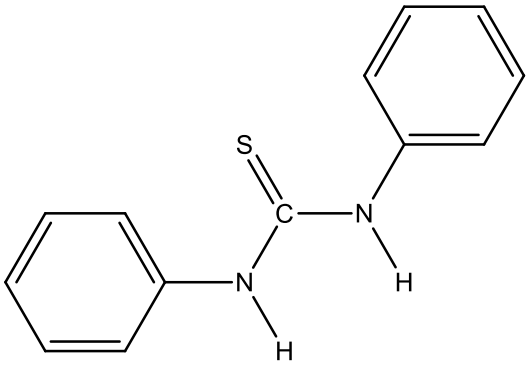
S
C
N
H
N
H

6

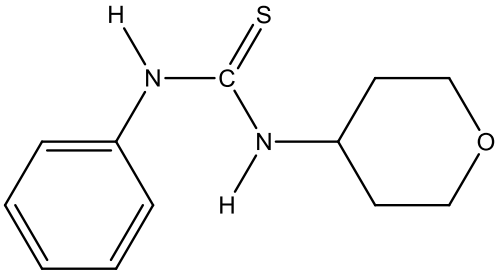
H
S
N
C
N
O
H

7

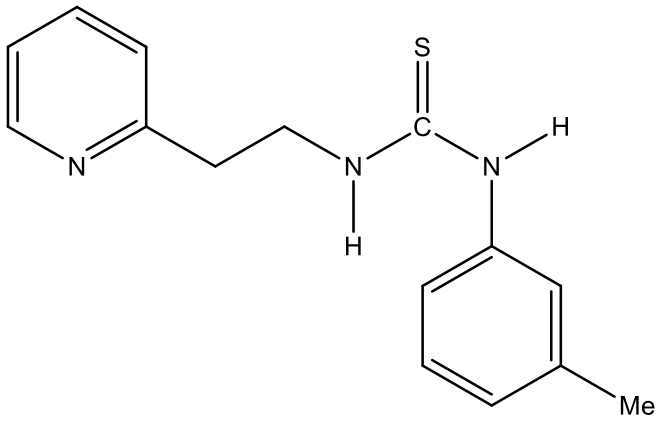
S
N
C
H
N
N
H
Me

8

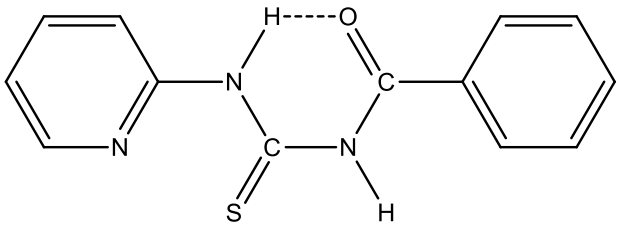
H
O
N
C
N
S
H

9

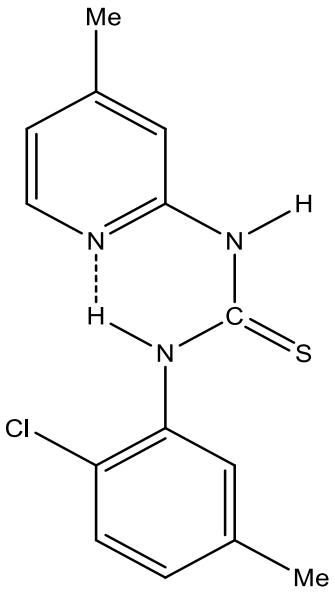
Me
H
N
N
H
C
N
S
Cl
Me

10

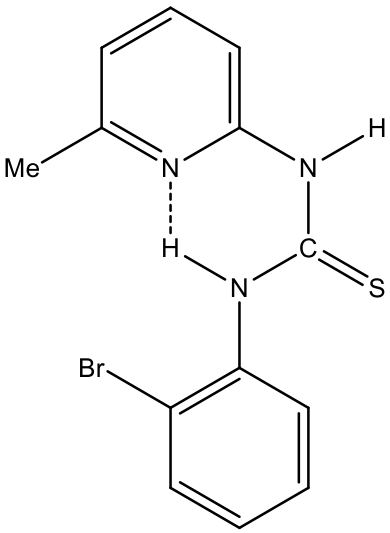
H
Me
N
N
H
C
N
S
Br

11

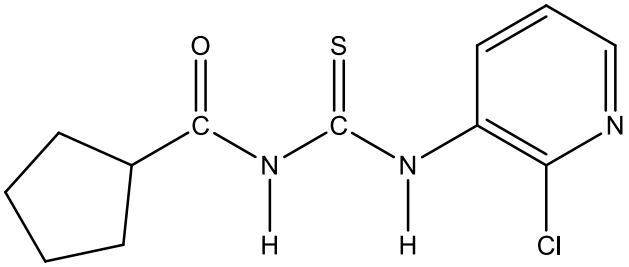

12

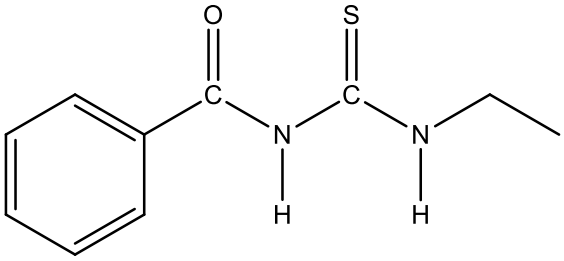

13

1.4 Coordination modes of thioureas

The flexible nature of thiourea ligands allow for a multitude of coordination possibilities using either the hard nitrogen or soft sulfur donor atoms[48]. The acyl thiourea derivatives, which bind predominantly through the sulfur and oxygen donor atoms to form monoanionic six-membered ring complexes of the type in **14** have been extensively investigated[45,49-52]. The *N,,N'* -disubstituted thioureas may bind as monodentate monoanionic ligands coordinating to the metal centre through the soft sulfur donor atom of the thiourea **15** or as neutral monodentate ligands coordinating through the thione sulfur atom **16**. A significant number of these types of compounds have been synthesised and reported in the literature[9,53,54]. The *N,S*-chelating thioureas, on the other hand, have been reported to form monoanionic complexes **17** and dianionic metal complexes **18** with variety of metal centres, including platinum[9,55], palladium[56], nickel[57] ruthenium, rhodium, iridium and osmium[58,59], gold(I)[60] gold(III)[61], aluminium[62], technetium[54] and chromium[63]. Apart from these binding modes, other bonding possibilities exist for thiourea ligands including as dianionic *N,S* bidentate ligands bridging through sulfur in dinuclear complexes **19**[64], as neutral bridging ligands through the sulfur donor atom **20**[65] or as tridentate ligands forming M-M bonded trinuclear centres 2**1**-**22**[66].

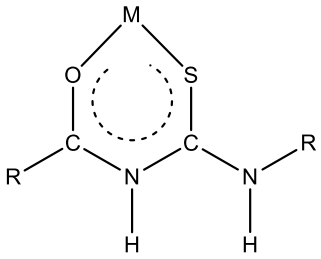

14

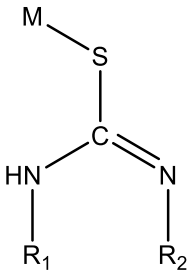

15

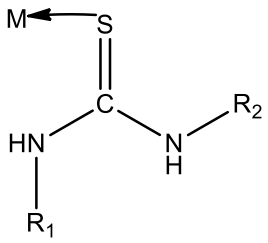

16

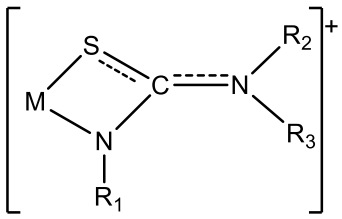

17

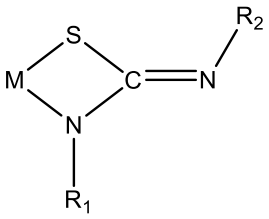

18

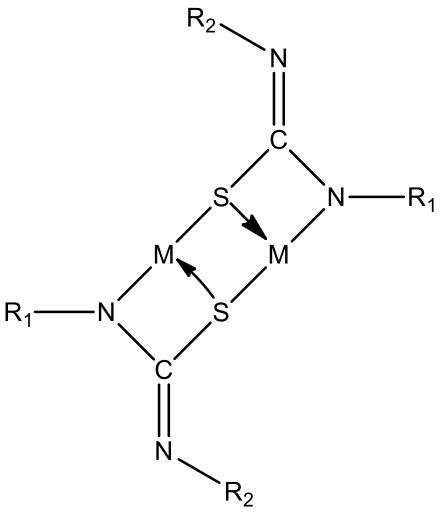

19

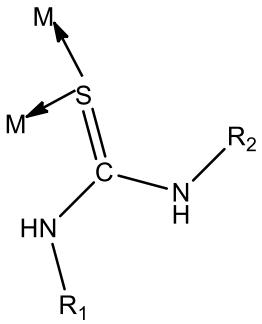

20

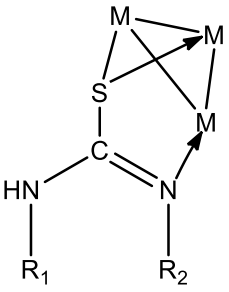

21

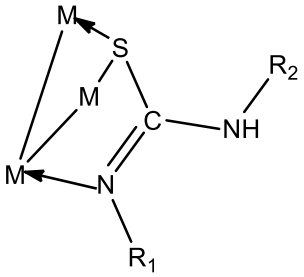

22

1.5 Coordination chemistry of thiourea monoanion and dianion ligands

1.5.1 *Synthesis and structure of platinum group metal complexes of thiourea dianions*

A range of synthetic methods has been applied in the synthesis of several platinum complexes containing bidentate thiourea dianion ligands in four-membered metallacyclic rings [55,57]. The two methods predominantly used for the synthesis of thiourea dianion and monoanion complexes are the silver(I) oxide and the triethylamine mediated synthesis methods.

1.5.2 *Silver(I) oxide-mediated synthesis*

Silver(I) oxide is a well-known facilitating reagent in the formation of new platinum carbon bonds. The first example of this process was reported in 1977[67]. Subsequently, other metal-ligand bonds have been formed using this method[5,48,68,69]. Silver(I) oxide has been considered to simultaneously serve as a halide abstracting agent (Ag^+) and a strong base (O^{2-}) which removes protons from the electron-withdrawing groups on the ligand. Silver(I) oxide reactions are typically carried out in air without exclusion of water as it is one of the by-products. The only other supposed by-product of the reaction is silver(I) chloride which is usually removed with the excess silver(I) oxide by filtration. The problem with silver(I) oxide-mediated reaction is that it can result in products having a slight purple tinge. This may be as a result of colloidal silver, from the decomposition of soluble silver-containing complexes which form during the reaction and can be removed by filtration through a fine glass filter paper.

1.5.3 *Triethylamine mediated synthesis*

The triethylamine mediated synthesis involves the addition of excess triethylamine base to the reaction mixture in refluxing methanol to afford the thiourea metal complex **Scheme 1.3**. The triethylamine abstracts the H^+ from the thiourea nitrogen to form the triethylammonium chloride salt and water. The complex is precipitated out of the methanol solution with water, filtered off and washed with water to remove triethylammonium chloride and excess amine. There have been previous reports on the successful synthesis of metal complexes of thioureas and other *N*,*S*-donor ligands using the triethylamine base and the analogous trimethylamine[9,37,57,70]. This method was explored for the synthesis of

metal-thiourea dianion complexes reported in this thesis. The products obtained in this case were very pure and obtained in high yield. ESI-mass spectral analysis of the complexes synthesised by this method showed high purity.

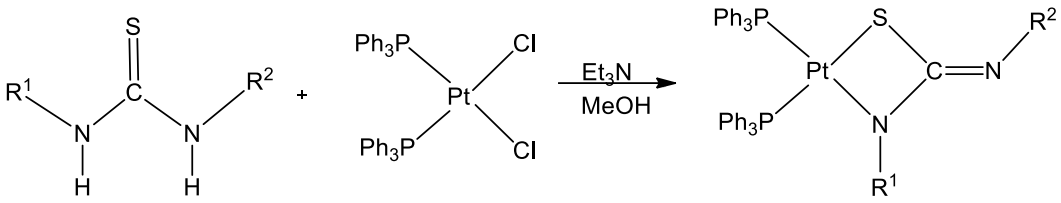

Scheme 1.3: Reaction scheme for the Et_3N mediated synthesis of platinum thiourea dianion complexes.

1.5.4 *Thiourea dianion complexes of platinum*

A number of thiourea dianion complexes of platinum have been successfully synthesised using different synthetic methods. In 1992, Okeya *et al.* synthesised the first thiourea dianion complex of bis(triphenylphosphine) platinum $[Pt\{SC(=NEt)NEt\}(PPh_3)_2]$ **23** by reacting equimolar quantities of $[Pt(acac)(PPh_3)_2](acac)$ (acac = acetylacetonate anion) and *N*,*N*'-diethylthiourea in refluxing methanol solution to afford yellow cubic crystals of the target complex. The absence of the ν(NH) bands in the IR and NH signals in the ^1H NMR indicated the dianionic nature of the ligand. The X-ray crystal structure of the compound confirmed the coordination geometry, where the *N, S*-donor atoms of the thiourea are coordinated to the platinum to form a distorted square planar chelate ring[55].

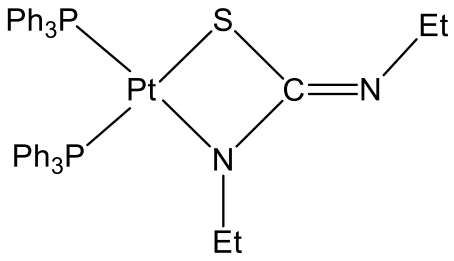

23

Later the same year Henderson and co-workers[71] reported a series of thiourea dianion complexes synthesised from the reaction of *cis*-[$PtCl_2L_2$] [L = PPh_3, $PMePh_2$, PEt_2Ph, $PPh_2(NEt_2)$ and L_2 = $Ph_2PCH_2CH_2PPh_2$ (dppe) with 1 molar equivalent of *N*,*N*'-diphenylthiourea and an excess of silver(I) oxide in refluxing dichloromethane solution to give the complexes **24-29** in reasonable yields. The $^{31}P\{^1H\}$ NMR analysis of the complexes **24-29** showed the simple second-order AB spin system with corresponding platinum coupling satellites consistent with phosphorus nucleus *trans* to sulfur and nitrogen. The single-crystal X-ray structure of the triphenylphosphine complex **24**, (**Figure 1.1**) showed that the four-membered metallacyclic {PtSCN} ring is planar with the two phenyl groups orientated orthogonally out of the plane of the metallacyclic ring.

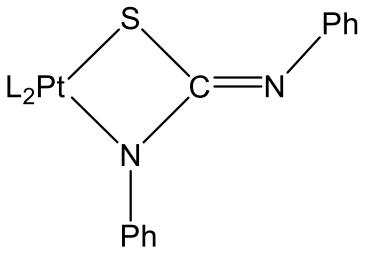

24 L = PPh_3

25 L = $PMePh_2$

26 L = PMe_2Ph

27 L = PEt_2Ph

28 L = $PPh_2(NEt_2)$

29 L_2 = dppe

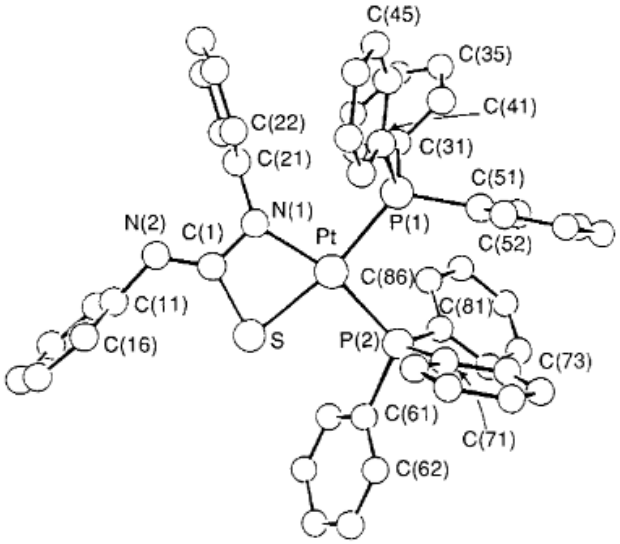

Figure 1.1: Molecular structure of [Pt{SC(=NPh)NPh}(PPh_3)$_2$] **22** showing the two phenyl substituents at right angles to the plane of the metallacyclic ring[71].

In a similar investigation, platinum(II) complexes derived from the thiourea dianion ligand $[MeNC(S)N(CN)]^{2-}$ were synthesised by reacting the platinum halide complex $[PtCl_2L_2]$ [L = tertiary phosphine or L_2 = cyclo-octa-1,5-diene (COD)] with the sodium salt of *N*-methyl-*N*'-cyanothiourea in refluxing dichloromethane and mediated by silver(I) oxide or trimethylamine to afford microcrystalline precipitates of the corresponding thiourea complexes in good yield[48]. The X-ray crystal structure of the COD derivative **30** revealed two independent molecules in the unit cell with some conformational differences in the COD ligands. The molecular structure of one of the molecules in **Figure 1.2** showed the expected square planar geometry with the platinum metal coordinated to a chelating COD ligand and the dianionic thiourea ligand. The authors noted that the NMR data showed only a single isomer of the complex for the two independent molecules with the cyano group directed away from the methyl substituent on the metallacyclic nitrogen and consistent with the formation of a thiourea dianionic complex containing asymmetrically substituted thioureas.

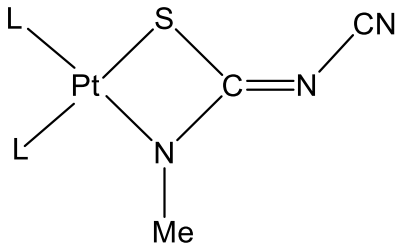

30 L-L = COD

31 L = PPh_3

32 L-L = DPPF

33 L-L = DPPE

34 L = PBu^n_3

35 L = $P(OPh)_3$

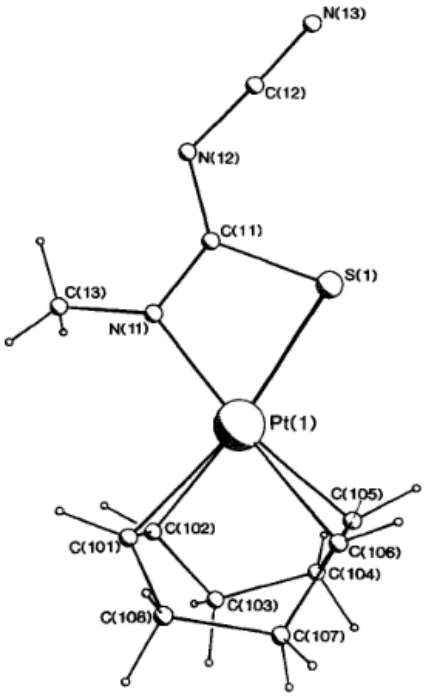

Figure 1.2: Molecular structure of [Pt{NMeC(=NCN)S}(COD)] **30**, showing the CN group directed away from the metallacyclic ring[48].

Recently a series of alkyl-substituted thiourea dianion platinum complexes of the type [Pt{SC(=NPh)NR}$(PPh_3)_2$] were reported by Spenceley and Henderson[37] where R is a straight or branched-chain alkyl group (R= Et, Me, Pr^n, Pr^i, Bu^n, Bu^t). The asymmetrically substituted thiourea dianion complexes were synthesised by the reaction of *cis*-[$PtCl_2(PPh_3)_2$] and the corresponding thioureas in refluxing methanol solution using triethylamine base (**Scheme 1.4**). The ^{1}H and ^{31}P{^{1}H} NMR spectra of the complexes showed the presence of isomers. The authors proposed a mechanism for the isomerisation and this involved the initial formation of the kinetically favoured distal isomer (**Scheme 1.4**) and subsequent isomerisation to the thermodynamically favoured proximal isomer when dissolved in $CDCl_3$ solution. The complex containing the branched-chain alkyl substituent Bu^t showed the opposite trend. X-ray crystal structure of the ethyl substituted complex **36b**, which crystallised from a dichloromethane solution by vapour diffusion of pentane, was determined. The square planar coordination geometry of the four-membered metallacycle confirmed the proximal isomeric configuration of the dianion complex. The ethyl group adjacent to the platinum metal is orientated out of the plane of the metallacyclic ring as evidenced by the Pt-N(1)-C(1)-(C_3) torsion angle of 104.3(4)^o (**Figure 1.3**).

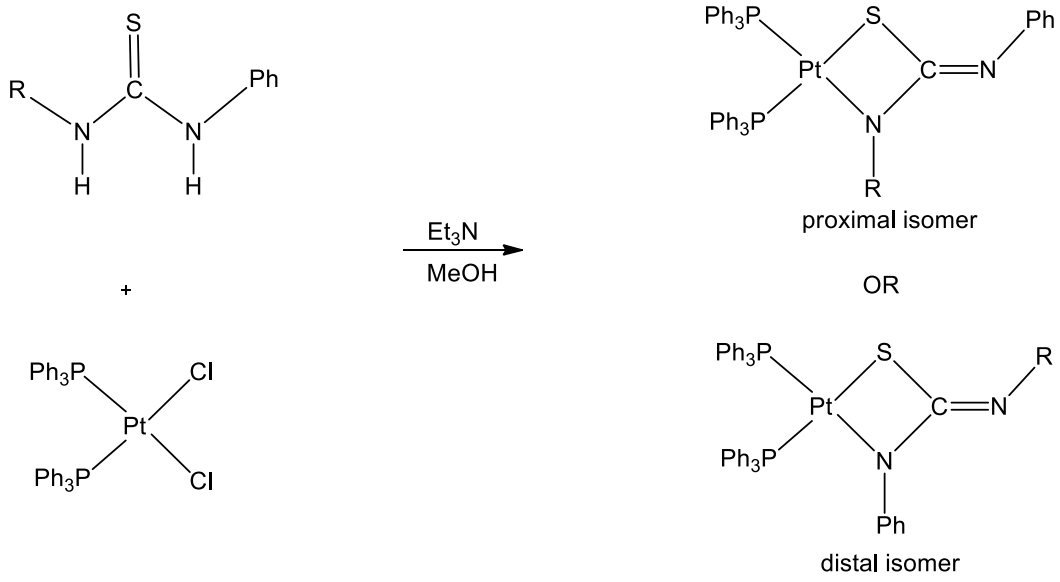

R = Me, **36a**; R = Et, **36b**; R = Pr^n, **36c**; R = Bu^n, **36d**; R = Bu^t, **36e**

Scheme 1.4: Reaction scheme for the formation of asymmetrically substituted thiourea dianion complexes **36** (**a-e**)[37]

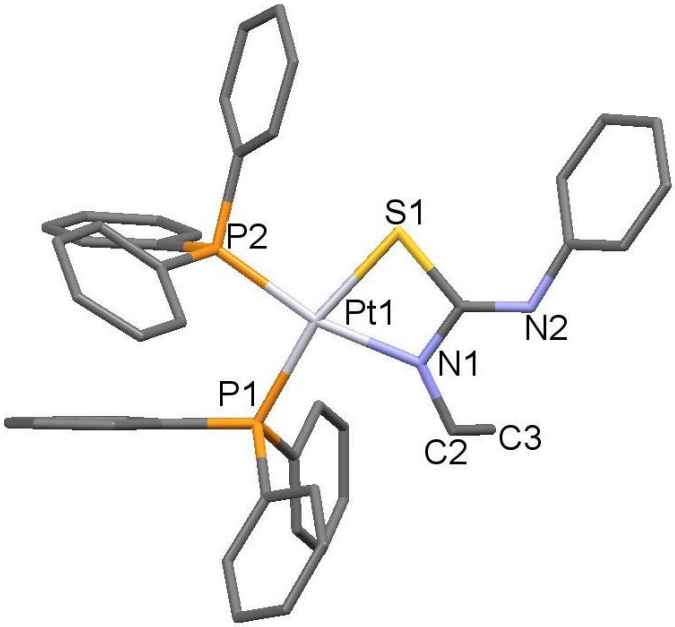

Figure 1.3: Molecular structure of ethyl substituted thiourea dianion complex [Pt{SC=(NEt)NPh}$(PPh_3)_2$]. Hydrogen atoms are omitted for clarity

1.5.5 *Thiourea dianion complexes of palladium*

Thiourea dianion complexes of palladium and nickel are very rare. Only a few reports of these complexes have been found in the literature. The *N*,*S*-palladium thiourea dianion complex [Pd(tol_2TU^{-2}-*N*,*S*)(tol_2TU-S)(dppm-P)] (**37a**) was synthesised in 1995[56] by the reaction of [Pd(tol_2TU^{-2}-*N*,*S*)$_2$] (tol_2TU=1,3–di(o-tolyl)-thiourea with dppm in dichloromethane solution where dppm = bis-(diphenylphosphino)methane. A refrigerated mixture of the complex and pentane afforded orange coloured cubic crystals of the dianion complex in high yield. $^{31}P\{^1H\}$ NMR analysis indicated a large difference in the chemical shifts of the two phosphorus nuclei (52 Hz) which confirmed the unidentate coordination of the dppm ligand. The complex was however observed to be unstable in organic solvents, disintegrating in dichloromethane solution to form the sulfur bridged palladium complex [(Pd(S)R_2TU^{-1})$_2$(dppm)] (R = o-tol) **37b**.

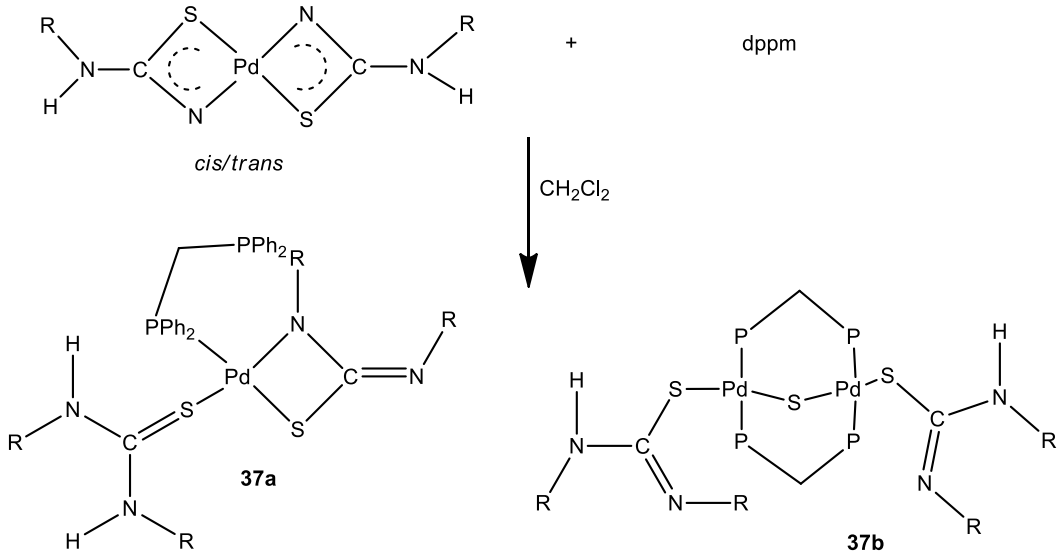

Scheme 1.5: Reaction scheme for the synthesis of palladium thiourea dianion complex [Pd(tol_2TU^{-2}-*N*,*S*)(tol_2TU-S)(dppm-P)][56] (R = o-tol)

1.5.6 *Thiourea monoanion complexes of platinum, palladium, nickel and gold*

A significant number of metal complexes containing the thiourea monoanion ligand have been reported in the literature. Only representative examples will be discussed in this chapter. Henderson and co-workers in 2001

reported the synthesis of a few thiourea monoanion complexes of platinum **38** and **39**. These compounds were synthesised from the reaction of *cis*-[$PtCl_2(PPh_3)_2$] and the corresponding thiourea in refluxing methanol. Addition of $NaBPh_4$ to the hot solution resulted in precipitation of the tetraphenylborate salts of the corresponding thiourea monoanion complexes in good yield[9]. The diethyl derivative, **39** was isolated previously as its hfac salt from the reaction of [Pt(hfac)$(PPh_3)_2$(hfac)] (hfac = 1,1,1,5,5,5-hexafluoro-2,4-pentanedionate anion) and 1,3-diethylthiourea in refluxing dichloromethane. $^{31}P\{^1H\}$ NMR spectra showed two resonances with coupling constant values similar to the ones reported in the literature[55]. Six other tri-substituted monoanionic complexes **40**-**46** were synthesised. The $^{31}P\{^1H\}$ NMR spectrum of the cyano-substituted complex showed the presence of a mixture of two isomers of the compound **40** and **41** with similar $^1J_{(PtP)}$ coupling constants of 3032 and 3305 Hz for **40** and 3031 and 3182 Hz for **41**.

The X-ray crystal structure of the azo-dye derivative **46** showed the monoanionic square planar coordination geometry of the complexes. The thiourea phenyl ring was reported to be out of the plane of N(1)-C(1)-N(2)-S ring by an angle of 60.9° while the planes of the two azo-dye phenyl rings are separated by an angle of 24.4°.

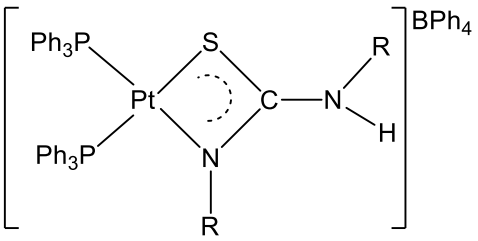

38 R = Ph

39 R = Et

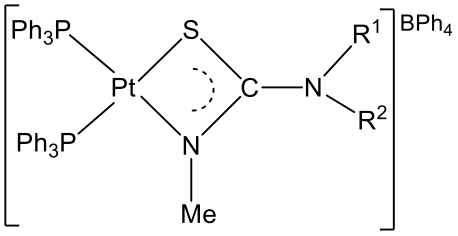

40 R^1 = CN, R^2 = H

41 R^1 = H, R^2 = CN

42 $R^1R^2 = (CH_2CH_2)_2O$

43 $R^1 = R^2 = CH_2Ph$

44 $R^1 = CH_2Ph$, R^2 = Et

45 R^1 = Me, $R^2 = CH_2$(9-anthracenyl)

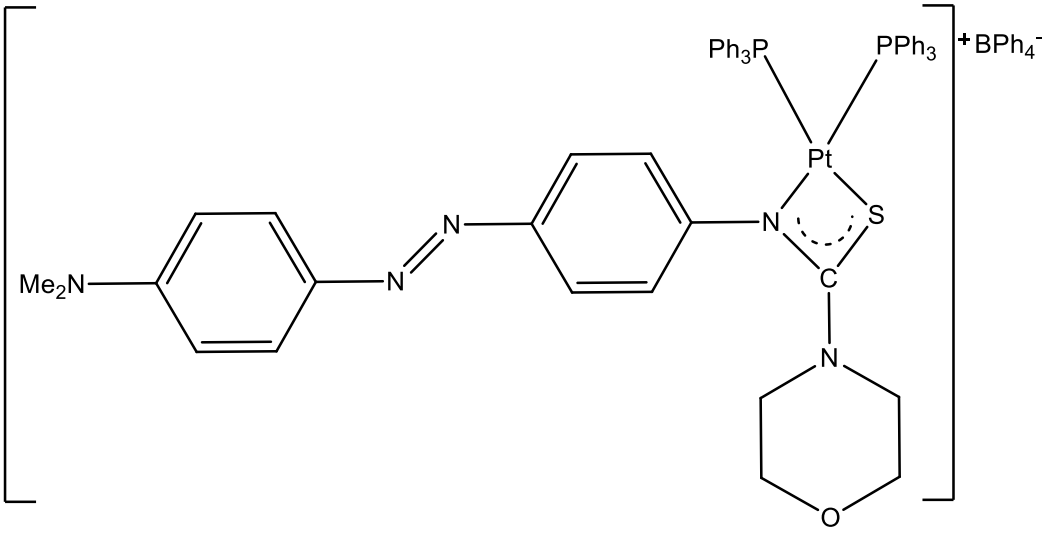

46

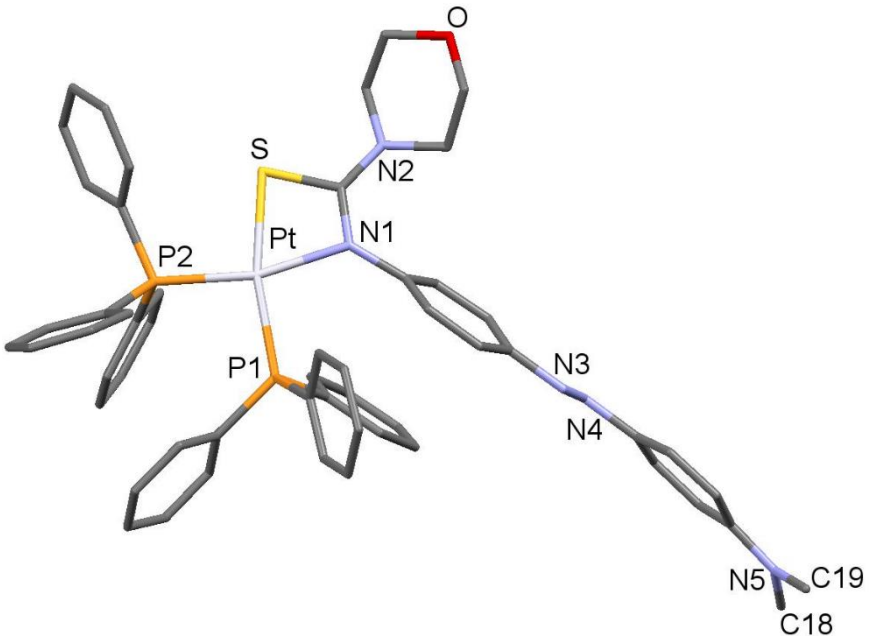

Figure 1.4: Molecular structure of the cationic thiourea monoanion complex **46**[9]. BPh_4 anion is omitted for clarity.

A series of platinum, palladium and nickel complexes of *N*-allyl-*N*'-pyrimidin-2-yl thiourea were synthesised by Kandil and co-workers[72]. The ligand was synthesised by the reaction of allylisothiocyanate with 2-aminopyrimidine. The

reaction of equimolar quantities of nickel(II), palladium(II) and platinum(II) chloride precursors and the *N*-allyl-*N*'-pyrimidin-2-yl thiourea ligand in refluxing ethanol for 24 hours resulted in the complexes **47**(**a-c**). Spectroscopic evidence revealed a 1:1 stoichiometry for the complexes. The coordination geometry of the complexes was confirmed by shifts in the infrared spectral bands of the ligand after coordination, indicating possible coordination through the nitrogen of the pyrimidine functional group.

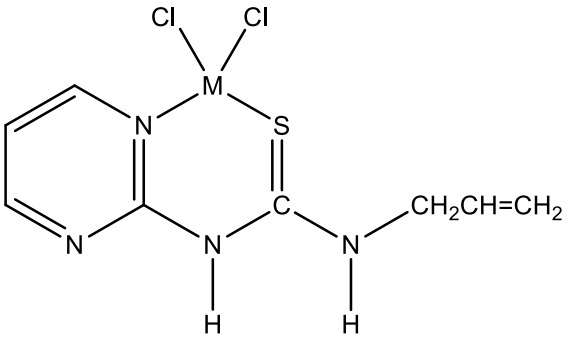

M = Ni, **47a**; M = Pd, **47b**; M = Pt, **47c**

Later in 2011, Bippus *et al*[73] synthesised some platinum monoanionic thiourea complexes containing the water-soluble PTA ligand (PTA = 1,3,5- triaza-7-phosphaadamantane). The complexes were synthesised from the reaction of *cis*-$[PtCl_2(PTA)_2]$ and $4\text{-}RC_6H_4NHC(S)NR^1{}_2$ and $4\text{-}ClC_6H_4NHC(S)NR$ (NR = 2–pyridylpiperazine) in the presence of a base to afford the mono-cationic platinum(II) complexes *cis*-$[Pt\{SC(NR^1)=NC_6H_4R\}(PTA)_2]^+$ [R^1 = Me, R = H, **48**; R^1 = Me, R= Cl, **49**; R^1 = Et, R= Cl **50** and *cis*-$[Pt\{SC(NR^1)= NC_6H_4R\}(PTA)_2]^+$ **51** [NR^1 = 2–pyridylpiperazine] as their PF_6 salts. The complexes were however found to be insoluble in water despite the presence of two molecules of the PTA ligand.

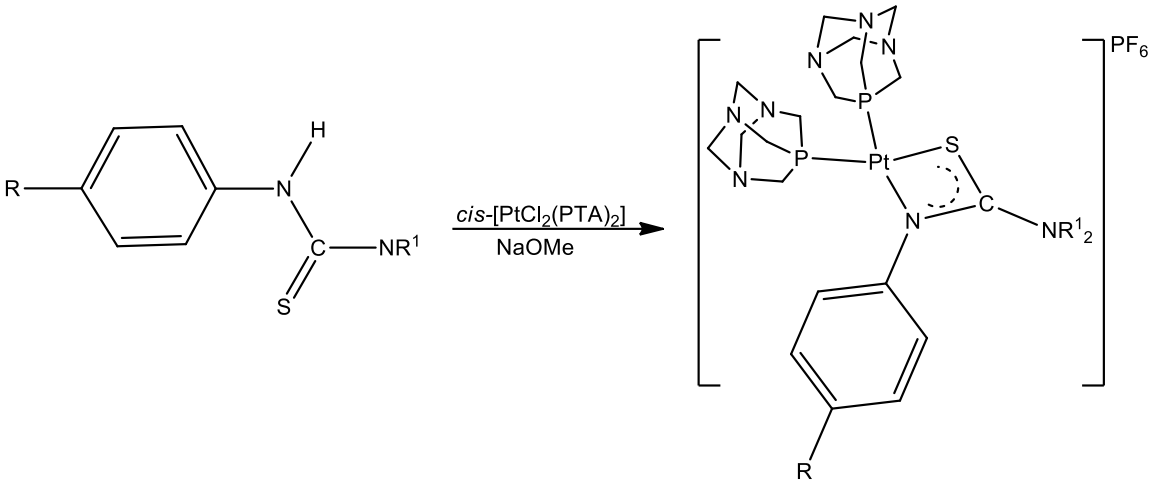

R^1 = Me, R= H; **48**, R^1 = Me, R = Cl; **49**, R^1 = Et, R = Cl; **50**, R = Cl, NR^1 = 2–pyridylpiperazine; **51**

Scheme 1.6: Reaction scheme for synthesis of PTA-substituted platinum complexes **48-51**

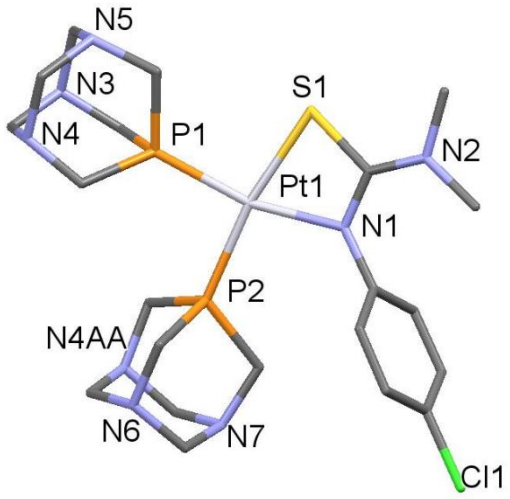

Figure 1.5: Molecular structure of *cis*-[Pt{SC=(NC_6H_4Cl)NMe_2}$(PTA)_2$]$^+$ **49**. PF_6 anion is omitted for clarity.

The molecular structure of the methyl-substituted complex **49**, (**Figure 1.5**) confirms the square planar configuration of the complex. The coordination sphere consists of a platinum centre bound to two PTA ligands and one deprotonated nitrogen and sulfur donor atoms of the thiourea ligand to give a four-membered metallacycle with an S(1)-Pt(1)-N(1) angle of 68.58(6)^o subtended at the platinum centre[73]. In the same year[57], a series of tri-substituted thiourea nickel complexes were reported. The monoanion complexes were synthesised by the reaction of

equimolar quantities of nickel(II) acetate, 1,2-bis-(diphenylphosphinoethane) (dppe) and a series of tri-substituted thiourea ligands $R^1NHC(S)R^2R^3$ in warm methanol and trimethylamine base resulting in the formation of orange coloured cationic complexes of the form $[Ni\{SC(NR^2R^3)NR^1\}(dppe)]^+$. Addition of excess $NaBPh_4$ to the hot solution gave orange coloured tetraphenylborate salts in good to moderate yields **52-63 (Scheme 1.7)**.

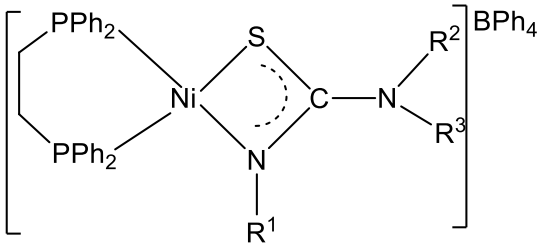

52 - 63

Complex	**R^1**	**R^2R^3**
52	Ph	Me, Me
53	Ph	Cy, Cy
54	Ph	$(CH_2)_4$
55	Ph	$(CH_2)_5$
56	Ph	$(CH_2CH_2)_2O$
57	Ph	$(CH_2CH_2)_2S$
58	Ph	CH_2Ph, (R)-CHMePh
59	Ph	Ph, H
60	Ph	Ph, H
61	Bu^n	Bu^n, H
62	*p*-$C_6H_4NO_2$	Me, Me
63	*p*-$C_6H_4NO_2$	$(CH_2CH_2)_2O$

Scheme 1.7: The nickel monoanion complexes and their different R substituents.

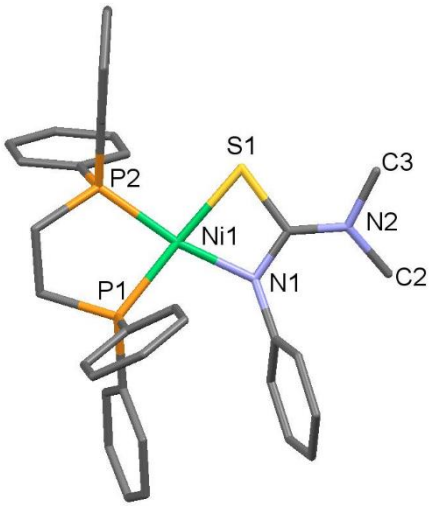

Figure 1.6: Molecular structure of the cationic nickel thiourea monoanion complex **52**. BPh_4 anion is omitted for clarity

1.5.7 *Gold(I) thiourea complexes*

Gold complexes and their coordination chemistry have received much attention lately. The gold(I) thiourea complexes are by far the most studied[74-77]. Most of the gold(I) thiourea complexes reported in the literature formed neutral or cationic complexes coordinating through the soft sulfur donor ligands of the thiourea moiety [60,74,75,77]. In 2003, a series of phosphine gold(I) complexes of thiourea ligands were synthesised and characterised by X-ray crystallography, NMR and IR spectroscopy. The complexes were synthesised by the reaction of R_3PAuCl (R=Me, Et, Cy, Ph, *o*-Tol, *m*-Tol) in refluxing methanol or acetonitrile with equivalent quantities of unsubstituted thiourea (HTu) to give crystalline products in moderate to high yields[75]. The X-ray crystal structure of the tri-cyclohexyl derivative of the complex was determined to confirm the coordination geometry structure of the complexes unequivocally. The molecular structure of the complex shown in **Figure 1.7** shows the P-Au-S chelation in an almost linear configuration with an angle of 168.54(9)^o. The phosphorus atom in the complex occupies the usual tetrahedral geometry with the attached cyclohexyl groups adopting the familiar chair conformations, as shown in **Figure 1.7**.

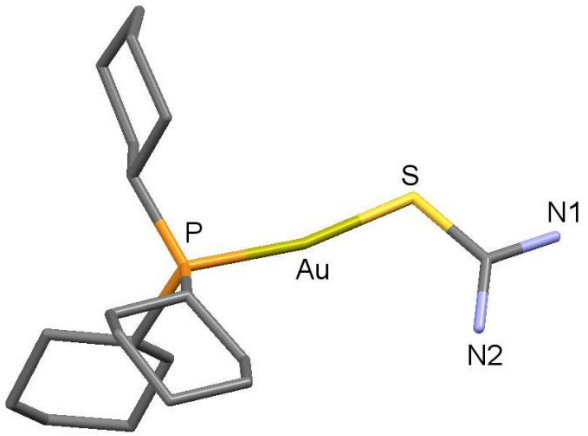

Figure 1.7: Molecular structure of thiourea gold(I) complex Cy_3PAuTu showing the chair conformational geometry of the Cy rings (Tu = thiourea)

Henderson and co-workers synthesised a series of monoanionic gold(I) thiourea complexes from the reaction of gold(I) phosphine complexes Ph_3PAuCl, Cy_3PAuCl, and the bisphosphine analogues $dppf(AuCl)_2$ [dppf = $Fe(\eta^5\text{-}C_5H_4PPh_2)_2$] and $dppe(AuCl)_2$ (dppe = $Ph_2PCH_2CH_2PPh_2$) with a number of trisubstituted thioureas in refluxing methanol solution and excess triethylamine base to give gold(I) complexes containing thiourea monoanion ligands[60]. Two disubstituted thiourea monoanionic gold complexes **74** and **75** were also synthesised with a monoanionic thiourea salt Na[MeNHC(S)NCN] and Ph_3PAuCl and $dppe(AuCl)_2$ in the absence of the triethylamine base.

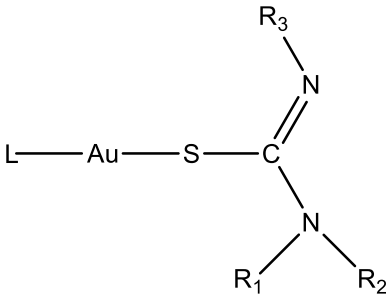

Complex	L	R_1R_2	R_3
64	PPh_3	$(CH_2CH_2)_2O$	Ph
65	PPh_3	$(CH_2CH_2)_2S$	Ph
66	PPh_3	$(CH_2Ph)_2$	Ph
67	PPh_3	Me_2	Ph
68	PPh_3	Me_2	*p*-$C_6H_4NO_2$
69	PPh_3	$(CH_2)_4$	Ph
70	PPh_3	$(CH_2)_5$	Ph
71	PPh_3	HMe	CN
72	PCy_3	Me_2	Ph
73	PCy_3	$(CH_2CH_2)_2O$	Ph

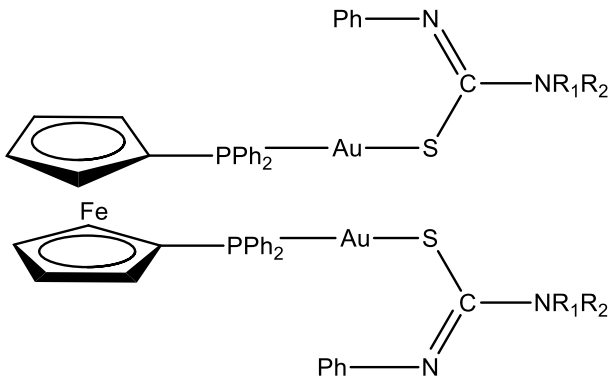

74 $R_2R_2 = (CH_2CH_2)_2O$

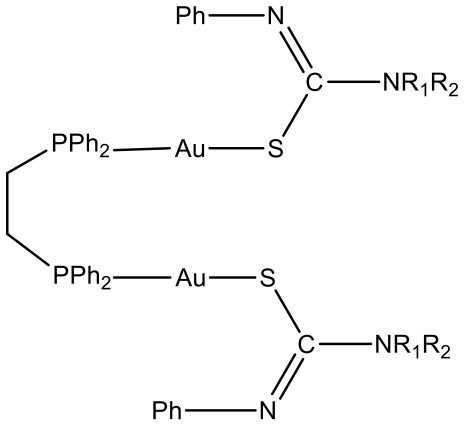

75 $R_2R_2 = (CH_2CH_2)_2O$, R_3 = Ph

76 R_2R_2 = HMe, R_3 = CN

The molecular structure of the morpholine-substituted mononuclear complex **64** showed a linear coordination sphere for the gold(I) centre comprising of the S and P donor atoms of the thiourea and PPh_3 ligands respectively. The structure was essentially planar, and the bond distances depicted the possibility of delocalisation of the thiolate π bonding system. The thiolate ligand of the gold(I) thiourea complex was observed to be orientated in such a way that the phenyl group of the thiourea is sitting directly above the gold(I) atom giving an Au–phenyl centroid bond distance of 3.449(18) Å **Figure 1.8**. The molecular structures of the other mononuclear complexes were reported to be similar to the structure described in **Figure 1.8**. The structures of the other complexes were confirmed by the use of ^{1}H, $^{31}P\{^{1}H\}$ NMR spectroscopy and ESI-mass spectrometry.

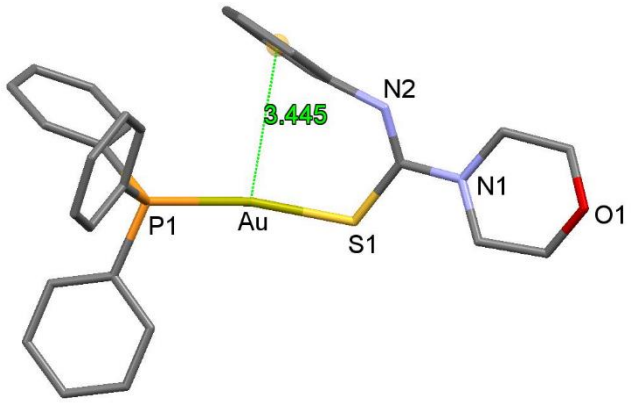

Figure 1.8: Molecular structure of gold(I) thiourea complex **64** showing the linear geometry of the gold(I) coordination sphere and the orientation of the phenyl group to the gold atom.

The dinuclear complexes showed similar coordination environment with the mononuclear complexes. The crystal structure of the dppf complex **74** (**Figure 1.9**) was reported to have crystallised with two similar but independent half molecules in the asymmetric unit with each molecule situated on a crystallographic centre of inversion. The planarity of the thiolate ligands were however found to exhibit some significant differences. The dppe substituted complex **75** also crystallised with two independent molecules in the asymmetric unit with similar geometric parameters as those found in the dppf substituted complex **74**.

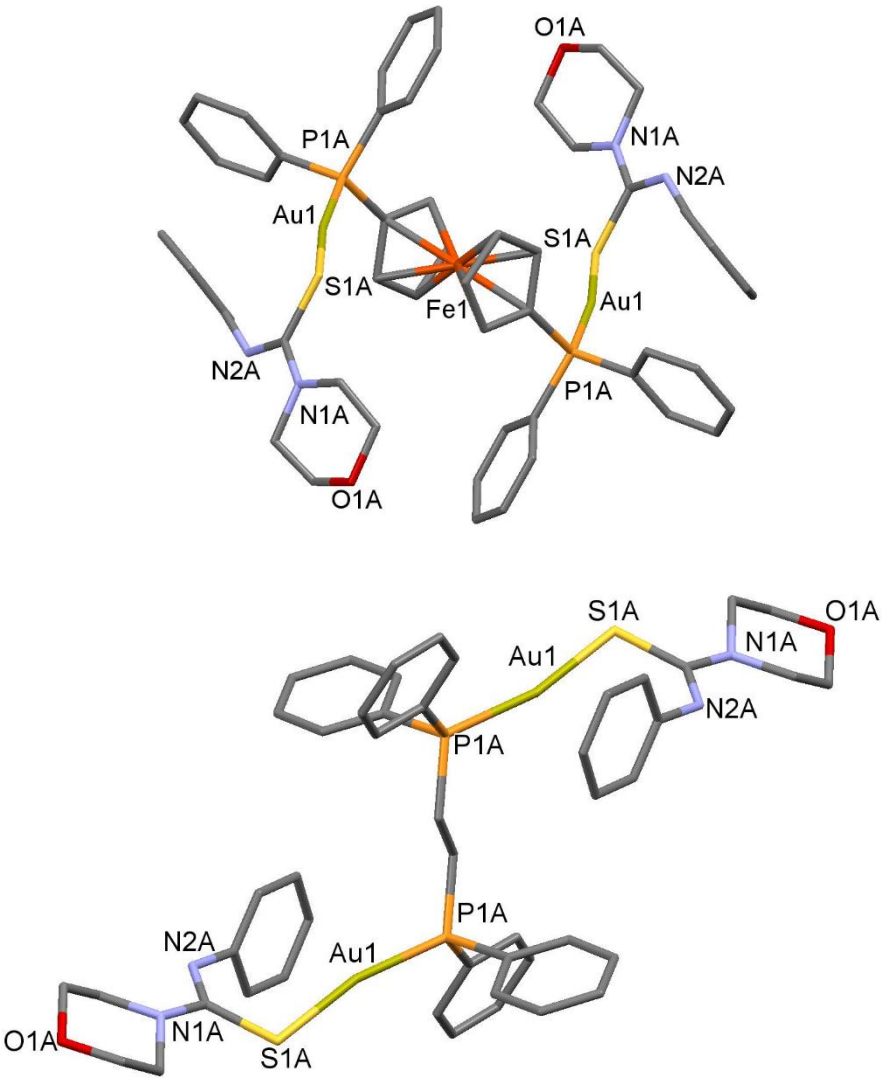

Figure 1.9: Molecular structures of dinuclear gold(I) thiourea monoanion complexes **74** (top) and **75** (bottom).

1.5.8 *Gold(III) thiourea complexes*

The number of publications on the coordination chemistry of the analogous gold(III) thiourea complexes is rather limited. Dinger and co-workers[78] in 1998 attempted the synthesis of cycloaurated gold(III) complexes of the di-substituted thiourea MeNHC(S)NHMe by reacting equimolar quantities of the ligand and gold(III) dihalide complexes [{$C_6H_3(CH_2NMe_2)$-2-R-5}AuX_2] (R = OMe, H:X = Cl) in refluxing dichloromethane and excess Ag_2O. This reaction conditions were successful in the synthesis of platinum(II) thiourea complexes but did not give the expected gold(III) thiourea complexes, notwithstanding the isoelectronic parity of Pt(II) and Au(III). The Au(III) thiourea reactions gave multimetallic gold(III)-silver(I)-sulfido aggregate cations [{[{$C_6H_3(CH_2NMe_2)$-2-R-5}Au(μ-S)]$_2$}AgX_2]$^+$(R = OMe, H; X = Cl, Br) formed from the thiourea desulfurisation.

Recently Smith *et al* reported the synthesis of a series of cycloaurated gold(III) thiourea complexes **77-80** (**Scheme 1.8**) by the reaction of two different gold(III) chloride complexes with equivalent amounts of $PhNHC(S)NCy_2$ or $PhNHC(S)NMe_2$ in refluxing methanol solution and trimethylamine base resulting in a bright yellow solution of the compounds, which were precipitated by the addition of excess $NaBPh_4$.

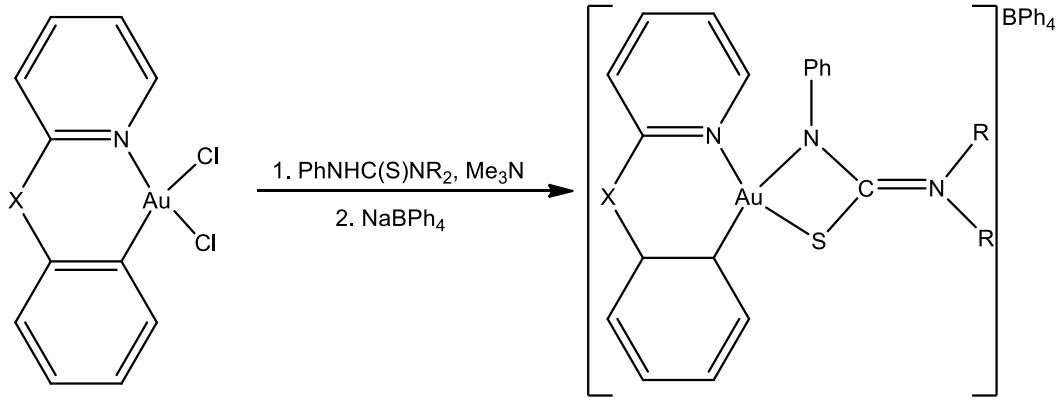

77 X = NH, R = Cy

78 X = NH, R = Me

79 X = CH_2, R = Me

80 X = NH, RR = $(CH_2CH_2)_2O$

Scheme 1.8: Synthesis of cycloaurated gold(III) complexes of trisubstituted thiourea ligands[78]

The X-ray crystal structure of the complex **77**, **Figure 1.10**, confirmed the cycloaurated anilinopyridylgold(III) complex containing the thiourea monoanion ligand and a BPh_4 counterion. The thiourea ligand was coordinated to the gold complex through the NPh and S donor atoms with the sulfur in a mutual *cis* position with the carbon donor atom of the anilinopyridyl ligand. The thiourea phenyl group in the complex is othorgonally oriented to the plane of the metallacyclic ring due to the steric bulk of the adjacent cyclohexyl group.

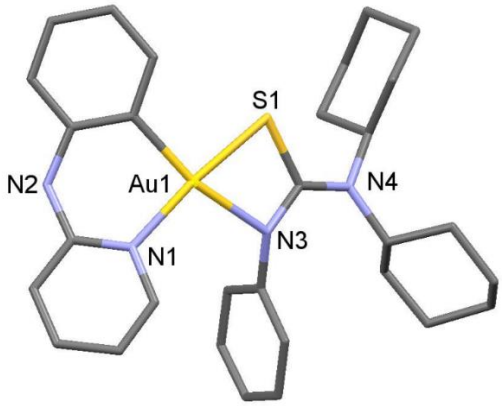

Figure 1.10: Molecular structure of the cation of cycloaurated gold(III) thiourea complex **77**.

1.6 Ruthenium, rhodium and iridium complexes of thioureas

The chemistry of the ruthenium η^6-arene complexes is very versed and well established. This is evident in the number of reviews exploring the different properties of this group of compounds[79-81]. Bennett *et al.* in 1997 reviewed the chemistry of ruthenium(0) and ruthenium(II) complexes coordinating to various ligands and incorporating a number of tertiary phosphines like PMe_2Ph, $PhMePh_2$ etc. The reactivity and structural properties of these compounds were also explored[79]. Among the η^6-arene ruthenium complexes, the piano stool complexes are probably the most studied, due to their ease of synthesis, chemical stability and the susceptibility to substitution, resulting in compounds with applications in catalysis, supramolecular assemblies, molecular devices, antimicrobial and anticancer activity. A recent review captured the supramolecular properties of these arene ruthenium complexes coordinated to a variety of ligands and their applications in different fields of chemistry including medicine, photochemistry and drug sensing[81]. The solubility, catalytic and biological properties of these half-

sandwich ruthenium arene complexes are on the most part as a result of the possibility of incorporating a variety of interesting functional groups bearing the desired properties on the ruthenium centre. A number of investigations exploring the structural, catalytic, solubility and biological properties of ruthenium arene PTA (RAPTA**)** complexes containing the water-soluble 1,3,5–triaza-7-phosphaadamantane ligand have been reported in the literature[82-87]. Recently a series of reviews capturing the supramolecular properties, reactivity and practical applications of these RAPTA complexes among other metal complexes were published[88-90].

During the late 1950's Fischer and co-workers started investigating the reactivity of ruthenium arene complexes [91,92]. They synthesised the first ruthenium complex by displacing the chloride anions from $RuCl_3$ in the presence of arenes using Lewis acids under reducing conditions. A few years later Winkhaus and Singer[93] reported the synthesis of polymeric Ru(II) half-sandwich π-arene complexes $[Ru(C_7H_8)Cl_2]_x$ and $[Ru(C_6H_6)Cl_2]_x$ from the dehydrogenation of cycloheptatriene and cyclohexadiene respectively with $RuCl_3.xH_2O$ in ethanol. The ruthenium(II) arene compounds formed by this method have been reported as chloride bridged structures in the solid-state, but the bridging chlorides may be easily cleaved in weakly coordinating solvents to yield a half sandwich compound with free coordination sites[94]. Beneth, Zelonka and Baird (1972) formed monomeric complexes of the type $[RuCl_2(arene)L]$ by reacting these ruthenium arene compounds with a range of monodentate tertiary arsines and pyridine ligands (**Scheme 1.9**)

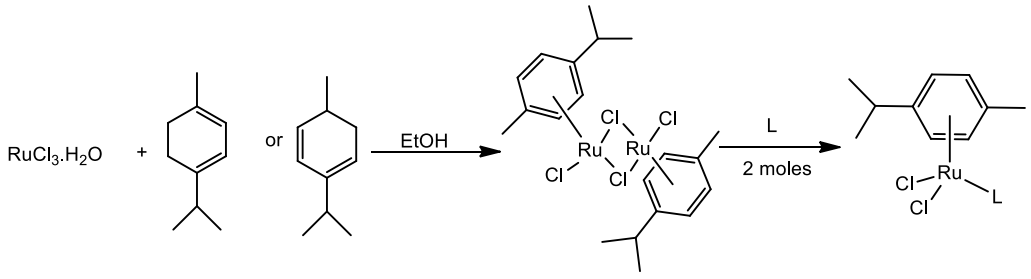

Scheme 1.9: Reaction scheme for the synthesis of monomeric ruthenium arene complex $[RuCl_2(arene)L]$

Analogous to the ruthenium arene complexes are the rhodium and iridium Cp*-derived complexes (Cp* = pentamethylcyclopentadienyl) which were being developed by Maitlis and co-workers[95-98] around the same time as their ruthenium arene counterparts. The reaction of complexes with silver(I) or sodium salts of non-coordinating counterions AgX (X= PF_6, BF_4, BPh_4 etc) extracted the chloride ions as AgCl or NaCl as the case may be, thus leaving a solvated half sandwich complex with access to the three labile coordination sites. This method was repeated with the [{Ru(arene)Cl(μ-Cl)}$_2$] complex to produce a series of monomeric compounds with the weakly coordinating solvent ligands [Ru(arene)S_3](X^-)$_2$] (S = solvent). These complexes allow all three coordination sites to be accessed by displacement of the solvent molecules. A number of ruthenium arene complexes has been prepared using this method[99,100].

The rhodium and iridium pentamethylcyclopentadienyl complexes are structurally related to the ruthenium arene complexes and are mostly investigated alongside each other. There are however not as many publications for the rhodium and iridium complexes in the literature as there are for the analogous ruthenium complexes. This is in part due to the high cost of the rhodium and iridium cyclopentadienyl starting complex. Nonetheless a significant number of publications exploring the reactivity, supramolecular and coordination chemistry of rhodium and iridium complexes incorporating a variety of ligands have been reported [101,102]. There are also other reports on the chemistry of ruthenium arene complexes and the cyclopentadienyl rhodium and iridium complexes incorporating the thiourea ligand. A greater percentage of these reports involve mostly the neutral or cationic acyl thiourea ligands[70,103-108]. There are only a few reports of ruthenium, rhodium and iridium complexes coordinated to thiourea dianion and monoanion ligands.

The early 1980s saw the rise in research into the chemistry of heterocumulenes such as CS_2, PhNCO, PhNCS, and OCS including their insertion reactions into metal-nitrogen (M-N) bonds. In 1983, Piraino *et al*[109] reported the results of insertion reactions of some heterocumulenes (OCS, CS_2, PhNCO, PhNCS) into the Rh-N bond of the rhodium complex [Rh(η-C_5Me_5)Cl(*p*-$MeC_6H_4N{=}CH{=}NC_6H_4Me$-*p*]. A formal insertion of the PhNCS into the Rh-N bond of the rhodium complex above resulted in a thioureido complex [Rh(η-C_5Me_5)Cl-{PhN=C[[N(C_6H_4Me-*p*)-CH=NC_6H_4Me-*p*]=S}]. The X-ray crystal structural

analysis of the complex in **Figure 1.11** confirmed the PhNCS insertion with a monomeric nature of the complex. The Rh(III) was coordinated by the chloride, sulfur and nitrogen atoms of the thioureido ligand and the η^5-bonded pentamethylcyclopentadienyl ligand. The coordination geometry of the complex could best be described as a three-legged piano stool with the rhodium atom sitting 0.572 Å away from the plane defined by the centre of gravity of the cyclopentadienyl ring and the sulfur and nitrogen atoms of the thioureido ligand. The chlorine atom is displaced on the same side by 2.846 Å. The deviations from the best mean plane of the thioureido ligand were similar to those reported for a related thioureido complex chloro-(*N*,*N*-dimethylthiocarbomoyl)(*N*,*N*′-dimethyl-*N*′-phenyl-thioureido)triphenylphosphinerhodium(III)[110].

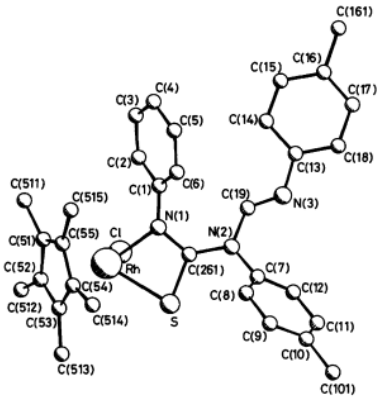

Figure 1.11: Molecular structure of the rhodium thiourea dianion complex [Rh(η-C_5Me_5)Cl{PhNC[[N(C_6H_4Me-*p*)-CH=NC_6H_4Me-*p*]=S}][109].

In the early 2000s, Robinson and co-workers started investigating the coordination geometry of *N*,*S*-chelated diphenylthioureido complexes of ruthenium, osmium and iridium prepared by the direct reaction of *N,N'*-diphenyl thiourea with the appropriate platinum metal hydride[58]. The reaction of [RuHCl(CO)(PPh_3)$_3$] with *N,N'*-diphenyl thiourea in refluxing benzene afforded the complex [RuCl{PhNC(NHPh)S}(CO)(PPh_3)$_2$], The $^{31}P\{^1H\}$ NMR spectrum showed a singlet indicative of either one of two possible *trans*-phosphine stereochemistries (Cl *trans* to S or NPh) but not enough evidence to distinguish between the two possible arrangements. The dihydrido derivative of the ruthenium complex [Ru(H_2)(CO)(PPh_3)$_3$] on the other hand reacted with the *N,N'*-diphenyl thiourea under more vigorous conditions (refluxing toluene) to afford the bis(thioureido) complex [Ru{PhNC(NHPh)S}$_2$(CO)(PPh_3)]. The X-ray crystal structure of the complex (**Figure 1.12)** showed an octahedral geometry around the ruthenium metal

centre and slightly distorted by the presence of two chelated ligands. The triphenylphosphine and carbonyl ligands occupied mutually *cis* positions and each situated *trans* to an NPh group of the chelated ligands with the sulfur atoms located in the remaining *trans*-coordinate sites. This geometric arrangement was reported to be similar to the one observed for corresponding guanidino complex containing the triphenylphosphine ligand $[Ru\{PhNC(NHPh)NPh\}_2CO(PPh_3)]$[111] and proposed for the corresponding dicarbonyl complex $[Ru\{PhNC(NHPh)S\}_2(CO)_2]$[112].

The reaction of the dichloride complex $[RuCl_2(PPh_3)_3]$ with diphenyl thiourea and triethylamine in refluxing toluene afforded the complex $[Ru\{PhNC(NHPh)S_2\}(PPh_3)_2]$[58]. The $^{31}P\{^1H\}$ NMR singlet peak established the magnetic equivalence of the PPh_3 ligands but was insufficient to determine the stereochemical isomer that was present from among the four possible stereochemical arrangements. However inference from related ruthenium(II) *N,S* chelates of the form $[Ru(N\text{-}S)_2(PPh_3)_2]$ pointed to a *trans*-S, *cis*-N arrangement. The reaction of the $[Ir(H)_3(PPh_3)_3]$ complex with *N,N'*-diphenyl thiourea in refluxing toluene gave the dihydride complex $[Ir(H)_2\{PhNC(NHPh)S\}(PPh_3)_2]$. The ^1H and $^{31}P\{^1H\}$ NMR pointed to the *cis*-hydrides *trans*-phosphines stereochemistry found for related iridium(III) complexes of the form $[Ir(H)_2(chelate)(PPh_3)_2]$ which has been reported to contain the asymmetrically coordinated *N,S* -thioureido ligand.

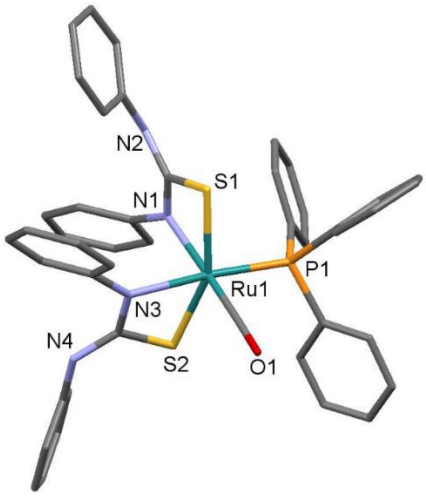

Figure 1.12: Molecular structure of the ruthenium complex $[Ru\{PhNC(NHPh)S\}_2(CO)(PPh_3)]$

Recently a series of Ru(II), Rh(III) and Ir(III) complexes of *N,S*-substituted mononuclear thiourea monoanion ligands containing 1,3-bis(3-picolyl) thiourea were synthesised by Kalidasan and co-workers[29].

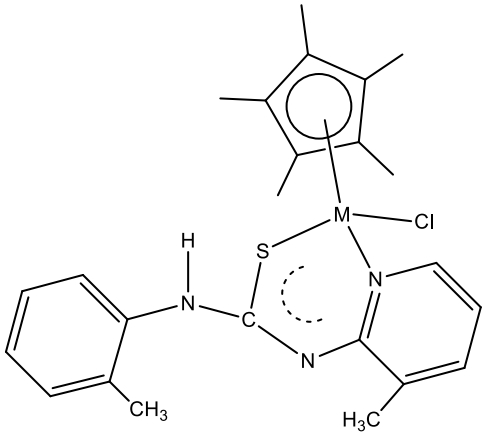

81 M = Rh **82** M = Ir

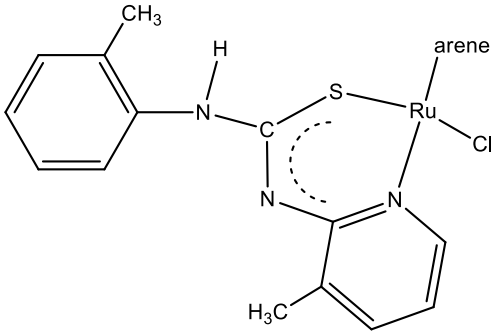

83 arene = cymene **84** benzene

The complexes were synthesised from $[Cp^*MCl_2]_2$ (M = Rh, Ir) and $[(\eta^6\text{-arene})RuCl_2]_2$ (arene = benzene) with 1:2 molar ratio of the 1,3-bis(3-picolyl)thiourea in methanol to give $[Cp^*Rh(L)Cl]^+$ **81**, $[Cp^*Ir(L)Cl]^+$ **82**, $[(\eta^6\text{-}p\text{-cymene})Ru(L)Cl]^+$ **83** and $[(\eta^6\text{-benzene})Ru(L)Cl]^+$ **84**. The cationic complexes crystallised out of solution as their PF_6^- salts in good yield. X-ray crystal structure analysis of the complexes revealed a three-legged piano-stool structure with the metal centre coordinated by the arene/Cp^* ligand, a chloride ligand and the *N*-*S*-chelated thiourea ligand as shown in the structures in **Figure 1.13**. The complexes show only *N,S*-coordination through the thiourea sulfur and the pyridine nitrogen of the thiourea ligand. This is in contrast to the organometallic *N*-phenyl-picolinamide complexes where the amide group provides an *N,N´*-coordination mode[113]. The six-membered metallacyclic ring formed has a bite angle of 86° resulting from the *pseudo*-octahedral arrangement. The complexes show some five-membered N-H-----N intramolecular hydrogen bonding. The H-N---H bond distance of 2.643 Å in **82** indicates a weaker hydrogen bond strength than **83** with an H-N----N bond distance of 2.59 Å.

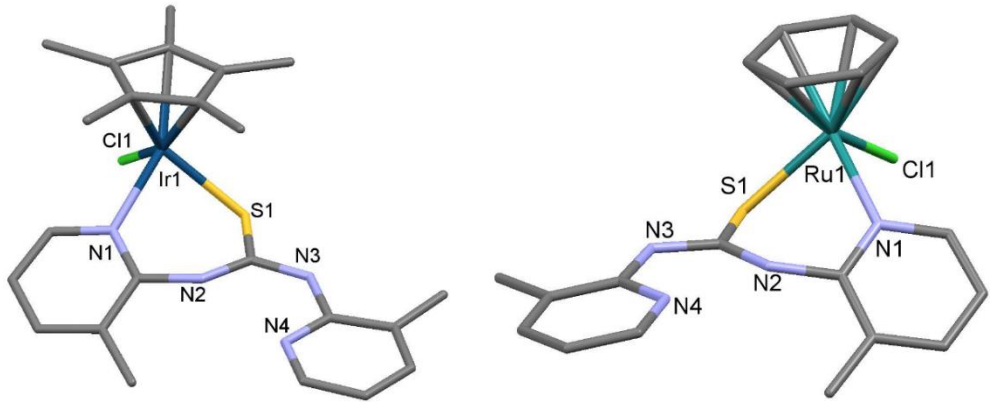

Figure 1.13: Molecular structures of iridium and ruthenium picolyl thiourea complexes **82** and **84**

In related research, Henderson *et al.* also reported a series of rhodium(III) and ruthenium(II) dianion complexes of substituted thioureas[64]. The complexes were synthesised from the reaction of dimeric rhodium and ruthenium complexes $[Cp^{*}RhCl(\mu\text{-}Cl)]_2$ and $[(\eta^6\text{-}p\text{-cymene})RuCl(\mu\text{-}Cl)]_2$ with two equivalents of the thiourea salt Na[MeNHC(S)NCN] and excess trimethylamine in refluxing methanol solution. Addition of distilled water to the hot solution resulted in the precipitation of red and orange crystalline solids for the rhodium and ruthenium complexes respectively. The ESI-mass spectral analysis of the complexes gave ions at *m/z* 703 (Rh) **85** and 699 (Ru) **86** assigned to $[M+H]^+$ for the dimeric species. The molecular structure of the ruthenium complex in **Figure 1.14** (top) confirmed the dimeric nature of the complexes, with the two η^6-*p*-cymene ruthenium groups connected by two thiourea dianion ligands. The thiourea bonds to one of the ruthenium metals through the sulfur and *N*-methyl groups with the sulfur bridging to the second ruthenium to give a puckered four-membered Ru-S-Ru-S metallacycle. This was in contrast to a planar configuration found in related dinuclear sulfur bridged complex $[(\eta^6\text{-}C_6H_3Me_3)Ru\{SC\text{-}Me_2CH(CO_2H)NH_2\}]_2$[114].

Similar synthetic methods were applied for the mononuclear complexes[64] **87** and **88** using the dimeric rhodium complex $[Cp^{*}RhCl(\mu\text{-}Cl)]_2$ and 2 equivalents of triphenylphosphine and Na[MeNHC(S)NCN] or PhNHC(S)NHPh. The complexes were confirmed by ESI-MS giving the expected $[M+H]^+$ ions. The $^{31}P\{^1H\}$ NMR spectra of the complexes also showed the expected peaks with single resonances showing $^1J_{(RhP)}$ coupling.

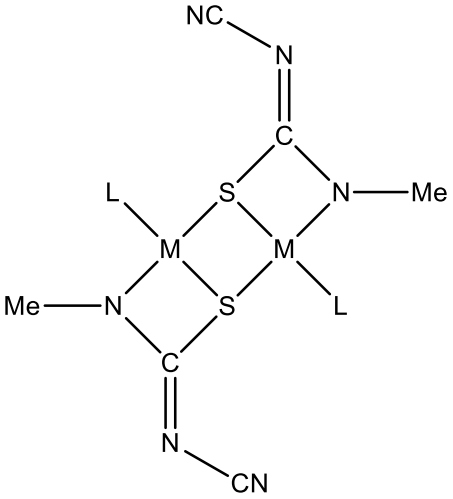

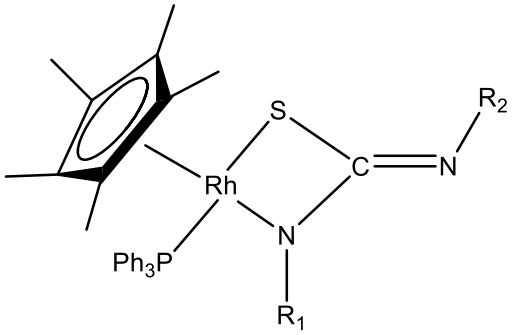

85 M = Rh, L = η^5-C_5Me_5 (Cp^*)

86 M = Ru, L = η^6-*p*-cymene

87 R_1 = Me, R_2 = CN

88 R_1 = R_2 = Ph

The mononuclear thiourea monoanion complexes containing monodentate *S*-bonded thiourea $[MeNHC(S)NCN]^-$ were also synthesised by the reaction of $[Cp^*RhCl(\mu\text{-}Cl)]_2$ with 2 equivalents of Na[MeNHC(S)NCN] and 1 equivalent of triphenylphosphine, triphenylarsine or triphenylstibine in methanol to give complexes **89**-**91** in good yield[64]. The phosphine substituted complex **89** was also obtained by the reaction of a solution of compound **87** with 2M aqueous hydrochloric acid. According to the report, a range of other bidentate mononuclear complexes were also synthesised from PhNHC(S)NHPh, $PhNHC(S)N(CH_2CH_2)_2O$, $PhNHC(S)NMe(CH_2Anth)$ (Anth = 9-anthracenyl) or $PhNHC(S)NBz_2$ (Bz = CH_2Ph) to give monoanionic complexes **92-96 .** ESI-mass spectrometry and $^{31}P\{^1H\}$ NMR spectroscopy confirmed the formation of the complexes.

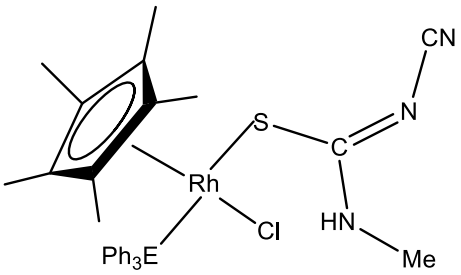

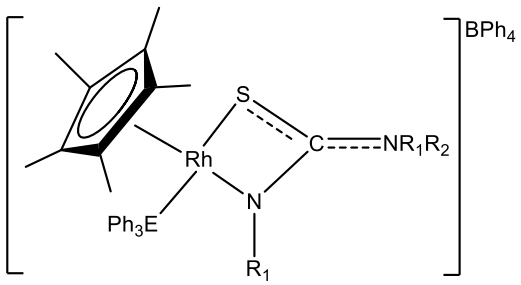

89 E = P
90 E = As
91 E = Sb

92 E = P, R_1R_2 = $(CH_2CH_2)_2O$
93 E = P, R_1 = (CH_2Anth), R_2 = Me
94 E = P, R_1 = R_2 = CH_2Ph
95 E = P, R_1 = Ph, R_2 = H
96 E = Sb, R_1R_2 = $(CH_2CH_2)_2O$

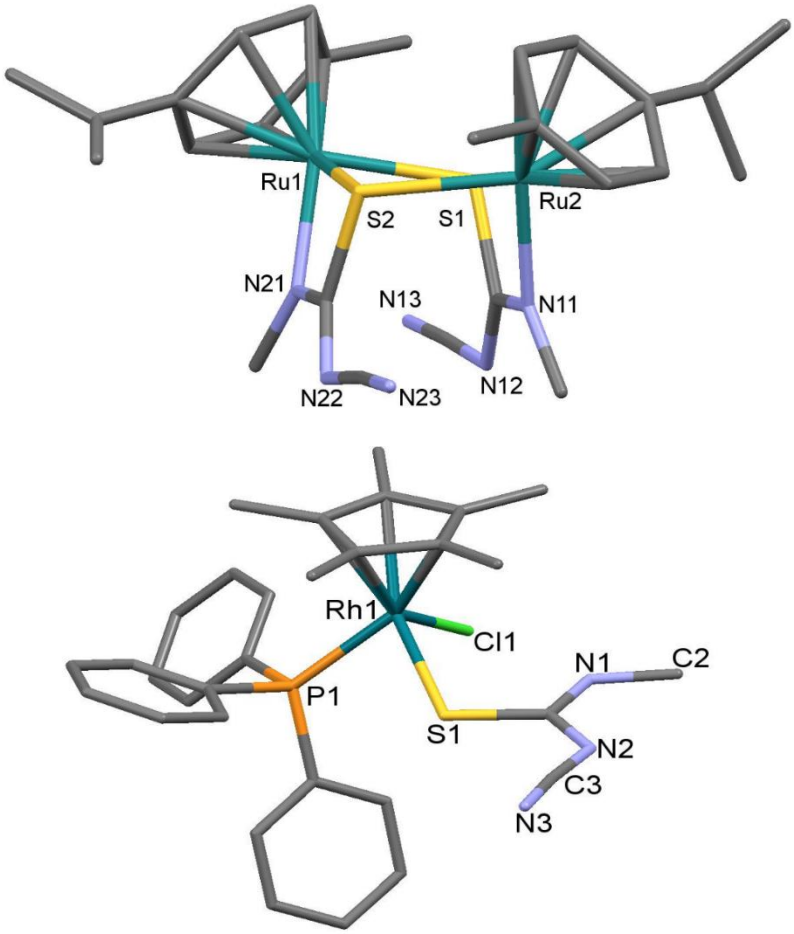

Figure 1.14: Molecular structure diagrams of thiourea anion complexes of ruthenium **86** (top) and rhodium **89** (bottom).

1.7 Coordination chemistry of complexes containing selenourea and thiosemicarbazone dianion ligands

Selenoureas and the thiosemicarbazones are related to thioureas. In the selenoureas, the sulfur in the thiourea is replaced with selenium while the thiosemicarbazones contain one nitrogen donor atom more than the corresponding thioureas and selenoureas. The structural similarities of the three group of ligands are shown in **Figure 1.15a-c**. The three ligands all coordinate bidentate to metal ions giving rise to four-membered metallacyclic rings.

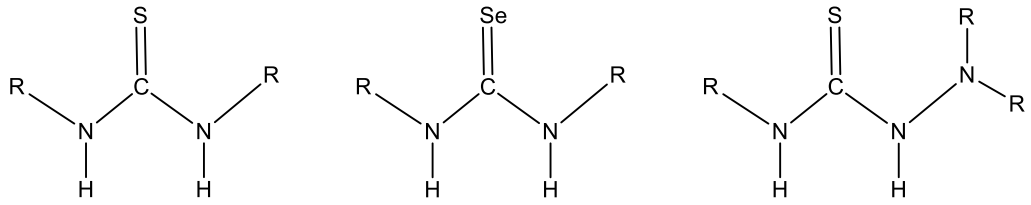

a **b** **c**

Figure 1.15: Structural similarities of thiourea (**a**) selenourea (**b**) and thiosemicarbazone (**c**).

1.7.1 *Platinum selenourea complexes*

The first selenourea dianion containing complex was reported by Henderson *et al.* in 2003. The complex was synthesised by the reaction of *cis*-[$PtCl_2(PPh_3)_2$] with one equivalent of *N,N'*-diphenylselenourea and excess trimethylamine in refluxing methanol solution. Precipitation with water gave a yellow air-stable platinum(II) selenourea dianion complex [Pt{SeC(=NPh)NPh}$(PPh_3)_2$] **97**[115]. $^{31}P\{^1H\}$ NMR spectrum of the complex showed two doublets due to inequivalent phosphine resonances. ^{195}Pt coupling constant values of 3068 and 3252 Hz resulting from the difference in *trans* influence of the Se and N donor groups were reported for the complex. The X-ray crystal structure of the complex confirmed the Pt-Se-N-C four-membered geometry of the dianion complex. The overall structural properties of the complex were reported to be similar to the analogous diphenyl thiourea complex [Pt{SC(=NPh)NPh}$(PPh_3)_2$][71]. This is the only selenourea ligand coordinating as a dianion that has been reported in the literature. There are however other reports of selenoureas coordinating to platinum group metals as neutral ligands.[116]

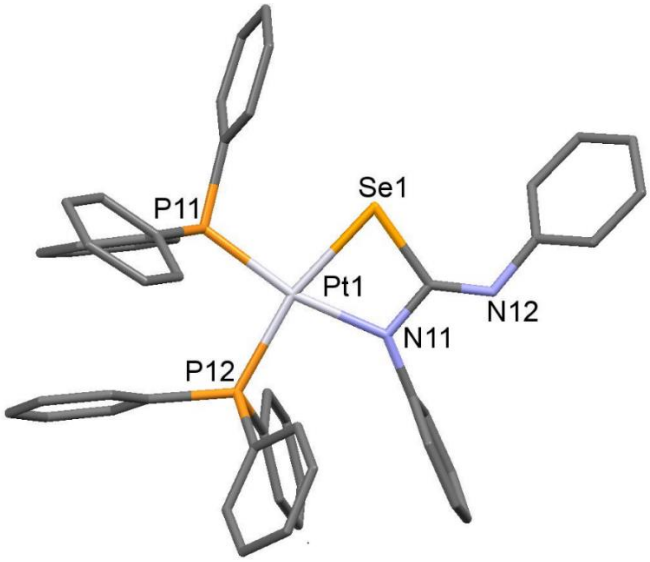

Figure 1.16: Molecular structure of the platinum selenourea dianion complex [Pt{SeC(=NPh)NPh}(PPh_3)$_2$].

1.7.2 *Monoanion and dianion complexes of thiosemicarbazones*

Several complexes containing thiosemicarbazone dianion and monoanion ligands in a four-membered metallacyclic ring system have been reported in the literature. In 1999, Burrows *et al.* started investigating the influence of intramolecular hydrogen bonding on the ligand coordination mode of a new breed of organo-phosphorus coordination compounds bearing the monoanionic thiosemicarbazone ligands[117]. The complexes were synthesised by addition of an ethanolic solution of the thiosemicarbazone ligand $R_1NHC(S)NHN(R_2)_2$ (R_1 = Me, R_2 = H; R_1 = Et, R_2 = H; R_1 = Me, R_2 = H) to a solution of 1 equivalent $[PtCl_2(dppe)]$ in the presence of NH_4PF_6 to afford the complexes **98 – 101**.

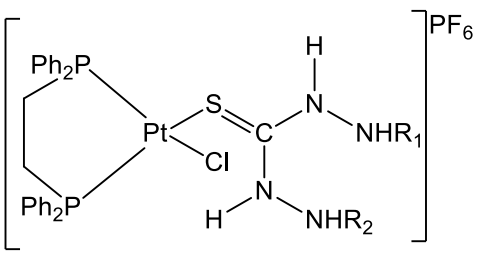

98, R_1 = Me, R_2 = H

99, R_1 = Et, R_2 = H

100, R_1 = Ph, R_2 = H

101, R_1 = Me, R_2 = Me

The X-ray crystal structure of the compound **101, Figure 1.17** was determined and found to be consistent with the observed $^{31}P\{^1H\}$ NMR data. The structure provided evidence for the formation of the above isomer of the complexes

rather than the opposite isomer where there is the possibility of intramolecular hydrogen bonding of the Cl to the two remote nitrogen atoms as shown in **102** below.

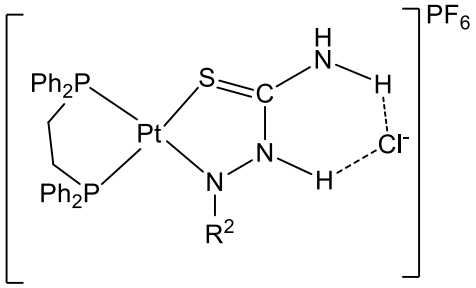

102

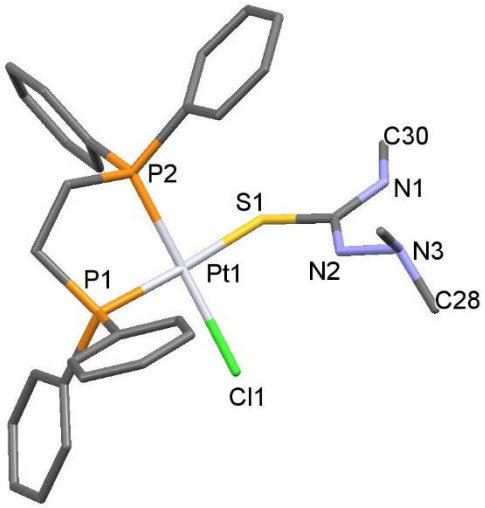

Figure 1.17: Molecular structure of the platinum thiosemicarbazone monoanion complex **101**. PF_6 ommitted for clarity.

Only a few dianion complexes of the thiosemicarbazone ligand have been synthesised and structurally characterised. Henderson and co-workers in 2003[61] reported the first set of thiosemicarbazone dianion complexes bonded to transition metals Pd, Pt and Au. The complexes were synthesised by reaction of *cis*-$[MCl_2(PPh_3)_2]$ (M = Pt or Pd) and $Ph_2NNHC(S)NHPh$ in the presence of trimethylamine base and refluxing methanol solution to afford bright yellow and maroon coloured platinum and palladium complexes **103** and **104** respectively.

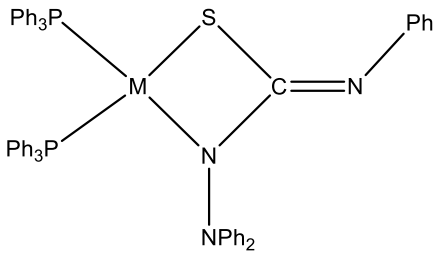

103 M = Pt **104** M = Pd

$^{31}P\{^{1}H\}$ NMR spectroscopy indicated the presence of two isomers of the complex **103**; a major isomer (**Figure 1.18a**) with the expected AB pattern corresponding to inequivalent phosphine resonances at 16.9 and 11.1 ppm and $^{1}J_{(PtP)}$ coupling constants of 3156 and 3147 Hz respectively and a minor isomer with $^{1}J_{(PtP)}$ coupling constants of 3038 and 3330 Hz consistent with *N,S*-donor ligands **Figure 1.18b**.

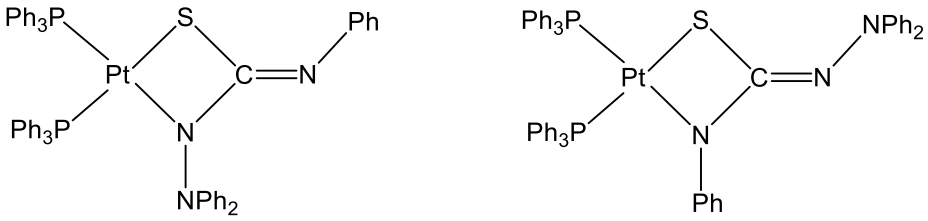

(**a**) (**b**)

Figure 1.18: Structures of the major (**a**) and minor (**b**) isomers of platinum thiosemicarbazone dianion complex $Pt\{SC(=NNPh_2)NPh\}(PPh_3)_2]$[61]

The X-ray crystal structure of the complex **103** (**Figure 1.19**) showed a square planar coordination geometry with the thiosemicarbazone ligand binding to the platinum metal centre through the sulfur and nitrogen bearing the substituted NPh_2 group of the ligand in a dianionic fashion. The authors suggested that the major isomer (**a**) formed in preference to the alternative isomer **(b**) because the NPh_2 group was sterically less bulky than the Ph group in the platinum coordination environment.

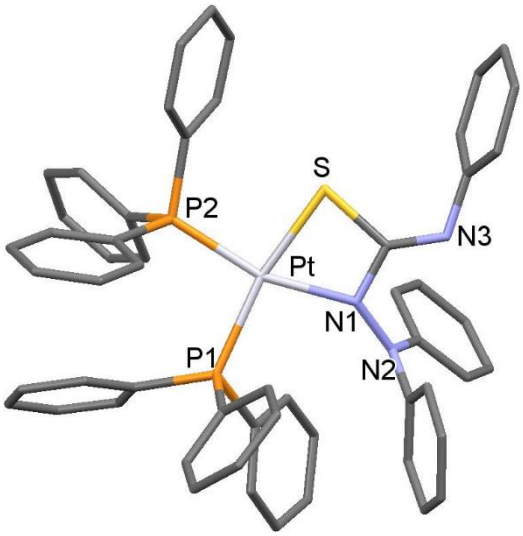

Figure 1.19: Molecular structure of the platinum thiosemicarbazone dianion complex **103**

In other to further investigate the steric preference theory, the authors synthesised another complex by substituting the sterically bulky phenyl group with a methyl group to give the complex **105**, where the other isomer was formed in preference to the triphenyl complex. The coordination geometry of the complex was confirmed with ^{1}H and $^{31}P\{^{1}H\}$ NMR spectroscopy. The palladium complex showed similar properties as the platinum complex, but there was no sign of isomerism in the $^{31}P\{^{1}H\}$ NMR spectrum of the palladium complex.

The Au(III) complex of the thiosemicarbazone ligand was synthesised using a method similar to that of the platinum complex using (2-anp)$AuCl_2$ (anp = anilinopyridyl) $Ph_2NNHC(S)NHPh$ and trimethylamine in refluxing methanol solution. The Au(III) dianion complex **106** was confirmed by ESI-MS spectrometry at low exit voltage of 60 V.

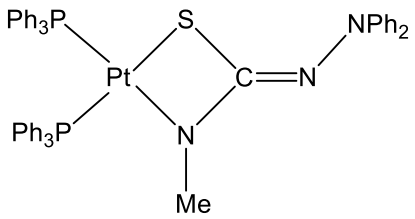

105

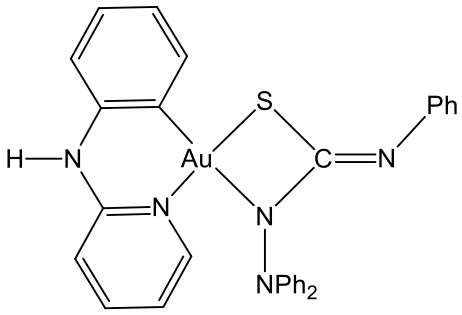

106

1.8 Thiourea dianion complexes of other metals

Apart from the thiourea dianion and monoanion complexes of the platinum group metals discussed above, thiourea dianion complexes of some main group and other transition metal complexes have been reported in the literature[62,118-120]. A thiourea dianion complex of molybdenum was reported in 1991[121]. The addition of a di-*p*-tolylcarbodiimide into the molybdenum sulfido bond of Cp_2MoS_2 in the presence of PMe_3 (**Scheme 1.10**) gave the dianion complex in good yield. The molecular structure of the complex was similar to other previously described four-membered metallacycles of the bis(cyclopentadienyl) molybdenum family [121,122].

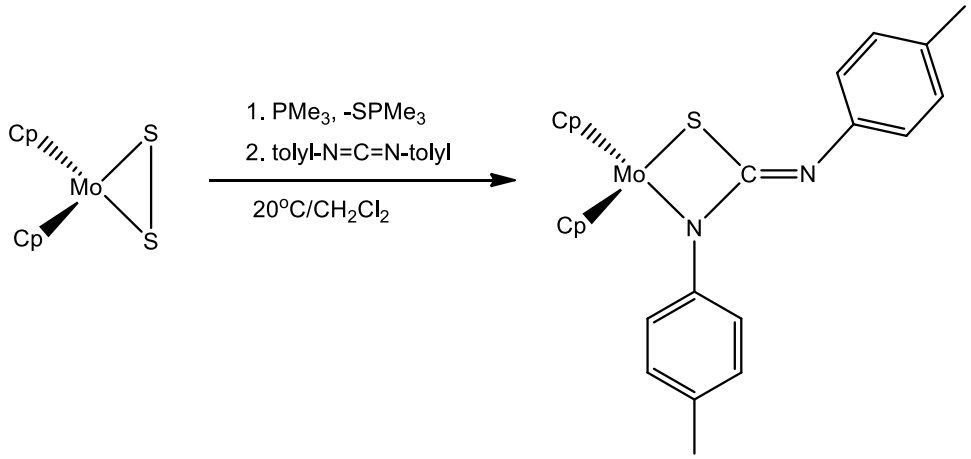

Scheme 1.10: Reaction scheme for the formation of [$Cp_2MoSC(=N\text{-tolyl})N\text{-tolyl}$] [Cp = η^5-C_5H_5]

The following year, a tris(thioureato)chromium(III) complex was synthesised by Bodensieck and co-workers[63]. The complex was obtained from the reaction of $Cr(CO)_6$ with *N,N'*-diphenylthiourea, which gives the known $Cr(CO)_5S=C(NHPh)_2$ complex at first, but undergoes decarbonylation on heating and further reacts with *N,N'*-diphenylthiourea to give the tris(thioureato)chromium(III) complex with three N,S chelating ligands arranged facially around the chromium as observed by X-ray crystallography.

Later in 1998, Coles *et al* reported two thiourea dianion complexes of aluminium. The complexes were synthesised from the methane elimination reaction of $AlMe_3$ and the thioureas [{$(RHN)_2C=S$}] (R = adamantyl or 2,6-$^i Pr_2$-Ph) to afford the dianion complexes [{RHNC(NR)S}$AlMe_2$] **108**[62] (**Scheme 1.11**)

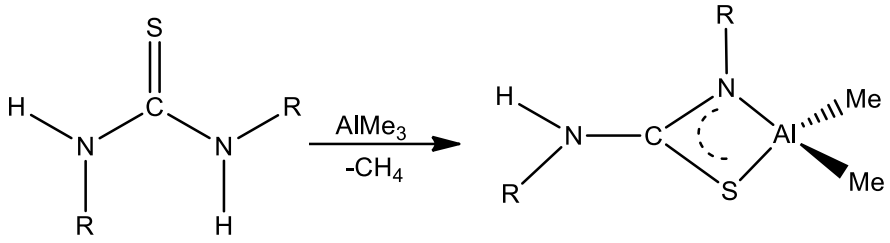

R = adamantyl; **108a,** R = 2,6-$^{i}Pr_2$-Ph; **108b**

Scheme 1.11: Reaction scheme for synthesis of [{R^1HNCS(NR^1)S}$AlMe_2$] by CH_4 elimination

The molecular structure of the adamantyl substituted complex **108a** (**Figure 1.20**) shows a distorted tetrahedral geometry at the aluminium centre. The N-Al-S-C metallacycle is approximately planar with the adamantyl groups orthogonally oriented to the plane of the metallacycle.

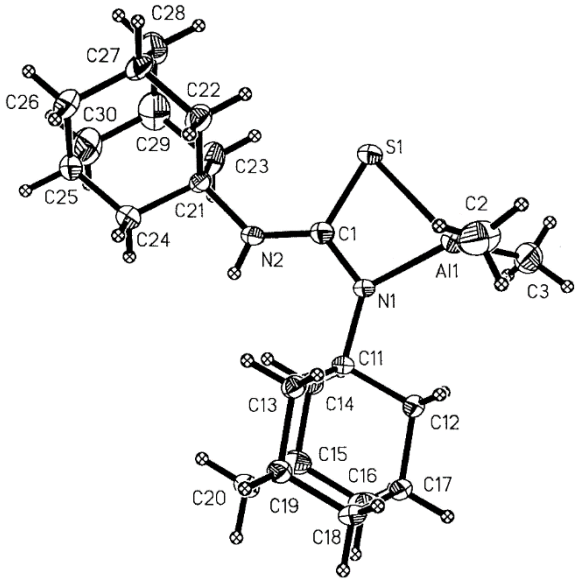

Figure 1.20: Molecular structure of the aluminium thiourea monoanion complex **108a**[62].

1.9 Computational chemistry methods

A number of computational chemistry methods will be used in this thesis to analyse and support experimental data. In this section, a brief overview of the different computational methods will be discussed.

1.9.1 *Density Functional Theory (DFT)*

Density Functional Theory is simply a solution to the electronic Schrödinger equation which involves the use of the electron density $\rho(r)$ rather than the usual wave function. For the many-electron system, the density is a much simpler function than the wave function. Density Functional Theory is an *ab initio* method (meaning from the beginning in Latin) that is they take input from the Schrödinger equation without experimental input. However, in some cases density functional expressions are fitted to some experimental datasets as well as to theoretical requirements[123].

1.9.2 *Geometry optimisation*

Geometry optimisation is a method to predict the three-dimensional arrangement of the atoms in a molecule using minimisation of model potential energy. The most straightforward way to explore potential energy surfaces is to characterise them in terms of their stationary points, where the gradient of the potential energy with respect to the atomic coordinates vanishes. These are the minima and saddle points. In order to locate these points, numerical methods for 'geometry optimisation' are used. As well as minima and saddlepoints, such methods can also be used to explore the reaction paths that connect them[124].

Optimisation of a local minimum on the potential energy surface is the simplest problem of this type. A starting structure i.e. a starting set of values of the atomic coordinates R is generated for the system being considered, and the aim is to find the nearby structure R_{eq} for which V(R) is a local minimum. Many algorithms are known for locating minima of functions. One option is to make a random change in the coordinates, ΔR, compute $V(R+\Delta R)$, and check to see if it is lower than the previous value of V. If yes, the change in structure is accepted, $R = R+\Delta R$, and one then repeats the process. If instead, the energy is higher than before, then the change is rejected, and one repeats the process without updating the structure. Provided that the maximum magnitude of ΔR is chosen to become smaller and smaller as one nears the minimum, this algorithm will eventually lead to R_{eq}.[123]

However, it is rather inefficient, and in practice, this approach is seldom used. The method just described only requires that one be able to calculate the potential energy at a given point. More efficient algorithms generally require that one also be able to calculate the gradient $\partial V/\partial R$. For most quantum mechanical

and molecular mechanical techniques, this can indeed be done, with relatively small additional computational effort above that needed to compute the energy itself. A simple procedure for geometry optimisation based on the availability of the gradient is the so-called steepest descent method. An initial structure R_o is chosen and the potential energy $V(R_o)$ and its gradient $\partial V(R_O)/\partial R$ are computed at that point. The lowest-energy structure along the linear direction defined by the point R_o and the direction of the gradient is then located. This is called a 'line search'. The potential energy and gradient at this new structure, R_1, is then obtained, and a new line search is performed along the direction defined by the new gradient. After several steps, this method which is involves repeatedly going as far as ''downhill'' as possible along the direction of the gradient, the steepest direction will get close to the nearest minimum on the surface. The minimisation will be considered to be converged when the size of the step taken and/or the magnitude of the gradient becomes smaller than some threshold[124].

More accurate methods for geometry optimisation use not only the gradient -the first derivative of energy with respect to the coordinates but also the Hessian - second derivative of the energy, shown in equation 1.1 below. This Hessian is a matrix since for n different coordinates $q_1 \ldots q_n$ there will be n × n matrix.

$$H_{ij} = \frac{\partial^2 V}{\partial q_i \partial q_j} \tag{1.1}$$

It is possible to generate a much better estimate of the position of the minimum given an initial position R_i and the gradient and Hessian at that position. This estimate is obtained from Newton's method (equation 1.2 where $\mathbf{H}^{-1}$ is the inverse of the Hessian matrix

$$R_{i+1} = R_i + \Delta R = R_i - \frac{\partial V(R_i)}{\partial R} \times \boldsymbol{H}^{-1} \tag{1.2}$$

Newton's method is a very challenging method to put into practice, because evaluating the full Hessian matrix is computationally demanding, and evaluating its matrix inverse can lead to numerical problems. Hence Newton's method is rarely applied as such in computational chemistry. However, many other 'second-order' methods are used. These methods are referred to as 'second-order' because they in some way take account of the second derivatives of the potential energy, usually in

some approximate way that avoids the need to calculate the exact Hessian matrix. Some examples of such methods are the conjugate gradient method and the BFGS method. The conjugate gradient method is similar to the steepest descent method described above in the sense that it involves line searches; however it does not follow the downhill direction for these searches. The direction is instead modified to take into account the outcome of previous steps. The BFGS suggested by researchers Broyden, Fletcher, Goldfard and Shano, uses equation 1.2 to update the structure at each step, but instead of evaluating $\mathbf{H}^{-1}$ matrix, an approximate matrix computed from the value of the gradient at the previous step is used. For quantum mechanical geometry optimisation of small systems of up to a few hundred atoms, BFGS or closely related methods are most often the best approaches. To minimise the time needed to carry out optimisation, one needs to minimise the number of times that the quantum mechanical energy and gradient are evaluated. This can be achieved by the use of approximate Hessian matrix $\mathbf{H}$[125].

Another factor that can improve the convergence of the optimisation procedure is a careful choice of the set of coordinates that are used to describe the structure of the system. The obvious choices are usually the Cartesian and internal coordinates of the atoms. The Cartesian coordinates have the advantage of leading to simple algorithms because the gradient of the energy is most readily obtained with respect to these coordinates whether one is using molecular mechanical or quantum mechanical potential energy method. The use of Cartesian coordinates does not always lead to smoothly converging optimisation because a small change of a given Cartesian coordinate can lead to either a large change in energy associated with a change in chemical bond length or small energy change usually associated with a change in dihedral angles. The internal coordinates (bond lengths, bond angles, dihedral angles, or other structural variables such as improper torsions) on the other hand often form a better basis for performing a geometry optimisation. This could perhaps be expected due to the reasonable accuracy of the molecular mechanics method which expresses potential energy in terms of relatively simple functions of such coordinates[126,127]. This also has its own complications: a natural set of internal coordinates can be overdetermined, that is it will contain more than the 3N-6 coordinates required to uniquely identify the structure. This results in redundancy of the internal coordinates. So when applying a geometry update step, either in a line search or a Newton step, this causes a problem, because the

combination of changes suggested by the algorithm for each of the internal coordinates will typically not correspond to any possible set of Cartesian coordinates. For example in a three-membered ring XYZ, in which one wishes to change each of the angles XYZ, YZX and ZXY, only changes that preserve the sum of angles as 180^{o} are feasible, yet a predicted structure will suggest changes to these angles independently. This requires an additional procedure during optimisation, to identify the change in coordinates that most closely satisfies all the ones predicted by the algorithm while also being consistent. There is however an additional step involved, which converts the gradient from Cartesian coordinates to internal coordinates. Despite these additional complications, optimisation in the space of redundant internal coordinates is usually preferred, because it is more efficient in terms of the number of potential energy and gradient evaluations needed to reach the minimum within a given convergence threshold.

1.9.3 *Vibrational frequencies*

Geometry optimisation yields a structure that is a minimum of the potential energy surface, which is a point where the gradient or first derivative of the potential energy with respect to displacements of the atoms is zero. The second derivative of the energy is not usually zero at the minimum. This second derivative is the Hessian matrix and provides information concerning infrared spectra and other aspects of vibrational frequency. The Hessian matrix, after weighting to take into account the masses of the different atoms can be used to generate a set of eigenvectors and eigenvalues that give a reasonably accurate description of the vibrational energy states of the system. The eigenvalues are related to the vibration frequencies for the molecule through a square root relationship. At the saddle point on the potential energy surface, one of the eigen values will be negative (leading to an imaginary frequency), where the corresponding eigenvector corresponds to the reaction coordinate leading away from the transition state (TS). Minima on the potential energy surface have only positive values. Calculation of vibrational frequencies is often used to determine certain properties of the potential energy surface including Zero-point energy, rotational, translational and Gibbs free energies.

1.9.4 *Non-covalent interactions*

Due to the rich and challenging bonding patterns in crystalline solids, it can be difficult to experimentally rationalise the different bonding distributions in

crystalline compounds, especially those exhibiting various degrees of non-covalent interactions. Consequently, researchers have increasingly turned to various theoretical approaches to investigate the nature and strength of non-covalent interactions. A number of these are based on topological analysis of the electron density [128-131], including the Electron Localisation Function (ELF)[132], the Quantum Theory of Atoms in Molecules (QTAIM) [133] and most recently the Non-Covalent Interaction index (NCI) [134].

1.9.5 *Non-covalent Interaction Index (NCI)*

1.9.5.1 The Reduced Density Gradient

The reduced density gradient (s) is a fundamental dimensionless quantity in density functional theory (DFT) used to describe the deviation from homogenous electron distribution[134,135]. Properties of the reduced gradient have been investigated in depth in the process of developing increasingly accurate functionals. The reduced density gradient originates from the generalised density gradient contribution to the Generalized Gradient Approximation (GGA) exchange energy, E_X^{GGA} from density functional theory,

$$E_X^{GGA} - E_X^{LDA} = \sum \int F(s)\rho^{\frac{4}{3}}(r)dr \qquad (1.3)$$

where F (s) is a function of *s* for a given spin with

$$s = \frac{1}{C_F}\frac{|\nabla\rho|}{\rho^{4/3}} \qquad (1.4)$$

C_F being the Fermi constant, $C_F = 2(3\pi^2)^{1/3}$ and the 4/3 exponent of the density ensuring that *s* is a dimensionless quantity. The reduced density accounts for local density inhomogeneities due to its differential behaviour depending on the chemical region of the molecule. The reduced density gradient assumes large values in the exponentially decaying density tails far from the nuclei, where the density denominator approaches zero more rapidly than the gradient numerator. Small values of s occur close to the nuclei, due to the combination of large densities and small density gradients. In the case of Gaussian basis sets, the lower bound on the reduced density gradient is zero, as occurs throughout a homogenous electron gas and at bond critical points.

The effect of bonding on the reduced density gradient is exceptionally easy to visualise when it is plotted as a function of the density. Graphs of *s* (ρ) assume the form of f (x) = $ax^{-1/3}$, where a is a constant. This can easily be proven from a slater type orbital (STO) model density. For a single atomic orbital ψ =$e^{-\alpha r}$, the density is ρ = $e^{-2\alpha r}$ and the gradient $\nabla\rho^2 = -2\alpha\rho$ such that

$$a^2 s(\rho) = \frac{1}{C_f}\frac{2\alpha\rho}{\rho^{4/3}} = \frac{2\alpha}{C_F}\rho^{-1/3} \qquad (1.5)$$

Where there is overlap between atomic orbitals, a spike in the s (ρ) diagram appears, **Figure 1.21a**. The points forming this spike can identify the interaction when they are mapped back to real space. This procedure is able to reveal non-covalent interactions.[136]

1.9.6 *The density second eigenvalue (The sign of the Laplacian)*

According to the divergence theorem[137], the sign of the Laplacian of the density $\nabla\rho^2$, indicates whether the net gradient flux is entering $\nabla\rho^2 < 0$, or leaving $\nabla\rho^2 > 0$, an infinitesimal volume around a reference point. Hence, it highlights whether the density is concentrated or depleted at that point, relative to the surrounding environment. To differentiate between different types of weak interactions one cannot resort to the sign of the Laplacian itself since it is dominated by the principal axis of variation and is positive for all closed-shell interactions[138].

To understand bonding in more detail, it is often useful to decompose the Laplacian into the contributions along the three axes of maximal variation. These components are the three eigenvalues λ_i of the electron-density Hessian matrix, such that $\nabla\rho^2$ t = $\lambda_1 + \lambda_2 + \lambda_3$, ($\lambda_1 < \lambda_2 < \lambda_3$). At points with zero gradients, analysis of the Hessian eigenvalues is analogous to determining the signature of the critical point. Thus, at nuclei (cups/maxima of ρ), all the eigenvalues are negative while at the centre of cages or holes (minima of ρ) all the eigenvalues are positive. In the remaining points of space $\lambda_3 > 0$, $\lambda_1 < 0$, and λ_2 can be either positive or negative. Within the NCI framework, the sign of λ_2 (i.e the perpendicular plane) enables identification of the interaction type. Attractive interactions appear at $\lambda_2 < 0$ whereas in the case where λ_2 is positive (as rings or cages), usually several atoms interact but are not bonded, which corresponds to steric crowding according to classical chemistry. Both van der Waals interactions and hydrogen bonds show negatives value of λ_2 at the critical point (with $\lambda_2 \leq 0$ for Van der Waals

interaction). This can be attributed to the homomorphic virial path associated with the bonding direction, which defines a line along which the potential-energy density is maximally negative. The nonbonding interactions such as steric crowding, on the other hand, result in depletion of the density such that $\lambda_2 > 0$. Analogously, the homeomorphisms ensure that these critical points (both ring and cage points) identify lines of minimally negative potential-energy density[139].

The introduction of the second eigenvalue helps to categorise the interactions into attractive and repulsive interactions. Characteristic densities of van der Waal interactions are much smaller than densities at which hydrogen bonds appear. However, steric clashes and hydrogen bonds span similar density ranges and overlap in plots of $s(\rho)$ against ρ as shown in the example for phenol dimer in **Figure 1.21a** a hydrogen-bonded complex that exhibits non–bonding interactions within each benzene ring and a stacking interaction between the benzene rings. There are thus three main interactions in this molecule: hydrogen bonding, Van der Waals interactions and steric clashes. The different types of interactions can now be distinguished by plotting the sign of the second eigenvalue sign λ_2 as the ordinate against the reduced gradient $s(\rho)$. Analysis of the sign of λ_2 thus helps to discern between the different types of weak interactions, whereas the density itself provides information about the strength of the interactions. The combination of both parameters gives the value of $\text{sign}(\lambda_2)\rho$. When the Hessian eigenvalues are considered, the different nature of these interactions is made manifest; the benzene ring interactions remain at positive values while the hydrogen bond interactions now lie at negative values, within the attractive region (**Figure 1.21b**). The NCI spikes nearest to zero density correspond to weakly dispersing interactions between the phenyl rings.

The noncovalent interactions discussed above can also be represented in three dimensions as reduced density gradient isosurfaces. These isosurfaces give rise to closed domains in the molecular space which highlights the spatial localisation of the interactions within the system as shown in **Figure 3.2c** for the phenol dimer discussed above. Since 3D isosurfaces are, by definition, regions of low reduced gradient, the density is nearly constant within these. An RGB (red-green-blue) colouring scheme is used in ranking the interactions. Red represents destabilising interactions, blue for stabilising interactions and green for delocalised weak interactions. The intensity of the colours corresponds to the strength of these

interactions. Noncovalent interactions of hydrogen-bonded thiourea ligands will be investigated with a locally developed program, Bonder, which provides numerically equivalent results to existing NCI codes such as NCIplot, NCImilano or Multifwn [139,140]. However, Bonder offers some advantages to these existing codes, particularly for larger molecules, in that it analyses each discrete non-covalent interaction separately, rather than constructing a single large sparse matrix, including the many regions where there are not non-covalent interactions.

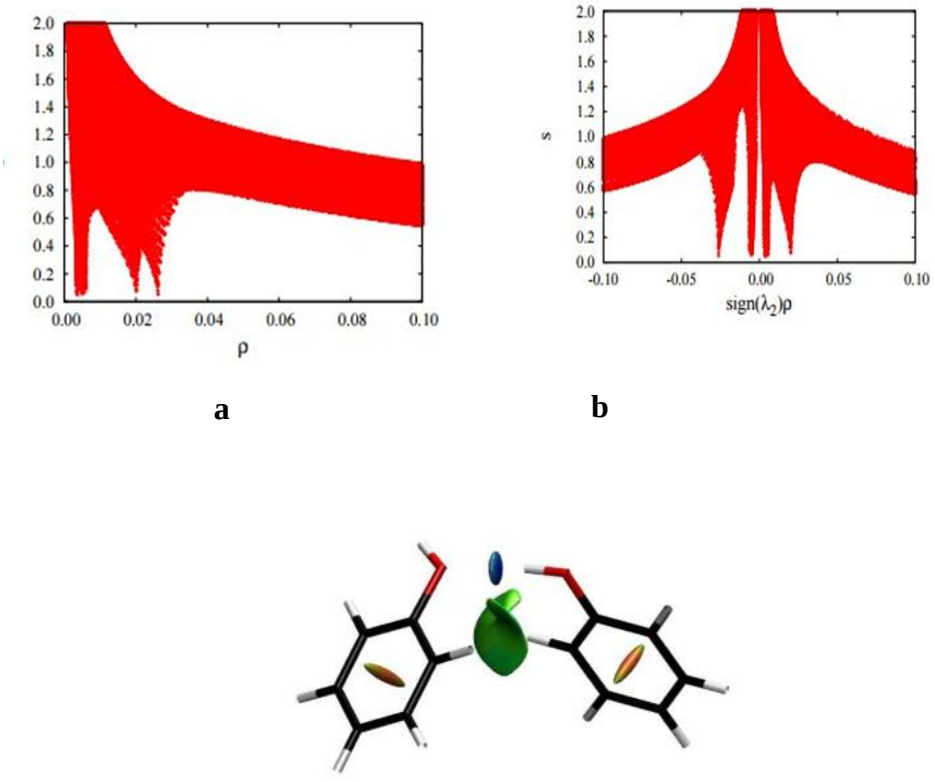

Figure 1.21: NCI plots of (**a**) s against ρ (**b**) s against sign(λ_2)ρ (**c**) NCI isosurface for phenol dimer. The s = 0.6 a.u. and isosurface are coloured according to BGR scheme over the range -0.03 < sign(λ_2)ρ < 0.03 a.u. Blue indicates strong interaction; green indicates weak interaction and red indicates strong repulsion.

1.10 Aims and objectives of this study

The main aim of this research was to synthesise some asymmetrically substituted thiourea ligands of the form in **109** and their platinum group metal complexes.

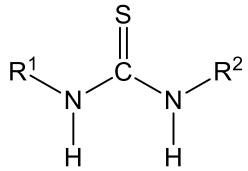

109

In the first part of the project, a range of thiourea ligands containing various pyridyl functional groups will be synthesised. The pyridyl functionality could provide additional nucleophilic nitrogen in the thiourea for possible coordination to the metal in the primary or secondary complex. This could result in changes in the geometry, physical, chemical and solvation properties of the resulting complexes. The second goal is the introduction of a methylene or ethylene spacer between the pyridyl functionality and the thiourea nitrogen. It is anticipated that this could alter the coordination geometry of the ligands in the complexes. Apart from that the methylene and ethylene spacers could act as spectroscopic handles for characterisation of the metal complexes formed from these ligands. Further, the steric properties of the ligands will be varied by introducing sterically different functional groups at the R^2 position. Subsequently the *N,S*-chelated platinum complexes of the pyridyl substituted thiourea ligands will be synthesised and structurally characterised and the possibility of isomerism in the complexes will be investigated using a combination of $^{31}P\{^1H\}$ NMR spectrometry and computational chemistry. The coordination chemistry of other platinum group metals (including palladium, nickel, ruthenium, rhodium and iridium) will be investigated and the reactivity, supramolecular and biological properties of this pyridyl substituted thiourea complexes will be explored.

Another important goal of the project is the synthesis and characterisation of a series of new asymmetrically substituted thiourea ligands by incorporating other functional groups like phosphonates, hydroxylates, silatranes at the terminal R group of the thioureas. The supramolecular properties and coordination chemistry of theses ligands towards platinum group metals will be explored.

The final part of the project is aimed at the synthesis of a series bisthiourea ligands and their platinum group metal complexes. The alkyl spacer group between these bisthiourea ligands will be varied to alter the proximity of the two thiourea groups. The coordination geometry and supramolecular properties of the resulting complexes will be investigated.

1.11 References

1. Rosenthal, U.; Burlakov, V. V.; Bach, M. A.; Beweries, T. *Chem. Soc. Rev.* **2007**, *36*, 719-728.
2. Klingler, R.; Huffman, J.; Kochi, J. *J. Am. Chem. Soc.* **1982**, *104*, 2147-2157.
3. Bleeke, J. R. *Chem. Rev.* **2001**, *101*, 1205-1228.
4. Li, B.; He, T.; Fan, Y.; Yuan, X.; Qiu, H.; Yin, S. *Chem. Commun.* **2019**, *55*, 8036-8059.
5. Dinger, M. Aspects of Metallacyclic Chemistry PhD Thesis, The University of Waikato, 1998.
6. Cook, T. R.; Stang, P. J. *Chem. Rev.* **2015**, *115*, 7001-7045.
7. McGuinness, D. S. *Chem. Rev.* **2010**, *111*, 2321-2341.
8. Zangrando, E.; Casanova, M.; Alessio, E. *Chem. Rev.* **2008**, *108*, 4979-5013.
9. Henderson, W.; Nicholson, B. K.; Rickard, C. E. F. *Inorg. Chim. Acta* **2001**, *320*, 101-109.
10. Venkatesh, P.; Pandeya, S. *Int. J. ChemTech Res.* **2009**, *1*, 733-741.
11. Hargrave, K. D.; Hess, F. K.; Oliver, J. T. *J. Med. Chem.* **1983**, *26*, 1158-1163.
12. Saeed, A.; Saeed, N.; Hummera, R.; Sadaf, R.; Hameed, A. *Chemistry* **2009**, *18*, 152-158.
13. Kurt, G.; Sevgi, F.; Mercimek, B. *Chemical Papers* **2009**, *63*, 548-553.
14. Sondhi, S.; Sharma, V. K.; Singhal, N.; Verma, R.; Shukla, R.; Raghubir, R.; Dubey, M. *Phosphorus, Sulfur Silicon Relat. Elem.* **2000**, *156*, 21-33.
15. Rosove, M. H. *West. J. Med.* **1977**, *126*, 339.
16. Masereel, B.; Lambert, D.; Dogné, J.; Poupaert, J.; Delarge, J. *Epilepsia* **1997**, *38*, 334-337.
17. Loev, B.; Bender, P. E.; Bowman, H.; Helt, A.; McLean, R.; Jen, T. *J. Med. Chem.* **1972**, *15*, 1024-1027.
18. Shakeel, A.; Altaf, A. A.; Qureshi, A. M.; Badshah, A. *J. Drug Des. Med. Chem.* **2016**, *2*, 10-20.
19. Trotti, A.; Colevas, A. D.; Setser, A.; Rusch, V.; Jaques, D.; Budach, V.; Langer, C.; Murphy, B.; Cumberlin, R.; Coleman, C. N. Development of a comprehensive grading system for the adverse effects of cancer treatment. Seminars in radiation oncology.13, 176-181.
20. Richter, C. P., *J. Am. Med. Assoc.* **1945**, *129*, 927-931.
21. Tunaz, H.; Uygun, N. *Turk. J. Agric. For.* **2004**, *28*, 377-387.
22. Brown, B.; Harris, R. *Pest Manage. Sci.* **1973**, *4*, 215-225.
23. Yonova, P.; Guleva, E. *Bulg. J. Plant Physiol.* **1997**, *23*, 72-79.

24. Madarász, J.; Bombicz, P.; Okuya, M.; Kaneko, S. *Solid State Ionics* **2001**, *141*, 439-446.

25. Wang, J.; Li, H.; Yu, X.; Zu, L.; Wang, W. *Org. Lett.* **2005**, *7*, 4293-4296.

26. Saeed, A.; Saeed, N.; Hummera, R.; Sadaf, R.; Hameed, A. *Chemistry* **2009**, *18*, 152-158.

27. Custelcean, R. *Chem. Commun.* **2008**, 295-307.

28. Custelcean, R.; Gorbunova, M. G.; Bonnesen, P. V. *Chem. Eur. J.* **2005**, *11*, 1459-1466.

29. Kalidasan, M.; Nagarajaprakash, R.; Rao, K. M. *Transition Met. Chem.* **2015**, *40*, 531-539.

30. Hollmann, K.; Oppermann, A.; Witte, M.; Li, S.; Amen, M.; Flörke, U.; Egold, H.; Henkel, G.; Herres-Pawlis, S. *Eur. J. Inorg. Chem.* **2017**, *2017*, 1266-1279.

31. Hollmann, K.; Oppermann, A.; Amen, M.; Flörke, U.; Egold, H.; Hoffmann, A.; Herres-Pawlis, S.; Henkel, G. *Zeit. Anorg. Allg. Chem.* **2016**, *642*, 660-669.

32. Maddani, M. R.; Prabhu, K. R. *J. Org. Chem.* **2010**, *75*, 2327-2332.

33. Huang, Y.-B.; Yi, W.-B.; Cai, C. Thiourea based fluorous organocatalyst. In *Fluorous Chemistry*; Springer, 2011; pp 191-212.

34. Koketsu, M.; Kobayashi, C.; Ishihara, H. *Heteroat. Chem* **2003**, *14*, 374-378.

35. Kumamoto, K.; Misawa, Y.; Tokita, S.; Kubo, Y.; Kotsuki, H. *Tetrahedron Lett.* **2002**, *43*, 1035-1038.

36. Li, Z.; Wang, Z.-Y.; Zhao, Y.-L.; Xing, Y.-L.; Zhu, W. *Phosphorus, Sulfur Silicon Relat. Elem.* **2005**, *180*, 2745-2750.

37. Spenceley, J. E.; Henderson, W.; Lane, J. R.; Saunders, G. C. *Inorg. Chim. Acta* **2015**, *425*, 83-91.

38. Smith, R.; Williams, R. *J. Med. Chem.* **1961**, *4*, 97-107.

39. Valdés-Martínez, J.; Hernández-Ortega, S.; Espinosa-Perez, G.; Presto, C. A.; Hermetet, A. K.; Haslow, K. D.; Ackerman, L. J.; Szczepura, L. F.; Goldberg, K. I.; Kaminsky, W. *J. Mol. Struct.* **2002**, *608*, 77-87.

40. Singh, A.; Bharty, M.; Bharati, P.; Bharti, A.; Singh, S.; Singh, N. *Polyhedron* **2015**, *85*, 918-925.

41. Kelman, D. R.; Szczepura, L. F.; Goldberg, K. I.; Kaminsky, W.; Hermetet, A. K.; Ackerman, L. J.; Swearingen, J. K.; West, D. X. *J. Mol. Struct.* **2002**, *610*, 143-150.

42. Kelman, D. R.; Claborn, K. A.; Kaminsky, W.; Goldberg, K. I.; West, D. X. *J. Mol. Struct.* **2002**, *642*, 119-127.

43. Yeşilkaynak, T.; Muslu, H.; Özpınar, C.; Emen, F. M.; Demirdöğen, R. E.; Külcü, N. *J. Mol. Struct.* **2017**, *1142*, 185-193.

44. Yesilkaynak, T.; Floerke, U.; Külcü, N.; Arslan, H. *Acta Crystallogr., Sect. E: Struct. Rep. Online* **2006**, *62*, 3934-3935.

45. Binzet, G.; Arslan, H.; Flörke, U.; Külcü, N.; Duran, N. *J. Coord. Chem.* **2006**, *59*, 1395-1406.

46. Asegbeloyin, J. N.; Oyeka, E. E.; Okpareke, O. C.; Ibezim, A. *J. Mol. Struct.* **2018**, *1153*, 69-77.

47. Oyeka, E. E.; Asegbeloyin, J. N.; Babahan, I.; Eboma, B.; Okpareke, O.; Lane, J.; Ibezim, A.; Bıyık, H. H.; Törün, B.; Izuogu, D. C. *J. Mol. Struct.* **2018**, *1168*, 153-164.

48. Henderson, W.; Nicholson, B. K. *Polyhedron* **1996**, *15*, 4015-4024.

49. Binzet, G.; Kavak, G.; Külcü, N.; Özbey, S.; Flörke, U.; Arslan, H. *J. Chem.* **2013**,

50. Özer, C. K.; Arslan, H.; VanDerveer, D.; Külcü, N. *Molecules* **2009**, *14*, 655-666.

51. Sacht, C.; Datt, M. S.; Otto, S.; Roodt, A. *J. Chem. Soc., Dalton Trans.* **2000**, 4579-4586.

52. Saeed, S.; Rashid, N.; Ali, M.; Hussain, R. *Eur. J. Chem.* **2010**, *1*, 200-205.

53. Bierbach, U.; Hambley, T. W.; Roberts, J. D.; Farrell, N. *Inorg. Chem.* **1996**, *35*, 4865-4872.

54. Braband, H.; Abram, U. *J. Organomet. Chem.* **2004**, *689*, 2066-2072.

55. Okeya, S.; Fujiwara, Y.; Kawashima, S.; Hayashi, Y.; Isobe, K.; Nakamura, Y.; Shimomura, H.; Kushi, Y. *Chem. Lett.* **1992**, 1823-1826.

56. Okeya, S.; Kameda, H.; Kawashima, H.; Shimomura, H.; Nishioka, T.; Isobe, K. *Chem. Lett.* **1995**, *24*, 501-502.

57. Yuen, H. Y.; Henderson, W.; Oliver, A. G. *Inorg. Chim. Acta* **2011**, *368*, 1-5.

58. Robinson, S. D.; Sahajpal, A.; Steed, J. W. *Inorg. Chim. Acta* **2000**, *306*, 205-210.

59. Henderson, W.; Nicholson, B. K.; Dinger, M. B.; Bennett, R. L. *Inorg. Chim. Acta* **2002**, *338*, 210-218.

60. Henderson, W.; Nicholson, B. K.; Tiekink, E. R. T. *Inorg. Chim. Acta* **2006**, *359*, 204-214.

61. Henderson, W.; Rickard, C. E. F. *Inorg. Chim. Acta* **2003**, *343*, 74-78.

62. Coles, M. P.; Swenson, D. C.; Jordan, R. F.; Young, V. G. *Organometallics* **1998**, *17*, 4042-4048.

63. Bodensieck, U.; Carraux, Y.; Stoeckli-Evans, H.; Süss-Fink, G. *Inorg. Chim. Acta* **1992**, *195*, 135-137.

64. Henderson, W.; Nicholson, B. K.; Dinger, M. B.; Bennett, R. L. *Inorg. Chim. Acta* **2002**, *338*, 210-218.

65. Seyfi, S.; Alizadeh, R.; Ganji, M. D.; Amani, V. *Polyhedron* **2017**, *134*, 302-315.

66. Bharati, P.; Bharti, A.; Nath, P.; Kumari, S.; Singh, N.; Bharty, M. *Inorg. Chim. Acta* **2016**, *443*, 160-169.

67. Cairns, M. A.; Dixon, K. R.; Smith, M. A. *J. Organomet. Chem.* **1977**, *135*, C33-C34.

68. Sim, S. A.; Saunders, G. C.; Lane, J. R.; Henderson, W. *Inorg. Chim. Acta* **2016**, *450*, 285-292.

69. Davies, D. L.; Fawcett, J.; Krafczyk, R.; Russell, D. R.; Singh, K. *J. Chem. Soc., Dalton Trans.* **1998**, 2349-2352.

70. del Campo, R.; Criado, J. J.; García, E.; Hermosa, M. R.; Jimenez-Sanchez, A.; Manzano, J. L.; Monte, E.; Rodrıguez-Fernández, E.; Sanz, F. *J. Inorg. Biochem.* **2002**, *89*, 74-82.

71. Henderson, W.; Kemmitt, R. D. W.; Mason, S.; Moore, M. R.; Fawcett, J.; Russell, D. R. *J. Chem. Soc., Dalton Trans.* **1992**, 59-66.

72. Kandil, S. S.; Katib, S. M.; Yarkandi, N. H. *Transition Met. Chem.* **2007**, *32*, 791-798.

73. Bippus, P.; Skocic, M.; Jakupec, M. A.; Keppler, B. K.; Mohr, F. *J. Inorg. Biochem.* **2011**, *105*, 462-466.

74. Yan, K.; Lok, C.-N.; Bierla, K.; Che, C.-M. *Chem. Commun.* **2010**, *46*, 7691-7693.

75. Isab, A. A.; Fettouhi, M.; Ahmad, S.; Ouahab, L. *Polyhedron* **2003**, *22*, 1349-1354.

76. Schwade, V. D.; Kirsten, L.; Hagenbach, A.; Schulz Lang, E.; Abram, U. *Polyhedron* **2013**, *55*, 155-161.

77. Piro, O. E.; Castellano, E. E.; Piatti, R. C.; Bolzán, A. E.; Arvia, A. J. *Acta Crystallogr., Sect. C: Cryst. Struct. Commun.* **2002**, *58*, 252-255.

78. Dinger, M. B.; Henderson, W.; Nicholson, B. K.; Robinson, W. *J. Organomet. Chem.* **1998**, *560*, 169-181.

79. Bennett, M. A. *Coord. Chem. Rev.* **1997**, *166*, 225-254.

80. Therrien, B. *Coord. Chem. Rev.* **2009**, *253*, 493-519.

81. Singh, A. K.; Pandey, D. S.; Xu, Q.; Braunstein, P. *Coord. Chem. Rev.* **2014**, *270-271*, 31-56.

82. Scolaro, C.; Bergamo, A.; Brescacin, L.; Delfino, R.; Cocchietto, M.; Laurenczy, G.; Geldbach, T. J.; Sava, G.; Dyson, P. J. *J. Med. Chem.* **2005**, *48*, 4161-4171.

83. Dutta, B.; Scolaro, C.; Scopelliti, R.; Dyson, P. J.; Severin, K. *Organometallics* **2008**, *27*, 1355-1357.

84. Casini, A.; Mastrobuoni, G.; Ang, W. H.; Gabbiani, C.; Pieraccini, G.; Moneti, G.; Dyson, P. J.; Messori, L. *ChemMedChem* **2007**, *2*, 631-635.

85. Allardyce, C. S.; Dyson, P. J.; Ellis, D. J.; Salter, P. A.; Scopelliti, R. *J. Organomet. Chem.* **2003**, *668*, 35-42.

86. Bolaño, S.; Gonsalvi, L.; Zanobini, F.; Vizza, F.; Bertolasi, V.; Romerosa, A.; Peruzzini, M. *J. Mol. Catal. A: Chem.* **2004**, *224*, 61-70.

87. Darensbourg, D. J.; Joo, F.; Kannisto, M.; Katho, A.; Reibenspies, J. H.; Daigle, D. J. *Inorg. Chem.* **1994**, *33*, 200-208.

88. Phillips, A. D.; Gonsalvi, L.; Romerosa, A.; Vizza, F.; Peruzzini, M. *Coord. Chem. Rev.* **2004**, *248*, 955-993.

89. Bravo, J.; Bolaño, S.; Gonsalvi, L.; Peruzzini, M. *Coord. Chem. Rev.* **2010**, *254*, 555-607.

90. Guerriero, A.; Peruzzini, M.; Gonsalvi, L. *Coord. Chem. Rev.* **2018**, *355*, 328-361.

91. Fischer, E.; Böttcher, R. *Zeit. Anorg. Allg. Chem.* **1957**, *291*, 305-309.

92. Fischer, E.; Fritz, H. P. *Angewandte Chemie* **1961**, *73*, 353-364.

93. Winkhaus, G.; Singer, H. *J. Organomet. Chem.* **1967**, *7*, 487-491.

94. Lenthall, J. T. Anion and platinum group metal binding of bis (thioureido) ligands, PhD Thesis, Durham University, 2007.

95. Kang, J. W.; Moseley, K.; Maitlis, P. M. *J. Am. Chem. Soc.* **1969**, *91*, 5970-5977.

96. Maitlis, P. M. *Acc. Chem. Res.* **1978**, *11*, 301-307.

97. White, C.; Thompson, S. J.; Maitlis, P. M. *J. Chem. Soc., Dalton Trans.* **1977**, 17, 1654-1661.

98. White, C.; Yates, A.; Maitlis, P.; Heinekey, D. *Inorg. Synth.* **1992**, 29, 228-234.

99. Bennett, M.; Huang, T. N.; Matheson, T.; Smith, A.; Ittel, S.; Nickerson, W. *Inorg. Synth.* **1982**, *21*, 74-78.

100. Bennett, M.; Matheson, T. *J. Organomet. Chem.* **1979**, *175*, 87-93.

101. Bolaño, S.; Plaza, M.; Bravo, J.; Castro, J.; Peruzzini, M.; Gonsalvi, L.; Ciancaleoni, G.; Macchioni, A. *Inorg. Chim. Acta* **2010**, *363*, 509-516.

102. Osswald, T.; Mikhel, I. S.; Rüegger, H.; Butti, P.; Mezzetti, A. *Inorg. Chim. Acta* **2010**, *363*, 474-480.

103. Pisiewicz, S.; Rust, J.; Lehmann, C. W.; Mohr, F. *Polyhedron* **2010**, *29*, 1968-1972.

104. Correa, R. S.; de Oliveira, K. M.; Delolo, F. G.; Alvarez, A.; Mocelo, R.; Plutin, A. M.; Cominetti, M. R.; Castellano, E. E.; Batista, A. A. *J. Inorg. Biochem.* **2015**, *150*, 63-71.

105. Barolli, J. P.; Maia, P. I. S.; Colina-Vegas, L.; Moreira, J.; Plutin, A. M.; Mocelo, R.; Deflon, V. M.; Cominetti, M. R.; Camargo-Mathias, M. I.; Batista, A. A. *Polyhedron* **2017**, *126*, 33-41.

106. Kalidasan, M.; Nagarajaprakash, R.; Forbes, S.; Mozharivskyj, Y.; Rao, K. M. *Zeit. Anorg. Allg. Chem.* **2015**, *641*, 715-723.

107. Koch, K. R.; Sacht, C.; Bourne, S. *Inorg. Chim. Acta* **1995**, *232*, 109-115.

108. Koch, K. R.; Bourne, S. *J. Mol. Struct.* **1998**, *441*, 11-16.

109. Piraino, P.; Bruno, G.; Tresoldi, G.; Faraone, G.; Bombieri, G. *J. Chem. Soc., Dalton Trans.* **1983**, 2391-2395.

110. Bosman, V.; Gal, A. *Crystl. Struct. Commun.* **1975**, *4*, 465.

111. Robinson, S. D.; Sahajpal, A.; Steed, J. *Inorg. Chim. Acta* **2000**, *303*, 265-270.

112. Holman,T.K.; Robinson, S.D.; Steed, J. *J. Chem. Soc., Dalton Trans.* **1999**, 15-18.

113. Meier, S. M.; Hanif, M.; Adhireksan, Z.; Pichler, V.; Novak, M.; Jirkovsky, E.; Jakupec, M. A.; Arion, V. B.; Davey, C. A.; Keppler, B. K. *Chem. Sci.* **2013**, *4*, 1837-1846.

114. Capper, G.; Davies, D. L.; Fawcett, J.; Russell, D. R. *Acta Crystallogr., Sect. C: Cryst. Struct. Commun.* **1995**, *51*, 578-580.

115. Henderson, W.; Nicholson, B. K.; Dinger, M. B. *Inorg. Chim. Acta* **2003**, *355*, 428-431.

116. Fregona, D.; Graziani, R.; Faraglia, G.; Caselato, U.; Sitran, S. *Polyhedron* **1996**, *15*, 2523-2533.

117. Burrows, A. D.; Coleman, M. D.; Mahon, M. F. *Polyhedron* **1999**, *18*, 2665-2671.

118. Gambino, D.; Benítez, J.; Otero, L. a.; Kremer, E.; Baran, E. J.; Piro, O. E. *Polyhedron* **1999**, *18*, 2099-2107.

119. Singh, R.; Dikshit, S. K. *Polyhedron* **1995**, *14*, 1799-1807.

120. Stocker, F. B.; Troester, M. A.; Britton, D. *Inorg. Chem.* **1996**, *35*, 3145-3153.

121. Pilato, R. S.; Eriksen, K. A.; Greaney, M. A.; Stiefel, E. I.; Goswami, S.; Kilpatrick, L.; Spiro, T. G.; Taylor, E. C.; Rheingold, A. L. *J. Am. Chem. Soc.* **1991**, *113*, 9372-9374.

122. Pilato, R. S.; Housmekerides, C. E.; Jernakoff, P.; Rubin, D.; Geoffroy, G. L.; Rheingold, A. L. *Organometallics* **1990**, *9*, 2333-2341.

123. Harvey, J. *Computational Chemistry*; Oxford University Press: United Kingdom, 2018; 139.

124. Schlegel, H. B. Geometry optimization on potential energy surfaces. In *Modern Electronic Structure Theory: Part I*; World Scientific, 1995; pp 459-500.

125. Schlegel, H. B. *Wiley Interdisciplinary Reviews: Computational Molecular Science* **2011**, *1*, 790-809.

126. Baker, J. *J. Comput. Chem.* **1993**, *14*, 1085-1100.

127. Schlegel, H. B. *Int. J. Quantum Chem.* **1992**, *44*, 243-252.

128. Bader, R. F. *Chem. Rev.* **1991**, *91*, 893-928.

129. Poater, J.; Duran, M.; Sola, M.; Silvi, B. *Chem. Rev.* **2005**, *105*, 3911-3947.

130. Noury, S.; Krokidis, X.; Fuster, F.; Silvi, B. *Comput. Chem. (Oxford)* **1999**, *23*, 597-604.

131. Zhou, F.; Liu, R.; Li, P.; Zhang, H. *New J. Chem.* **2015**, *39*, 1611-1618.

132. Silvi, B.; Savin, A. *Nature* **1994**, *371*, 683-686.

133. Bader, R. F.; Nguyen-Dang, T. *Adv. Quantum Chem.* **1981**, *14*, 63-124.

134. Johnson, E. R.; Keinan, S.; Mori-Sanchez, P.; Contreras-Garcia, J.; Cohen, A. J.; Yang, W. *J. Am. Chem. Soc.* **2010**, *132*, 6498-6506.

135. Cohen, A. J.; Mori-Sánchez, P.; Yang, W. *Science* **2008**, *321*, 792-794.

136. Contreras-García, J.; Yang, W.; Johnson, E. R. *J. Phys. Chem. A* **2011**, *115*, 12983-12990.

137. Arfken, G. B.; Weber, H. J.; Harris, F. E. *Mathematical methods for physicists: A comprehensive guide*, 7th ed.; Academic Press: Amsterdam, Netherlands, 2011.

138. Bader, R. F.; Essén, H. *J. Chem. Phys.* **1984**, *80*, 1943-1960.

139. Narth, C.; Maroun, Z.; Boto, R. A.; Chaudret, R.; Bonnet, M.-L.; Piquemal, J.-P.; Contreras-García, J. A complete NCI perspective: From new bonds to reactivity. In *Applications of Topological Methods in Molecular Chemistry*; R. Remi Chauvin; C. Christine Lepetit; B. Bernard Silvi and E. Alikhani, Eds.; Springer: Switzerland, 2015; pp 491-527.

140. Otero-de-la-Roza, A.; Johnson, E. R.; Contreras-García, J. *Phys. Chem. Chem. Phys.* **2012**, *14*, 12165-12172.

Chapter 2

Platinum complexes of some pyridyl-substituted thiourea monoanion and dianion ligands

2.1 Introduction

Among bidentate *N,S*-ligands, the *N*-substituted pyridyl thiourea ligands have been of interest in both pharmaceutical and industrial processes. Their metal complexes have been utilised for several decades as synthetic precursors in coordination[1,2], supramolecular and materials chemistry[3-5]. The antimicrobial properties of this group of compounds and their metal complexes are well documented in the literature[6-8]. The presence of the pyridine nitrogen in *N*-(2-pyridyl)thioureas make them susceptible to intermolecular and intramolecular hydrogen bonding. Hydrogen bonding in *N*-(2-pyridyl)thioureas was first confirmed by NMR spectroscopy some years ago[9]. Recently the crystal structure of *N*-(2-pyridyl)-*N′*-phenylthiourea was determined, showing both intramolecular N′-H·····N and intermolecular N-H····S hydrogen bonding interaction in the crystal lattice[10] (**Figure 2.1**). Subsequently, hydrogen bonding interactions were reported in other disubstituted *N*-(2-pyridyl)-*N′*-aryl thioureas including *N*-(2-pyridyl)-*N′*-tolylthioureas[11], *N*-2(4,6-lutidyl)-*N′*-tolylthioureas[12], *N*-(5-bromo-2-pyridyl)-*N′*-2-(2,5-dimethoxyphenylethyl)thiourea[13], *N*-(2-pyridyl)-*N′*-(4-methoxyphenyl) thiourea[14], *N*-(2-pyridyl)-*N′*-2-methoxyphenylthioureas and *N*-(2-pyridyl)-*N′*-tolylthioureas.[15] A number of other compounds containing the *N*-(2-picolyl)- and *N*-(4,6-lutidyl)-*N′*-phenyl thioureas were also reported.[16]

Due to the versatility of the coordination options available in the pyridyl substituted thiourea ligands, a significant number of complexes have been formed between this group of ligands and a variety of transition metal centres including platinum and palladium[17], copper[18], mercury[19], cobalt and nickel[20], ruthenium, rhodium and iridium[3]. Despite the increasing number of asymmetrically substituted complexes of platinum reported in the literature, there are only a few reports of the pyridyl substituted thiourea dianion and monoanion complexes of platinum[17]. The

present chapter explores the synthesis, structure and the effect of different pyridyl substituents on isomerism in platinum complexes of some asymmetrically substituted thiourea monoanion and dianion ligands. The possibility of the pyridyl nitrogen acting as an additional donor site for the platinum metal in the first complex or to other metals in a secondary complex informed the interest in the pyridyl substituted thiourea complexes. Apart from that, there is also a possibility of protonation or alkylation of the pyridyl group in solution and this could alter the solubility property of the complexes, which may enhance the potential anti-microbial and anti-cancer properties of the compounds. Further, the effect of an ethylene or methylene spacer between the pyridyl and thiourea functionalities on the coordination geometry and supramolecular properties of the platinum complexes will be explored.

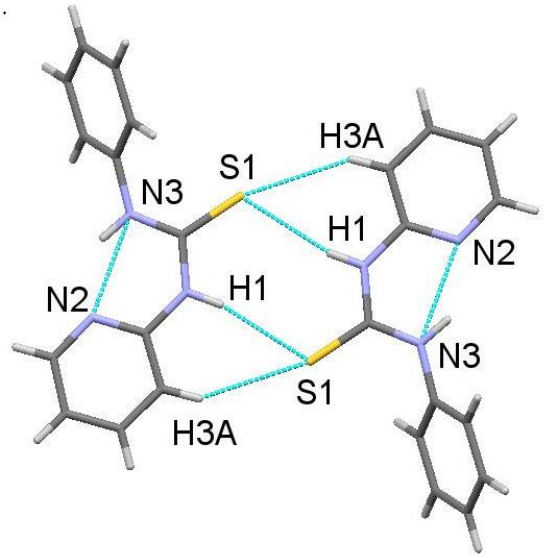

Figure 2.1: Crystal structure of *N*-(2-pyridyl)-*N′*-phenylthiourea showing intermolecular and intramolecular hydrogen bonding.

2.2 Results and discussion

2.2.1 *Synthesis of asymmetrically di-substituted thiourea ligands*

A range of pyridyl-substituted thiourea ligands were synthesised from the reaction of phenyl isothiocyanate, *p*-nitrophenyl isothiocyanate and *p*-methoxyphenyl isothiocyanate and the corresponding pyridyl amines in refluxing diethyl ether to afford the semi-crystalline products in high yield (70-95%)

(**Scheme 2.1**). These thiourea ligands have been made previously using different literature methods [10,21-23].

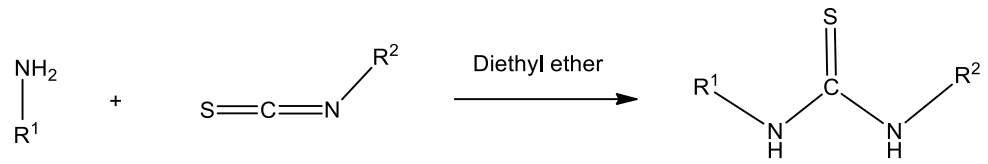

Ligand	R^1	R^2
1a	Py	Ph
1b	Py	*p*-C_6H_4OMe
1c	Py	*p*-$C_6H_4NO_2$
1d	(CH_2)Py	Ph
1e	(CH_2)Py	*p*- $C_6H_4NO_2$
1f	$(CH_2)_2$Py	Ph
1g	$(CH_2)_2$Py	*p*-C_6H_4OMe
1h	$(CH_2)_2$Py	*p*-$C_6H_4NO_2$

Scheme 2.1: Reaction scheme for the synthesis of asymmetrically substituted thiourea ligands.

2.2.2 *Platinum complexes of asymmetrically substituted pyridyl thiourea dianions*

The reaction of the phosphine complex *cis*-$[PtCl_2(PPh_3)_2]$ with some asymmetrically di-substituted thiourea ligands in the presence of triethylamine in refluxing methanol at different reaction times of between 20 and 60 min (**Table 2.7**) gave a clear yellow solution. Addition of water (70 mL) resulted in a precipitate of the appropriate thiourea dianion complex (**Scheme 2.2**).

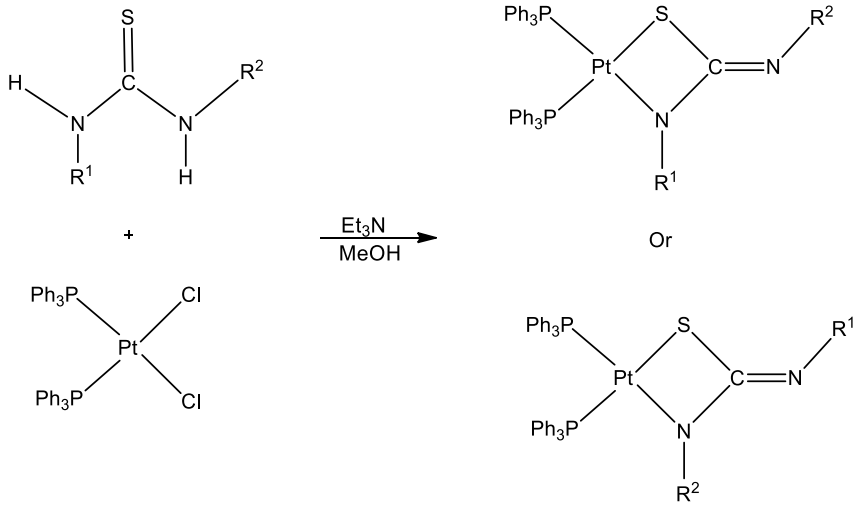

Compound	R^1	R^2
2a	Py	Ph
2b	Py	*p*-C_6H_4OMe
2c	Py	*p*-$C_6H_4NO_2$
2d	(CH_2)Py	Ph
2e	(CH_2)Py	*p*-$C_6H_4NO_2$
2f	$(CH_2)_2$Py	Ph
2g	$(CH_2)_2$Py	*p*-C_6H_4OMe
2h	$(CH_2)_2$Py	*p*-$C_6H_4NO_2$

Scheme 2.2: Reaction scheme for the synthesis of platinum thiourea dianion complexes.

The first platinum pyridyl thiourea dianion complex [Pt{SC(NPh)NPy}](PPh_3)$_2$] **2a** was synthesised from the reaction of *cis*-[$PtCl_2$(PPh_3)$_2$] and PyNHC(S)NHPh **1a** in refluxing methanol solution. ESI-mass spectral data showed that the immediately isolated yellow solid formed on addition of water was the pure complex with a dominant isotope peak for $[M+H]^+$ with *m/z* 946.97 at a low capillary exit voltage (CEV) of 60 V. The experimental isotope pattern showed excellent agreement with the calculated pattern (**Figure 2.2**). Increasing the CEV to 150 V resulted in fragmentation of the dianion complex, giving rise to fragment ions at *m/z* 684.95 $[M-PPh_3+H]^+$ and 1631.88 $[2M-PPh_3+H]^+$ attributable to loss of one PPh_3 ligand from the monomer and dimer respectively. Also appearing in the spectrum is a fragment ion with *m/z* 717.96. This has been identified in some other platinum complexes containing the triphenylphosphine ligand as the orthometallated species $[Pt(PPh_2C_6H_4)(PPh_3)]^+$ [24]

2.1. Complexes containing triphenylphosphine ligands have been reported to undergo orthometallation at higher exit voltages to give the species observed at *m/z* 717.96 [25]. Further increase in the CEV above 150 V resulted in an ion *m/z* 1915.87 identified as a sodium adduct of the platinum complex dimer $[2M+Na]^+$. Addition of a small quantity of NaCl to the solution of the complex resulted in an increase in the intensity of the molecular ion peak confirming the peak as the sodium adduct of the complex. The *m/z* values for the different ions formed for this complex and the other complexes reported here at various capillary exit voltages are presented in **Table 2.1.**

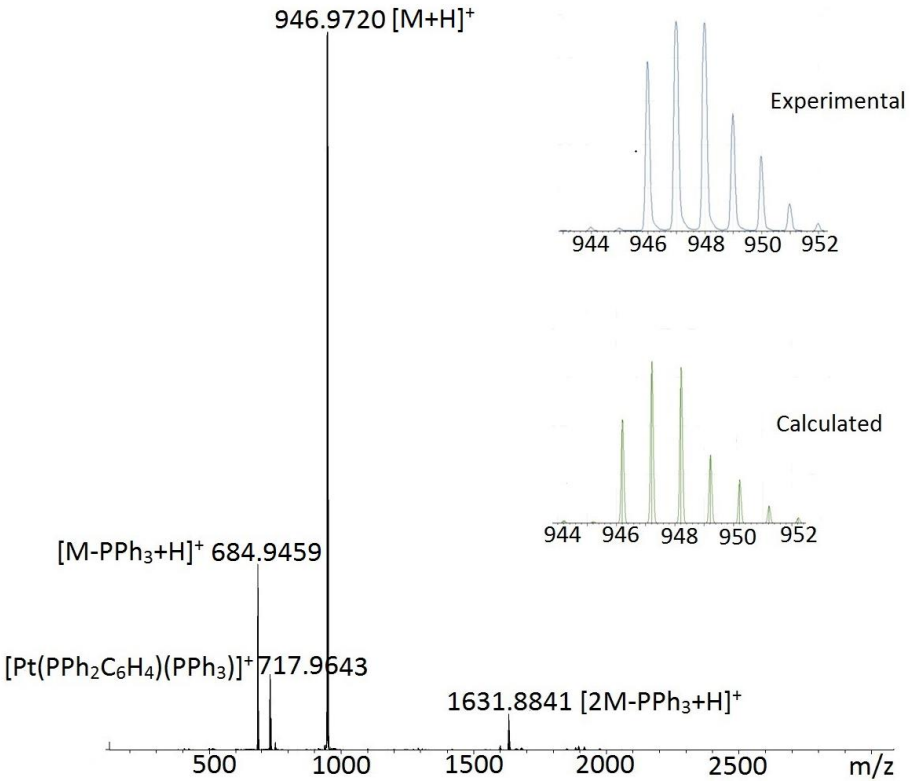

Figure 2.2: ESI-mass spectrum of thiourea dianion complex $[Pt\{SC(=NPh)NPy\}(PPh_3)_2]$ **2a** at CEV 150 V. Experimental and calculated isotope patterns are shown.

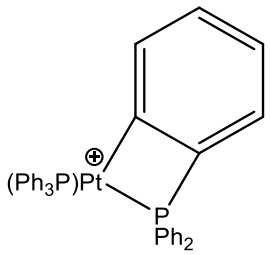

2.1

Table 2.1: Positive–ion electrospray mass spectral data for the thiourea dianion complexes **2a-2h**

Complexes	**Capillary exit voltage (V)**	***m/z* (%) ions**
$[Pt\{SC(NPh)NPy\}(PPh_3)_2]$ **(2a)**	60	947 (100) $[M+H]^+$, 1631 (2) $[2M-PPh_3+H]^+$.
	150	685 (35) $[M-PPh_3+H]^+$, 718 (12) $[Pt(PPh_2C_6H_4)(PPh_3)]^+$, 947 (100) $[M+H]^+$,1631 (6) $[2M-PPh_3+H]^+$.
	180	649 (62) $[M-PPh_3+H]^+$, 718 (12) $[Pt(PPh_2C_6H_4)(PPh_3)]^+$, 947 (99) $[M+H]^+$, 1916 (3) $[2M+Na]^+$.
$[Pt\{SC(NC_6H_4OMe)NPy)\}(PPh_3)_2]$ (**2b)**	60	977 (100) $[M+H]^+$.
	150-180	715 (6) $[M-PPh_3+H]^+$, 977 (99) $[M+H]^+$, 1691 (8) $[2M-PPh_3+H]^+$.
$[Pt\{SC(NC_6H_4NO_2)NPy\}(PPh_3)_2]$ **(2c)**	60	992 (100) $[M+H]^+$.
	120-150	946 (22) $[M-NO_2+H]^+$, 992 (100) $[M+H]^+$, 1722 (16) $[2M-PPh_3+H]^+$,1983(6) $[2M+H]^+$.
	180	718 (12) $[Pt(PPh_2C_6H_4)PPh_3]^+$, 729 (14) $[M-PPh_3+H]^+$,946 (22) $[M-NO_2+H]^+$, 992 (100) $[M+H]^+$.
$[Pt\{SC(NPh)NCH_2Py\}(PPh_3)_2]$ **(2d)**	60	961 (100) $[M+H]^+$.
	120-150	699 (13) $[M-PPh_3+H]^+$, 961 (100) $[M+H]^+$, 1201 (11) $[2M-Py(CH_2)NCSNPh+H]^+$.
	180	699 (81) $[M-PPh_3+H]^+$, 961 (100) $[M+H]^+$, 718 (24)

		$[Pt(PPh_2C_6H_4)(PPh_3)]^+$, 1944 (2) $[2M+Na+H]^{2+}$.
	240	699 (100) $[M-PPh_3+H]^+$, 961 (54) $[M+H]^+$, 718 (41) $[Pt(PPh_2C_6H_4)(PPh_3)]^+$, 1944 (2) $[2M+Na+H]^{2+}$.
$[Pt\{SC(NC_6H_4NO_2)NCH_2Py\}(PPh_3)_2]$ **(2e)**	60	1005.95 (100) $[M+H]^+$, 2012 (2) $[2M+H]^+$.
	120-150V	483 (2) $[M-2PPh_3+H]^+$, 718 (14) $[Pt(PPh_2C_6H_4)(PPh_3)]^+$, 744 (28) $[M-PPh_3]^+$, 2012 (6) $[2M+H]^+$.
$[Pt\{SC(NPh)N(CH_2)_2Py\}(PPh_3)_2]$ **(2f)**	60	975 (100) $[M+H]^+$.
	120	713 (74) $[M-PPh_3+H]^+$, 975 (100) $[M+H]^+$.
	180	451 (12) $[(M-PPh_3)_2+H]^+$, 713 (62) $[M-PPh_3+H]^+$, 975 (100) $[M+H]^+$.
$[Pt\{SC(NC_6H_4OMe)N(CH_2)_2Py)\}(PPh_3)_2]$**(2g)**	60	1005 (100) $[M+H]^+$.
	120-180	1005 (100) $[M+H]^+$, 955 (2) $[M-MeO+H]^+$, 742 (3) $[M-PPh_3+H]^+$.
	240	1005 (100) $[M+H]^+$, 481 (12) $[M-(PPh_3)_2+H]^+$.
$[Pt\{SC(NC_6H_4NO_2)N(CH_2)_2Py\}(PPh_3)_2]$**(2h)**	60	1020 (100) $[M+H]^+$.
	120	758 (13) $[M-PPh_3+H]^+$, 1020 (100) $[M+H]^+$, 1363 (4) $[M-PPh_4NS+H]^+$.
	180	496 (7) $[M-(PPh_3)_2+H]^+$, 718 (48) $[Pt(PPh_2C_6H_4)(PPh_3)]^+$, 758 (41) $[M-PPh_3+H]^+$, 1020 (100) $[M+H]^+$.

The ^{1}H NMR spectrum of a sample of the dianion complex [Pt{SC(NPy)NPh}(PPh_3)$_2$] **2a** in $CDCl_3$ showed overlapping peaks and was somewhat complicated. This suggests the possibility of the presence of more than one isomer of the complex in the NMR solution. The $^{31}P\{^{1}H\}$ NMR spectrum of a freshly dissolved sample of the complex recorded after 30 min. of dissolution showed the expected AB doublets (two doublets) pattern for two inequivalent PPh_3 ligands coordinated to platinum with resonances at 17.6 and 12.4 ppm and $^{1}J_{(PtP)}$ coupling constants of 3178 and 3341 Hz respectively (**Figure 2.3a**). These values are comparable to the coupling constant values for thiourea dianion complex [Pt{SC(=NCN)NMe}(PPh_3)$_2$] (**2.2**)[24] with coupling constant values of 3137 and 3308 Hz but slightly higher than the values for the triphenyl-substituted thiosemicarbazone complex [Pt{SC($NNPh_2$)NPh}(PPh_3)$_2$] **2.3**[26] with coupling constants of 3156 Hz and 3147 Hz. A spectrum collected after 120 min. of dissolution showed another set of AB phosphine signals with about 10 % intensity of the first set of peaks having phosphorus resonance peaks at 16.6 ppm and 11.8 ppm. Another spectrum collected after 12 hr in solution, showed that the minor isomers had grown up to about 40% of the first set of isomers along with their ^{195}Pt satellite peaks having coupling constants of 3067 and 3279 Hz respectively (**Figure 2.3b)**. The sample was left in solution and the isomerisation monitored by $^{31}P\{^{1}H\}$ NMR spectroscopy. A spectrum recorded after exactly 12 days showed the presence of another set of AB doublets at 15.3 ppm and 10.4 ppm with $^{1}J_{(PtP)}$ coupling constants of 3180 and 3339 Hz respectively. These third set of peaks had similar intensities as the peaks for the second isomer (**Figure 2.3 c**). The coupling constants for these new set of peaks were similar to that of the two initial isomers.

Theoretical $^{31}P\{^{1}H\}$ NMR calculations were used to tentatively assign the first and major peaks as the proximal isomer of the complex (**2.4**) while the second set of peaks were assigned as a distal isomer of the complex (**2.5**). Chemical shifts for the third set of peaks were observed to be close to that of the distal isomer indicating the possibility of another form of isomerism in the complex. This is probably due to the pyridyl substituent at the distal position interchanging between the *cis* and *trans*-positions with respect to the sulfur, resulting in another isomer of the complex (**2.6**).

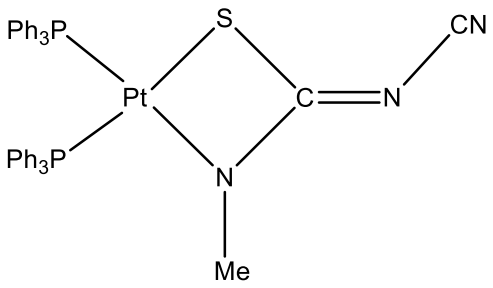

2.2

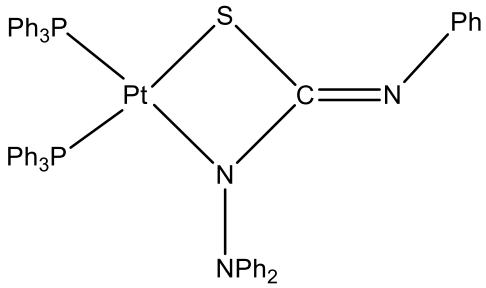

2.3

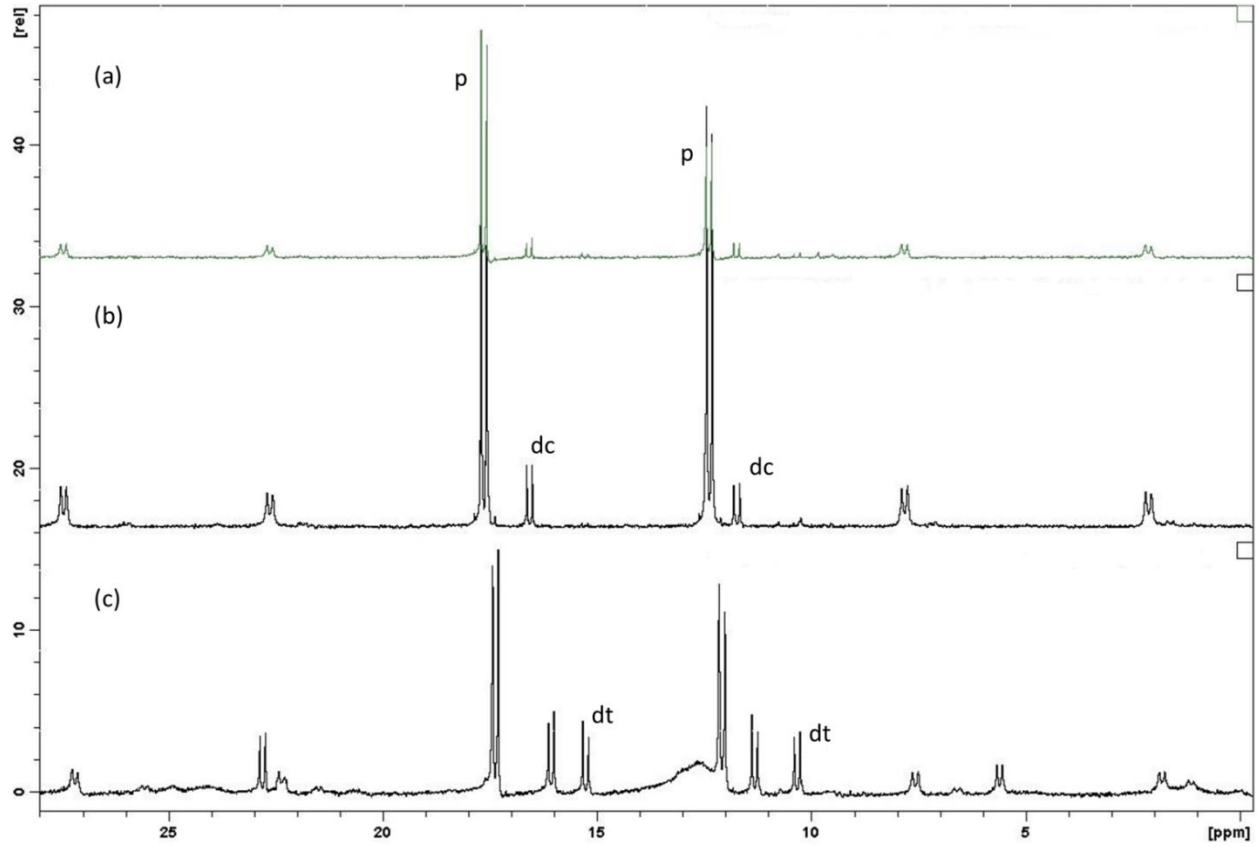

Figure 2.3: $^{31}P\{^{1}H\}$ NMR spectra of pyridyl thiourea dianion complex [Pt{SC(=NPh)NPy}(PPh_3)$_2$], (a) After 30 min (b) 12 hours (c) 12 days in solution p = proximal isomer, and d = distal isomer. Satellite peaks due to ^{195}Pt coupling are lower intensity peaks on both sides of the major peaks.

Another possible explanation for the presence of the third set of peaks in the above spectrum could be the presence of an entirely different complex resulting from the *in-situ* generation of hydrochloric acid from the $CDCl_3$ NMR solution and subsequent chlorination of the original complex to get the chloride substituted complex **2.7**. The $^{1}J_{(PtP)}$ coupling constant for the chloro-substituted complex should

be different from those of the other two isomers of the complex (**2.4** and **2.5**) due to the difference in *trans* influence between the nitrogen and chloride donor ligands. A search through the literature revealed $^{1}J_{(PtP)}$ coupling constant values of 3770 and 3950 Hz for a Pt-P bond trans to Cl in $[PtCl(sac)(PPh_3)_2]$ (sac = saccharin)[27] and $[PtCl(debarb)(PPh_3)_2]$ (debarb = 5,5-diethylbarbituric acid)[28] respectively. The $^{31}P\{^{1}H\}$ NMR spectrum of the *cis*-$[PtCl_2(PPh_3)_2]$ starting complex also gave $^{1}J_{(PtP)}$ coupling constant of 3679 Hz for a Pt-P bond *trans* to a chloride. $^{1}J_{(PtP)}$ coupling constants of 3180 and 3339 Hz recorded for the third set of AB peaks (**Table 2.2**) rules out the possibility of a chloro-substituted complex **2.7** in the NMR solution.

Apart from the chloro-substituted complex, there is also the possibility of platinum coordination to the pyridyl nitrogen resulting in the formation of a six-membered platinum dianion complex, **2.8**. The $^{1}J_{(PtP)}$ coupling constants for Pt-P bond *trans* to pyridyl nitrogen has been reported as 3552 and 3609 Hz for platinum monoanion complexes *cis*-$[Pt(debarb)(py)(PPh_3)_2]BPh_4$[28] and $[\{Fe(\eta^5\text{-}C_5H_4PPh_2)(Spy)\}]BF_4$ [29]. The $^{1}J_{(PtP)}$ coupling constants for the third set of peaks in the $^{31}P\{^{1}H\}$ NMR spectrum of the complex **2a**, were however observed to be lower than the values reported for P-Pt *trans* to Py and a lot closer to values recorded for the second (minor) and first (major) isomers (**Table 2.2**). So the third set of peaks in the NMR spectrum of the pyridyl-substituted complex $[Pt\{SC(=NPh)NPy\}(PPh_3)_2]$ **2a** (**Figure 2.3c**) is possibly due to *E/Z* isomerisation in the complex**.** It was not entirely clear however why the same E/Z isomerisation was not observed when the pyridyl substituent was at the proximal position to generate the *trans*-isomer, **2.9**. The FTIR spectra of the complex showed characteristic bands between 1520 and 1650 cm^{-1} corresponding to $\upsilon C{=}N$ stretching vibrations of the amidate bond and another spectrum taken from an evaporated NMR solution showed the IR bands in the same region. There was no evidence of the formation of a different complex in the NMR solution.

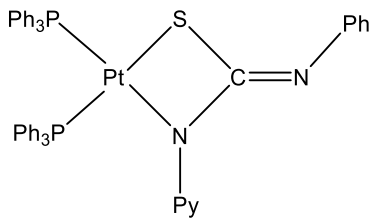

2.4 Proximal isomer

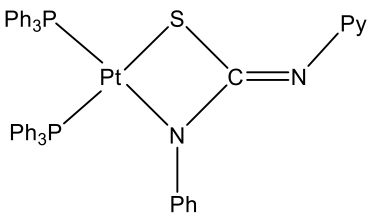

2.5 Distal isomer

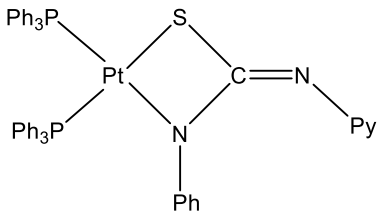

2.6 distal isomer (*trans*)

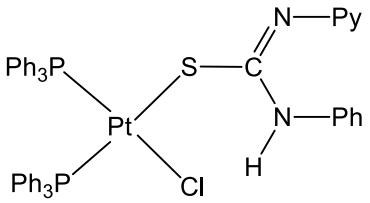

2.7 chloro-substituted complex

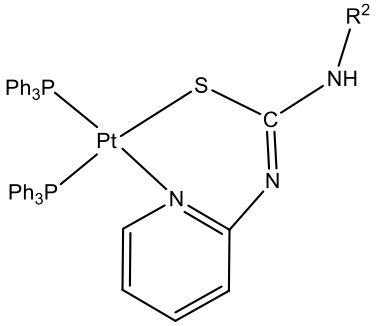

2.8 Pyridyl coordination complex

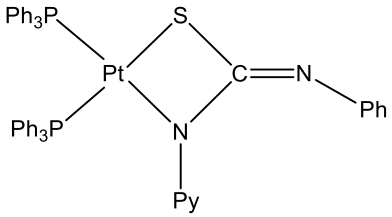

2.9 Proximal isomer (*trans*)

Table 2.2: A summary of the $^{31}P\{^{1}H\}$ NMR data [δ/ppm, with $^{1}J_{(PtP)}$ in parentheses] for the complexes $[Pt\{SC(=NR^{1})NR^{2}\}(PPh_3)_2]$ containing substituted thiourea dianions.

R^1	R^2	Distal isomer (*cis*)	Distal isomer (*trans*)	Proximal Isomer
Py	Ph	16.6(3067), 11.8(3279)	15.3(3180), 10.40(3339)	17.6(3178), 12.4(3341)
Py	*p*-C_6H_4OMe	16.7(3291), 11.7(3334)	15.6(3181), 10.4(3426)	17.7(3176), 12.5(3318)
Py	*p*-$C_6H_4NO_2$	14.9(3222), 9.7(3386)		17.5(3175), 11.9(3338)
Py(CH_2)	Ph	13.6(3238), 9.1(3448)		18.2(3055), 13.6(3194)
Py(CH_2)	*p*-$C_6H_4NO_2$			17.6(3109), 13.1(3245)
Py(CH_2)$_2$	Ph	13.4(3210), 9.3(3483)		18.3(3119), 13.4(3221)
Py(CH_2)$_2$	*p*-C_6H_4OMe	14.0(3259), 9.4(3338)		18.3(3216), 13.6(3338)
Py(CH_2)$_2$	*p*-$C_6H_4NO_2$	13.6(3215), 9.2(3403)		18.2(3105), 12.8(3194)

In order to investigate the thermodynamic aspect of the isomerisation process, Density Functional Theory calculations were employed to determine the difference in the Gibbs free energy ΔG ($GPt_{dist} - GPt_{prox}$) between the possible isomers of the complex, where Pt_{prox} is the proximal isomer and Pt_{dist} is the distal isomer. It has been previously reported that the more stable isomer will be lower in energy and thus more abundant in a solution of the complex[30]. This will probably result in this isomer having a greater population than the isomer with the higher

Gibbs free energy at equilibrium. The calculated Gibbs free energy difference ΔG ($GPt_{dist} - GPt_{prox}$) for two isomers of the complex $[Pt\{SC(NPh)NPy\}(PPh_3)_2]$ **2a** (**Figure 2.4**) was found to be 24.93 kJ mol^{-1} indicating that the proximal isomer is lower in energy than the distal isomer by this amount and thus kinetically more stable. The results from the NMR and Gibbs free energy calculations indicate a possible formation of the kinetically stable proximal isomer which subsequently isomerises into a mixture of the proximal and distal isomers as indicated in the NMR results.

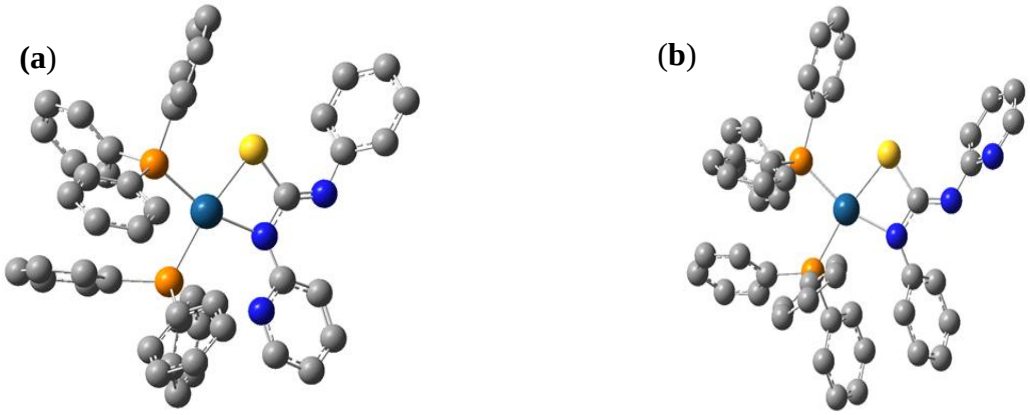

Figure 2.4: Optimised structures of (**a**) proximal and (**b**) distal isomers of the complex $[Pt\{SC(=NPy)NPh\}(PPh_3)_2]$ **2a**.

The effect of solvent on the isomerisation process was also investigated by synthesising a fresh sample of the $[Pt\{SC(NPh)NPy\}(PPh_3)_2]$ complex and isolating a small proportion of the reaction mixture while the rest was left in the methanol solution for 12 days at room temperature before precipitation with water. The two isolated samples were observed to have slightly different shades of yellow with the sample isolated after 12 days deeper in colour. The $^{31}P\{^1H\}$ NMR analysis of the immediately isolated sample showed the presence of only the proximal isomer of the complex after 30 min. of dissolution. The sample isomerised into a mixture of two isomers after 120 minutes and subsequently into a mixture of three isomers after 12 days. The $^{31}P\{^1H\}$ NMR spectrum of the sample isolated after 12 days showed the presence of two isomers of the complex on dissolution in $CDCl_3$ solution, which indicate that the sample had isomerised, though to a lesser degree in the methanol solution than the $CDCl_3$ solution. The third isomer was also observed after leaving the sample in solution for another 5 days. Complete

conversion from the proximal to the distal isomer was not observed for any of the two samples even after leaving them in the solution for 90 days. DFT calculations were also used to estimate the effect of different solvents on the Gibbs free energies of the proximal and distal isomers of the complex, and the results showed only a slight difference on changing the solvent (from chloroform to methanol to water).

To further investigate the isomerisation process, two other derivatives of the pyridyl complex were synthesised by substituting the phenyl group on the complex **2a** with *p*-methoxyphenyl and *p*-nitrophenyl functional groups to obtain the complexes $[Pt\{SC(NC_6H_4OMe)NPy\}(PPh_3)_2]$ **2b** and $[Pt\{SC(NC_6H_4NO_2)NPy\}(PPh_3)_2]$ **2c** respectively. The ESI-mass spectral analysis of the complexes gave single $[M+H]^+$ peaks for the dianion complexes **2b** and **2c** at low capillary exit voltage (60 V), **Table 2.1.** Satisfactory micro-analytical data were obtained for the two complexes. $^{31}P\{^1H\}$ NMR spectra of a freshly prepared sample of $[Pt\{SC(=NC_6H_4OMe)NPy\}(PPh_3)_2]$ **2b** determined after 30 min. of dissolution of the complex in $CDCl_3$ showed phosphorus resonance peaks at 17.65 and 12.64 ppm with ^{195}Pt satellites and coupling constants of 3171 and 3318 Hz.

A second spectrum taken 10 days later showed the presence of two other sets of phosphorus resonance peaks close to each other and up-field of the first set of peaks with about 30 % intensity of the first set of peaks. The peaks had phosphorus resonances at 16.73 ppm and 11.77 ppm with $^1J_{(PtP)}$ coupling constants of 3291 and 3334 Hz respectively and 15.58 ppm and 10.40 ppm with coupling constants of 3181 and 3426 Hz respectively. The first set of peaks were assigned as the proximal isomers (where the pyridyl functional group is attached to the nitrogen adjacent to the platinum metal) as predicted by theoretical $^{31}P\{^1H\}$ NMR calculations. The other two peaks up-field of the proximal isomer were assigned as the distal isomers of the complex (where the pyridyl functional group is attached to the nitrogen remote to the platinum metal). The coupling constants for the two distal isomers were observed to be similar and close to the coupling constants recorded for the proximal isomer (**Table 2.2**). The coupling constants are also similar to those reported for a related dianion complex $[Pt\{SC(=NBu^t)NPh\}(PPh_3)_2]$ [30]. The ESI-mass spectral analysis of the NMR solution of this complex after isomerisation also gave the molecular ion for the dianion complex **2b**. The results from the spectroscopic analysis of this complex also point to the formation of the *cis* and *trans* distal isomeric forms of the complex, similar to the phenyl substituted

complex [Pt{SC(=NPh)NPy}(PPh_3)$_2$] **2a**. To the best of our knowledge, this is the first report of the possibility of *E/Z* isomerism in platinum complexes of thiourea dianions. $^{31}P\{^1H\}$ NMR investigation for the *p*-nitrophenyl substituted complex [Pt{SC($NC_6H_4NO_2$)NPy}(PPh_3)$_2$] **2c** exhibited similar isomerisation trend to **2a** and **2b**. This involved the formation of an initial proximal isomer with phosphorus resonances at 17.4 and 11.9 ppm and $^1J_{(PtP)}$ coupling constants of 3223 and 3386 Hz respectively and a minor distal isomer after 6 days in solution with resonances at 14.9 and 9.70 ppm and having coupling constants of 3223 and 3386 Hz respectively. These coupling constants were similar to the ones observed for the phenyl **2a** and *p*-methoxyphenyl **2b** derivatives of this complex. There was however no evidence of the formation of a third isomer for the *p*-nitrophenyl-substituted complex **2c** after 26 days in solution, but rather a decomposition of the complex as evidenced by the presence of several unidentified peaks in the $^{31}P\{^1H\}$ NMR spectrum.

Spectroscopic and theoretical investigations for this group of pyridyl-substituted complexes suggest a plausible mechanism for the initial formation of a kinetically stable dianion complex with the pyridyl functional group at the proximal position. This is a direct opposite of what was observed with a previous investigation where the alkyl substituent was located at the distal position for the initial complex[30]. The first stage involves the formation of an S-bonded monodentate thiourea complex, probably due to the high affinity of platinum metal for soft sulfur donor ligands. The second stage of the process is the deprotonation of an NH bond, resulting in cyclisation through the formation of the Pt-N bond. The NHPy proton is expected to be more acidic than the NHPh, NHC_6H_4OMe or $NHC_6H_4NO_2$ protons, because of the lone pair of electrons on the nitrogen of the pyridyl functional group. The possibility of the NPy group preferentially reacting to form the proximal isomer with a coordinated Pt-NPy group is very high.

2.2.3 *Crystallographic analysis of pyridyl substituted complexes 2a and 2b*

Crystals of the complexes **2a** and **2b** were grown by vapour diffusion of diethyl ether into a dichloromethane solution of the compounds. Bright yellow crystals of the complexes precipitated out of the solution after about 4 and 6 days for **2a** and **2b** respectively. X-ray structure determination confirmed their proximal isomeric configuration. Selected bond lengths and angles for both complexes are

presented in **Table 2.3,** while the molecular structures are shown in **Figure 2.5**. The molecular structures of the complexes showed the expected four-membered metallacyclic ring with the platinum *S,N*-chelated by an *N*-pyridyl-*N*-phenylcarbamimidothioato anion and also bonded to two phosphorus atoms of the triphenylphosphine ligand (PPh_3) in a distorted square planar geometry. The coordination geometries are similar to other structurally characterised platinum thiourea complexes [Pt{SC(=NEt)NEt}$(PPh_3)_2$] **2.10a**[31] and [Pt{SC(=NPh)NPh}$(PPh_3)_2$] **2.10b**[32]. The root mean square (r.m.s.) deviation of the NP_2S square plane are 0.1040 and 0.0638 Å for **2a** and **2b** and the platinum atom lies out of the plane by 0.053 and 0.115 Å for **2a** and **2b** respectively. *S,N*-chelate *cis*-angles in the two complexes has acute values of 69.79(7)^o **2a** and 69.51(13)^o **2b**, while the angles subtended by the phosphorus atoms are 98.58(3) and 96.64(5) for **2a** and **2b** respectively. The P(2)–Pt(1)–N(1) and S(1)–Pt(1)–P(1) *trans*-angles in the two complexes are similar and they deviate from the ideal 180^o by approximately 15^o. The four-membered chelate ring in the structures of **2a** and **2b** are similar and nearly planar with fold angles of 5.74^o and 3.20^o respectively between the N(1)–Pt(1)–S(1) and N(1)–C(1)–S(1) least-squares planes. The angles subtended at the thiolate-S(1) and metallacyclic-N(1) atoms are as expected with the more sterically encumbered Pt(1)–N(1)–C(1) angles wider than the acute Pt(1)–S(1)–C(1) angles in the two complexes. The pyridyl rings bonded to N(1) at the proximal positions of the two complexes are out of the plane of the metallacyclic ring by 29.8^o and 27^o for **2a** and **2b** respectively.

The phenyl and *p*-methoxyphenyl groups bonded to N(2) at the distal position are twisted and out of the plane of the metallacyclic ring by 52.2^o and 72.8^o for [Pt{SC(=NPh)NPy}$(PPh_3)_2$] **2a** and [Pt{SC(=NC_6H_4OMe)NPy}$(PPh_3)_2$] **2b** respectively. The Pt(1)–P(1) bonds in the two complexes are different; 2.3143(7) Å **2a,** 2.2777(7) Å **2b** and slightly longer than the Pt(1)–P(2) bond lengths; 2.2581(7) Å **2a,** 2.2464(7) Å **2b.** This is due to the greater *trans* influence of the sulfur-donor atom relative to nitrogen. This trend has been reported for the related diphenyl-substituted thiourea dianion complex [Pt{SC(=NPh)NPh}$(PPh_3)_2$] **2.10b**, (Pt–P); 2.308(1) and 2.247(1) Å[32], but not as much in the diethyl thiourea analogue [Pt{SC(=NEt)NEt}$(PPh_3)_2$] **2.10a** (Pt–P); 2.274(6) and 2.269(6) Å[31]. The delocalisation of electron density around the chelate ring is evident by comparing the geometric parameter in **2a** with those in the precursor ligand 1-phenyl-3-

(pyridin-2-yl) thiourea (**Figure 2.1**). The C(1)–S(1) and C(1)-N(2) bonds in **2a** 1.803(3) and 1.285(4) Å respectively were considerably elongated and shortened, when compared with the corresponding parameters in the ligand with 1.682(3) and 1.336(4) Å. The C(1)–N(1)-pyridyl bond lengths 1.371(4) and 1.381(4) Å remain similar however. The S(1)–C(1)–N(2) 129.9(2)^{o} and N(1)–C(1)–N(2) bond angles in **2a** are systematically wider than the corresponding angles in the free ligand; 124.61(2) and 116.80(3)^{o}. The narrow S(1)–C(1)–N(1) angle of 104.9(2) in **2a** expands to 118.60(2)^{o} in the free ligand.

Table 2.3: Selected bond lengths (Å) and angles (^{o}) for the proximal isomer [Pt{SC(=NPh)NPy}(PPh_3)$_2$] **2a** and [Pt{SC(=NC_6H_4OMe)NPy}(PPh_3)$_2$] **2b**

[Pt{SC(=NPh)NPy}(PPh_3)$_2$] (**2a**)			
Pt(1) – P(1)	2.3143(7)	N(1) – C(8)	1.392(4)
Pt(1) – P(2)	2.2581(7)	N(3) – C(8)	1.333(4)
Pt(1) – S(1)	2.3278(7)	N(3) – C(12)	1.340(4)
Pt(1) – N(1)	2.073(2)	N(2) – C(1)	1.285(4)
S(1) – C(1)	1.790(3)	N(2) – C(2)	1.415(4)
N(1) – C(1)	1.381(4)	N(1) – Pt(1) – S(1)	69.79(7)
P(1) – Pt(1) – P(2)	98.58(3)	C(1) – S(1) – Pt(1)	82.16(10)
S(1) – Pt(1) – P(1)	165.56(2)	C(1) – N(2) – Pt(1)	102.91(18)
S(1) – Pt(1) – P(2)	93.72(3)	C(8) – N(2) – Pt(1)	129.9(2)
N(2) – Pt(1) – P(2)	98.30(7)	N(1) – C(1) – S(1)	104.9(2)
N(1) – Pt(1) – P(2)	163.04(7)	N(2) – C(1) – S(1)	127.3(2)
[Pt{SC(=NC_6H_4OMe)NPy}(PPh_3)$_2$] **2b**			
Pt(1) – S(1)	2.3212(7)	N(1) – C(9)	1.446(4)
Pt(1) – P(1)	2.2777(7)	N(1) – C(1)	1.352(4)
Pt(1) – P(2)	2.2464(7)	N(2) – C(1)	1.296(4)
Pt(1) – N(1)	2.059(3)	N(2) – C(2)	1.409(4
S(1) – C(1)	1.803(3)	N(1) – Pt(1) – P(2)	163.89(13)
S(1) – Pt(1) – P(1)	165.60(5)	C(1) – S(1) – Pt(1)	82.0(2)
P(2) – Pt(1) – P(1)	96.64(5)	N(1) – C(1) – S(1)	105.0(4)
P(2) – Pt(1) – S(1)	94.49(5)	N(2) – C(1) – S(1)	129.1(5)
N(1) – Pt(1) – P(1)	98.98(13)	N(2) – C(1) – N(1)	125.8(6)
N(1) – Pt(1) – S(1)	69.47(13)	N(1) – C(1) – S(1)	69.51(13)

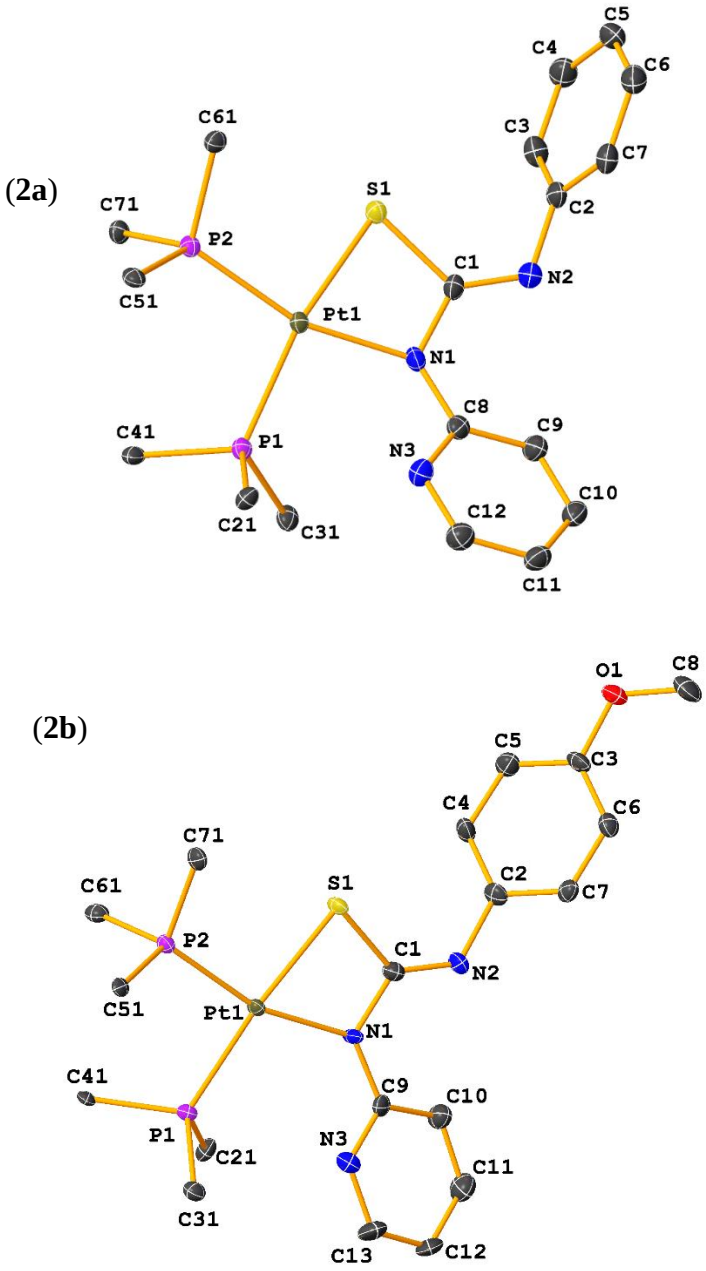

Figure 2.5: Molecular structures of pyridyl-substituted complexes [Pt{SC(=NPh)NPy}(PPh_3)$_2$] **2a** and [Pt{SC(=NC_6H_4OMe)NPy}(PPh_3)$_2$] **2b**. Thermal ellipsoids are drawn at 50% probability level and only *ipso* carbons of the PPh_3 ligand are shown for clarity.

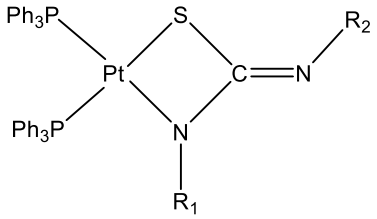

2.10 a, $R_1 = R_2 = Et$

2.10 b, $R_1 = R_2 = Ph$

2.10 c, $R_1 = Et$, $R_2 = Ph$

2.2.4 *Further investigation of isomerism in platinum complexes of pyridyl-substituted thiourea dianions*

Two methylene pyridyl-substituted complexes [Pt{SC(NPh)NCH$_2$Py}(PPh$_3$)$_2$] **2d** and [Pt{SC(NC$_6$H$_4$NO$_2$)NCH$_2$Py}(PPh$_3$)$_2$] **2e** were synthesised by substituting the pyridyl functional group in complexes **2a** and **2c** with the methylene pyridyl functional group (R^1 = CH$_2$Py). The idea was to vary the steric properties of the substituted functional groups and thus investigate its effect on isomerism. It was anticipated that the CH$_2$ spacers would increase the bulk and flexibility of the potentially coordinating pyridyl group as well as provide a spectroscopic handle to further characterise the resulting complexes by ^{1}H NMR spectroscopy. The complexes were synthesised using the appropriate thiourea ligands and *cis*-[PtCl$_2$(PPh$_3$)$_2$]. The products were isolated in reasonable yields by precipitation with water. The ESI-mass spectral analysis at low capillary exit voltage (60 V) gave single pseudo-molecular $[M+H]^+$ ions corresponding to the protonated dianion complexes (**Table 2.1**). Good microanalytical data were obtained for the complexes. DFT calculations on the complexes gave positive Gibbs free energy differences for the two complexes; 12.60 kJ mol^{-1} **2d** and 23.70 kJ mol^{-1} **2e** predicting that the proximal isomer of the complex was the most kinetically favoured in both cases.

The ^{1}H NMR spectrum of a freshly dissolved sample of **2d** in CDCl$_3$ showed the presence of a doublet at 4.40 ppm characteristic of equivalent methylene protons coupling to phosphorus. A $^4J_{(PH)}$ coupling constant of 5.6 Hz was recorded for the complex. The platinum coupling was seen as two small peaks at the foot of the doublet. The recorded $^3J_{(PtH)}$ coupling constant of 43 Hz is similar to coupling constant reported for the ethyl-substituted thiourea dianion complex [Pt{SC(=NPh)NEt}(PPh$_3$)], 44 Hz, **2.10c** [30]. The presence of the $^3J_{(PtH)}$ coupling is an indication that the methylenepyridyl functional group is attached to the nitrogen coordinated to the platinum, indicating that the kinetically stable proximal isomer of the complex was the one initially isolated from synthesis. A second spectrum recorded after 120 min. showed the presence of another doublet just downfield of the first methylene doublet at 4.80 ppm (**Figure 2.6**). The $^3J_{(HH)}$ coupling constant of 4 Hz was observed resulting from the coupling between the methylene proton and a pyridyl proton. No $^3J_{(PtH)}$ coupling was observed for this isomer, indicating

that the methylene protons for this isomer was probably at the distal position and too far away from the platinum to engage in $^{3}J_{(PtH)}$ coupling.

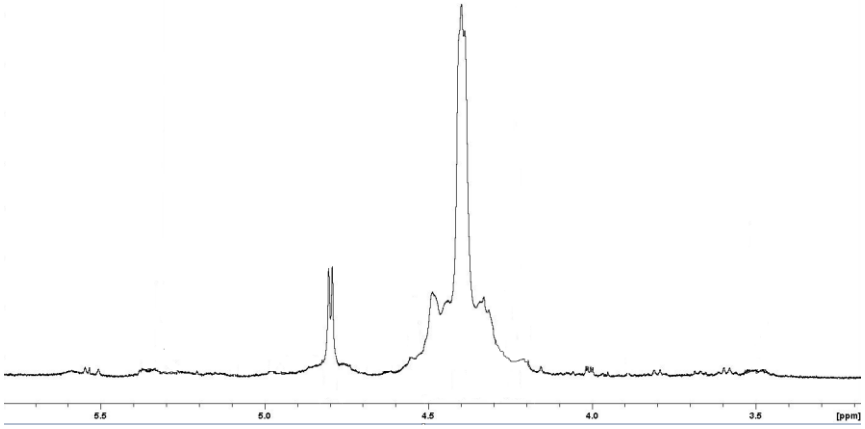

Figure 2.6: ^{1}H NMR spectrum of [Pt{SC(NPh)NCH$_2$Py}(PPh$_3$)$_2$] **2d** showing the signals for the proximal and distal isomers at 4.40 and 4.80 ppm, respectively.

Similar ^{1}H NMR data was obtained for the freshly dissolved sample of the complex **2e** in $CDCl_3$ with a doublet at 4.3 ppm corresponding to equivalent methylene protons coupling to phosphorus with $^{4}J_{(PH)}$ coupling constant of 5 Hz and two small peaks at the base of the doublet characteristics of satellite peaks for $^{3}J_{(PtH)}$ coupling with coupling constant of 45.5 Hz. The coupling constant values are similar to those reported for platinum dianion complex [Pt{SC(=NPh)NEt}(Ph$_3$P)$_2$] **2.10c**, $^{3}J_{(PtH)}$ = 47 Hz [30] and the cyano-substituted dianion complex [Pt{SC(=NCN)NMe}(PPh$_3$)$_2$] **2.2**, $^{4}J_{(PH)}$ = 4 Hz [24]. There was no evidence of isomerism in the complex **2e** even after leaving the sample in $CDCl_3$ solution for 26 days. ^{31}P{^{1}H} NMR spectrum of a freshly prepared sample of the complex **2d** showed the formation of an initial kinetically favoured proximal isomer, which slowly transformed into the distal isomeric form of the complex after 96 days of dissolution in $CDCl_3$ solution. A series of spectra showing the different stages of isomerism in the complex are presented in **Figure 2.7.** The ^{31}P{^{1}H} NMR spectrum of the *p*-nitrophenyl substituted complex **2e** showed only one set of phosphorus resonances for the complex in $CDCl_3$ solution. The complex did not show any sign of isomerisation. The ^{31}P{^{1}H} NMR chemical shifts and the corresponding ^{195}Pt coupling constants for the two complexes are presented in **Table 3.**

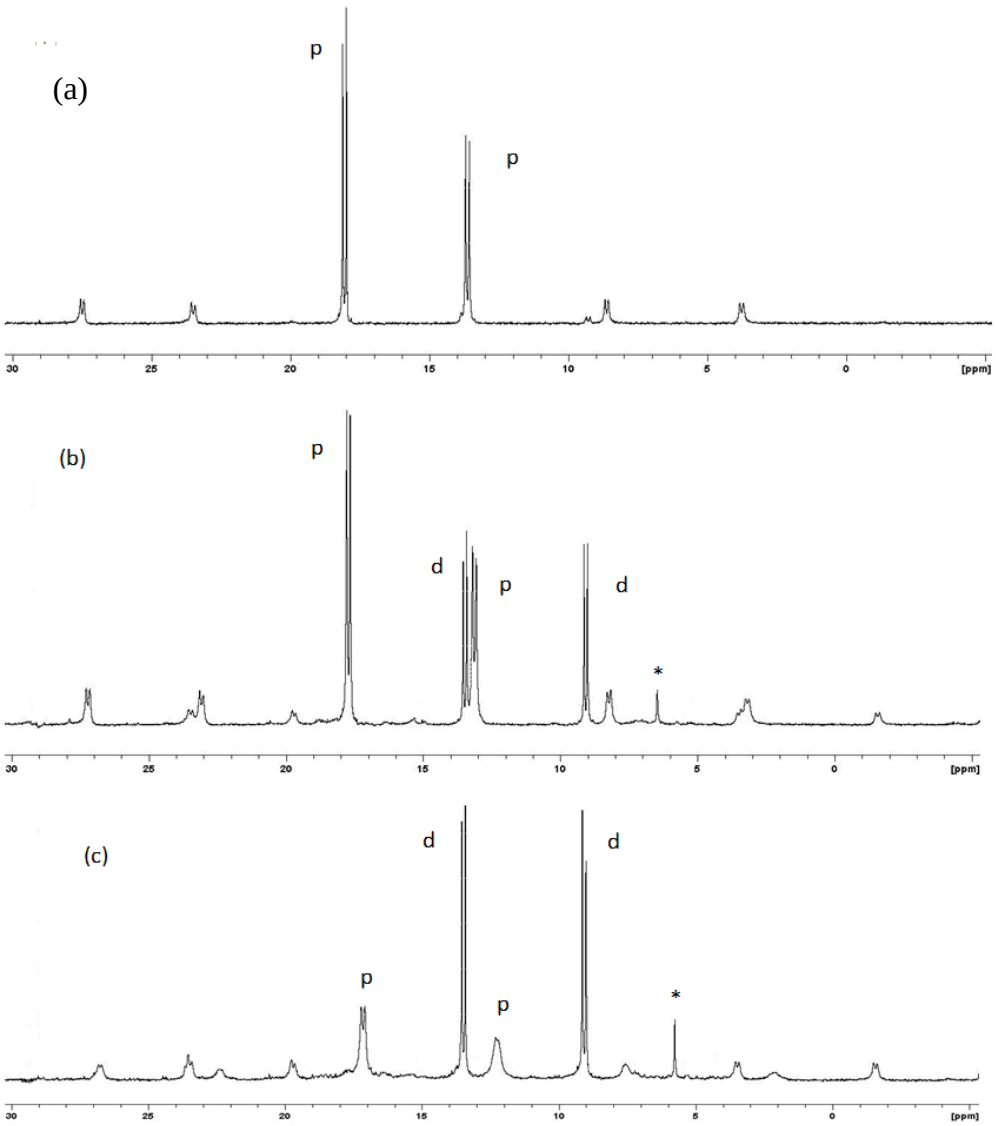

Figure 2.7: $^{31}P\{^{1}H\}$ NMR spectra of [Pt{SC(=NPh)N(CH_2)Py}(PPh_3)$_2$] **2d** showing the various stages of the isomerisation process (a) Freshly dissolved sample, (b) after 12 days in solution, (c) after 96 days in solution. p = proximal isomer, d = distal isomer * = unknown

2.2.5 *The X-ray crystallographic analysis of platinum thiourea dianion complexes 2d and 2e*

Crystals of the complexes **2d** and **2e** suitable for X-ray diffraction were isolated. The complexes crystallised in the triclinic and monoclinic crystal system with one molecule of dichloromethane and water of crystallisation respectively. The molecular structures of the complexes **2d** and **2e** in **Figures 2.8** and **2.9**, respectively, confirmed the prediction of the theoretical and spectroscopic

evidence that the proximal isomeric form of the complex was kinetically more stable. Some selected bond lengths and angles for the two complexes are presented in **Table 2.4**. There appears to be a lot of similarities in the structural and electronic features of the two methylenepyridyl substituted dianion complexes, so only significant differences between the structures will be discussed. The structures showed the expected square planar geometry characteristic of platinum dianion complexes as has been established in complexes **2a** and **2b** discussed prior. The metallacyclic ring for the two complexes are slightly puckered between the N(1)–Pt(1)–S(1) and N(1)–C(1)–S(1) least-squares planes with fold angles of 13.5 and 8.2^{o} for **2d** and **2e** respectively.

The methylenepyridyl group in **2d** defined by the C(2)–C(3)–C(4)–C(5)–C(6)–C(7) plane is nearly orthogonal to the Pt(1)–N(1)–C(1)–S(1) plane of the metallacyclic ring with a fold angle of 86.4^{o}. This is probably in a bid to avoid steric interaction with the adjacent triphenylphosphine ligand. The methylene pyridyl functional group for the *p*-nitrophenyl derivative **2e** is out of the plane of the metallacyclic ring by 57.4^{o}. These angles observed for **2d** and **2e** are higher and quite different from the values reported for related pyridyl substituted complexes **2a**; 29.8^{o} and **2b**; 27.1^{o}. The Pt(1)–P(1) bonds for the complexes are slightly longer than the Pt(1)–P(2) bonds: Pt(1)–P(1) 2.2948(7) Å; Pt(1)–P(2) 2.2516(7) Å **2d**, Pt(1)–P(1) 2.2790(14) Å; Pt(1)–P(2) 2.2511(17) Å **2e**, understandably in accordance with the trend in *trans*-influence established for related complexes **2a** and **2b.** The bond lengths and angles the complexes **2d** and **2e** are similar to the ones observed for related pyridyl substituted complexes **2a** and **2b**. The geometric parameters for these complexes are presented in **Table 2.4**.

Table 2.4: Selected bond lengths (Å) and angles (°) for methylenepyridyl substituted complexes [Pt{SC(=NPh)NCH$_2$Py}(PPh$_3$)$_2$] **2d**; [Pt{SC(=NC$_6$H$_4$NO$_2$)NCH$_2$Py}(PPh$_3$)$_2$] **2e**

[Pt{SC(=NPh)N(CH$_2$)Py}(PPh$_3$)$_2$] **2d**			
Pt(1) – S(1)	2.3252(7)	N(1) – C(1)	1.356(4)
Pt(1) – P(1)	2.2948(7)	N(1) – C(8)	1.446(3)
Pt(1) – P (2)	2.2516(7)	N(2) – C(1)	1.293(4)
Pt(1) – N(1)	2.076(2)	S(1) – C(1)	1.802(3)
P(1) – Pt(1) – S(1)	166.52(2)	C(1) – S(1) – Pt(1)	80.73(9)
P(2) – Pt(1) – S(1)	95.56(2)	C(1) – N(1) – Pt(1)	101.84(18)
P(2) – Pt(1) – P(1)	97.46(2)	C(8) – N(1) – Pt(1)	135.12(19)
N(1) – Pt(1) – S(1)	70.02(7)	N(1) – C(1) – S(1)	105.82(19)
N(1) – Pt(1) – P(1)	97.02(7)	N(2) – C(1) – S(1)	129.50(2)
N(1) – Pt(1) – P(2)	165.51(7)	N(2) – C(1) – N(1)	124.40(3)
[Pt{SC(=NC$_6$H$_4$NO$_2$)N(CH$_2$)Py}(PPh$_3$)$_2$] **2e**			
Pt(1) – S(1)	2.3308(13)	N(1) – C(1)	1.356(7)
Pt(1) – P(2)	2.2511(17)	N(1) – C(8)	1.436(8)
Pt(1) – P(1)	2.2790(14)	C(1) – N(2)	1.286(8)
Pt(1) – N(1)	2.084(4)	S(1) – C(1)	1.811(7)
P(2) – Pt(1) – S(1)	95.84(5)	N(1) – Pt(1) – P(1)	97.35(14)
P(1) – Pt(1) – S(1)	166.74(5)	C(1) – S(1) – Pt(1)	81.11(19)
P(1) – Pt(1) – P(2)	96.97(5)	N(1) – C(1) – S(1)	105.70(4)
N(1) – Pt(1) – S(1)	70.00(13)	N(2) – C(1) – S(1)	128.80(5)
N(1) – Pt(1) – P(2)	165.55(13)	N(2) – C(1) – N(1)	125.30(6)

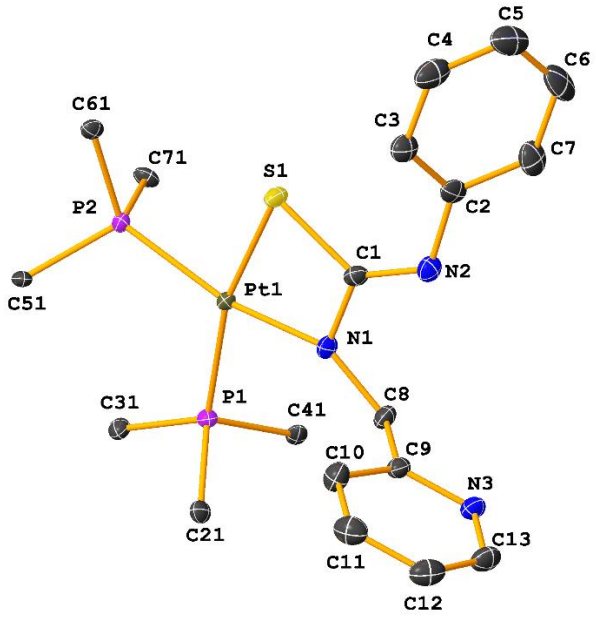

Figure 2.8: Molecular structure of methylenepyridyl substituted platinum complex [Pt{SC(=NPh)NCH$_2$Py}(PPh$_3$)$_2$] **2d**. Thermal ellipsoids are drawn at 50% probability and only *ipso* carbons of the PPh$_3$ ligand are shown for clarity.

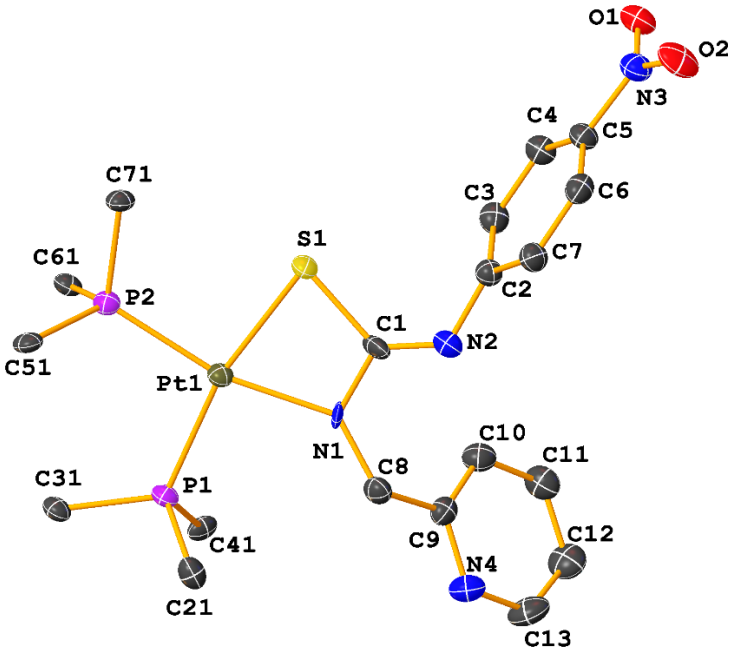

Figure 2.9: Molecular structure of methylenepyridyl substituted platinum complexes [Pt{SC(=$NC_6H_4NO_2$)NPy}(PPh_3)$_2$] **2e**. Thermal ellipsoids are drawn at 50% probability and only *ipso* carbons of the PPh_3 ligand are shown for clarity.

2.2.6 *Isomerism in ethylenepyridyl substituted thiourea dianion complexes*

The effect of the length of the pyridyl carbon chain on isomerism was further investigated by substituting the pyridyl functional group on the pyridyl thiourea complex **2a-2c** with the ethylenepyridyl functionality to afford the ethylene pyridyl substituted thiourea dianion complexes, [Pt{SC(=NPh)N$(CH_2)_2$Py}(PPh_3)$_2$] **2f**, [Pt{SC(=$NC_6H_4NO_2$)N$(CH_2)_2$Py}(PPh_3)$_2$] **2g** and [Pt{SC(=NC_6H_4OMe)N$(CH_2)_2$Py}(PPh_3)$_2$] **2h**. DFT calculations on the phenyl-substituted ethylenepyridyl complex **2f** showed a positive ΔG (GPt_{dist} – GPt_{prox}) value of +10.68 kJ mol^{-1}. This is slightly lower than the values obtained for the methylenepyridyl **2d** (+12.59 kJ mol^{-1}) and pyridyl derivative **2a** (+24.93 kJ mol^{-1}). These results indicate a decrease in the Gibbs free energy difference between isomers as the length of the alkyl chain of the pyridyl functional group in the proximal position increases as shown by the blue bars in the bar chart presented in **Figure 2.10**. This is probably because the steric bulk of the pyridyl group is further away from the rest of the complex with the ethylene spacer in the Py$(CH_2)_2$ group. The bar chart depicts an opposite trend for the *p*-methoxyphenyl (red bars) and *p*-

nitrophenyl (green bars) substituted complexes, where there are observed increases in Gibbs free energy difference with increase in the alkyl carbon spacer.

The effect of substitution of the R^2 group at the distal position of the complex with different functional groups on Gibbs free energy difference between the isomers was also plotted on the chart in **Figure 2.10**. For the pyridyl substituted derivatives, there was an observed decrease in ΔG on substitution of the phenyl group on the distal position with *p*-methoxyphenyl functional group from +24.9 kJ mol^{-1} to +17.8 kJ mol^{-1} and a further decrease on substitution with *p*-nitrophenyl functional groups to +7.04 kJ mol^{-1}. The trend indicates that an increase in the electron-withdrawing property of the functional group at the distal position results in a decrease in the Gibbs free energy difference for the complexes. The opposite trend was observed for the methylenepyridyl and ethylene pyridyl derivatives as there were a marked increase in the calculated Gibbs free energy difference as the electron-withdrawing properties of the substituents at the distal position increased from the phenyl to the *p*-methoxyphenyl and *p*-nitrophenyl substituents.

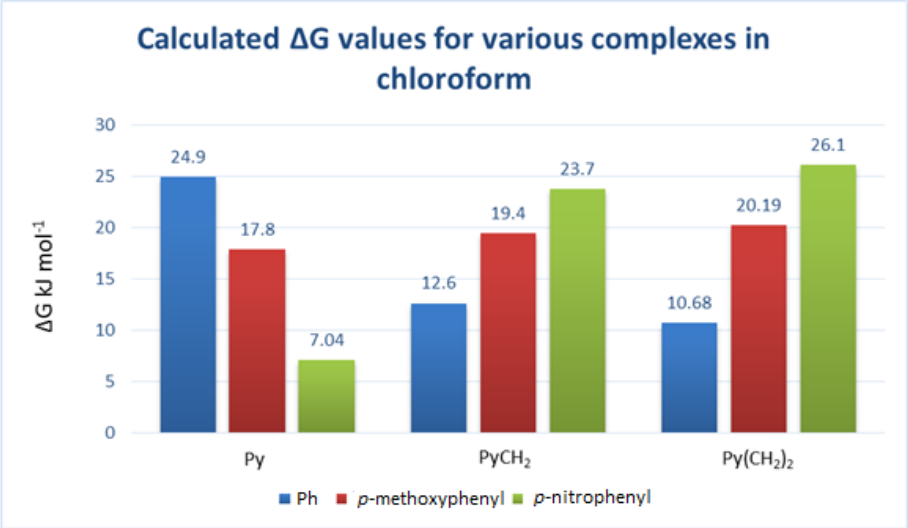

Figure 2.10: A bar chart showing the variation in calculated Gibbs free energy change for two isomers of the various complexes with changes in steric and electronic properties. Py = pyridyl.

The ^{1}H NMR spectrum of the phenyl-substituted ethylenepyridyl complex **2f** showed an overlap of peaks for the ethylene protons making the spectrum almost impossible to interpret.

The $^{31}P\{^{1}H\}$ NMR spectrum of a freshly dissolved sample of the phenyl-substituted complex **2f** showed the presence of a mixture of two isomers of equal intensity (**Figure 2.11**) with phosphorus resonances at 18.7 and 13.4 ppm and $^{1}J_{(PtP)}$ 3210 and 3483 Hz for the proximal isomer. The distal isomer showed resonances at 13.6 and 9.4 ppm and $^{1}J_{(PtP)}$ coupling constants of 3119 and 3221 Hz. The *p*-methoxyphenyl substituted complex **2g** showed a set of phosphorus resonances at 18.3 ppm and 13.6 ppm with $^{1}J_{(PtP)}$ coupling constants of 3216 Hz and 3434 Hz respectively. Another set of AB resonance peaks appeared after 2 days in solution at 14.02 and 9.41 ppm with $^{1}J_{(PtP)}$ coupling constants of 3257 and 3434 Hz. A spectrum obtained after 88 days showed that the proximal isomer had completely isomerised into the distal form of the complex (**Figure 2.12**). Similar sets of AB phosphorus resonance peaks at 18.34 and 12.84 ppm and $^{1}J_{(PtP)}$ coupling constants of 3119 and 3221 Hz were observed for the *p*-nitrophenyl substituted complex **2h** and was assigned as the proximal isomer of the complex. Another set of peaks at 13.64 and 9.26 ppm with $^{1}J_{(PtP)}$ coupling constants of 3210 and 3483 Hz respectively were observed after 4 days of isomerisation and were assigned as the distal isomer of the complex.

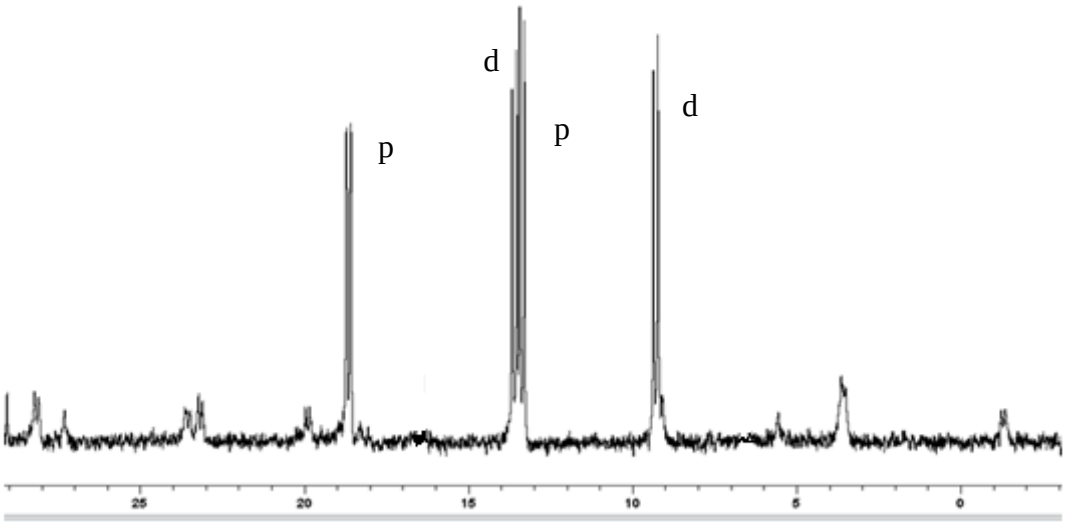

Figure 2.11: $^{31}P\{^{1}H\}$ NMR spectrum of $[Pt\{SC(NPh)N(CH_2)_2Py\}(PPh_3)_2]$ **2f** showing a mixture of proximal and distal isomers, p = proximal isomer, d = distal isomer.

The path of isomerisation for the thiourea dianion complexes discussed above did not seem to be affected by the length of the alkyl spacer on the pyridyl functional group. The isomerisation times were however observed to have decreased as the length of the alkyl spacer on the pyridyl functional group increased from the phenyl substituted pyridyl complex **2a** which took about 15 days to attain a stable mixture of three isomers to the methylene derivative (**2d**) which needed 96 days for the proximal isomer to completely convert to the distal isomeric form of the complex. Further increase in length of the alkyl spacer however showed an increase in the rate of isomerisation as it took only 3 days to for the ethylene derivative **2f** to form a stable mixture of two isomers of equal intensity in $CDCl_3$ solution. This is probably due to the lengthening of the alkyl chain of the pyridyl functionality which took the pyridyl group further away from the immediate vicinity of the adjacent triphenylphosphine ligand, thus reducing steric interaction. Similar trends were observed for *p*-methoxyphenyl and *p*-nitrophenyl substituted derivatives.

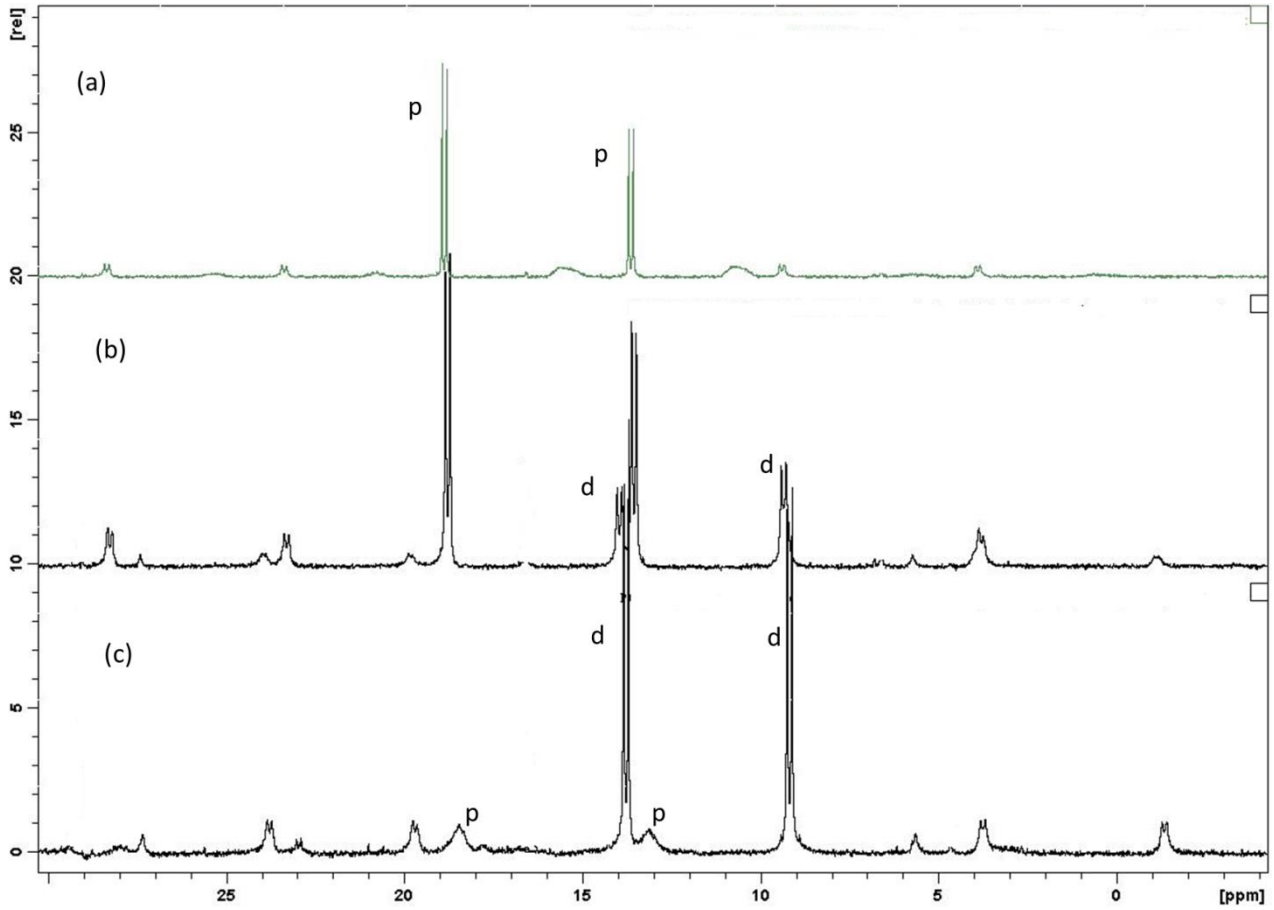

Figure 2.12: $^{31}P\{^{1}H\}$ NMR spectra of [Pt{SC(=NC$_6$H$_4$OMe)N(CH$_2$)$_2$Py}(PPh$_3$)$_2$] **2g** showing the different stages of the isomerisation process, p = proximal isomer, d = distal isomer.

2.2.1 *The X-ray crystallographic analysis of platinum thiourea dianion complexes 2f-2h*

Crystals of the three complexes **2f-2h** suitable for X-ray crystallography were obtained after about 7 days of dissolution by vapour diffusion of diethyl ether into a saturated dichloromethane solution of the complexes and used for X-ray crystallographic analysis. The complexes crystallised in the monoclinic crystal system with one molecule of dichloromethane solvent of crystallisation in the structure of **2h**. Molecular structures of the complexes presented in **Figures 2.13-2.15** showed that all the three complexes **2f-2h** showed similar NP_2S square planar geometry as the pyridyl substituted derivative **2a** discussed earlier in the chapter. The ethylene pyridyl functional group in the three complexes are bound to nitrogen proximal to the metallacyclic ring as predicted by theoretical Gibbs free energy calculations and experimental NMR analysis.

Due to the obvious similarities in the structural and geometric parameters (**Table 2.5-2.6**) of the complexes only the structure of the *p*-methoxyphenyl substituted complex **2g** will be discussed as a representative complex and any significant differences with the structures of **2f** and **2h** will be mentioned. The four-membered metallacyclic ring in the complex **2g** is slightly puckered with a fold angle of 13.61^o between the least square planes defined by N(1)–Pt(1)–S(1) and N(1)–C(1)–S(1). This is significantly higher than the fold angles recorded for the pyridyl substituted derivative of this complex **2b**, 3.12^o. The thiourea core is of the complex is essentially planar with the highest deviation from the N(1)–S(1)–C(1)–N(2) least-square plane equal to 0.007 Å [N(2)]. The dihedral angle between pyridyl group at the proximal position and plane of the metallacyclic ring is 33.46(11)^o. This is the highest in the ethylenepyridyl series (**2f** = 9.20(14)^o, **2h** = 5.113(13)^o), but significantly lower than the dihedral angles in the methylene substituted complex [Pt{SC(=NPh)N(CH_2)Py}(PPh_3)$_2$] **2d**, 86.40(8)^o and a previously reported dianion complex [Pt{SC(=NPh)NPh}(PPh_3)$_2$] (**2.10b**), 76.20(13)^o. The *p*-methoxyphenyl group at the distal position is twisted out of the plane of the metallacycle by 54.24^o. This is similar to equivalent angles in **2f**; 57.48(8)^o, **2h**; 64.28(18), the pyridyl derivative of the compound **2b**; 57.6^o and the previously reported asymmetrically substituted complex [Pt{SC(=NPh)NEt}(PPh_3)$_2$] (50.47(11)^o)[30]. The overall structural features of the *p*-methoxyphenyl substituted complex **2g** bear a close resemblance to the previously reported phenyl

disubstituted thiourea dianion complex [Pt{SC(=NPh)NPh}(PPh_3)$_2$] (**2.10b**), However the thiourea S(1)–C(1), C(1)–N(1) and C(1)–N(2) bond lengths in (**2.10b**) 1.782(5) Å, 1.348(7) Å and 1.277(6) Å are slightly shorter than those in (**2g**) 1.795(6) Å, 1.377(7) Å and 1.281(8) Å.

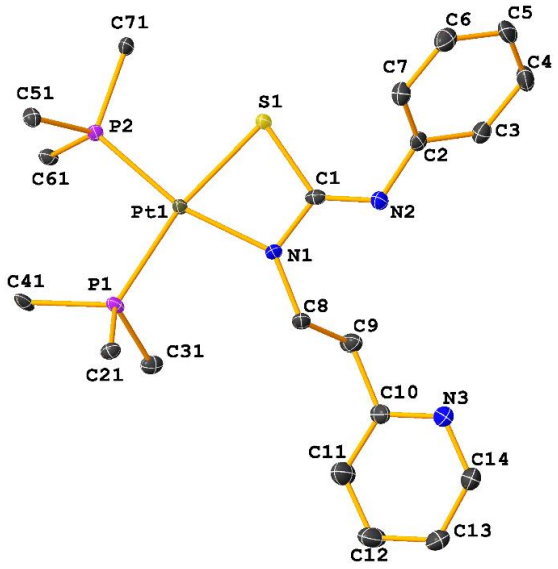

Figure 2.13: Molecular structure of the phenyl substituted ethylenepyridyl complex [PtSC{(=NPh)N(CH_2)$_2$Py}(PPh_3)$_2$] **2f**. Ellipsoids are drawn at 50% probability and only *ipso* carbons of the PPh_3 ligand are shown for clarity.

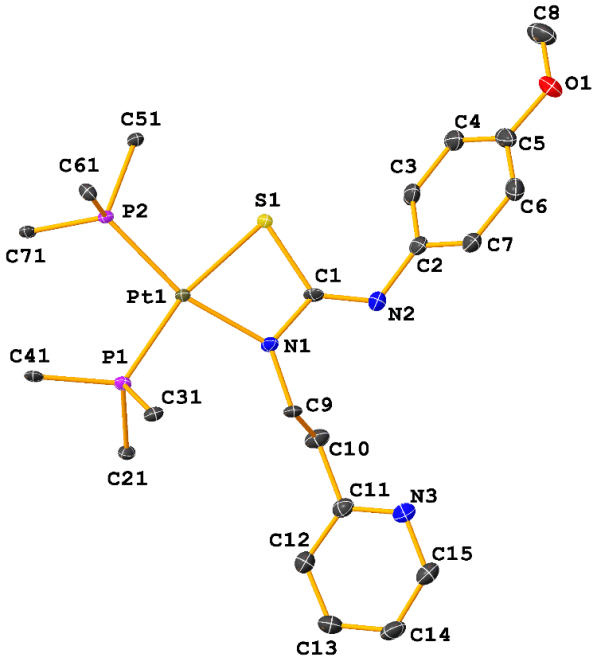

Figure 2.14: Molecular structure of the *p*-methoxyphenyl-substituted ethylenepyridyl complex [Pt{SC(=NC_6H_4OMe)N(CH_2)$_2$Py}(PPh_3)$_2$] **2g**. Thermal ellipsoids are drawn at 50% probability. Only *ipso* carbons of the PPh_3 ligand are shown for clarity.

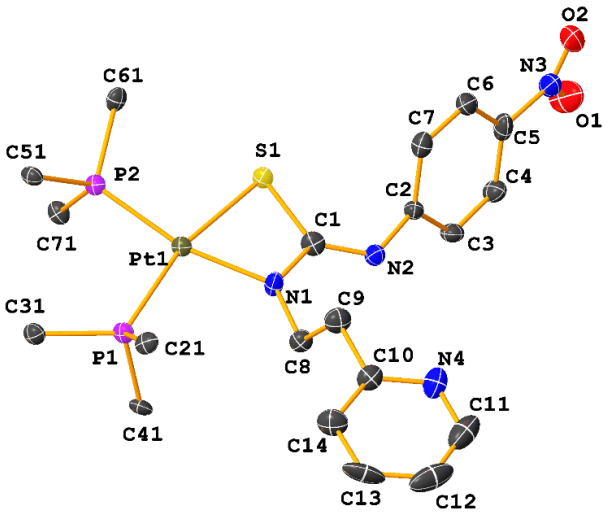

Figure 2.15: Molecular structure of the *p*-nitrophenyl substituted ethylenepyridyl complex [PtSC{=NC$_6$H$_4$(NO$_2$)N(CH$_2$)$_2$Py}(PPh$_3$)$_2$] **2h**. Only *ipso* carbons of the PPh$_3$ ligand are shown for clarity. Ellipsoids are at 50% probability.

Table 2.5: Selected bond lengths (Å) and angles (°) for ethylenepyridyl substituted complexes [Pt{SC(=NPh)N(CH$_2$)$_2$Py}(PPh$_3$)$_2$] **2f**; [Pt{SC(=NC$_6$H$_4$OMe)N(CH$_2$)$_2$Py}(PPh$_3$)$_2$] **2g**

[Pt{SC(=NPh)N(CH$_2$)$_2$Py}(PPh$_3$)$_2$] **2f**			
Pt(1) – S(1)	2.3337(9)	N(1) – C(1)	1.354(4)
Pt(1) – P(1)	2.2881(8)	N(1) – C(8)	1.455(4)
Pt(1) – P(2)	2.2495(8)	N(2) – C(1)	1.287(4)
Pt(1) – N(1)	2.066(3)	S(1) – C(1)	1.808(3)
C(2) – N(2)	1.401(3)	N(3) – C(10)	1.342(5)
P(1) – Pt(1) – S(1)	167.65(2)	C(1) – S(1) – Pt(1)	80.75(8)
P(2) – Pt(1) – S(1)	95.27(2)	C(1) – N(1) – Pt(1)	103.09(15)
P(2) – Pt(1) – P(1)	96.83(2)	C(8) – N(1) – Pt(1)	135.12(19)
N(1) – Pt(1) – S(1)	70.16(6)	N(1) – C(1) – S(1)	105.90(19)
N(1) – Pt(1) – P(1)	97.89(6)	N(2) – C(1) – S(1)	128.60(19)
N(1) – Pt(1) – P(2)	165.06(6)	N(2) – C(1) – N(1)	125.5(2)
[Pt{SC(=NC$_6$H$_4$OMe)N(CH$_2$)$_2$Py}(PPh$_3$)$_2$] **2g**			
Pt(1) – S(1)	2.3444(13)	N(1) – C(1)	1.377(7)
Pt(1) – P(2)	2.263(15)	N(1) – C(9)	1.388(8)
Pt(1) – P(1)	2.3093(14)	C(1) – N(2)	1.281(8)
Pt(1) – N(1)	2.077(5)	S(1) – C(1)	1.795(6)
P(2) – Pt(1) – S(1)	94.49(5)	N(1) – Pt(1) – P(1)	98.98(13)
P(1) – Pt(1) – S(1)	165.60(5)	C(1) – S(1) – Pt(1)	82.0(2)
P(1) – Pt(1) – P(2)	96.64(5)	N(1) – C(1) – S(1)	105.0(4)
N(1) – Pt(1) – S(1)	69.47(13)	N(2) – C(1) – S(1)	129.1(5)
N(1) – Pt(1) – P(2)	163.89(13)	N(2) – C(1) – N(1)	125.8(6)

Table 2.6: Selected bond lengths (Å) and angles (°) for ethylenepyridyl substituted complex [Pt{SC(=$NC_6H_4NO_2$)N(CH_2)$_2$Py}(PPh_3)$_2$] **2h**

[Pt{SC(=$NC_6H_4NO_2$)N(CH_2)$_2$Py}(PPh_3)$_2$] **2h**			
Pt(1) – S(1)	2.3419(13)	N(1) – C(1)	1.340(7)
Pt(1) – P(1)	2.2891(13)	N(1) – C(8)	1.448(7)
Pt(1) – P(2)	2.2502(13)	N(2) – C(1)	1.303(7)
Pt(1) – N(1)	2.073(4)	S(1) – C(1)	1.797(6)
C(2) – N(2)	1.385(7)	N(3) – C(10)	1.346 (7)
P(1) – Pt(1) – S(1)	165.36(14)	C(1) – S(1) – Pt(1)	80.08(19)
P(2) – Pt(1) – S(1)	96.52(5)	C(1) – N(1) – Pt(1)	102.2(3)
P(2) – Pt(1) – P(1)	97.42(5)	C(8) – N(1) – Pt(1)	137.5(4)
N(1) – Pt(1) – S(1)	69.91(13)	N(1) – C(1) – S(1)	107.2(4)
N(1) – Pt(1) – P(1)	96.22(13)	N(2) – C(1) – S(1)	128.5(4)
N(1) – Pt(1) – P(2)	166.36(14)	N(2) – C(1) – N(1)	125.93(4)

2.2.2 *Isomerism in pyridyl substituted thiourea monoanion complex 2i*

The thiourea monoanion complex was synthesised from equimolar quantities of *cis*-[$PtCl_2(PPh_3)_2$] and the thiourea ligand $PyCH_2NHC(S)NHPh$ in refluxing methanol and excess triethylamine. Addition of excess solid $NaBF_4$ followed by water afforded a bright yellow semi-crystalline product of the complex **2i** in high purity and yield. Satisfactory microanalytical data were obtained for the complex. The ESI-MS spectrum for the complex at a capillary exit voltage of 60 V gave a single pseudo molecular $[M]^+$ ion peak with *m/z* 961.22 for the monoanion complex $[Pt\{SC(NHCH_2Py)NPh\}(PPh_3)_2]^+$. The experimental isotope pattern for the complex corresponds to its calculated isotope pattern. The theoretical Gibbs free energy calculations for this complex gave a negative difference in Gibbs free energy ΔG ($GPt_{dist} - GPt_{prox}$) between the two possible isomers; the proximal isomer (when the methylene pyridyl functional group is attached to the platinum adjacent nitrogen) and the distal isomer (when the methylenepyridyl group is attached to the nitrogen remote to the platinum). The result (-6.8 $kJmol^{-1}$) suggested the initial formation of a kinetically stable distal isomer for this complex. This is probably because of the absence of steric hindrance between the methylenepyridyl functional group and the triphenylphosphine in the distal isomer of the complex (**Figure**

2.16a) as against the proximal isomer where PPh_3 tends to hinder the free rotation of the methylenepyridyl functional group. (**Figure 2.16b**).

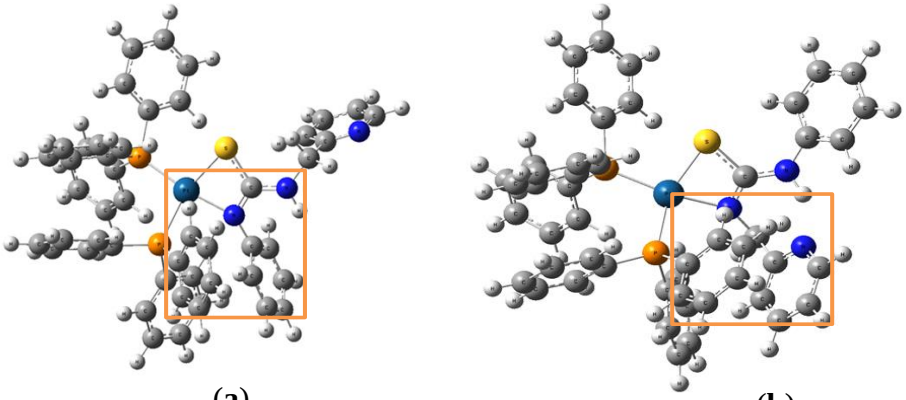

(a) **(b)**

Figure 2.16: Optimised structures of the complex **2i** (**a**) distal isomer showing the free rotation of the $PyCH_2$ group (**b**) proximal isomeric configuration showing possible hindrance of the $PyCH_2$ group from free rotation by adjacent PPh_3.

The ^1H NMR spectrum (**Figure 2.17**) of a freshly prepared sample of the complex in $CDCl_3$ showed a singlet at $\delta = 5.3$ ppm for the NH proton and another singlet at $\delta = 4.4$ ppm for two methylene protons. The absence of satellite peaks for Pt-H coupling suggests that the isomer was the distal isomeric form of the complex. Another spectrum collected after 8 days showed the presence of another peak at $\delta = 3.9$ ppm. The $^3J_{(PtH)}$ coupling satellite peaks for this isomer was too small and obscured in the baseline. The acidic NH protons for the distal and proximal isomers were observed at $\delta = 3.66$ ppm and $\delta = 5.32$ ppm respectively. The position of the NH protons peaks were confirmed by addition of D_2O to the NMR solution resulting in the disappearance of the NH proton peaks from the NMR spectrum

The $^{31}P\{^1H\}$ NMR spectrum of a freshly prepared sample of the thiourea monoanion complex showed initial AB resonance peaks corresponding to two inequivalent phosphorus environments at 13.3 and 8.9 ppm respectively (**Figure 2.18**). $^1J_{(PtP)}$ coupling constants for the peaks were determined as 3247 and 3456 Hz respectively. Another spectrum collected after 8 days of dissolution showed the presence of the second set of peaks downfield of the first peaks with $\delta = 15.9$ and 10.3 ppm. The $^1J_{(PtP)}$ coupling constants of 3190 and 3420 Hz respectively were recorded for the isomer. Using evidence from the theoretical free energy calculations and experimental NMR determinations, the initial and major isomers

were designated as the kinetically favoured distal isomers of the complex, while the second and minor isomers were designated as the thermodynamically favoured proximal isomers. The $^{1}J_{(PtP)}$ coupling constant values for this complex were slightly higher than those observed for the dianion analogue of this complex (**2e**) with coupling constants 3055 and 3194 Hz for the proximal isomer, while 3238 and 3448 Hz were recorded as the distal isomer of the complex. Similar coupling constant values were reported for related di-substituted phenyl thiourea monoanion complex [Pt{SC(NHPh)NPh}$(PPh_3)_2$]BPh_4 (3198 and 3490 Hz) and its diethyl analogue [Pt{SC(NHEt)NEt}$(PPh_3)_2$]BPh_4 (3233 and 3352 Hz) [33].

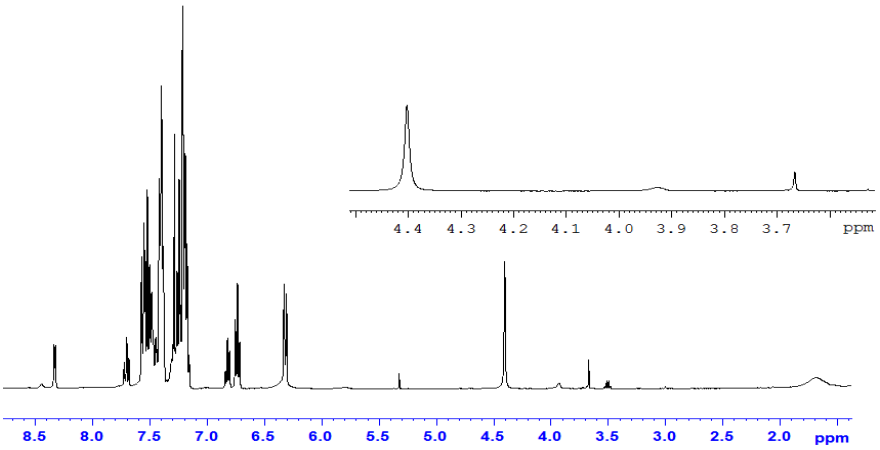

Figure 2.17: ^{1}H NMR spectrum of a freshly dissolved sample of the complex [Pt{SC(=NHCH$_2$Py)NPh)}$(PPh_3)_2$] **2i** showing the absence of Pt – H coupling (insert).

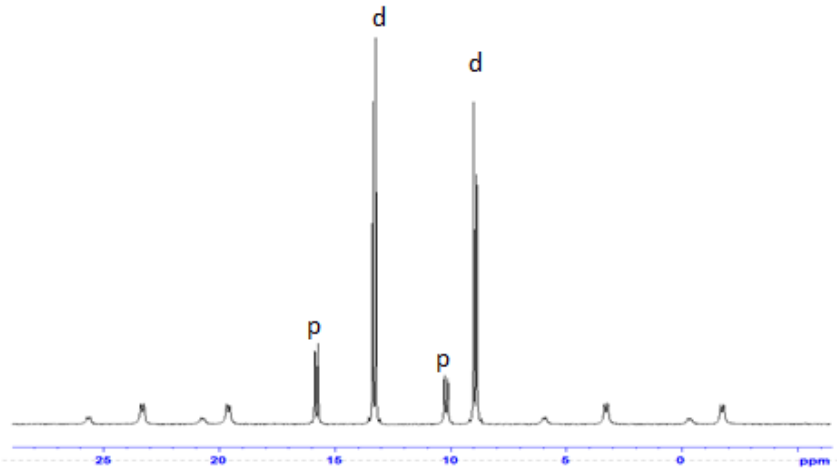

Figure 2.18: $^{31}P\{^{1}H\}$ NMR spectrum of [Pt{SC(=NHCH$_2$Py)NPh}$(PPh_3)_2$] **2i** showing the isomerisation process, from the distal to the proximal form p = proximal isomer, d = distal isomer.

X-ray crystallographic analysis of bright yellow crystals of the monoanionic complex obtained by vapour diffusion of diethyl ether into a dichloromethane solution of the complex for about 10 days confirmed the distal isomeric configuration of the complex. The molecular structure of the complex, shown in **Figure 2.19**, differs from the other complexes **2a - 2h**, in that the complex is the salt $[Pt\{SC(=NHCH_2Py)NPh)\}(PPh_3)_2]BF_4$ where the thiourea ligand is bonded to the platinum atom through the *N,S* donor atoms and two phosphorus atoms from the PPh_3 ligand occupy the other end of the almost square planar geometry. Apart from that, there is a juxtaposition of the N-bound substituents, such that metallacyclic N(1) atom bears the phenyl group and the imine -N(2) now bears the protonated methylene pyridyl functionality. The metallacyclic ring is essentially planar with two different Pt–P bond lengths. The Pt(1)–P(1) bond (2.2895(5) Å) is expectedly longer than the Pt(1)–P(2) bond (2.2429(5) Å), due to the greater *trans* influence of the sulfur donor atom relative to the nitrogen donor atom consistent with the $^{31}P\{^1H\}$ NMR data. A similar trend was reported for the thiourea dianion analogue of this complex $[Pt\{SC(=NPh)NCH_2Py\}(PPh_3)_2]$ **2d** with slightly shorter bond lengths; Pt(1)–P(1) 2.2948(7) Å and Pt(1)–P(2) 2.2516(7) Å. A number of other thiourea dianion and monoanion complexes $[Pt\{SC(=NPh)NCN\}(PPh_3)_2]$[24], $[Pt\{SC(=NPh)NPh\}(PPh_3)_2]$[34], $[Pt\{SC(NHPh)NPh\}(PPh_3)_2]BPh_4$ and $[Pt\{SC(NHMe)NMe\}(PPh_3)_2]BPh_4$[33], exhibiting a similar trend has been reported in the literature.

The substituted phenyl and methylenepyridyl groups are almost orthogonal to the plane of the metallacyclic ring by 80.03^o and 79.74^o respectively. The coordinated thiourea ligand defined by S(1)–N(1)–C(1)–N(2) is planar to within 0.09 Å. The S(1)–C(1) and C(1)–N(2) bond distances are suggestive of electron delocalisation in the thiourea ligand. The S(1)–C(1) and C(1)–N(1) bond distances of 1.759(2) and 1.319(3) Å in **2i** are shortened when compared with the values recorded for the neutral thiourea dianion complexes **2d [**1.802(3) Å, 1.340(7) Å] and **2e** [1.811(7) Å, 1.340(7) Å]. The exocyclic C(1)–N(2) bonds reveal an opposite trend, where the bond in the thiourea monoanion complex **2i** 1.327(3) Å show a considerable increase in length compared to corresponding bonds in related thiourea dianion complexes [**2d** 1.293(4) Å and **2e** 1.286(8) Å]. The above parameters suggest partial double bond characteristics of C(1)–S(1) and C(1)–N(2) bonds of the monoanion complex **2i**. Similar electron delocalisation properties have

been reported for other complexes containing the thiourea monoanion ligand coordinating *via* the *N,S* donor atoms[33,35,36].

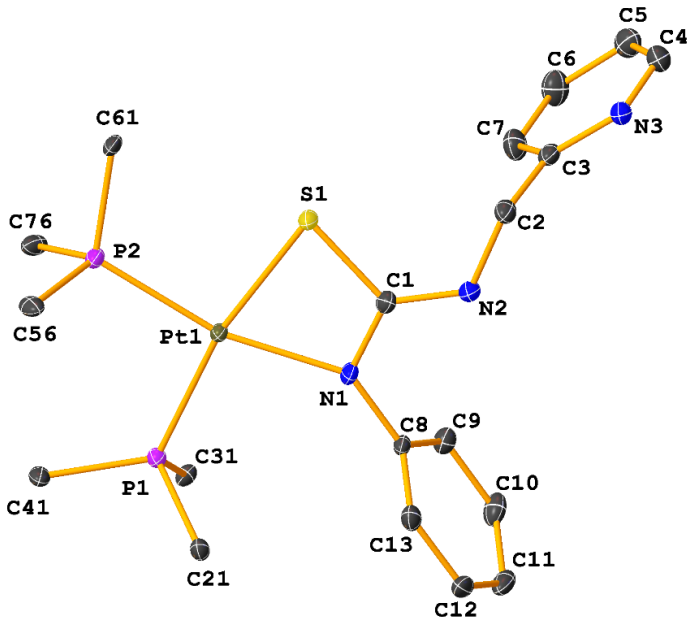

Figure 2.19: Molecular structure of [Pt{SC(=NHCH$_2$Py)NPh}(PPh$_3$)$_2$]BF$_4$ **2i** showing the methylenepyridyl functional group in the distal position. Ellipsoids were drawn at 50% probability. BF_4^- anion was omitted and only *ipso* carbons of the PPh$_3$ ligand are shown for clarity.

Table 2.7: Selected bond lengths and angles for **2i** with estimated standard deviations in parentheses**.**

[Pt{SC(=NHCH$_2$Py)NPh))}(PPh$_3$)$_2$]BF$_4$ **2i**			
Pt(1) – S(1)	2.3439(5)	N(1) – C(8)	1.436(3)
Pt(1) – P(2)	2.2429(5)	N(1) – C(1)	1.319(3)
Pt(1) – P(1)	2.2895(5)	N(2) – C(1)	1.327(3)
Pt(1) – N(1)	2.1087(17)	C(2) – N(2)	1.455(3)
S(1) – C(1)	1.759(2)	N(1) – Pt(1) – P(1)	99.39(5)
P(2) – Pt(1) – S(1)	95.168(18)	C(1) – S(1) – Pt(1)	80.02(7)
P(1) – Pt(1) – S(1)	168.767(18)	C(8) – N(1) – Pt(1)	139.22(13)
P(1) – Pt(1) – P(2)	96.064(18)	C(1) – N(1) – Pt(1)	100.07(13)
N(1) – Pt(1) – S(1)	69.38(5)	C(1) – N(1) – C(8)	120.07(17)
N(1) – Pt(1) – P(2)	164.31(5)		

The structural similarities of the crystal structures of the complexes reported in this thesis, especially in terms of the square planar geometry are highlighted in the structure overlay diagram in **Figure 2.20**. The structure shows an overlaid metallacyclic ring with relatively small differences in the structural characteristics of the various substituents.

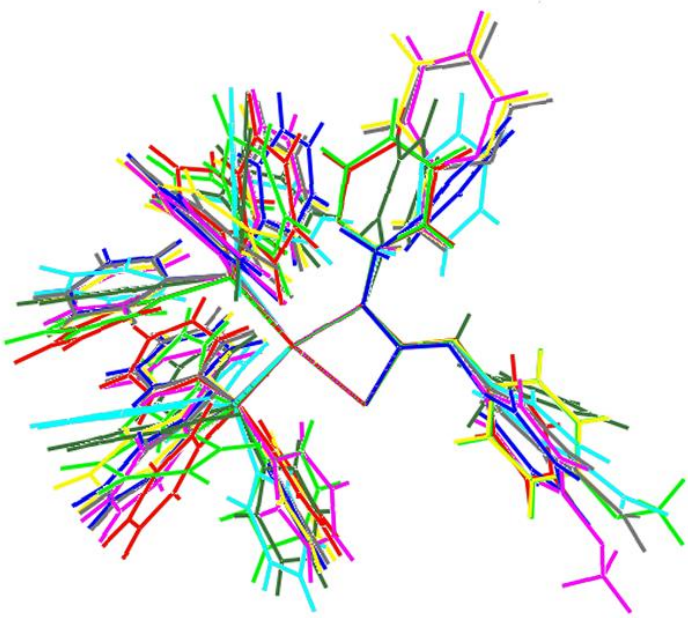

Figure 2.20: Structural overlay of thiourea dianion and monoanion complexes highlighting the similarities and the differences in the structure of the complexes.

2.3 Conclusions

Thiourea dianion and monoanion complexes of the type $[Pt\{SC(=NR_1)NR_2\}(PPh_3)_2]$ and $[Pt\{SC(=NPh)NH(CH_2)Py\}(PPh_3)_2]^+$ were successfully synthesised and characterised by ESI-MS, NMR and single-crystal X-ray crystallography. Theoretical Gibbs free energy calculations and NMR investigations revealed the initial formation of a kinetically stable proximal isomer which isomerised into the thermodynamically favoured distal isomer or a stable mixture of both at equilibrium for the thiourea dianion complexes. The monoanion complex, on the other hand, showed an initial distal isomeric configuration which subsequently isomerised into a stable mixture of the proximal and distal isomer. The pyridyl-substituted thiourea dianion complexes $[Pt\{SC(=NPy)NPh\}(PPh_3)_2]$ (**2a**) and $[Pt\{SC(=NC_6H_4OMe)NPy\}(PPh_3)_2]$ (**2b**) showed evidence of *E/Z* isomerisation when the pyridyl functional group was attached to the nitrogen

remote to the platinum metal centre. This is the first report of the possibility of *E/Z* isomerism in platinum complexes of thiourea dianions. The isomerisation process was found to be a function of the difference in Gibbs free energy between the possible isomers of the complexes, while the degree of isomerisation was dependent on the nature and size of the functional groups attached to the nitrogen at the proximal and distal positions of the complexes. X-ray crystallographic analysis confirmed the neutral nature of the dianionic complexes **2a-2b**; **2d-2h** with the pyridyl functional group coordinated to the nitrogen at the proximal position. The monoanion complex **2i** showed a juxtaposition of the pyridyl functionality to the distal position. The robustness of the various substituents did not result in any obvious structural advantages for the complexes. The only significant difference in the complexes is the variability in the dihedral angles between the chelate and pyridyl rings which are separated by as much as an ethylene spacer in some of the complexes.

2.4 Experimental

2.4.1 *General experimental methods*

2-Pyridylamine, 2-methylene(pyridylamine), 2-ethylene(pyridylamine), phenyl isothiocyanate, *p*-nitrophenyl isothiocyanate, *p*-methoxyphenyl isothiocyanate, triphenylphosphine (PPh_3), sodium tetrafluoroborate and triethylamine were purchased from Sigma Aldrich Chemical Company and used without further purification. Dichloromethane, diethyl ether and methanol ethanol, acetonitrile, and petroleum spirits were supplied as drum solvents by Ajax Chemical Company Limited. $PtCl_2COD$ (COD = cyclo-octadiene) was taken from a laboratory sample [30]. Elemental analyses of all compounds were performed by the Campbell Microanalytical Laboratory, Department of Chemistry, University of Otago. ESI-mass spectral data were recorded in positive ion mode on a Bruker Microtof instrument. Samples were prepared by dissolving the solid in a few drops of dichloromethane and diluting with methanol. Infrared spectra were recorded as KBr discs on a Perkin-Elmer Spectrum 100 Fourier Transform Infrared Spectrometer with a wavenumber range of 4000 – 400 cm^{-1}, $^{31}P\{^1H\}$ and ^1H NMR spectra were recorded on a Bruker Avance (III) 400 MHz instrument in $CDCl_3$ solution (unless otherwise stated) at 300 K referenced to external 85% H_3PO_4 and TMS respectively. Coupling constants (J) are in Hertz. Melting points were recorded on a Reichert–

Jung Thermovar instrument as solid samples on glass slides. Detailed explanation of methods are presented in the appendix

2.4.2 *Preparation of cis-[$PtCl_2(PPh_3)_2$] precursor complex*

$PtCl_2COD$ (1.00 g) was dissolved in CH_2Cl_2 (20 mL) in a 100 mL round-bottomed flask. While stirring (1.40 g, 2.00 mole equivalent) PPh_3 solid, was added and stirred for 5 minutes, then petroleum spirit (50 mL) was added to precipitate the product. The product was filtered using a number 3 sintered glass frit, washed with petroleum spirit (2 x 10 mL) and dried overnight in a vacuum. Yield: 2.55 g, 90%. $^{31}P\{^1H\}$ NMR: 14.43 ppm, $^1J_{(PtP)}$; 3673 Hz.

2.4.3 *Computational chemistry calculations*

2.4.3.1 Geometry Optimisation and harmonic frequency calculations

Density functional theory (DFT) calculations were carried out using Gaussian 2009 [37] on the University of Waikato's high-performance computer. Initial input geometries were adapted from the crystal structure of [Pt{SC(=NPh)NPy}$(PPh_3)_2$] (Py = 2-pyridyl). The pyridyl group was subsequently replaced with 2-methylene pyridyl ($PyCH_2$) and 2-ethylene pyridyl ($Py(CH_2)_2$) in the proximal and distal positions. The phenyl group in the thiourea was later replaced with *p*-nitrophenyl and *p*-methoxyphenyl groups in the second and third set of calculations in both the proximal and distal positions. All DFT calculations were completed with the MO6-2X density function using 6311+G(2d,2p) basis set for all main group elements and the LANL2DZ basis set and effective core potential (ECP) for platinum. This level of theory was found to have the highest congruency with the bond lengths and angles of the [PtSC(=NPh)NPy$(PPh_3)_2$] crystal structure. Geometry optimisation and harmonic frequency calculations were run with the default criteria. The geometries of the complexes were also optimised in the presence of an implicit solvent using the IEFPCM method. The effect of different implicit solvent environment on the Gibbs free energy of the different isomers were investigated. The solvent optimised geometries were then used to calculate the NMR chemical shifts with the GIAO method also in the presence of implicit solvent. The reference NMR shifts for TMS and H_3PO_4 were also obtained using the MO6-2X/ at the 6311+G(2d,2p) level of theory with GIAO method in the presence of an implicit

solvent. The effect of different functionals on the Gibbs free energy of the isomers was also investigated.

2.4.4 *Synthesis of thiourea ligands*

Thiourea ligands (**1a-g**) with the general formula $R^1NHC(S)NHR^2$ were prepared in high yields by a modified literature method [10,22]. Equimolar quantities of phenyl isothiocyanate, *p*-nitrophenyl isothiocyanate or *p*-methoxyphenyl isothiocyanate and the appropriate primary amine were refluxed in diethyl ether for 2 hours and cooled to get a suspension of the semi-crystalline product. The products were washed with diethyl ether and recrystallised from ethyl acetate. These compounds have been synthesised and characterised previously [9,10,21-23]. Valdes-Martinez and co-workers reported the X-ray, NMR, IR and U.V data for the phenyl, *p*-methoxyphenyl and *p*-nitrophenyl derivatives of ethylenepyridyl[22] and methylenepyridyl[23]substituted thioureas. The NMR and IR spectral data for the pyridyl thiourea derivatives were also reported[10,21]. The melting points and ESI–mass spectral data for this group of compounds has been reported for the first time here.

(**1a**). 1-phenyl-3-(pyridin-2-yl)thiourea (PyNHC(S)NHPh) Synthesised from a mixture of phenylisothiocyanate (3 mL, 25 mmol) and 2-pyridylamine (2.353 g, 25 mmol) in diethyl ether (25 mL). A colourless precipitate was obtained and recrystallised from ethyl acetate to give white crystalline solid. Yield: 3.96 g, 76 %. M.p: 162-164ºC, ESI-MS: calculated *m/z* = 230.06 experimental *m/z* = 230.08 $[M+H]^+$.

(**1b**). 1-(4-methoxyphenyl)-3-(2-(pyridin-2-yl))thiourea **(**$PyNHC(S)NHC_6H_4OMe$) Synthesised using the same method as in (**1a**) from a mixture of *p*-methoxyphenyl isothiocyanate ($MeOC_6H_4NCS$) (1.38 mL, 10 mmol) and 2-pyridylamine (0.98 g, 10 mmol) in diethyl ether (20 mL) and recrystallised from ethyl acetate to give bright cream coloured crystals. Yield: 1.98 g, 86 %. M.p: 188-190ºC. ESI-MS: calculated *m/z* = 282.08, experimental *m/z* = 282.08; $[M+Na]^+$.

(**1c**). 1-(4-nitrophenyl)-3-(pyridin-2-yl)thiourea ($PyNHC(S)NHC_6H_4NO_2$) Synthesised from 2-pyridylamine (0.94 g, 10 mmol) and *p*-nitrophenyl isothiocyanate ($NO_2C_6H_4NCS$) (1.80 g, 10 mmol) in diethyl ether (20 mL) resulting in a deep yellow precipitate which was recrystallised from ethyl acetate to give

bright yellow crystals. Yield: 2.45 g, 89 %. M.p: 165-170^{o}. ESI-MS: calculated *m/z* = 297.05, experimental *m/z* = 297.06 $[M+Na]^{+}$.

(**1d**). 1-phenyl-3-(pyridin-2-ylmethyl)thiourea ($Py(CH_2)NHC(S)NHPh$) Synthesised from phenylisothiocyanate (2.6 mL, 25 mmol) and 2-methylene(pyridylamine) (2.556 mL, 25 mmol) using the same method as for (**1a**) and recrystallised from ethyl acetate to give off white crystals. Yield: 4.21 g, 91 %. M.p: 100-102^{o}C, ESI-MS: calculated *m/z* = 266.08, experimental *m/z* = 266.09 $[M+Na]^{+}$.

(1e). 1-(4-nitrophenyl)-3-(pyridin-2-yl)methyl)thiourea ($Py(CH_2)NHC(S)NHC_6H_4NO2$) Synthesised from *p*-nitrophenylisothiocyanate (1.80 g, 10 mmol) ($NO_2C_6H_5NCS$) and 2-methylene(pyridyl amine) (1.022 mL, 10 mmol) in diethyl ether (20 mL) and recrystallised from ethyl acetate to give pale yellow crystals. Yield: 2.51 g, 86 %. M.p: 168-172^{o}C, ESI-MS: calculated *m/z* = 289.07, experimental *m/z* = 289.06 $[M+H]^{+}$.

(1f). 1-phenyl-3-(2-(pyridin-2-yl)ethyl)thiourea ($Py(CH_2)_2NHC(S)NHPh$) Synthesised as in (**1a**) from phenylisothiocyanate (1.80 mL, 15 mmol) and 2-ethylene(pyridylamine) (1.78 mL, 15 mmol) in diethyl ether (25 mL) and recrystallised from ethyl acetate to give white crystals. Yield: 3.21 g, 89 %. M.p: 97-100^{o}C; ESI-MS: calculated *m/z* = 280.10, experimental *m/z* = 280.11 $[M+Na]^{+}$.

(1g). 1-(4-methoxyphenyl)-3-(2-(pyridin-2-yl)ethyl)thiourea ($Py(CH_2)_2NHC(S)NHC_6H_4OMe$) Synthesised using the same method as in (**1e**) from a mixture of *p*-methoxyphenylisothiocyanate ($MeOC_6H_4NCS$) (1.38 mL, 10 mmol) and 2-pyridylethylamine (1.20 mL, 10 mmol) in diethyl ether (20 mL) and recrystallised from ethyl acetate to give a bright cream coloured powder. Yield: 2.78 g, 97 %. M.p: 100-102^{o}C, ESI-MS: calculated *m/z* = 288.12, experimental *m/z* = 288.14 $[M+H]^{+}$.

(1h). 1-(4-nitrophenyl)-3-(2-(pyridin-2-yl)ethyl)thiourea ($Py(CH_2)_2NHC(S)NHC_6H_4NO_2$) Synthesised using the same method as (**1e**) from a mixture of *p*-nitrophenyl isothiocyanate ($NO_2C_6H_4NCS$) (1.80 g, 10 mmol) and 2-ethylene(pyridylamine) (1.20 mL, 1 mmol) in diethyl ether (20 mL) and recrystallised from ethyl acetate to give bright yellow crystals. Yield: 3.11 g, 89 %. M.p: 146-150^{o}C and ESI-MS: calculated *m/z* = 303.08, experimental *m/z* = 303.08 $[M+H]^{+}$.

2.4.5 *Synthesis of thiourea dianion complexes*

Equimolar quantities of *cis*-[$PtCl_2(PPh_3)_2$] and PhNHC(S)NHR, $NO_2C_6H_4NHC(S)NHR$ or $MeOC_6H_4NHC(S)NHR$ where R= Py, $PyCH_2$, $Py(CH_2)_2$ were suspended in methanol (20 mL) in a 100 mL round bottom flask with a magnetic stirrer and refluxed for 5 min. resulting in a clear colourless solution. Et_3N (5 mL) was added and the resulting mixture refluxed for 20 to 60 min. resulting in a clear yellow solution. Distilled water (70 mL) was added with stirring and the suspension cooled to room temperature. The resulting precipitate was filtered on a Buchner funnel, washed successively with cold distilled water (20 mL) and diethyl ether (5 mL) and then dried under vacuum. The details for specific experiments are presented in **Table 2.8**.

Table 2.8: Reaction times and conditions for the synthesis of thiourea dianion complexes**.**

	R^2	R^1	$R^2NHC(S)NHR^1$		$PtCl_2(PPh_3)_2$		Reflux Time min	Yield %
			mg	mmol	mg	mmol		
2a	Ph	Py	27	0.12	80	0.1	20	92
2b	*p*-C_6H_4OMe	Py	26	0.10	63	0.08	35	64
2c	*p*-$C_6H_4NO_2$	Py	32.8	0.12	95	0.12	45	46
2d	Ph	$Py(CH_2)$	24	0.10	80	0.1	20	78
2e	*p*-$C_6H_4NO_2$	$Py(CH_2)$	34.5	0.12	95	0.12	40	67
2f	Ph	$Py(CH_2)_2$	25.7	0.10	80	0.1	30	87
2g	*p*-C_6H_4OMe	$Py(CH_2)_2$	28	0.10	63	0.08	35	72
2h	*p*-$C_6H_4NO_2$	$Py(CH_2)_2$	30.2	0.10	80	0.1	45	61

2.4.6 *Characterisation of platinum thiourea dianion complexes*

[Pt{SC(NPh)NPy}(PPh_3)$_2$] ***(2a)***

Elemental analysis: Found %; C 60.55, H 4.23, N 4.40. $C_{48}H_{39}N_3P_2PtS$; requires %; C 60.88, H 4.15, N 4.44. Melting point: 158-162^{o}C. ESI-MS: Calculated *m/z:* 947.21 $[M+H]^+$, experimental *m/z*: capillary exit voltage (CEV); 60 V; 946.97 (100%) $[M+H]^+$, 1630.81(2%) $[2M-PPh_3+H]^+$, 150-180 V 684.96 (5%) $[M-PPh_3+H]^+$, 717.96 (12%) $[Pt(PPh_2C_6H_4)PPh_3]^+$, 946.97 (100%) $[M+H]^+$, 1915.89 (3%) $[2M+Na]^+$. NMR: Distal isomer (*cis*): $^{31}P\{^1H\}$ NMR δ ppm: 16.6 [$^1J_{(PtP)}$ =

3067 Hz, $^{2}J_{(pp)}$ = 22 Hz] and δ 11.8 [$^{1}J_{(PtP)}$ = 3279 Hz, $^{2}J_{(PP)}$ = 22 Hz]. Distal isomer (*trans*): $^{31}P\{^{1}H\}$ NMR δ ppm: 15.33 [$^{1}J_{(PtP)}$ = 3180 Hz, $^{2}J_{(PP)}$ = 22 Hz] and 10.40 [$^{1}J_{(PtP)}$ = 3339 Hz, $^{2}J_{(PP)}$ = 22 Hz]. Proximal isomer: $^{31}P\{^{1}H\}$ δ ppm: 17.6 [$^{1}J_{(PtP)}$ = 3178 Hz, $^{2}J_{(PP)}$ = 21 Hz] and 12.4 [$^{1}J_{(PtP)}$ = 3341 Hz, $^{2}J_{(PP)}$ = 21 Hz]. ^{1}H NMR δ ppm: (Pt_{dist} and Pt_{prox}) 8.04 [d, 1H J = 8.7 Hz, Ar], 7.720 [m, 1H], 7.50 [m, 14H], 7.15 [m, 14H], 7.0 [m, 7H] 6.85 [m, 1H], 6.5 [m, 1H, Ar]. FTIR (cm^{-1}): 3424(w), 3053(w), 2922(w), 1599(w), 1588(w), 1552(s), 1507(w), 1482(w), 1459(s), 1329(m), 1284(m), 1182(w), 1149(m), 1097(m), 1026(w), 998(w), 982(m), 899(w), 784(m), 693(s), 545(s), 526(s), 514(m), 495(w), 463(w), 422(w).

[Pt{SC(NC_6H_4OMe)NPy)}(PPh_3)$_2$] ***(2b)***

Elemental analysis %: Found; C 59.67, H 4.25, N 4.68 $C_{51}H_{44}N_4O_2P_2PtSCl_2$; requires: C 60.25, H 4.23, N 4.30. Melting point: 110-118ºC. ESI-MS: Calculated *m/z:* 976.21 $[M+H]^+$, experimental *m/z*: CEV; 60 V 976.11 (100%) $[M+H]^+$, 150-180 V 715.05 (6%) $[M-PPh_3+H]^+$, 976.11 (100%) $[M+H]^+$, 1691.15 (8%) $[2M-PPh_3+H]^+$. NMR: Distal isomer (*cis*): $^{31}P\{^{1}H\}$ NMR δ ppm: 16.73 [$^{1}J_{(PtP)}$ = 3291 Hz, $^{2}J_{(PP)}$ = 21 Hz] and δ 11.77 [$^{1}J_{(PtP)}$ = 3334 Hz, $^{2}J_{(PP)}$ = 21 Hz]. Distal isomer (*trans*): $^{31}P\{^{1}H\}$ NMR δ ppm 15.58 [$^{1}J_{(PtP)}$ = 3181 Hz, $^{2}J_{(PP)}$ = 21 Hz] and 10.40 ppm [$^{1}J_{(PtP)}$ = 3426 Hz, $^{2}J_{(PP)}$ = 21 Hz]. Proximal isomer: $^{31}P\{^{1}H\}$ NMR δ ppm: 17.65 [$^{1}J_{(PtP)}$ = 3176 Hz, $^{2}J_{(PP)}$ = 22 Hz] and 12.46 [$^{1}J_{(PtP)}$ = 3318 Hz, $^{2}J_{(PP)}$ = 21 Hz]. ^{1}H NMR δ ppm; 3.76 [s, 3H, OCH_3] 6.01-8.56 [m, 41H, Ar]. FTIR (cm^{-1}): 3437(br), 3050(m), 2830(w), 1593(s), 1562(s), 1537(w), 1502(s), 1461(s), 1422(m), 1331(s), 1281(m), 1237(s), 1179(w), 1147(m), 1097(s), 998(w), 924(m), 827(m), 776(m), 743(s), 694(s), 619(w), 544(s), 524(m), 516(w), 499(w), 464(w).

[Pt{SC($NC_6H_4NO_2$)NPy}(PPh_3)$_2$] ***(2c)***

Elemental analysis: Found %; C 57.97, H 3.65, N 5.60. $C_{48}H_{38}N_4O_2P_2PtS$; requires %: C 58.12, H 3.86. N 5.65. Melting point: 160-179ºC decomposed. ESI-MS: Calculated *m/z*: 992.18 $[M+H]^+$. experimental: CEV 60 V; 991.95(100%) $[M+H]^+$, 120-150 V 945.98 (22%) $[M-NO_2+H]^+$, 991.97 (100%) $[M+H]^+$, 1721.82 (2%) $[2M-PPh_3+H]^+$, 1982.84 (7%) $[2M+H]^+$, 180 V; 717.96 (12%) $[Pt(PPh_2C_6H_4)PPh_3]^+$, 729.14 (14%) $[M-PPh_3+H]^+$, 945.98 (28%) $[M-NO_2+H]^+$, 991.95 (100%) $[M+H]^+$. NMR: Distal isomer: $^{31}P\{^{1}H\}$ NMR δ ppm: 14.9 [$^{1}J_{(PtP)}$ = 3222 Hz, $^{2}J_{(pp)}$ = 22 Hz] and δ 9.7 ppm, [$^{1}J_{(PtP)}$ = 3386 Hz, $^{2}J_{(PP)}$ = 22 Hz]. ^{1}H NMR

δ ppm: 6.12-8.45 [m, 38H]. Proximal isomer: $^{31}P\{^{1}H\}$ NMR δ ppm 17.5 [$^{1}J_{(PtP)}$ = 3175 Hz, $^{2}J_{(PP)}$ = 22 Hz] and 11.9 [$^{1}J_{(PtP)}$ = 3338 Hz, $^{2}J_{(PP)}$ = 22 Hz]. ^{1}H NMR δ ppm: 6.12-8.45 [m, 38H]. FTIR (cm^{-1}): 3446(s), 3050(w), 1858(m), 1531(m), 1480(w), 1460(s), 1434(s), 1422(m), 1321(s), 1283(m), 1255(w), 1183(w), 1155(m), 1107(w), 1095(w), 1026(w), 998(w), 926(m), 873(w), 852(m), 778(w), 742(s), 693(s), 651(w), 618(w), 579(w), 544(s), 524(m), 515(w), 499(m), 421(w).

[Pt{SC(NCH$_2$Py)NPh}(PPh$_3$)$_2$] ***(2d)***

Elemental analysis: Found %; C 57.74, H 4.19, N 4.03. $C_{50}H_{43}N_3P_2PtSCl_2$; requires %: C 57.62, H 4.37, N, 3.96. Melting point: 180-188ºC. ESI-MS: Calculated *m/z*: 960.88 $[M+H]^+$, experimental *m/z*: CEV 60 V; 960.97 (100%) $[M+H]^+$, 120-150 V; 698.95 (13%) $[M-PPh_3+H]^+$, 960.97 (100%) $[M+H]^+$, 1200.97 (11%) $[2M-PyCH_2NCSN+H]^+$, 180-240 V; 698.95 (81%) $[M-PPh_3+H]^+$, 717.97 (24%) $[Pt(PPh_2C_6H_4)PPh_3]^+$, 961.01 (100%) $[M+H]^+$, 1943.91 (2%) $[2M+Na+H]^{2+}$. NMR: Distal isomer; $^{31}P\{^{1}H\}$ NMR δ ppm: 13.6 [$^{1}J_{(PtP)}$ = 3238 Hz, $^{2}J_{(PP)}$ = 22 Hz] and 9.13 [$^{1}J_{(PtP)}$ = 3448 Hz, $^{2}J_{(PP)}$ = 21 Hz]. ^{1}H NMR δ ppm: 7.95 [d, 1 H, J = 5.2 Hz, Ar], 7.5 [m, 7H], 7.40 [m, 8H], 7.20 [m, 13H], 7.0 [m, 8H], 6.85 [m, 2H, Ar], 4.40 [s, 2H, CH_2]. Proximal isomer; $^{31}P\{^{1}H\}$ NMR δ ppm: 18.2 [$^{1}J_{(PtP)}$ = 3055 Hz, $^{2}J_{(PP)}$ = 21 Hz] and 13.6 [$^{1}J_{(PtP)}$ = 3194 Hz, $^{2}J_{(PP)}$ = 22 Hz]. ^{1}H NMR δ ppm: 7.95 [d, 1H, J = 5.2 Hz, Ar], 7.5 [m, 7H), 7.40 [m, 8H), 7.20 [m, 13H], 7.0 [m, 8H], 6.85 [m, 2H, Ar], 4.79 [q, 2H, CH_2, J = 4.11 Hz, J = 43 Hz]. FTIR (cm^{-1}): 3383(br), 3051(m), 2923(w), 1591(w), 1551(s), 1479(m), 1434(s), 1314(m), 1203(m), 1158(w), 1094(s), 1069(w), 1084(s), 1059(w), 997(m), 869(w), 743(s), 693(s), 545(s), 525(m), 514(w), 498(w), 426(w).

[Pt{SC(NC$_6$H$_4$NO$_2$)NCH$_2$Py}(PPh$_3$)$_2$] ***(2e)***

Elemental analysis: Found %; C 58.78, H 3.96, N 5.39. $C_{49}H_{40}N_4O_2P_2PtS$; requires %: C, 58.50; H, 4.01; N, 5.57. Melting point: 190-198ºC. ESI-MS: Calculated *m/z*: 1005.88 $[M+H]^+$, experimental *m/z*: CEV 60 V; 1005.95 (100%) $[M+H]^+$, 2011.82 (2%) $[2M+H]^+$, 120-150 V; 482.91 (3%) $[M-(PPh_3)_2+H]^+$, 717.97 (14%) $[Pt(PPh_2C_6H_4)PPh_3]^+$, 743.95 (57%) $[M-PPh_3+H]^+$, 1005.97 (100%) $[M+H]^+$, 2011.82 (2%) $[2M+H]^+$, 180 V; 482.91 (100%) $[M-PPh_3+H]^+$, 717.97 (71%) $[Pt(PPh_2C_6H_4)PPh_3]^+$, 743.95 (14%) $[M-PPh_3+H]^+$,1005.95 (26%) $[M+H]^+$. NMR: Proximal isomer; $^{31}P\{^{1}H\}$NMR δ ppm: 17.6 [$^{1}J_{(PtP)}$ = 3109 Hz, $^{2}J_{(PP)}$ = 21 Hz] and 13.10 [$^{1}J_{(PtP)}$ = 3245 Hz, $^{2}J_{(PP)}$ = 21 Hz]. ^{1}H NMR δ ppm: 4.42 [q, 2H, CH_2, J= 4.6

Hz, J = 44.51 Hz], 6.41-8.65 [m, 38H, Ar]. FTIR (cm^{-1}): 3437(s), 3054(w), 2922(w), 1591(w), 1512(s), 1435(s), 1364(w), 1309(s), 1222(w), 1169(w), 1108(s), 1058(w), 999(w), 890(m), 847(m), 747(m), 694(s), 617(w), 546(m), 526(m), 515(w), 498(w), 419(w).

[Pt{SC(NPh)N(CH_2)$_2$Py}(PPh_3)$_2$] ***(2f)***

Elemental analysis: Found %; C 61.08, H 4.38, N 4.28. $C_{50}H_{43}N_3P_2PtS$; requires %: C 61.59, H 4.45, N 4.31. Melting point: 191-202^{o}C decomposed. ESI-MS: : Calculated *m/z*: 974.89 $[M+H]^+$, experimental *m/z* : CEV 60 V; 974.94 (100%) $[M+H]^+$, 120-150 V; 712.93 (74%) $[M-PPh_3+H]^+$, 974.95 (100%) $[M+H]^+$, 180 V; 450.92 (12%) $[M-(PPh_3)_2+H]^+$, 712.93 (62%) $[M-(PPh_3)_2+H]^+$, 974.96 (100%) $[M+H]^+$. NMR: Distal isomer; $^{31}P\{^1H\}$ NMR δ ppm: 13.6 [$^1J_{(PtP)}$ = 3210 Hz, $^2J_{(PP)}$ = 22 Hz] and 9.3 [$^1J_{(PtP)}$ = 3483 Hz, $^2J_{(PP)}$ = 21 Hz]. ^1H NMR δ ppm: 3.49 [t, 2H, CH_3, J = 13 Hz], 2.92 [t, 2H, J = 11 Hz]. Proximal isomer; $^{31}P\{^1H\}$ NMR δ ppm: 18.3 [$^1J_{(PtP)}$ = 3119 Hz, $^2J_{(PP)}$ = 21 Hz] and 13.4 [$^1J_{(PtP)}$ = 3221 Hz, $^2J_{(PP)}$ = 21 Hz] ^1H NMR δ ppm: 3.29 [dd, 2H, J = 11 Hz, J = 20 Hz], 2.74 [t, 2H, CH_2, J = 7.8 Hz). FTIR (cm^{-1}): 3437(s), 3047(m), 2930(w), 1597(w), 1589(w), 1561(s), 1479(s), 1435(s), 1320(m), 1283(w), 1202(m), 1093(s), 1070(w), 1049(w), 1027(w), 998(m), 899(m), 842(w), 746(m), 692(s), 629(w), 548(s), 526(w), 518(w), 497(m), 421(w).

[Pt{SC(NC_6H_4OMe)N(CH_2)$_2$Py)}(PPh_3)$_2$] ***(2g)***

Elemental analysis %: Found; C 60.67, H 4.52, N 4.10 $C_{51}H_{44}N_4O_2P_2PtSCl_2$; requires: C 60.95, H 4.51, N 4.18. Melting point: 240-250^{o}C decomposed. ESI-MS: Calculated *m/z*: 1005.22 $[M+H]^+$, experimental *m/z*: CEV 60 V; 1005.14 (100%) $[M+H]^+$ 120-150 V; 742.06 (6%) $[M-PPh_3+H]^+$, 955.115 (100%) $[M-OCH_3+H]^+$, 1005.14 (100%) $[M+H]^+$, 180 V; 481.01 (23%) $[M-(PPh_3)_2+H]^+$, 1005.15 (100%) $[M+H]^+$. NMR: Distal isomer; $^{31}P\{^1H\}$ NMR δ ppm: 14.02 [$^1J_{(PtP)}$ = 3259 Hz, $^2J_{(PP)}$ = 21 Hz] and 9.41 [$^1J_{(PtP)}$ = 3338 Hz, $^2J_{(PP)}$ 22 Hz]. ^1H NMR δ ppm: 3.18 [m, 2H, CH_2, J = 6 Hz], 3.46 [t, 2H, CH_2, J = 6 Hz), 3.74 (s, 3H, CH_3). Proximal isomer; $^{31}P\{^1H\}$ NMR δ ppm: 18.3 [$^1J_{(PtP)}$ = 3216 Hz, $^2J_{(PP)}$ = 21 Hz] and 13.6 [$^1J_{(PtP)}$ = 3434 Hz, $^2J_{(PP)}$ = 22 Hz]. ^1H NMR δ ppm: 3.24 [dd, 2H, CH_2, J = 6 Hz, J = 22 Hz)], 2.9 [t, 2H CH_2, J = 6 Hz], 3.65 [s, 3H, CH_3]. FTIR (cm^{-1}): 3447(br), 3054(w), 2932(w), 1633(w), 1565(s), 1501(s), 1480(m), 1435(s), 1279(w), 1236(m), 1182(w), 1096(s), 1029(w), 999(w), 899(w), 830(w), 745(m), 693(s), 619(w), 547(s), 525(s), 516(w), 497(w), 464(w).

[Pt{SC($NC_6H_4NO_2$)N(CH_2)$_2$Py}(PPh_3)$_2$] ***(2h)***

Elemental analysis %: Found; C 56.79, H 3.97, N 5.28 $C_{51}H_{44}N_4O_2P_2PtSCl_2$; requires: C 55.44, H 4.01, N 5.07. Melting point: 225-240^oC decomposed. ESI-MS: Calculated *m/z*: 1019.92 $[M+H]^+$ experimental *m/z*: CEV 60 V; 1019.98 (100%), $[M+H]^+$ 2011.82 (5%) $[2M+H]^+$, 120-150 V; 757.92 (13%) $[M-PPh_3+H]^+$, 1020.01 (100%) $[M+H]^+$, 180 V; 495.91 (100%) $[M-(PPh_3)_2+H]^+$, 717.95 (48%) $[Pt(PPh_2C_6H_4)PPh_3]^+$, 757.96 (41%) $[M-PPh_3+H]^+$, 1020.01 (100%) $[M+H]^+$ 240 V; 777.95 (11%) $[M-PPh_3+H]^+$. NMR Distal isomer: $^{31}P\{^1H\}$ NMR δ: 13.63 ppm [$^1J_{(PtP)}$ = 3215 Hz, $^2J_{(PP)}$ = 22Hz] and δ 9.26 ppm [$^1J_{(PtP)}$ = 3403 Hz, $^2J_{(PP)}$ = 21Hz] , ^1H NMR δ ppm: 3.56 [m, 2H; J = 8 Hz]. Proximal isomer: $^{31}P\{^1H\}$ NMR δ ppm: 18.20 [$^1J_{(PtP)}$ = 3105 Hz, $^2J_{(PP)}$ = 21 Hz] and 12.82 [$^1J_{(PtP)}$ = 3194 Hz, $^2J_{(PP)}$ = 21 Hz]. ^1H NMR δ ppm: 3.26 [m, 2H, J = 6.5 Hz, J = 20 Hz], 2.63 [t, 2H, J = 8 Hz]. FTIR (cm^{-1}): 3443(s), 3054(w), 2924(w), 1591(w), 1513(s), 1435(w), 1313(s), 1214(w), 1170(w), 1108(m), 1027(w), 999(w), 851(m), 745(m), 693(s), 617(w), 546(m), 526(m), 515(w), 499(w), 421(w).

2.4.7 *Synthesis and characterisation of the platinum thiourea monoanion complex [Pt{SC(NHCH$_2$Py)NPh}(PPh_3)$_2$](BF_4) 2i*

The thiourea monoanion complex **2i** was synthesised by the reaction of equimolar quantities of *cis*-[$PtCl_2(PPh_3)_2$] (80 mg, 0.1 mmol) and $PyCH_2NHCSNHPh$ (25 mg, 0.1 mmol) in 15 mL of methanol solvent. The reaction was stirred for about five minutes to give a clear colourless solution. Et_3N (2 mL) was added and the mixture refluxed for about 25 minutes. Solid $NaBF_4$ (0.1 g, 1 mmol excess) was added and the reaction mixture refluxed for another 15 minutes before water (70 mL) was added to precipitate the product. The bright yellow solid obtained was filtered in a Buchner funnel and washed successively with water (10 mL), methanol (2 mL) and diethyl ether (5 mL). The final product was dried overnight under vacuum. Bright yellow crystals of the complex formed after 4 days of diffusing diethyl ether into a dichloromethane solution of the product. Yield; 60 %. Elemental analysis %: Found; C 52.62, H 3.91, N 4.67. $C_{49}H_{42}N_3P_2PtSBF_4$ requires; C 52.97, H 3.91, N 3.71. Melting point: 129-140^oC. ESI-MS: Calculated *m/z*: 961.22 $[M]^+$, experimental *m/z*; CEV 60 V; 961.12 (100%) $[M]^+$, 1201.13 (3%) $[2M-(PPh_3)_2]^{2+}$, 150 V; 699.05 (67%) $[M-PPh_3]^+$, 962.10 (100%) $[M]^+$, 1201.13 (5%) $[2M-Pt(PPh_3)_2]^+$, 180 V; 699.05 (97%) $[M-(PPh_3)]^+$, 718.06 (13%) $[Pt(PPh_2C_6H_4)(PPh_3)]^+$, 962.11 (100%)

$[M+H]^+$, 1201.15 (3%) $[2M\text{-}Pt(PPh_3)_2]^{2+}$. NMR: Distal isomer; $^{31}P\{^1H\}$ NMR δ ppm: 13.3 [$^1J_{(PtP)}$ = 3246 Hz, $^2J_{(PP)}$ = 22 Hz] and 9.0 ppm [$^1J_{(PtP)}$ = 3456 Hz, $^2J_{(PP)}$ = 21 Hz]. ^1H NMR δ ppm: 5.3 [s, 1H, NH], 4.4 [s, 2H, CH_2]. Proximal isomer; $^{31}P\{^1H\}$ NMR δ ppm: 15.8 [$^1J_{(PtP)}$ = 3190 Hz, $^2J_{(PP)}$ = 21 Hz] and 10.24 [$^1J_{(PtP)}$ = 3420 Hz, $^2J_{(PP)}$ 22 Hz]. ^1H NMR δ ppm: 5.66 [s, 1H], 3.9 [d, 2H, $^3J_{(PtH)}$ obscured in the base line). FTIR (cm^{-1}): 3451(br), 3056(w), 1635(m), 1595(w), 1574(m), 1497(w), 1481(m), 1436(s), 1335(w), 1186(m) 1158(m), 1096(w), 1084(s), 1057(w), 998(w), 913(m), 747(m), 693(s), 619(w) 547(m), 526 (s), 517(m), 498(w).

2.4.8 *Single crystal X-ray structure determinations*

Crystal data and refinement details for the investigated complexes are included in **Tables 2.9-2.10.** Intensity were measured at T = 100 K on a SuperNova Dual AtlasS2 diffractometer fitted with Cu Kα radiation (λ=1.54184 Å). Data reduction, including absorption correction, was accomplished with CrysAlisPro[38]. The structures were solved by direct-methods[39] and refined (with anisotropic displacement parameters and C-bound H atoms in the riding model approximation) on F^2 [40]. For **2i**, the N-bound H atom was located from a difference map and refined with N−H = 0.88±0.01 Å. In the final cycles of the refinement of each of **2b**, **2d**, **2e**, **2f**, **2h** and **2i**, and a number of reflections were omitted owing to poor agreement; details are given in the CIF's. A residual electron density peak in **2e**, evident after the complex molecule was refined, was modelled as a water molecule of crystallisation consistent with the spectroscopic and microanalytical data. As the O-bound H atoms could not be located unambiguously, owing to the poor resolution of the site (the atom was refined isotropically in the final cycles) these were not included in the model. With the exception of **2e** and **2i**, the structures featured large residual electron density peaks with the maximum of these always located near the Pt atom; details are given in the CIF's. The molecular structure diagrams were generated in Olex 2[41] and Mercury [42.]

Table 2.9: Crystallographic and structure refinement parameters for platinum complexes **2a**, **2b**, **2c**, **2d.**

Complexes	**2a**	**2b.**CH_2Cl_2	**2d.**CH_2Cl_2	**2e**.H_2O
Formula	$C_{48}H_{39}N_3P_2PtS$	$C_{49}H_{41}N_3OP_2SPt$	$C_{50}H_{44}N_3P_2PtSCl_2$	$C_{51}H_{41}N_2O_3P_2PtS$
Formula weight (g/mol)	946.91	1061.86	1046.87	1022.00
Temperature /K	99.99(10)	100.4(7)	99.96(12)	99.98(6)
Wavelenght /Å	1.54184	1.54184	1.54184	1.54184
Crystal System	Monoclinic	Monoclinic	Triclinic	Monoclinic
Space group	$P2_{1/}n$	$P2_1/c$	P-1	$P2_1/c$
a/Å	12.97790(10)	10.09620(10)	11.2041(4)	18.0588(14)
b/Å	19.13100(10)	17.3291(2)	13.3287(4)	11.048876(2)
c/Å	15.99760(10)	24.7899(2)	15.8165(4)	32.999(3)
α/º	90	90	97.172(2)	90
β/º	97.2740(10)	91.4110(10)	105.098(2)	138.729(15)
γ/º	90	90	103.704(3)	90
Volume /$Å^3$)	3939.92(5)	4335.88(7)	2171.26(12)	4343.0 (10)
Z	4	4	2	4
ρcalc g/cm^3	1.596	1.6270	1.601	1.5583
F(000)	1888.0	2120.0	1046.0	2044.0
Crystal Size/mm^3	0.262x0.1807x0.103	0.211 × 0.115 × 0.082	0.155x0.082x0.044	0.295 × 0.163 × 0.115
2Θ(º)	7.238 - 147.948	7.134 - 147.794	5.906 - 147.77	7422 – 148.698
Goof	1.058	1.052	1.053	1.135
R-Factor (%)	2.54	4.72	2.46	4.72
Reflections used	7872	8575	8536	8739
Total reflections	37263	29968	24189	40322
Abs correction	Guassian	multiscan	Guassian	multiscan

Table 2.10: Crystallographic and structure refinement parameters for platinum complexes **2f, 2g, 2h** and **2i,**

Complexes	**2f**	**2g**	**2h.**CH_2Cl_2	**(2i)**
Formula	$C_{50}H_{43}N_3P_2PtS$	$C_{51}H_{46}N_3OP_2PtS$	$C_{51}H_{44}Cl_2N_4O_2P_2PtS$	$C_{49}H_{42}BF_4N_3P_2PtS$
Formula weight (g/mol)	974.96	1006.04	1104.89	1048.75
Temperature /K	99.96(13)	100.4(8)	100.00(10)	100.00(10)
Wavelength /Å	1.54184	1.54184	1.54184	1.54184
Crystal System	Monoclinic	Monoclinic	Monoclinic	triclinic
Space group	C_2/c	$P2_1/c$	$P2_1/n$	P-1
a/Å	30.7383(3)	13.51630(16)	17.6890(2)	10.5640(3)
b/Å	11.4819(10)	28.6178(3)	11.4524(2)	13.1413(3)
c/Å	23.5515(3)	12.0288(16)	23.2628(3)	17.3734(4)
α/°	90	90	90	72.162(2)
β/°	92.7720(10)	112.5101(14)	98.7992	78.805(2)
γ/°	90	90	90	73.609(2)
Volume/Å^3)	8302.40(13)	4298.35(10)	4657.25(11)	2187.23(10)
Z	8	4	4	2
ρ_{calc} g/cm^3	1.5600	1.5545	1.5758	1.5924
F(000)	3904.0	2010.9	2208.0	1044.0
Crystal Size/mm^3	0.08 x 0.054 x 0.05	0.24 × 0.12 × 0.08	0.211 × 0.069 × 0.052	0.305 × 0.158 × 0.115
2Θ(°)	7.516 - 148.018	7.08 to 148.32	5.864 - 148.004	5.38 - 147.902
Goof	1.054	1.054	1.035	1.083
R-Factor (%)	2.10	2.84	4.06	4.69
Ind. Reflections	8169	8623	9093	8759
Total reflections	23800	39312	25914	39629
Abs correction	Guassian	multiscan	Guassian	Guassian

2.5 References

1. Satpathy, K. C.; Panda, A. K.; Mishra, R.; Mohapatra, A. *Synth. React. Inorg. Met.-Org. Chem.* **1989**, *19*, 23-31.

2. Kashyap, B. C.; Banerji, S. K.; Taneja, A. D. *Current Science* **1976**, *45*, 81-83.

3. Kalidasan, M.; Nagarajaprakash, R.; Rao, K. M. *Transition Met. Chem.* **2015**, *40*, 531-539.

4. Hollmann, K.; Oppermann, A.; Witte, M.; Li, S.; Amen, M.; Flörke, U.; Egold, H.; Henkel, G.; Herres-Pawlis, S. *Eur. J. Inorg. Chem.* **2017**, *2017*, 1266-1279.

5. Hollmann, K.; Oppermann, A.; Amen, M.; Flörke, U.; Egold, H.; Hoffmann, A.; Herres-Pawlis, S.; Henkel, G. *Zeit. Anorg. Allg. Chem.* **2016**, *642*, 660-669.

6. El-Ayaan, U. *J. Mol. Struct.* **2011**, *998*, 11-19.

7. Isab, A. A.; Nawaz, S.; Saleem, M.; Altaf, M.; Monim-ul-Mehboob, M.; Ahmad, S.; Evans, H. S. *Polyhedron* **2010**, *29*, 1251-1256.

8. Pisiewicz, S.; Rust, J.; Lehmann, C. W.; Mohr, F. *Polyhedron* **2010**, *29*, 1968-1972.

9. Kascheres, A.; Ueno, M. *J. Heterocycl. Chem.* **1991**, *28*, 2057-2058.

10. West, D.; Hermetet, A. K.; Ackerman, L.; Valdés-Martínez, J.; Hernández-Ortega, S. *Acta Crystallogr., Sect. C: Cryst. Struct. Commun.* **1999**, *55*, 811-813.

11. Valdés-Martínez, J.; Hernàndez-Ortega, S.; West, D. X.; Ackerman, L. J.; Swearingen, J. K.; Hermetet, A. K. *J. Mol. Struct.* **1999**, *478*, 219-226.

12. Valdés-Martınez, J.; Hernández-Ortega, S.; Ackerman, L.; Li, D.; Swearingen, J.; West, D. *J. Mol. Struct.* **2000**, *524*, 51-59.

13. Sudbeck, E. A.; Jennissen, J. D.; Venkatachalam, T. K.; Uckun, F. M. *Acta Crystallogr., Sect. C: Cryst. Struct. Commun.* **1999**, *55*, 2122-2124.

14. Szczepura, L. F.; Eilts, K. K.; Hermetet, A. K.; Ackerman, L. J.; Swearingen, J. K.; West, D. X. *J. Mol. Struct.* **2002**, *607*, 101-110.

15. Valdés-Martínez, J.; Hernández-Ortega, S.; Espinosa-Perez, G.; Presto, C. A.; Hermetet, A. K.; Haslow, K. D.; Ackerman, L. J.; Szczepura, L. F.; Goldberg, K. I.; Kaminsky, W. *J. Mol. Struct.* **2002**, *608*, 77-87.

16. Giesen, J. M.; Claborn, K. A.; Goldberg, K. I.; Kaminsky, W.; West, D. X. *J. Mol. Struct.* **2002**, *613*, 223-233.

17. El-Ayaan, U. *J. Mol. Struct.* **2011**, *998*, 11-19.

18. Saxena, A.; Dugan, E. C.; Liaw, J.; Dembo, M. D.; Pike, R. D. *Polyhedron* **2009**, *28*, 4017-4031.

19. Vassilev, G.; Davarski, K. *Dokladi Na Bolgarskata Akademiya Na Naukite* **1986**, *39*, 103-106.

20. West, D. X.; Van Roekel, S. A.; Bunting, R. K. *Transition Met. Chem.* **1988**, *13*, 53-57.

21. Szczepura, L. F.; Eilts, K. K.; Hermetet, A. K.; Ackerman, L. J.; Swearingen, J. K.; West, D. X. *J. Mol. Struct.* **2002**, *607*, 101-110.

22. Valdés-Martínez, J.; Hernández-Ortega, S.; Ackerman, L. J.; Li, D. T.; Swearingen, J. K.; West, D. X. *J. Mol. Struct.* **2000**, *524*, 51-59.

23. Valdés-Martínez, J.; Hernández-Ortega, S.; Rubio, M.; Li, D. T.; Swearingen, J. K.; Kaminsky, W.; Kelman, D. R.; West, D. X. *J. Chem. Crystallogr.* **2004**, *34*, 533-540.

24. Henderson, W.; Nicholson, B. K. *Polyhedron* **1996**, *15*, 4015-4024.

25. Scheffknecht, C.; Rhomberg, A.; Müller, E. P.; Peringer, P. *J. Organomet. Chem.* **1993**, *463*, 245-248.

26. Henderson, W.; Rickard, C. E. F. *Inorg. Chim. Acta* **2003**, *343*, 74-78.

27. Henderson, W.; Nicholson, B. K.; McCaffrey, L. J. *Inorg. Chim. Acta* **1999**, *285*, 145-148.

28. Raymond, D. *J. Chem. Soc., Dalton Trans.* **1996**, 1897-1903.

29. De Castro, V.; De Lima, G. M.; Porto, A. O.; Siebald, H. G.; de Souza Filho, J. D.; Ardisson, J.; Ayala, J. D.; Bombieri, G. *Polyhedron* **2004**, *23*, 63-69.

30. Spenceley, J. E.; Henderson, W.; Lane, J. R.; Saunders, G. C. *Inorg. Chim. Acta* **2015**, *425*, 83-91.

31. Okeya, S.; Fujiwara, Y.; Kawashima, S.; Hayashi, Y.; Isobe, K.; Nakamura, Y.; Shimomura, H.; Kushi, Y. *Chem. Lett.* **1992**, 1823-1826.

32. Henderson, W.; Kemmitt, R. D. W.; Mason, S.; Moore, M. R.; Fawcett, J.; Russell, D. R. *J. Chem. Soc., Dalton Trans.* **1992**, 59-66.

33. Henderson, W.; Nicholson, B. K.; Rickard, C. E. F. *Inorg. Chim. Acta* **2001**, *320*, 101-109.

34. Dinger, M. B. Aspects of Metallacyclic Chemistry, PhD Thesis, The University of Waikato, 1998.

35. Yuen, H. Y.; Henderson, W.; Oliver, A. G. *Inorg. Chim. Acta* **2011**, *368*, 1-5.

36. Henderson, W.; Nicholson, B. K.; Dinger, M. B.; Bennett, R. L. *Inorg. Chim. Acta* **2002**, *338*, 210-218.

37. Frisch, M.; Trucks, G.; Schlegel, H.; Scuseria, G.; Robb, M.; Cheeseman, J.; Scalmani, G.; Barone, V.; Mennucci, B.; Petersson, G. *Inc., Wallingford CT* **2009**

38. Rigaku Oxford Diffraction CrysAlisPro Software System, version 1.171. 38.41 l, Rigaku Coorporation. Oxford, UK, (2015).

39. Sheldrick, G. M. *Acta Crystallogr., Sect. C: Struct. Chem.* **2015**, *71*, 3-8.

40. Sheldrick, G. M. *Acta Crystallogr., Sect. A: Found. Adv* **2015**, *71*, 3-8.

41. Dolomanov, O. V.; Bourhis, L. J.; Gildea, R. J.; Howard, J. A. K.; Puschmann, H. *J. Appl. Crystallogr.* **2009**, *42*, 339-341.

42. Macrae, C. F.; Bruno, I. J.; Chisholm, J. A.; Edgington, P. R.; McCabe, P.; Pidcock, E.; Rodriguez-Monge, L.; Taylor, R.; Streek, J. v. d.; Wood, P. A. *J. Appl. Crystallogr.* **2008**, *41*, 466-470.

Chapter 3

Palladium and nickel complexes of pyridyl-substituted thiourea dianion and monoanion complexes

3.1 Introduction

Palladium and nickel complexes containing organophosphorus ligands have been the subject of a considerable amount of research, due to their numerous applications in organic synthesis as well as catalysis[1-6]. The oxidative carbonylation of alkynes by palladium–iodide thiourea catalysts has been well documented in the literature[7-10] and the role of palladium tetramethylthiourea chloride catalyst in bis(methoxycarbonylation) of terminal olefins has also been reported[11]. The affinity of palladium and nickel for sulfur-containing compounds has endeared their phosphine containing complexes to thiolate ligands, including the thioureas[12-16]. The possibility of substitution of the amine protons of the thioureas with a variety of functional groups, leading to compounds with interesting chemical and physical properties, has made thioureas one of the most versatile organo-thiolate compounds.

In the previous Chapter, platinum complexes of some pyridyl-substituted thiourea monanion and dianion ligands were explored. Differences in steric properties of the substituents at the metallacyclic and imine nitrogens resulted in isomerism in some of the complexes. In this Chapter, the reactivity of the pyridyl-substituted thiourea ligands reported in Chapter two towards palladium and nickel was investigated. The effect of different asymmetric substituents on the chemical, structural and supramolecular properties of the resulting complexes were explored. Further, metal complexes containing similar but sterically different organophosphorus ligands; $[PdCl_2(PPh_3)_2]$ and $[PdCl_2(dppe)]$ (PPh_3 = triphenylphosphine; dppe = bis-(diphenylphosphino)ethane) were synthesised, and the effect of the steric bulk of the organophosphorous ligands on the chemical and supramolecular properties of the complexes was investigated. The pyridyl substituents in the thiourea ligands were substituted with the methylene- and ethylene-pyridyl functional groups. This was in a bid to introduce some variation

in the steric nature of the ligands in the complexes, which could alter the bonding geometry and probably their physical and chemical properties.

3.2 Results and discussion

3.2.1 *Thiourea monoanion and dianion complexes of palladium and nickel*

A series of pyridyl-substituted thiourea complexes of palladium and nickel **3a-3l** were synthesised by the reaction of equimolar quantities of pyridyl-substituted thiourea ligands of the form $R^1NHC(S)NHR^2$ (where $R^1 = Py(CH_2)_n$; n = 0,1,2; R^2 = Ph or *p*-$C_6H_4NO_2$) with $[PdCl_2(dppe)]$, $[PdCl_2(PPh_3)_2]$ or $[NiCl_2(dppe)]$. The complexes were synthesised in a refluxing methanol solution in the presence of excess Et_3N. The cationic complexes **3a, 3d, 3f-l**, precipitated as BPh_4 salts by addition of excess solid $NaBPh_4$ to the hot reflux solution. Complexes **3b-c** were isolated by addition of excess $NaBF_4$, while **3f** was isolated with excess NH_4PF_6. Complex **3e** was isolated as a dianion complex.

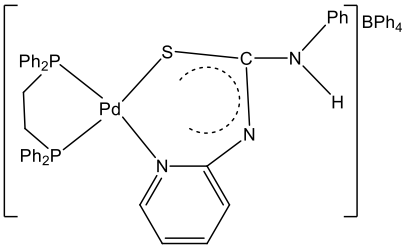

3a

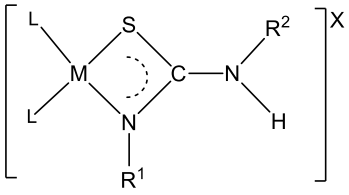

3b-d; **3f-l**

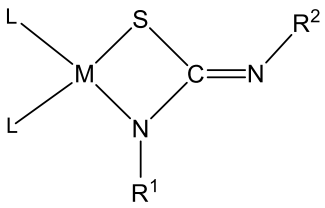

3e

Compound	L^2/L_2	M	R^1	R^2	X
3b	dppe	Pd	CH_2Py	Ph	BF_4
3c	dppe	Pd	Ph	$(CH_2)_2Py$	BF_4
3d	dppe	Pd	*p*-$C_6H_4NO_2$	$(CH_2)_2Py$	BPh_4
3e	dppe	Pd	Py	*p*-$C_6H_4NO_2$	-
3f	$(PPh_3)_2$	Pd	Py	Ph	BPh_4
3g	$(PPh_3)_2$	Pd	CH_2Py	Ph	BPh_4
3h	$(PPh_3)_2$	Pd	$(CH_2)_2Py$	Ph	BPh_4
3i	dppe	Ni	Py	Ph	BPh_4
3j	dppe	Ni	$(CH_2)_2Py$	Ph	BPh_4
3k	dppe	Ni	Py	*p*-$C_6H_4NO_2$	BPh_4
3l	dppe	Ni	$(CH_2)_2Py$	*p*-$C_6H_4NO_2$	BPh_4

Scheme 3.1: Reaction scheme for the synthesis of palladium and nickel thiourea complexes (L= PPh_3 or L_2 = dppe)

3.2.2 *Spectroscopic characterisation of the complexes*

ESI-mass spectral analysis of the complexes at relatively low capillary exit voltage (CEV 60 V) showed the presence of $[M]^+$ ions, where M = [Pd{SC(NR^1)NHR^2(dppe)}]. For example, the spectrum for the pyridyl substituted complex [Pd{SC=(NPh)NH$(CH_2)_2$Py}(dppe)] **3c** (**Figure 3.1**) showed the presence of a single molecular ion peak at *m/z* 760.04 (CEV 60 V). The experimental isotope pattern for the complex corresponds to the calculated pattern (insert). Increase in the capillary exit voltage for this complex to 120 and 180 V resulted in many unidentifiable fragment peaks. Similar ESI-MS results were obtained for palladium **3a-b, 3c-e** and nickel complexes **3i-l,** containing the bis-diphenylphosphinoethane ligand (dppe) (**Table 3.1**)

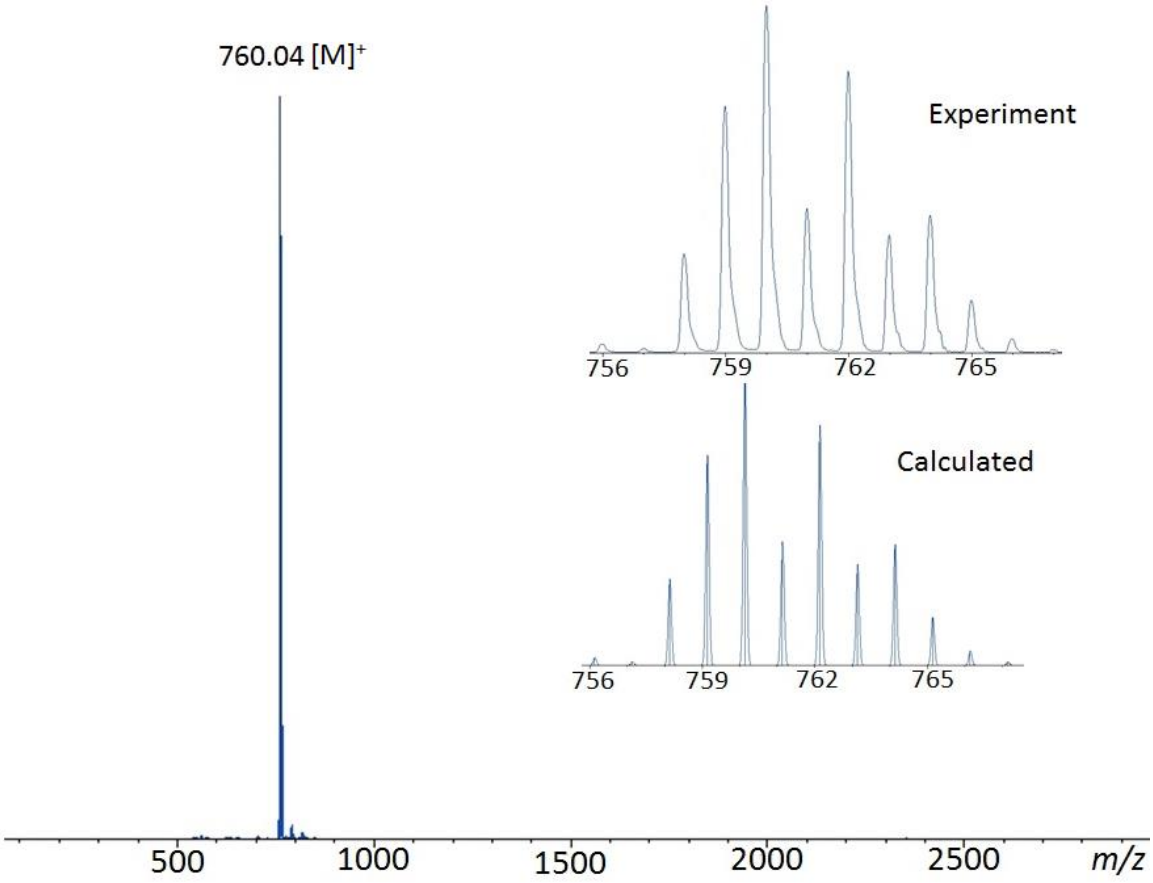

Figure 3.1: ESI-mass spectrum of palladium thiourea complex [Pd{SC(NPh}$N(CH_2)_2$Py)$(PPh_3)_2$]BPh_4 **3c** at capillary exit voltage 60 V. Inserts are experimental and calculated isotope patterns.

Table 3.1: ESI-MS data of palladium and nickel pyridyl-substituted thiourea complexes at varying capillary exit voltage.

Complexes	**Capillary exit voltage (V)**	***m/z*(%) ions**
[Pd{SC(NPy)NHPh}(dppe)]BPh_4 (**3a**)	60	732 (100) $[M]^+$
[Pd{SC(NPh)$NHCH_2$Py}(dppe)]BF_4(**3b**)	60	746 (100) $[M]^+$
[Pd{SC(NPh)$NH(CH_2)_2$Py}(dppe)]BF_4 (**3c**)	60	760 (100) $[M]^+$
[Pd{SC($NC_6H_4NO_2$)$NH(CH_2)_2$Py}(dppe)]BPh_4 (**3d**)	60	805 (100) $[M]^+$
[Pd{SC(NPy)$NHC_6H_4NO_2$}(dppe)] (**3e**)	60	777 (100) $[M+H]^+$
[Pd{SC(NPy)NPh}$(PPh_3)_2$]BPh_4 (**3f**)	60	858 (100) $[M]^+$
	120	596 (47) $[M\text{-}PPh_3]^+$ 858 (100) $[M]^+$, 1193(3) $[2M\text{-}(PPh_3)_2]^{2+}$
	180	596 (47) $[M\text{-}PPh_3]^+$, 858(100) $[M]^+$, 1193(3) $[2M\text{-}(PPh_3)_2]^{2+}$, 1455(3) $[2M\text{-}PPh_3]^{2+}$
[Pd{SC(NCH_2Py)NPh}$(PPh_3)_2$]BPh_4 (**3g**)	60	872 (100) $[M]^+$
	120	610 (79) $[M\text{-}PPh_3]^+$, 872(100) $[M]^+$
[Pd{SC(N$(CH_2)_2$Py)NPh}$(PPh_3)_2$]BPh_4 (**3h**)	60	624 (12) $[M\text{-}PPh_3]^+$, 886(100) $[M]^+$
[Ni{SC(NPy)NHPh}(dppe)]BPh_4 **(3i**)	60	684 (100) $[M]^+$
[Ni{SC(NPh)$NH(CH_2)_2$Py}(dppe)]BPh_4 **(3j**)	60	712 (100) $[M]^+$
[Ni{SC($NC_6H_4NO_2$)NHPy}(dppe)]BPh_4 (**3k**)	60	729 (100) $[M]^+$
[Ni{SC($NC_6H_4NO_2$)$NH(CH_2)_2$Py}(dppe)]BPh_4 (**3l**)	60	757 (100) $[M]^+$

The PPh_3 substituted palladium complex $[Pd\{SC(NPy)NPh\}(PPh_3)_2]BPh_4$ **3f** showed a single molecular ion peak at CEV 60 V. Increase in the capillary exit voltage to 120 V resulted in the loss of one PPh_3 ligand (**Figure 3.2 a**). Further increase in the exit voltage to 180 V resulted in fragmentation of the complex (**Figure 3.2 b**). Similar fragmentation pattern was recorded for analogous complex **3g**.

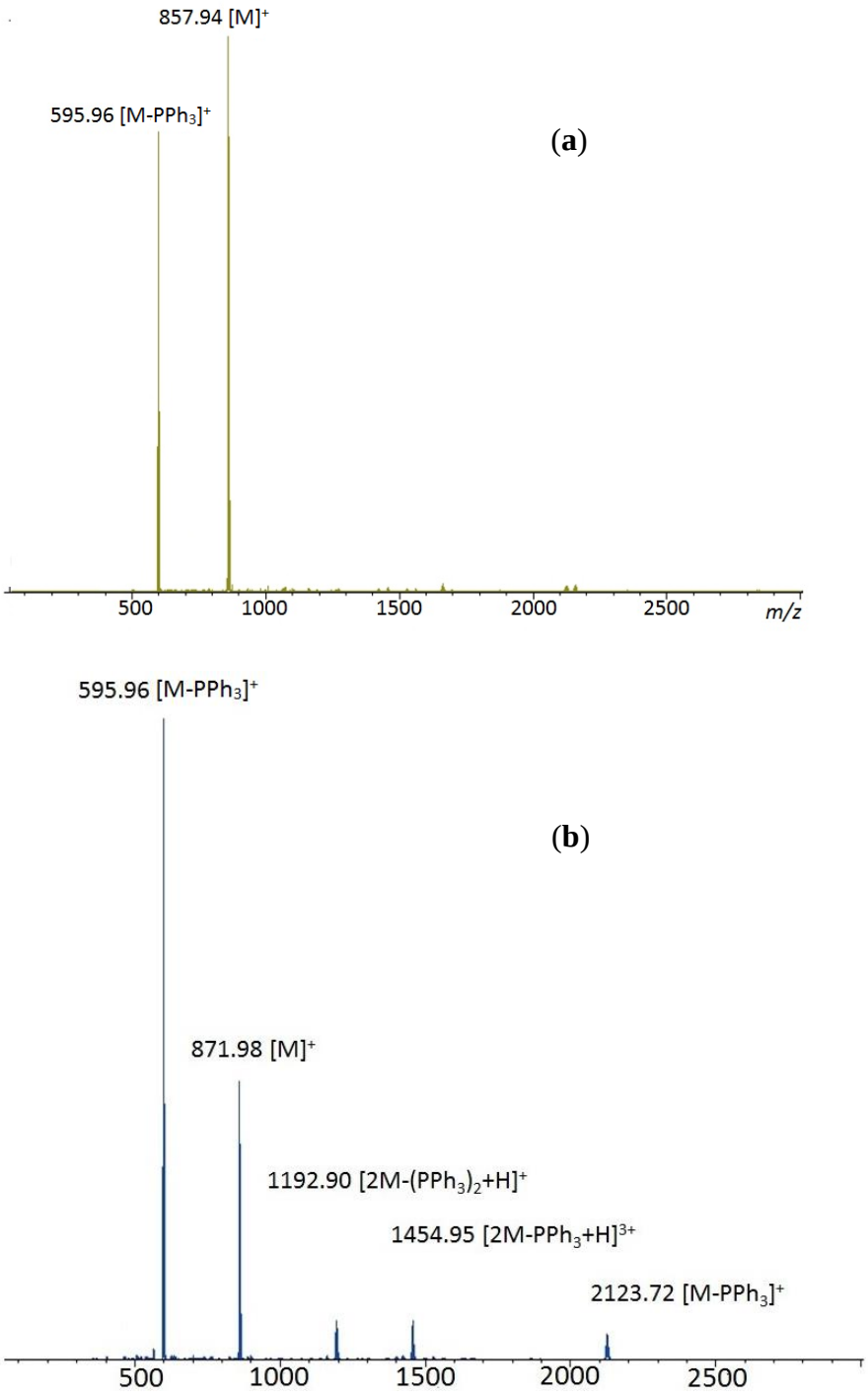

Figure 3.2: ESI-mass spectra of $[Pd\{SC(NPy)NPh\}(PPh_3)_2]BPh_4$ **3f** showing fragmentation at different capillary exit voltages (**a**) 120 V and (**b**) 180 V

The ^{1}H NMR spectrum of a freshly dissolved sample of the palladium thiourea complex **3a** showed a multiplet at δ = 1.82 - 2.05 ppm resulting from the four ethylene protons of the dppe ligand. A multiplet, appearing at 5.99 - 8.16 ppm, was assigned to the aromatic protons of the dppe and thiourea ligands. The ^{1}H NMR spectrum of the methylene-substituted complex **3b** showed the presence of a multiplet at δ = 2.8 ppm, characteristic of the four ethylene protons of the dppe ligand. The doublet at δ = 4.60 ppm was assigned to the methylene protons of the thiourea ligand. The group of multiplets at δ = 6.3 - 8.4 ppm are characteristic of aromatic protons of the dppe and thiourea ligands. Similar values were recorded for the other dppe-containing palladium complexes **3c-e** and nickel complexes **3i-l,** consistent with literature reports[13,17].

The $^{31}P\{^{1}H\}$ NMR spectrum of the complex **3a** showed two sets of doublets from the coupling of phosphorus resonances for the two inequivalent phosphorus environments. The first set appeared at 65.13 ppm and 62.67 ppm, with a $^{2}J_{(PP)}$ coupling constant of 17 Hz. The complex was left in the NMR solution for 6 days. Another spectrum collected after six days of dissolution showed the presence of another set of peaks at 66.56 ppm and 56.02 ppm, with a $^{2}J_{(PP)}$ coupling constant of 27 Hz (**Figure 3.3**).

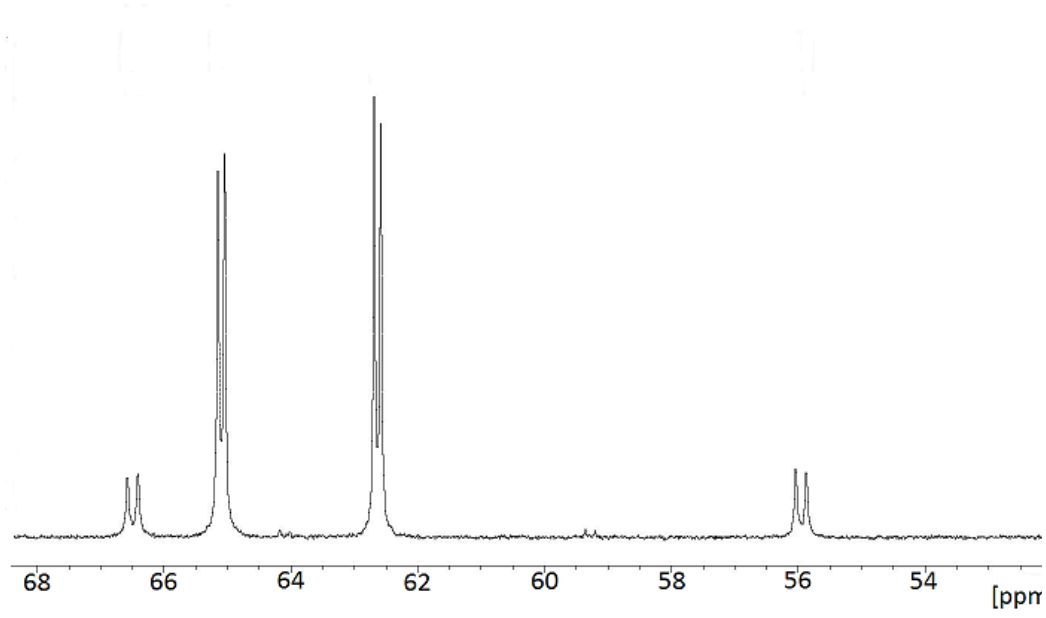

Figure 3.3: $^{31}P\{^{1}H\}$ NMR spectrum of the pyridyl and phenyl-substituted thiourea palladium complex **3a** after standing in the NMR solution for 6 days.

The presence of two sets of phosphorus resonance peaks in the spectrum indicated the possibility of isomerism in the complex. Spenceley *et al.* recently investigated isomerism in platinum thiourea dianion complexes[18]. The possibility of isomerism in pyridyl substituted thiourea complexes of platinum was also investigated in the previous chapter, and two major isomeric forms of the complexes were noted; the proximal and distal isomers. The proximal isomer was observed when the substituent bearing the pyridyl functional group was bonded to the metallacyclic nitrogen adjacent to the platinum metal centre, whereas the distal isomer was observed when the substituent bearing the pyridyl functionality was bonded to the imine nitrogen remote to the platinum centre. In line with this observation, and because the palladium complexes investigated here are similar to the platinum complexes, the two sets of peaks observed in the palladium complex **3a** above were tentatively assigned as the proximal and distal isomeric forms of the complex (**Figure 3.4**), However, evidence from the crystal structure of the complex **3a** indicates the presence Pd-N(pyridyl) coordination, resulting in a six-membered ring. As a result of this, it is unlikely that the two isomers observed in the $^{31}P\{^{1}H\}$ NMR spectrum would be the proximal and distal isomers as described in **Figure 3.4a-b**. There is however a possibility of *E/Z* isomerism at the N-distal substituents as shown in **Figures 3.4 c-d** or the presence of both the four-membered or six-membered species in the NMR solution.

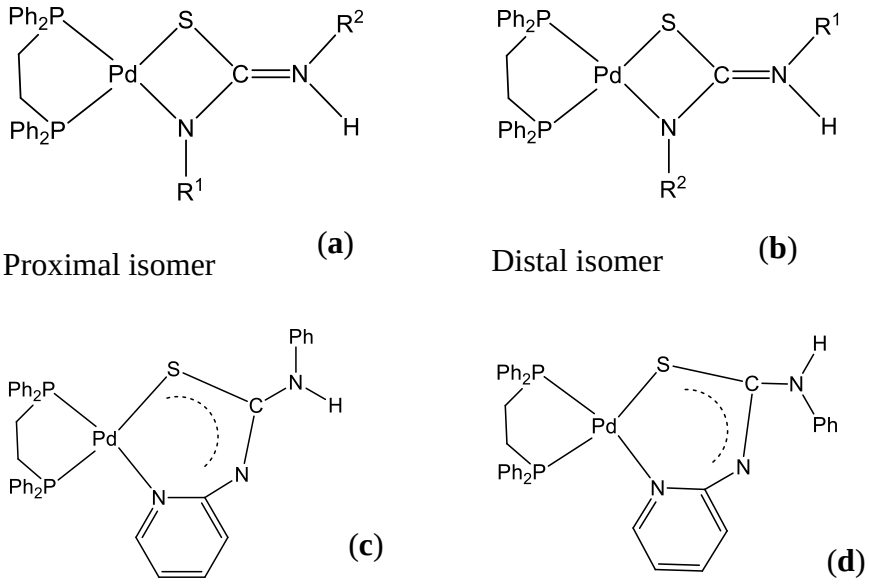

R^1 = $Py(CH_2)_n$; n = 0,1,2, R^2 = Ph, or *p*-$C_6H_4NO_2$

Figure 3.4: Possible isomers of the pyridyl-substituted thiourea palladium complexes.

$^{31}P\{^{1}H\}$ NMR spectrum of the methylenepyridyl substituted complex **3b** showed similar AB doublets to the pyridyl-substituted derivative **3a**. The peaks were observed at 63.70 ppm and 59.04 ppm, with $^{2}J_{(PP)}$ coupling constant of 24 Hz. Another set of peaks were observed just downfield of the first set of peaks at 59.58 ppm and 57.48 ppm, after about 6 days of the dissolution of the complex. $^{2}J_{(PP)}$ coupling constants of 26 and 27 Hz respectively were recorded for the complex. These coupling constant values are also close to the values recorded for the pyridyl-substituted complex **3a**. However due to absence of the Pd-P coupling constant information for these complexes it is difficult to correctly ascertain the geometry of the complexes or the type of isomerism taking place in the complexes. The ethylene pyridyl derivative **3c**, on the other hand, showed only one set of AB phosphorus resonances at 63.24 ppm and 58.48 ppm with $^{2}J_{(PP)}$ coupling constant of 26 Hz and 27 Hz respectively. There was no sign of a second isomer even after leaving the complex in the NMR solution for several days. The phosphorus resonances of all the complexes and their corresponding $^{2}J_{(PP)}$ coupling constants are presented in **Table 3.2**. The table shows significant differences in the phosphorus resonances and coupling constant values of the dppe and PPh_3 substituted complexes.

^{1}H NMR spectra of the nickel thiourea complexes were similar to those reported for their palladium counterparts. The pyridyl and phenyl-substituted complex **3j** showed two sets of multiplets at 2.42 and 5.99 ppm for ethylene protons of the dppe ligand and the aromatic protons of the dppe and thiourea ligand. The ethylenepyridyl and phenyl-substituted complex **3k** showed multiplets at 1.92 ppm for the dppe ethylene protons. Another set of peaks at 2.83 ppm was assigned to the two CH_2 protons of the thiourea ligand closest to N-H. The doublet at 3.53 ppm corresponds to the second CH_2 proton of the thiourea. The dppe and thiourea aromatic protons are shown as a set the multiplets at 6.33 ppm. The $^{31}P\{^{1}H\}$ NMR data for the nickel complexes in (**Table 3.2)** show very similar phosphorus resonances for the four nickel complexes **3i-3j.** There was no evidence of isomerism in any of the nickel complexes.

The infrared spectra of the palladium and nickel complexes are similar. Characteristic bands were evident among the complexes. The ν(C-S) bands appeared around 600-700 cm^{-1} for most of the complexes, ν(C=N) bands appeared around 1500 cm^{-1}, while ν(N-H) bands were observed around 3200 cm^{-1} for most of the complexes. The N-H bending vibrations were observed around 1600 cm^{-1}.

Table 3.2: $^{31}P\{^{1}H\}$ NMR resonances and coupling constants for palladium and nickel complexes **3a-l**

Complexes	**$^{31}P\{^{1}H\}$ NMR Chemical shifts in ppm ($^{2}J_{(PP)}$ coupling constants in Hz)**	
	Isomer 1	**Isomer 2**
[Pd{SC(NHPh)NPy}(dppe)]BPh_4 (**3a**)	66.56(27); 56.20(27)	65.13(18); 62.67(17)
[Pd{SC(NPh)NHCH_2Py}(dppe)]BF_4(**3b**)	63.70(24); 59.04(24)	59.58(26); 57.48(26)
[Pd{SC(NPh)NH(CH_2)$_2$Py}(dppe)]BF_4 (**3c**)	63.24(26); 58.67(25)	
[Pd{SC(N$C_6H_4NO_2$)NH(CH_2)$_2$Py}(dppe)]BPh_4 **(3d**)		59.27(34); 51.05(35)
[Pd{SC(N$C_6H_4NO_2$)NHPy}(dppe)](**3e**)	64.86(25); 59.20(25)	
[Pd{SC(NPy)NHPh}(PPh_3)$_2$]BPh_4 (**3f**)	33.2(26); 28.5(25)	
[Pd{SC(NCH_2Py)NHPh}(PPh_3)$_2$]BPh_4 (**3g**)	34.25(28); 26.17(26)	
[Pd{SC(N(CH_2)$_2$ Py)NHPh}(PPh_3)$_2$]BPh_4 (**3h**)	33.09(29); 26.05(29)	
[Ni{SC(NHPh)NPy}(dppe)]BPh_4 (**3i**)		61.52(50); 59.33(51)
[Ni{SC(NPh)NH(CH_2)$_2$Py}(dppe)]BPh_4 (**3j**)		61.51(50); 59.83(51)
[Ni{SC(N$C_6H_4NO_2$)NHPy}(dppe)] (**3k)**		62.43(48); 59.26(48)
[Ni{SC(N$C_6H_4NO_2$)NH(CH_2)$_2$Py}(dppe)] (**3l)**		62.44(51); 58.90(51)

3.2.3 *X-ray crystallographic studies*

3.2.3.1 Palladium thiourea complexes

In order to unambiguously establish the geometry of the complexes, good quality bright yellow crystals of four of the pyridyl substituted complexes suitable for X-ray crystallographic analysis were isolated by diffusing diethyl ether into saturated dichloromethane solutions of the complexes [Pd{SC(NHPh)NPy}(dppe)]BPh_4 **3a**, [Pd{SC(NPh)NH$(CH_2)_2$Py}(dppe)]BF_4 **3c**, [Pd{SC($NC_6H_4NO_2$)NPy)}(dppe)]BPh_4 **3d**, [Pd{SC($NC_6H_4NO_2$)NH$CH_2)_2$}(dppe)] (**3e**). The pyridyl substituted complexes **3a** (BPh_4), **3c** (BF_4) crystallised in the triclinic crystal system as tetraphenylborate and tetrafluoroborate salts respectively, while **3d** crystallised in the orthorhombic crystal system as a tetraphenylborate salt. In addition, complexes **3d** and **3e** contained solvent molecules of crystallisation in the asymmetric unit. The molecular structure of the cationic complex **3a** is shown in **Figure 3.5**, while selected bond lengths and angles are presented in **Table 3.3**.

The molecular structure of the complex **3a** shows a square planar arrangement with the Pt metal coordinated to the thiolate-S and pyridyl-N donor atoms of the monoanionic thiourea ligand. The remaining positions of the slightly distorted NP_2S square plane are occupied by the two phosphorus atoms of the dppe ligand. The root mean square deviation from the P(1)–P(2)–N(3)–S(1) plane is 0.088 Å, with the palladium metal lying 0.099 Å out of this plane. The Pd(1)–N(3)–C(8)–N(2)–C(1)–S(1) metallacycle has a six-membered ring geometry with a puckered boat configuration and an r.m.s. deviation of 0.445 Å, with the thiolate S-donor ligand being the most deviated (0.667 Å). The six-membered metallacyclic arrangement is quite different from the four-membered metalacyclic ring found in the analogous platinum thiourea complex [Pt{SC(NPh)NPy}$(PPh_3)_2$] **(2a)** reported in the previous Chapter (**Figure 2.5a**), where the Pt-metal is bound to the pyridyl-substituted thiourea N-donor ligand. Most other square planar thiourea monoanion complexes of the platinum group metals reported in the literature appear to have the four-membered metallacyclic ring geometry[13,19-22]. The inter-planar angle between the least square planes P(1)–Pt(1)–P(2) and S(1)–(N3)–C(1)–N(2)–C(8) is 71.34º. The phenyl substituent at the distal position of the complex is orthogonally out of the plane of the metallacyclic least square plane Pd(1)–S(1)–C(1)–N(2)–C(8)–N(3) by 89.98º. The Pd(1)–P(1) bond length of 2.2650(5) Å is slightly longer than the

Pd(1)–P(2) bond length 2.240(5) Å. This is as a result of the greater *trans* influence of the sulfur donor atom relative to nitrogen. Similar bond lengths have been reported for a platinum thiosemicarbazide monoanion complex [PtCl{SC(NHMe)NHNMe$_2$-*S*}(dppe)]PF$_6$ containing the dppe ligand; Pt(1)–P(1) 2.217(4) Å, Pt(1)–P(2) 2.249(4) Å[23].

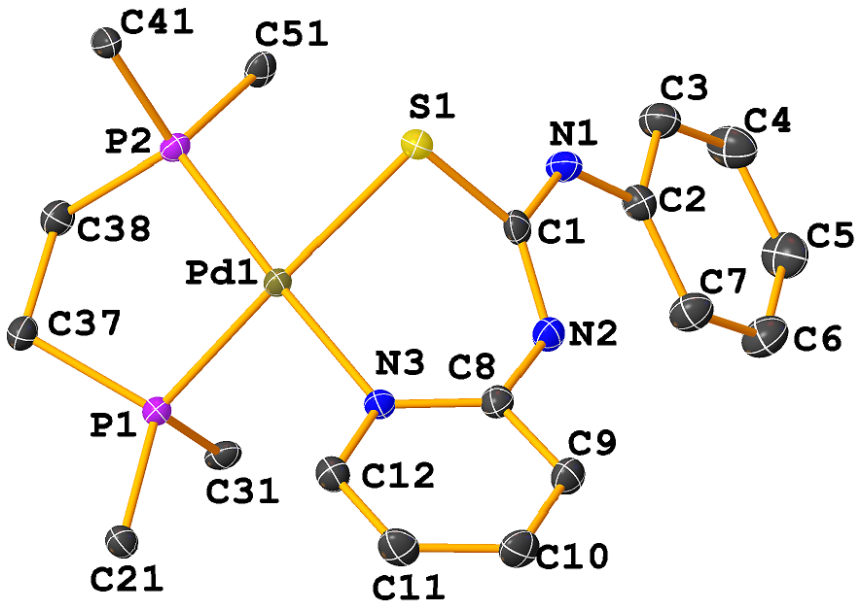

Figure 3.5: Molecular structure of the pyridyl and phenyl substituted complex [Pd{SC(NHPh)NPy}(dppe)]BPh$_4$ **3a**. Only ipso carbons of the dppe ligand are shown and BPh$_4$ anion is omitted for clarity. Ellipsoids are drawn at 50% probability.

The metallacyclic C(1)–N(2) bond distance of 1.300(3) Å is slightly shorter than the exocyclic C(1)–N(1) bond length of 1.361 Å. This is probably due to the partial double bond character of the C(1)–N(2) bond resulting from electron delocalisation from the protonated thiourea NH. The *cis* angles in P(1)-P(2)-S(1)-N(3) square plane are similar with acute values of 85.78(5)^o for the S,N-chelate and 84.92(19)^o for the angle between the phosphorus atoms. The *trans*-angles defined by S(1)–Pd(1)–P(1) and N(1)–Pd(1)–P(2) deviate from the ideal 180^o by 10^o and 3^o respectively.

The crystal structure of **3a** does not show any conventional hydrogen bonding interactions, however, the structure is held together in the crystal lattice by a number of noncovalent interactions. The two-molecule aggregates of the complex shown in **Figure 3.6** are held together by phosphane-phenyl-C–H$\cdots$S(thiolate),

thiourea-N–H·····S(thiolate) and thiourea-C–H·····S(thiolate) interactions in a tripod geometric orientation. At the rear ends are two thiourea-π---π(phosphanephenyl) interactions.

Table 3.3: Selected bond lengths and angles for the pyridyl and phenyl substituted monoanionic complex **3a**

Parameters	**Å / º**	**Parameters**	**Å / º**
Pd(1) – S(1)	2.356(5)	N(1) – C(2)	1.418(3)
Pd(1) – P(2)	2.240(5)	N(1) – C(1)	1.361(3)
Pd(1) – P(1)	2.265(5)	N(3) – C(8)	1.358(3)
Pd(1) – N(3)	2.110(17)	P(1) – C(37)	1.834(2)
S(1) – C(1)	1.784(2)	P(2) – C(38)	1.843(2)
N(2) – C(1)	1.300(3)	N(3) – Pd(1) – P(1)	97.41(5)
P(2) – Pd(1) – S(1)	91.808(19)	C(1) – S(1) – Pd(1)	122.28(19)
P(2) – Pd(1) – P(1)	84.916(19)	C(1) – N(2) – C(8)	85.46(7)
P(1) – Pd(1) – S(1)	170.167(19)	C(1) – N(1) – H(1)	130.50(18)
N(3) – Pd(1) – S(1)	85.780(5)	C(1) – N(1) – C(2)	118.76(14)
N(3) – Pd(1) – P(2)	177.560(5)	C(12) – N(3) – Pd(1)	121.40(14)

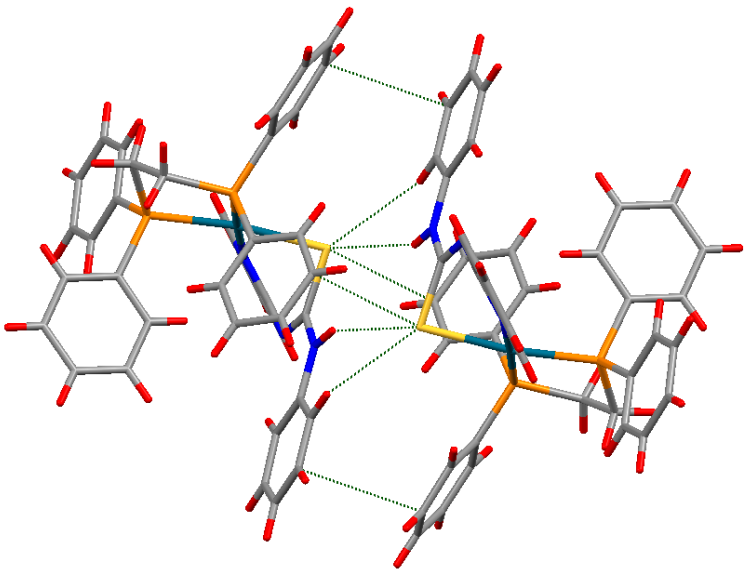

Figure 3.6: Noncovalent interactions in the structure of the pyridyl-substituted complex **3a** showing the NH---S, CH----S, C----S and C-----H interactions in the crystal lattice. Non-participating hydrogen atoms are excluded for clarity.

The molecular structure of the phenyl and ethylenepyridyl-substituted complex **3c** is presented in **Figure 3.7**, while selected bond lengths and angles are presented in **Table 3.4**. The structure shows a distorted square planar geometry for the complex with the palladium metal coordinated to the thiourea ligand through the nitrogen and sulfur donor atoms in a four-membered metallacyclic ring. The pyridyl nitrogen was not involved in coordination as was observed in the previous complex **3a**. The ethylenepyridyl functional group in this complex is bound to the protonated imine nitrogen at the distal position (that is the nitrogen remote to the palladium metal centre). This is probably to avoid steric interaction with the adjacent diphenylphosphine group. A similar coordination geometry was observed for the platinum monoanion complex **2i** reported in Chapter 2 of this thesis. The palladium coordination environment is slightly puckered with a fold angle of 10.45^{o} between the least-square planes defined by P(1)–Pd(1)–P(2) and S(1)–C(1)–N(1). The metallacyclic four-membered Pd(1)–S(1)–C(1)–N(1) ring is essentially planar with an r.m.s. deviation of 0.037 Å and the Pd metal is deviated out of the metallacyclic plane by the same value. These values are smaller than the values found in the pyridyl-substituted complex **3a** (0.009 and 0.445 Å) respectively.

The ethylenepyridyl substituent is orthogonally out of the plane of the metallacyclic ring defined by Pd(1)–S(1)–C(1)–N(1) by 75.55^{o}. The phenyl substituent attached to the metallacyclic nitrogen adjacent to the palladium metal centre is also nearly orthogonal to the plane of the metallacyclic ring by an angle of 74.65^{o}. This is probably as a result of steric interaction with the adjacent diphenyl phosphine ligand. Similar orientations were reported for a related thiourea platinum complex [Pt{(SC(=NPh)NPh}(PPh_3)$_2$] bearing a di-substituted metallacyclic ring and an adjacent triphenylphosphine ligand with near orthogonal angles of 82.87^{o} and 87.93^{o} for the two phenyl substituents respectively[24]. The difference in Pd(1)–P(1) 2.2733(6) Å and Pd(1)–P(1) 2.2503(6) Å bond lengths is a clear indication of the different *trans*-influence of the S- and N-donor ligands in the complex. The lengths of the bonds around the metallacycle are slightly different to the values observed for the pyridyl substituted complex **3a**. For example, the metallacyclic C(1)–N(1) bond distance in **3c** [1.329(3) Å] was found to be equivalent to the exocyclic C(1)–N(2) bond length [1.332(3) Å]. This is probably as a result of electron delocalisation along the metallacyclic ring resulting in lengthening of the supposedly C(1)–N(1) double bond. This is in contrast to the pyridyl-substituted

complex **3a,** where the metallacyclic C–N bond, 1.300 Å is significantly shorter than the exocyclic C–N bond, 1.361(3). The *cis*-angles in the square plane are expectedly acute with values of 69.82(6)^{o} and 84.96(2)^{o} for the S(1)–Pd(1)–N(1) and P(1)–Pd(1)–P(2). The deviation of the *trans* angles from linearity are only 7 and 9^{o} for S(1)–Pd(1)–P(1) and N(1)–Pd(1)–P(2) respectively.

Molecular packing in the complex indicates the presence of some intermolecular hydrogen bonding interactions between the thiourea N-H and the pyridyl nitrogen of a rotated molecule of the complex to form hydrogen-bonded dimer, **Figure 3.8**. The structure of the dimer is such that the ethylenepyridyl functional group is oriented perpendicularly to the plane of metallacycle in opposite directions, while the thiolate group in the complex are *trans* to one another.

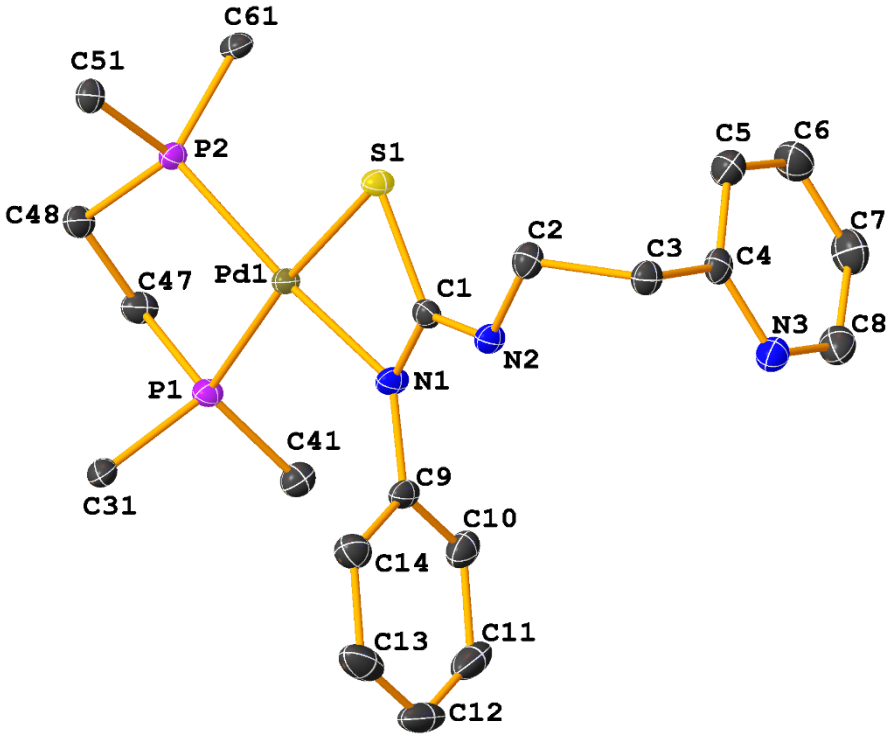

Figure 3.7: Molecular structure of the ethylenepyridyl-substituted complex [Pd{SC(NPh)NH$(CH_2)_2$Py}(dppe)]BF_4 **3c**. Only ipso carbons of the dppe ligand are shown and BF_4 anion was omitted for clarity. Thermal ellipsoids are drawn at 50% probability.

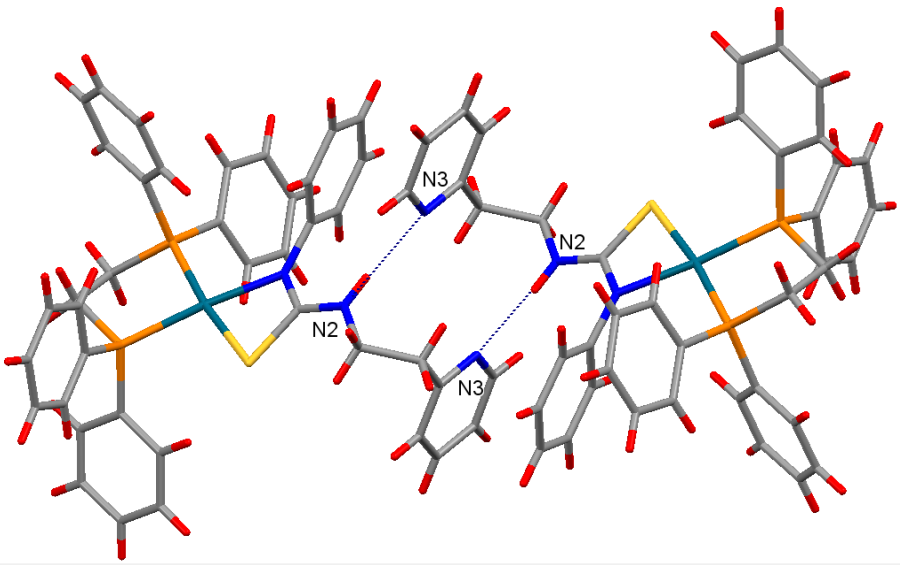

Figure 3.8: Hydrogen bonded structure of **3c** showing NH……N intermolecular interactions.

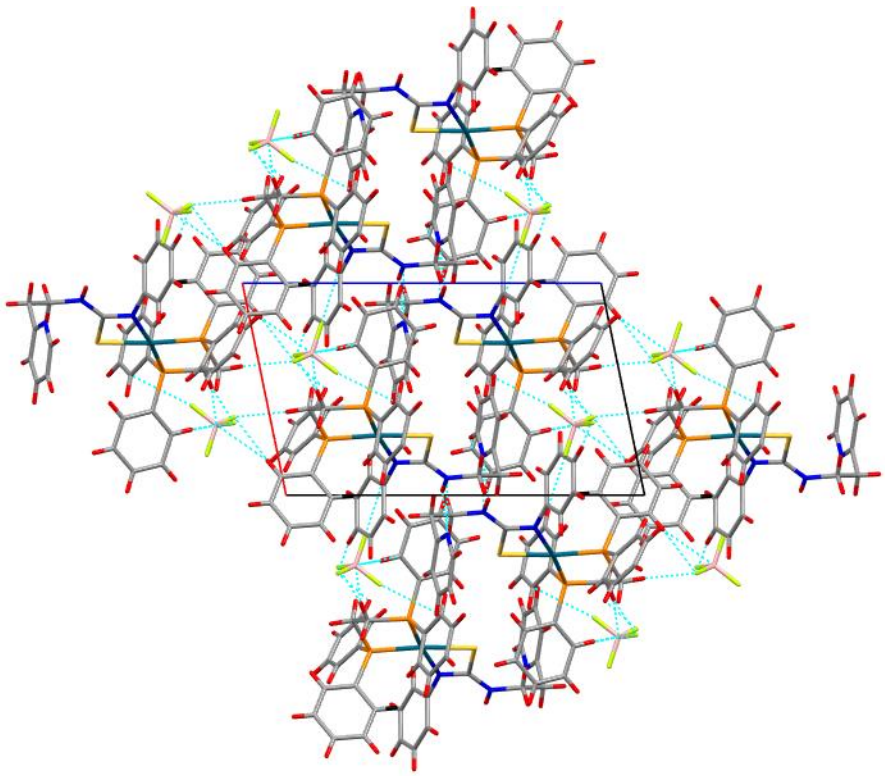

Figure 3.9: Molecular packing in the crystal structure of **3c**: a view of the unit cell contents in projection down the b-axis. The supramolecular chains are sustained by NH….N hydrogen bonds and linked together into a three-dimensional architecture by phosphane-phenyl CH----F (BF_4 anion) interactions.

The *p*-nitrophenyl and ethylenepyridyl-substituted complex **3d** crystallised from the monoclinic crystal system as a CH_2Cl_2 solvate with one BPh_4 anion in the asymmetric unit. The molecular structure of the complex is presented in **Figure 3.10.** The square planar metallacyclic geometry of the complex has some resemblance to that in **3c**, consisting of two phosphorus atoms and a palladium metal, coordinated to the sulfur and nitrogen donor atoms of the thiourea ligand. The orientation of the substituted functional groups is also similar to that in **3c**, where the pyridyl-containing functional group is bound to the protonated imine nitrogen at the distal end of the metallacyclic ring. This is quite different from the orientation observed in **3a** where the distal position is occupied by the *N*-phenyl functionality and the pyridyl group is at the proximal position. The *p*-nitrophenyl substituent in the present complex **3d** is bound to the nitrogen proximal to metallacyclic ring. In the platinum dianion analogue of this complex containing the triphenylphosphine ligand [Pt{SC(=$NC_6H_4NO_2$)NPy}(PPh_3)$_2$], reported in Chapter 2 and shown in **3.1**, there is a juxtaposition of the *N*-substituted ethylenepyridyl and *p*-nitrophenyl functionalities. This is probably due to differences in the steric bulk of the *N*-bound substituents.

The palladium coordination environment in this complex **3d** is similar to that found in **3c**, with an inter-planar angle of 8.57^o between the least square planes defined by P(1)–Pd(1)–P(2) and S(1)–C(1)–N(1). The metallacyclic ring is planar to a root mean square (r.m.s.) deviation of 0.025 Å. This is slightly smaller than the r.m.s. deviation in **3c** (0.037 Å). The palladium atom lies 0.04 Å out of the Pd(1)–S(1)–C(1)–N(1) metallacyclic plane. The *p*-nitrophenyl and ethylene pyridyl substituents bonded to the metallacyclic and imine nitrogen are out of the Pd(1)–S(1)–C(1)–N(1) least square plane by 52.21^o and 49.60^o respectively. The orientation of the ethylenepyridyl substituent is such that the pyridyl group is aligned close to the thiourea nitrogen to engage in intramolecular N-H------N-pyridyl hydrogen bonding. The general structural features of this compound are closely related to that of the phenyl-substituted analogue in (**3c**), where the ethylene pyridyl functional group also twists itself out of the plane of the metallacycle to engage in intermolecular hydrogen bonding.

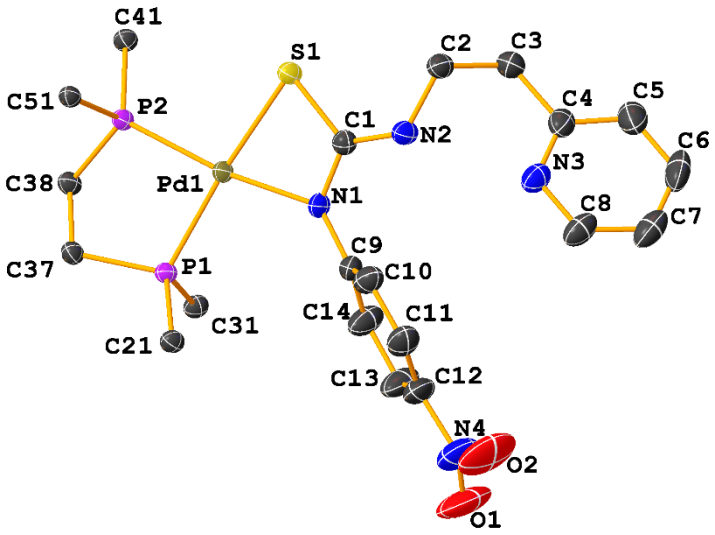

Figure 3.10: Molecular structure of the ethylenepyridyl and *p*-nitrophenyl-substituted complex **3d**. Only ipso carbons of the dppe ligand are shown for clarity. Thermal ellipsoids are drawn at 50% probability. BPh_4 anion and CH_2Cl_2 solvent are omitted for clarity.

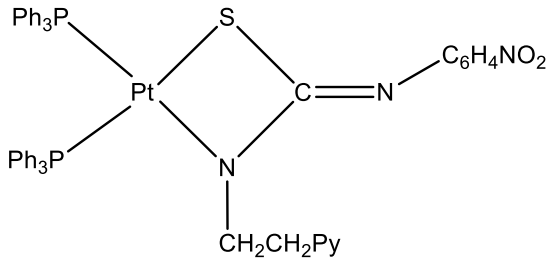

3.1

The bond lengths and angles in complexes **3c** and **3d** are also similar (**Table 3.4**). For instance, the metallacyclic C-N bonds in the complexes are similar; 1.336(3) Å **3d**, 1.329(3) Å **3c** and both exhibit dual single and double bond characteristics, probably due to electron delocalisation in the metallacyclic ring. Apart from that, the C–S bond lengths in the two complexes are similar; 1.760(2) Å **3c**, 1.752(3) Å **3d**, and slightly shorter than the average C–S bond in the tolyl–substituted palladium thiourea complex $[Pd_2(\mu\text{-}S)(\mu\text{-}dppm)_2(tolTu^{-1}\text{-}S)_2]$,1.777(8) Å[22] but longer than the C=S bond in the free thiourea ligand, 1.693(1) Å[25].

The supramolecular architecture of the complex **3d** in the asymmetric unit shows the presence of NH⋯N intramolecular hydrogen bonding; this is shown as orange coloured dashed lines in the molecular packing structure presented in **Figure 3.11**. The three-dimensional structure is also held together by some other

intermolecular interactions including; phosphane-phenyl CH·····π(pyridyl), phosphane-phenyl CH·····O(*p*-nitrophenyl), pyridyl CH·····π(BPh_4-phenyl), phosphane-phenyl CH·····Cl(CH_2Cl_2) and CH_2Cl_2 CH·····S(thiolate).

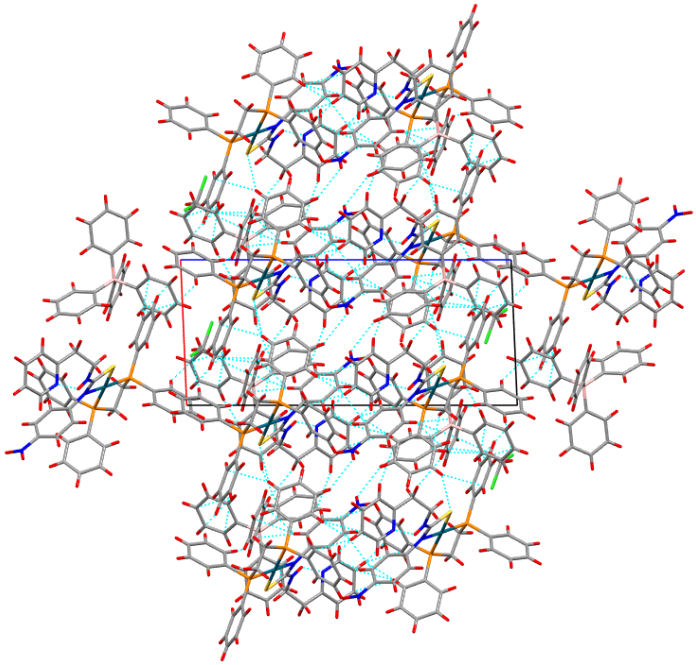

Figure 3.11: Molecular packing in the crystal of **3d**; a view of the unit cell contents in projection down the b-axis. The intramolecular hydrogen bonding interactions are shown in dashed orange lines, while the intermolecular interactions are shown in blue dashed lines.

The structure of the neutral thiourea dianion complex [Pd{SC=($NHC_6H_4NO_2$)NPy}(dppe)].CH_2Cl_2 **3e** (**Figure 3.12)** showed the expected four-membered metallacyclic ring formed by the palladium metal and the dianionic thiourea ligand. The palladium coordination sphere is slightly puckered with a fold angle of 15.10^o between the P(1)–Pd(1)–P(2) and S(1)–C(1)–N(1) least square planes. The *p*-nitrophenyl substituent in this complex is bonded to the nitrogen remote from the palladium coordination environment. This is a direct opposite of what was observed for the ethylenepyridyl-substituted monoanion complex **3d** discussed in the preceding section, where the *p*-nitrophenyl substituent was bonded to the metallacyclic nitrogen adjacent to the palladium metal. However, the *p*-nitrophenyl substituents in the two complexes adopt similar geometric positions by rotating out of plane of the metallacylic ring by 52.21 and 64.14^o in [Pd{SC=($NH(CH_2)_2Py$)$NC_6H_4NO_2$}dppe] **3d** and [Pd{SC=($NHC_6H_4NO_2$)NPy}dppe] **3e** respectively. The pyridyl substituent in the

complex **3e** is only slightly twisted out of the Pd(1)–S(1)–C(1)–N(1) plane by a fold angle of 6.34°, while the ethylenepyridyl group in **3d** is out by 49.60°. This complex, by virtue of the proximal position of the *N*-pyridyl substituent, could potentially coordinate *via* the pyridyl nitrogen to form a six-membered ring as in **3a**, but the molecular structure of the complex in **Figure 3.12** paints a different picture. The fact that the complex **3e** is a neutral complex while **3a** is a monoanion could account for the difference in the conformational arrangement of the two complexes in the solid-state.

There are also slight differences in the geometric parameters between the two complexes **3a** and **3e**. For instance, the Pd(1)–P(1) 2.2853(3) Å and Pd(1)–P(2) 2.2404(6) Å bond distances in **3e** are different and slightly longer than the values reported for the six-membered monocation complex **3a** Pd(1)–P(1) 2.2650(5) and Pd(1)–P(2) 2.240(5) Å. Apart from that, the *cis*-angles subtended by the thiourea S and N on the one hand, and the dppe phosphorus atoms, on the other hand, have acute values of 71.32(5)° and 86.23(2)° respectively and the equivalent angles in **3a** are 85.78(5)° and 84.916(19)° respectively. The *trans*-angles P(2)–Pd(1)–S(1) and P(1)–Pd(1)–N(1) are deviated from linearity by 4° and 10° respectively, in **3e**. The values are very similar to the angles reported for related compounds **3d** P(2)–Pd(1)–S(1) (5°) and P(2)–Pd(1)–N(1) (10°) and **3a** P(2)-Pd(1)-N(3) (2°), while P(1)–Pd(1)–S(1) is approximately 10°.

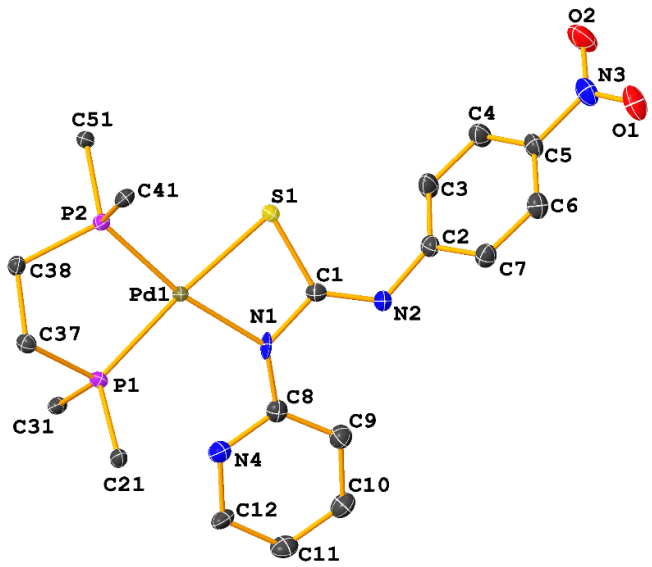

Figure 3.12: Molecular structure of the pyridyl and *p*-nitrophenyl-substituted complex **3e**. Only ipso carbons of the dppe ligand are shown for clarity. Thermal ellipsoids are drawn at 50% probability**.**

The single bond character of the metallacyclic C(1)–N(1) in the dianion complex **3e** is confirmed by the bond length 1.406(3) Å which is expectedly longer than the equivalent bond in the monoanion complexes **3a**; 1.300(3), **3c**; 1.329(3) Å and **3d**; 1.336(3) Å. The S(1)–C(1) bond length in **3e** is also elongated by a value of 0.04 Å compared to **3d** and **3c.** This apparently leads to a shortening of the exocyclic C(1)–N(2) in **3e** 1.286(3) Å compared to 1.316(3) Å and 1.332(3) Å in **3d** and **3c** respectively. This is a clear indication of the double bond character of C(1)–N(2) bond in the dianionic complex **3e** compared to the delocalised bonds in the monoanionic complexes **3d** and **3c.** The overall structural configuration of the complex **3e** is related to those in the platinum thiourea complexes **2a-2h** containing pyridyl substituted dianion ligands and reported in Chapter two of this thesis.

Apart from the apparent juxtaposition of the metallacyclic N-bound substituents in **3a** and **3e**, (where the pyridyl-bearing substituents are bonded to the palladium adjacent metallacyclic nitrogen) to **3c** and **3d (**where the pyridyl bearing substituents are bonded to the remote protonated *N*-imine nitrogen). The only obvious structural differences in the four structures presented above would be the six-membered boat like configuration of the chelate ring in **3a**, compared to the four-membered chelate rings in **3c-e**. The steric differences in the N-bearing substituents do not result in any obvious structural implications in the four complexes. However, the presence of the ethylene spacer between the pyridyl and N-H functional groups results in intermolecular and intramolecular hydrogen bonding interactions in **3c** and **3d** respectively. The dihedral angles between the metallacyclic ring and pyridyl ring separated by as much as an ethylene spacer in some cases are; **3a**; 53.6^{o}, **3c**; 74.65^{o}, **3d**; 49.60^{o}, **3e**; 6.34^{o} tend to be smaller than the corresponding dihedral angles for the phenyl or *p*-nitrophenyl substituents, **3a**; 89.8^{o}, **3c** 75.55^{o}, **3d**; 52.21^{o}, **3e**; 64.14^{o}.

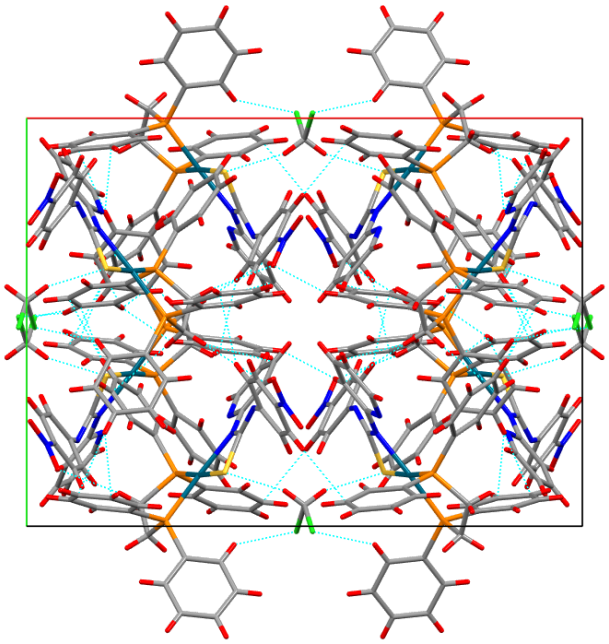

Figure 3.13: Molecular packing in the crystal of **3e**, a view of the unit cell contents in projection down the a-axis. The blue dashed lines show intermolecular phosphane-phenyl CH……O(p-nitrophenyl), phosphane-phenyl CH……Cl(CH_2Cl_2), phosphane-phenyl CH……π(CH_2Cl_2), solvent CH…….S(thiolate) interactions.

Table 3.4: Selected bond lengths and angles for palladium thiourea complexes, **3c-3e**

Bond lengths (Å) and angles (º)	**3c**	**3d**	**3e**
Pd(1) – S(1)	2.3694(5)	2.3586(6)	2.3350(5)
Pd(1) – P(1)	2.2733(6)	2.2424(6)	2.2853(5)
Pd(1) – P(2)	2.2503(6)	2.2636(6)	2.2404(6)
Pd(1) – N(1)	2.0802(19)	2.096(2)	2.0928(18)
S(1) – C(1)	1.760(2)	1.752(3)	1.797(2)
N(2) – C(1)	1.332(3)	1.316(3)	1.286(3)
N(2) – C(2)	1.460(3)	1.457(3)	1.392(3)
N(1) – C(9)	1.419(3)	1.404(3)	1.335(3)
N(1) – C(1)	1.329(3)	1.336(3)	1.406(3)
P(1) – Pd(1) – S(1)	173.23(2)	174.85(2)	175.22(2)
P(2) – Pd(1) – S(1)	101.74(2)	100.86(2)	98.493(19)
P(2) – Pd(1) – P(1)	84.95(2)	84.13(2)	86.23(2)
N(1) – Pd(1) – S(1)	69.82(6)	70.36(6)	71.32(5)
N(1) – Pd(1) – P(1)	103.45(6)	104.57(6)	103.94(5)
N(1) – Pd(1) – P(2)	171.04(6)	170.49(6)	169.72(5)
C(1) – S(1) – Pd(1)	78.59(8)	78.61(9)	80.57(7)
C(1) – N(1) – Pd(1)	100.11(15)	98.45(16)	99.31(14)
C(1) – N(1) – C(9)	122.6(2)	121.3(2)	133.66(15)
C(9) – N(1) – Pd(1)	134.02(15)	138.72(17)	126.84(19)

3.2.3.2 Nickel thiourea complexes

Two cationic nickel thiourea complexes [Ni{SC(=NPh)NH$(CH_2)_2$Py}(dppe)]BPh_4 (**3j**) and [Ni(dppe) {SC(=N$C_6H_4NO_2$)NH$(CH_2)_2$Py}]BPh_4 (**3l**) crystallised as tetraphenylborate salts in the triclinic crystal system and P-1 space group. The *p*-nitrophenyl substituted derivative of the complex crystallised with a molecule of dichloromethane solvent in the asymmetric unit. The molecular structures of the complexes presented in **Figures 3.14** and **3.15** for **3j** and **3l** respectively show square planar arrangements involving two phosphorus atoms of the dppe ligand and the thiourea S,N atoms in a metallacyclic ring. The P_2SN coordination environment in **3j** is slightly puckered to about 3.72^o between the plane P(1)–P(1)–N(1)–S(1) and Ni(1)–S(1)–N(1)–C(1), while (**3l**) is planar to 0.00^o. The P(1)–Ni(1) and P(2)–Ni(1) bond distances are slightly different in both complexes. This is a clear indication of the different *trans* influence of the thiolate and nitrogen donor ligands for both complexes. The similarity in the length of the metallacyclic and exocyclic C-N bonds distances [1.329(3) and 1.325(18) Å **3j**; 1.332(2) and 1.314(3) Å **3l**] is a pointer to the delocalisation of electron density around the metallacyclic ring and the chelated thiourea ligand. This is similar to the values reported for the metallacyclic 1.332(3) Å and exocyclic 1.3397(2) Å C-N bonds in *N*-alkyl substituted nickel thiourea complex [Ni{SC(NMe_2)NPh}(dppe)]BPh_4[13] and related cationic palladium complexes **3a**, **3c** and **3d** in the previous section. These values are, however different from the values recorded for the dianionic palladium complex **3e**, where there was a clear difference in the bond distances between the two C-N bonds; [N(1)–C(1) = 1.406(3) Å and N(2)–C(1) = 1.286(3) Å] indicating single and double bonds respectively. The C(1)-S(1) bond distances in the two complexes [1.7461(18) Å; **3j** and 1.7452(19) Å; **3l**] are similar, but shorter the than C-S bond in the dimethyl substituted nickel thiourea complex, [Ni{SC(NMe_2)NPh}(dppe)]BPh_4, 1.755(3) Å[13], and longer than the C=S double bond in PyNHC(S)NHPh 1.690(4) Å and Py$(CH_2)_2$NHCSNH$C_6H_4NO_2$ 1.693(1) Å thiourea ligands[25,26]. The Ni(1)-S(1)-N(1)-C(1) metallacycle showed a greater r.m.s. deviation from planarity in **3j** (0.037 Å) than in **3l** (0.029 Å), and the deviation of the Ni atom from the metallacycle followed an opposite trend: **3j** (0.023Å) and **3l** (0.055 Å).The pyridyl bearing substituents in the two complexes are bonded to the protonated imine nitrogen remote from the metallacyclic ring. This is different from the palladium complexes, where there was a switch in the position of the pyridyl bearing

substituent between the adjacent metallacyclic nitrogen and the protonated imine nitrogen as the steric nature of the substituents varied. The main structural differences between the two complexes **3j** and **3l** are the magnitude of the dihedral angles between the ethylene-pyridyl functional group and the metallacyclic ring in **3j** (8^{o}) compared to that in **3l** (48^{o}). Apart from that, there is a *cis* and *trans* orientation of the N-pyridyl functional group in **3j** and **3l** respectively, resulting in N-H···N intramolecular hydrogen bonding in **3l** but not in **3j**. Other geometric parameters in the complexes are similar; for example, the dihedral angles between the phenyl and *p*-nitrophenyl functional groups in **3j** and **3l** and the plane of the metallacyclic ring are 77^{o} and 69^{o} respectively. The metallacyclic S-Ni-N *cis* angles in the two complexes are similar; 74.34(5)^{o} and 74.80(5)^{o} for **3j** and **3l** respectively. The P(1)-Ni(1)-S(1) *trans*-angles in the two complexes are deviated from the idealised 180^{o} by 2^{o} and 3^{o} for **3j** and **3l** respectively, while the P(2)-Ni(1)-N(1) *trans*-angles are out of the ideal values by 12 and 10^{o} in **3j** and **3l** respectively. The structural and conformational differences in the two complexes are depicted in the structure overlay in **Figure 3.16**.

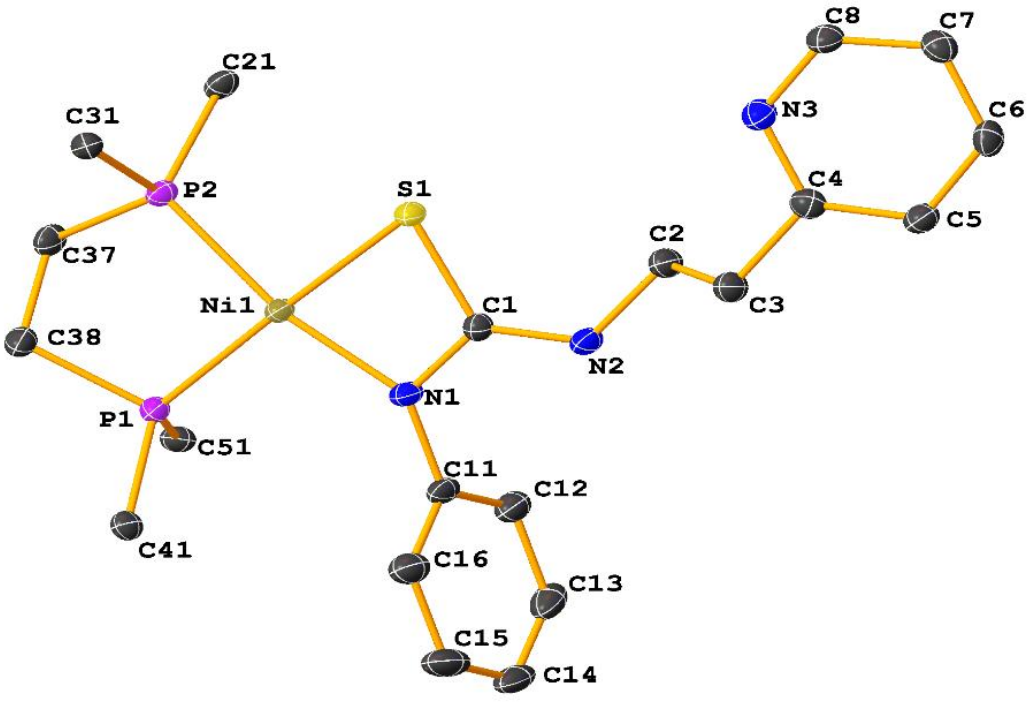

Figure 3.14: Molecular structure of the ethylenepyridyl and phenyl substituted cationic nickel complex **3j**. Only ipso carbons of the dppe ligand are shown for clarity. Thermal ellipsoids are drawn at 50% probability.

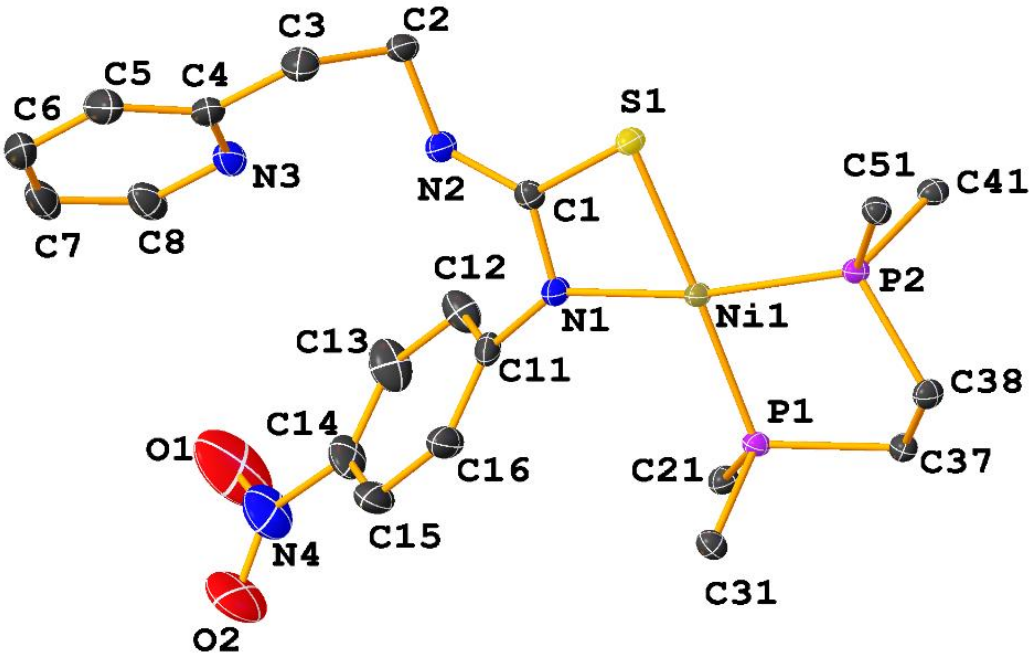

Figure 3.15: Molecular structure of the ethylenepyridyl and *p*-nitrophenyl substituted cationic nickel complex **3l**. Only ipso carbons of the dppe ligand are shown for clarity. Thermal ellipsoids are drawn at 50% probability.

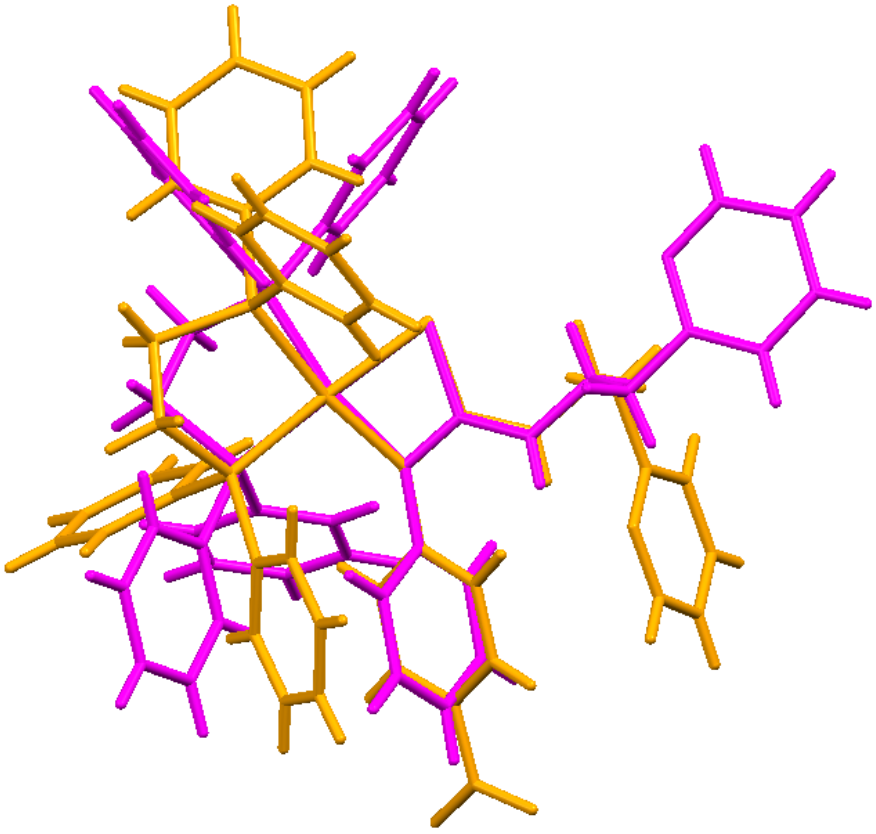

Figure 3.16: Structure overlay of the two nickel thiourea monoanionic complexes, highlighting the difference in the orientation of the pyridyl functional groups in **3j**, orange color and **3l** magenta.

Table 3.5: Selected bond lengths and angles for nickel thiourea monoanion complexes **3j** and **3l**

Bond lengths (Å) and angles (°)	**3j**	**3l**
Ni(1) – S(1)	2.2277(5)	2.2303(5)
Ni(1) – P(2)	2.1534(5)	2.1538(5)
Ni(1) – P(1)	2.1862(5)	2.1635(5)
Ni(1) – N(1)	1.9185(16)	1.9246(15)
Ni(1) – C(1)	2.4888(18)	2.4917(19)
S(1) – C(1)	1.7461(18)	1.7452(19)
N(2) – C(1)	1.325(2)	1.314(3)
N(2) – C(2)	1.464(2)	1.456(2)
N(1) – C(11)	1.419(3)	1.420(2)
N(1) – C(1)	1.329(3)	1.333(2)
P(1) – Ni(1) – S(1)	178.05(2)	176.71(19)
P(2) – Ni(1) – S(1)	94.538(19)	96.85(2)
P(1) – Ni(1) – P(2)	87.38(2)	86.12(2)
N(1) – Ni(1) – S(1)	74.34(5)	103.94(5)
N(1) – Ni(1) – P(2)	168.45(5)	170.42(5)
N(1) – Ni(1) – P(2)	103.77(5)	102.12(5)
N(1) – Ni(1) – C(1)	31.50(6)	31.97(6)
C(1) – S(1) – Ni(1)	74.49(6)	76.54(7)
C(1) – N(1) – Ni(1)	98.90(11)	98.16(12)
C(1) – N(1) – C(11)	121.17(15)	120.13(16)

3.3 Conclusions

A series of palladium and nickel complexes of asymmetrically-substituted thiourea ligands were successfully synthesised and characterised. ESI-mass spectral data for the complexes showed molecular ion fragments for loss of the bulky PPh_3 ligand at CEV above 120 V, for the PPh_3 substituted palladium complexes. $^{31}P\{^1H\}$ NMR of the pyridyl and phenyl substituted complex **3a** indicated the possibility of *E/Z* isomerism. The X-ray crystal structure showed a six-membered boat-like conformation for the palladium complex **3a**, while the other palladium, **3c-e** and nickel complexes **3j** and **3l** showed the usual four-membered distorted square planar configuration. There is an apparent juxtaposition of the pyridyl bearing functional groups between the metallacyclic and imine nitrogen of the thiourea ligands in both palladium and nickel complexes as the steric properties of the substituents changed. Introduction of an alkyl spacer between the pyridyl and thiourea functional groups of the ligand resulted in both intermolecular and intramolecular hydrogen bonding interactions between the thiourea N-H and pyridyl nitrogen. Molecular aggregation

of the crystal structures of the complexes revealed the presence of a range of non-covalent interactions in the unit cell, including $\pi^{\cdots}\pi$ and C-H$^{\cdots}$F interactions.

3.4 Experimental

3.4.1 *Synthesis of palladium and nickel thiourea complexes*

0.1 mmol equivalents of the complexes [$PdCl_2$(dppe)], [$PdCl_2(PPh_3)_2$] or [$NiCl_2$(dppe)] and asymmetrically substituted thiourea ligands of the type; PhNHC(S)NHR or $C_6H_4NO_2$NHC(S)NHR where R = Py, Py(CH_2) Py(CH_2)$_2$ (Py= pyridyl), was suspended in methanol (20 mL) in a 100 mL round bottom flask with a magnetic stirrer and refluxed for 5 min. to give a clear solution. Et_3N (2 mL) was added and the resulting mixture refluxed for 90 min. resulting in a clear solution. Solid $NaBF_4$ or $NaBPh_4$ (0.35 mmol, excess) was added to the hot solution. The cationic complexes precipitated out of the solution. In **3e**, the addition of distilled water (70 mL) precipitated the product. The suspension was cooled to room temperature and the resulting products were filtered on a Büchner funnel, washed successively with distilled water (20 mL), diethyl ether (10 mL) and then dried overnight under vacuum. [$PdCl_2(PPh_3)_2$] and [$PdCl_2$(dppe)] precursor complexes were synthesised by a method similar to the one used for *cis*-[$PtCl_2(PPh_3)_2$] and reported in Chapter two. [$NiCl_2$(dppe)] complex was synthesised using a known literature method[27].

3.4.2 *Characterisation of complexes*

*[Pd{SC(=NPy)NHPh}(dppe)]BPh_4 (**3a**)*

[$PdCl_2$(dppe)] (58 mg, 0.1 mmol), PyNHC(S)NHPh (23 mg, 0.1 mmol). Yield: 60 mg; 75 %, melting range: 120-125 ^oC. Elemental analysis %: calculated for $C_{62}H_{54}BN_3P_2PdS$; C 70.76, H 5.17, N 3.99, found; C 70.58, H 5.32, N 4.01. ESI-MS: Calculated *m/z*; 732.10 $[M]^+$, experimental *m/z*; CEV 60 V; 732.08 (100 %) $[M]^+$. $^{31}P\{^1H\}$ NMR δ ppm: isomer 1; 66.56 [$^2J_{(PP)}$ = 27 Hz] and 56.2 [$^2J_{(PP)}$ = 27 Hz]; isomer 2; 65.13 [$^2J_{(PP)}$ = 18 Hz] and 62.67 [$^2J_{(PP)}$ = 17 Hz]. ^1H NMR δ ppm: 6.5-8.1 [m, 36H, Ar], 1.9 [m, 4H, dppe]. FTIR (cm^{-1}): 3415(br) 3362(m), 3053(m), 1639(w), 1602(m), 1578(m), 1558(s), 1509(s), 1462(s), 1435(s), 1312(m), 1220(m), 1146(m), 1106(s), 1021(m), 877(m), 811(m), 774(m), 705(s), 689(s), 612(s), 534(s), 480(m).

[Pd{SC(=NPh)NHCH$_2$Py}(dppe)]BF$_4$ ***(3b)***

[PdCl$_2$(dppe)] (58 mg, 0.1 mmol), Py(CH$_2$)NHC(S)NHPh (24 mg, 0.1 mmol). Yield: 42 mg; 64 %, melting range: 132-145 ^{o}C. Elemental analysis %: calculated for $C_{39}H_{36}BF_4N_3P_2PdS$; 56.17, H 4.35, N 5.03, found; C 56.31, H 4.29, N 5.05. ESI-MS: Calculated *m/z*; 746.11 $[M]^+$, experimental *m/z* (CEV 60 V); 745.98 (100 %) $[M]^+$. $^{31}P\{^1H\}$ NMR δ ppm: proximal isomer; 59.58 [$^2J_{(PP)}$ = 26 Hz] and 57.48 [$^2J_{(PP)}$ = 26 Hz], distal isomer; 63.70 [$^2J_{(PP)}$ = 24 Hz] and 59.04 [$^2J_{(PP)}$ = 24 Hz]. ^1H NMR ($CDCl_3$) δ ppm: 6.3-8.4 [m, 32H, Ar], 4.60 [s, 2H, CH$_2$], 2.80 [d, 4H, CH$_2$ (dppe); J = 10 Hz]. FTIR (cm^{-1}): 3371(br), 3054(m) 2922(m), 1593(m), 1562(s), 1485(m), 1436(s), 1362(m), 1331(m), 1284(m), 1187(w), 1059(s), 950(w), 878(m), 819(m), 749(s), 691(s), 530(s), 483(m).

[Pd{SC(=NPh)NHPy(CH$_2$)$_2$}(dppe)]BF$_4$ ***(3c)***

[PdCl$_2$(dppe)] (58 mg, 0.1 mmol), Py(CH$_2$)$_2$NHC(S)NHPh (25.7 mg, 0.1 mmol). Yield 53 mg; 63.8 %, melting range: 146-152 ^{o}C, Elemental analysis %: calculated for $C_{40}H_{38}BF_4N_3P_2PdS$; C 56.66, H 4.52, N 4.96, found; C 56.24, H 4.41, N 4.89. ESI-MS: Calculated *m/z*; 760.13 $[M]^+$, experimental *m/z* (CEV 60 V); 759.98 (100 %) $[M]^+$. NMR: $^{31}P\{^1H\}$ NMR δ ppm: 63.24 [$^2J_{(PP)}$ = 26 Hz] and 58.67 [$^2J_{(PP)}$ = 25 Hz]. ^1H NMR δ ppm: 6.4-8.3 [m; Ar-H], 3.68 [t; 2H CH$_2$, J = 10 Hz], 2.98 [t, 2H CH$_2$, J = 11.4 Hz], 2.78 [m; 4H, CH$_2$ (dppe), J = 10.8 Hz]. FTIR (cm^{-1}): 3415(br) 2923(m), 1638(w), 1617(w), 1594(m), 1574(m), 1563(m), 1484(m), 1436(s), 1326(m), 1241(m), 1106(m), 1051(s), 998(m), 824(m), 719(m), 691(s), 530(s), 480(m)

[Pd{SC(=NC$_6$H$_4$NO$_2$)NPy(CH$_2$)$_2$}(dppe)]BPh$_4$ ***(3d)***

[PdCl$_2$(dppe)] (58 mg, 0.1 mmol), Py(CH$_2$)$_2$NC(S)NC$_6$H$_4$NO$_2$ (32 mg, 0.1 mmol). Yield: 62 mg; 69 %, melting range: 166-172 ^{o}C. Elemental analysis %: calculated for $C_{64}H_{57}BN_4O_2P_2PdS$; C 68.30, H 5.11, N 4.98, found; C 68.12, H 5.08, N 4.82. ESI-MS: Calculated *m/z*; 805.11, experimental *m/z* (CEV 60 V); 805.14(100 %) $[M]^+$. $^{31}P\{^1H\}$ NMR δ ppm; 64.86 [$^2J_{(PP)}$ = 25 Hz] and 59.2 [$^2J_{(PP)}$ = 25 Hz]. ^1H NMR δ ppm; 1.99 [m, 4H, CH$_2$ (dppe)], 2.95 [t, 2H, CH$_2$; J = 6 Hz], 3.69 [t, 2H, CH$_2$; J = 5.7 Hz], 6.5-7.9 [m, 64H, Ar-H], 8.08 [t, 1H, NH(CH$_2$), J = 5.74 Hz]. FTIR (cm^{-1}): 3415(br), 2916(s), 2850(s), 1668(m), 1638(w), 1618(m), 1537(s), 1493(m), 1420(m), 1312(s), 1105(m), 839(m), 689(m), 525(s), 480(m).

*[Pd{SC(=NPy)NC$_6$H$_4$NO$_2$}(dppe)] (**3e**)*

[PdCl$_2$(dppe)] (86 mg, 0.15 mmol), PyNHC(S)NHC$_6$H$_4$NO$_2$ (44 mg, 0.16 mmol). Yield: 72.16 mg; 55 %, melting range: 136-114 ^{o}C. Elemental analysis %: calculated for $C_{62}H_{55}BN_4O_2P_2PdS$; C 67.86, H 4.87, N 5.52 , found; C 67.58, H 4.92, N 5.49. ESI-MS: Calculated *m/z*; 777.08, experimental *m/z* (CEV 60 V); 777.13 (100 %). $^{31}P\{^1H\}$ NMR δ ppm: 59.27 [$^2J_{(PP)}$ = 34 Hz] and 51.05 [$^2J_{(PP)}$ = 35 Hz]. ^1H NMR δ ppm: 6.23-8.32 [m, 51H, Ar], 2.25-2.40 [m, 4H, CH$_2$ dppe]. FTIR (cm^{-1}): 3415(br), 3054(w), 2916(s), 2850(s) 1668(m), 1618(m), 1583(w) 1537(s), 1493(m), 1458(m), 1420(m), 1312(s), 1228(m), 1232(w), 1106(m), 1028(w), 998(w), 839(m), 743(m), 689(m), 525(s), 480(m).

*[Pd{SC(=NPy)NHPh}(PPh$_3$)$_2$]BPh$_4$ (**3f**)*

[PdCl$_2$(PPh$_3$)$_2$] (56 mg, 0.08 mmol), PyNHC(S)NHPh (22 mg, 0.1 mmol). Yield: 40 mg; 51 %, melting range: 140-152 ^{o}C. Elemental analysis %: calculated for $C_{72}H_{60}N_3P_2PdS$; C 70.76, H 5.17, N 3.99, found %; C 70.72, H 5.19, N 4.02. ESI-MS: Calculated *m/z* ; 858.15, experimental *m/z* (CEV 60 V); 857.99 (100%) $[M]^+$, (CEV 120 V) 595.91 (47%) $[M\text{-}PPh_3]^+$, 857.99 (100 %) $[M]^+$, 1192.87 (3%) $[2M\text{-}(PPh_3)]^{2+}$, 1454.91 (3 %) $[2M\text{-}PPh_3]^{2+}$. $^{31}P\{^1H\}$ NMR δ ppm: 33.2 [$^2J_{(PP)}$ = 26 Hz] and 28.5 [$^2J_{(PP)}$ = 25 Hz]. ^1H NMR (CDCl$_3$) δ ppm: 6.4-8.0 [m, 60H, Ar-H]. FTIR (cm^{-1}): 3412(br), 3053(m), 2983(w), 1600(w), 1563(m), 1493(w), 1463(s), 1433(s), 1349(w), 1310(m), 1223(w), 1149(m), 1149(w), 1096(m), 999(m), 843(m), 742(s), 704(s), 691(s), 612(m), 532(s), 510(m), 459(w).

*[Pd{SC(=NCH$_2$Py)NHPh}(Ph$_3$P)$_2$]BPh$_4$ (**3g**)*

[PdCl$_2$(PPh$_3$)$_2$] (56 mg, 0.08 mmol), PyCH$_2$NHC(S)NHPh (24 mg, 0.1 mmol). Yield: 35 mg; 45 %, melting range: 148-156 ^{o}C. Elemental analysis %: calculated for $C_{67}H_{57}BN_3P_2PdS$; C 72.14, H 5.15, N 3.77, found; C 72.16, H 5.19, N 3.78. ESI-MS: Calculated *m/z* 872.16, experimental *m/z* (CEV 60 V); 871.97 (100 %) $[M]^+$, (CEV 120 V); 609.94 (79 %) $[M\text{-}PPh_3]^+$, 871.97 (100 %) $[M]^+$. $^{31}P\{^1H\}$ NMR δ ppm: 34.25 [$^2J_{(PP)}$ = 28 Hz] and 26.17 [$^2J_{(PP)}$ = 26 Hz]. ^1H NMR δ ppm: 3.26 [d, CH$_2$ (NH); J = 5.8 Hz], 6.4-8.0 [m, 60 H, Ar-H]. FTIR (cm^{-1}): 3551(br), 3473(br), 3413(m), 3053(w) 2983(w), 1638(w), 1617(m), 1562(w), 1535(w), 1480(s), 1435(s), 1407(w), 1328(w) 1312(w), 1247(w), 1184(w), 1149(w), 1095(s), 999(m) 846(m), 743(s), 703(s), 688(m), 612(m), 520(s), 509(m), 493(w).

*[Pd{SC(=N(CH$_2$)$_2$Py)NHPh}(Ph$_3$P)$_2$]BPh$_4$ (**3h**)*

[PdCl$_2$(PPh$_3$)$_2$] (56 mg, 0.08 mmol), Py(CH$_2$)$_2$NHC(S)NHPh (25 mg, 0.1 mmol). Yield: 67 mg; 83 %, melting range: 172-195 ^{o}C. Elemental analysis %: calculated for $C_{68}H_{59}BN_3P_2PdS$; C 72.31, H 5.27, N 3.72. found; C 72. 37, H 5.26, N 3.69. ESI-MS: Calculated *m/z* 886.18, experimental *m/z* (CEV 60 V); 623.95(12 %) [M-PPh$_3$]$^+$, 885.98 (100 %) [M]$^+$. ^{31}P{^{1}H} NMR δ ppm: 34.09 [^{2}J$_{(PP)}$ = 29 Hz] and 26.05 [^{2}J$_{(PP)}$ = 29 Hz]. ^{1}H NMR δ ppm: 6.11-7.8 [m, 55 H, Ar-H), 2.81 [t, 2H, CH$_2$; J = 5.9 Hz], 2.45 [dd, 2H, CH$_2$; J = 7.6 Hz, ^{3}J$_{(PH)}$ = 21 Hz]. FTIR (cm^{-1}): 3416(br), 3134(m), 3035(m) 2984(w), 1638(s), 1618(m) 1592(w), 1562(s), 1479(s), 1434(s), 1349(m) 1327(m), 1248(w), 1180(w), 1149(m), 1095(m), 1031(m), 998(m), 840(m) 741(s), 704(s), 691(m), 604(s), 520(m), 492(w).

*[Ni{SC(=NPy)NHPh}(dppe)]BPh$_4$ (**3i**)*

[NiCl$_2$(dppe)] (37 mg, 0.07 mmol), PyNHC(S)NHPh (23 mg, 0.1 mmol). Yield: 35 mg; 59 %, melting range: 182-186 ^{o}C. Elemental analysis %: calculated for $C_{62}H_{54}BN_3NiP_2S$; C 74.12, H 5.42, N 4.17, found; C 74.09, H 5.38, N 4.23. ESI-MS: Calculated *m/z* 684.13, experimental *m/z*; (CEV 60 V) 683.98 (100 %) [M]$^+$. ^{31}P{^{1}H} NMR δ ppm: 61.52 [^{2}J$_{(PP)}$ = 50 Hz] and 59.33 [^{2}J$_{(PP)}$ = 51 Hz]. ^{1}H NMR δ ppm: 2.42 [m, 4H, CH$_2$ (dppe)], 5.99-8.04 [m, 52H, Ar-H]. FTIR (cm^{-1}): 3415(br), 3375(w), 3054(w) 2983(m), 1603(w), 1579(w), 1558(m), 1510(s), 1462(s), 1435(s), 1312(w), 1221(w), 1147(m), 1104(m), 998(s), 875(w), 742(m), 706(s), 690(s) 533(s), 481(m).

*[Ni{SC(=N(CH$_2$)$_2$Py)NHPh}(dppe)]BPh$_4$ (**3j**)*

[NiCl$_2$(dppe)] (37 mg, 0.07 mmol), Py(CH$_2$)$_2$NHC(S)NHPh (26 mg, 0.1 mmol). Yield: 45 mg; 71 %, melting range: 188-192 ^{o}C. Elemental analysis %: calculated for $C_{64}H_{58}BN_3NiP_2S$; C 74.44, H 5.66, N 4.07, found; C 74.62, H 5.68, N 4.02. ESI-MS: Calculated *m/z* 712.16, experimental *m/z*; (CEV 60 V) 712.08 (100 %) [M]$^+$. ^{31}P{^{1}H} NMR δ ppm: 61.52 [^{2}J$_{(PP)}$ = 50 Hz] and 59.33 [^{2}J$_{(PP)}$ = 51 Hz]. ^{1}H NMR δ ppm: 1.92 [m, 4H, CH$_2$ (dppe); J = 6.5 Hz, ^{3}J$_{(PH)}$ = 27 Hz], 2.83 [d, 2H CH$_2$, J = 5.7 Hz], 3.53 [dd, 2H CH$_2$, J = 5.7, 8.2 Hz], 6.3-7.9 [m, 27H, Ar-H). FTIR (cm^{-1}): 3437(br), 3353(w), 3054(m) 2982(m), 1594(w), 1567(s), 1483(m), 1435(s), 1344(m), 1221(w), 1149(w), 1103(s), 998(m), 875(w), 746(w), 706(s), 690(s), 612(s), 533(s), 482(m).

*[Ni{SC(=NPy)NHC$_6$H$_4$NO$_2$}(dppe)]BPh$_4$ (**3k**)*

[NiCl$_2$(dppe)] (37 mg, 0.07 mmol), PyNHC(S)NHC$_6$H$_4$NO$_2$ (28 mg, 0.1 mmol). Yield: 46 mg; 89 %, melting range: 216-220 ^{o}C. Elemental analysis %: calculated for $C_{62}H_{53}BN_4NiO_2P_2S$; C 70.95, H 5.09, N 5.34, found; C 70.88, H 5.12, N 5.28. ESI-MS: Calculated *m/z* 729.12, experimental *m/z*; (CEV 60 V) 728.97 (100 %) $[M]^+$. $^{31}P\{^1H\}$ NMR δ ppm: 62.43 [$^2J_{(pp)}$ = 48 Hz] and 59.26 [$^2J_{(PP)}$ = 48 Hz]. ^1H NMR ($CDCl_3$) δ ppm: 1.98 [m, 4H CH_2 (dppe), J = 5.7, 23 Hz], 6.53-8.27 [m 49H, Ar-H]. FTIR (cm^{-1}): 3473(br), 3413(w), 3080(w) 2927(w), 1607(s), 1595(s), 1559(s), 1532(m), 1488(s), 1463(s) 1425(s), 1407(s), 1349(m) 1344(m), 1247(m), 1220(w), 1148(s), 1112(m), 1019(s), 850(s), 781(s), 749(m), 688(m), 618(m), 532(w), 495(w).

*[Ni{SC(=NH(CH$_2$)$_2$Py)N(C$_6$H$_4$NO$_2$)}(dppe)]BPh$_4$ (**3l**)*

[NiCl$_2$(dppe)] (79 mg, 0.15 mmol), Py(CH$_2$)$_2$NHC(S)NHC$_6$H$_4$NO$_2$ (45 mg, 0.15 mmol).Yield: 89 mg; 71 %, melting range: 172-180 ^{o}C. Elemental analysis %: calculated for $C_{64}H_{57}BN_4NiO_2P_2S$; C 71.33, H 5.33, N 5.20, found; C 70.98, H 5.36, N 5.18. ESI-MS: Calculated *m/z* 757.15, experimental *m/z*; (CEV 60 V) 756.98(100 %) $[M]^+$. $^{31}P\{^1H\}$ NMR δ ppm; 62.44 [$^2J_{(PP)}$ = 51 Hz] and 58.90 [$^2J_{(PP)}$ = 51 Hz]. ^1H NMR δ ppm: 1.86 [m, 4H (CH_2) (dppe)], 2.85 [d, 2H (CH_2) J = 11 Hz], 3.50 [d, 2H (CH_2), J = 6.3 Hz], 6.48-7.96 [m, 50H, Ar-H]. FTIR (cm^{-1}): 3437(br), 3353(w), 3054(m) 2982(m), 1594(w), 1567(s), 1483(m), 1435(s), 1344(m), 1221(w), 1149(w), 1103(s), 998(m), 875(w),746(w), 706(s), 690(s), 612(s), 533(s), 482(m).

3.4.3 *X-ray crystallographic analyses*

Crystal data and refinement details for the investigated complexes are included in **Table 3.6** and **3.7**. The intensity was measured at T = 100 K on a SuperNova Dual Atlas S2 diffractometer fitted with Cu Kα radiation (λ=1.54184 Å). Data reduction, including absorption correction, was accomplished with CrysAlisPro[28]. The structures were solved by intrinsic phasing method on ShelXT[29] and refined (with anisotropic displacement parameters and C-bound H atoms in the riding model approximation) on F^2 [30]. Some residual electron density peaks in **3d** and **3e**, evident after the complex molecule was refined, were modelled as H_2O molecule and CH_2Cl_2 solvents of crystallisation. The molecular structure diagrams were

generated with Olex11 Draw [31] with 50% displacement ellipsoids, while molecular aggregation and packing diagrams were generated in Mercury[32]

Table 3.6: Crystallographic refinement parameters for complexes, **3a**, **3c** and **3d**

Complexes	**3a**	**3c**	**3d**
Formula	$C_{62}H_{54}BN_3P_2PdS$	$C_{40}H_{38}BF_4N_3P_2PdS$	$C_{38}H_{34}N_4O_2P_2PdS$
Formula weight g/mol	1052.29	847.94	820.61
Temperature /K	100.01(10)	100.0(3)	100.3(7)
Crystal System	triclinic	triclinic	orthorhombic
Space group	P-1	P-1	Pbcn
a/ Å	11.5969(3)	9.5485(2)	21.7422(3)
b/ Å	14.9686(3)	12.6418(3)	15.9554(3)
c/ Å	16.0266(4)	15.9336(5)	20.2577(3)
α/º	82.103(2)	83.332(2)	90
β/º	71.956(2)	78.332(2)	90
γ/º	74.956(2)	89.068(2)	90
Volume/Å ^{3}	2538.73(11)	1870.81(8)	7027.2(18)
Z	2	2	8
ρ_{calc}g/cm^3	1.377	1.505	1.5511
μ/mm^{-1}	4.262	5.784	6.711
F (000)	1088	864.0	
Crystal Size/mm^3	0.262x0.149x0.124	0.131x0.163x0.211	0.18x0.14x0.12
2Θ(º)	8.212 to 147.85	7.04 to 148.	6.88-146
Goof	1.055	1.040	1.036
R-Factor (%)	3.07	3.03	2.80
Reflections used	10139	7462	27398
Total reflections	45711	35255	6986
Abs correction	Gaussian	multiscan	multiscan

Table 3.7: Crystallographic refinement parameters for complexes, **3e**, **3j** and **3l**

Complexes	**3e**	**3j**	**3l**
Formula	$C_{65}H_{59}BCl_2N_4O_2P_2PdS$	$C_{64}H_{59}BN_3NiP_2S$	$C_{66}H_{59}BCl_2N_3NiO_2P_2S$
Formula weight g/mol	1210.27	1033.66	1160.58
Temperature /K	100.01(10)	99.98(10)	99.99
Crystal system	triclinic	triclinic	triclinic
Space group	P-1	P-1	P-1
a/ Å	9.3208(2)	10.4982(3)	9.3401(2)
b/ Å	14.4565(3)	12.2111(4)	14.3393(4)
c/ Å	21.0976(4)	21.1514(6)	21.1146(5)
α/°	88.034(2)	96.164(3)	91.478(2)
β/°	87.555(2)	92.156(2)	93.528(2)
γ/°	89.739(2)	100.728(3)	90.425(2)
Volume/(Å^3)	2838.55(10)	2644.09(14)	2821.48(12)
Z	2	2	2
ρ_{calc} g/cm^3	1.416	1.298	1.366
μ/mm^{-1}	4.765	1.803	2.631
F (000)	1248.0	1086.0	1210.0
Crystal Size/mm^3	0.202 x 0.183 x 0.082	0.192 x 0.111 x 0.097	0.142 x0.084x 0.041
2Θ(°)	7.3 - 148.1	7.418 - 148.274	7.368 - 148.076
Goof	1.037	1.058	0.871
R-Factor (%)	3.55	3.53	3.59
Reflections used	11291	10313	11226
Total reflections	40120	29604	41521
Abs correction	Gaussian	multiscan	Gaussian

3.5 References

1. Aguilar, D.; González, G.; Villuendas, P.; Urriolabeitia, E. P. *J. Organomet. Chem.* **2014**, *767*, 27-34.
2. Barzegar-Kiadehi, S. R.; Golbon Haghighi, M.; Jamshidi, M.; Notash, B. *Inorg. Chem.* **2018**, *57*, 5060-5073.
3. Bielsa, R.; Navarro, R.; Soler, T.; Urriolabeitia, E. P. *Dalton Trans.* **2008**, 1203-1214.
4. Dervisi, A. *Annual Reports Section A(Inorganic Chemistry)* **2009**, *105*, 248-260.
5. Grushin, V. V. *Chem. Rev.* **2004**, *104*, 1629-1662.
6. Negishi, E.; Takahashi, T.; Baba, S.; Van Horn, D. E.; Okukado, N. *J. Am. Chem. Soc.* **1987**, *109*, 2393-2401.
7. Gabriele, B.; Salerno, G.; Costa, M.; Chiusoli, G. P. *J. Organomet. Chem.* **1995**, *503*, 21-28.
8. Vizer, S. A.; Yerzhanov, K. B.; Al Quntar, A. A. A.; Dembitsky, V. M. *Tetrahedron* **2004**, *60*, 5499-5538.
9. Nan, Y.; Miao, H.; Yang, Z. *Org. Lett.* **2000**, *2*, 297-299.
10. Wu, X.-F.; Neumann, H.; Beller, M. *Chem. Rev.* **2012**, *113*, 1-35.
11. Liu, B.; Tian, H. *Chem. Lett.* **2005**, *34*, 686-687.
12. Su, W.; Cao, R.; Hong, M.; Wu, D.; Lu, J. *J. Chem. Soc., Dalton Trans.* **2000**, 1527-1532.
13. Yuen, H. Y.; Henderson, W.; Oliver, A. G. *Inorg. Chim. Acta* **2011**, *368*, 1-5.
14. Binzet, G.; Gumus, I.; Dogen, A.; Flörke, U.; Kulcu, N.; Arslan, H. *J. Mol. Struct.* **2018**, *1161*, 519-529.
15. del Campo, R.; Criado, J. J.; García, E.; Hermosa, M. a. R.; Jimenez-Sanchez, A.; Manzano, J. L.; Monte, E.; Rodrıguez-Fernández, E.; Sanz, F. *J. Inorg. Biochem.* **2002**, *89*, 74-82.
16. Kandil, S. S.; Katib, S. M.; Yarkandi, N. H. *Transition Met. Chem.* **2007**, *32*, 791-798.
17. Hayter, R. G. *J. Am. Chem. Soc.* **1962**, *84*, 3046-3053.
18. Spenceley, J. E.; Henderson, W.; Lane, J. R.; Saunders, G. C. *Inorg. Chim. Acta* **2015**, *425*, 83-91.
19. Henderson, W.; Nicholson, B. K.; Dinger, M. B.; Bennett, R. L. *Inorg. Chim. Acta* **2002**, *338*, 210-218.
20. Henderson, W.; Nicholson, B. K.; Rickard, C. E. F. *Inorg. Chim. Acta* **2001**, *320*, 101-109.
21. Henderson, W.; Rickard, C. E. F. *Inorg. Chim. Acta* **2003**, *343*, 74-78.

22. Okeya, S.; Kameda, H.; Kawashima, H.; Shimomura, H.; Nishioka, T.; Isobe, K. *Chem. Lett.* **1995**, *24*, 501-502.

23. Burrows, A. D.; Coleman, M. D.; Mahon, M. F. *Polyhedron* **1999**, *18*, 2665-2671.

24. Henderson, W.; Kemmitt, R. D. W.; Mason, S.; Moore, M. R.; Fawcett, J.; Russell, D. R. *J. Chem. Soc., Dalton Trans.* **1992**, 59-66.

25. Valdés-Martínez, J.; Hernández-Ortega, S.; Ackerman, L. J.; Li, D. T.; Swearingen, J. K.; West, D. X. *J. Mol. Struct.* **2000**, *524*, 51-59.

26. Giesen, J. M.; Claborn, K. A.; Goldberg, K. I.; Kaminsky, W.; West, D. X. *J. Mol. Struct.* **2002**, *613*, 223-233.

27 Booth, G.; Chatt, J. *J. Chem. Soc.* **1965**, 3238-3241.

28. Rigaku Oxford Diffraction CrysAlisPro Software System, version 1.171. 38.41 l, Rigaku Coorporation. Oxford, UK, (2015).

29. Sheldrick, G. M. *Acta Crystallogr., Sect. A: Found. Adv* **2015**, *71*, 3-8.

30. Sheldrick, G. M. *Acta Crystallogr., Sect. C: Struct. Chem.* **2015**, *71*, 3-8.

31. Dolomanov, O. V.; Bourhis, L. J.; Gildea, R. J.; Howard, J. A. K.; Puschmann, H. *J. Appl. Crystallogr.* **2009**, *42*, 339-341.

32. Macrae, C. F.; Bruno, I. J.; Chisholm, J. A.; Edgington, P. R.; McCabe, P.; Pidcock, E.; Rodriguez-Monge, L.; Taylor, R.; Streek, J. v. d.; Wood, P. A. *J. Appl. Crystallogr.* **2008**, *41*, 466-47.

Chapter 4

Ruthenium, rhodium and iridium complexes of pyridyl-substituted thiourea ligands

4.1 Introduction

Half-sandwich arene Ru, Cp*Rh and Cp*Ir complexes are a versatile class of organometallic compounds that have found potential applications in many areas [1,2]. This is due to their ease of synthesis, high yield, high stability and excellent solubility in both organic and aqueous solutions[3]. The metal precursors for this group of compounds are usually dimers of the form $[(\eta^6\text{-}C_6Me_6/\text{benzene/cymene})RuCl_2]_2$ and $[Cp^*MCl_2]_2$ (M = Rh, Ir). These dimers undergo a variety of chloride-bridge cleavage reactions resulting in the formation of neutral or cationic mononuclear complexes. These compounds have been found to possess biological as well as industrial applications [4-6]. Ruthenium arene complexes have displayed remarkable activity in medicinal chemistry as potential metal-based anti-cancer drugs[7-11]. The most prominent of these complexes are $[Ru(\eta^6\text{-arene})Cl(en)]^+$ (en = ethylenediamine)[12] and $[Ru(cymene)Cl_2(PTA)$ (RAPTA) (PTA = 1,3,5-triaza-7-phosphaadamantane)[13,14]. The ethylenediamine-substituted ruthenium(II)-arene complexes and their derivatives have been reported to bind to DNA, thus leading to cytotoxicity towards cancer cells[15]. The RAPTA compounds and their derivatives, on the other hand, have been the subject of several cytotoxicity and anti-cancer studies and found to possess excellent activity [14,16,17].

The pentamethylcyclopentadienyl rhodium and iridium complexes have also been studied for their antitumor and anti-proliferative activities[18-20]. The nature of the arene or Cp* ligand, the functionality of the chelating ligands and the leaving group is also a factor in the reactivity, chemical and biological properties of these Ru, Rh and Ir complexes [3,4]. The choice of pyridyl ligands in this chapter is significant in the sense that the pyridyl functionality increases the selectivity of the ligand towards the metal with a possibility of altering the geometric, chemical and biological properties of the resulting complexes. A number of ruthenium, rhodium and iridium complexes containing pyridyl thiourea ligands have been reported in the literature[3,4,21,22].

A review of the coordination chemistry of Ru, Rh and Ir thiourea complexes in Chapter 1 show that most of these complexes contain the monodentate S-bonded thiourea ligands or the bidentate thiourea ligands binding through N, S donor atoms, and containing one or more chloride anions in the complex. In this chapter, the synthesis of half sandwich arene ruthenium, rhodium and iridium complexes containing pyridyl thiourea ligands (arene = *p*-cymene and C_6Me_6 for Ru; Cp* for Rh and Ir) is reported. The effect of a methylene and ethylene spacer between the pyridyl and thiourea functionality on the geometry and supramolecular properties of the complexes is explored. Further, the effect of substitution of the chlorido-ligand with the bulky PPh_3 ligand on the coordination geometry of the half sandwich complexes is investigated.

4.2 Results and discussion

4.2.1 *Ruthenium thiourea complexes*

The reaction of dimeric ruthenium complex $[(\eta^6\text{-}C_6Me_6)RuCl_2]_2$ with 2 molar equivalents of pyridyl substituted ligands $Py(CH_2)_nNHC(S)NHR$ (n = 0, 2 and R = Ph, C_6H_4OMe) and excess triethylamine in refluxing methanol, followed by the addition of solid NH_4PF_6 and water resulted in mononuclear ruthenium bis(thiourea) complexes **4a**-**4b** and mononuclear tridentate ruthenium thiourea complexes **4c**-**4d** (**Scheme 4.1**), depending on the length of the alkyl spacer.

The complex **4a** gave a *pseudo*-molecular ion peak at *m/z* 721.07 in the positive ion electrospray ionisation (ESI) mass spectrum at capillary exit voltage (CEV) of 60 V. This peak was assigned to $[M+H]^+$ ions of the neutral bis(thiourea) complex, M = $[(\eta^6\text{-}C_6Me_6)Ru\{SC(=NPy)NPh\}\{SC(NPy)NHPh\}]$ **4a**. A higher capillary exit voltage of 150 V resulted in fragmentation of the complex to give molecular ion peak at *m/z* 492.04, $[M\text{-}PyNC(S)NHPh]^+$ formed by loss of one molecule of the ligand (as a monoanion) from the neutral complex (**Figure 4.1**). Further increase of the CEV to 180 V did not result in further fragmentation of the complex. The *p*-methoxyphenyl substituted pyridyl thiourea complex **4b** showed similar molecular ions at *m/z* 782.05 and 522.04 for the $[M+H]^+$ and $[M\text{-}PyNCSNHC_6H_4OMe]^+$ ions respectively (**Table 4.1**).

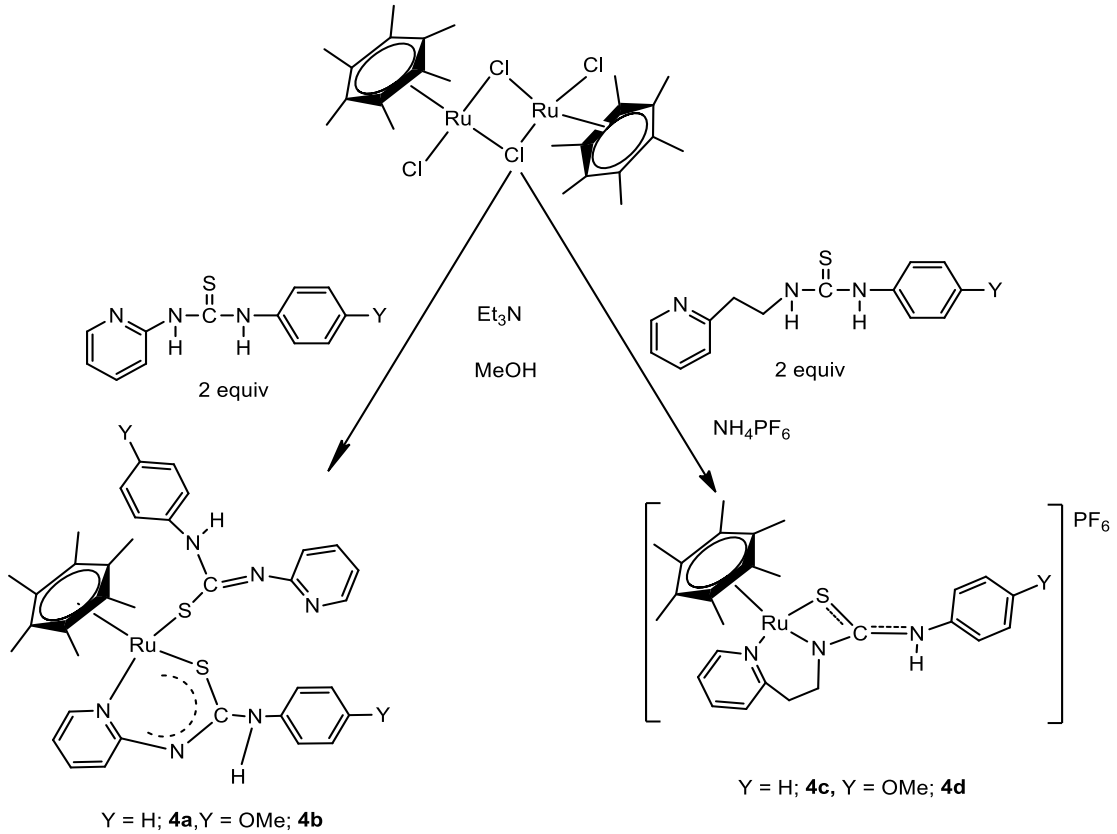

Scheme 4.1: Reaction scheme for the synthesis of mononuclear ruthenium bis (thiourea) complexes **4a**-**4b** and mononuclear tridentate ruthenium thiourea complexes **4c**-**4d**.

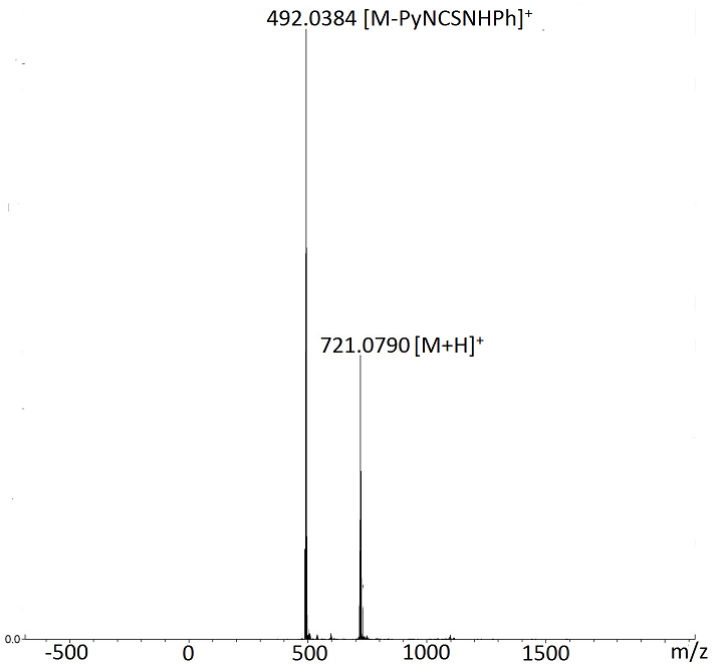

Figure 4.1: ESI-mass spectrum of the neutral dinuclear ruthenium thiourea complex **4a** [(η^6-C_6Me_6)Ru{SC(=NPy)NHPh}{SC(NPy)NHPh}] at CEV 150 V showing the peak for loss of the second bound ligand.

In two other similar but seperate synthesis, the pyridyl groups in the thiourea ligands used in **4a** and **4b** were substituted with the ethylenepyridyl functional group, and the effect of the ethylene spacer on the coordination geometry of the complexes was investigated. The ligands were reacted with the ruthenium dimer $[(\eta^6\text{-}C_6Me_6)RuCl_2]_2$ under the same reaction conditions as **4a** and **4b** (**Scheme 4.1)** to give complexes **4c** and **4d**. The ESI-mass spectra of the complexes showed molecular ion peaks $[M]^+$ with *m/z* 519.98 and 549.98 for **4c** and **4d** at CEV of 60 V. These ions are assignable to the mononuclear ruthenium thiourea complexes $[(\eta^6\text{-}C_6Me_6)Ru\{SC(=N(CH_2)_2Py)NHX\}]PF_6$ (where X = Ph or C_6H_4OMe) as opposed to the bis(thiourea) complexes formed in **4a** and **4b** (**Scheme 4.1**).

^{1}H NMR spectra of the ruthenium bis(thiourea) complexes **4a** and **4b** showed a singlet peaks above 8.5 and 5.0 ppm, assignable to the two NH protons of the thiourea. The presence of multiple NH protons in the NMR spectra of the compounds was a confirmation of the presence of two thiourea ligands in the complexes, indicating that one thiourea is monodentate to the metal centre. The mono-ligand complexes **4c** and **4d** showed peaks for NH protons around 5.0 ppm only. The peaks for the ligand phenyl protons were observed between 6.50-7.99 ppm in all the complexes **4a**-**4d**. The pyridyl protons were observed as a group of doublets and triplets around 8.10-8.52 ppm. The ethylene substituted complexes **4c**-**4d** showed peaks around 2.0-3.0 ppm, assignable to the CH_2 protons of the ethylene spacer and the *p*-methoxy substituted complexes **4b** and **4d** showed singlets around 3.80-3.90 ppm, characteristic of the CH_3 protons of the *p*-methoxyphenyl ligands. In all four complexes, there was a singlet around 1.70–2.20 ppm assignable to the CH_3 protons of the C_6Me_6 arene ring.

The FTIR spectra of the complexes **4a** and **4b** showed multiple intense bands around 3500 - 3300 cm^{-1} for N-H stretching frequencies of the thiourea ligand. The mononuclear complexes **4c** and **4d**, on the other hand, showed only weak bands around the same region. The absorption bands around 1520 – 1450 cm^{-1} of all four complexes are characteristic of $\nu_{C=N}$ pyridyl stretching frequencies and bands around 845 and 530 cm^{-1} assignable to P-F stretching and rocking frequencies respectively confirm the formation of PF_6 salts of the complexes **4c** and **4d**.

Table 4.1: ESI-mass spectral data of ruthenium thiourea complexes **4a** – **4r**

Complexes	**Capillary exit voltage (V)**	***m/z* (%) ions**
$[(\eta^6\text{-}C_6Me_6)Ru\{SC(=NPy)NHPh\}\{SC(NPy)NHPh\}]$ (**4a**)	60	721 (100) $[M+H]^+$
	150	492 (100) $[M\text{-}PyNCSNHPh]^+$, 721(100) $[M+H]^+$
	180	492 (100) $[M\text{-}\ PyNCSNHPh]^+$
$[(\eta^6\text{-}C_6Me_6)Ru\{SC(=NPy)NHC_6H_4OMe\}\{SC(NPy)NHC_6H_4OMe\}]$(**4b**)	60	522 (58) $[M\text{-}PyNCSNHC_6H_4OMe]^+$, 781 (100) $[M+H]^+$
	150	522 (100) $[M\text{-}PyNCSNHC_6H_4OMe]^+$, 781 (46) $[M+H]^+$
	180	522 (100) $[M\text{-}PyNCSNHC_6H_4OMe]^+$
$[(\eta^6\text{-}C_6Me_6)Ru\{SC(=N(CH_2)_2Py)NHPh\}]PF_6$ (**4c**)	60-180	519.98 (100) $[M]^+$
$[(\eta^6\text{-}C_6Me_6)Ru\{SC(=N(CH_2)_2\ Py)NHC_6H_4OMe\}]PF_6$ (**4d**)	60-180	549.99 (100) $[M]^+$
$[(\eta^6\text{-}C_6Me_6)Ru\{SC(=N(Py)NHPh\}(PPh_3)]BF_4$ (**4e**)	60	754.20 (100) $[M]^+$
	150	754 (82) $[M]^+$, 492 (89) $[M\text{-}PPh_3]^+$
	180	492 (100) $[M\text{-}PPh_3]^+$
$[(\eta^6\text{-}C_6Me_6)Ru\{SC(=NCH_2Py)NHPh\}PPh_3]BF_4$ (**4f**)	60	768 (100) $[M]^+$
	150	506 (82) $[M\text{-}PPh_3]^+$, 768 (28)
	180	506 (100) $[M\text{-}PPh_3]^+$, 768 (5) $[M]^+$
$[(\eta^6\text{-}C_6Me_6)Ru\{SC(=N(Py)NHC_6H_4NO_2\}(PPh_3)]BF_4$ (**4g**)	60	799 (100) $[M]^+$, 1097 $[M+L+Na]^+$(L= $PyNCSNHC_6H_4NO_2$)
	150	537 (82) $[M\text{-}PPh_3]^+$, 799 (82) $[M]^+$
	180	537 (100) $[M\text{-}PPh_3]^+$
$[(\eta^6\text{-}C_6Me_6)Ru\{SC(=NCH_2(Py)NHC_6H_4NO_2\}(PPh_3)]BF_4$ (**4h**)	60	551 (12) $[M\text{-}PPh_3]^+$, 813 (100) $[M]^+$
	150	551 (89) $[M\text{-}PPh_3]^+$, 813 (29) $[M]^+$
	180	551 (100) $[M\text{-}PPh_3]^+$

Complexes	**Capillary exit voltage (V)**	***m/z* (%) ions**
$[(\eta^6\text{-}C_6Me_6)Ru\{SC(=N(CH_2)_2(Py)NHPh\}(PPh_3)]BF_4$ (**4i**)	60	520 (15) $[M\text{-}PPh_3]^+$, 782 (100) $[M]^+$
	150	520 (100) $[M\text{-}PPh_3]^+$, 782 (12) $[M]^+$
$[(\eta^6\text{-}C_6Me_6)Ru\{SC(=N(CH_2)_2Py)NHC_6H_4NO_2\}(PPh_3)]BF_4$ (**4j**)	60	565 (10) $[M\text{-}PPh_3]^+$, 827(100) $[M]^+$
	150	565 (100) $[M\text{-}PPh_3]^+$, 827 (14) $[M]^+$
$[(\eta^6\text{-}C_6Me_6)Ru\{SC(=NPy)NHC_6H_4OMe\}(PPh_3)]PF_6$ (**4k**)	60	522 (12) $[M\text{-}PPh_3]^+$, 784 (100) $[M]^+$
	150	522 (100) $[M\text{-}PPh_3]^+$, 784 (64) $[M]^+$
$[(\eta^6\text{-}p\text{-cymene})Ru\{SC(=NPy)NPh\}(PPh_3)]BF_4$ (**4l**)	60	726 (100) $[M]^+$
	150	464 (100) $[M\text{-}PPh_3]^+$, 726 (82) $[M]^+$
$[(\eta^6\text{-}p\text{-cymene})Ru\{SC(=NCH_2Py)NPh\}(PPh_3)]BF_4$ (**4m**)	60	740 (100) $[M]^+$
	180	478 (100) $[M\text{-}PPh_3]^+$, 740 (82) $[M]^+$
$[(\eta^6\text{-}p\text{-cymene})Ru\{SC(=N(CH_2)_2Py)NHPh\}(PPh_3)]PF_6$ (**4n**)	60	754 (100) $[M]^+$
	150	754 (82) $[M]^+$, 492 (89) $[M\text{-}PPh_3]^+$
$[(\eta^6\text{-}p\text{-cymene})Ru\{SC(=NPy)NHC_6H_4NO_2\}(PPh_3)]PF_6$ (**4o**)	60	771 (100) $[M]^+$
	150	509 (100) $[M\text{-}PPh_3]^+$ 771 (78) $[M]^+$
$[(\eta^6\text{-}p\text{-cymene})Ru\{SC(=NPy)NHC_6H_4OMe\}(PPh_3)]PF_6$ (**4p**)	60	756 (100) $[M]^+$
	150	494 (100) $[M\text{-}PPh_3]^+$, 756 (74) $[M]^+$
$[(\eta^6\text{-}p\text{-cymene})Ru\{SC(=N(CH_2)_2\,Py)NHC_6H_4OMe\}(PPh_3)]PF_6$ (**4q**)	60	784 (100) $[M]^+$
	150	522 (100) $[M\text{-}PPh_3]^+$, 784 (56) $[M]^+$

4.2.2 *X-ray crystal structures of thiourea complexes 4a and 4c*

In order to unambiguously establish the structures of the complexes **4a-4d**, crystals of the complexes **4a** and **4c** suitable for X-ray crystallography were obtained by diffusing diethyl ether into a saturated dichloromethane solution of each complex. Complex **4a** crystallised as a neutral complex with one molecule of water of crystallisation in the asymmetric unit. The molecular structure of the compound is presented in **Figure 4.2**, while selected bond lengths and angles are presented in **Table 4.3**. The molecular structure of the complex features a regular three-legged piano stool in which three coordination sites on the ruthenium metal are occupied by the η^6-C_6Me_6 arene ligand acting as the seat of the piano stool. The remaining coordination sites on the metal are taken up by two thiourea ligands, one coordinating to the metal through the pyridyl nitrogen N(3) and thiolate sulfur S(1) and another molecule of the ligand coordinates through the thiolate sulfur S(2) in a monoanionic fashion to form a *pseudo*-octahedral Ru(arene)L_2 complex (L= thiourea monoanion).

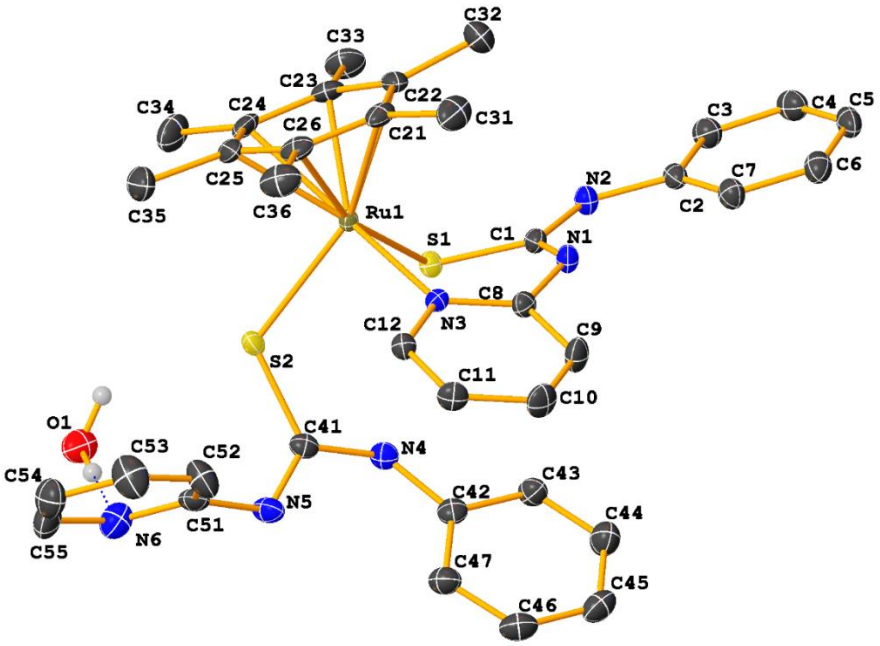

Figure 4.2: Molecular structure of ruthenium bis(thiourea) complex [(η^6-C_6Me_6)Ru{SC(NPy)NHPh}{SC(=NPy)NHPh}] **4a**. Ellipsoids are drawn at 50% probability level. Hydrogen atoms were omitted for clarity.

The six-membered ring formed by the Ru-N,S coordination is substantially puckered to a root mean square deviation (r.m.s.) of 0.345 Å. The metal to arene centroid ring distance is 1.712(11) Å. The Ru(1)-S(1) bond 2.387(5) Å is slightly shorter than the Ru(1)-S(2) 2.410(5) Å. These bond distances are consistent with the k^2-N,S coordination of thiourea derivatives and in close agreement with reported values[23]. The C-S bonds in the complex are similar (C(1)-S(1) = 1.757(2) Å and C(41)-S(2) = 1.773(2) Å) indicating that they possess partial single and double bond characteristics[3,4,24-26]. The bond angles around the metal centre S(1)-Ru(1)-N(3); 90.04(4)^o, N(3)-Ru(1)-S(2); 84.10(5)^o, S(1)-Ru(1)-S(2); 89.977(17)^o are all very close to 90^o, indicating the *pseudo*-octahedral geometry of the complexes. The angles subtended at S(1) and S(2) are 99.03(7)^o and 114.34(7)^o respectively.

The ethylenepyridyl substituted complex **4c, Figure 4.3**, crystallised in the monoclinic $P2_1/c$ crystal system with one molecule of the PF_6 anion. A three-legged piano stool structure of the complex is evident in the molecular structure of the complex in **Figure 4.3**. The η^6-C_6Me_6 arene-bound ruthenium is also coordinated to the ethylenepyridyl thiourea ligand in an *N, N, S* tridentate fashion, using the pyridyl N, the thiourea N and thioate S atoms. The ruthenium coordination environment in the complex also features a *pseudo*-octahedral geometry with bite angles of 78.41(2)^o and 67.32(7)^o for the six-membered Ru-N(3)-C(10)-C(9)-C(8)-N(1) and four-membered Ru(1)-N(1)-C(1)-S(1) rings, respectively. The metallacyclic ring has a boat configuration with an 8-membered ring separated into N,N, and N,S bonded metallacycles. The six-membered Ru-N(3)-C(10)-C(9)-C(8)-N(1) ring is essentially puckered to an r.m.s. deviation of 0.381 Å and the four-membered Ru(1)-N(1)-C(1)-S(1) is planar to 0.033 Å. The Ru(1)-S(1) and Ru(1)-N(3) pyridyl bond lengths in the complex **4c** (2.4018 and 2.115(3) Å) are close to the values reported for the neutral dianion complex **4a** and other arene thiourea complexes in the literature[22,26,27]. The bond angles around the ruthenium coordination sphere for the complex **4c** are N(3)-Ru(1)-S(1) 86.72(7)^o, N(1)-Ru(1)-N(3) 78.42(11)^o, N(1)-Ru(1)-S(1) 67.32(72)^o and are expectedly narrower than the corresponding angles in the analogous complex **4a**. The Ru(1)-S(1)-C(1) bond angle 79.55(11)^o in **4c** is significantly smaller than the ones in **4a** by 19.48^o and 34.79^o probably because the ligand in **4c** is tridentate rather than bidentate.

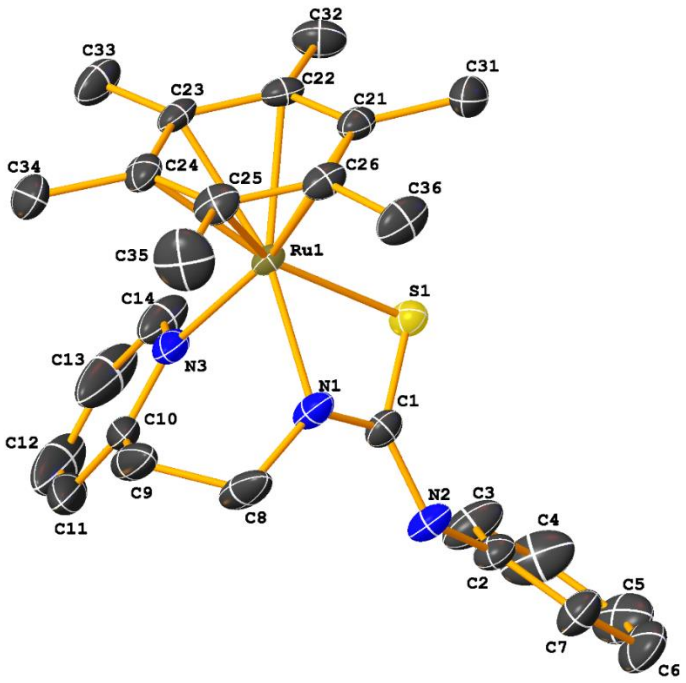

Figure 4.3: Molecular structure of the mononuclear tridentate thiourea complex of ruthenium **4c**. Ellipsoids are drawn at 50% probability level. Hydrogen atoms, diethyl ether solvent and PF_6 anion are omitted for clarity.

Apart from the distinct structural and geometric differences in the crystal structure of the complexes **4a** and **4c**, the most significant difference in the crystal structure of the two complexes is the presence of a number of intermolecular and intramolecular hydrogen bonding interactions in the crystal structure of **4a** and the absence of it in the structure of **4c**. This may be attributed to the presence of a second ligand in the structure of **4a,** which provides a few uncoordinated functional and hydrogen bond donating N-H groups that can be exploited for intermolecular hydrogen bonding interactions.

Further, the tridentate mode of coordination of the thiourea ligand in **4c** and **4d** can be attributed to the presence of the ethylene spacer, which allows the ligand to wrap around to engage in tridentate coordination, a feat that is practically impossible in the ligands without CH_2 spacer (**4a** and **4b**). The packing diagram of **4a** in **Figure 4.4** features N-H----S intramolecular hydrogen bonding between the thiourea nitrogen of one ligand and thiolate sulfur of the second molecule (green dotted lines). Holding the packing structure together are some intermolecular hydrogen bonding interactions inter-connected by one molecule of water of crystallisation. These interactions include the N-H---O hydrogen bonds between the

thiourea N-H and oxygen of the water of crystallisation (shown as blue dotted lines), the O-H----N hydrogen bonding interactions between O-H group of the water and pyridyl functional group of the ligand (sky blue dotted lines) and O-H---S hydrogen bond interactions (shown as purple coloured dotted lines).

Table 4.2: Geometric parameters for ruthenium thiourea complexes **4a** and **4c**

Parameters (Å, º)	**4a**	**Parameters (Å, º)**	**4c**
Ru(1) – S(1)	2.402(7)	Ru(1) – S(1)	2.3878(5)
Ru(1) – N(3)	2.115(3)	Ru(1) – N(3)	2.1202
Ru(1) – N(1)	2.091(2)	C(1) – N(1)	1.301(3)
C(1) – N(1)	1.309(4)	N(2) – C(1)	1.368(3)
N(2) – C(1)	1.299(4)	S(1) – C(1)	1.757(2)
S(1) – C(1)	1.723(3)	Ru(1) – S(2)	2.4103
N(2) – Ru(1) – S(1)	67.32(7)	C(41) – S(2)	1.773(2)
N(1) – Ru(1) – S(1)	67.32(7)	S(1) – Ru(1) – S(2)	89.977(17)
N(1) – Ru(1) – N(2)	78.42(11)	N(3) – Ru(1) – S(1)	84.10(5)
C(1) – S(1) – Ru(1)	124.61(3)	C(1) – S(1) – Ru(1)	127.66(16)
N(1) – C(1) – S(1)	109.10(15)	N(1) – C(1) – S(1)	127.66(16)
N(2) – C(1) – N(3)	123.40(3)	N(2) – C(1) – N(1)	119.52(18)
N(2) – C(1) – S(1)	126.00(2)	N(2) – C(1) – S(1)	112.81(15)

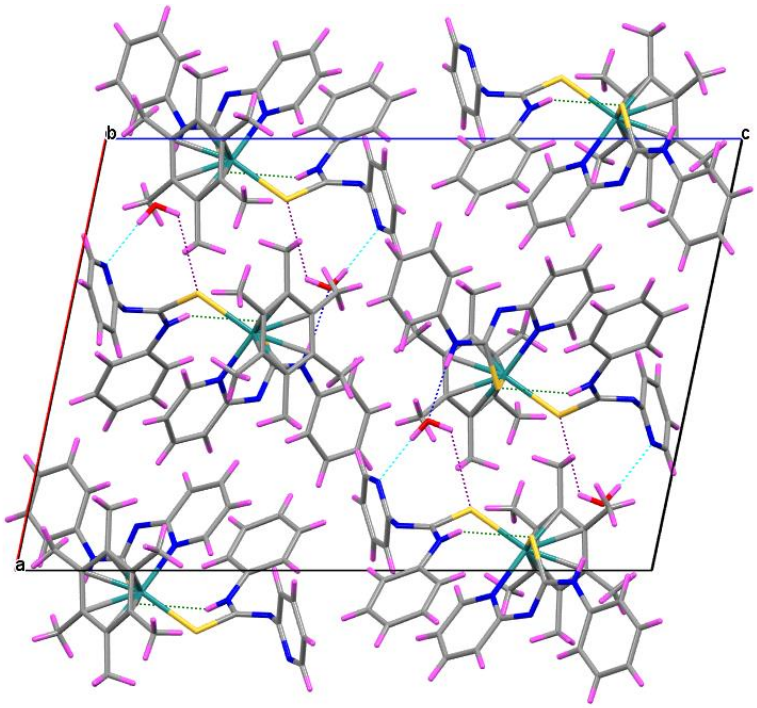

Figure 4.4: Molecular packing diagram of bis(thiourea) complex **4a** showing the intermolecular and intramolecular hydrogen bonding interactions in the crystal structure of the compound

The packing diagram of the mononuclear tridentate complex, **4c** in **Figure 4.5** shows four molecules of the mononuclear complex and four molecules of the hexafluorophosphate anion with eight molecules of disordered diethyl ether solvent spread around the crystal lattice. There were no hydrogen bonding interactions observed in the packing structure of the compound, probably due to the tridentate bonding geometry of the complex **4c,** where most of the functional groups in the ligand are involved in the coordination with the ruthenium metal and there are no NH hydrogen bonding donors or residual hydrogen bonding solvents to engage in hydrogen bonding interactions.

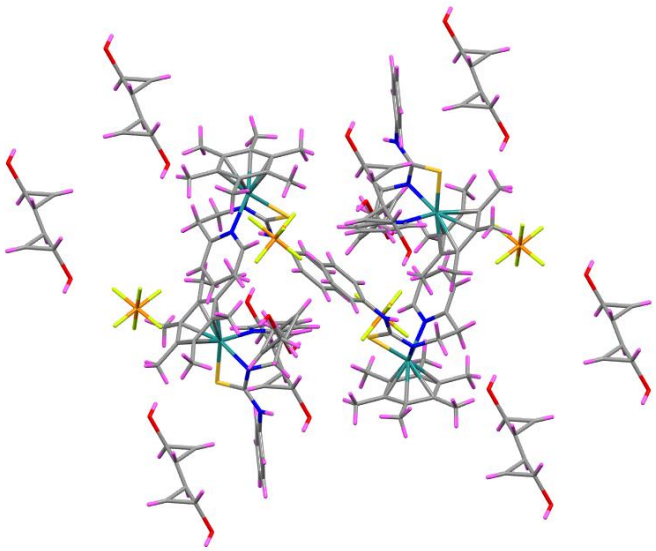

Figure 4.5: Molecular packing diagram of the mononuclear ruthenium thiourea complex **4c**.

4.2.3 *Mononuclear PPh_3-substituted thiourea complexes*

In another series of syntheses, dimeric ruthenium complexes $[(\eta^6\text{-}C_6Me_6)RuCl_2]_2$ and $[(\eta^6\text{-}p\text{-cymene})RuCl_2]_2$ were refluxed with 2 molar equivalents of pyridyl substituted ligands $Py(CH_2)_nNHC(S)NHR$ (n = 0, 1, 2 and R = Ph, C_6H_4OMe) with triphenylphosphine (PPh_3) and excess triethylamine in refluxing methanol. Solid NH_4PF_6 or $NaBF_4$ was added to the hot solution and water was used to precipitate the complexes **4e-4p**, **Scheme 4.2**.

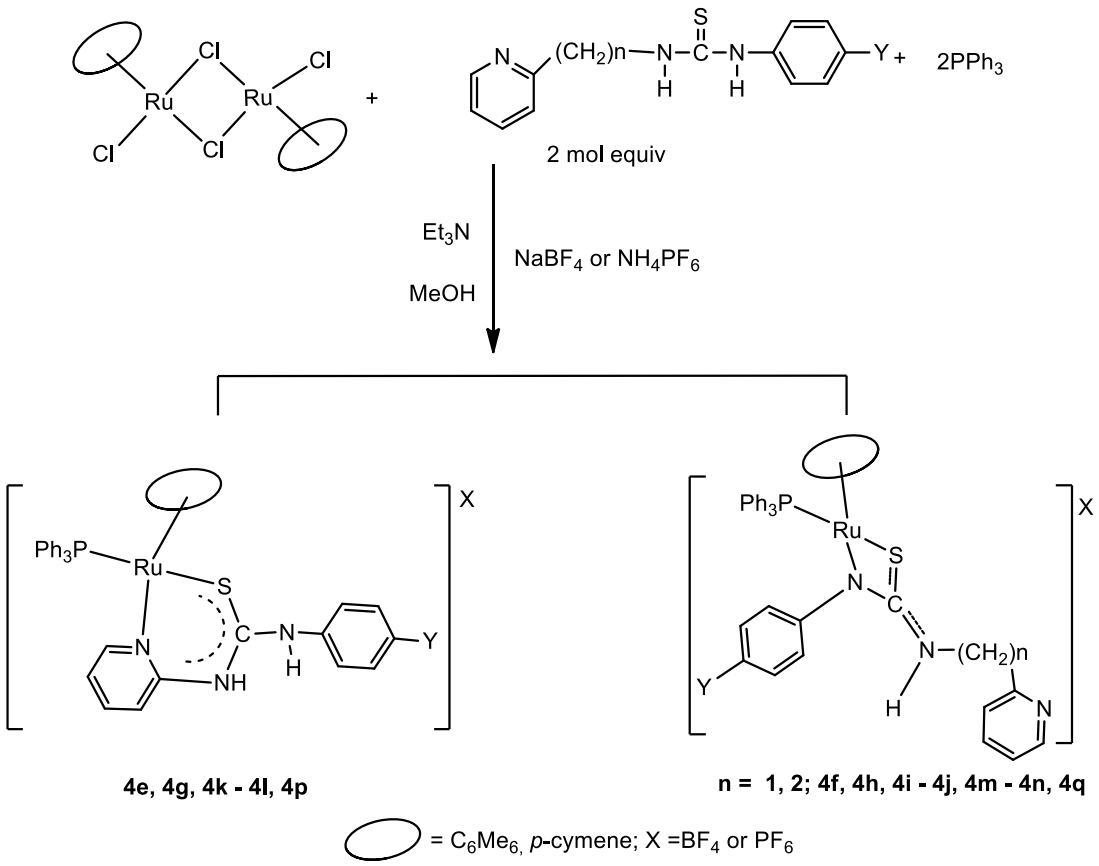

complex	arene	n	Y	X
4e	C_6Me_6	0	H	BF_4
4f	C_6Me_6	1	H	BF_4
4g	C_6Me_6	0	NO_2	BF_4
4h	C_6Me_6	1	NO_2	BF_4
4i	C_6Me_6	2	H	BF_4
4j	C_6Me_6	2	NO_2	BF_4
4k	C_6Me_6	0	OCH_3	PF_6
4l	*p*-cymene	0	H	BF_4
4m	*p*-cymene	1	H	BF_4
4n	*p*-cymene	2	H	BF_4
4o	*p*-cymene	0	NO_2	PF_6
4p	*p*-cymene	0	OCH_3	PF_6
4q	*p*-cymene	2	OCH_3	PF_6

Scheme 4.2: Reaction scheme for the synthesis of PPh_3-substituted ruthenium thiourea complexes

The ESI-mass spectra of the complexes **4e**-**4q** showed molecular ion peaks for cationic mononuclear complexes $[M]^+$ at a low capillary exit voltage (CEV) of 60 V. Increasing the CEV to 150 V resulted in additional peaks assignable to the

loss of the labile PPh_3 ligand from the mononuclear complex. For example, the ESI-mass spectra of mononuclear ruthenium complexes **4e**, **4g** and **4q** showed molecular ion $[M]^+$ peaks at *m/z* 754.20, 799.18, and 756.05 respectively at CEV of 60 V. Additional peaks at *m/z* 492.04, 537.08, 494.01 assignable to $[M\text{-}PPh_3]^+$ for **4e**, **4g** and **4q** respectively were observed at higher CEV of up to 150 V, **Table 4.1**.

The loss of the labile PPh_3 ligand from complexes on fragmentation in the mass spectrometer have been reported previously for ruthenium [Ru(η^6-*p*-cym){k^2-S,O-2,6-$F_2C_6H_3C(O)NHC(S)NEt_2$}(PPh_3)][28] and rhodium [Cp*Rh{SC(=NPh)NHPh}(PPh_3)]$^+$ [27] complexes. The ESI-mass spectrum of the ruthenium pyridyl and phenyl substituted complex, **4l** is presented in **Figure 4.6** as a representative example.

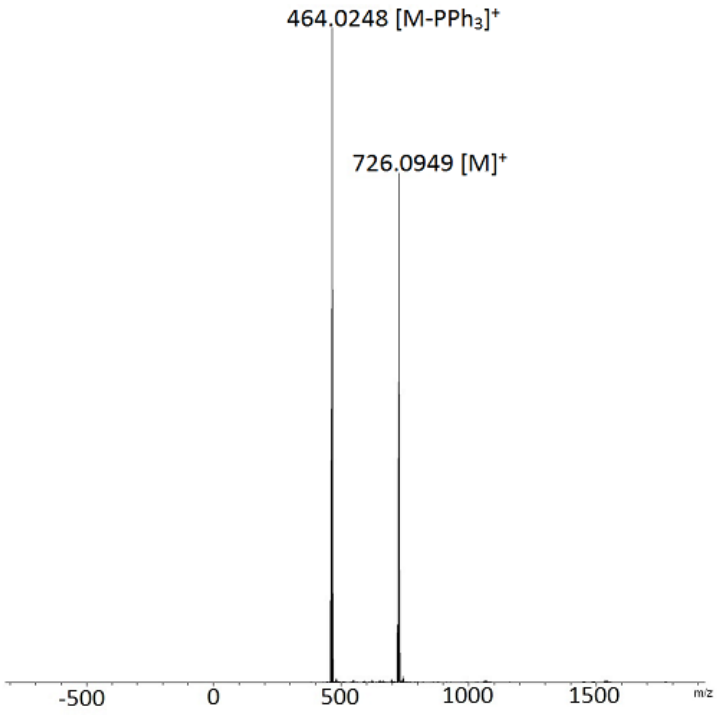

Figure 4.6: ESI-mass spectrum of pyridyl and phenyl-substituted ruthenium complex **4l**, M = [(η^6-*p*-cymene)Ru{SC(=NPy)NPh}(PPh_3)]$^+$

The proton NMR spectra of mononuclear complexes **4e-4k** containing hexamethylbenzene (C_6Me_6) are similar to the spectra reported for related complexes **4a-4d**. In complexes **4e-4k**, the peaks for the hexamethylbenzene ligand appear as a singlet around 1.86-2.25 ppm and NH protons are observed around 4.0-5.9 ppm. The aromatic region of the spectra for these complexes (**4e-4k)** showed

more peaks than the corresponding spectra in **4a**-**4d**. This is probably due to the presence of the PPh_3 ligand in **4e**-**4k**. $^{31}P\{^1H\}$ NMR spectra of the complexes showed singlets around 39.22 - 42.50 ppm assignable to the phosphorus of the PPh_3 ligand. Additional phosphorus peaks were observed as a septet at -143.5 ppm for **4k**, resulting from the PF_6 anion. The septet is due to $^1J_{P\text{-}F}$ coupling.

The ^1H NMR spectra of the *p*-cymene substituted complexes **4l**-**4q** show a doublet around 1.00 ppm assignable to the isopropyl CH_3 protons, singlets around 1.50-2.60 ppm for methyl protons of the cymene ligand and a septet around 2.50-3.20 ppm assignable to the methine proton of the isopropyl functionality. Methylene proton signals are observed as a singlet and a triplet at 2.14 and 2.21 ppm, respectively for **4m** and **4n**. A singlet assignable to CH_3 protons of the *p*-methoxyphenyl group was observed at 3.89 ppm in the proton NMR spectra of **4q**. The *p*-cymene CH protons appear as doublets around 4.80-5.9 ppm in the complexes **4l**-**4q**. The aromatic protons of the thiourea and PPh_3 ligands appear around 6.2-8.0 ppm while the pyridyl protons of the thiourea are observed between 8.10 and 8.5 ppm. Similar proton NMR signals have been reported for ruthenium arene complexes containing the *p*-cymene ligand[3,21,22,26].

The most significant features of the FTIR spectra of the hexamethylbenzene complexes **4e**-**4k** and *p*-cymene complexes **4l**-**4q** are the presence of strong bands around 3400-3300 cm^{-1} assigned to vibrational stretching frequencies of the thiourea N-H protons. Other bands around 1600-1450 cm^{-1} and 625 cm^{-1} assignable to C=N and C-S stretching frequencies are also prominent in the spectra of most of the complexes. P-F stretching frequency vibrations from the PF_6 counter ions were also recorded around 650 and 550 cm^{-1} in **4q**.

4.2.4 *X-ray crystal structure analyses of complexes 4e-4q*

In order to unambiguously determine the coordination geometry of ruthenium arene complexes **4e**-**4q** and also investigate the effect of the alkyl-pyridyl spacer on the bonding geometry of the complexes, crystal structures of complexes **4f**, **4i**, **4k**, **4l** and **4n** were obtained. The molecular structures of the compounds are presented in **Figures 4.7-4.9**, while selected bond lengths and angles are presented in **Tables 4.3** and **4.4**. All the complexes crystallised as salts with BF_4 anions in **4f**, **4i**, **4l** and **4n** and PF_6 in **4k**. The crystal structure of all the complexes featured the regular 'piano stool' geometry in which the coordination

sites around the ruthenium metal is occupied by the arene ligand (arene = *p*-cymene /C_6Me_6) in a η^6 manner, a terminal PPh_3 ligand and a chelating N,S thiourea ligand, resulting in a *pseudo*-octahedral geometry around the ruthenium metal centre. The molecular structures of the complexes show that the thiourea ligands coordinate to the ruthenium metal centre through the N(3)-pyridyl in **4l** and **4k** or the thiourea N(1) in **4f**, **4i** and **4n** and thiolate sulfur S(1) in a bidentate fashion. This bidentate mode of coordination resulted in the formation of four-membered rings in **4f**, **4i** and **4n** and six-membered rings in **4k** and **4l**. The arene rings (arene = C_6Me_6 or *p*-cymene) in the complexes are planar, and the metallacyclic ring in the complexes are planar to a root mean square deviation of 0.019 Å; **4f**, 0.021 Å; **4i**, 0.0308 Å; **4l**, 0.01 Å; **4n**. The six-membered metallacyclic ring in the complex **4k** is however substantially puckered with a root mean square deviation of 0.413 Å and a dihedral angle of 45.25^o between the S(1)-Ru(1)-N(3) and S(1)-C(1)-N(1)-C(12) least square planes. The metal to centroid bond distances in the complexes are 1.768 Å; **4f**, 1.751 Å; **4i**, 1.775 Å; **4k**, 1.750 Å; **4l** and 1.729 Å (**4n**). The introduction of methylene and ethylene spacers between the pyridyl and thiourea groups of the ligands results in the juxtaposition of the pyridyl ring from the proximal position (adjacent to the ruthenium metal centre) in the six-membered ring complexes **4k** and **4l**, to the distal position (remote from the ruthenium metal centre) in the methylene and ethylene substituted complexes **4f**, **4i** and **4n**, containing the four-membered metallacycle. Apart from that, the size of the dihedral angles between the pyridyl rings and the metallacyclic ring ranges from 18.25(6)^o and 21.10(2)^o in pyridyl substituted six-membered **4l** and **4k** respectively to the four-membered **4f**; 48.93(4)^o, **4i;** 46.31(2)^o and **4n**; 29.40(11)^o, where the pyridyl rings are separated from the metallacyclic ring by as much as a methylene spacer in **4f** and an ethylene spacer in **4i** and **4n**.

The C(1)-S(1) bond distances in the complexes are similar; 1.734(6) Å; **4f**, 1.737(3) Å; **4i**, 1.746(3) Å ; **4k**, 1.745(3) Å ; **4l**, and 1.741(2) Å indicating electron delocalisation around the metallacyclic ring on coordination of the ligand. The Ru(1)-S(1) bond distances in the complexes **4f**; 2.4001(15) Å, **4i**; 2.400(7) Å, **4n**; 2.406(5) Å are similar and comparatively longer than the corresponding bonds in **4k**; 2.3515(6) Å and **4l**; 2.3491(7) Å. These bond distances are comparable to the values reported for other ruthenium arene complexes containing four and six-membered rings[4,26,29]. The Ru(1)-P(1) bond distances in the complexes are 2.327(6),

2.346(8), 2.323(7), 2.336(8), 2.352(15) Å for **4f**, **4i**, **4k**, **4l**, and **4n** respectively. These values are slightly shorter than Ru(1)-P(1) bond lengths reported for an imidazolium substituted ruthenium arene thiourea complex $[Ru(arene)(L)(PPh_3)Cl]PF_6$[30] (2.369 Å) (L= imidazolidine thione) and another structurally related complex $[Ru(\eta^6\text{-}p\text{-cymene})(PPh_3)(PTA)Cl]^+$ [31] (2.359 Å). The Ru-Cl bonds in these two complexes and other previously reported complexes are, however much more elongated[3,22,25]

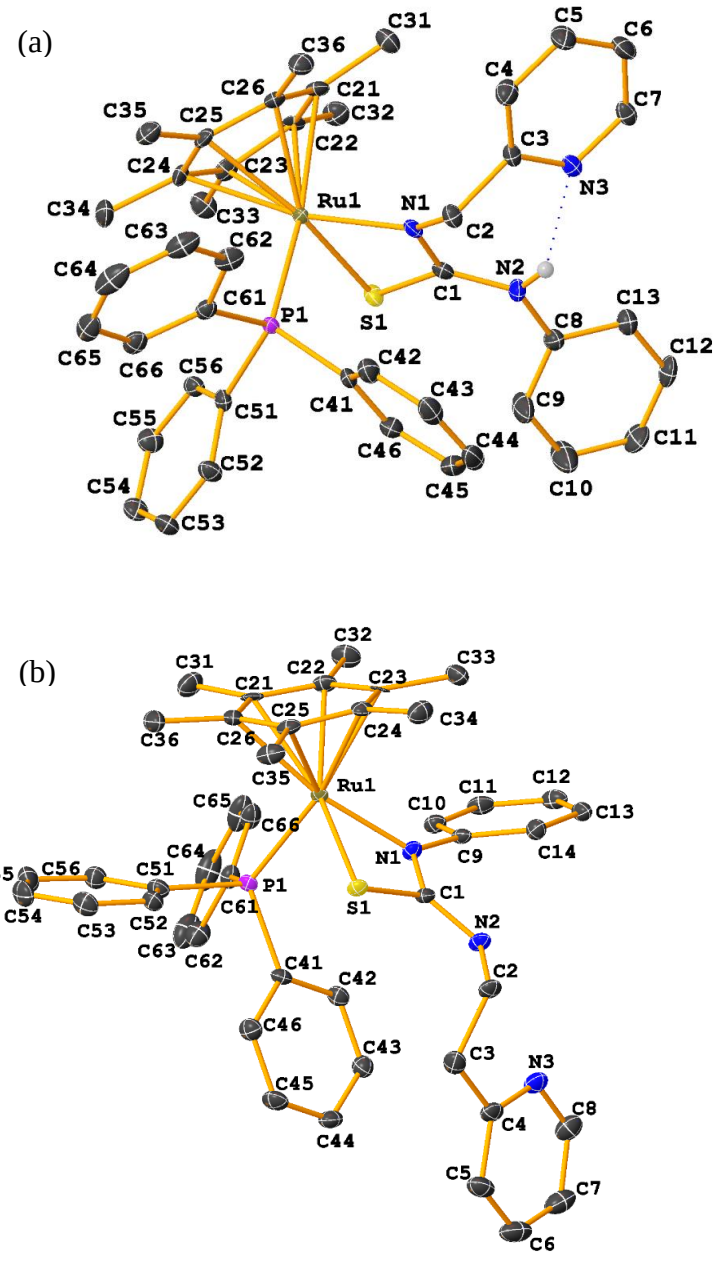

Figure 4.7: Molecular structures of (a) phenyl and methylenepyridyl substituted ruthenium complex **4f** $[(\eta^6\text{-}C_6Me_6)Ru\{SC(=NCH_2Py)NHPh\}PPh_3]BF_4$ (b) phenyl and ethylenepyridyl substituted ruthenium complex **4i** $[(\eta^6\text{-}$

C_6Me_6)Ru{SC(=N(CH_2)$_2$(Py)NHPh}(PPh_3)]BF_4. Hydrogen atoms and BF_4 anions are omitted for clarity. Ellipsoids are drawn at 50% probability.

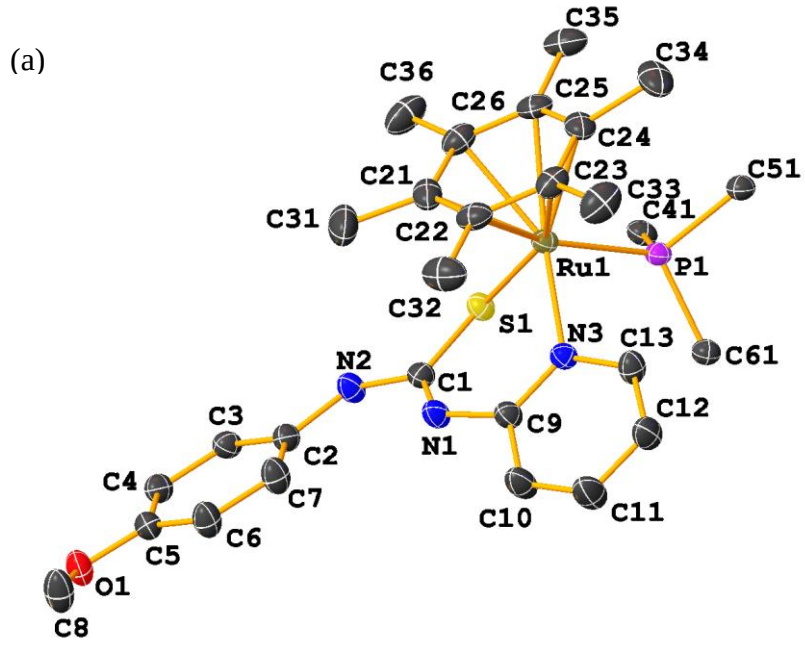

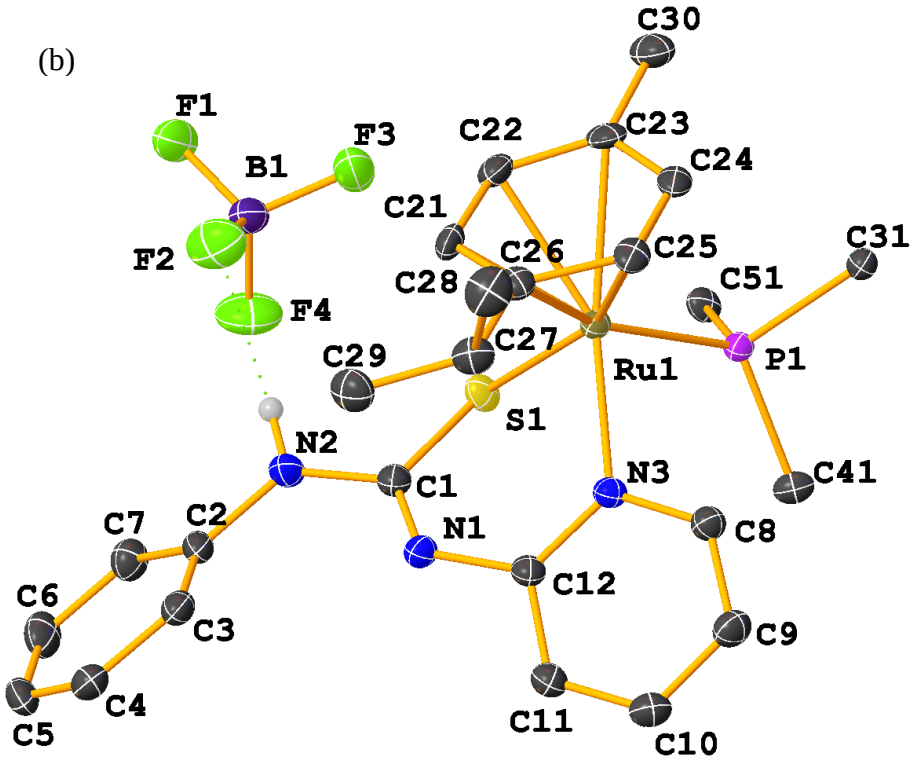

Figure 4.8: Molecular structures of (a) *p*-methoxyphenyl and pyridyl substituted ruthenium complex **4k**, [(η^6-C_6Me_6)Ru{SC(NPy)NHC_6H_4OMe}(PPh_3)]PF_6 (b) phenyl and ethylene pyridyl substituted ruthenium complex **4l** [(η^6-*p*-cymene)Ru{SC(NPy)NHPh}(PPh_3)]BF_4. Hydrogen atoms are omitted for clarity and BF_4 anion is included in structure to show hydrogen bonding interaction. Only *ipso* carbons of the PPh_3 is shown for clarity. Ellipsoids are drawn at 50% probability.

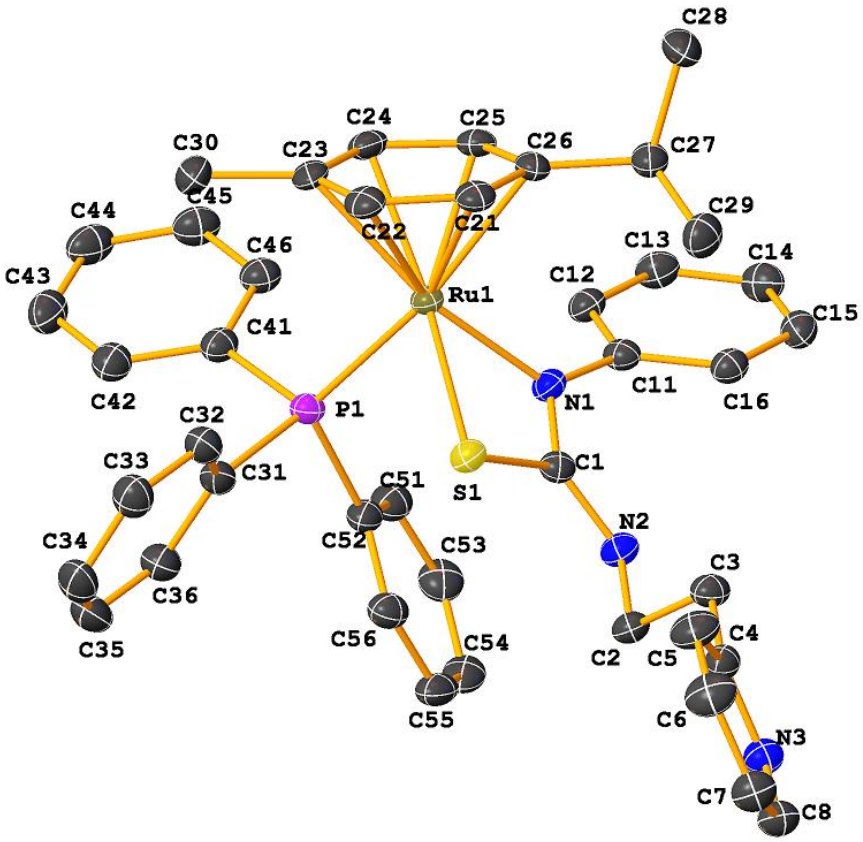

Figure 4.9: Molecular structure of phenyl and ethylenepyridyl substituted ruthenium complex **4n** [(η^6-*p*-cymene)Ru{SC(NH(CH_2)$_2$Py)NPh}(PPh_3)]BF_4 Hydrogen atoms and BF_4 anions are omitted for clarity. Ellipsoids are drawn at 50% probability.

The N(1)-Ru(1)-S(1) bond angles in the complexes with four-membered metallacyclic rings; **4f**, 67.14(15)^o, **4i** 67.11(2)^o, and **4n** 67.120(5)^o, are significantly narrower than the corresponding N(3)-Ru(1)-S(1) bond angles in six-membered **4k** 85.78(7)^o and **4l**, 85.66(7)^o. Similarly, the P(1)-Ru(1)-S(1) angles in **4f**; 86.19(5) and **4i**; 86.72(2)^o are larger than the corresponding angles in **4k**; 83.48(2)^o and **4l**; 84.31(3)^o. The angles subtended at the thiolate S(1) and C(1) atoms of the six-membered metallacyclic ring for complexes **4k**, 101.81(10)^o, 128.9(2)^o and **4l**, 100.62(11)^o, 128.10(2)^o are also more elongated than the equivalent angles in **4f**; 80.40(2), 109.9(5), **4i**; 80.76(10), 109.4(2) and **4n**; 80.49(7), 109.10^o.

Table 4.3: Geometric parameters for ruthenium thiourea complexes **4f, 4i** and **4n**

Bond lengths (Å) and angles (º)	**4f**	**4i**	**4n**
Ru(1) – P(1)	2.3267(16)	2.346(8)	2.352(15)
Ru(1) – S(1)	2.4001(15)	2.400(7)	2.406(5)
Ru(1) – N(1)	2.110(5)	2.116(5)	2.103(17)
C(1) – N(1)	1.313(8)	1.321(4)	1.320(3)
N(2) – C(1)	1.358(8)	1.333(4)	1.339(3)
S(1) – C(1)	1.734(6)	1.737(3)	1.741(2)
P(1) – Ru(1) – S(1)	86.19(5)	86.72(2)	83.424(18)
N(1) – Ru(1) – S(1)	67.14(15)	67.11(2)	67.120(5)
N(1) – Ru(1) – P(1)	88.07(15)	88.72(7)	89.11(5)
C(1) – S(1) – Ru(1)	80.40(2)	80.76(10)	80.49(7)
C(1) – N(1) – Ru(1)	102.5(4)	102.58(5)	103.26(13)
N(1) – C(1) – S(1)	109.9(5)	109.4(2)	109.10(15)
N(1) – C(1) – N(2)	123.3(6)	127.5(3)	127.70(19)
N(2) – C(1) – S(1)	126.8(5)	123.10(2)	123.15(16)

Table 4.4: Geometric parameters for ruthenium thiourea complexes **4k** and **4l**

Bond lengths (Å) and angles (º)	**4k**	**4l**
Ru(1) – P(1)	2.3626(7)	2.3365(8)
Ru(1) – S(1)	2.3515(7)	2.3491(7)
Ru(1) – N(3)	2.115(2)	2.125(2)
C(1) – N(1)	1.298(4)	1.299(4)
N(2) – C(1)	1.360(4)	1.367(4)
S(1) – C(1)	1.746(3)	1.745(3)
P(1) – Ru(1) – S(1)	83.48(2)	84.31(3)
N(3) – Ru(1) – S(1)	85.78(7)	85.66(7)
N(3) – Ru(1) – P(1)	90.85(7)	91.13(7)
C(1) – S(1) – Ru(1)	101.81(10)	100.62(11)
N(1) – C(1) – S(1)	128.9(2)	128.10(2)
N(1) – C(1) – N(2)	119.6(3)	120.10(3)
N(2) – C(1) – S(1)	111.5(2)	111.30(2)

4.2.5 *Rhodium and iridium thiourea complexes*

Mononuclear thiourea complexes of rhodium and iridium were synthesised by reacting the $[Cp^*MCl_2]_2$ dimer (where M = Rh, Ir) with 2 molar equivalents of asymmetrically disubstituted thioureas of the type $Py(CH_2)_nNHC(S)NHPh$ in refluxing methanol solution to give neutral complexes **4r**-**4w** (**Scheme 4.3**). In another series of syntheses, 2 molar equivalents of the PPh_3 ligand was added to the reaction solution. Solid $NaBF_4$ (excess) was added to the hot solution to give complexes **4x**-**4ze**, **Scheme 4.3**.

ESI-mass spectra of the complexes **4r**-**4w** showed molecular ion peaks for the cationic species $[M\text{-}Cl]^+$ at a capillary exit voltage of 60 V. For example, the pyridyl and phenyl substituted rhodium complex **4r** showed $[M\text{-}Cl]^+$ peak at *m/z* 465.97. Also appearing alongside the $[M\text{-}Cl]^+$ peaks in the spectra are peaks assignable to molecular ions for the protonated neutral complexes $[M+H]^+$. Molecular ion peaks for $[2M+H]^+$ aggregate ions were also observed as low-intensity peaks for complexes **4v** and **4u.** The ESI-mass spectrum of the rhodium thiourea complex **4r** at CEV 150 V is presented in **Figure 4.10** as a representative example.

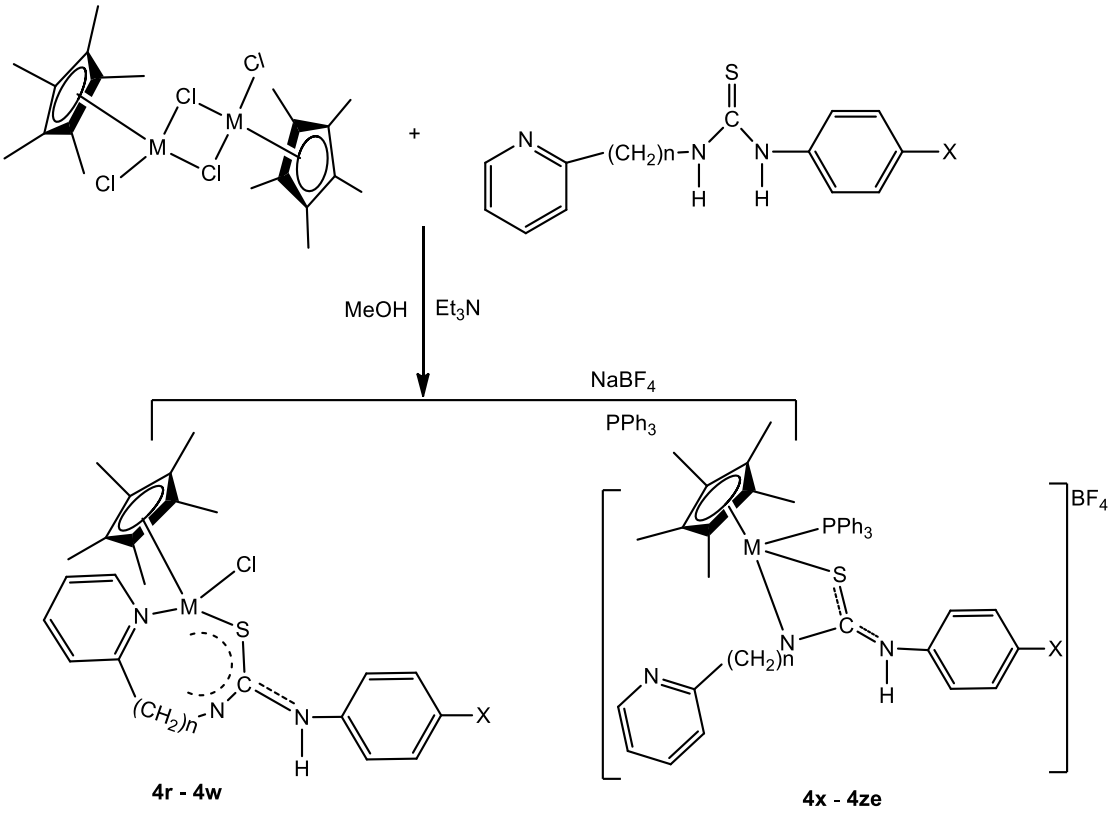

Complexes	M	n	X
4r	Rh	0	H
4s	Ir	0	H
4t	Rh	2	H
4u	Ir	2	H
4v	Rh	0	OCH_3
4w	Ir	0	OCH_3
4x	Rh	0	H
4y	Ir	0	H
4z	Rh	1	H
4za	Ir	1	H
4zb	Rh	2	H
4zc	Ir	2	H
4zd	Rh	2	OCH_3
4ze	Ir	2	OCH_3

Scheme 4.3: Reaction scheme for mononuclear rhodium and iridium thiourea complexes

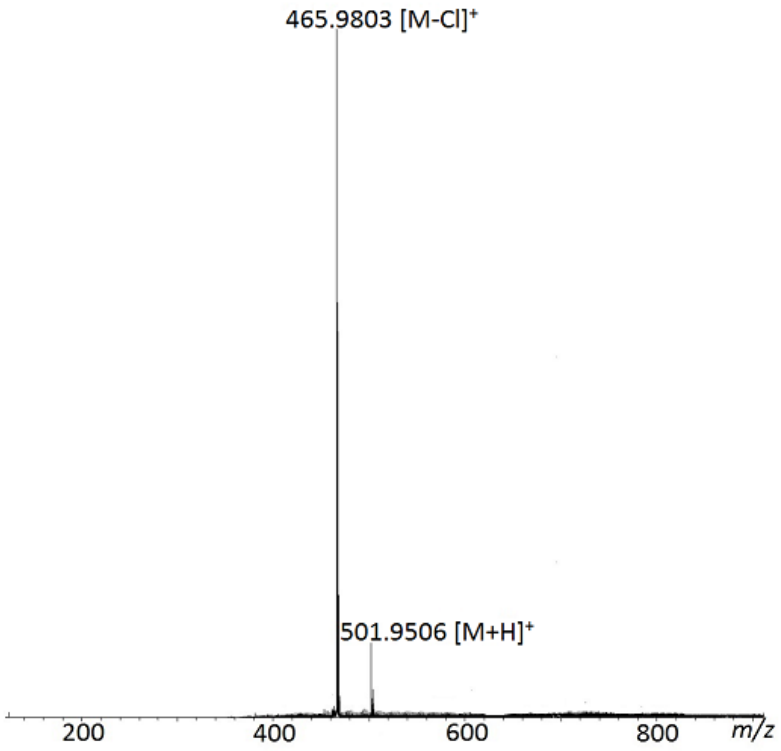

Figure 4.10: ESI-mass spectrum of pyridyl and phenyl-substituted ruthenium complex **4r,** M = [Cp*Rh{SC(=NPy)NPh}Cl]

ESI-mass spectra of the PPh_3 substituted complexes **4x**–**4ze** show molecular ions $[M]^+$ for the cationic complexes at a low CEV of 60 V. Increasing the CEV to 120 V resulted in peaks assignable to $[M\text{-}PPh_3]^+$ ions for loss of the labile PPh_3 ligand from the cationic complexes. Similar fragmentation behaviour was observed for the monomeric ruthenium complexes discussed in the preceding section and other arene complexes such as $[Ru(\eta^6\text{-cymene})(PPh_3)\{k^2\text{-N,S-PhNC(S)NMe}_2\}]BPh_4$[32], and $[(\eta^5\text{-Cp*})RhCl\{SC(=NCN)NHMe\}PPh_3]$[27] reported in the literature.

Proton NMR spectra of the complexes **4r**–**4ze**, showed distinctive singlets around 1.30–1.65 ppm in all the complexes. These peaks integrated to 15 protons of the Cp* ligand. Other peaks corresponding to bridging alkyl protons of the pyridyl thiourea ligands were observed around 1.70-3.50 ppm in **4t**, **4u**, **4z**–**4ze**. Methyl protons of the *p*-methoxyphenyl substituents were recorded around 3.80 – 3.96 ppm in **4v**, **4w**, **4zd** and **4ze**. In all the complexes, the NH protons appeared as singlets around 4.50-5.99 ppm. The peaks for the aromatic protons of the thiourea ligands and the attached PPh_3 ligands were observed around 6.02-10.05 ppm in all the complexes.

$^{31}P\{^1H\}$ NMR spectra of the PPh_3 substituted complexes showed singlets around 5-15 ppm for the iridium thiourea complexes and doublets around 30-45 ppm for the rhodium complexes resulting from phosphorus-rhodium coupling ($^1J_{(PRh)}$). Average $^1J_{(PRh)}$ coupling constant values of 149.50 Hz were recorded for the complexes. Similar coupling constant values have been reported for rhodium complexes of the diphenyl substituted thiourea monoanion complex in **4.2**[27].

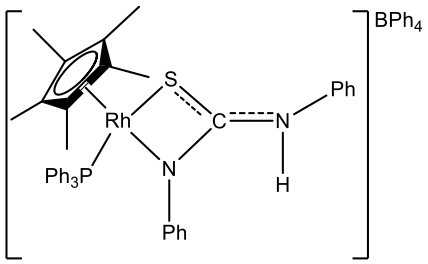

4.2

FTIR spectra of the complexes showed vibrational bands around 3480-3300 cm^{-1} for all the complexes **4r**–**4ze** attributed to NH protons of the thiourea ligands. This is an indication of the presence of at least one uncoordinated NH group in each of the complexes.

4.2.6 *X-ray crystallographic analysis of rhodium and iridium thiourea complexes*

In order to gain a broader understanding of the coordination modes of the various pyridyl substituted thioureas to iridium and rhodium, crystals of the complexes **4r**, **4s**, **4y**, **4z**, **4zb** and **4ze** were obtained. The molecular structure of the mononuclear neutral complexes **4r** and **4s** presented in **Figure 4.11** feature the regular 3-legged piano-stool arrangement, similar to the ones found in mononuclear ruthenium complex **4k**. The coordination sites around the metal in this case, are taken up by a η^5 Cp* ring, an N,S coordinating thiourea ligand and chloride anion in a distorted *pseudo*-octahedral geometry. In a related complex **4y**, (**Figure 4.12**) the chloride anion is substituted with a neutral PPh_3 ligand to give a mono-cationic thiourea complex $[(Cp^*)Ir\{SC(N(Py)NPh\}(PPh_3)]BF_4$.

The crystal structures of the three complexes **4r**, **4y** and **4s** feature a bidentate mode of coordination, through the N-pyridyl and thiolate-S of the thiourea ligand to give six-membered chelate rings. The metallacyclic rings in the complexes are slightly puckered to an r.m.s deviation of 0.375, 0.382 and 0.311 Å for **4r**, **4s** and **4y** respectively. The dihedral angles between the six-membered chelate rings and the adjacent pyridyl rings are 29.9^o, 26.04^o, 23.50^o for **4r, 4s,** and **4y** respectively. The metal to centroid (arene) distance in **4y**, 1.837 Å is slightly longer than those in **4r**, 1.793 Å and **4s**; 1.789 Å. The M-S(1) bond distances in **4r**, 2.376(11) Å and **4s**; 2.379(18) Å are similar and longer than the corresponding bond in **4y** and related rhodium and iridium complexes of a picolyl thiourea ligand, **4.3**.[22]

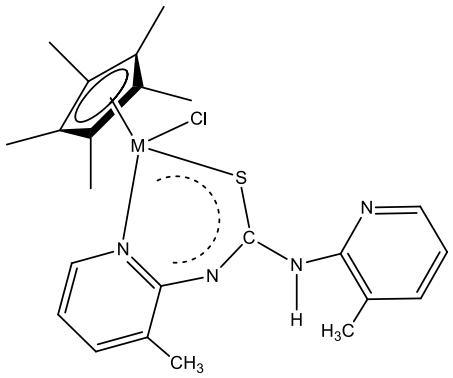

4.3 (M = Rh, Ir)

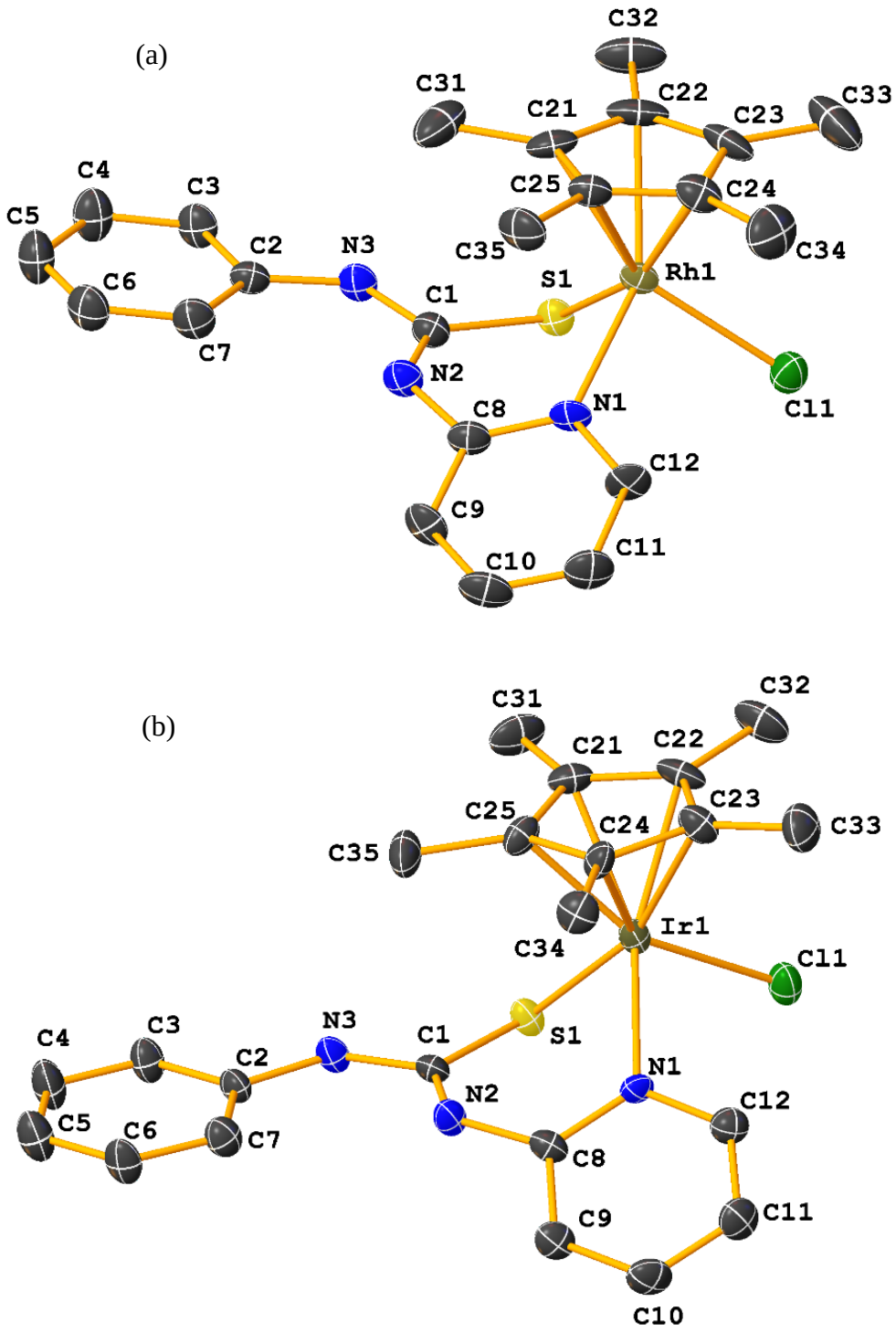

Figure 4.11: Molecular structures of (a) phenyl and pyridyl substituted rhodium thiourea complex **4r**, [(η^5-Cp*)Rh{SC(=NPy)NHPh}Cl] (b) phenyl pyridyl substituted iridium thiourea complex, **4s** [(η^5-Cp*)Ir{SC(=NPy)NHPh}Cl] Hydrogen atoms are omitted for clarity. Ellipsoids are drawn at 50% probability.

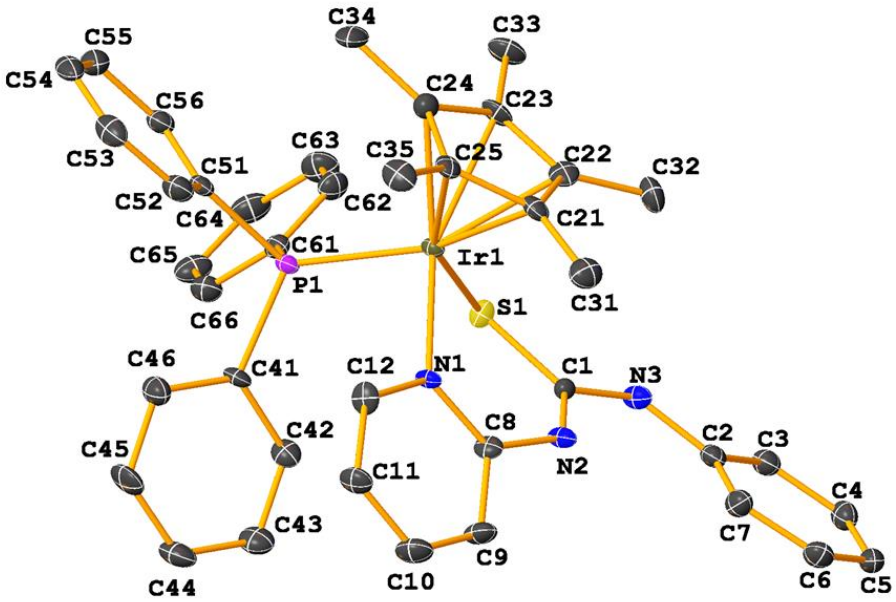

Figure 4.12: Molecular structure of phenyl and pyridyl substituted iridium complex [(Cp*)Ir{SC(N(Py)NHPh}(PPh_3)]BF_4 **4y.** Hydrogen atoms and BF_4 anions are omitted for clarity. Ellipsoids are drawn at 50% probability.

Similarly, the M-N(1) bonds in **4r** and **4s** are progressively longer than the corresponding M-N(1) bonds in **4y**, **Table 4.5**. This is probably due to the steric effect of the large PPh_3 ligand bound to the metal in **4y**. The C(1)–S(1) bonds in the three complexes are similar **4r**; 1.756(5) Å, **4s**; 1.767(7) Å, **4y**; 1.749(7) Å and significantly longer than the average C–S thione double bond length of 1.654 Å. This is an indication of electron delocalisation in the chelate ring. The C(1)-N(2) bonds connected to the pyridyl in the complexes **4r**; 1.296(7), **4s**; 1.288 and **4y**; 1.292(8) Å are systematically shorter than the C(1)-N(3) bonds in **4r**; 1.375(6) Å, **4s**; 1.369(8) Å, **4y**; 1.371(8) Å. This is an indication of the double and single bond character of the C(1)-N(2) and C(1)-N(3) bonds respectively, thus placing the proton on C(1)-N(3)-Ph. The angles subtended at the metal centre in the complexes are very close to 90°, consistent with the bite angles in a *pseudo*-octahedral geometry[4]. The S(1)- M(1)-P(1) angle in **4y** 85.50(6)° is however, smaller than the corresponding S(1)- M(1)-Cl(1) angles in **4r**, 90.22(3)° and **4s**, 88.48(6)°. The bulky nature of the PPh_3 ligand in **4y** may be responsible for this disparity in bond angles. The opposite trend applies to all the other angles subtended at the metal centre. For example, the N(1)- M(1)-S(1) angles in **4r**; 83.24(11)°, and **4s**; 82.55(15)° are significantly smaller than the corresponding angle in **4y**; 88.25(15)°. The angles

subtended at the thiolate S(1) atom follow a similar trend with the C(1)-S(1)-M(1) angles in **4y** larger than those in **4r** and **4s** by approximately 3°. The angles at the N(1) are equivalent in the three complexes and equal to 123°. Apart from the structural and geometric differences in the structures of complexes **4r**, **4s** and **4y** discussed above, the structural orientation of the complexes results in intermolecular hydrogen bonding in the structure of **4r** and **4s** but not in **4y**. Intermolecular hydrogen-bonded dimers of **4s** are shown in **Figure 4.13**.

Crystal structures of alkyl-pyridyl substituted thiourea complexes **4z**, **4zb** and **4ze** were also obtained. In these structures, the pyridyl substituent of the thiourea ligand was replaced with methylenepyridyl group in **4z** and the ethylene pyridyl group for **4zb** and **4ze**. The molecular structures of the compounds presented in **Figures 4.14 - 4.16** show a piano stool arrangement similar to the ones found in **4y**, however the coordination environment in these complexes features a more strained pseudo-octahedral geometry which involves a Cp* arene ligand, a large PPh_3 ligand and an N,S bonded thiourea nitrogen and thione sulfur of the ligand in a four-membered chelate ring.

Table 4.5: Geometric parameters for rhodium and iridium thiourea complexes **4r**, **4s**, and **4y**

Bond lengths (Å) and angles (°)	**4r (Rh)**	**4s (Ir)**	**4y (Ir)**
M(1) – Cl(1)/P(1)	2.413(12)	2.409(18)	2.317(17)
M(1) – S(1)	2.376(11)	2.379(18)	2.370(17)
M(1) – N(1)	2.102(4)	2.110(5)	2.098(5)
N(3) – C(1)	1.375(6)	1.369(8)	1.371(8)
N(2) – C(1)	1.296(7)	1.288(8)	1.292(8)
S(1) – C(1)	1.756(5)	1.767(7)	1.749(7)
S(1) – M(1) – Cl(1)/P(1)	90.22(3)	88.48(6)	85.50(6)
N(1) – M(1) – S(1)	83.24(11)	82.55(15)	88.25(15)
N(1)– M(1) – Cl(1)/P(1)	89.87(11)	87.92(16)	91.11(16)
C(1) – S(1) – M(1)	97.09(16)	97.2(2)	100.0(2)
C(8)/C(9) – N(1) – M(1)	123.1(3)	122.7(4)	123.6(4)
N(3) – C(1) – S(1)	112.6(4)	112.5(5)	112.6(5)
N(3) – C(1) – N(2)	119.8(4)	120.6(6)	119.2(6)
N(2) – C(1) – S(1)	127.6(4)	126.9(5)	128.1(5)

Note: M = Rh or Ir

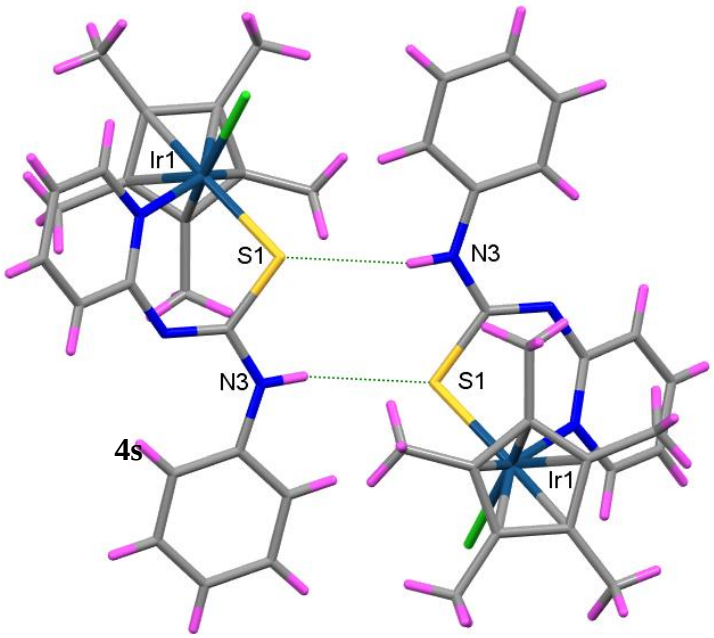

Figure 4.13: Intermolecular hydrogen bonding in the crystal structure of **4s**, resulting in a hydrogen-bonded dimer.

The four-membered metallacyclic rings formed in these complexes are planar to a r.m.s. deviation of 0.027, 0.001, and 0.0027 Å for **4z**, **4zb** and **4ze** respectively. This is a significant shift from the more puckered six-membered metallacycle in **4r**, **4s** and **4y**. The molecular structure of the complexes shows that the pyridyl nitrogen is not involved in the coordination with the metal, which is probably due to the presence of the methylene and ethylene spacers in the thiourea ligands and the difficulty in forming seven or eight-membered rings. The pyridyl rings separated from the metallacycle by a methylene group in **4z** and as much as an ethylene in **4zb** and **4ze** has much larger dihedral angles; **4z** 65.06(11)^{o}, **4zb** 85.56(5)^{o}, **4ze** 43.08(2)^{o} when compared with the corresponding angles in **4r**, **4s** and **4y** with an average value of 23^{o}. The bond lengths and angles in these complexes are comparable to the values reported for **4y**, and other complexes reported in the literature[4,26,27,30]. The N(1)-Rh(1)-S(1) and C(1)-S(1)-Rh(1) in **4z**, **4zb** and **4ze** are however significantly smaller than the values reported for **4y**, probably due to the strain in coordination sphere from the four-membered ring formed by these complexes as opposed to the 6-membered ring in **4y**.

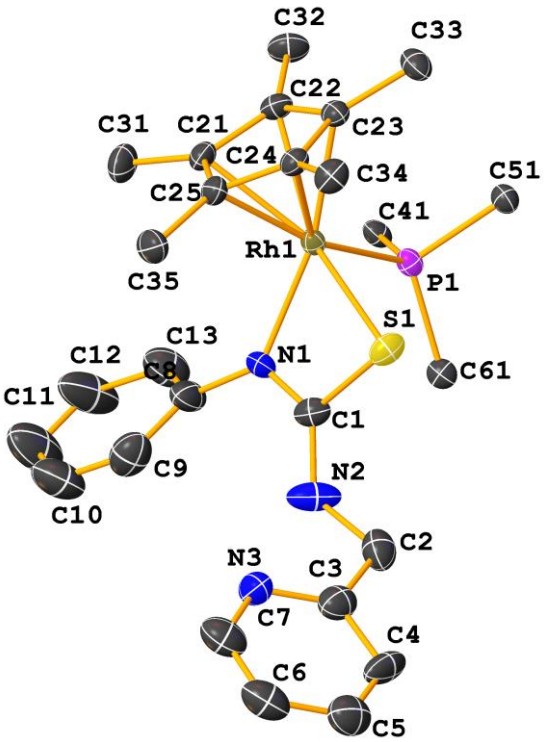

Figure 4.14: Molecular structure of phenyl and methylenepyridyl-substituted rhodium thiourea complex **4z**, $[(\eta^5\text{-Cp*})Rh\{SC(=NHCH_2Py)NPh\}PPh_3]BF_4$ Hydrogen atoms and BF_4 anions are omitted for clarity. Ellipsoids are drawn at 50% probability. Only ipso carbon atoms are shown for clarity.

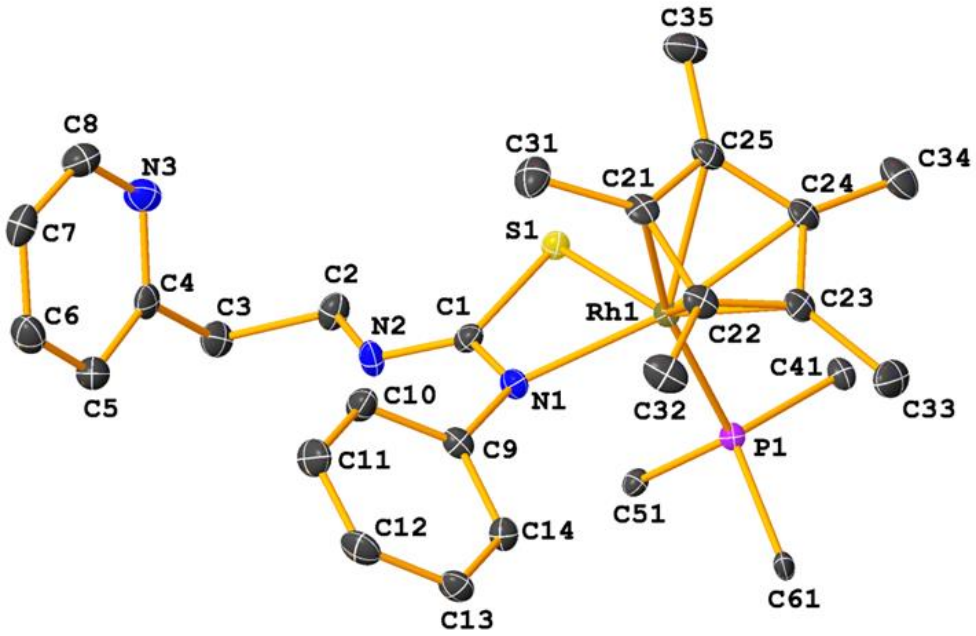

Figure 4.15: Molecular structure of phenyl and ethylenepyridyl-substituted rhodium thiourea complex **4ze**, $[(\eta^5\text{-Cp*})Rh\{SC(=NH(CH_2)_2Py)NPh\}PPh_3]BF_4$. Hydrogen atoms and BF_4 anions are omitted for clarity. Ellipsoids are drawn at 50% probability. Only ipso carbon atoms are shown for clarity.

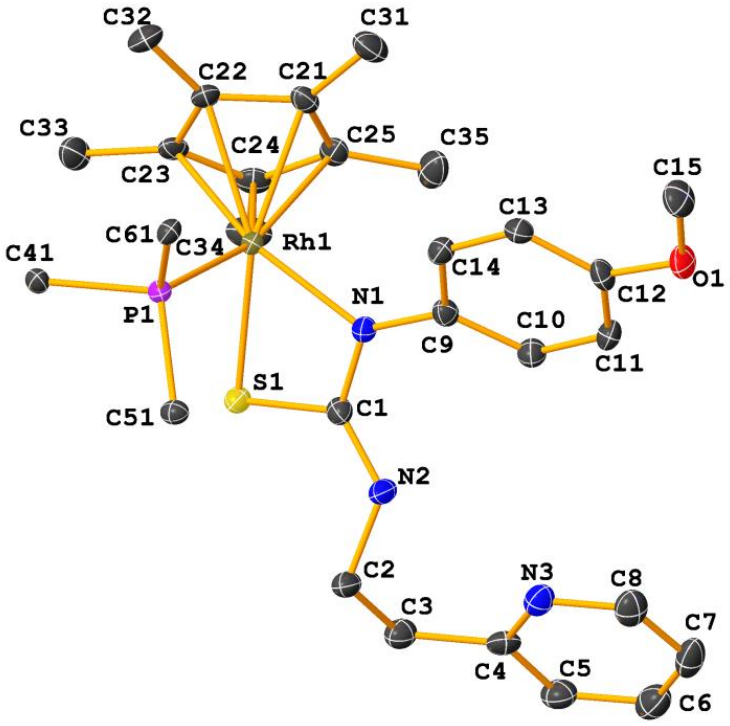

Figure 4.16: Molecular structure of *p*-methoxyphenyl and ethylenepyridyl-substituted rhodium thiourea complex **4z**, [(η^5-Cp*)Rh{SC(=NH(CH_2)$_2$Py)NC_6H_4OMe}PPh_3]. Hydrogen atoms and BF_4 anions are omitted for clarity. Ellipsoids are drawn at 50% probability. Only ipso carbon atoms are shown for clarity.

Table 4.6: Geometric parameters for rhodium thiourea complexes **4z**, **4zb** and **4ze**

Bond lengths (Å) and angles (º)	**4z**	**4zb**	**4ze**
Rh(1) – P(1)	2.333(10)	2.344(5)	2.333(5)
Rh(1) – S(1)	2.389(9)	2.409(5)	2.411(6)
Rh(1) – N(1)	2.119(3)	2.109(5)	2.117(17)
C(1) – N(1)	1.305(5)	1.317(3)	1.318(3)
N(2) – C(1)	1.330(5)	1.333(3)	1.334(3)
S(1) – C(1)	1.7444(4)	1.744(2)	1.746(2)
P(1) – Rh(1) – S(1)	88.39(3)	87.11(19)	86.51(18)
N(1) – Rh(1) – S(1)	67.70(5)	67.32(5)	67.30(5)
N(1) – Rh(1) – P(1)	90.83(10)	92.10(5)	92.77(5)
C(1) – S(1) – Rh(1)	79.16(13)	80.13(8)	80.13(17)
C(1) – N(1) – Rh(1)	101.50(3)	102.72(14)	102.37(13)
N(1) – C(1) – S(1)	110.80(3)	109.95(16)	109.95(16)
N(1) – C(1) – N(2)	126.84(4)	126.8(2)	126.17(19)
N(2) – C(1) – S(1)	122.4(3)	123.43(16)	123.84(17)

4.3 Conclusions

A series of pyridyl substituted thiourea complexes of ruthenium, rhodium and iridium were synthesised and characterised by ESI-mass spectrometry, NMR and single-crystal X-ray crystallography. The compounds formed both neutral and cationic mononuclear complex. Substitution of the chloride ion in the complexes with a bulkier PPh_3 ligand resulted in changes in the geometric parameters around the metal coordination sphere, while substitution of the pyridyl functional group with a methylene pyridyl and ethylene pyridyl groups resulted in an eight-membered bidentate chelate ring in **4c** or juxtaposition of the pyridyl functionality from the proximal to the distal position and formation of a four-membered chelate ring.

4.4 Experimental

4.4.1 *Synthesis of ligands and complexes*

Refer to Chapter two for general experimental procedures, instrumentation and synthesis of the thiourea ligands. The complexes were synthesised by reacting $[(\eta^6\text{-}C_6Me_6)RuCl_2]_2$ or $[Cp^*MCl_2]_2$ (where M = Rh or Ir) with 2 mole equiv of thiourea ligands of the type $Py(CH_2)_nNHC(S)NHR$ (n = 0, 2 and R = Ph, C_6H_4OMe, $C_6H_4NO_2$) and triethylamine (2 mL) in refluxing methanol solution (20 mL) for 120 min.. The complexes were precipitated by addition of 0.3 mmol of $NaBF_4$ or NH_4PF_6 and distilled water (70 mL) for cationic complexes, and water alone for neutral complexes. The compounds were filtered, washed with methanol (5 mL), diethyl ether (10 mL) and dried overnight in a desiccator under vacuum.

4.4.2 Characterisation of complexes

*$[(\eta^6\text{-}C_6Me_6)Ru\{SC(=NPy)NHPh\}\{SC(NPy)NHPh]$ **(4a)***

$[(\eta^6\text{-}C_6Me_6)RuCl_2]_2$ (67 mg, 0.11 mmol) and PyNHC(S)NHPh (48 mg, 0.20 mmol). Yield: 72 mg, 62%. Elemental analysis %: calculated for $C_{36}H_{38}N_6RuS_2$; C, 60.06; H, 5.32; N, 11.67, found; C, 60.04; H, 5.32, N, 11.71. ESI-MS: Calculated *m/z*; 721.08 $[M+H]^+$, experimental *m/z*: CEV 60 V, 721.07 (100%) $[M+H]^+$, CEV 150 V, 492.04 (100%) $[M\text{-}C_{12}H_{10}NS]^+$, 721.01 (52%) $[M+H]^+$, CEV 180 V, 492.04 (100%) $[M\text{-}C_{12}H_{11}NS]^+$. ^1H NMR δ ppm: 1.89 [d, 18H, CH_3, C_6Me_6; J = 22.4 Hz], 6.29 [d, 1H, NH, J = 3.8 Hz], 6.7-6.9 [m, 2H, Ar-H], 7.01-7.23 [m, 3H, Ar-H], 7.36-7.6 [m, 2H, Ar-H], 7.7 [d, 1H, Ar-H; J = 7.8 Hz], 8.62 [s, H, NH]. FTIR (cm^{-1}):

3552(m), 3478(br), 3415(s), 3240(m), 2923(w), 1638(w), 1616(m), 1561(s), 1496(s), 1460(s), 1435(s), 1384(s), 1313(s), 1228(m), 1149(s), 1108(w), 1084(m), 925(m), 844(s), 770(s), 694(s), 624(s), 557(m), 479(w).

[(η^6-C_6Me_6)Ru{SC(=N Py)NHC$_6$H$_4$OMe}{SC(H Py)NHC$_6$H$_4$OMe}]PF_6 (***4b***)

[(η^6-C_6Me_6)$RuCl_2$]$_2$ (67 mg, 0.11 mmol) and PyNHC(S)NHC$_6$H$_4$OMe (56 mg, 0.20 mmol). Yield; 80 mg, 66%. Elemental analysis %: calculated for $C_{38}H_{43}F_6N_6O_2PRuS_2$; C, 49.29; H, 4.68; N, 9.08, found; C, 49.30; H, 4.68; N, 9.06. ESI-MS: Calculated *m/z*; 781.05 $[M+H]^+$, experimental *m/z*: CEV 60 V, 522.02 (58%) $[M-C_{13}H_{12}N_3OS]^+$, 781.05 (100%) $[M+H]^+$, CEV 150 V, 522.04 (100%) $[M-C_{13}H_{12}N_3OS]^+$, 781.07 (46%) $[M+H]^+$. ^{1}H NMR δ ppm: 1.95 [s, 18 H, CH_3, C_6Me_6], 3.82 [s, 3H, CH_3OMe], 3.89 [s, 3H, CH_3OMe], 4.05 [s, 1H, NH], 6.65-7.06 [m, 2H, Ar-H], 7.31-7.18 [m, 2H, Ar-H], 7.65 [m, 6H, Ar-H], 7.86 [t, 2H, Ar-H; J = 8.2 Hz], 8.17 [m, 1H, Ar-H], 8.20- 8.49 [d, 2H, Ar-H; J = 5.3 Hz], 10.84 [s, 1H, NH]. FTIR (cm^{-1}): 3437(br), 3001(w) 2920(w), 1609(w), 1579(m), 1542(m), 1508(s), 1464(s), 1430(w), 1385(m), 1299(m), 1246(m), 1182(w), 1150(s), 1112(m), 1030(m), 926(w), 845(s) 781(m), 740(m), 557(s), 525(w).

*[(η^6-C_6Me_6)Ru{SC(=NH(CH_2)$_2$Py)NPh}]PF_6 (**4c**)*

[(η^6-C_6Me_6)$RuCl_2$]$_2$ (67 mg, 0.11 mmol) and Py(CH_2)$_2$NHC(S)NHPh (52 mg, 0.20 mmol). Yield: 86 mg, 71 %. Elemental analysis %: calculated for $C_{30}H_{42}F_6ON_3PRuS$; C, 48.77; H, 5.73; N, 5.69, found; C, 48.90; H, 5.86, N, 5.41. ESI-MS: Calculated *m/z*; 520.02 $[M]^+$, experimental *m/z*: CEV 60-180 V, 519.98 (100%) $[M]^+$. ^{1}H NMR δ ppm: 2.12 [s, 18H CH_3, C_6Me_6], 2.83 [m, 2H, CH_2], 3.19 [d, 2H, CH_2, d = 15.40 Hz], 4.48 [s, 1H, NH], 6.96 [d, 3H, Ar-H; J = 7.2 Hz], 7.01 [t, 1H, Ar-H; J = 7.7 Hz], 7.17 [t, 3H, Ar-H; J = 7.9 Hz], 7.45 [d, 1H, Ar-H; J = 7.3 Hz], 7.79 [t, 2H, Ar-H; J = 7.8 Hz], 8.49 [d, 1H, Ar-H; J = 5.51]. FTIR (cm^{-1}): 3467(br), 3012(w), 2925(m), 1598(m), 1561(s), 1499(m), 1474(w), 1440(w), 1386(m), 1300(s), 1243(w), 1159(w), 1111(w), 1069(m), 1017(m), 843(s), 762(s), 696(s), 624(w), 558(m), 500(m).

*[(η^6-C_6Me_6)Ru{SC(=NH(CH_2)$_2$ Py)NC_6H_4OMe]PF_6 (**4d**)*

[(η^6-C_6Me_6)$RuCl_2$]$_2$ (67 mg, 0.11 mmol) and Py(CH_2)$_2$NHC(S)NHC_6H_4OMe (56 mg, 0.20 mmol). Yield; 126 mg, 95 %. Elemental analysis %: calculated for $C_{27}H_{34}F_6N_3OPRuS$; C, 46.68; H, 4.93; N, 6.05, found; C, 46.63; H, 4.95; N, 6.02. ESI-MS: Calculated *m/z*; 550.01 $[M]^+$, experimental *m/z*: CEV 60-180 V, 549.99 (100%) $[M]^+$. ^{1}H NMR δ ppm: 2.11 [s, 18 H, CH_3, C_6Me_6] 2.54-2.69 [m, 2H, CH_2], 2.74-2.87 [m, 2H, CH_2] 5.01 [m, 1H, NH], 3.82 [s, 3H, CH3], 6.67-7.09 [m, 3H, Ar-H], 7.05-7.18 [m, 1H, Ar-H], 7.65 [m, 3H, Ar-H], 7.86 [t, 2H, Ar-H; J = 8.2 Hz], 8.17 [m, 1H, Ar-H], 8.25 [m, 2H, Ar-H], 8.47 [d, 1H, Ar-H; J = 5.3 Hz]. FTIR (cm^{-1}): 3552(m), 3478(br), 3415(m), 3236(w), 2934(m), 1638(m), 1617(s), 1561(s), 1511(s), 1473(m), 1441(m), 1385(s), 1292(m), 1246(s), 1178(s), 1109(m), 1031(s), 843(s), 767(m), 628(s), 557(s), 485(m).

*[(η^6-C_6Me_6)Ru{SC(=N(Py)NHPh}(PPh_3)]BF_4 (**4e**)*

[(η^6-C_6Me_6)$RuCl_2$]$_2$ (67 mg, 0.11 mmol) and PyNHC(S)NHPh (46 mg, 0.20 mmol), PPh_3 (54 mg, 0.21 mmol). Yield: 60 mg, 51 %. Elemental analysis %: calculated for $C_{42}H_{43}BF_4N_3PRuS$; C, 60.0; H, 5.16; N, 5.00, found; C, 60.02; H, 5.16, N, 4.97. ESI-MS: Calculated *m/z*; 754.20 $[M]^+$, experimental *m/z*: CEV 60 V, 754.20 (100 %) $[M]^+$, CEV 150 V, 754.20 (82%) $[M]^+$, 492.09 (89%) $[M\text{-}PPh_3]^+$, CEV 180 V, 492.04 (100%) $[M\text{-}PPh_3]^+$, 754.20 (2%) $[M]^+$. ^{1}H NMR δ ppm: 1.89 [s, 18H, CH_3, C_6Me_6], 4.9 [s, 1H, NH], 6.62 [m, 1H, Ar-H], 6.77 [d, 1H, Ar-H, J = 8.2 Hz], 6.94 [t, 4H, Ar-H, J = 7.5 Hz], 7.1 [t, 2H, Ar-H, J = 7.3 Hz], 7.24-7.26 [m, 1H, Ar-H, J = 7.1 Hz], 7.35 [t, 6H, Ar-H; J = 7.8 Hz], 7.44 [t, 3H, Ar-H, J = 6.9 Hz], 7.49 [t, 3H, Ar-H, d = 8.30 Hz], 7.65 [m, 2H Ar-H,], 7.75 [t, 2H, Ar-H, J = 6.8 Hz], 8.36 [d, 1H, Ar-H, J = 5.9 Hz]. $^{31}P\{^1H\}$ NMR δ ppm: 39.22 [s, PPh_3]. FTIR (cm^{-1}): 3552(m), 3478(br), 3415(s), 3238(w), 2924(w), 1637(w), 1608(m), 1569(s), 1497(s), 1456(s), 1436(m), 1385(s), 1330(s) 1299(s), 1235(s), 1143(s), 1114(m), 1068(m), 933(m), 855(s), 783(m), 750(s), 701(s), 621(s), 525(s), 499(m).

*[(η^6-C_6Me_6)Ru{SC(=NHCH_2Py)NPh}PPh_3]BF_4 (**4f**)*

[(η^6-C_6Me_6)$RuCl_2$]$_2$ (67 mg, 0.11 mmol) and PyCH_2NHC(S)NHPh (48 mg, 0.20 mmol), PPh_3 (54 mg, 0.21 mmol). Yield: 80 mg, 73 %. Elemental analysis %: calculated for $C_{44}H_{47}BCl_2F_4N_3PRuS$; C, 56.24; H, 5.04; N, 4.47, found; C, 56.42; H, 5.16, N, 4.49. ESI-MS: Calculated *m/z*; 768.10 $[M]^+$, experimental *m/z*: CEV 60

V, 768.05 (100 %) $[M]^+$, CEV 150 V, 506.11 (82%) $[M\text{-}PPh_3]^+$, 768.21 (28%) $[M]^+$, CEV 180 V, 506.12 (100%) $[M\text{-}PPh_3]^+$, 768.20 (5%) $[M]^+$. ^1H NMR δ ppm: 1.81 [d, 18H, CH_3, C_6Me_6; J = 19.02 Hz], 3.43 [dd, 2H, CH_2; J = 15.4 Hz, J = 3.1 Hz], 4.25 [dd, 1H, NH; J = 15.1 Hz, J = 4.6 Hz], 6.53 [t, 1H, Ar-H, J = 8.38 Hz], 7.07-7.20 [m, 6H, Ar-H], 7.26-7.55 [m, 14H, Ar-H], 7.70 [m, 3H, Ar-H], 7.94 [m, 1H, Ar-H], 8.43 [t, 1H, Ar-H, J = 5.4 Hz]. $^{31}P\{^1H\}$ NMR δ ppm: 42. 68 [s, PPh_3]. FTIR (cm^{-1}): 3438(br), 3057(m), 2918(m), 1633(w), 1591(s), 1570(w), 1550(m), 1479(s), 1434(m), 1382(m), 1327(s) 1271(s), 1168(m), 1106(s), 1066(w), 996(w), 841(m), 752(s), 695(s), 522(s), 490(w).

$[(\eta^6\text{-}C_6Me_6)Ru\{SC(=NH(Py)NC_6H_4NO_2\}(PPh_3)]BF_4$ ***(4g)***

$[(\eta^6\text{-}C_6Me_6)RuCl_2]_2$ (67 mg, 0.11 mmol) and $PyNHC(S)NHC_6H_4NO_2$ (54 mg, 0.20 mmol), PPh_3 (54 mg, 0.21 mmol). Yield: 119 mg, 69 %. Elemental analysis %: calculated for $C_{42}H_{42}BF_4N_4O_2PRuS$; C, 56.95; H, 4.78; N, 6.33, found; C, 56.97; H, 4.81, N, 6.29. ESI-MS: Calculated *m/z*; 799.18 $[M]^+$, experimental *m/z*: CEV 60 V, 799.18 (100 %) $[M]^+$, 1097.21 $[M+L+Na]^+$(L=$PyNC(S)NHC_6H_4NO_2$), CEV 150 V, 537.08 (82%) $[M\text{-}PPh_3]^+$, 799.18 (82%) $[M]^+$, CEV 180 V, 537.04 (100%) $[M\text{-}PPh_3]^+$. ^1H NMR δ ppm: 1.89 [s, 18H, CH_3, C_6Me_6], 2.09 [t, 1H, NH; J = 4.23 Hz], 6.67 [t, 1H, Ar-H, J = 6.95], 6.87 [d, 1H, Ar-H; J = 7.88 Hz], 6.95 [dd, 4H, Ar-H, J = 8.82 Hz],], 7.1 [t, 1H, Ar-H; J = 6.95 Hz], 7.46 [dd, 4H, Ar-H, J = 8.81, 7.6 Hz], 7.5 [t, 1H, Ar-H; J = 7.7 Hz], 7.44 [t, 3H, Ar-H, J = 6.85 Hz], 7.49 [t, 3H, Ar-H, J = 8.30 Hz], 7.65 [m, 3H], 7.75 [t, 2H, Ar-H; J = 6.82 Hz], 8.36 [d, 1H, Ar-H, J= 5.9 Hz]. $^{31}P\{^1H\}$ NMR δ ppm: 41.12 [s, PPh_3]. FTIR (cm^{-1}): 3428(br), 3051(m), 2920(w), 1597(s), 1570(s), 1546(m), 1497(s), 1455(s), 1436(w), 1385(m), 1329(s), 1299(s), 1236(m), 1143(s), 1144(s), 1084(m), 1064(m), 933(m), 854(s), 781(m), 750(s), 699(s), 620(w), 525(s), 499(m).

$[(\eta^6\text{-}C_6Me_6)Ru\{SC(=NHCH_2(Py)NC_6H_4NO_2\}(PPh_3)]BF_4$ ***(4h)***

$[(\eta^6\text{-}C_6Me_6)RuCl_2]_2$ (67 mg, 0.11 mmol) and $PyCH_2NHC(S)NHC_6H_4NO_2$ (58 mg, 0.20 mmol), PPh_3 (54 mg, 0.21 mmol). Yield: 126 mg, 71 %. Elemental analysis %: calculated for $C_{43}H_{45}BF_4N_4O_2PRuS$; C, 57.34; H, 4.78; N, 6.33, found; C, 56.97; H, 4.81, N, 6.29. ESI-MS: Calculated *m/z*; 813.20 $[M]^+$, experimental *m/z*: CEV 60 V, 551.09 (12%) $[M\text{-}PPh_3]^+$, 813.19 (100 %) $[M]^+$, CEV 150 V, 551.09 (89%) $[M\text{-}PPh_3]^+$, 813.19 (29%) $[M]^+$, CEV 180 V, 551.10 (100%) $[M\text{-}PPh_3]^+$. ^1H NMR δ ppm:

2.11 [s, 18H, CH_3, C_6Me_6], 2.34 [d, 2H, CH_2, J = 8.2 Hz], 5.62 [t, 1H, NH; J = 7.8 Hz], 6.82 [d, 1H, Ar-H; J = 8.8 Hz], 6.98-7.87 [m, 21 H, Ar-H, J = 7.2 Hz], 7.90 [t, 3H, Ar-H; J = 8.2 Hz], 8.36 [d, 1H, Ar-H, J = 5.2 Hz]. $^{31}P\{^1H\}$ NMR δ ppm: 37.62 [s, PPh_3]. FTIR (cm^{-1}): 3438(br), 3057(m), 2919(m), 1633(w), 1591(s), 1570(w), 1550(m), 1485(s), 1434(m), 1385(m), 1327(s) 1271(s), 1168(m), 1106(s), 1066(w), 999(w), 845(m), 752(s), 697(s), 525(s), 495(w).

$[(\eta^6\text{-}C_6Me_6)Ru\{SC(=NH(CH_2)_2Py)NPh\}(PPh_3)]BF_4$ ***(4i)***

$[(\eta^6\text{-}C_6Me_6)RuCl_2]_2$ (67 mg, 0.11 mmol) and $Py(CH_2)_2NHC(S)NHPh$ (52 mg, 0.20 mmol), PPh_3 (54 mg, 0.21 mmol). Yield: 152 mg, 87 %. Elemental analysis %: calculated for $C_{44}H_{47}BF_4N_3PRuS$; C, 60.83; H, 5.45; N, 4.84, found; C, 60.88; H, 5.35; N, 4.80. ESI-MS: Calculated *m/z*; 782.10 $[M]^+$, experimental *m/z*: CEV 60 V; 520.07 (15%) $[M\text{-}PPh_3]^+$, 782.13 (100%) $[M]^+$, CEV 150 V, 520.07 (100%) $[M\text{-}PPh_3]^+$, 782.13 (12%) $[M]^+$. ^1H NMR δ ppm: 2.01 [s, 18H, CH_3, C_6Me_6], 2.72 [m, 2H, CH_2], 3.34 [t, 2H, CH_2, J = 9.3 Hz], 5.01 [s, 1H, NH], 6.65 [d, 1H, Ar-H; J = 7.8 Hz], 6.9-7.65 [m, 19 H, Ar-H, J = 9.2 Hz], 7.92 [t, 3H, Ar-H; J = 8.6 Hz], 8.48 [d, 1H, Ar-H, J = 5.6 Hz]. $^{31}P\{^1H\}$ NMR δ ppm: 41.20 [s, PPh_3]. FTIR (cm^{-1}): 3446(br), 3055(w), 2925(m), 1595(m), 1555(s), 1483(s), 1435(s), 1328(m), 1308(w), 1219(w), 1158(w), 1084(s), 1056(s), 829(w), 843(w), 754(s), 699(s), 524(s), 494(w).

$[(\eta^6\text{-}C_6Me_6)Ru\{SC(=NH(CH_2)_2(Py)NC_6H_4NO_2\}(PPh_3)]BF_4$ ***(4j)***

$[(\eta^6\text{-}C_6Me_6)RuCl_2]_2$ (67 mg, 0.11 mmol) and $Py(CH_2)_2NHC(S)NHC_6H_4NO_2$ (60 mg, 0.21 mmol), PPh_3 (54 mg, 0.20 mmol). Yield: 152 mg, 87 %. Elemental analysis %: calculated for $C_{44}H_{46}BF_4N_3O_2P_2RuS$; C, 51.14; H, 3.76; N, 7.56, found; C, 51.18; H, 3.91; N, 7.50. ESI-MS: Calculated *m/z*; 827.15 $[M]^+$, experimental *m/z*: CEV 60 V; 565.07 (10%) $[M\text{-}PPh_3]^+$, 827.17 (100%) $[M]^+$, CEV 150 V, 565.06 (100%) $[M\text{-}PPh_3]^+$, 827.15 (14%) $[M]^+$. ^1H NMR ($CDCl_3$) δ ppm: 2.16 [s, 18H, CH_3, C_6Me_6], 2.86 [dd, 2H, CH_2, J = 11.2 Hz, 6.9 Hz], 3.03 [t, 2H, CH_2, J = 8.9 Hz], 4.06 [s, 1H, NH], 6.85 [d, 1H, Ar-H; J = 7.9 Hz], 7.2-7.72 [m, 22H, Ar-H, J = 8.82 Hz], 7.88 [t, 3H, Ar-H; J = 9.1 Hz], 8.55 [d, 1H, Ar-H, J = 4.40 Hz]. $^{31}P\{^1H\}$ NMR ($CDCl_3$) δ ppm: 42.40 [s, PPh_3]. FTIR (cm^{-1}): 3430(br), 3052(m), 2921(w), 1591(s), 1555(m), 1494(s), 1434(m), 1384(m), 1326(s), 1269(s), 1170(s), 1106(s), 1065(w), 998(w), 893(m), 846(m), 752(s), 698(s), 525(s), 496(w).

[(η^6-C_6Me_6)Ru{SC(=NPy)NHC$_6$H$_4$OMe}(PPh_3)]PF_6 ***(4k)***

[(η^6-C_6Me_6)$RuCl_2$]$_2$ (67 mg, 0.1 mmol) and PyNHC(S)NHC$_6$H$_4$OMe (61 mg, 0.24 mmol), PPh_3 (54 mg, 0.21 mmol). Yield: 151 mg, 82 %. Elemental analysis %: calculated for $C_{43}H_{45}F_6N_3OP_2RuS$; C, 55.60; H, 4.88; N, 4.52, found; C, 55.58; H, 4.91; N, 4.50. ESI-MS: Calculated *m/z*; 784.10 $[M]^+$, experimental *m/z*: CEV 60 V; 522.04 (12%) $[M\text{-}PPh_3]^+$, 784.09 (100%) $[M]^+$, CEV 150 V, 522.04 (100%) $[M\text{-}PPh_3]^+$, 784.09 (64%) $[M]^+$. ^{1}H NMR δ ppm: 1.27 [s, 18H, CH_3, C_6Me_6], 3.89 [s, 3H, CH_3], 6.84-7.01 [m, 3H, Ar-H], 7.46-7.56 [m, 4H, Ar-H], 7.67-7.76 [m, 3H, Ar-H], 8.0 [dd, 1H, Ar-H; J = 8.3 Hz], 8.25 [dd, 1H, Ar-H, J = 4.9, 8.6 Hz], 8.80 [s, 1H, Ar-H], 13.45 [s, 1H, NH]. $^{31}P\{^1H\}$ NMR δ ppm: 38.76 [s, PPh_3], -143.32 to 143.7 [sp, PF_6]. FTIR (cm^{-1}): 3552(m), 3474(br), 3414(m), 3187(m), 3038(m), 2959(w), 1605(m), 1594(m), 1537(s), 1508(s), 1478(s), 1456(m), 1432(s), 1385(m), 1349(m), 1318(m), 1240(s), 1191(s), 1145(s), 1030(s), 999(w), 930(m), 843(s), 778(s), 742(s), 698(s), 631(s), 557(s), 524(s), 511(m).

[(η^6-p-cymene)Ru{SC(=NPy)NHPh}(PPh_3)]BF_4 ***(4l)***

[(η^6-*p*-cymene)$RuCl_2$]$_2$ (61 mg, 0.1 mmol) and PyNHC(S)NHPh (46 mg, 0.20 mmol), PPh_3 (54 mg, 0.21 mmol). Yield: 126 mg, 78 %. Elemental analysis %: calculated for $C_{40}H_{39}BN_3PRuS$; C, 59.12; H, 4.84; N, 5.17, found; C, 59.20; H, 4.82, N, 5.15. ESI-MS: Calculated *m/z*; 726.16 $[M]^+$, experimental *m/z*: CEV 60 V, 726.19 (100%) $[M]^+$, CEV 150 V, 464.03 (100%) $[M\text{-}PPh_3]^+$, 726.09 (82%) $[M]^+$. ^{1}H NMR δ ppm: 1.02 [d, 3H, $CH_3(Me_2CH)$; J = 6.6 Hz], 1.15 [d, 3H, $CH_3(Me_2CH)$; J = 7.0 Hz], 1.72 [s, 3H, CH_3], 2.43 [m, 1 H, CH Me_2], 5.02 [d, 1H, cym; J = 7.6 Hz], 5.16 [d, 1H, cym; J = 6.9 Hz], 5.4 [d, 1H, cym; J = 5.80], 5.50 [d, 1H, cym; J = 6.20 Hz], 5.77 [s, 1 H, NH], 6.26 [d, 1 H, Ar-H, J = 6.1 Hz], 6.74 [d, 2H, Ar-H], 6.9-8.3 [m, 21 H, Ar-H], $^{31}P\{^1H\}$ NMR δ ppm: 39.96 [s, PPh_3]. FTIR (cm^{-1}): 3478(br), 3414(s), 3055(m) 2927(m), 1638(m), 1617(s), 1568(m), 1508(s), 1458(s), 1434(s), 1384(m), 1312(m), 1226(m), 1152(m), 1084(s), 1060(s), 929(w), 750(s), 696(s), 614(m), 527(s), 496(w).

[(η^6-p-cymene)Ru{SC(=NHCH$_2$Py)NPh}(PPh$_3$)]BF$_4$ ***(4m)***

[(η^6-*p*-cymene)RuCl$_2$]$_2$ (61 mg, 0.11 mmol) and PyCH$_2$NHC(S)NHPh (48 mg, 0.20 mmol), PPh$_3$ (54 mg, 0.21 mmol). Yield: 106 mg, 65 %. Elemental analysis %: calculated for $C_{41}H_{43}BN_3PRuS$; C, 66.56; H, 5.59; N, 5.68, found; C, 66.54; H, 5.62, N, 5.65. ESI-MS: Calculated *m/z*; 740.18 $[M]^+$, experimental *m/z*: CEV 60 V, 740.18 (100%) $[M]^+$, CEV 150 V, 478.05 (100%) $[M\text{-}PPh_3]^+$, 740.12 (82%) $[M]^+$. ^{1}H NMR δ ppm: 1.12 [d, 3H, CH$_3$(Me$_2$CH); J = 8.2 Hz], 1.18 [d, 3H, CH$_3$(Me$_2$CH); J = 7.9 Hz], 1.72 [s, 3H, CH$_3$], 2.14 [s, 2H, CH$_2$], 2.53 [m, 1 H, CH Me$_2$], 4.98 [d, 1H, cym; J = 6.9 Hz], 5.22 [d, 1H, cym; J = 6.7 Hz], 5.51 [d, 1H, cym; J = 6.90], 5.60 [d, 1H, cym; J = 7.2 Hz], 5.87 [s, 1 H, NH], 6.46 [d, 2H, Ar-H, J = 7.8 Hz], 6.7-7.95 [m, 24 H, Ar-H], ^{31}P{^{1}H} NMR δ ppm: 38.12 [s, PPh$_3$]. FTIR (cm^{-1}): 3411(br), 3056(w), 2964(w), 1633(w), 1592(s), 1549(w), 1484(s), 1436(s), 1385(w), 1327(m), 1249(m), 1156(w), 1084(s), 1031(w), 855(w), 755(s), 696(s), 619(w), 527(s), 458(w).

[(η^6-p-cymene)Ru{SC(=NH(CH$_2$)$_2$Py)NPh}(PPh$_3$)]BF$_4$ ***(4n)***

[(η^6-*p*-cymene)RuCl$_2$]$_2$ (61 mg, 0.1 mmol) and Py(CH$_2$)$_2$NHC(S)NHPh (52 mg, 0.20 mmol), PPh$_3$ (54 mg, 0.21 mmol). Yield: 117 mg, 70 %. Elemental analysis %: calculated for $C_{42}H_{43}BF_4N_3PRuS$; C, 60.00; H, 5.16; N, 5.00, found; C, 60.03; H, 5.12, N, 4.98. ESI-MS: theoretical *m/z*; 754.20, experimental *m/z*: CEV 60V, 754.14 (100%) $[M]^+$, CEV 150V; 492.06 (100%) $[M\text{-}PPh_3]^+$, 754.14 (52%) $[M]^+$. ^{1}H NMR (CDCl$_3$) δ ppm: 0.99 [d, 3H, CH$_3$(Me$_2$CH); J = 6.9 Hz], 1.12 [d, 3H, CH$_3$(Me$_2$CH); J = 7.4 Hz], 1.51 [s, 3H, CH$_3$], 2.21 [t, 4H, CH$_2$; J = 7.6 Hz], 2.53 [m, 1 H, CHMe$_2$], 4.97 [d, 1H, cym; J = 7. Hz], 5.12 [d, 1H, cym; J = 7.8 Hz], 5.52 [d, 1H, cym; J = 7.6 Hz], 5.72 [d, 1H, cym; J = 6.6 Hz], 5.79 [s, 1 H, NH], 6.56 [d, 2 H, Ar-H, J = 8.1 Hz], 6.74 [d, 3H, J = 8.9 Hz, Ar-H], 6.9-8.2 [m, 20 H, Ar-H], ^{31}P{^{1}H} NMR δ ppm: 38.16 [s, PPh$_3$]. FTIR (cm^{-1}): 3367(br), 3056(w), 2962(w), 1596(s), 1562(w), 1497(s), 1474(s), 1386(w), 1386(m), 1301(s), 1158(w), 1089(w), 1029(s), 840(s), 760(s), 695(s), 557(s), 498(m).

[(η^6-p-cymene)Ru{SC(=NPy)NHC$_6$H$_4$NO$_2$}(PPh$_3$)]PF$_6$ ***(4o)***

[(η^6-*p*-cymene)RuCl$_2$]$_2$ (61 mg, 0.11 mmol), and PyNHC(S)NHC$_6$H$_4$NO$_2$ (56 mg, 0.23 mmol), PPh$_3$ (54 mg, 0.21 mmol). Yield: 125 mg, 73 %. Elemental analysis %: calculated for $C_{40}H_{38}F_6N_4O_2P_2RuS$; C, 52.46; H, 4.18; N, 6.12, found; C, 52.43;

H, 4.17, N, 6.12. ESI-MS: Calculated *m/z*; 771.11, experimental *m/z*: CEV 60V, 771.08 (100%) $[M]^+$, CEV 150V; 509.00 (100%) $[M\text{-}PPh_3]^+$, 771.07 (78%) $[M]^+$. ^1H NMR δ ppm: 1.04 [d, 3H, $CH_3(Me_2CH)$; J = 6.9 Hz], 1.15 [d, 3H, $CH_3(Me_2CH)$; J = 8.0 Hz], 1.68 [s, 3H, CH_3], 2.40 [m, 1 H, CH Me_2], 5.06 [d, 1H, cym; J = 7.2 Hz], 5.21 [d, 1H, cym; J = 6.8 Hz], 5.42 [d, 1H, cym; J = 6.20 Hz], 5.56 [d, 1H, cym; J = 7.1 Hz], 5.82 [s, 1 H, NH], 6.26 [d, 1 H, Ar-H, J = 7.7 Hz], 6.79 [d, 2H, Ar-H, J = 7.8 Hz], 6.96-8.12 [m, 20H, Ar-H], $^{31}P\{^1H\}$ NMR δ ppm: 37.82 [s, PPh_3]. FTIR (cm^{-1}): 3408(br), 3058(w) 2927(w), 1598(m), 1570(m), 1497(s), 1459(s), 1328(s), 1300(m), 1243(w), 1148(s), 1111(s), 1092(w), 932(w), 841(s), 750(s), 696(s), 618(w), 557(s), 526(s), 498(w).

$[(\eta^6$-p-cymene)Ru{SC(=NPy)NHC_6H_4OMe}$(PPh_3)]PF_6$ ***(4p)***

$[(\eta^6$-*p*-cymene)$RuCl_2]_2$ (61 mg, 0.11 mmol) and PyNHC(S)NHC_6H_4OMe (61 mg, 0.24 mmol), PPh_3 (52 mg, 0.21 mmol). Yield: 121 mg, 76 %. Elemental analysis %: calculated for $C_{41}H_{41}F_6N_3OP_2RuS$; C, 54.66; H, 4.59; N, 4.66, found; C, 54.62; H, 4.59; N, 4.70. ESI-MS: Calculated *m/z*; 756. 05 $[M]^+$, experimental *m/z*: CEV 60 V; 756.06 (100%) $[M]^+$, CEV 150 V, 494.01 (100%) $[M\text{-}PPh_3]^+$, 756.05 (74%) $[M]^+$. ^1H NMR δ ppm: 1.10 [d, 3H, $CH_3(Me_2CH)$; J = 7.6 Hz], 1.15 [d, 3H, $CH_3(Me_2CH)$; J = 8.2 Hz], 1.70 [s, 3H, CH_3], 2.46 [m, 1 H, CH Me_2], 3.88 [s, 3H, OCH_3], 5.1 [d, 1H, cym; J = 6.1 Hz], 5.25 [d, 1H, cym; J = 6.9 Hz], 5.46 [d, 1H, cym; J = 6.81 Hz], 5.70 [d, 1H, cym; J = 6.36 Hz], 5.96 [s, 1 H, NH], 6.46 [d, 2 H, Ar-H; J = 8.1 Hz], 6.9-7.86 [m, 20 H, Ar-H]. $^{31}P\{^1H\}$ NMR δ ppm: 38.12 [s, PPh_3]. FTIR (cm^{-1}): 3478(br), 3415(s), 3236(w), 3001(w), 2933(m), 1637(m), 1579(m), 1542(m), 1508(s), 1464(s), 1430(m), 1385(s), 1299(s), 1247(s), 1181(w), 1150(s), 1112(m), 1069(m), 1031(s), 927(m), 844(s), 782(s), 740(s), 695(s), 705(m), 626(s), 558(s), 524(w).

$[(\eta^6$-p-cymene)Ru{SC(=NH$(CH_2)_2$ Py)NC_6H_4OMe}$(PPh_3)]PF_6$ ***(4q)***

$[(\eta^6$-*p*-cymene)$RuCl_2]_2$ (61 mg, 0.11 mmol) and Py$(CH_2)_2$NHC(S)NHC_6H_4OMe (56 mg, 0.24 mmol), PPh_3 (54 mg, 0.21 mmol). Yield: 146 mg, 83%. Elemental analysis %: calculated for $C_{43}H_{45}F_6N_3OP_2RuS$; C, 55.60; H, 4.88; N, 4.52, found; C, 55.58; H, 4.91; N, 4.50. ESI-MS: Calculated *m/z*; 784.10 $[M]^+$, experimental *m/z*: CEV 60, 784.09 (100%) $[M]^+$, CEV 150 V, 522.04 (100%) $[M\text{-}PPh_3]^+$, 784.09 (56%) $[M]^+$. ^1H NMR δ ppm: 1.14 [d, 3H, $CH_3(Me_2CH)$; J = 6.7 Hz], 1.17 [d, 3H,

$CH_3(Me_2CH)$; J = 7.2 Hz], 1.59 [s, 3H, CH_3], 2.24 [s, 2 H, CH_2], 2.43 [m, 1 H, CH Me_2], 3.89 [s, 3H, OCH_3], 4.83 [d, 1H, cym; J = 6.9 Hz], 5.28 [d, 1H, cym; J = 6.7 Hz], 5.46 [d, 1H, cym; J = 6.20 Hz], 5.50 [d, 1H, cym; J = 6.40 Hz], 5.90 [s, 1 H, NH], 6.56 [d, 1 H, Ar-H, J = 8.4 Hz], 6.8-8.16 [m, 24 H, Ar-H]. $^{31}P\{^1H\}$ NMR δ ppm: 38.66 [s, PPh_3]. FTIR (cm^{-1}): 3414(br), 3056(m), 2960(w), 1568(s), 1504(s), 1435(s), 1325(m), 1290(m), 1245(s), 1180(s), 1118(m), 1091(s), 999(m), 840(s), 750(s), 721(m), 696(s), 639(w), 557(s), 527(s), 495(w).

*[Cp*Rh{SC(=NPy)NHPh}Cl]* ***(4r)***

$[Cp^*RhCl_2]_2$ (62 mg, 0.11 mmol) and PyNHC(S)NHPh (46 mg, 0.21 mmol). Yield: 57 mg, 42 %. Elemental analysis %: calculated for $C_{22}H_{25}N_3RhSCl$; C, 52.65; H, 5.02; N, 8.37, found; C, 52.67; H, 4.98, N, 8.36. ESI-MS: Calculated *m/z*; 466.01 $[M\text{-}Cl]^+$, experimental *m/z*: CEV 60V, 465.97 (100%) $[M\text{-}Cl]^+$, CEV 150V; 466.09 (100%) $[M\text{-}Cl]^+$, 501.94 (12%) $[M+H]^+$. ^1H NMR δ ppm: 1.76 [s, 15H, CH_3 Cp*], 5.93 [s, 1H, NH], 6.08 [d, 2H, Ar-H; J = 8.2 Hz], 7.34 [t, 1H, Ar-H; J = 7.5 Hz], 7.60 [m, 2H, Ar-H], 7.76 [m, 1H, Ar-H; d = 9.6 Hz], 8.54 [d, 1H, Ar-H; J = 5.0 Hz] FTIR(cm^{-1}): 3417(br), 3360(br), 3284(m), 3050(w), 2916(m), 1601(m), 1563(s), 1519(s), 1495(s), 1461(s), 1428(s), 1376(m), 1310(s), 1225(s), 1146(s), 1109(w), 1018(m), 918(m), 774(s), 741(s), 693(s), 587(m), 507(w), 409(w).

*[Cp*Ir{SC(=NPy)NHPh}Cl]* ***(4s)***

$[Cp^*IrCl_2]_2$ (80 mg, 0.1 mmol) and PyNHC(S)NHPh (46 mg, 0.2 mmol). Yield: 79 mg, 62 %. Elemental analysis %: calculated for $C_{22}H_{25}N_3IrSCl$; C, 44.70; H, 4.26; N, 7.11, found; C, 44.67; H, 4.24, N, 7.13. ESI-MS: Calculated *m/z*; 556.10, experimental *m/z*: CEV 60V, 556.08 (100%) $[M\text{-}Cl]^+$, 1112.16 (22%) $[2M+H]^+$, CEV 150V; 556.03 (100%) $[M\text{-}Cl]^+$, 592.08 (16%) $[M+H]^+$. ^1H NMR δ ppm: 1.63 [s, 15H, CH_3 Cp*], 5.82 [s, 1H, NH], 6.12 [d, 2H, Ar-H; J = 9.2 Hz], 7.16-7.40 [m, 2H, Ar-H], 7.56 [m, 1H, Ar-H; J = 8.2 Hz], 8.29 [d, 1H, Ar-H; J = 5.4 Hz]. FTIR (cm^{-1}): 3360(br), 3054(w), 2920(m), 1602(m), 1580(w), 1564(s), 1496(s), 1461(s), 1430(s), 1380(m), 1309(s), 1225(m), 1149(m), 1126(w), 1020(m), 919(m), 774(s), 693(s), 588(m), 520(w), 506(w).

*[Cp*Rh{SC(=NH(CH$_2$)$_2$Py)NPh}Cl] (**4t**)*

[Cp*RhCl$_2$]$_2$ (62 mg, 0.11 mmol) and Py(CH$_2$)$_2$NHC(S)NHPh (52 mg, 0.21 mmol). Yield: 52 mg, 46 %. Elemental analysis %: calculated for $C_{24}H_{29}ClN_3IrS$; C, 54.38; H, 5.53, N, 7.94, found; C, 54.33; H, 5.56, N, 7.91. ESI-MS: Calculated *m/z*; 494.11 $[M\text{-}Cl]^+$, experimental *m/z*: CEV 60V, 494.09 (100%) $[M\text{-}Cl]^+$, CEV 150V; 494.07 (100%) $[M\text{-}Cl]^+$, 529.19 (96%) $[M+H]^+$. ^{1}H NMR δ ppm: 1.42 [s, 15H, CH$_3$ Cp*], 2.96 [t, 2H CH$_2$; J = 6.9 Hz], 3.03 [dd, 2H, CH$_2$; J = 7.6 Hz, 8.2 Hz], 5.48 [s, 1H, NH], 6.08 [d, 2H, Ar-H; J = 8.2 Hz], 7.0 [t, 2H, Ar-H; J = 7.6 Hz], 7.15 [m, 2H, Ar-H], 7.50-7.80 [m, 2H, Ar-H], 8.64 [d, 1H, Ar-H; J = 6.2 Hz]. FTIR (cm^{-1}): 3432(br), 3068(w), 2918(m), 1634(w), 1588(s), 1566(s), 1485(s), 1442(m), 1380(m), 1305(s), 1246(w), 1156(m), 1083(s), 1032(m), 890(m), 763(s), 697(s), 626(m), 503(m).

*[Cp*Ir{SC(=NH(CH$_2$)$_2$Py)NPh}Cl] (**4u**)*

[Cp*IrCl$_2$]$_2$ (80 mg, 0.11 mmol) and Py(CH$_2$)$_2$NHC(S)NHPh (52 mg, 0.21 mmol). Yield: 44 mg, 33 %. Elemental analysis %: calculated for $C_{24}H_{29}ClN_3IrS$; C 46.55; H, 4.72; N, 6.79, found; C, 49.58; H, 4.73, N, 7.95. ESI-MS: Calculated *m/z*; 584.17, experimental *m/z*: CEV 60V, 584.18 (100%) $[M\text{-}Cl]^+$, 1167.39 (22%) $[2M\text{-}Cl]^+$, CEV 150 V. 584.18 (100%) $[M\text{-}Cl]^+$. H NMR δ ppm: 1.61 [s, 15H, CH$_3$ Cp*], 2.96 [t, 2H CH$_2$; J = 8.2 Hz], 3.03 [dd, 2H CH$_2$; J = 7.6 Hz], 4.08 [t, 4H, CH$_2$; J = 8.2 Hz], [d, 4H, Ar-H; J = 8.2 Hz], 7.0 [t, 2H, Ar-H; d = 7.5 Hz], 7.15 [m, 10H, Ar-H], 7.60 [m, 2H, Ar-H], 7.82 [m, 1H, Ar-H; J = 9.6 Hz], 8.64 [d, 1H, Ar-H; J = 5.0 Hz]. FTIR (cm^{-1}): 3415(br), 3057(w), 2919(m), 1637(w), 1596(s), 1567(s), 1485(s), 1437(m), 1380(m), 1305(s), 1246(w), 1155(m), 1083(s), 1031(m), 899(m), 760(s), 696(s), 626(m), 503(m).

*[Cp*Rh{SC(=NPy)NHC$_6$H$_4$OMe}Cl] (**4v**)*

[Cp*RhCl$_2$]$_2$ (62 mg, 0.11 mmol) and PyNHC(S)NHC$_6$H$_4$OMe (52 mg, 0.20 mmol). Yield: 90 mg, 79 %. Elemental analysis %: calculated for $C_{23}H_{27}ClN_3ORhS$; C, 51.94; H, 5.12; N, 7.90, found; C, 51.89; H, 5.10, N, 7.91. ESI-MS: Calculated *m/z*; 496.09 $[M\text{-}Cl]^+$, experimental *m/z*: CEV 60V, 496.10 (100%) $[M\text{-}Cl]^+$, 531.06 (13%) $[M+H]^+$, CEV 150 V; 496.18 (100%) $[M\text{-}Cl]^+$. ^{1}H NMR δ ppm: 1.63 [s, 15H, CH$_3$ Cp*], 3.85 [s, 3H, OCH$_3$], 5.86 [s, 1H, NH], 6.8-7.01 [m, 10H, Ar-H], 7.20-7.40 [m, 7H, Ar-H], 7.50-7.96 [m, 5H, Ar-H], 8.02 [d,

1H, Ar-H; J = 9.02 Hz], 10.12 [d, 1H, Ar-H, J = 5.7 Hz]. FTIR (cm^{-1}): 3471(br), 3415(m), 3051(w), 2918(w), 1637(w), 1606(w), 1569(s), 1505(s), 1478(m), 1435(s), 1372(s), 1329(m), 1290(s), 1247(s), 1181(m), 1064(s), 1034(w), 898(s), 838(s), 780(m), 753(s), 694(s), 638(w), 525(s), 509(s), 492(m) 456(w).

*[Cp*Ir{SC(=NPy)NHC$_6$H$_4$OMe}Cl] (**4w**)*

[Cp*IrCl$_2$]$_2$ (62 mg, 0.11 mmol) and PyNHC(S)NHC$_6$H$_4$OMe (52 mg, 0.21 mmol). Yield: 36 mg, 31 %. Elemental analysis %: calculated for $C_{23}H_{27}ClIrN_3OS$; C, 44.47; H, 4.38; N, 6.76, found; C, 44.48; H, 4.36, N, 6.75. ESI-MS: Calculated *m/z*; 586.15, experimental *m/z*: CEV 60V, 586.17 (100%) $[M-Cl]^+$, 621.12 $[M+H]^+$, CEV 50 V, 586.12 (100%) $[M-Cl]^+$. ^{1}H NMR δ ppm: 1.51 [s, 15H, CH_3, Cp*], 3.82 [s, 3H, OCH_3], 5.67 [s, 1H, NH], 6.05-7.16 [m, 8H, Ar-H], 7.30-7.48 [m, 7H, Ar-H], 7.62-7.91 [m, 5H, Ar-H], 8.16 [d, 1H, Ar-H; J = 8.32 Hz], 9.1 [d, 1H, Ar-H; J = 6.2]. FTIR (cm^{-1}): 3462(br), 3413(m), 3058(w), 2816(w), 1635(w), 1605(w), 1575(s), 1504(s), 1476(m), 1432(s), 1369(s), 1328(m), 1290(s), 1245(s), 1180(m), 1065(s), 1040(w), 896(s), 835(s), 782(m), 751(s), 698(s), 632(w), 525(s), 506(s), 490(m) 454(w).

*[Cp*Rh{SC(=NPy)NHPh}(PPh$_3$)]BF$_4$ (**4x**)*

[Cp*RhCl$_2$]$_2$ (62 mg, 0.11 mmol) and PyNHC(S)NHPh (46 mg, 0.20 mmol), PPh_3 (52 mg, 0.21 mmol). Yield: 64 mg 76 %. Elemental analysis %: calculated for $C_{40}H_{40}BF_4N_3PRhPS$; C, 58.91; H, 4.94; N, 5.15, found; C, 58.91; H, 4.96, N, 5.18. ESI-MS: Calculated *m/z*; 728.49, experimental *m/z*: CEV 60V, 728.52 (100%) $[M]^+$, CEV 150; 466.33 (100%) $[M-PPh_3]^+$, 728.52 (99.2%) $[M]^+$. ^{1}H NMR δ ppm: 1.52 [s, 15H, CH_3 Cp*], 5.4 [s, 1H NH], 6.7 [t, 1H, Ar-H; J = 7.29 Hz], 6.91 [dd, 1H, Ar-H; J = 8.2 Hz], 7.01 [m, 4H, Ar-H], 7.12 [t, 2H, Ar-H; J = 7.2 Hz], 7.3 [m, 6H, Ar-H], 7.40-7.72 [m, 10H, Ar-H], 8.24 [dd, 1H, Ar-H; J = 4.8, 7.8 Hz]. ^{31}P{^{1}H} NMR δ ppm: 35.12 [d, PPh_3; J = 149 Hz]. FTIR (cm^{-1}): 3436(br), 3337(w), 2921(w), 1602(m), 1563(s), 1535(w), 1509(s), 1496(w), 1457(s), 1437(s), 1380(m), 1314(s), 1223(m), 1150(s), 1083(s), 1058(s), 838(w), 782(m) 750(s), 696(s), 616(w), 526(s), 510(m), 496(w).

*[Cp*Ir{SC(=NPy)NHPh}(PPh$_3$)]BF$_4$* ***(4y)***

[Cp*IrCl$_2$]$_2$ (80 mg, 0.12 mmol) and PyNHC(S)NHPh (46 mg, 0.21 mmol), PPh$_3$ (0.20 mmol, 52 mg). Yield: 130 mg, 74 %. Elemental analysis %: Calculated, for $C_{40}H_{40}BF_4N_3IrPS$; C, 53.10; H, 4.46; N, 4.64, found; C, 53.12; H, 4.46, N, 4.65. ESI-MS: Calculated *m/z*; 818.05, experimental *m/z*: CEV 60V, 818.07 (100%) $[M]^+$, CEV 150 V; 555.97 (100%) $[M\text{-}PPh_3]^+$, 818.06 (92.2%) $[M]^+$. ^{1}H NMR δ ppm: 1.56 [s, 15H, CH_3 Cp*], 5.23 [s, 1H NH], 6.78 [t, 1H, Ar-H; J = 7.5 Hz], 6.96 [dd, 1H, Ar-H; J = 8.2 Hz], 7.01 [m, 4H, Ar-H], 7.12 [t, 2H, Ar-H; J = 7.2 Hz], 7.3 [m, 6H, Ar-H], 7.53-7.90 [m, 9H, Ar-H], 8.27 [dd, 1H, Ar-H; J = 5.2 Hz]. ^{31}P{^{1}H} NMR δ ppm: 6.12 [s, PPh$_3$]. FTIR (cm^{-1}): 3435(br), 3058(w), 2919(m), 1603(m), 1565(s), 1510(s), 1496(m), 1458(s), 1438(s), 1383(m), 1314(s), 1225(m), 1152(s), 1083(s), 1059(m), 1029(w), 932(w), 849(w), 781(m), 750(s), 697(s), 589(w), 532(s), 513(m), 500(w).

*[Cp*Rh{SC(=NHCH$_2$Py)NPh}(PPh$_3$)]BF$_4$* ***(4z)***

[Cp*RhCl$_2$]$_2$ (60 mg, 0.11 mmol) and PyCH$_2$NHC(S)NHPh (0.20 mmol, 48 mg), PPh$_3$ (52 mg, 0.21 mmol). Yield: 76 mg, 95 %. Elemental analysis %: calculated for $C_{41}H_{42}BF_4RhN_3PS$; C, 59.36; H, 5.10; N, 5.07, found; C, 59.40; H, 5.09, N, 5.08. ESI-MS: Calculated *m/z*; 744.01, experimental *m/z*: CEV 60V, 741.99 (100%) $[M]^+$, CEV 150 V; 479.95 (98%) $[M\text{-}PPh_3]^+$, 741.98 (76.2%) $[M]^+$. ^{1}H NMR δ ppm: 1.4 [d, 15H, CH_3, Cp*; J = 3.2 Hz], 1.47 [d, 2H CH_2; J = 3.12 Hz], 4.33 [s, 1H, NH], 6.80 [t, 1H, Ar-H; J = 8.8 4Hz], 6.99 [d, 2H, Ar-H; J = 7.45 Hz], 7.1-7.24 [m, 6H, Ar-H], 7.30-7.38 [m, 6H, Ar-H], 7.38-7.55 [m, 5H, Ar-H], 7.70 [dd, 2H, Ar-H, J = 7.73, J = 1.82], 7.90 [m, 1H, Ar-H] 8.45 [d, 1H, Ar-H; J = 4.8 Hz]. ^{31}P{^{1}H} NMR δ ppm: 38.79 ppm [d, PPh$_3$; J = 150 Hz]. FTIR (cm^{-1}): 3417(br), 3056(m), 2920(m), 1618(w), 1594(m), 1559(s), 1480(s), 1435(s), 1374(m), 1334(m), 1283(w), 1247(w), 1158(m), 1084(s), 1055(s), 998(w), 747(s), 696(s), 526(s), 509(s), 494(w).

*[Cp*Ir{SC(=NHCH$_2$Py)NPh}(PPh$_3$)]BF$_4$* ***(4za)***

[Cp*IrCl$_2$]$_2$ (80 mg, 0.11 mmol) and PyCH$_2$NHC(S)NHPh (48 mg, 0.20 mmol,), PPh$_3$ (54 mg, 0.21 mmol). Yield: 114 mg, 63 %. Elemental analysis %: Calculated, for $C_{41}H_{42}BF_4IrN_3PS$; C, 53.59; H, 4.61; N, 4.57, found; C, 53.60; H, 4.60, N, 4.55. ESI-MS: Calculated *m/z*; 832.09, experimental *m/z*: CEV 60V, 832.05 (100%) $[M]^+$, CEV 150 V; 569.99 (98%) $[M\text{-}PPh_3]^+$, 832.06 (96.2%) $[M]^+$. ^{1}H NMR δ ppm:

1.46 [d, 15H, CH_3, Cp*; J = 3.6 Hz], 1.62 [d, 2H, CH_2; J = 6.12 Hz], 5.33 [s, 1H, NH], 6.70 [t, 1H, Ar-H; J = 7.6 Hz], 6.92 [d, 2H, Ar-H; J = 8.25 Hz], 7.1-7.34 [m, 6H, Ar-H], 7.39 [m, 6H, Ar-H], 7.42-7.55 [m, 5H, Ar-H], 7.72 [dd, 2H, Ar-H, J = 7.73, 1.82 Hz], 7.87 [m, 1H, Ar-H] 8.48 [d, 1H, Ar-H; J = 5.6 Hz]. $^{31}P\{^1H\}$ NMR δ ppm: 10.26 ppm. FTIR (cm^{-1}): 3552(m), 3450(br), 3057(m), 2983(w), 1630(w), 1594(s), 1562(s), 1483(s), 1435(s), 1343(m), 1309(w), 1247(w), 1186(w), 1156(w), 1124(m), 1084(s), 1029(m), 999(w), 753(s), 698(s), 612(s), 533(s), 513(s), 498(w).

*[Cp*Rh{SC(=NH(CH₂)₂Py)NPh}(PPh₃)]BF₄* ***(4zb)***

$[Cp^*RhCl_2]_2$ (62 mg, 0.11 mmol) and $Py(CH_2)_2NHC(S)NHPh$ (52 mg, 0.20 mmol), PPh_3 (52 mg, 0.21 mmol). Yield: 120 mg, 72 %. Elemental analysis %: calculated for $C_{42}H_{44}BF_4N_3RhPS$; C, 59.80; H, 5.26; N, 4.98, found; C, 59.77; H, 4.96, N, 4.95. ESI-MS: Calculated *m/z*; 756.09, experimental *m/z*: CEV 60V, 756.10 (100%) $[M]^+$, CEV 150 V; 494.11 (98%) $[M\text{-}PPh_3]^+$, 756.12 (96.2%) $[M]^+$. ^1H NMR δ ppm: 1.39 [s, 15H, CH_3, Cp*], 2.67 [t, 2H CH_2; J = 10.8 Hz], 2.82 [m, 2H CH_2], 5.40 [m, 1H, NH], 6.89 [d, 2H, Ar-H; J = 7.5 Hz], 7.10-7.20 [m, 5H, Ar-H], 7.30-7.36 [m, 3H, Ar-H], 7.38-7.48 [m, 11H, Ar-H], 7.63-7.72 [m, 2H, Ar-H], 8.24 [d, 1H, Ar-H; d = 4.9 Hz]. $^{31}P\{^1H\}$ NMR δ ppm: 38.80 ppm [d, PPh_3; J = 149 Hz]. FTIR (cm^{-1}): 3417(br), 3056(m), 2920(m), 1618(w), 1594(m), 1559(s), 1480(s), 1435(s), 1374(m), 1334(m), 1283(w), 1247(w), 1158(m), 1084(s), 1055(s), 998(w), 747(s), 696(s), 526(s), 509(s), 494(w).

*[Cp*Ir{SC(=NH(CH₂)₂Py)NPh}(PPh₃)]BF₄* ***(4zc)***

$[Cp^*IrCl_2]_2$ (80 mg, 0.11 mmol) and $Py(CH_2)_2NHC(S)NHPh$ (52 mg, 0.20 mmol), PPh_3 (52 mg, 0.21 mmol). Yield: 82 mg, 53 %. Elemental analysis %: calculated, for $C_{42}H_{44}BF_4IrN_3PS$; C, 54.07; H, 4.75; N, 4.50, found; C, 54.10; H, 4.74, N, 4.52. ESI-MS: Calculated *m/z*; 846.05, experimental *m/z*: CEV 60V, 846.08 (100%) $[M]^+$, CEV 150 V; 584.06 (98%) $[M\text{-}PPh_3]^+$, 846.06 (96.2%) $[M]^+$. ^1H NMR δ ppm: 1.46 [s, 15H, CH_3 Cp*], 2.74 [t, 2H CH_2; J = 9.6 Hz], 2.90 [dd, 2H CH_2; J = 8.2 Hz, 6.7 Hz], 5.4 [t, 1H, NH; J = 9.8 Hz], 6.92 [d, 2H, Ar-H; J = 8.2 Hz], 7.15 [d, 3H, Ar-H; J = 7.5 Hz], 7.21 [d, 2H, Ar-H; J = 8.1 Hz], 7.30 [t, 3H, Ar-H; J = 7.7 Hz], 7.45 [m, 11H, Ar-H], 7.68 [t, 2H, Ar-H; J = 7.2 Hz], 8.15 [d, 1H, Ar-H; J = 5.6 Hz]. $^{31}P\{^1H\}$ NMR δ ppm: 10.70 [s, PPh_3]. FTIR (cm^{-1}): 3414(br), 3055(m), 2918(m), 1595(m), 1563(s), 1482(s), 1435(s), 1375(w), 1341(m), 1310(w),

1248(w), 1156(m), 1056(m), 999(w), 752(s), 697(s), 626(m), 533(s), 512(s), 460(w).

*[Cp*Rh{SC(=NH(CH$_2$)$_2$Py)NC$_6$H$_4$OMe}(PPh$_3$)]BF$_4$* ***(4zd)***

[Cp*RhCl$_2$]$_2$ (62 mg, 0.11 mmol) and Py(CH$_2$)$_2$NHC(S)NHC$_6$H$_4$OMe (58 mg, 0.20 mmol), PPh$_3$ (52 mg, 0.21 mmol). Yield: 90 mg, 72 %. Elemental analysis %; calculated, for C$_{43}$H$_{46}$BF$_4$N$_3$O$_2$RhS; C, 59.12; H, 5.31; N, 4.81, found; C, 59.15; H, 5.30, N, 4.84. ESI-MS: Calculated *m/z*; 786.22, experimental *m/z*: CEV 60V, 786.15 (100%) [M]$^+$, CEV 150 V; 524.13 (100%) [M-PPh$_3$]$^+$, 786.15 (100%) [M]$^+$. ^{1}H NMR δ ppm: 1.38 [d, 15H, CH$_3$ Cp*; J = 3.17 Hz], 1.17 [m, 2H, CH$_2$], 2.80 [m, 2H, CH$_2$], 3.85 [s, 3H, CH$_3$], 5.65 [m, 1H, NH], 6.85 [m, 5H, Ar-H], 7.15 [m, 4H, Ar-H], 7.30-7.54 [m, 16H, Ar-H], 7.60-7.70 [m, 3H, Ar-H], 8.27 [d, 1H, Ar-H; J = 5.8 Hz]. ^{31}P{^{1}H} NMR δ ppm: 38.6 [d, PPh$_3$; J = 150 Hz]. FTIR (cm^{-1}): 3471(br), 3415(m), 3077(w), 2918(w), 1637(w), 1569(s), 1505(s), 1478(s), 1435(s), 1372(m), 1329(m), 1290(s), 1247(s), 1181(m), 1051(m), 898(s), 838(s), 780(m), 753(s), 694(s), 638(m), 579(m), 525(s), 509(s), 492(s), 455(m).

*[Cp*Ir{SC(=NH(CH$_2$)$_2$Py)NC$_6$H$_4$OMe}(PPh$_3$)]BF$_4$* ***(4ze)***

[Cp*IrCl$_2$]$_2$ (80 mg, 0.11 mmol) and Py(CH$_2$)$_2$NHC(S)NHC$_6$H$_4$OMe (52 mg, 0.20 mmol), PPh$_3$ (52 mg, 0.21 mmol). Yield: 96 mg, 72 %. Elemental analysis %: calculated for C$_{43}$H$_{46}$BF$_4$IrN$_3$OPS; C, 53.64; H, 4.82; N, 4.36, found; C, 53.68; H, 4.83, N, 4.39. ESI-MS: Calculated *m/z*; 876.22, experimental *m/z*: CEV 60V, 876.20 (100%) [M]$^+$, CEV 150 V; 614.19 (100%) [M-PPh$_3$]$^+$, 872.20 (100%) [M]$^+$. ^{1}H NMR δ ppm: 1.49 [s, 15H, CH$_3$ Cp*], 1.86 [m, 2H, CH$_2$], 2.80 [dd, 2H, CH$_2$; J = 6.2 Hz. 8.9 Hz], 3.82 [s, 3H, CH$_3$], 6.14 [d, 1H, NH; J = 7.5 Hz], 6.86 [dd, 4H, Ar-H; J = 9.7 Hz], 6.89 [dd, 5H, Ar-H; J = 9.2 Hz], 7.40-7.70 [m, 12H, Ar-H], 8.34 [d, 1H, Ar-H; J = 6.15 Hz]. ^{31}P{^{1}H} NMR δ ppm: 5.47 [s, PPh$_3$]. FTIR (cm^{-1}): 3415(br), 3261(w), 3077(w), 2964(w), 1637(w), 1606(w), 1569(s), 1505(s), 1372(m), 1329(m), 1290(s), 1247(s), 1216(m), 1181(m), 1149(w), 1064(s), 956(w), 898(s), 838(s), 780(s), 753(s), 694(s), 638(m), 579(w), 525(s), 509(s), 492(m), 456(w).

4.4.3 *X-ray crystallography*

Crystals of the complexes suitable for X-ray crystallography were obtained by vapour diffusion of diethyl ether into a saturated dichloromethane solution of the complexes. Diffraction data were collected at 100 K on an Agilent (Supernova, single-source at offset Atlas) diffractometer equipped with an EOS CCD area detector and a 4-axis KAPPA goniometer. Graphite monochromated Cu-Kα radiation (λ=1.54184 Å) was used. Data integration, scaling, and empirical absorption correction was carried out using the CrysAlis-Pro program package[33]. The structures were solved with intrinsic phasing method in ShelXT[34] and refined by Matrix-least-square against F^2 on ShelXL[35]. The non-hydrogen atoms were refined anisotropically, and hydrogen atoms were placed at idealised positions and refined using the riding model. Some residual electron density peaks remaining in structures were modelled as H_2O of crystallisation in **4a**, disordered diethyl ether solvent in **4c**, and dichloromethane solvent in **4f** and **4l**. The crystal structure of **4y** had a disorder at the C(1) carbon atom, and that was refined isotropically. All calculations were implemented in OLEX2 program package[36]. Important crystallographic and refinement parameters are presented in **Tables 4.7-4.9**.

Table 4.7: Crystallographic and structure refinement parameters for ruthenium thiourea complexes **4a**, **4c**, **4f**, **4i**, and **4k**

Identification code	**4a**	**4c**	**4f**	**4i**	**4k**
Empirical formula	$C_{36}H_{38}N_6RuS_2.H_2O$	$C_{27}H_{34}N_3F_6OPRuS.CH_3CH_2OCH_2CH_3$	$C_{44}H_{43}BN_3F_4PRuS.CH_2Cl_2$	$C_{44}H_{47}BF_4N_3PRuS$	$C_{43}H_{45}F_6N_3OP_2RuS$
Formula weight g/mol	737.93	720.71	949.65	868.75	928.89
Temperature/K	99.97(13)	99.94(19)	293(2)	99.97(19)	100.01(10)
Crystal system	monoclinic	monoclinic	monoclinic	triclinic	monoclinic
Space group	$P2_1/n$	$P2_1/c$	$P2_1/n$	P-1	$P2_1/n$
a/Å	15.61100(10)	8.77692(10)	10.7669(10)	9.4717(3)	9.0164(2)
b/Å	9.56840(10)	16.4992(2)	27.1486(3)	14.4341(4)	21.8580(5)
c/Å	22.5163(2)	20.9583(3)	15.2222(2)	15.1670(4)	20.4264(5)
α/°	90	90	90	87.100(2)	90
β/°	101.8250(10)	99.8550(10)	107.0340(10)	83.795(2)	91.310(2)
γ/°	90	90	90	72.212(2)	90
Volume/$Å^3$	3291.94(5)	2987.60(7)	4254.35(9)	1962.53(10)	4024.59(16)
Z	4	4	4	2	4
ρ_{calc} g/cm^3	1.489	1.602	1.483	1.470	1.533
μ/mm^{-1}	5.352	5.997	5.402	4.575	4.963
F(000)	1528.0	1472.0	1944.0	896.0	1904.0
Crystal size/mm^3	0.157 x 0.121 x 0.061	0.203 x 0.084 x 0.078	0.127 x 0.086 x 0.051	0.194 x 0.123 x 0.072	0.14 x 0.12 x 0.08
2Θ range for data °	7.686 -148.024	6.858 -148.012	6.892-148.086	8.626-148.032	8.09-156.554
Reflections collected	31685	28490	31978	29042	34742
Independent reflections	6584	5980	8472	7737	8039
Data/restraints/parameters	6584/0/415	5980/0/386	8472/0/529	7737/0/502	8039/0/521
Goodness-of-fit on F^2	1.063	1.038	1.118	1.052	1.093
Final R indexes [$I \geq 2\sigma(I)$]	R_1 = 0.0262, wR_2 = 0.0592	R_1 = 0.0353, wR_2 = 0.0964	R_1 = 0.0694, wR_2 = 0.2107	R_1 = 0.0392, wR_2 = 0.1037	R_1=0.0377, wR_2 = 0.0974
Final R indexes [all data]	R_1 = 0.0306, wR_2 = 0.0611	R_1 = 0.0415, wR_2 = 0.1015	R_1 = 0.0947, wR_2 = 0.2233	R_1 = 0.0433, wR_2 = 0.1069	R_1 = 0.0483, wR_2 = 0.1074

Table 4.8: Crystallographic and structure refinement parameters for thiourea complexes **4l**, **4n**, **4r**, **4s**, and **4y**

Identification code	**4l**	**4n**	**4r**	**4s**	**4y**
Empirical formula	$C_{41}H_{41}BF_4N_3PRuS.CH_2Cl_2$	$C_{42}H_{43}BF_4N_3PRuS$	$C_{22}H_{25}ClN_3RhS$	$C_{22}H_{25}ClIrN_3S$	$C_{40}H_{40}BF_4IrN_3PS$
Formula weight g/mol	897.58	840.70	501.87	591.16	904.79
Temperature/K	99.9(4)	99.96(13)	99.97(11)	101(1)	99.9(5)
Crystal system	monoclinic	monoclinic	triclinic	triclinic	monoclinic
Space group	$P2_1/c$	$P2_1/n$	P-1	P-1	$P2_1/n$
a/Å	20.9720(4)	9.80260(10)	7.2737(3)	7.2808(5)	8.7312(2)
b/Å	10.85740(10)	18.10980(10)	11.2948(4)	11.3186(6)	18.4606(4)
c/Å	18.8819(3)	21.6883(2)	13.2667(5)	13.3313(5)	22.3323(4)
α/°	90	90	78.722(3)	78.560(4)	90
β/°	115.042(2)	95.1760(10)	76.715(3)	75.935(5)	96.600(2)
γ/°	90	90	83.745(3)	83.503(5)	90
Volume/$Å^3$	3895.28(12)	3834.47(6)	1037.93(7)	1042.06(10)	3575.74(13)
Z	4	4	2	2	4
ρ_{calc} g/cm^3	1.531	1.456	1.606	1.884	1.681
μ/mm^{-1}	5.863	4.664	8.868	14.610	8.661
F(000)	1832.0	1728.0	512.0	576.0	1800.0
Crystal size/mm^3	0.161 × 0.125 × 0.106	0.2013 × 0.1364 × 0.0653	0.154 × 0.098 × 0.076	0.107 × 0.083 × 0.053	0.364 × 0.178 × 0.069
2Θ range for data	9.31 to 148.19	6.37 to 148.072	6.956 to 147.748	6.946 to 147.734	7.97 to 147.99
Reflections collected	22539	37151	19045	11602	32646
Independent reflections	7703	7694	4120	4093	7182
Data/restraints/parameters	7703/0/490	7694/0/481	4120/0/258	4093/0/258	7182/0/455
Goodness-of-fit on F^2	1.024	1.054	1.152	1.066	1.194
Final R indices [$I \geq 2\sigma(I)$]	R_1 = 0.0396, wR_2 = 0.0968	R_1 = 0.0278, wR_2 = 0.0699	R_1 = 0.0469, wR_2 = 0.1250	R_1 = 0.0395, wR_2 = 0.0899	R_1 = 0.0491, wR_2 = 0.1335
Final R indices [all data]	R_1 = 0.0516, wR_2 = 0.1066	R_1 = 0.0346, wR_2 = 0.0750	R_1 = 0.0565, wR_2 = 0.1294	R_1 = 0.0518, wR_2 = 0.0962	R_1 = 0.0491, wR_2 = 0.1335

Table 4.9: Crystallographic and structure refinement parameters for rhodium thiourea complexes **4z, 4zb** and **4ze**

Identification code	**4z**	**4zb**	**4ze**
Empirical formula	$C_{41}H_{42}BF_4N_3PRhS$	$C_{42}H_{44}BF_4N_3PRhS$	$C_{43}H_{46}BF_4N_3OPRhS$
Formula weight g/mol	829.52	843.55	873.63
Temperature/K	99.9(4)	101.3(7)	100.01(10)
Crystal system	monoclinic	triclinic	monoclinic
Space group	C2/c	P-1	$P2_1/c$
a/Å	23.3588(3)	9.9998(4)	14.52353(16)
b/Å	17.59322(13)	13.2758(4)	19.79480(12)
c/Å	19.2426(2)	15.4283(5)	15.13400(14)
α/°	90	87.343(2)	90
β/°	112.1006(14)	73.244(3)	115.5136(13)
γ/°	90	76.888(3)	90
Volume/$Å^3$	7326.85(15)	1909.69(11)	3926.60(8)
Z	8	2	4
ρ_{calc} g/cm^3	1.504	1.467	1.4777
μ/mm^{-1}	5.177	4.975	4.880
F(000)	3408.0	868.0	1808.1
Crystal size/mm^3	0.22 x 0.18 x 0.12	0.22 x 0.18 x 0.12	0.12 x 0.08 x 0.05
2Θ range for data /°	7.16 to 148.078	6.838 to 148.098	7.86 to 148.06
Reflections collected	34975	34988	37263
Independent reflections	7276	7636	7788
Data/restraints/parameters	7276/0/474	7636/0/483	7788/0/502
Goodness-of-fit on F^2	1.087	1.082	1.057
Final R indexes [$I \geq 2\sigma(I)$]	R_1 = 0.0481, wR_2 = 0.1110	R_1 = 0.0334, wR_2 = 0.0688	R_1 = 0.0273, wR_2 = 0.0571
Final R indexes [all data]	R_1 = 0.0529, wR_2 = 0.1126	R_1 = 0.0392, wR_2 = 0.0747	R_1 = 0.0349, wR_2 = 0.0594

4.5 References

1. Orhan, E.; Garci, A.; Therrien, B. *Inorg. Chim. Acta* **2015**, *438*, 5-9.
2. Therrien, B. *Coord. Chem. Rev.* **2009**, *253*, 493-519.
3. Kalidasan, M.; Nagarajaprakash, R.; Forbes, S.; Mozharivskyj, Y.; Rao, K. M. *Zeit. Anorg. Allg. Chem.* **2015**, *641*, 715-723.
4. Adhikari, S.; Hussain, O.; Phillips, R. M.; Kaminsky, W.; Kollipara, M. R. *Appl. Organomet. Chem.* **2018**, *32*, 4362.
5. Süss-Fink, G. *J. Organomet. Chem.* **2014**, *751*, 2-19.
6. Zeng, L.; Gupta, P.; Chen, Y.; Wang, E.; Ji, L.; Chao, H.; Chen, Z.-S. *Chem. Soc. Rev.* **2017**, *46*, 5771-5804.
7. Jakupec, M. A.; Kandioller, W.; Schoenhacker-Alte, B.; Trondl, R.; Berger, W.; Keppler, B. K. Trends and Perspectives of Ruthenium Anticancer Compounds (Non-PDT). In *Ruthenium Complexes: Photochemical and Biomedical Applications*; Wiley-VCH: USA, 2018; pp 271-291.
8. Yang, Y.; Guo, L.; Tian, Z.; Liu, X.; Gong, Y.; Zheng, H.; Ge, X.; Liu, Z. *Chem. - Asian J.* **2018**
9. Pettinari, R.; Marchetti, F.; Di Nicola, C.; Pettinari, C.; Galindo, A.; Petrelli, R.; Cappellacci, L.; Cuccioloni, M.; Bonfili, L.; Eleuteri, A. M. *Inorg. Chem.* **2018**, 14123-14133.
10. Schmitt, F.; Kasparkova, J.; Brabec, V.; Begemann, G.; Schobert, R.; Biersack, B. *J. Inorg. Biochem.* **2018**, *184*, 69-78.
11. Li, C.; Ip, K.-W.; Man, W.-L.; Song, D.; He, M.-L.; Yiu, S.-M.; Lau, T.-C.; Zhu, G. *Chem. Sci.* **2017**, *8*, 6865-6870.
12. Aird, R.; Cummings, J.; Ritchie, A.; Muir, M.; Morris, R.; Chen, H.; Sadler, P.; Jodrell, D. *Br. J. Cancer* **2002**, *86*, 1652-1657.
13. Chatterjee, S.; Kundu, S.; Bhattacharyya, A.; Hartinger, C. G.; Dyson, P. J. *J. Biol. Inorg. Chem.* **2008**, *13*, 1149.
14. Guerriero, A.; Peruzzini, M.; Gonsalvi, L. *Coord. Chem. Rev.* **2017**
15. Su, W.; Peng, B.; Li, P.; Xiao, Q.; Huang, S.; Gu, Y.; Lai, Z. *Appl. Organomet. Chem.* **2017**, *31*, 3610.
16. Bravo, J.; Bolaño, S.; Gonsalvi, L.; Peruzzini, M. *Coord. Chem. Rev.* **2010**, *254*, 555-607.
17. Phillips, A. D.; Gonsalvi, L.; Romerosa, A.; Vizza, F.; Peruzzini, M. *Coord. Chem. Rev.* **2004**, *248*, 955-993.
18. Geldmacher, Y.; Oleszak, M.; Sheldrick, W. S. *Inorg. Chim. Acta* **2012**, *393*, 84-102.
19. Millett, A. J.; Habtemariam, A.; Romero-Canelón, I.; Clarkson, G. J.; Sadler, P. J. *Organometallics* **2015**, *34*, 2683-2694.
20. Lucas, S. J.; Lord, R. M.; Wilson, R. L.; Phillips, R. M.; Sridharan, V.; McGowan, P. C. *Dalton Trans.* **2012**, *41*, 13800-13802.

21. Adhikari, S.; Palepu, N. R.; Sutradhar, D.; Shepherd, S. L.; Phillips, R. M.; Kaminsky, W.; Chandra, A. K.; Kollipara, M. R. *J. Organomet. Chem.* **2016**, *820*, 70-81.

22. Kalidasan, M.; Nagarajaprakash, R.; Rao, K. M. *Transition Met. Chem.* **2015**, *40*, 531-539.

23. Meier, S. M.; Hanif, M.; Adhireksan, Z.; Pichler, V.; Novak, M.; Jirkovsky, E.; Jakupec, M. A.; Arion, V. B.; Davey, C. A.; Keppler, B. K. *Chem. Sci.* **2013**, *4*, 1837-1846.

24. Bharati, P.; Bharti, A.; Bharty, M.; Maiti, B.; Butcher, R.; Singh, N. *Polyhedron* **2013**, *63*, 156-166.

25. Sheeba, M. M.; Muthu Tamizh, M.; Farrugia, L. J.; Endo, A.; Karvembu, R. *Organometallics* **2014**, *33*, 540-550.

26. Adhikari, S.; Hussain, O.; Phillips, R. M.; Kollipara, M. R. *J. Organomet. Chem.* **2018**, *854*, 27-37.

27. Henderson, W.; Nicholson, B. K.; Dinger, M. B.; Bennett, R. L. *Inorg. Chim. Acta* **2002**, *338*, 210-218.

28. Pisiewicz, S.; Rust, J.; Lehmann, C. W.; Mohr, F. *Polyhedron* **2010**, *29*, 1968-1972.

29. Shadap, L.; Diamai, S.; Banothu, V.; Negi, D.; Adepally, U.; Kaminsky, W.; Kollipara, M. R. *J. Organomet. Chem.* **2019**, *884*, 44-54.

30. Hanif, M.; Nawaz, M.; Babak, M.; Iqbal, J.; Roller, A.; Keppler, B.; Hartinger, C. *Molecules* **2014**, *19*, 8080-8092.

31. Scolaro, C.; Chaplin, A. B.; Hartinger, C. G.; Bergamo, A.; Cocchietto, M.; Keppler, B. K.; Sava, G.; Dyson, P. J. *Dalton Trans.* **2007**, 5065-5072.

32. Alagöz, C.; Brauer, D. J.; Mohr, F. *J. Organomet. Chem.* **2009**, *694*, 1283-1288.

33. Rigaku Oxford Diffraction CrysAlisPro Software System, version 1.171. 38.41 l, Rigaku Coorporation. Oxford, UK, (2015).

34. Sheldrick, G. M. *Acta Crystallogr., Sect. A: Found. Adv* **2015**, *71*, 3-8.

35. Sheldrick, G. M. *Acta Crystallogr., Sect. C: Struct. Chem.* **2015**, *71*, 3-8.

36. Dolomanov, O. V.; Bourhis, L. J.; Gildea, R. J.; Howard, J. A. K.; Puschmann, H. *J. Appl. Crystallogr.* **2009**, *42*, 339-341.

Chapter 5

Platinum and palladium complexes of phosphonate-, hydroxyalkyl- and -silatrane-functionalised thioureas

5.1 Introduction

The versatility of thiourea ligands is due in part to the ease of synthesis and the possibility of modifying their nitrogen binding substituents to generate a wide range of steric and electronic properties in the target compounds[1]. The physical and chemical properties can be tuned to the desired product. A good number of substituted thioureas has been applied as broad-spectrum anti-HIV, antiviral, high-density lipoprotein (HDL) elevating, antibacterial, and analgesic agents[2-4]. These thioureas have also been applied in agriculture as pesticides[5] and fungicides[6], in the industry as anticorrosives, antioxidants, fire retardants and as components of polymeric products[7,8].

This chapter explores the synthesis, structure and non-covalent interaction properties of some disubstituted thiourea ligands containing hydroxyalkyl, phosphonate, and silatrane functional groups and their platinum and palladium complexes. A search through the literature indicates that the chemistry of thioureas containing phosphonate donor ligands has been understudied. The hydroxyalkyl thioureas, on the other hand, have been explored as tyrosinase inhibitors and applied in the development of whitening agents[9]. A number of these hydroxyalkyl thioureas has been reported in the literature[8,10]. However, there are no reports on the complexes of these group of compounds.

The silatranes are a class of cyclic organosilicon esters containing a dative transannular bond (N-Si) between the hypervalent silicon atom and nitrogen[11-13]. The resulting cage-like structure (**5.1**) has a pentacoordinate organosilicon in a distorted bipyramidal geometry. Silatranes have continued to receive attention due to their high stability, unique structural architecture, and broad applications in agriculture and biology[14-17].

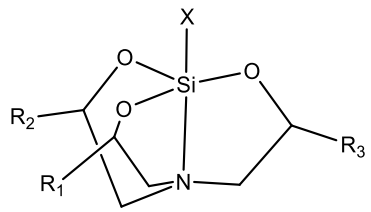

5.1

Apart from that, there have been numerous reports on the applications of these classes of compounds in metal binding and anion sensing[18,19]. There is however no record of platinum group coordination complexes of these groups of thiourea ligands in the literature.

5.2 Results and discussion

5.2.1 *Synthesis and structure of the phosphonate thiourea ligands*

The phosphonate thiourea ligands **1i** and **1j** were prepared by the reaction of equimolar amounts of diethyl 4-aminobenzyl-1-phosphonate $(EtO)_2P(O)CH_2C_6H_4NH_2$ and phenyl isothiocyanate or *p*-nitrophenyl isothiocyanate respectively in DMF.

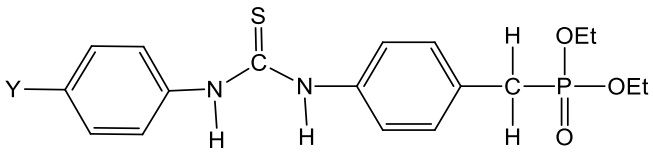

Y = H; **1i**, Y = NO_2; **1j**

The ESI-mass spectra of the ligands showed *pseudo*-molecular ion peaks at *m/z* 401 and 446 respectively, for $[M+Na]^+$ of **1i** and **1j**. The ^1H NMR spectra of the ligands showed two small peaks above 8 ppm attributable to the two N-H protons of the thiourea. Peaks around 6-8 ppm, assignable to aromatic protons were observed in both ligands. The peaks around 4 ppm in both compounds, which integrated as four protons, were assigned as the CH_2-O-P protons of the phosphonate ester. A doublet around 3 ppm is assignable to CH_2 protons between P and the substituted phenyl group. A triplet appearing around 1.2 ppm in the two ligands were assigned to the 6 CH_3 protons of the phosphonate ester. The $^{31}P\{^1H\}$ NMR spectra of the two ligands showed singlet peaks at 28 and 26 ppm for **1i** and **1j** respectively. The FTIR spectra of the ligands showed bands around 3200, 1050, 1300 and 970 cm^{-1} for N-H, C-N, P=O and P-OR vibrations respectively[20,21].

Crystals of the ligands **1i** and **1j** suitable for X-ray crystallography were isolated by recrystallising the compounds in a 3:1 ethanol-water mixture. The molecular structures of the thioureas **1j** and **1i** are shown in **Figure 5.1**, while selected bond parameters are presented in **Table 5.1**.

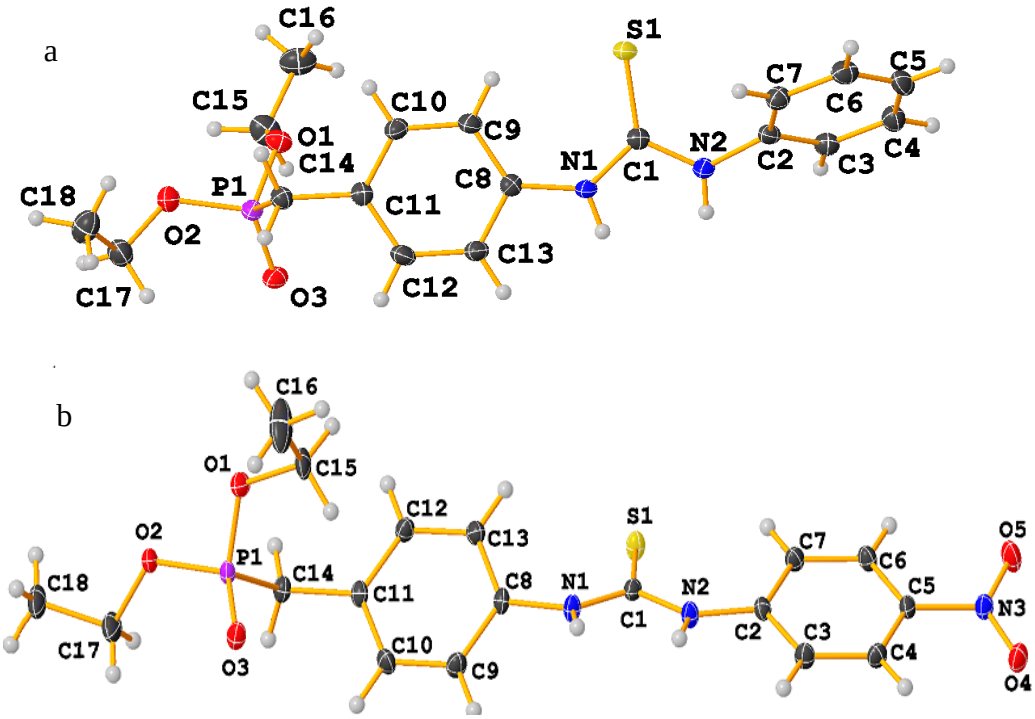

Figure 5.1: Molecular structures of phosphonate thioureas; (a) $(EtO)_2P(O)CH_2C_6H_4NHC(S)NHPh$ **1i** and (b) $(EtO)_2P(O)CH_2C_6H_4NHC(S)NHC_6H_4NO_2$ **1j**.

The molecular structure of the phenyl **1i** and *p*-nitrophenyl **1j** substituted phosphonate thiourea ligands have similar geometric configurations with the P=O and C=S acceptor functional groups pointing in opposite directions in both compounds, resulting in a *trans-trans* configuration for the thiourea functionality. The dihedral angles between the thiourea planes and the substituted phenyl and *p*-nitrophenyl planes are 57.87 and 17.81° in **1i** and **1j** respectively. The substituted phosphonate ester contains a phosphorus atom tetrahedrally coordinated to two EtO groups, one phosphonate O and the carbon atom of the bridging methylene. The two alkyl groups in the ester adopt different conformations with respect to the phosphorus atom. The C(15)-C(16) ethyl group in 1i adopts an -antiperiplanar conformation with a P(1)-O(1)-C(15)-C(16) torsion angle of -178.78°, while the C(17)-C(18) alkyl chain adopts a + anticlinal conformation from P(1)-O(2)-C(117)-

C(18) torsion angle of 110.69º. Similar conformations were found in 1j with torsion angles -124.90º for P(1)-O(1)-C(15)-C(16) and 172.32º P(1)-O(2)-C(117)-C(18) corresponding to a -anti-clinal and +antiperiplanar confirmations respectively. The *trans-trans* conformation in thioureas has been reported to form mostly the zigzag hydrogen-bonded thiourea chain motif [22], however, due to the flexibility of the thioureas and the presence of a competing P=O acceptor functional group, the strong hydrogen bond donating N-H functional groups align themselves orthogonally to the plane of the P=O acceptor group resulting in a bifurcated hydrogen-bonded dimer, **Figure 5.2**. The thione S in the thiourea **1i** is twisted out of the plane of the hydrogen bond donating thiourea N-H functional group and thus not involved in hydrogen bond formation. In the thiourea **1j**, the *p*-NO_2 group is involved in intermolecular C-H---O short-range interactions with one of the methylene carbons of the phosphonate ester of another molecule of the ligand to form a cyclic dimer. Each of the dimers is further linked by long-range C-H----S intermolecular interaction, resulting in a continuous zigzag chain of cyclic dimers (**Figure 5.3**).

Table 5.1: Geometric parameters for thiourea ligands **1i** and **1j**

Bond Parameters (Å,º)	**1i**	**1j**
P(1) – O(2)	1.5850(13)	1.5736(16)
P(1) – O(1)	1.5691(12)	1.5679(16)
P(1) – O(3)	1.4780(13)	1.4810(16)
P(1) – C(14)	1.7908(18)	1.799(2)
S(1) – C(1)	1.6780(18)	1.667(2)
O(2) – C(17)	1.453(2)	1.7452(19)
O(1) – C(15)	1.4562(2)	1.465(3)
N(1) – C(8)	1.414(2)	1.422(3)
N(2) – C(1)	1.355(2)	1.420(2)
N(1) – C(2)	1.425(3)	1.333(2)
N(1) – C(1)	1.363(2)	1.359(3)
N(2) – C(2)	1.425(2)	1.402(3)
C(15) – C(16)	1.492(3)	1.494(4)
C(18) – C(17)	1.504(3)	1.496(5)
O(1) – P(1) – O(2)	101.65(7)	170.42(5)
O(2) – P(1) – O(3)	113.51(7)	114.70(9)
O(1) – P(1) – O(3)	114.72(7)	114.58(9)
C(14) – P(1) – O(2)	107.52(8)	107.66(10)
C(17) – O(2) – P(1)	121.49(12)	120.43(14)
C(15) – O(1) – P(1)	120.92(8)	120.13(16)
C(1) – N(1) – C(8)	132.78(15)	132.15(19)
C(2) – N(2) – C(1)	126.95(15)	128.66(19)
N(1) – C(1) – S(1)	125.96(13)	124.00(16)
N(2) – C(1) – S(1)	122.60(13)	125.56(17)
N(2) – C(1) – N(1)	111.44(15)	110.39(19)

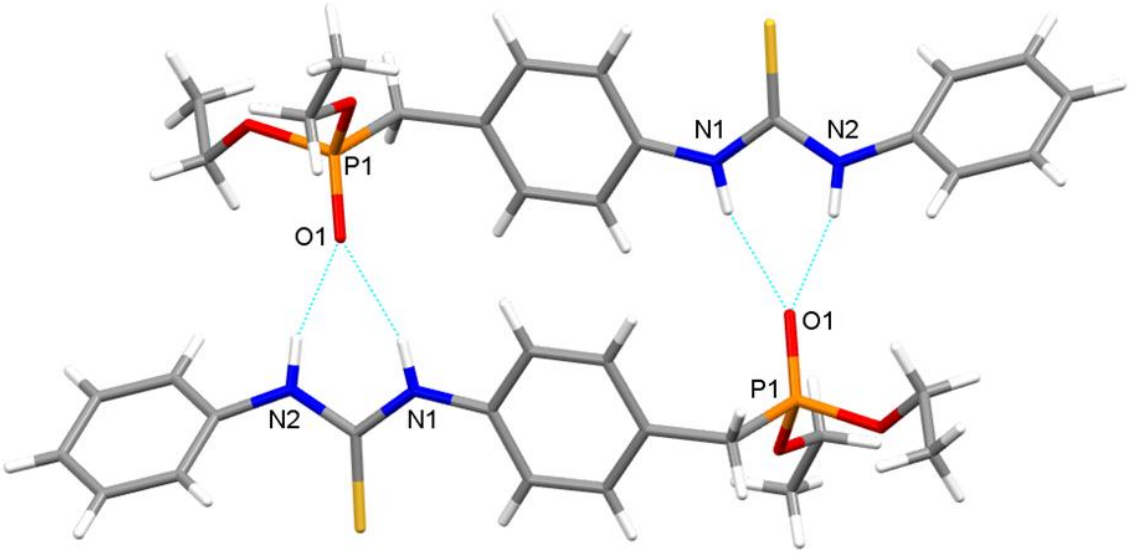

Figure 5.2: Bifurcated hydrogen-bonded dimeric structure of phosphonate and phenyl-substituted thiourea ligand **1i**, D….A: N1…O3; 2.896 Å, N2…O3; 2.931 Å. D-H…A: N1-H1...O3; 156.03º, N2-H2...O3; 161.79º.

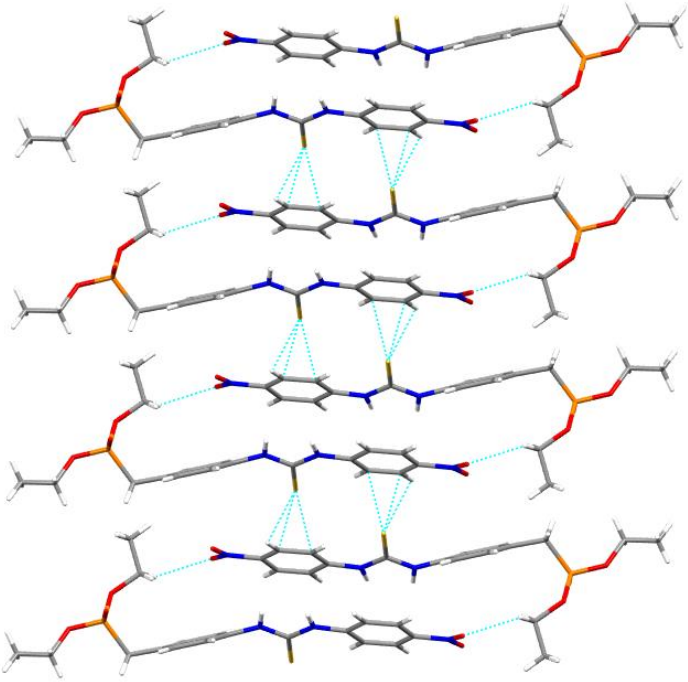

Figure 5.3: Intermolecular phosphonate ester-C-H----O(*p*-nitrophenyl) and thiourea-C-S---H(phenyl) interactions in the crystal structure of **1j** resulting in a chain of cyclic dimers.

5.2.2 *Non-covalent interactions in phosphonate-substituted thioureas 1i and 1j*

The theory of the non-covalent interaction technique has been discussed in Chapter 1. Non-covalent interactions in diethyl 4-(3-phenyl thioureido) benzyl phosphonate **1i** and diethyl 4-(3-(4-nitrophenyl) thioureido)benzylphosphonate **1j** were analysed using the locally developed Bonder program. Input geometries were taken from the crystal structures of the ligands, and the wave function files were generated at the DFT level of theory using the ωB97XD functional and the 6-311++G(d,p)** basis set. The 3-D isosurface troughs and the 2-D electron density plots for **1i** are presented in **Figure 5.4**, while those of **1j** are presented in appendix 2 **(Figure B1**). The intermolecular attractive hydrogen bonding interaction between the thiourea NH groups and the phosphonate oxygens in **1i** appear as two blue peaks at the high-density end of the 2-D electron density bonder plots with density values of $\rho = 0.018$ a.u.; $\lambda_2 < 0$. These correspond to the two blue pill-like troughs on the 3-D isosurface plots (**Figure 5.3**). Similar hydrogen bonding interactions appear at $\rho = 0.023$ a.u.; $\lambda_2 < 0$ on the 2-D electron density plots for the *p*-nitro thiourea derivative **1j** (**Figure B1**, appendix 2).

The low-density low gradient peak at $\rho = 0.015$au, $\lambda_2 > 0$ in the 2-D plot of **1i** correspond to the green isosurface trough between the two pill-like hydrogen bonding isosurfaces and results from the weak intramolecular interaction between the two adjacent N-H protons. The other strong attractive interaction in the dimer is the non-bonding intramolecular C-H---SC interactions. The 3-D almond-shaped isosurface trough for this interaction in **1i** shows a tricoloured system, indicating the presence of three different types of interaction. The upper blue part represents a more directional attractive interaction possessing significant bicentric character and corresponding to the low density low reduced gradient peak at $\rho = 0.017$ a.u. ; $\lambda_2 < 0$. The middle part of the almond-shaped isosurface is a light blue part corresponding to the low-density low gradient peak at $\rho = 0.015$ a.u. ; $\lambda_2 < 0$. There is also the red lower end of the isosurface with density ($\rho = 0.015$a.u. ; $\lambda_2 > 0$). The tricolour nature of these interactions shows the transition from bi-centricity to multicentricity of intramolecular interactions resulting in the formation of intramolecular ring systems. A separate 3-D isosurface representation and corresponding 2-D bonder plot for this interaction are presented in the appendix **Figure B2**, to clearly illustrate the tricoloured nature of the C-H---S interaction.

In addition to these tricoloured isosurfaces, there are also some green-coloured flat-shaped isosurfaces found at density $\rho < 0015$ a.u. They correspond to the C-H---O, C-H---π and C-H---N intramolecular stabilising interactions. Separate 2D bonder plots and 3D isosurface representation for these interactions are presented in the appendix, **Figure B3**. Further down the sign$\lambda(\rho)$ axis of the 2-D electron density plots are the peaks for the highly repulsive benzene ring interactions with high-density values $\rho = 0.022$ a.u. and $\lambda_2 > 0$, corresponding to the red cigar-shaped isosurfaces at the centre of the benzene rings, **Figure 5.4**. These interactions are a result of highly repulsive steric strain within the benzene rings. The repulsive benzene ring interactions have little or no effect on the supramolecular architecture of the compounds. The highly attractive NH----OP hydrogen bonding and the weakly attractive multicentric CH---OS and CH---OP interactions, on the other hand, are instrumental to the rearrangement of the hydrogen-bonded supramolecular architecture of the thioureas.

The 2-D and 3-D electron density plots for the *p*-nitro-substituted thiourea **1j**, (**Figure B1** of appendix 2**)** contain some intramolecular CH---O bicentric interactions between the terminal phenyl C-H and O of the *p*-nitro group. These interactions correspond to the almond-shaped bicoloured isosurfaces resulting from symmetric interactions with density values of $\rho = 0.018$ a.u. ; $\lambda_2 < 0$ and $\rho = 0.018$ a.u.; $\lambda_2 > 0$ for the stabilising and non-stabilising interactions respectively. These interactions are responsible for the cyclic dimers in the crystal packing of **1j** (**Figure 5.3**). Similar symmetric interactions were reported for multicentric NH---π and CH----O interactions in the solid-state structure of *N*-acetyl-phenylalanyl-amide (NAPA)[23], *N*,*N*-diethyl-*N*'-palmitoylthiourea[24] and 2-{[2-(phenylsulfonyl)hydrazinylidene]methyl} benzoic acid[25].

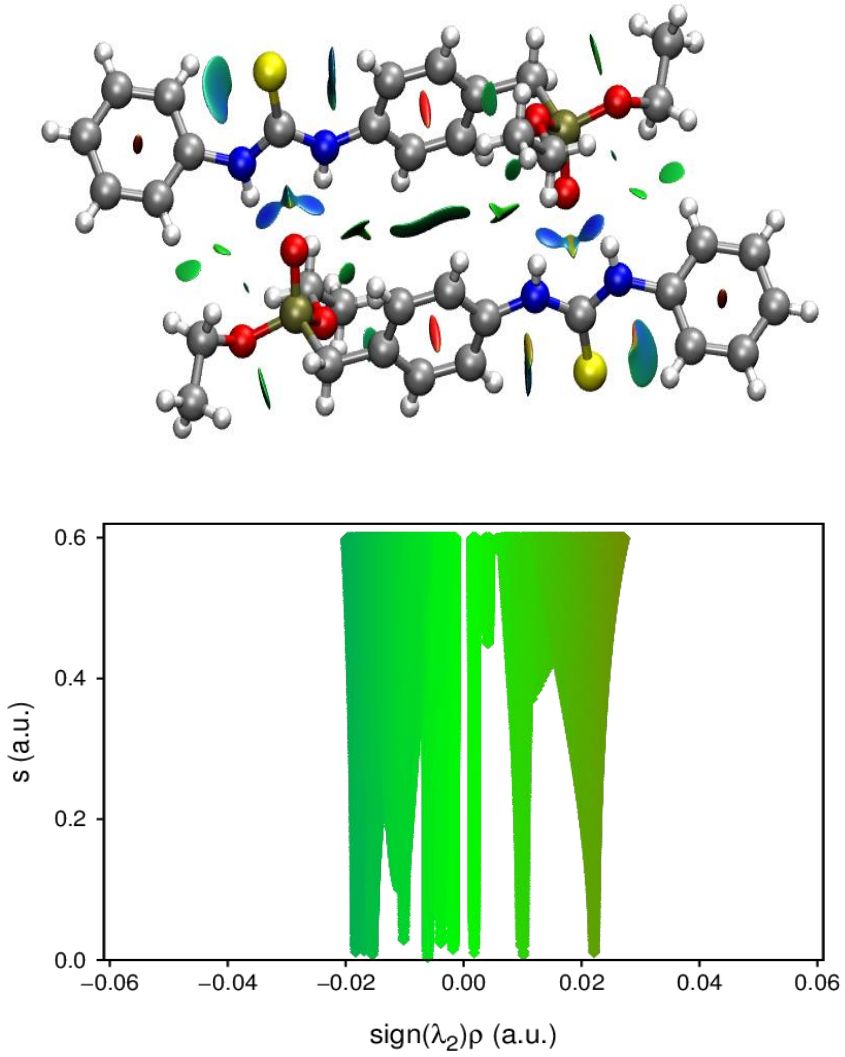

Figure 5.4: The 2-D density plots for the phosphonate thiourea dimer **1i** (bottom) and the corresponding 3-D isosurface representations (top) (s = 0.5au) (-0.05 < sign(λ_2) ρ < 0.05au)

5.2.3 *Synthesis of hydroxyalkyl substituted thiourea ligands*

The hydroxyalkyl thioureas **1k** and **1l** were synthesised by following a modified literature procedure[10]. The reaction of 1:1 molar equivalent of the appropriate hydroxyalkylamine with phenyl isothiocyanate in diethyl ether gave the ligands **1k** and **1l** in moderate to high yields.

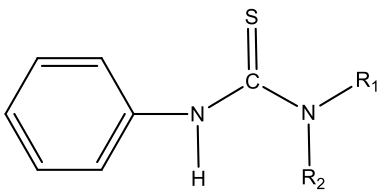

R_1 = H, R_2 = CH_2CH_2OH; (**1k**)

R_1 = R_2 = CH_2CH_2OH; (**1l**)

The ESI-mass spectra of the ligands in methanol solvent with added sodium formate at a capillary exit voltage of 150 V showed intense peaks at *m/z* 219 and 263 for the $[M+Na]^+$ ions of **1k** and **1l** respectively. The ^1H NMR spectra of the two ligands in DMSO-d_6 showed the expected peaks around 9.50 ppm corresponding to hydroxyl protons. Singlets appearing between 7.0-8.0 ppm were assigned to NH protons of the thiourea moiety and multiplets around 6-7 ppm were associated with the aromatic protons in the phenyl rings of the thiourea. The peaks observed around 3-4 ppm in the thioureas are attributed to CH_2 protons. The hydroxyalkyl thiourea **1k** has been previously obtained as the unexpected product of a multicomponent reaction of phenyl isothiocyanate, malononitrile, and 2-aminoethanol under reflux. Only the crystal structure of the compound was reported[8]. Attempts to obtain crystals of **1l** suitable for X-ray crystallography were unsuccessful.

5.2.4 *Synthesis of silatrane substituted thioureas*

Silatrane-substituted thioureas **1m-1o** were synthesised by a literature method[11]. The reaction of 3-aminopropylsilatrane with the corresponding isothiocyanate gave the ligands in good yields.

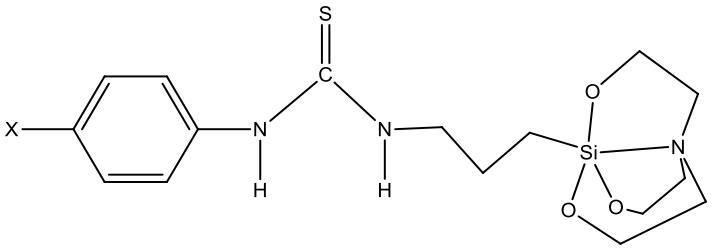

X = H; **1m**, X = NO_2; **1n**, X = OMe; **1o**

These silatrane-substituted thioureas have been synthesised previously and structurally characterised[11]. The experimental data for this group of ligands reported in the experimental section are in agreement with the literature values.

5.2.5 *Platinum and palladium complexes of phosphonate, hydroxyalkyl, and silatrane thioureas*

The complexes were synthesised using the same general method. Equimolar amounts of *cis*-$[PtCl_2(PPh_3)_2]$ or $[PdCl_2(dppe)]$ and thiourea ligands **1i-1o** were refluxed in methanol solution with excess triethylamine base. The complexes **5a-5j**

were isolated by the addition of solid $NaBF_4$ (excess) to the hot solution. **Schemes 5.1-5.3.**

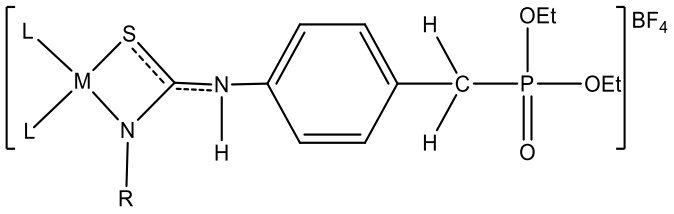

Compound	L-L	M	R
5a	$(PPh_3)_2$	Pt	Ph
5b	$(PPh_3)_2$	Pt	*p*-$C_6H_4NO_2$
5h	dppe	Pd	Ph
5i	dppe	Pd	*p*-$C_6H_4NO_2$

Scheme 5.1: Pt and Pd complexes of phosphonate thiourea ligands

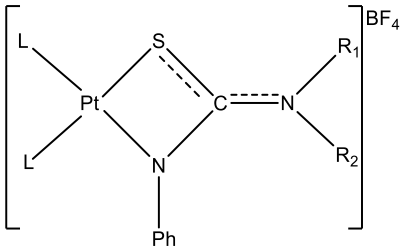

Compound	L-L	M	R_1	R_2
5c	$(PPh_3)_2$	Pt	C_2H_5OH	H
5d	$(PPh_3)_2$	Pt	C_2H_5OH	C_2H_5OH
5j	dppe	Pd	C_2H_5OH	H
5k	dppe	Pd	C_2H_5OH	C_2H_5OH

Scheme 5.2: Pt and Pd complexes of hydroxyalkyl-substituted thiourea ligands

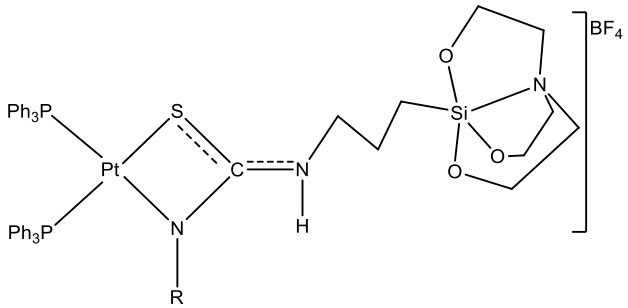

R = Ph; **5e**, R = *p*-$C_6H_4NO_2$; **5f**, R = *p*-C_6H_4OMe; **5g**

Scheme 5.3: Platinum complexes of silatrane-substituted thiourea ligands

The ESI-mass spectra of the platinum complexes in methanol solution at a capillary exit voltage of 60 V showed molecular ion peaks for the cationic complexes $[M]^+$, **Table 5.2**. At a higher capillary exit voltage in the range of 120-180 V, peaks corresponding to the loss of a PPh_3 ligand from the cationic complex $[M\text{-}PPh_3]^+$, appeared in the spectra of all platinum thiourea complexes **5a-5g**. Also present in the spectra of all the platinum compounds is the peak corresponding to the cyclometalated platinum species $[Pt(PPh_2C_6H_4)PPh_3]^+$ with *m/z* 718, **Figure 5.5**. This cyclometallated platinum species has been observed in previously reported platinum complexes[26,27]. The spectra of platinum complexes **5b** and **5d** showed peaks assignable to the dimeric species of the corresponding cationic complexes, $[2M\text{-}H]^+$. The palladium complexes **5h-5k**, on the other hand, showed peaks only assignable to the *m/z* values for cationic species $[M]^+$, **Table 5.2**.

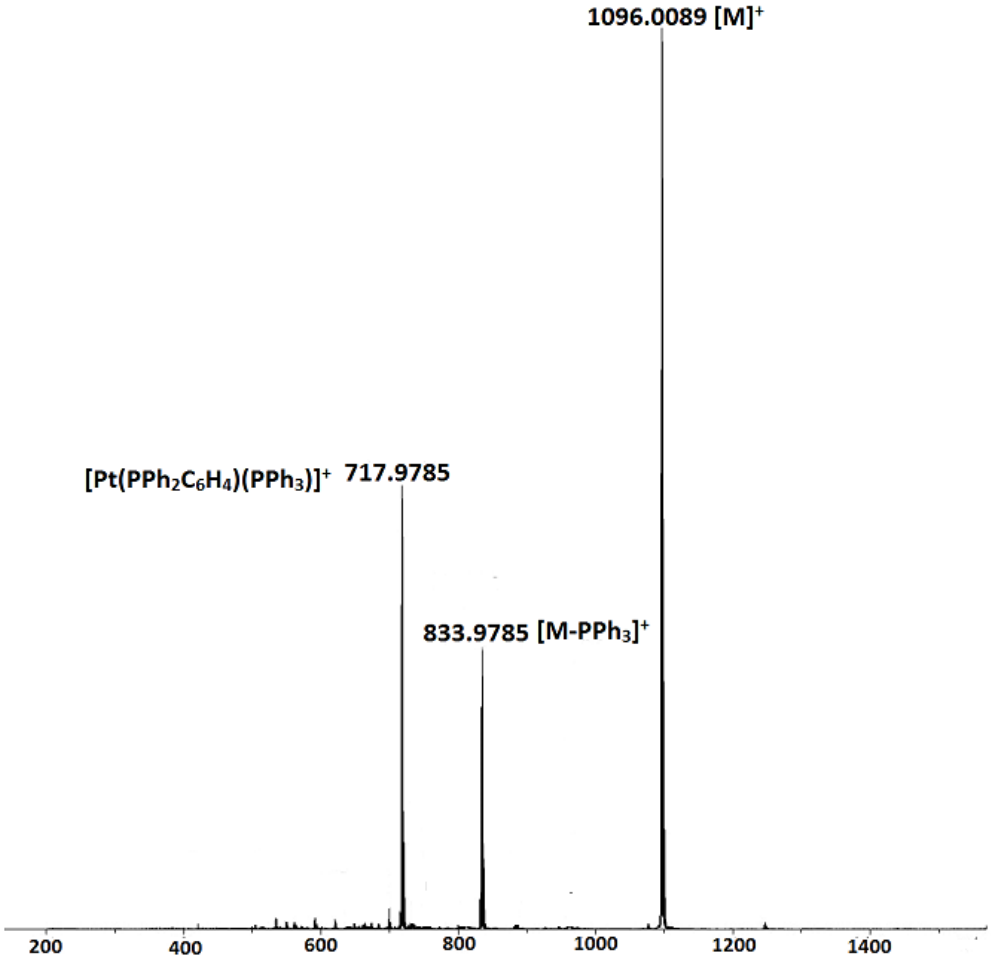

Figure 5.5: ESI-mass spectrum of $[M]BF_4$ platinum thiourea complex $[Pt\{SC(NPh)NHC_6H_4(CH_2)P(O)(OEt)_2\}(PPh_3)_2]BF_4$ **5a** at capillary exit voltage of 120 V.

Table 5.2: ESI-MS data of platinum and palladium complexes of phosphonate, hydroxyalkyl, and silatrane–substituted thiourea complexes **5a-5k**

Complexes	**Capillary exit voltage (V)**	***m/z* (%) ions**
$[Pt\{SC(NPh)NHC_6H_4CH_2P(O)(EtO)_2\}(PPh_3)_2]BF_4$ (**5a**)	60	1096 (100) $[M]^+$
	120 - 180	718 (68) $[Pt(PPh_2C_6H_4)(PPh_3)]^+$, 834 (32) $[M\text{-}PPh_3]^+$, 1096 (100) $[M]^+$,
$[Pt\{SC(NC_6H_4NO_2)NHC_6H_4CH_2P(O)(EtO)_2\}(PPh_3)_2]BF_4$ (**5b**)	60	1141 (100) $[M]^+$
	120 - 180	718 (12) $[Pt(PPh_2C_6H_4)(PPh_3)]^+$, 879 (3) $[M\text{-}PPh_3]^+$, 1141 (100) $[M]^+$, 2282 (6) $[2M]^+$
$[Pt\{SC(NPh)NHC_2H_4OH\}(PPh_3)_2]BF_4$ (**5c**)	60	914 (100) $[M]^+$, 1827 (7) $[2M\text{-}H]^+$
	120 - 180	651 (12) $[M\text{-}PPh_3]^+$, 718 (24) $[Pt(PPh_2C_6H_4)(PPh_3)]^+$, 914 (100) $[M]^+$, 1827 (7) $[2M\text{-}H]^+$
$[Pt\{SC(NPh)N(C_2H_4OH)_2\}(PPh_3)_2]BF_4$ (**5d**)	60	958 (100) $[M]^+$
	120 - 180	696 (22) $[M\text{-}PPh_3]^+$, 718 (32) $[Pt(PPh_2C_6H_4)(PPh_3)]^+$, 958 (47) $[M]^+$
$[Pt\{SC(NPh)NHC_9H_{18}NO_3Si\}(PPh_3)_2]BF_4$ (**5e**)	60 - 150	1085 (100) $[M]^+$
	180	718 (24) $[Pt(PPh_2C_6H_4)(PPh_3)]^+$, 822 (100) $[M\text{-}PPh_3]^+$, 1085 (27) $[M]^+$
$[Pt\{SC(NC_6H_4NO_2)NHC_9H_{18}NO_3Si\}(PPh_3)_2]BF_4$ (**5f**)	60 - 150	1131 (100) $[M]^+$
	180	718 (12) $[Pt(PPh_2C_6H_4)(PPh_3)]^+$, 869 (80) $[M\text{-}PPh_3]^+$, 1131 (100) $[M]^+$
$[Pt\{SC(NC_6H_4OMe)NHC_9H_{18}NO_3Si\}(PPh_3)_2]BF_4$ (**5g**)	60 - 150	1116 (100) $[M]^+$
	180	718 (12) $[Pt(PPh_2C_6H_4)(PPh_3)]^+$, 854 (10) $[M\text{-}PPh_3]^+$, 1116 (97) $[M]^+$
$[Pd\{SC(NPh)NHC_6H_4CH_2P(O)(EtO)_2\}(dppe)]BF_4$ (**5h**)	60	881 (100) $[M]^+$
	120 - 180	746 (22) $[M\text{- }P(O)(EtO)_2]^+$, 881 (100) $[M]^+$
$[Pd\{SC(NC_6H_4NO_2)NHC_6H_4CH_2(EtO)_2P(O)\}(dppe)]BF_4$ (**5i**)	60	926 (100) $[M]^+$
	120 - 180	779 (42) $[M\text{- }P(O)(EtO)_2]^+$, 926 (100) $[M]^+$
$[Pt\{SC(NPh)NHC_2H_4OH\}(dppe)]BF_4$ (**5j**)	60 - 180	699 (100) $[M]^+$
$[Pt\{SC(NPh)N(C_2H_4OH)_2\}(dppe)]BF_4$ (**5k**)	60 - 150	743 (100) $[M]^+$

The $^{31}P\{^{1}H\}$ NMR spectrum of the phenyl and phosphonate substituted thiourea complex **5a**, collected after 30 min. of dissolution of the complex in $CDCl_3$ showed two doublets at 16.66 and 11.95 ppm with $^{1}J_{(PtP)}$ coupling constants of 3072 and 3269 Hz respectively. Another spectrum collected after 180 mins of dissolution showed another set of doublets further downfield and having chemical shifts of 16.47 and 11.72 ppm with $^{1}J_{(PtP)}$ coupling constants of 3068 and 3257 Hz respectively, **Figure 5.6**. The similarity in the $^{31}P\{^{1}H\}$ NMR shifts is anticipated due to the similarity of the N-bound substituents. However, comparing the spectrum with those of the pyridyl substituted thiourea complexes reported in Chapter 2, (where the most downfield peaks were assigned as the proximal isomers by comparing with calculated values) the first and second set of peaks in this spectrum were assigned to as resulting from the proximal and distal isomers of the complex, shown in **5.1** (**a**) and (**b**). Two singlets at 27.12 and 27.26 ppm were also assigned to P atom of phosphonate ester for the distal and proximal isomers respectively.

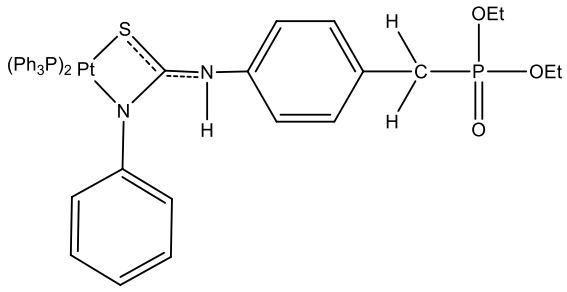

5.1(**a**)

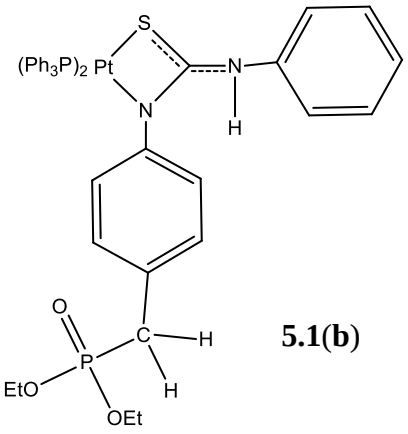

5.1(**b**)

The *p*-nitrophenyl derivative of the phosphonate substituted platinum thiourea complex **5b** showed similar $^{31}P\{^{1}H\}$ NMR resonances to those in **5a**, **Table 5.3**.

Apart from the phosphonate substituted complexes, the $^{31}P\{^{1}H\}$ NMR spectrum of the hydroxyalkyl-substituted complex **5c** (**Scheme 5.2**) showed two sets of doublets with chemical shifts, and coupling constants closer to values observed in the phosphonate substituted complexes. These values are assignable to the proximal and distal isomers of the complex in **5.2** (**a**) and (**b**) and presented in **Table 5.3**.

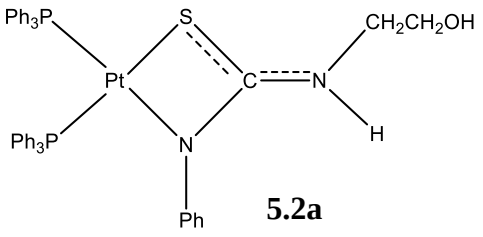

5.2a

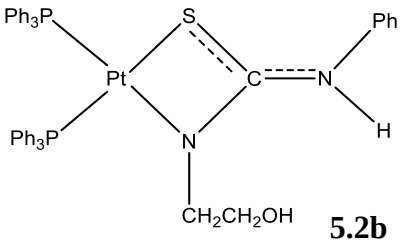

5.2b

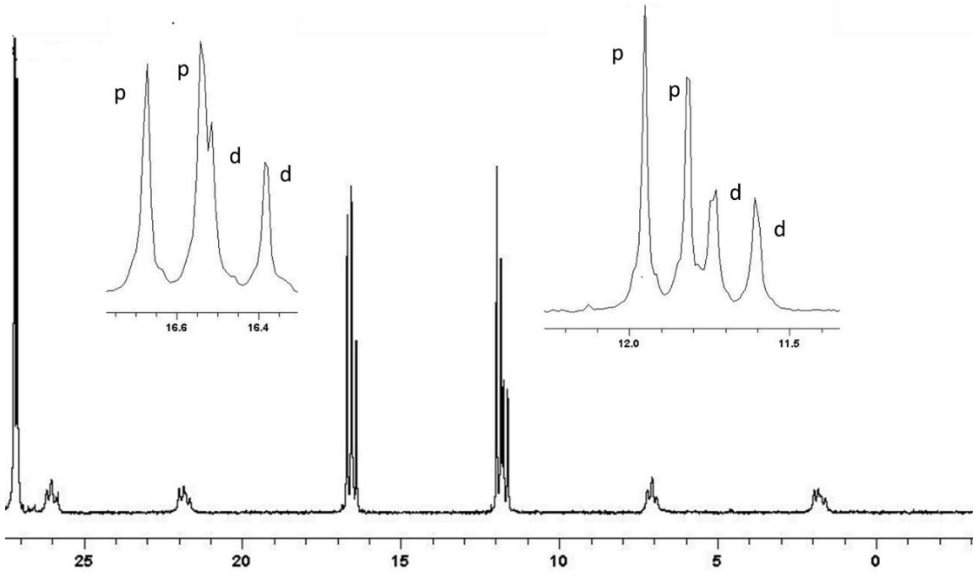

Figure 5.6: $^{31}P\{H\}$ NMR spectrum of platinum thiourea complex $[Pt\{SC(NPh)NHC_6H_4CH_2P(O)(OEt)_2\}(PPh_3)_2]BF_4$ **5a** after 180 mins of dissolution in $CDCl_3$. Inserts are expanded phosphorus resonance peaks showing proximal (p) and distal (d) isomers of the complex in solution

The $^{31}P\{^1H\}$ NMR of the bis(hydroxyethyl)-substituted derivative **5d** did not show any sign of isomerisation, even after the complex was left in the NMR solution for several days. This is expected, due to the steric impossibility of having bis(hydroxyethyl) substituent at the proximal position. So, the isomer shown by **5.3** was assigned as the only possible isomer of the complex. The chemical shifts are presented in **Table 5.3.**

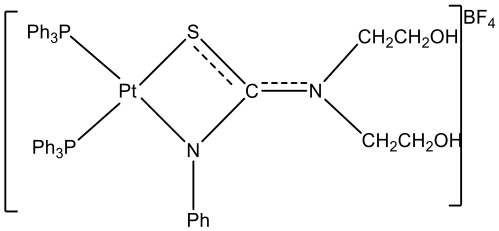

5.3

Table 5.3: $^{31}P\{^{1}H\}$ NMR chemical shift values and corresponding $^{1}J_{(PtP)}$ coupling constants

Complexes	**$^{31}P\{^{1}H\}$ NMR Chemical shifts in ppm (coupling constant)**	
	Proximal isomer	**Distal Isomer**
5a	11.95(3269); 16.66(3072); 27.26	11.72(3257); 16.47(3068); 27.12
5b	11.22(3335); 17.04(3051); 27.71	11.21(3315); 16.18(3053); 27.04
5c	12.68(3237); 18.10(3136)	9.50(3417); 14.32(3208)
5d		9.37(3410); 15.00(3268)
5e		9.44(3456); 13.73(3234)
5f		9.41(3421); 14.39(3221)
5g		9.42(3423); 14.01(3227)

The silatrane-substituted platinum complexes, **5e-5g** (**Scheme 5.3**) showed only one set of doublets in their $^{31}P\{^{1}H\}$ NMR spectra after several days in solution, indicating that only one isomer of the complex existed in solution. This is probably due to the bulky nature of the silatrane functional group. The single isomer was assigned as the distal isomer by comparing their chemical shifts with those of the-bis(hydroxyethyl)-substituted complex, **5d (Table 5.2**). $^{31}P\{^{1}H\}$ NMR spectra of the phosphonate and hydroxyethyl substituted palladium complexes **5h-5k**, were recorded in $CDCl_3$ solution. The spectra showed that the phosphonate and hydroxyethyl-substituted palladium complexes had two sets of doublets like their platinum analogues, while the bis(hydroxyethyl) derivative had one set of doublets as was observed in the platinum complex analogue, **5d**. The chemical shifts of the different isomers of the palladium complexes **5h-k** are presented in **Table 5.3**.

Table 5.4: $^{31}P\{^{1}H\}$ NMR chemical shifts and corresponding $^{1}J_{(PP)}$ coupling constants

Complexes	**$^{31}P\{^{1}H\}$ NMR Chemical shifts in ppm**	
	Proximal isomer	**Distal Isomer**
5h	55.46(35); 50.24(36); 59.62	55.12(36); 48.60(36); 58.04
5i	58.50(37); 50.24(36); 60.70	56.89(36); 49.60(37); 59.79
5j	62.60(27); 57.91(26)	55.34(29); 52.30(30)
5k		60.90(33); 54.66(33)

The FTIR spectra of the phosphonate substituted complexes showed strong bands around 1300 cm^{-1} indicating that the P=O functional group was not involved in the coordination process[20]. The hydroxyethyl substituted complexes also showed broad OH bands around 3400 cm^{-1} resulting from the hydroxyl groups of the hydroxyalkyl thiourea ligand. The C=S stretching and rocking frequencies bands observed around 1450 and 750 cm^{-1} in the spectra of the ligands was observed to have moved to lower frequencies in the spectra of the complexes, indicating the involvement of the thione sulfur of the ligand in the complex formation[28].

5.2.6 *X-ray crystal structures of complexes 5c, 5d, and 5e*

Crystals of platinum complexes of the hydroxyalkyl thioureas **5c-5d** and silatrane-substituted thiourea **5e**, suitable for X-ray crystallography were isolated by vapour diffusion of diethyl ether into a saturated dichloromethane solution of the complex. The crystal structure determination showed that the three crystals formed salts with one BF_4 anion each. In addition to the BF_4 anion, **5e** crystallised with a diethyl ether solvent disordered in two positions and sitting on an inversion centre in the asymmetric unit. All three complexes **5c-5e** crystallised in the monoclinic *P2₁* crystal system in the distal isomeric forms of the compounds. This is the isomer where the hydroxyalkyl or silatrane functional groups are bound to the nitrogen remote to the metallacyclic ring.

The hydroxyethyl-substituted complex $[Pt\{SC(NPh)NHC_2H_5OH\}(PPh_3)_2]BF_4$ **5c** contains a platinum atom S,N chelated to the N-hydroxyethyl thiourea anion, with the remaining positions in the almost square planar arrangement occupied by two phosphorus atoms of the triphenylphosphine ligands. The molecular structure of the complex and selected geometric parameters are presented in **Figure 5.7** and **Table 5.5**, respectively. The r.m.s. deviation of the resulting NP_2S square plane is 0.080 Å, and the platinum atom lies 0.030 Å out of the plane. The *cis*-angles in the square plane range from the narrower 68.01(14)° for the S-N chelate angles to a wider 98.00(5)° for the angle subtended by the phosphorus atoms. These values are similar to the values reported for the trisubstituted platinum complex

$[Pt\{SC(=N(CH_2CH_2)_2O)NC_6H_4N=NC_6H_4NMe_2\}(PPh_3)_2]BPh_4$ (68.68(7)°, 97.42(7)° [1], and the disubstituted pyridyl thiourea complex $[Pt\{SC(=NPh\}NCH_2Py(PPh_3)_2]$ [69.33(5)°, 96.06(18)°] reported in Chapter 2 of this thesis. The P(2)-Pt(1)-

N(1) and S(1)-Pt(1)-P(1) *trans* angles in the complex **5c** deviate from the ideal 180° by approximately 16 and 14° respectively.

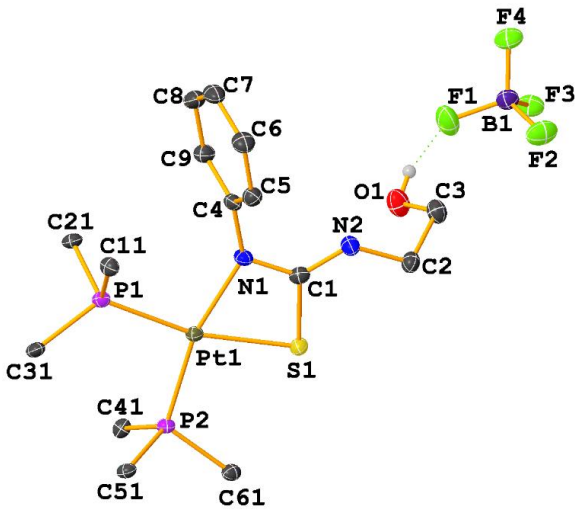

Figure 5.7: Molecular structure of the hydroxyethyl-substituted complex $[Pt\{SC(NPh)NHC_2H_5OH\}(PPh_3)_2]BF_4$ **5c**. Only ipso carbon atoms of the PPh_3 ligand are shown for clarity. Ellipsoids are at 50% probability.

The difference in the Pt(1)-P(1) 2.2837(17) Å and Pt(1)-P(2) 2.2455(16) Å bond lengths, is a clear indication that the sulfur donor atom has a greater *trans*-influence than the nitrogen donor atom[29]. This is consistent with the ^{31}P NMR assignments. The angles subtended at the thiolate S(1), and N(1) atoms of the chelate ring are as expected with the Pt(1)-S(1)-C(1) at 79.70(2)° and the more sterically encumbered Pt(1)-N(1)-C(1) wider with an angle of 100.7(4)°. The N-bound phenyl ring is oriented 67.17(3)° out of the plane of the chelate ring, while the alkyl chain of the hydroxyethyl functional group adopts an anti-clinal conformation as shown by the C(1)-N(2)-C(2)-C(3) torsion angle of 117.70(4)°.

The orientation of the hydroxyethyl functional group in the crystal results in intermolecular hydrogen bond between the OH group and the fluorine atom of the adjacent BF_4 counter ion The delocalisation of electron density around the chelate ring on complexation is confirmed by comparing the geometric parameters of the complex **5c** with those of the precursor thiourea ligand[8]. The C(1)-S(1) and C(1)-N(2) bond lengths in the complex **5c** 1.751(3) Å and 1.327(3) Å were considerably elongated and shortened, compared to the equivalent bonds in the precursor thiourea ligand with corresponding bond lengths of 1.707(2) Å and 1.333(3) Å. The C(1)-N(1) bond length in **5c** is shortened 1.325(5) Å compared

with the equivalent bond in the thiourea ligand 1.344(3) Å. Also reflecting the delocalisation of π-electron density are changes in the magnitude of the angles around the C(1) carbon atom. In the complex **5c**, the S(1)-C(1)-N(2); 123.23(4)^o and N(1)-C(1)-N(2); 126.29(4)^o angles are systematically wider than the corresponding angles in the ligand, S(1)-C(1)-N(2); 122.89(16)^o and N(1)-C(1)-N(2); 118.68(19)^o. Apart from that, the endocyclic S(1)-C(1)-N(1) angle in the complex **5c**, 110.45(18)^o is wider than the thiourea ligand 118.42(16)^o.

Table 5.5: Geometric parameters for crystal structures of **5c, 5d,** and **5e**

Bond parameters	**5c**	**5d**	**5e**
Pt(1) – S(1)	2.3502(6)	2.3377(8)	2.3611(17)
Pt(1) – P(1)	2.2802(6)	2.2969(8)	2.2837(17)
Pt(1) – P(2)	2.2532(6)	2.2423(9)	2.2455(16)
Pt(1) – N(1)	2.103(2)	2.125(3)	2.114(5)
S(1) – C(1)	1.751(3)	1.756(4)	1.772(7)
N(2) – C(1)	1.327(3)	1.332(5)	1.310(9)
N(2) – C(2)	1.460(3)	1.489(5)	1.452(9)
N(1) – C(1)	1.325(3)	1.329(5)	1.310(8)
P(1) – Pt(1) – S(1)	166.39(5)	166.76(3)	166.38(6)
P(2) – Pt(1) – S(1)	95.60(5)	95.35(3)	95.60(6)
P(1) – Pt(1) – P(2)	98.00(5)	95.42(5)	98.00(6)
N(1) – Pt(1) – S(1)	69.01(14)	69.54(8)	69.07(16)
N(1) – Pt(1) – P(2)	164.35(15)	164.84(9)	164.41(16)
N(1) – Pt(1) – P(1)	97.38(14)	99.70(9)	97.31(16)
C(1) – S(1) – Pt(1)	79.70(2)	79.94(13)	79.80(2)
C(1) – N(1) – Pt(1)	100.7(4)	98.5(2)	100.7(4)
N(2) – C(1) – S(1)	123.2(2)	122.7(5)	124.8(5)
N(1) – C(1) – S(1)	110.45(18)	110.8(3)	110.3(5)
N(1) – C(1) – N(1)	126.3(2)	126.3(4)	124.9(6)

The bis(hydroxyethyl)-substituted platinum complex **5d** is structurally similar to the hydroxyethyl derivative in **5c**. The NP_2S square plane in **5d** is slightly more planar than **5c**, with r.m.s. deviation of 0.077 Å. The silatrane-substituted thiourea platinum complex **5e** has the most planar four membered ring with a r.m.s. deviation of 0.024 Å. Selected geometric parameters for **5d** and **5e** are presented in **Table 5.5**, while their molecular structures are shown in **Figures 5.8** and **5.9**, respectively.

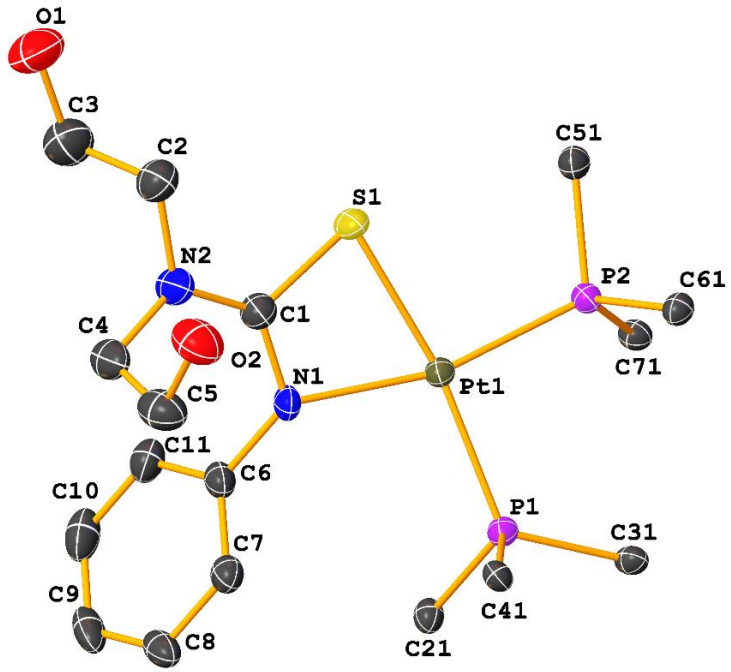

Figure 5.8: Molecular structure of bis(hydroxyethyl)-substituted complex $Pt\{SC(NPh)N(C_2H_5OH)_2\}(PPh_3)_2]BF_4$ **5d**. The BF_4 anion is omitted, and only ipso carbon atoms of the PPh_3 ligand are shown for clarity. Ellipsoids are drawn at 50% probability

The S-Pt-N *cis*-angles in **5d** 69.54(16)^o and **5e** 69.07(16)^o are similar and slightly wider than that in **5c** 68.01(14)^o. The P(1)-Pt(1)-P(2) angles in **5c** and **5e** are equivalent 98.00(6)^o, while the corresponding angle in **5d** is narrower by 3^o. The deviations of the *trans*-angles in **5d** and **5e** from the ideal 180^o are similar and very close to the values recorded for the deviations in **5c.** The Pt(1)-P(1) bond lengths in **5d**, 2.2969(9) Å and **5e** 2.2837(17) Å are systematically longer than the Pt(1)-P(2) bonds in both complexes **5d**; 2.2423(9) Å and **5e**; 2.2455(16) Å, due to the greater *trans*-influence of the thiolate donor group to the nitrogen[30,31]. The π-electron density delocalisation around the metallacyclic C(1) carbon atom of the complexes results in the elongation of the thiolate S(1)-C(1) bonds and shortening of the C(1)-N(2) bonds. There are slight variations in the magnitude of the angles around the metallacycle for the three complexes, **Table 5.4**, but this does not result in any obvious structural implication for the complexes. The only significant difference in the crystal structure of the complexes **5c**, **5d** and **5e** is the magnitude of the dihedral angles between the Pt(1)-S(1)-C(1)-N(1) chelate rings and the N-bound phenyl rings. The N-bound phenyl ring in **5e** is orthogonally out of the plane of the four-membered chelate ring with an angle of 89.37^o. The phenyl rings in **5d**

and **5e** are deviated by much narrower angles of 67.17° and 59.03°. The C(1)-N(2)-C(2)-C(3) 116.35(6)° torsion angle in **5d** adopts a +anti-clinal conformation similar to the corresponding angle in **5c**, while C(1)-N(2)-C(4)-C(5) torsion angle 63.73(5)° of the second hydroxyethyl group in **5d** adopts a +syn-clinal conformation. The propyl chain of the silatrane functional group in **5e** also adopts a -syn-clinal conformation with a torsion angle of -83.22(5)°, thus orientating the silatrane-O to accept an intermolecular hydrogen bond from the thiourea N-H (**Figure 5.9**). The presence of N-H·····O intramolecular and O-H·····F intermolecular hydrogen bonding interactions in the crystal structures of **5e** and **5c** respectively and none in **5d** is an indication of the changes in supramolecular properties that could arise with changes in thiourea functionality.

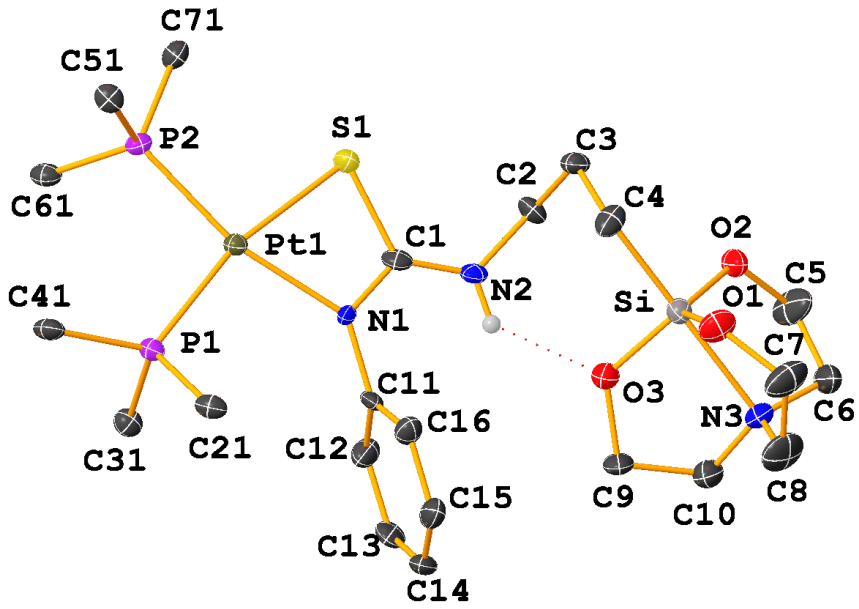

Figure 5.9: Molecular structure of the siltrane-substituted complex $[Pt\{SC(NPh)NH(CH_2)_3Si(OCH_2CH_2)_3N\}(PPh_3)_2]BF_4$ **5e**. BF_4 anion was omitted, and only ipso carbon atoms of the PPh_3 ligand are shown for clarity. Ellipsoids are drawn at 50% probability.

5.3 Conclusions

A series of phosphonate-, hydroxyethyl-, and silatrane-substituted thioureas were synthesised and characterised. The X-ray crystal structure of the phosphonate substituted thioureas showed the formation of unusual hydrogen-bond motifs, resulting from noncovalent interactions in competing functional groups. Platinum and palladium complexes of these thioureas were synthesised and characterised.

The $^{31}P\{^{1}H\}$ NMR spectra of the phosphonate and monohydroxyethyl-substituted complexes showed the presence of two isomers of the complex in $CDCl_3$ solution, while the bis(hydroxyethyl) and silatrane-substituted complexes showed only a single isomer. The X-ray crystal structures of the hydroxyethyl, bis(hydroxyethyl) and silatrane-substituted platinum thiourea complexes **5c**, **5d** and **5e** showed that the compounds crystallised as BF_4 salts, in the distal isomeric form of the complexes. The difference in the *N*-substituted functional groups does not result in any apparent geometric or structural discrepancy in the almost square planar structure of the complexes. The intermolecular hydrogen bonding in **5e** and **5d** are however an indication of the robustness of the bis(hydroxyalkyl) and silatrane substituted complexes.

5.4 Experimental

5.4.1 *Synthesis and characterisation of thiourea ligands*

(1i). *Diethyl 4-(3-phenyl thioureido) benzyl phosphonate*

$(EtO)_2P(O)CH_2C_6H_4NHC(S)NHPh$

Diethyl 4-aminobenzyl-1-phosphonate, ethanolamine, di-ethanolamine and DMF were purchased from Sigma Aldrich Chemical Company. Refer to Chapter 2 for sources of isothiocyanates and solvents. Diethyl 4-aminobenzyl-1-phosphonate (1 g, 0.0041 mol, 1 equiv.) in DMF 20 mL was reacted with phenyl isothiocyanate (0.54 mL, 0.0045 mol, 1 equiv.) in a 100 mL round bottom flask in the fume hood. The resulting yellowish-brown mixture was left to stir overnight. The product was isolated by adding distilled water (35 mL) dropwise to the reaction mixture until an off-white product precipitated out of the solution. The product was filtered and washed with water (15 mL) and petroleum spirits (10 mL). The product was recrystallised from hot ethanol (25 mL) to give colorless crystals. Yield, 1.21g; 60 %, melting range; 140-142^{o}C. Elemental analysis: calculated; C 57.13; H 6.13; N 7.40, found; C 57.38, H 6.23, N 7.39 %. ESI-MS: *m/z* 379.12 (28%) $[M+H]^+$, 401.12 (100%) $[M+Na]^+$, 779.22 (82%) $[2M+Na]^+$, 1157.23 (16.69%) $[3M+Na]^+$. $^{31}P\{^{1}H\}$ NMR δ ppm: 27.55. ^{1}H NMR δ ppm; 8.62 [s, 1H, NH], 8.51 [s, 1H; NH], 7.0-8.0 [m, 8H; Ph], 4.31 [m, 4H, CH_2-OEt], 3.17 [d, 2H, CH_2-P; J = 22 Hz], 1.25 [t, 6H, CH_3; J = 7.1 Hz]. FTIR (cm^{-1}) 3322(s), 3236(m), 2986(m), 2940(w), 1641(w), 1595(s), 1541(s), 1513(s), 1498(s), 1450(w), 1350(m), 1312(w), 1257(s),

1214(s), 1162(w), 1050(w), 1028(s), 975(s), 903(w), 842(s), 780(w), 696(s), 618(w), 550(s), 494(w).

(1j). *Diethyl 4-(3-4-nitrophenylthioureido)benzyl phosphonate*

$(EtO)_2P(O)(CH_2)C_6H_4NHC(S)NHC_6H_4NO_2$

The procedure is the same as above using diethyl 4-aminobenzyl-1-phosphonate (0.5 g, 0.0021 mol, 1 equiv.) and *p*-nitrophenyl isothiocyanate (0.456 g, 0.00225 mol, 1 equiv.). Yield; 0.8 g; 83 %, melting range: 180-183^{o}C. Elemental analysis: calculated; C 51.06, H 5.24, N 9.92, found: C 51.10, H 5.32; N 9.98 %. ESI-MS: *m/z* 446 (100%) $[M+Na]^+$, 869 (14.7%) $[2M+Na]^+$, 1292 (5.6%) $[3M+Na]^+$. $^{31}P\{^1H\}$ NMR $CDCl_3$ δ ppm; 26.45 . ^1H NMR δ ppm; 10.4 [s, 1H, NH], 10.3 [s, 1H, NH], 6.0-8.3 [m, 8H, Ph], 4.02 [m, 4H, CH_2-OEt], 3.17 [d, 2H, CH_2-P; J = 21 Hz], 1.2 [t, 6H, CH_3; J = 6.9 Hz]. FTIR (cm^{-1}): 338(s), 3234(s), 3193(s), 3098(br), 2983(s), 2905(w), 1660(s), 1595(s), 1540(s), 1507(s), 1413(s), 1450(w), 1330(s), 1312(w), 1249(s), 1205(s), 1174(s), 1112(s), 1056(w), 1017(s), 981(s), 854(w), 834(s), 772(s), 752(s), 719(s), 628(m), 566(s), 517(s), 498(m), 473(w).

(1k). *1-(2-Hydroxyethyl)-3-phenylthiourea (PhNHC(S)NHCH$_2$CH$_2$OH)*

This ligand was synthesised using a modified literature method[10]. Ethanolamine (0.5 mL, 8.3 mmol) and phenyl isothiocyanate (1.1 mL, 9.1 mmol) were refluxed in acetonitrile (10 mL). The solution was cooled for 30 mins and then filtered, the solid washed with diethyl ether (10 mL) and dried under vacuum to give feathery white crystals. Yield: 1.43 g, 88 %, melting range; 136-137 ^{o}C. ESI-MS: *m/z* 219.04 (100%) $[M+Na]^+$. ^1H NMR (DMSO-d_6) δ ppm; 9.58 [s, 1H, NH], 7.68 [s, 1H, NH], 7.43-7.09 [m, 5H, Ph], 4.86 [m, 1H, OH], 3.55[m, 4H, CH_2]. FTIR (cm^{-1}): 3361(s), 3189(m), 2999(w), 2948(w), 1636(w), 1594(m), 1545(s), 1522(w), 1486(m), 1427(w), 1374(w), 1308(m), 1253(m), 1220(w), 1178(m), 1128(m), 1056(s), 929(s), 908(w), 784(w), 721(s), 690(s), 606(s), 573(w), 477(m).

(1l). *1-(2,2-di-hydroxyethyl)-3-phenylthiourea (PhNHC(S)N(CH$_2$CH$_2$OH)$_2$)*

Diethanolamine (0.5 g, 4.76 mmol) was suspended in diethyl ether (35 mL) with a slight excess of phenyl isothiocyanate (0.6 mL, 5.23 mmol). The resulting pale-yellow solution was stirred for 24 h. Diethyl ether was removed using a rotary evaporator, producing a pale-yellow solid, which was washed with petroleum

spirits (10 mL) and dried overnight in a vacuum. Yield: 1.09 g, 84 %, melting range; 94-95^{o}C. ESI-MS: *m/z* 263.07 (100%) $[M+Na]^{+}$. ^{1}H NMR (DMSO-d_6) δ ppm; 9.72 [s, 1H, NH], 6.94-7.33 [m, 5H, Ph], 5.32 [s, 2H. OH], 3.83-3.90 [t, 4H CH_2O; J = 5.6 Hz], 3.73 [t, 4H, CH_2N; J = 5 Hz]. FTIR (cm^{-1}): 3271(br), 3146(s), 2948(w), 2848(w), 1634(s), 1599(s), 1572(s), 1499(s), 1485(s), 1406(s), 1365(s), 1216(s), 1089(s), 1034(s), 902(w), 759(m), 701(m), 606(s), 560(m), 516(w), 420(w).

(1m). *1-(-3-(2,8,9-Trioxa-5-aza-1-sila-bicyclo[3.3.3.]undecane-1-yl)propyl)-3-phenyl thiourea. ($PhNHC(S)NHC_9H_{18}NO_3Si$)*

This compound was synthesised according to the method reported in the literature[32]. 3-Aminopropylsilatrane (0.70 g, 3.01 mmol) was dissolved in chloroform (25 mL) and solution of phenyl isothiocyanate (0.36 g, 3 mmol) in chloroform (5 mL) was added dropwise with stirring. The mixture was stirred under reflux for 4 h. After cooling, the solvent was evaporated under vacuum and the pale colored solid was precipitated with hexane (20 mL). Yield: 0.87 g; 79 %. Melting range: 172-174^{o}C. ESI-MS: *m/z* 368.07 (100%) $[M+H]^{+}$. ^{1}H NMR (DMSO-d_6) δ ppm; 7.48-7.05 [m, 4H, Ar-H], 7.03 [s, 1H, NH, Ar-H], 4.44 [s, 1H, NH-CH_2], 3.62 [t, 6H, OCH_2; J = 5.7 Hz], 3.38 [m, 2H, CCH_2N], 2.78 [t, 6H, NCH_2; J = 5.7 Hz], 1.56 [m, 2H, CH_2], 0.24 [t, 2H, $SiCH_2$; J = 8.6 Hz. $^{13}C\{^{1}H\}$NMR (DMSO-d_6/$CDCl_3$) δ ppm: 179.74 (C=S), 117.24-139.33 (Ar-C), 58.75, (OCH_2) 50.09 (NCH_2), 47.50 (CH_2NH), 24.42 (CCH_2C), 14.07 ($SiCH_2$). FTIR (cm^{-1}): 3484(w), 3390(w), 3264(br), 3217(br), 2925(s), 2876(s), 1962(w), 1595(s), 1541(br), 1453(s), 1351(s), 1315(m), 1275(w), 1172(m), 1127(br), 1017(s), 973(s), 939(s), 910(s), 877(s), 825(w), 763(br), 711(m), 619(s), 586(m), 503(s).

(1n). *1-(-3-(2,8,9-Trioxa-5-aza-1-sila-bicyclo[3.3.3.]undecane-1-yl)propyl)-3-(4-nitrophenyl thiourea. ($O_2NC_6H_4NHC(S)NHC_9H_{18}NO_3Si$)*

This silatrane thiourea was synthesised following the same procedure as described for the phenyl derivative in **(1m**). In this case *p*-nitrophenyl isothiocyanate (0.54 g, 3 mmol) and 3-aminopropylsilatrane (0.70 g, 3.01 mmol) were used. The yellow colored product was precipitatating with diethyl ether (25 mL) after 120 min.. Yield: 1.02 g; 82 %. Melting range: 203-205^{o}C. ESI-MS *m/z* = 413 (100%) $[M+H]^{+}$, 335 (87%) $[M+Na]^{+}$. ^{1}H NMR (DMSO-d_6/$CDCl_3$) δ ppm; 8.05-8.20 [m, 4H, Ar-H], 7.57 [s, 1H, NHAr], 6.91 [s, 1H, NH(CH_2)], 3.69 [t, 6H, OCH_2; J = 5.7 Hz],

3.16 [m, 2H, CCH_2N], 2.80 [t, 6H NCH_2; J = 5.7 Hz], 1.53 [m, 2H, CCH_2C], 0.44 [t, 2H, $SiCH_2$; J = 8.6 Hz]. $^{13}C\{^1H\}$ NMR (DMSO-d_6/$CDCl_3$) δ ppm: 178.32 [C=S], 154.00 [CNO_2], 122.59-128.33 [Ar-C], 57.56 [OCH_2], 56.81 [NCH_2], 44.67 [$C(CH_2N)$], 24.53 [$C(CH_2C)$], 12.77 [$SiCH_2$]. FTIR (cm^{-1}): 3413(br), 3201(s), 2973(w), 2955(w), 2881(w), 1927(w), 1663(m), 1612(m), 1598(s), 1518(br), 1455(s), 1393(m), 1346(m), 1247(s), 1214(m), 1149(s), 1118(s), 1081(s), 1018(s), 987(s), 949(s), 912(s), 874(m), 860(s), 792(m), 708(w), 623(s), 568(s), 532(w), 498(s).

(1o). *1-(-3-(2,8,9-Trioxa-5-aza-1-sila-bicyclo[3.3.3.]undecane-1-yl)propyl)-3(-4-methoxyphenyl) thiourea. ($C_6H_4OMeNHC(S)NHC_9H_{18}NO_3Si$)*

This silatrane thiourea was synthesised using similar a similar method as the one described for the phenyl derivative (**1m**). In this case (0.39 g, 3.01 mmol) of *p*-methoxyphenyl isothiocyanate and (0.70 g, 3.01 mmol) 3-aminopropylsilatrane were used. The white colored product was obtained by addition of diethyl ether (15 mL) to the reaction solution. Yield: 0.85 g; 71 %. Melting range: 167-170°C. ESI-MS: *m/z* 398.07 (100%) $[M+H]^+$. ^1H NMR (DMSO-d_6/$CDCl_3$) δ ppm: 6.70-7.29 [m, 4H, Ar-H], 5.89 [s, 1H, NH], 4.37 [s, 1H, NCH_2], 3.72 [s, 3H, OCH_3], 3.65 [t, 6H, OCH_2; J = 5.7 Hz], 3.03 [m, 2H, CCH_2N], 2.80 [t, 6H, CH_2N; J = 5.7 Hz], 1.46 [m, 2H, CCH_2C]. $^{13}C\{^1H\}$ NMR (DMSO-d_6/$CDCl_3$) δ ppm: 178.32 (C=S), 155.20 [C=O], 153.54 [(COMe)], 112.59-132.33 [(Ar-C)], 58.56 [OCH_2], 56.88 [OCH_3] 51.61 [NCH_2], 43.47 [CCH_2N], 25.83 [CCH_2C], 13.57 [$SiCH_2$]. FTIR (cm^{-1}) 3303(s), 3160(s), 2966(w), 2880(w), 1873(m), 1609(w), 1509(br), 1454(w), 1401(w), 1381(m), 1329(m), 1272(w), 1184(m), 1170(m), 1094(br), 1024(br), 1018(w), 987(s), 937(s), 909(s), 825(s), 755(br), 707(s), 620(m), 572(s), 518(s), 495(s).

5.4.2 *Synthesis and characterisation of thiourea complexes*

*$[Pt\{SC(NPh)NHC_6H_4CH_2P(O)(OEt)_2\}(PPh_3)_2]BF_4$ (**5a**)*

cis-$[PtCl_2(PPh_3)_2]$ (80 mg, 0.1 mmol) was suspended in ethanol (25 mL) and $(EtO)_2P(O)CH_2C_6H_4NHC(S)NHPh$ (**1i**) (38 mg, 0.1 mmol) was added. The mixture was stirred until a clear solution was observed. Triethylamine (0.5 mL) was added to the solution and was allowed to reflux for 1 hour. Solid $NaBF_4$ (329 mg, 0.3 mmol) was added to the hot solution and distilled water (70 mL) was added to

precipitate the yellowish product. The product was filtered and dried overnight in a desiccator, under vacuum. Yield 98 mg, 79 %. Elemental analysis %: calculated for $C_{54}H_{52}N_3O_3P_2PtS$; C 74.12, H 5.42, N 4.17, found; C 74.09, H 5.38, N 4.2. ESI-MS: Calculated *m/z*; 1096.20 $[M]^+$, experimental *m/z*: CEV 60 V, 1096.18 (100%) $[M]^+$, CEV 120-180 V, 834.13 (32%) $[M\text{-}PPh_3]^+$, 718.0 (68) $[Pt(PPh_2C_6H_4)(PPh_3)]^+$ 1096.20 (100%) $[M]^+$. Distal isomer: $^{31}P\{^1H\}$ NMR δ ppm; 16.47 [$^1J_{(PtP)}$ = 3068 Hz, $^2J_{(PP)}$ = 22 Hz] and 11.72 [$^1J_{(PtP)}$ = 3257 Hz, $^2J_{(PP)}$ = 22 Hz], 27.12 [s, P(O)]. ^1H NMR δ ppm; 1.13 [t, 6H, CH_3; J = 7.2 Hz], 2.88 [d, 2H, CH_2; J = 21 Hz], 3.87 [m, 4 H, CH_2-ester], 6.4-7.51 [m, 40 H, Ar-H]. Proximal isomer: $^{31}P\{^1H\}$ NMR δ ppm; 16.66 [$^1J_{(PtP)}$ 3074 Hz, $^2J_{(PP)}$ 22 Hz] and 11.95 [$^1J_{(PtP)}$ 3269 Hz, $^2J_{(PP)}$ 21 Hz], 27.26 [s, P(O)]. ^1H NMR δ ppm: 1.22 [t, 6H, CH_3; J = 8.2 Hz], 3.07 [d, 2H, CH_2; J = 22 Hz], 3.87 [m, 4 H, CH_2-ester], 6.4-7.51 [m, 40 H, Ar-H]. FTIR (cm^{-1}): 3421(br), 3051(m), 2982(m), 2925(w), 1592(w) 1548(s), 1503(m), 1482(m), 1436(s), 1312(m), 1234(s), 1161(w), 1096(s), 1052(w), 1025(s), 957(s), 849(m), 745(s), 592(w), 546(s), 525(s), 514(w), 497(w).

*$[Pt\{SC(NC_6H_4NO_2)NHC_6H_4CH_2P(O)(OEt)_2\}(PPh_3)_2]BF_4$ (**5b**)*

This complex was synthesised following the same method as **5a** from *cis*-$[PtCl_2(PPh_3)_2]$ (80 mg, 0.1 mmol) and $(EtO)_2P(O)CH_2C_6H_4NHC(S)NHC_6H_4NO_2$ (**1j**) (42 mg, 0.1 mmol). Yield 87 mg; 89 %. Elemental analysis %: calculated for $C_{54}H_{51}N_3O_5P_3PtS$; C 56.79, H 4.50, N 3.68, found; C 55.23, H 4.59, N 3.79. ESI-MS: Calculated *m/z*; 1141.14 $[M]^+$, experimental *m/z*; CEV 60 V, 1141.12 (100%) $[M]^+$, CEV 150 V, 718.06 (12%) $[Pt(PPh_2C_6H_4)(PPh_3)]^+$, 879.10 (3%) $[M\text{-}PPh_3]^+$, 2282.22 (3%) $[2M\text{-}H]^+$. Distal isomer: $^{31}P\{^1H\}$ NMR δ ppm; 16.18 [$^1J_{(PtP)}$ = 3055 Hz, $^2J_{(PP)}$ = 22 Hz] and 11.21 [$^1J_{(PtP)}$ = 3315 Hz, $^2J_{(PP)}$ = 22 Hz], 27.04 ppm [s, P(O)]. ^1H NMR; 1.13 [t, 6H, CH_3; J = 5.9 Hz], 3.09 [d, 2H, CH_2; J = 20 Hz], 3.87 [m, 2 H, CH_2-ester] 6.4-7.51 [m, 39 H, Ar-H]. Proximal isomer: $^{31}P\{^1H\}$ NMR δ ppm; 17.04 [$^1J_{(PtP)}$ = 3051 Hz, $^2J_{(PP)}$ 22 Hz] and 11.22 [$^1J_{(PtP)}$ = 3335 Hz, $^2J_{(PP)}$ = 22 Hz], 27.71 [s, P(O)]. ^1H NMR δ ppm; 1.16 [t, 6H, CH_3; J = 6.4 Hz], 2.84 [d, 2H, CH_2; J = 21 Hz], 3.87 [m, 4 H, CH_2-ester], 6.4-7.51 [m, 39 H, Ar-H], FTIR (cm^{-1}): 3422(br), 3053(m) 2980(m), 2905(w), 1588(w), 1500(s), 1482(w), 1436(s), 1411(w), 1312(s), 1247(m), 1171(w), 1099(s), 1052(m), 1025(s), 957(s), 852(s) 746(m), 693(s), 617(w), 545(s), 525(s), 514(w), 497(w).

*[Pt{SC(NPh)NHC$_2$H$_5$OH}(PPh$_3$)$_2$]BF$_4$ (**5c**)*

From *cis*-[PtCl$_2$(PPh$_3$)$_2$] (80 mg, 0.1 mmol) and PhNHC(S)NHC$_2$H$_5$OH (20 mg, 0.1 mmol). Yield 52 mg; 62 %. Elemental analysis %: calculated for C$_{45}$H$_{40}$N$_2$OP$_2$PtS; C 59.14, H 4.41, N 3.07, found; C 59.12, H 4.42, N 3.08. ESI-MS: Calculated *m/z*; 914.20 [M]$^+$, experimental *m/z*: CEV 60 V, 914.17 (100%) [M]$^+$, 1827.17 (7%) [2M-H]$^+$, CEV 120-180 V, 651.06 (12%) [M-PPh$_3$]$^+$, 718.09 (24%) [Pt(PPh$_2$C$_6$H$_4$)(PPh$_3$)]$^+$, 914.15 (100%) [M]$^+$, 1827.17 (7%) [2M-H]$^+$. Distal isomer: ^{31}P{^{1}H} NMR δ ppm; 14.32 [^{1}J$_{(PtP)}$ = 3208 Hz, ^{2}J$_{(PP)}$ = 20 Hz] and 9.50 [^{1}J$_{(PtP)}$ = 3417 Hz, ^{2}J$_{(PP)}$ = 20 Hz], ^{1}H NMR δ ppm; 2.19 [s, 1H, OH], 2.79 [t, 2H, CH$_2$; J = 4.5 Hz], 3.05 [m, 2H, CH$_2$], 6.85-7.60 [m, 35H, Ar-H], Proximal isomer: ^{31}P{^{1}H} NMR δ ppm; 18.10 [^{1}J$_{(PtP)}$ 3136 Hz, ^{2}J$_{(PP)}$ 22 Hz] and 12.68 [^{1}J$_{(PtP)}$ 3237 Hz, ^{2}J$_{(PP)}$ 22 Hz]. ^{1}H NMR δ ppm; 2.36 [s, 1H, OH], 2.72 [t, 2H, CH$_2$; J = 4.5 Hz], 3.64 [m, 2H, CH$_2$], 6.78-7.56 [m, 35H, Ar-H]. FTIR (cm^{-1}): 3444(br), 3054(w), 2919(w), 2850(w), 1632(br), 1595(w), 1551(s), 1481(s), 1435(s), 1354(w), 1309(w), 1202(m), 1162(w), 1096(s), 1029(m), 998(m), 967(m), 897(w), 873(w), 745(s), 693(s), 619(w), 547(s), 525(s), 515(m), 500(w).

*[Pt{SC(NPh)N(C$_2$H$_5$OH)$_2$}(PPh$_3$)$_2$]BF$_4$ (**5d**)*

From *cis*-[PtCl$_2$(PPh$_3$)$_2$] (80 mg, 0.1 mmol) and PhNHC(S)N(C$_2$H$_5$OH)$_2$ (**1l**) (24 mg, 0.1 mmol). Yield 61 mg; 72 %. Elemental analysis %: calculated for C$_{47}$H$_{45}$BF$_4$N$_2$O$_2$P$_2$PtS; C 53.98, H 4.34, N 2.68, found; C 54.02, H 4.32, N 2.69 ESI-MS: Calculated *m/z*; 958.12 [M+H]$^+$, experimental *m/z*: CEV 60 V, 958.12 (100%) [M]$^+$, CEV 120-180 V, 696.10 (22%) [M-PPh$_3$]$^+$, 718.09 (32%) [Pt(PPh$_2$C$_6$H$_4$)(PPh$_3$)]$^+$, 958.10 (100%) [M]$^+$. ^{31}P{^{1}H} NMR δ ppm: 15.00 [^{1}J$_{(PtP)}$ = 3268 Hz, ^{2}J$_{(PP)}$ = 22 Hz] and 9.37 [^{1}J$_{(PtP)}$ = 3410 Hz, ^{2}J$_{(PP)}$ = 22 Hz]. ^{1}H NMR δ ppm: 3.26 [s, 1H, OH], 3.53 [t, 1H, OH], 3.88 [m, 4H, CH$_2$], 3.89 [m, 4H,CH$_2$], 6.18 [d, 2H, Ar-H; J = 4.4 Hz], 6.64 [t, 1H, Ar-H; J = 3.2 Hz], 7.1-7.26 [m, 14H, Ar-H], 7.30-7.54 [m, 16H, Ar-H], 7.60-7.73 [m, 2H, Ar-H]. FTIR (cm^{-1}): 3442(br), 3052(w) 2924(w), 2854(w), 1643(br), 1590(w), 1539(m), 1481(m), 1435(s), 1385(w), 1311(w), 1268(w), 1184(m), 1097(s), 1027(w), 998(m), 897(w), 846(w), 746(s), 693(s), 639(m), 614(w), 543(s), 524(w), 515(s), 499(w).

*[Pt{SC(NPh)NHC$_9$H$_{18}$NO$_3$Si}(PPh$_3$)$_2$]BF$_4$ (**5e**)*

From *cis*-[PtCl$_2$(PPh$_3$)$_2$] (80 mg, 0.1 mmol) and PhNHC(S)NHC$_9$H$_{18}$NO$_3$Si (**1m**) (37 mg, 0.1 mmol). Yield 75 mg; 74 %. Elemental analysis %: calculated for

$C_{56}H_{64}BF_4N_3O_4P_2PtSSi$; C 53.94, H 5.17, N 3.38, found; C 53.52, H 5.12, N 3.36 ESI-MS: Calculated *m/z*; 1085.10 $[M]^+$, experimental *m/z*: CEV 60-150 V, 1085.07 (100%)$[M]^+$, CEV 180 V, (22%) $[M\text{-}PPh_3]^+$, 718.09 (24%) $[Pt(PPh_2C_6H_4)(PPh_3)]^+$, 822.07 (100%) $[M\text{-}PPh_3]^+$ 1085.09 (27%) $[M]^+$. $^{31}P\{^1H\}$ NMR δ ppm; 13.73 [$^1J_{(PtP)}$ = 3234 Hz, $^2J_{(PP)}$ = 22 Hz] and 9.44 [$^1J_{(PtP)}$ = 3456 Hz, $^2J_{(PP)}$ = 22 Hz]. ^1H NMR δ ppm: 1.07 [t, 2H, CH_2; J = 6.8 Hz], 1.27 [m, 6H, CH_2], 1.52 [m, 2H, CH_2], 3.05 [dd, 2H, CH_2; J = 6.4 Hz], 3.50 [t, 6H, CH_2; J = 5.8 Hz], 6.15-6.27 [m, 3H, Ar-H], 6.70 [m, 2H, Ar-H], 6.80 [t, 1H, Ar-H; J = 7.3 Hz], 7.13-7.25 [m, 14H, Ar-H], 7.34-7.42 [m, 16H, Ar-H]. FTIR (cm^{-1}): 3369(br), 3054(m), 2928(w), 2879(w), 1595(m), 1573(s), 1482(s), 1436(s), 1375(w), 1333(w), 1266(w), 1185(w), 1120(w), 1097(s), 999(m), 913(m), 843(w), 749(s), 692(s), 693(s), 621(w), 547(s), 526(s), 498(m).

*$[Pt\{SC(NC_6H_4NO_2)NHC_9H_{18}NO_3Si\}(PPh_3)_2]BF_4$ (**5f**)*

From *cis*-$[PtCl_2(PPh_3)_2]$ (80 mg, 0.1 mmol) and $O_2NC_6H_4NHC(S)NHC_9H_{18}NO_3Si$ (**1n**) (41 mg, 0.1 mmol). Yield 78 mg; 64 %. Elemental analysis %: calculated for $C_{52}H_{53}BF_4N_4O_5P_2PtSSi$; C 51.28, H 4.39, N 4.60, found; C 51.28, H 4.41, N 4.64. ESI-MS: Calculated *m/z*; 1131.02 $[M]^+$, experimental *m/z*: CEV 60-150 V, 1131.00 (100%) $[M]^+$, CEV 180 V, 718.09 (12%) $[Pt(PPh_2C_6H_4)(PPh_3)]^+$, 869.02 (80%) $[M\text{-}PPh_3]^+$ 1131.02 (47%) $[M]^+$. $^{31}P\{H\}$ NMR δ ppm: 14.31 [$^1J_{(PtP)}$ = 3221 Hz, $^2J_{(PP)}$ = 22 Hz] and 9.41 ppm [$^1J_{(PtP)}$ = 3421 Hz, $^2J_{(PP)}$ = 22 Hz]. ^1H NMR δ ppm: 0.97 [t, 2H, CH_2; J = 7.2 Hz], 1.15 [m, 6H, CH_2], 1.72 [m, 2H, CH_2], 3.15 [dd, 2H, CH_2; J = 7.1 Hz], 3.65 [t, 6H, CH_2; J = 6.4 Hz], 6.0-6.5 [m, 4H, Ar-H], 6.80 [m, 2H, Ar-H], 6.94 [t, 1H, Ar-H; J = 6.9 Hz], 7.25-7.30 [m, 12H, Ar-H], 7.40-7.52 [m, 10H, Ar-H]. FTIR (cm^{-1}): 3382(br), 3056(m), 2926(w), 2877(w), 1594(m), 1571(s), 1516(s), 1483(m), 1436(s), 1341(s), 1210(w), 1123(w), 1085(s), 999(w), 939(w), 910(s), 862(w), 754(s), 693(s), 618(w), 548(s), 526(s), 498(m).

*$[Pt\{SC(NC_6H_4OMe)NHC_9H_{18}NO_3Si\}(PPh_3)_2]BF_4$ (**5g**)*

From *cis*-$[PtCl_2(PPh_3)_2]$ (80 mg, 0.1 mmol) and $C_6H_4OMeNHC(S)NHC_9H_{18}NO_3Si$ (**1o**) (40 mg, 0.1 mmol). Yield 87 mg; 84 %. Elemental analysis %: calculated for $C_{53}H_{56}BF_4N_3O_4P_2PtSSi$; C 53.25, H 4.88, N 3.45, found; C 53.20, H 4.79, N 3.39. ESI-MS: Calculated *m/z*; 1116.03 $[M]^+$, experimental *m/z*: CEV 60-150 V, 1116.02 (100%) $[M]^+$, CEV 180 V, 717.90 (12%) $[Pt(PPh_2C_6H_4)(PPh_3)]^+$, 854.00 (10%) $[M\text{-}PPh_3]^+$ 1116.04 (97%) $[M]^+$. $^{31}P\{^1H\}$NMR δ ppm; 14.01 [$^1J_{(PtP)}$ = 3227 Hz, $^2J_{(PP)}$ 22 Hz] and 9.42 [$^1J_{(PtP)}$ = 3423 Hz, $^2J_{(PP)}$ = 21 Hz]. ^1H NMR δ ppm: 0.85 [d, 2H, CH_2;

J = 6.25 Hz], 1.26 [m, 2H, CH_2], 2.76 [t, 6H, CH_2; J = 5.9 Hz], 3.06 [d, 2H, CH_2; J = 6.5 Hz], 3.52 [t, 6H, CH_2, J = 5.9 Hz, 3.69 [s, 3H, OCH_3], 6.07-6.20 [m, 6H, Ar-H], 7.15-7.26 [m, 6H, Ar-H], 7.32-7.44 [m, 14H, Ar-H], 7.45-7.57 [m, 10H, Ar-H]. FTIR (cm^{-1}): 3373(br), 3055(m), 2933(m), 2879(w), 1578(s), 1506(s), 1482(s), 1437(s),1375(w), 1335(w), 1293(w), 1246(s), 1181(w), 1097(s), 999(w), 940(m), 911(m), 840(m), 750(s), 693(s), 618(w), 548(s), 526(s), 497(m).

[Pd{SC(NPh)NHC$_6$H$_4$CH$_2$P(O)(OEt)$_2$}(dppe)]BF$_4$ ***(5h)***

From [$PdCl_2$(dppe)] (58 mg, 0.1 mmol) and $(EtO)_2P(O)CH_2C_6H_4NHC(S)NHPh$ (**1i**) (38 mg, 0.1 mmol). Yield 72 mg; 79 %. Elemental analysis %: calculated for $C_{44}H_{45}N_2O_3P_3PdS$; C 56.97, H 5.15, N 3.18, found; C 56.89, H 5.21, N 3.17. ESI-MS: Calculated *m/z*; 881.02 $[M]^+$, experimental *m/z*: CEV 60 V, 880.96 (100%) $[M]^+$, CEV 150 V, 745.98 (22%) $[M\text{-}(EtO)_2P(O)]^+$, 880.97 (100%) $[M]^+$. Distal isomer: $^{31}P\{^1H\}$ NMR δ ppm; 55.12 [$^2J_{(PP)}$ = 36 Hz] and 48.60 [$^2J_{(PP)}$ = 36 Hz], 58.04 [s, P(O)]. ^1H NMR δ ppm; 1.21 [t, 6H, CH_3; J = 8.9 Hz], 2.12 [m 4H, dppe], 2.50 [d, 2H, CH_2; J = 21 Hz], 3.69 [m, 4 H, CH_2-ester], 7.0-7.98 [m, 29 H, Ar-H]. Proximal isomer: $^{31}P\{^1H\}$ NMR δ ppm; 55.46 [$^2J_{(PP)}$ = 35 Hz] and 50.24 [$^2J_{(PP)}$ = 36 Hz], 59.62 [s, P(O)]. ^1H NMR δ ppm; 1.31 [t, 6H, CH_3; J = 7.9 Hz], 2.20 [m, 4H, dppe], 2.59 [d, 2H, CH_2; J = 22 Hz], 3.72 [m, 4 H, CH_2-ester], 7.1-7.8 [m, 29 H, Ar-H]. FTIR (cm^{-1}): 3447(br), 3135(m), 3054(m) 2983(w), 2922(w), 1631(w), 1579(s), 1480(s), 1435(s), 1407(w), 1385(w), 1265(m), 1101(s), 1064(w), 1031(m), 1025(s), 997(m), 875(m), 840(w), 821(s), 742(s), 705(s), 689(s), 612(s), 532(s), 478(m).

[Pd{SC(NC$_6$H$_4$NO$_2$)NHC$_6$H$_4$CH$_2$P(O)(OEt)$_2$}(dppe)]BF$_4$ ***(5i)***

[$PdCl_2$dppe] (58 mg, 0.1 mmol) and $(EtO)_2P(O)CH_2C_6H_4NHC(S)NHC_6H_4NO_2$ (**1j**) (42 mg, 0.1 mmol). Yield 92 mg; 92 %. Elemental analysis %: calculated for $C_{44}H_{44}N_3O_5P_3PdS$; C 57.06, H 4.79, N 4.51, Found; C 57.02, H 4.82, N 4.48 ESI-MS: Calculated *m/z*; 926.12 $[M]^+$, experimental *m/z*: CEV 60 V, 925.95 (100%) $[M]^+$, CEV 150 V, 786.98 (42%) $[M\text{-}(EtO)_2P(O)]^+$, 925.97 (100%) $[M]^+$. Distal isomer: $^{31}P\{^1H\}$ NMR δ ppm; 56.89 [$^2J_{(PP)}$ = 36 Hz] and 49.60 [$^2J_{(PP)}$ = 37 Hz], 59.79 [s, P(O)]. ^1H NMR δ ppm; 1.19 [t, 6H, CH_3; J = 7.6 Hz], 1.98 [m 4H, dppe], 2.46 [d, 2H, CH_2; J = 20 Hz], 3.69 [m, 4 H, CH_2-ester], 7.15-8.10 [m, 23 H, Ar-H]. Proximal isomer: 58.50 [$^2J_{(PP)}$ = 37 Hz] and 50.24 [$^2J_{(PP)}$ = 36 Hz], 60.70[s, P(O)]. ^1H NMR δ ppm; 1.26 [t, 6H, CH_3; J = 8.2 Hz], 2.08 [m 4H, dppe], 2.55 [d, 2H, CH_2;

J = 22 Hz], 3.69 [m, 4 H, CH_2-ester], 7.11-8.22 [m, 24 H, Ar-H]. FTIR (cm^{-1}): 3451(br), 3135(m), 3054(m) 2985(m), 2920(w), 2825(w), 1625(w), 1579(m), 1507(w), 1479(s), 1435(s), 1385(m), 1329(s), 1267(w), 1180(w), 1103(s), 1065(w), 1031(m), 998(s), 842(s) 742(m), 706(s), 690(m), 613(m), 532(s), 479(m).

[Pd{SC(NPh)NHC$_2$H$_5$OH}(dppe)]BF$_4$ ***(5j)***

From [$PdCl_2$(dppe)] (116 mg, 0.2 mmol) and PhNHNC(S)NCH_2CH_2OH (**1j**) (40 mg, 0.2 mmol). Yield: 102 mg; 82 %. Elemental analysis %: calculated for $C_{35}H_{35}BF4\,N_2O_5P_2PdS$; C 53.42, H 4.48, N 3.56, found; C 53.36, H 4.51, N 3.49. ESI-MS: Calculated *m/z*; 699.10 $[M]^+$, experimental *m/z*: CEV 60 V, 699.12 (100%) $[M]^+$, CEV 150 V, 699.13 (100%) $[M]^+$. Distal isomer: $^{31}P\{^1H\}$NMR δ ppm; 55.34 [$^2J_{(PP)}$, = 29 Hz] and 52.30 [$^2J_{(PP)}$ = 30 Hz], ^1H NMR δ ppm; 2.47 [m, 4H, CH_2, dppe; J = 8.9 Hz], 3.14 [t, 2H, CH_2, J = 4.6 Hz], 3.40 [t, 2H, CH_2, J = 6.3 Hz], 3.66 [s, 1H, OH], 6.85-7.60 [m, 26H, Ar-H]. Proximal isomer: $^{31}P\{^1H\}$ NMR δ ppm; 62.60 [$^2J_{(PP)}$ = 27 Hz] and 57.91 [$^2J_{(PP)}$ = 26 Hz], ^1H NMR δ ppm; 2.62 [m, 4H, dppe], 3.30 [t, 2H, CH_2; J = 5.2 Hz], 3.61 [t, 2H, CH_2; J = 6.6 Hz], 3.66 [s, 1H, OH], 6.85-7.60 [m, 25H, Ar-H]. FTIR (cm^{-1}): 3450(br), 2922(w), 2852(w), 1635(br), 1568(m), 1485(m), 1435(s), 1384(w), 1329(w), 1233(w), 1185(w), 1004(m), 1062(w), 998(w), 876(w), 846(w), 748(m), 717(w), 691(s), 618(w), 530(s), 483(s).

[Pd{SC(NPh)N(C$_2$H$_5$OH)$_2$}(dppe)]BF$_4$ ***(5k)***

From [$PdCl_2$(dppe)] (58 mg, 0.1 mmol) and PhNHNC(S)$N(CH_2CH_2OH)_2$ (24 mg, 0.1 mmol) (**1l**). Yield: 63 mg; 86 %. Elemental analysis %: calculated for $C_{37}H_{39}BF4N_2O_5P_2PdS$; C 53.48, H 4.73, N 3.37, found; C 53.48, H 4.78, N 3.37. ESI-MS: Calculated *m/z*; 743.10 $[M]^+$, experimental *m/z*: CEV 60 -150 V, 743.12 (100%) $[M]^+$. $^{31}P\{^1H\}$ NMR δ ppm; 60.90 [$^2J_{(PP)}$ = 33 Hz] and 54.66 [$^2J_{(PP)}$ = 33 Hz]. ^1H NMR; 2.50 [m, 4H, CH_2, dppe], 3.44 [t, 4H, CH_2; J = 8.9 Hz], 3.62 [t, 4H, CH_2; J = 8.5 Hz], 3.7 [s, 2H, OH], 6.51 [m, 2H, Ar-H], 6.80 [t, 3H, Ar-H; J = 6.8 Hz], 7.13 [m, 7H, Ar-H], 7.35-7.40 [m, 6H, Ar-H], 7.54-7.61 [m, 5H, Ar-H], 7.70-7.80 [m, 3H, Ar-H]. FTIR (cm^{-1}): 3448(br), 2924(w), 2852(w), 1636(br), 1537(s), 1485(m), 1436(s), 1383(w), 1310(w), 1218(w), 1186(w), 1105(w), 1084(s), 997(w), 882(w), 749(w), 692(s), 613(w), 534(s), 486(m).

5.4.3 *Single crystal X-ray structure determinations*

Crystal data and refinement details for the investigated complexes are in **Table 5.6.** Intensity measurements were carried out at T = 100 K on a SuperNova Dual AtlasS2 diffractometer fitted with Cu Kα radiation (λ = 1.54184). Data reduction, including absorption correction, was accomplished with CrysAlisPro[33]. The structures were solved by the intrinsic phasing method on ShelxT[34] and refined (with anisotropic displacement parameters and C-bound H atoms in the riding model approximation) on F^2 [35]. In the final cycles of the refinement of each of **1i**, **1j**, **5d**, and **5e**, a number of reflections were omitted owing to the poor agreement. A residual electron density peak in **5e**, evident after the complex molecule was refined, was modelled as a disordered diethyl ether solvent of crystallisation. With the exception of **1i** and **1j**, the structures featured large residual electron density peaks with the maximum of these always located near the Pt atom. The molecular structure diagrams were generated with OLEX2 draw[36], with 50% displacement ellipsoids and the packing diagrams were drawn with Mercury[37].

Table 5.6: Crystallographic and data refinement parameters for thiourea ligands **1i** and **1j**, and platinum complexes **5c, 5d** and **5e**

Code	**1i**	**1j**	**5c**	**5d**	**5e**
Empirical formula	$C_{18}H_{23}N_2O_3PS$	$C_{18}H_{22}N_3O_5PS$	$C_{45}H_{41}BF_4N_2OP_2PtS$	$C_{47}H_{45}BF_4N_2O_2P_2PtS$	$C_{54.5}H_5 4BF_4N_3O_{3.3}P_2PtSSi$
Formula weight (g/mol)	378.43	423.43	1001.75	1045.80	1208.38
Temperature (K)	99.97(10)	100.69(10)	100.01(10)	100.0(5)	99.9(6)
Crystal system	triclinic	triclinic	monoclinic	monoclinic	monoclinic
Space group	P-1	P-1	$P2_1/n$	$P2_1/c$	$P2_1/c$
a(Å)	9.6029(4)	7.8125(4)	16.3227(2)	9.9138(8)	16.9715(4)
b(Å)	9.9633(4)	10.7595(5)	15.3246(10)	26.5791(2)	16.7680(3)
c(Å)	10.6440(4)	12.7527(6)	16.7064(2)	16.3042(19)	18.8709(5)
α(°)	72.776(4)	78.665(4)	90	90	90
β(°)	81.061(3)	84.080(4)	99.9670(10)	93.8970(8)	105.351
γ(°)	75.843(4)	69.437(4)	90	90	90
Volume($Å^3$)	939.38(7)	983.42(8)	4115.85(8)	4286.23(7)	5178.6(2)
Z	2	2	4	4	4
ρcal(g/cm^3)	1.3378	1.4298	1.6165	1.6205	1.5498
(μ)/mm^{-1}	2.500	2.547	8.055	7.780	6.766
F (000)	402.3643	446.6261	1983.6	2079.9	2424.5
Crystal Size	0.1748 x 0.1117 x 0.1011	0.257 x 0.112 x 0.07	0.242 x 0.22 x 0.128	0.18 x 0.16 x 0.12	0.233 x 0.171 x 0.083
Θ(°)	4.3500 - 73.9900	3.5110 - 73.8740	7-148.08	6.66 - 148.02	7.16 - 147.72
R-Factor (%)	3.69	3.76	2.13	2.91	5.2
Reflections used	3329	3245	8272	8557	10125
Total reflections	3753	3899	38770	41137	28634
Completeness to Θ	100.00	99.89	100	100	99
Abs correction type	multi-scan	multi-scan	multi-scan	multi-scan	multi-scan
Goof	1.055	1.051	1.026	1.053	1.033

5.5 References

1. Henderson, W.; Nicholson, B. K.; Rickard, C. E. F. *Inorg. Chim. Acta* **2001**, *320*, 101-109.
2. Struga, M.; Kossakowski, J.; Kedzierska, E.; Fidecka, S.; Stefan, J. *Chem. Pharm. Bull.* **2007**, *55*, 796-799.
3. Kilcigil, G. A.; Altanlar, N. *Turk. J. Chem.* **2006**, *30*, 223-228.
4. Patel, R. B.; Chikhalia, K. H.; Pannecouque, C.; Clercq, E. d. *J. Braz. Chem. Soc.* **2007**, *18*, 312-321.
5. Wang, N.; Budde, W. L. *Anal. Chem.* **2001**, *73*, 997-1006.
6. Arslan, H.; Flörke, U.; Külcü, N.; Kayhan, E. *Turk. J. Chem.* **2006**, *30*, 429-440.
7. Katritzky, A. R.; Gordeev, M. F. *J. Chem. Soc, Perkn. Trans. 1* **1991**, 2199-2203.
8. Abdelhamid, A. A.; Mohamed, S. K.; Akkurt, M.; Singh, K.; Potgieter, H. *Acta Crystallogr., Sect. E: Struct. Rep. Online* **2012**, *68*, 1162-1162.
9. Choi, H.; Shim, Y. S.; Han, B. H.; Kang, S. K.; Sung, C. K. *Acta Crystallogr., Sect. E: Struct. Rep. Online* **2012**, *68*, 530-530.
10. Choi, H.; Shim, Y. S.; Han, B. H.; Kang, S. K.; Sung, C. K. *Acta Crystallogr., Sect. E: Struct. Rep. Online* **2010**, *66*, 2487-2488.
11. Singh, G.; Saroa, A.; Rani, S.; Girdhar, S.; Sahoo, S.; Choquesillo-Lazarte, D. *Polyhedron* **2016**, *112*, 51-60.
12. Singh, G.; Saroa, A.; Rani, S.; Choquesillo-Lazarte, D.; Sahoo, S. *Arabian J. Chem.* **2017**, *10*, 523-531.
13. Voronkov, M. *Pure Appl. Chem.* **1966**, *13*, 35-60.
14. Singh, G.; Arora, A.; Mangat, S. S.; Rani, S.; Kaur, H.; Goyal, K.; Sehgal, R.; Maurya, I. K.; Tewari, R.; Choquesillo-Lazarte, D. *Eur. J. Med. Chem.* **2016**, *108*, 287-300.
15. Singh, G.; Kaur, G.; Singh, J. *Inorg. Chem. Commun.* **2018**, *88*, 11-20.
16. Singh, G.; Saroa, A.; Girdhar, S.; Rani, S.; Choquesillo‐Lazarte, D.; Sahoo, S. C. *Appl. Organomet. Chem.* **2015**, *29*, 549-555.
17. Chuit, C.; Corriu, R. J.; Reye, C.; Young, J. C. *Chem. Rev.* **1993**, *93*, 1371-1448.
18. Singh, G.; Girdhar, S.; Singh, A.; Saroa, A.; Lakhi, J. S.; Khullar, S.; Mandal, S. K. *New J. Chem.* **2018**, *42*, 6315-6321.
19. Singh, G.; Rani, S. *Eur. J. Inorg. Chem.* **2016**, *2016*, 3000-3011.
20. Smirnova, I.; Cuisset, A.; Hindle, F.; Mouret, G.; Bocquet, R.; Pirali, O.; Roy, P. *J. Phys. Chem. B* **2010**, *114*, 16936-16947.
21. Zakaria, S. A.; Muharam, S. H.; Yusof, M. S. M.; Khairul, W. M.; Kadir, M. A.; Yamin, B. M. *M. J. of Anal. Scien.* **2011**, *15*, 37-45.

22. Custelcean, R. *Chem. Commun.* **2008**, 295-307.

23. Chaudret, R.; De Courcy, B.; Contreras-Garcia, J.; Gloaguen, E.; Zehnacker-Rentien, A.; Mons, M.; Piquemal, J.-P. *Phys. Chem. Chem. Phys.* **2014**, *16*, 9876-9891.

24. Asegbeloyin, J. N.; Oyeka, E. E.; Okpareke, O. C.; Ibezim, A. A. *J. Mol. Struct.* **2018**, *1153*, 69-77

25. Asegbeloyin, J. N.; Izuogu, D. C.; Oyeka, E. E.; Okpareke, O. C.; Ibezim, A. *J. Mol. Struct.* **2019**, *1175*, 219-229.

26. Henderson, W.; Kemmitt, R. D. W.; Mason, S.; Moore, M. R.; Fawcett, J.; Russell, D. R. *J. Chem. Soc., Dalton Trans.* **1992**, 59-66.

27. Henderson, W.; Nicholson, B. K. *Polyhedron* **1996**, *15*, 4015-4024.

28. Kennedy, B. P.; Lever, A. B. P. *Can. J. Chem.* **1972**, *50*, 3488-3507.

29. Appleton, T. C.; Clark, H. C.; Manzer, L. C. *Coord. Chem. Rev.* **1973**, *10*, 335-422.

30. Manojlovic-Muir, L.; Muir, K.-W. *Inorg. Chim. Acta* **1974**, *10*, 47-49.

31. Pidcock, A.; Richards, R.; Venanzi, L. *J. Chem. Soc. A: Inorg., Phys., Theo.* **1966**, 1707-1710.

32. Cazacu, M.; Shova, S.; Turta, C.; Simionescu, B. C. *Polyhedron* **2012**, *33*, 119-1.

33. Rigaku Oxford Diffraction CrysAlisPro Software System, version 1.171. 38.41 l, Rigaku Coorporation. Oxford, UK, (2015).

34. Sheldrick, G. M. *Acta Crystallogr., Sect. A: Found. Adv* **2015**, *71*, 3-8.

35. Sheldrick, G. M. *Acta Crystallogr., Sect. C: Struct. Chem.* **2015**, *71*, 3-8.

36. Dolomanov, O. V.; Bourhis, L. J.; Gildea, R. J.; Howard, J. A. K.; Puschmann, H. *J. Appl. Crystallogr.* **2009**, *42*, 339-341.

37. Macrae, C. F.; Bruno, I. J.; Chisholm, J. A.; Edgington, P. R.; McCabe, P.; Pidcock, E.; Rodriguez-Monge, L.; Taylor, R.; Streek, J. V.; Wood, P. A. *J. Appl. Crystallogr.* **2008**, *41*, 466-470.

Chapter 6

Platinum, palladium and nickel complexes of bisthiourea ligands

6.1 Introduction

The coordination chemistry of thiourea ligands has been established[1-7]. In previous research[8], the stereochemistry and coordination geometries of nickel(II) complexes of bisthiourea ligands of the form $PhNHCSNH(CH_2)_nNHC(S)NHPh$ (where n = 2-10) were investigated. The complexes were synthesised by reacting a range of nickel halide salts (NiX_2, X= Cl, Br and I) and thiourea ligands in ethanol or butanol solvent under reflux to give monomeric or polymeric products. The results from the electronic spectra and magnetic susceptibility measurements were used to predict the stereochemistry and coordination geometry of the complexes. The authors predicted that the complexes formed mostly tetrahedral paramagnetic and square planar diamagnetic complexes depending on the length of the methylene spacer between the two thiourea groups. The authors also presumed that the ligands coordinated through the sulfur of the thiourea ligands resulting in tetrahedral (NiS_2X_2), tetragonal (NiS_4X_2) and square planar (NiS_2X_2) complexes. The bisthiourea ligands formed the most stable complexes when n = 1 and 2 because the sulfur atoms were closer together and could coordinate to the same Ni atom. Due to poor solubility, crystal structures of these compounds could not be obtained.

More recently, platinum group metal complexes of several bifunctional thiourea derivatives including $PhNHC(S)NHCH_2CH_2PPh_2$ has been reported in the literature[9]. The ligand coordinated to palladium through the phosphorus and thiourea functions to form a seven-membered ring in a boat like conformation. The chloride counter ion in this complex forms a hydrogen bond with the thiourea functional group. Further, two bifunctional thiourea derivatives $C_6H_{12}(NMeCSNMe_2)_2$ and $C_2H_4(NMeCSNMe_2)_2$ were reported as part of a project on the modification of platinum antitumor complexes with sulfur ligands[10]. ^{195}Pt NMR spectroscopy of the dinuclear complexes $[\{Pt(en)_2\text{-}\mu\text{-}3\text{-}S,S)](NO_3)_2$ and $[\{Pt(en)Cl\}_2\text{-}\mu\text{-}4\text{-}S,S)](NO_3)_2.0.5EtOH$ showed the presence of a mixed donor $[PtN_2ClS]$ coordination geometry for the complexes.

In this chapter, the synthesis and structure of several related alkyl-bridged bisthiourea ligands and their platinum, palladium and nickel complexes using the organo-phosphorus *cis*-[$PtCl_2(PPh_3)_2$] and [MCl_2(dppe)] starting precursors (where M = Pd, Ni) was explored. This Chapter aims to investigate the coordination properties of these complexes and the effect of the length of the bridging alkyl carbon chain on the coordination geometry of the resulting complexes using X-ray crystallographic techniques.

6.2 Results and discussion

6.2.1 *Synthesis of bisthiourea ligands*

The bisthiourea ligands used in this chapter were synthesised using a modified literature procedure[11]. The reaction of corresponding α, β diaminoalkanes $H_2NC_6H_4$-CH_2-$C_6H_4NH_2$ (**1p**), $H_2N(CH_2)_nNH_2$; n = 4, 6, 8, 12 and two equivalents of phenyl isothiocyanate in DMF solution, under reflux gave the mostly white products. Bisthiourea ligands (**1q**-**1s**) **Scheme 6.1** have been synthesised previously but have not been fully characterised[12, 13].

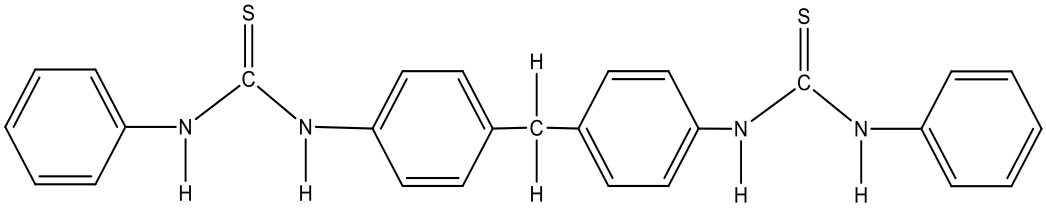

(**1p**)

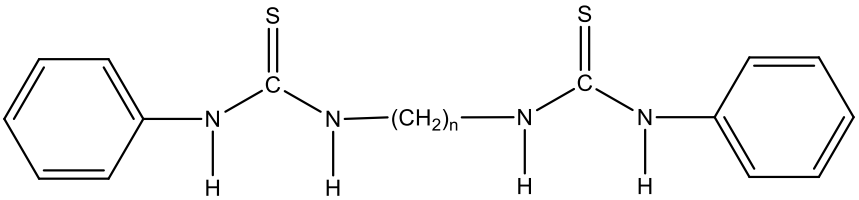

n = 2; (**1q**), n = 4; (**1r**), n = 6; (**1s**), n = 8; (**1t**), n = 12; (**1u**)

Scheme 6.1: Reaction scheme for the synthesis of bis(thiourea) ligands

ESI-mass spectrometry, NMR and FTIR spectroscopies were used to characterise the bifunctional thiourea ligands. The ESI-mass spectra of the ligands showed that the compounds ionised by loss of one NH proton to give $[M-H]^+$ ions. The proton NMR spectra of the ligands in DMSO-d_6 showed peaks above 8.0 ppm, resulting from NH protons of the thiourea secondary amides. These assignments were confirmed by the addition of D_2O solvent to the NMR solution, followed by vigorous shaking. The NMR spectra of the resulting NMR solution showed that the peaks for the secondary amine protons had disappeared. Other peaks below 4.0 ppm can be assigned to CH_2 protons of the bridging alkyl carbon chain. The associated integration values on the spectrum correspond to the expected figures. The FTIR spectra of the ligands showed absorption bands around 3300 and 1600 cm^{-1} corresponding to stretching and bending vibrations of the N-H functional group, respectively. Absorption bands around 1450 and 750 cm^{-1} are due to C=S stretching and rocking vibrations, while the bands around 1490-1500 cm^{-1} are a result of the stretching vibrations of the N-C-N group[,13].

6.2.2 Bisthiourea complexes

Platinum, palladium and nickel complexes of bisthiourea ligand **1p** were synthesised by refluxing 1 mol equivalent of the ligand with 2 mol equivalents of the metal complex *cis*-$[PtCl_2(PPh_3)_2]$ and $[MCl_2(dppe)]$, (where M = Pd or Ni) in methanol for 2 h. The dicationic complex formed was isolated by addition of $NaBPh_4$ to the hot solution. The mass spectrum of the isolated platinum complex (**6a**) showed *pseudo* molecular ion peaks at *m/z* 953 for a dication $[M]^{2+}$ of the dichelated complex. The dichelated complex is formed when the two ends of the bifunctional thiourea ligand are bound to the platinum metal, **Figure 6.1**(**a**). The spectrum also showed another peak at *m/z* 1187.34 for the monochelated complex as a monocation. The monochelated complex is formed when only one end of the bifunctional thiourea is coordinated to the platinum metal, **Figure 6.1(b**). **Figure 6.2**(**a**) shows the ESI-mass spectrum of the complex **6a** after 2h of reflux in methanol solution. The spectrum clearly shows that the complex formed after two hours has a mixture of both the monochelated and dichelated complexes.

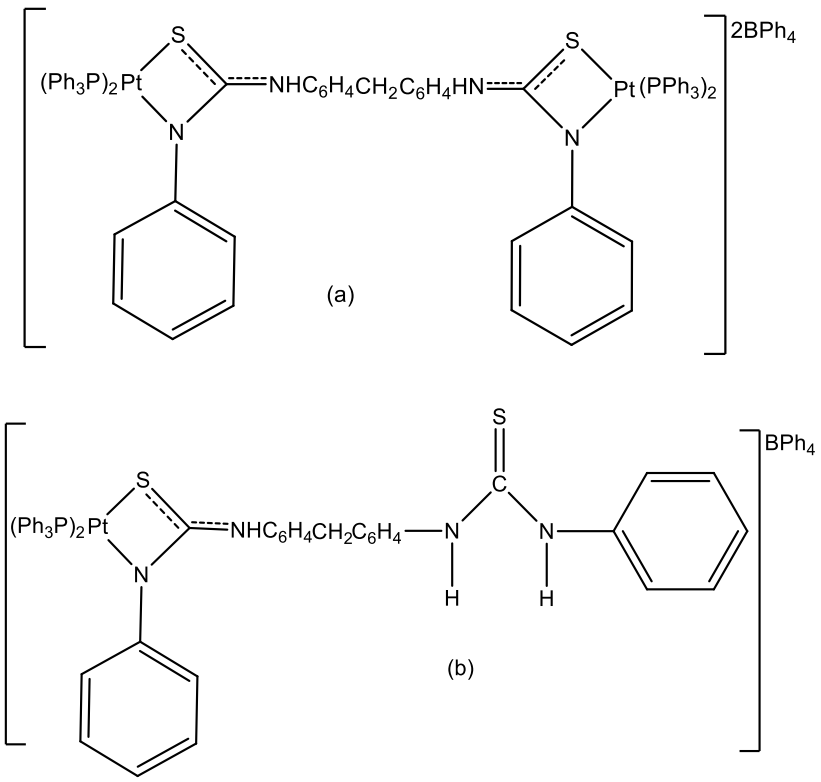

Figure 6.1: (a) Dichelated and (b) Monochelated platinum complexes of the bisthiourea ligand (**1p**).

The presence of peaks for the dichelated and monochelated complexes in the spectrum in **Figure 6.2a** was suspected to be a result of the incomplete chelation of the two ends of the bisthiourea ligand due to short reaction time or insufficient amount of the *cis*-$[PtCl_2(PPh_3)_2]$ starting complex. In other to investigate this, another reaction was set up with a slight excess of the *cis*-$[PtCl_2(PPh_3)_2]$ starting complex and the reflux time was increased from 2 h to 8 h. The reaction progress was monitored using ESI-mass spectrometry. Aliquots of the reaction solution was removed every 2 h after the first 3 h to monitor the disappearance of the peak for the monochelated complex from the spectra. A sample taken after about 7 h showed only the peak for the dichelated complex (**Figure 6.2b**), indicating that the reaction had reached completion. The reaction was refluxed for another hour and the product isolated by addition of $NaBPh_4$. The mass spectrum of the isolated sample measured at a capillary exit voltage of 60 V showed the peak for the dichelated complex.

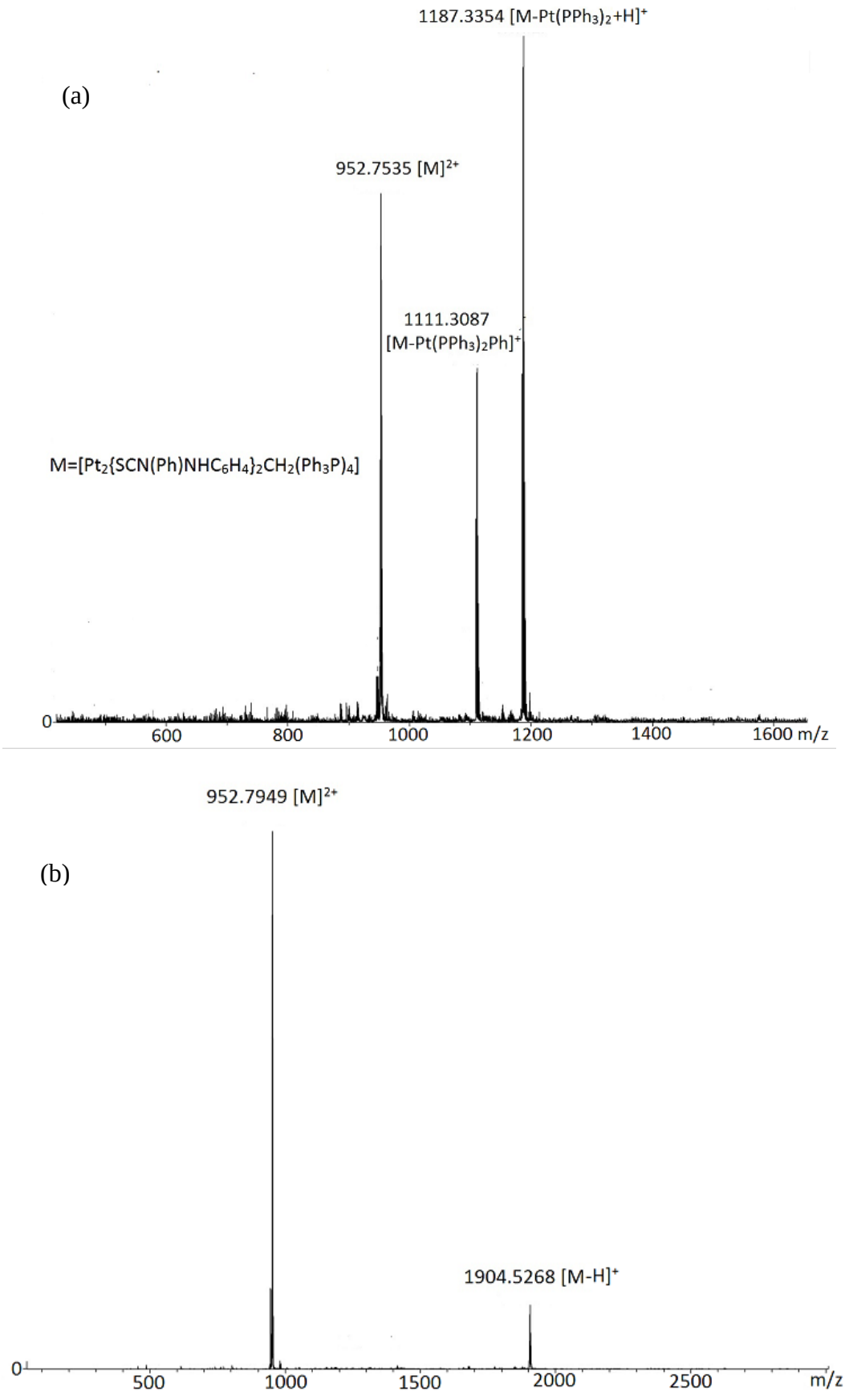

Figure 6.2: (a) ESI-mass spectrum of the complex $[\{(PtSC(NPh)NHC_6H_5)_2CH_2\}(PPh_3)_4]\cdot 2BPh_4$ **6a** refluxed for 2 hours with 1:2 ligand to metal mole ratio. (b) ESI-mass spectrum of the complex

$[\{(PtSC(NPh)NHC_6H_5)_2CH_2\}(PPh_3)_4]\cdot 2BPh_4$ **6a**, refluxed for 8 hours with an excess of the *cis*-$[PtCl_2(PPh_3)_2]$ starting complex. Both spectra were recorded at a capillary exit voltage of 60 V, (M = dichelated complex).

When the capillary exit voltage was increased to 120 V, the spectrum showed the presence of both the dichelated and monochelated complexes at different intensities. The percentage intensities of the molecular ion peaks recorded for this complex at different exit voltages are presented in **Table 6.1**.

Table 6.1: ESI-MS data of platinum, palladium and nickel bisthiourea complexes

Complexes	**Capillary exit voltage (V)**	***m/z*(%) ions**
$[Pt_2\{(SC(NPh)NHC_6H_4)_2CH_2\}(PPh_3)_4]\cdot 2BPh_4$ (**6a**)	60	953 (100) $[M]^{2+}$, 1905 (8) $[M-H]^+$
	120 - 180	719 (49) $[Pt(PPh_2C_6H_4)(PPh_3)]^+$, 1187 (7) $[M-(PPh_3)_2Pt]^+$, 1905 (3) $[M-H]^+$
$[Pd_2\{(SC(NPh)NHC_6H_4)_2CH_2\}(dppe)_2]\cdot 2BPh_4$ (**6b**)	60	738 (100) $[M]^{2+}$, 971 (42) $[M-(dppeNi)]^+$
	120 - 180	738 (100) $[M]^{2+}$, 971(47) $[M-(dppeNi)]^+$, 1795 (6) $[M]^+BPh_4^-$
$[Ni_2\{(SC(NPh)NHC_6H_4)_2CH_2(dppe)_2]\cdot 2BPh_4$ (**6c**)	60	690 (100) $[M]^{2+}$, 923 (12) $[M-(dppeNi)]^+$
	120 - 180	690 (100) $[M]^{2+}$, 923(22) $[M-(dppeNi)]^+$, 1699 (13) $[M]^+BPh_4^-$.
$[Pt_2\{SC(NPh)NH\}_2(CH_2)_4(PPh_3)_4]\cdot 2BPh_4$ (**6d**)	60	898 (100) $[M]^{2+}$, 1042 (42) $[M-Pt(PPh_3)_2S]^+$, 1076 (15) $[M-Pt(PPh_3)_2+H]^+$, 2113 (5) $[M]^+BPh_4^-$,
	120 - 150	719 (52) $[Pt(PPh_2C_6H_4)(PPh_3)]^+$, 898 (100) $[M]^{2+}$, 1042 (47) $[M-Pt(PPh_3)_2S]^+$, 1076 (19) $[M-Pt(PPh_3)_2S]^+$, 1530 (7) $[M-PPh_3]^+$, 2113(5) $[M]^+BPh_4^-$,
	180	718 (18) $[Pt(PPh_2C_6H_4)(PPh_3)]^+$, 898 (100) $[M]^{2+}$, 1042 (32) $[M-Pt(PPh_3)_2S]^+$, 1076 (12%) $[M-Pt(PPh_3)_2S]^+$, 2113 (5) $[M]^+BPh_4^-$
$[Pt_2\{SC(NPh)NH\}_2(CH_2)_6(PPh_3)_4]\cdot 2BPh_4$ (**6e**)	60	912 (96) $[M]^{2+}$, 2142 (7) $[M]^+BPh_4^-$
	120 - 180	719 (68) $[Pt(PPh_2C_6H_4)(PPh_3)]^+$, 912 (96) $[M]^+$), 2142 (12) $[M]^+BPh_4^-$
$[Pt_2\{SC(NPh)NH\}_2(CH_2)_8(PPh_3)_4]\cdot 2BPh_4$ (**6f**)	60	926 (100) $[M]^{2+}$, 2170(8) $[M]^+BPH_4^-$
	120 - 180	719 (42) $[Pt(PPh_2C_6H_4)(PPh_3)]^+$, 925 (96) $[M]^{2+}$, 2170(8) $[M]^+BPh_4^-$
$[Pt_2\{SC(NPh)NH\}_2(CH_2)_{12}(PPh_3)_4]\cdot 2BPh_4$ (**6g**)	60	955(100) $[M]^{2+}$, 2226 (3) $[M]^+BPh_4^-$
	120 - 180	719 (68) $[Pt(PPh_2C_6H_4)(PPh_3)]^+$, 954 (100) $[M]^{2+}$, 1188 (3) $[M-Pt(PPh_3)_2+H]^+$ 2226 (3) $[M]^+BPh_4^-$
$[Pd_2\{SC(NPh)NH\}_2(CH_2)_4(dppe)_2]\cdot 2BPh_4$ (**6h**)	60	683 (100) $[M]^{2+}$
	120 - 180	683 (100) $[M]^{2+}$, 1685 (28) $[M]^+BPh_4^-$
$[Pd_2\{SC(NPh)NH\}_2(CH_2)_6(dppe)_2]\cdot 2BPh_4$ (**6i**)	60	697 (100) $[M]^{2+}$
	120 - 180	697 (100) $[M]^{2+}$, 1713 (32) $[M]^+BPh_4^-$

$[Pd_2\{SC(NPh)NH\}_2(CH_2)_8(dppe)_2]\cdot 2BPh_4$ (**6j**)	60	711 (100) $[M]^{2+}$
	120 - 180	711 (100) $[M]^{2+}$, 1221 (7.2) $[M\text{-}(Pd(dppe)S)]^{+}$, 1742 (5) $[M]^{+}BPh_4^{-}$
$[Pd_2\{SC(NPh)NH\}_2(CH_2)_{12}](dppe)_2\cdot 2BPh_4$ (**6k**)	60	739 (100) $[M]^{2+}$, 973 (12) $[M\text{-}Pd(dppe)]^{+}$, 1796 (5) $[M]^{+}BPh_4^{-}$
	120 - 180	739 (100) $[M]^{2+}$, 973 (12) $[M\text{-}Pd(dppe)]^{+}$, 1796 (22) $[M]^{+}BPh_4^{-}$
$[Ni_2\{SC(NPh)NH\}_2(CH_2)_4(dppe)_2]\cdot 2BPh_4$ (**6l**)	60	650 (100) $[M]^{2+}$, 812 (52) $[M\text{-}Ni(dppe)]^{+}$
	120 - 180	650 (100) $[M]^{2+}$, 813 (52) $[M\text{-}Ni(dppe)]^{+}$, 1589 (26) $[M]^{+}BPh_4^{-}$,
	240	813 (100) $[M\text{-}Ni(dppe)]^{+}$, 1589 (56) $[M]^{+}BPh_4^{-}$
$[Ni_2\{SC(NPh)NH\}_2(CH_2)_6(dppe)_2]\cdot 2BPh_4$ (**6m**)	60	649 (100) $[M]^{2+}$, 841 (46) $[M\text{-}Ni(dppe)]^{+}$
	120 - 180	649 (100) $[M]^{2+}$, 841 (46) $[M\text{-}Ni(dppe)]^{+}$, 1617 (23) $[M]^{+}BPh_4^{-}$
	240	649 (35) $[M]^{2+}$, 841 (100) $[M\text{-}Ni(dppe)]^{+}$, 1617 (25) $[M]^{+}BPh_4^{-}$
$[Ni_2\{SC(NPh)NH\}_2(CH_2)_8(dppe)_2]\cdot 2BPh_4$ (**6n**)	60	663 (100) $[M]^{2+}$, 869 (14) $[M\text{-}Ni(dppe)]^{+}$
	120 - 180	663 (70) $[M]^{2+}$, 869 (100) $[M\text{-}Ni(dppe)]^{+}$, 1645 (3) $[M]^{+}BPh_4$,
	240	663 (68) $[M]^{2+}$, 869 (100) $[M\text{-}(dppeNi)]^{+}$, 1645 (8) $[M]^{+}BPh_4$.
$[Ni_2\{SC(NPh)NH\}_2(CH_2)_{12}(dppe)_2]\cdot 2BPh_4$ (**6o**)	60	691 (100) $[M]^{2+}$, 925 (20) $[M\text{-}Ni(dppe)]^{+}$, 1701 (3) $[M]^{+}BPh_4$
	120 - 240	691 (100) $[M]^{2+}$, 925 (12) $[M\text{-}Ni(dppe)]^{+}$, 1701 (63) $[M]^{+}BPh_4$.

The proton NMR spectrum of the complex **6a** was very complex and could not be easily interpreted. The $^{31}P\{^{1}H\}$ NMR spectrum of the complex in $CDCl_3$, on the other hand, showed the presence of multiplets around 13 ppm, and 9 ppm with coupling constants of 3207 Hz and 3480 Hz respectively (**Figure 6.3a**). The inserts are expanded multiplets. The multiplets were suspected to be probably due to isomerism in the complex on dissolution in $CDCl_3$ solution. Due to the long spacer between the two platinum centres, the possibility of coupling between the P atoms located on the different platinum atoms was ruled out.

The palladium **6b** and nickel **6c**, dppe complexes of the bisthiourea ligand, **1p** were also synthesised using a similar method to **6a**. The ESI-mass spectra of the palladium and nickel complexes showed molecular ion peaks as those for the dichelated and monochelated complexes even after refluxing for up to 8 h. The molecular ion peaks for the complexes at different capillary exit voltages are presented in **Table 6.1**. The $^{31}P\{^{1}H\}$ NMR spectra of the Pd and Ni complexes also showed multiplets like those observed in the platinum complexes. The multiplets for the isomers in the Pd and Ni complexes were much more defined than those in the platinum complex, **Figure 6.3**. This is probably due to the absence of metal-phosphorus coupling in the palladium and nickel complexes. The infrared spectra data for the complexes showed that the bands around 3300 cm^{-1} in the ligands, ascribed to NH stretching frequencies had disappeared or moved to lower frequencies in the spectra of the complex, indicating an involvement of the NH group in coordination. The bands around 1590 cm^{-1} ascribed to NH bending vibrations, however, remained intact in the spectra of the complexes. This is probably due to the remaining thiourea NH that was not involved in coordination with the metal. Other bands around 1490 cm^{-1} ascribed to stretching vibrations of the N-C-N functional group were also observed in the spectra of the complexes. The disappearance or lowering of bands observed around 1450 and 750 cm^{-1} is a strong indication that the C=S group was involved in coordination with the metal. In other ascertain the coordination geometry of these complexes, several attempts were made to grow crystals of these complexes without any success.

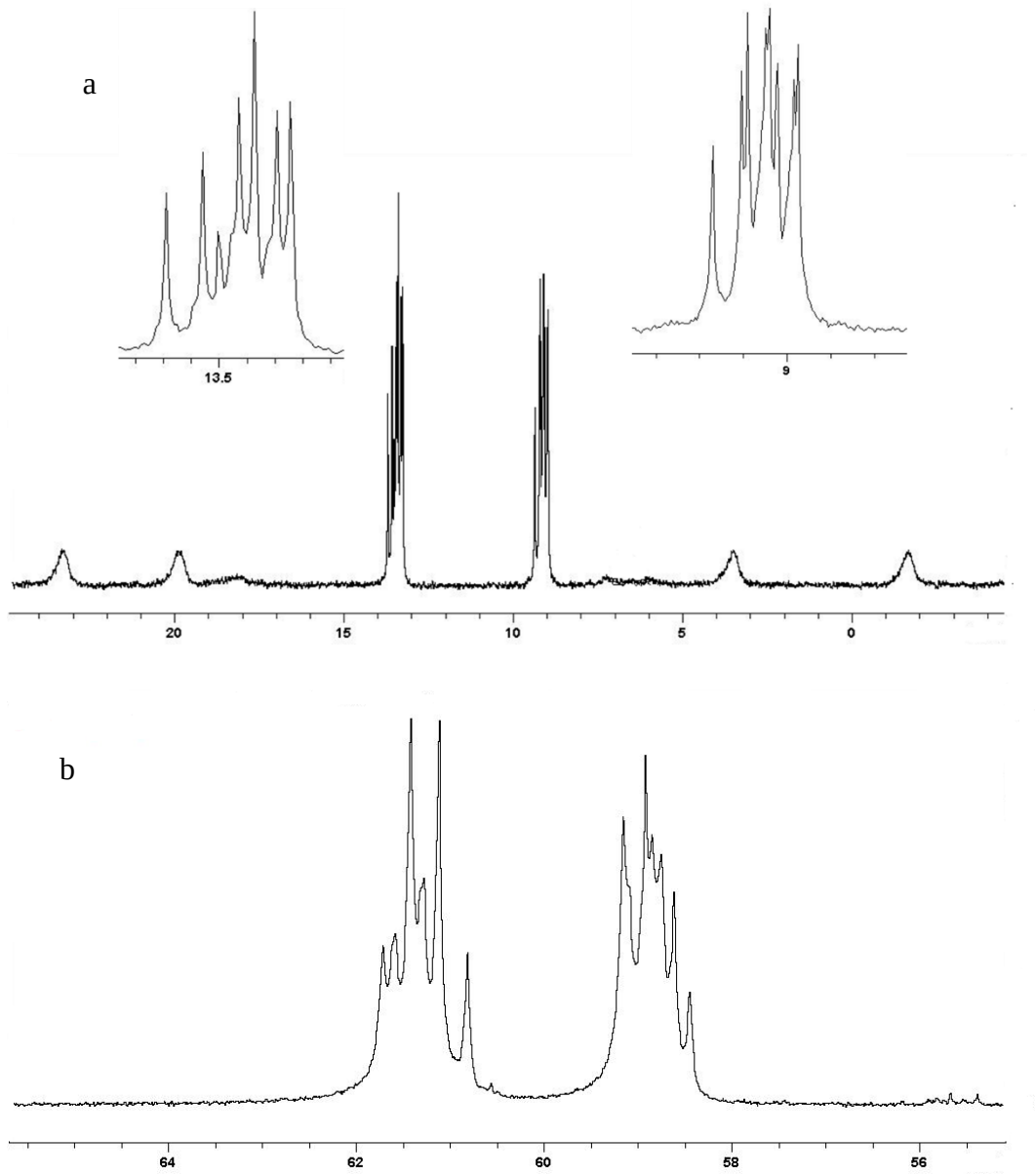

Figure 6.3: $^{31}P\{^{1}H\}$ NMR spectra of (a) platinum bisthiourea complex **6a** (b) nickel bisthiourea complex **6c** in $CDCl_3$ showing the multiplets resulting from the isomerisation

6.2.3 *Complexes of alkyl bridged bisthiourea ligands*

Platinum complexes of the alkyl-bridged bisthioureas ligands **1q-1u** were synthesised by reacting the *cis*-$[PtCl_2(PPh_3)_2]$ with the corresponding ligands in refluxing methanol solution for 8 h to give complexes **6d-6h**, **Scheme 6.2.**

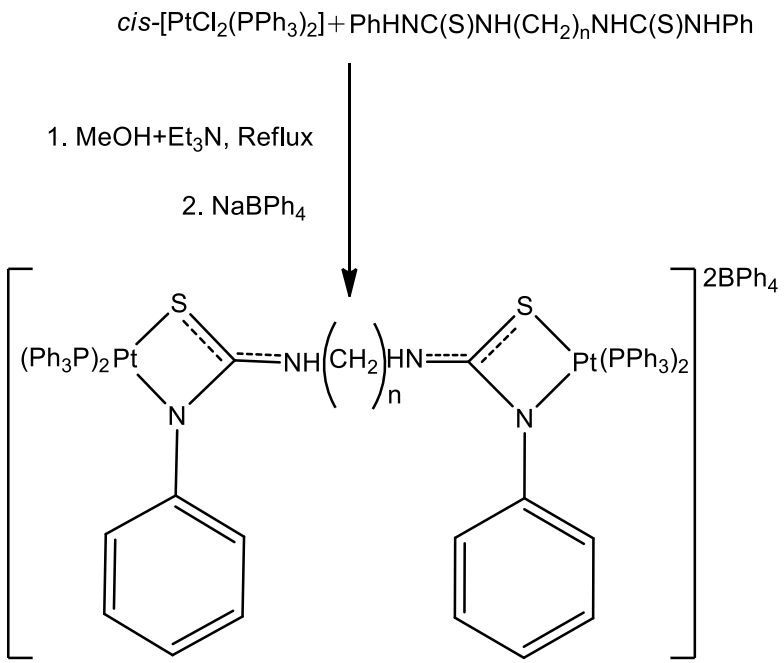

n = 4; **6d**, n = 6; **6e**, n = 8; **6f**, n =12; **6h**

Scheme 6.2: Synthesis of platinum bisthiourea complexes **6d-6h**

The ESI-mass spectra of the butylene bridged bisthiourea complex **6d** at a low capillary exit voltage of 60 V showed the molecular ion peaks for the dichelated complex as a dication at *m/z* 897.47 $[M]^{2+}$. Also appearing in the spectrum as a minor peak with the intensity of about 15% of the major is the peak for the monochelated complex as a monocation with *m/z* 1076 $[M\text{-}Pt(PPh_3)_2+H]^+$. This is a clear indication that the small amount of the monochelated complex was as a result of incomplete complexation of the bisthiourea ligand. Another spectrum collected at higher capillary exit voltage 150 V, with peaks at *m/z* 1042 for $[M\text{-}Pt(PPh_3)_2S]^+$ tends to suggest the possibility of fragmentation of the complex on increasing the capillary exit voltage on the mass spectrometer. Further increase of the capillary exit voltage voltage to 180 V resulted in more fragmentation of the complex to give additional peaks at 718.89 for the cyclometallated platinum species $[Pt(PPh_2C_6H_4)(PPh_3)]^+$, other peaks at *m/z* 1530 for loss of PPh_3 ligand, $[M\text{-}PPh_3]^+$ and *m/z* 2113 for $[MBPh_4]^+$ were also identified in the spectrum at 180 V.

The ESI-mass spectra of the hexylene **6e**, octylene **6f** and dodecylene bridged (**6h**) platinum complexes showed similar peaks to the ones in the complex **6d**. The *m/z* values for the different complexes at varying capillary exit voltages are also presented in **Table 6.1**. The only notable difference in the spectra of the

complexes is that complexes **6e** and **6f** did not show any peaks for the monochelated species while the compound **6g** showed the molecular ion peak for the monochelated complex at *m/z* 1188. Because the synthesis was carried out with the equivalent amount of reactants at the same reaction time of 8 h. It is fair to assume that several factors may be responsible for the presence of either the dichelated and monochelated species in the mass spectra of the complexes. These factors may include the following; ligand to metal mole ratio, the reaction time and temperature, and fragmentation of the complexes in the spectrometer at high capillary exit voltage.

The $^{31}P\{^{1}H\}$ NMR analysis of the platinum bisthiourea complexes **6d-6g** was carried out in $CDCl_3$ solution. The NMR of the butylene bridged complex **6d** showed the presence of doublets at 13.58 and 9.22 ppm with two platinum coupling satellite peaks on each side of the parent peaks. The $^{1}J_{(PtP)}$ coupling constants for those peaks were recorded as 3234 and 3462 Hz respectively. The NMR solution was left several days, and another NMR spectrum was collected. The spectrum did not show any sign of isomerism in the complex. The $^{31}P\{^{1}H\}$ NMR spectra of the other alkyl bridged complexes **6e-6g** showed similar chemical shifts and coupling constants as **6d**. The chemical shifts and their corresponding $^{1}J_{(PtP)}$ coupling constants are presented in Table 6.2. The table shows slight changes in the chemical shifts for the complexes as the length of the bridging carbon chain increases from n = 4; **6d** to n = 12; **6g**, in no particular order.

Table 6.2: $^{31}P\{^{1}H\}$ NMR chemical shifts for alkyl bridged platinum bisthiourea complexes and their corresponding $^{1}J_{Pt\text{-}P}$ coupling constants.

Complexes	**Chemical shifts ppm ($^{1}J_{(PtP)}$ coupling constants Hz)**
$[Pt_2\{SC(NPh)NH\}_2(CH_2)_4(PPh_3)_2]\cdot 2BPh_4$ (**6d**)	13.54(3234), 9.22(3462)
$[Pt_2\{SC(NPh)NH\}_2(CH_2)_6(PPh_3)_4]\cdot 2BPh_4$ (**6e**)	13.46(3241), 9.23(3461)
$[Pt_2\{SC(NPh)NH\}_2(CH_2)_8(PPh_3)_4]\cdot 2BPh_4$ (**6f**)	13.42(3232), 9.23(3470)
$[Pt_2\{SC(NPh)NH\}_2(CH_2)_{12}(PPh_3)_4]\cdot 2BPh_4$ (**6g**)	13.40(3241), 9.21(3461)

6.2.4 *Crystal structure determinations*

Crystals suitable for X-ray crystallography were isolated by vapour diffusion of diethyl ether into a saturated dichloromethane solution of the hexylene bridged platinum bisthiourea complex **6e**. The compound crystallised from the *P2₁/c* space group with a half-molecule of the cationic complex in the asymmetric unit. The asymmetric unit also contains one molecule each of BPh_4 anion, H_2O and CH_2Cl_2 of crystallisation. The symmetry elements showed that the bisthiourea complex is sitting on a centre of inversion, with one half of the molecule equivalent to the other half and generated by symmetry.

The molecular structure of one half of the compound formulated as $[Pt\{SC=(NPh)N(CH_2)_3\}(Ph_3P)_2]$ **Figure 6.4**, has the platinum(II) atom S-N chelated by a phenyl-N´-propylenecarbamimidothioato anion, with the remaining positions in the almost square planar geometry, occupied by two phosphorus atoms of the triphenylphosphine ligands. The root mean square (r.m.s.) deviation of the resulting NP_2S square plane is 0.05 Å, and the platinum atom lies 0.068 Å out of that plane. The *cis*-angles around the square plane has values of 69.40(11)^o and 98.82(4)^o for the angles subtended by the S-N and phosphorus donor atoms respectively. These values are closer to the values reported for an N, S-chelated platinum thiourea monoanion complex[1] with 68.68(7), and 97.42(3)^o respectively. The *trans*-angles, i.e. S(1)-Pt(1)-P(1) and P(2)-Pt(1)-N(1) deviate from the ideal 180^o by approximately 14 and 17^o respectively. The Pt(1)-P(1) bond *trans* to the thiolate S(1) atom; 2.295(11) Å is longer than the Pt(1)-P(2) bond *trans* to the N(1) atom; 2.259(11) Å. This is an obvious indication of a greater *trans*-influence of the thiolate S(1) compared to the N-donor atom. This is a common feature of N-S chelated platinum thiourea complexes with phosphorus donor ligands[14-16].

The four-membered metallacyclic ring in the complex is planar with an r.m.s. deviation of 0.031 Å. The angles subtended at the less sterically encumbered thiolate S(1) donor group are wider than the ones subtended at the metalacyclic N atom. The Pt(1)-S(1)-Cl acute angle of 80.14(17)^o is therefore expectedly smaller than the Pt(1)-N(1)-C(1) angle of 100.2(3)^o, while the angle involving the N-bound phenyl substituent is almost 40^o wider. The thiolate C(1)-S(1) bond length of 1.762(5) Å is longer than the average C-S bond in alkyl-substituted bisthiourea ligands 1.690 Å[12,13,17], while the C(1)-N(2) exocyclic bond is shortened to 1.318(7)

Å when compared to the average C(1)-N(2); 1.3363 Å in the free ligand[12,17]. The angles around the C(1) carbon reflect the redistribution of electron density on the coordination of the bisthiourea ligands. The angles involving the exocyclic N(2) atom; S(1)-C(1)-N(2), 122.88(17)^{o} and N(1)-C(1)-N(2), 127.21(12)^{o} are wider than the equivalent angles in the free bisthiourea ligand, that is 122.29^{o} and 117.79^{o}[12]. The dihedral angle between the metalacyclic r.m.s. plane and the N(1)-bound phenyl ring is 69.28(11)^{o}. This is far smaller than the angle reported for [Pt{SC(=NPh)NPh}(PPh_3)$_2$] (87.93°)[18]. The N(2)-bound alkyl group has a wider dihedral angle 81.52(7)^{o}.

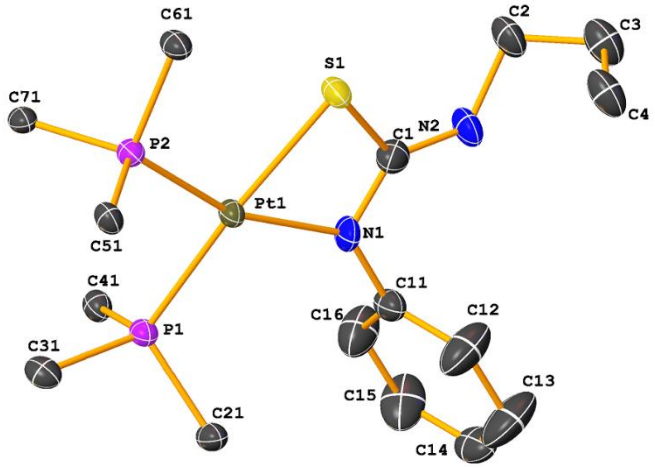

Figure 6.4: Molecular structure of platinum bisthiourea complex [Pt_2{SC=(NPh)NH}$_2$(CH_2)$_6$(PPh_3)$_4$]·2BPh_4 **6e** showing one half of the molecule in the asymmetric unit. Only one-half of the structure and ipso carbons of PPh_3 ligand are shown for clarity. BPh_4 anion also omitted for clarity. Ellipsoids are drawn at 50% probability

Table 6.3: Table of geometric parameters for platinum bisthiourea complex **6e**.

Parameters	**Bond lengths Å**	**Parameters**	**Bond angles ^{o}**
Pt(1) – S(1)	2.3454(11)	P(1) – Pt(1) – S(1)	165.76(4)
Pt(1) – P(1)	2.2948(11)	P(2) – Pt(1) – S(1)	93.40(4)
Pt(1) – P(2)	2.2595(11)	P(1) – Pt(1) – P(2)	98.82(4)
Pt(1) – N(1)	2.106(4)	N(1) – Pt(1) – S(1)	69.40(11)
S(1) – C(1)	1.762(5)	N(1) – Pt(1) – P(2)	162.80(11)
N(2) – C(1)	1.318(7)	N(1) – Pt(1) – P(1)	98.21(11)
N(2) – C(2)	1.466(2)	C(1) – S(1) – Pt(1)	80.14(17)
N(1) – C(11)	1.425(6)	C(1) – N(1) – Pt(1)	100.2(3)
N(1) – C(1)	1.327(6)	C(1) – N(1) – C(11)	119.7(4)

6.2.5 *Palladium and nickel complexes of alkyl bridged bisthiourea ligands (1q-1u)*

The palladium and nickel complexes of the bisthiourea ligands **1q-1u** were also synthesised using similar methods as the platinum complexes. The metal precursors, $[MCl_2(dppe)]$ (where M=Pd or Ni) was refluxed with the corresponding bisthiourea ligand to give bisthiourea complexes **6h-6o** (**Scheme 6.3**).

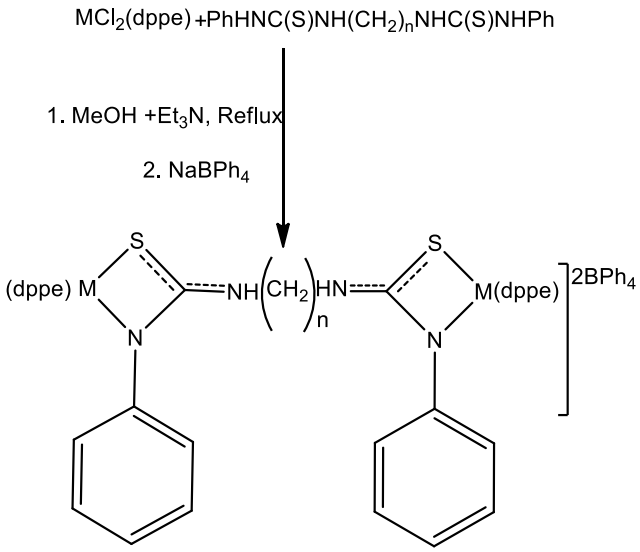

M = Pd; n = 4, **6h**; n = 6, **6i**; n = 8, **6j**; n = 12, **6k**; M = Ni; n = 4, **6l**; n = 6, **6m**; n = 8, **6n**; n = 12, **6o**

Scheme 6.3: Reaction scheme for the synthesis of palladium and nickel bisthiourea complexes **6h-o**

The ESI-mass spectra of the palladium complexes **6h** and **6i** showed molecular ion peaks for the dichelated complexes as a dication at low capillary exit voltage of 60 V. Increase in the capillary exit voltage up to 180 V showed peaks for the monocation with one BPh_4^- anion. No peaks were observed from the monochelated derivative of these two complexes. The ESI-mass spectra of the other palladium complexes **6j-k** and nickel complexes **6l-o** showed peaks for the dichelated and monochelated derivatives at both low and high capillary exit voltages up to 250 V (**Table 6.1**). These results corroborate an assertion earlier in section **6.2.3**, that several factors were responsible for the presence or absence of the monochelated species on the mass spectra of these bisthiourea complexes.

The $^{31}P\{^{1}H\}$ NMR spectra of the palladium and nickel bisthiourea complexes **6h-o** were determined in $CDCl_3$. The chemical shifts and the $^{2}J_{(PP)}$ coupling constants are presented in **Table 6.4**.

Table 6.4: Chemical shifts and $^{2}J_{(PP)}$ coupling constant values for palladium and nickel bisthiourea complexes **6h-6o**.

Complexes	**Chemical shifts ppm ($^{2}J_{(PP)}$ coupling constants Hz)**
$[Pd_2\{SC(NPh)NH\}_2(CH_2)_4(dppe)_2]\cdot 2BPh_4$ (**6h**)	62.55(28), 58.15(28)
$[Pd_2\{SC(NPh)NH\}_2(CH_2)_6(dppe)_2]\cdot 2BPh_4$ (**6i**)	62.69(28), 58.34(28)
$[Pd_2\{SC(NPh)NH\}_2(CH_2)_8(dppe)_2]\cdot 2BPh_4$ (**6j**)	62.78(27), 58.43(28)
$[Pd_2\{SC(NPh)NH\}_2(CH_2)_{12}(dppe)_2]\cdot 2BPh_4$ (**6k**)	62.84(28), 58.47(28)
$[Ni_2\{SC(NPh)NH\}_2(CH_2)_4(dppe)_2]\cdot 2BPh_4$ (**6l**)	61.52(50), 59.06(51)
$[Ni_2\{SC(NPh)NH\}_2(CH_2)_6(dppe)_2]\cdot 2BPh_4$ (**6m**)	61.55(50), 59.17(50)
$[Ni_2\{SC(NPh)NH\}_2(CH_2)_8(dppe)_2]\cdot 2BPh_4$ (**6n**)	61.54(50), 59.18(50)
$[Ni_2\{SC(NPh)NH\}_2(CH_2)_{12}(dppe)_2]\cdot 2BPh_4$ (**6o**)	61.56(50), 59.20(50)

The chemical shifts from the $^{31}P\{^{1}H\}$ NMR data presented in **Table 6.4** above show that the palladium complexes contained two doublets each around 62 and 58 ppm and a coupling constant of 28 Hz for all the palladium complexes **6h-6k**. Similarly, the nickel bisthiourea complexes **6l-6o** also showed two doublets each around 61 and 59 ppm respectively, with coupling constant values of 50 Hz. The NMR data in **Table 6.5** above showed slight changes in the value of the chemical shifts as the length of the alkyl bridge increased from one complex to the other. The chemical shifts for palladium complexes **6h-6k** showed slight increases in chemical shifts as the length of the bridging alkyl carbon chain increased from n = 4 in **6h** to n = 12 in **6k**. There were also slight, but non-significant changes in the chemical shift values for the nickel complexes **6l-o** as the length of the bridging alkyl carbon chain changed with no trend as in the palladium counterparts. Generally, it was observed that the length of the bridging alkyl carbon chain has no significant effect on the NMR chemical shifts of the bisthiourea complexes.

6.2.6 *Crystal structure of palladium bisthiourea complex 6k*

The palladium bisthiourea complex $[Pd_2\{SC=(NPh)NH\}_2(CH_2)_6(dppe)_2]\cdot 2BPh_4$ **6k** crystallised from a dichloromethane-diethyl ether solvent mixture with one molecule of the dichelated complex and two BPh_4 anions in the asymmetric unit. The symmetry elements of the structure do not include a centre of inversion, which implies that there might be differences in the geometric parameters of the square planes at each end of the bisthiourea complex. The molecular structure of the complex in **Figure 6.5** shows a slightly distorted square plane geometry on both ends of the complex. The square planes consist of the thiolate-S and N-donor atoms and two phosphorus atoms from the dppe ligand. The r.m.s. deviation of the N(1)-S(1)-P(1)-P(2) and N(4)-S(2)-P(3)-P(4) square planas are 0.070 and 0.027 Å respectively. The palladium atoms Pd(1) and Pd(2) deviate from the N(1)-S(1)-P(1)-P(2) and N(4)-S(2)-P(3)-P(4) square planes by 0.039 and 0.010 Å. The *cis* angles subtended by the P(1), P(2) and S(1), N(1) donor atoms have acute values of 85.36(2) and 70.82(6)^o respectively, while the angles subtended by P(4), P(3) and S(2), N(4) end of the structure are narrower; 84.70(3) and 70.20(7)^o. The *trans* angles in the N(1)-S(1)-P(1)-P(2) defined by P(1)-Pd(1)-N(1) and P(2)-Pd(1)-S(1) are deviated from the ideal 180^o by 10 and 7^o respectively. On the other end of the structure, the *trans* angles represented by P(3)-Pd(2)-N(4) and P(4)-Pd(2)-S(2) deviate from the ideal 180^o by approximately 7^o. The Pd-P bond lengths *trans* to thiolate-S are longer than the Pd-P bond lengths *trans* to N-donor atoms (**Table 6.5**). This is a visible indication of the greater *trans*-influence of the thiolate S, over the phenyl substituted *N*-donor atoms.

The four-membered metallacycle comprising of Pd(1)-S(1)-C(1)-N(1) has r.m.s. deviation of 0.091 Å which is almost twice the value of the r.m.s. deviation of the second metallacyclic ring defined by Pd(2)-S(2)-C(58)-N(4), 0.05 Å. The angles at the thiolate donor groups S(1) and S(2) has acute values of 77.74(10) and 77.92(10)^o respectively and are expectedly smaller than the angles at the more sterically encumbered N(1) and N(4) donor atoms with values of 98.06(19) and 99.68(18)^o. These angles are in turn smaller than the angles involving the N-bound phenyl groups adjacent to the Pd metal centre in the two metallacycles with values of 135.59(18)^o and 135.10(18)^o.

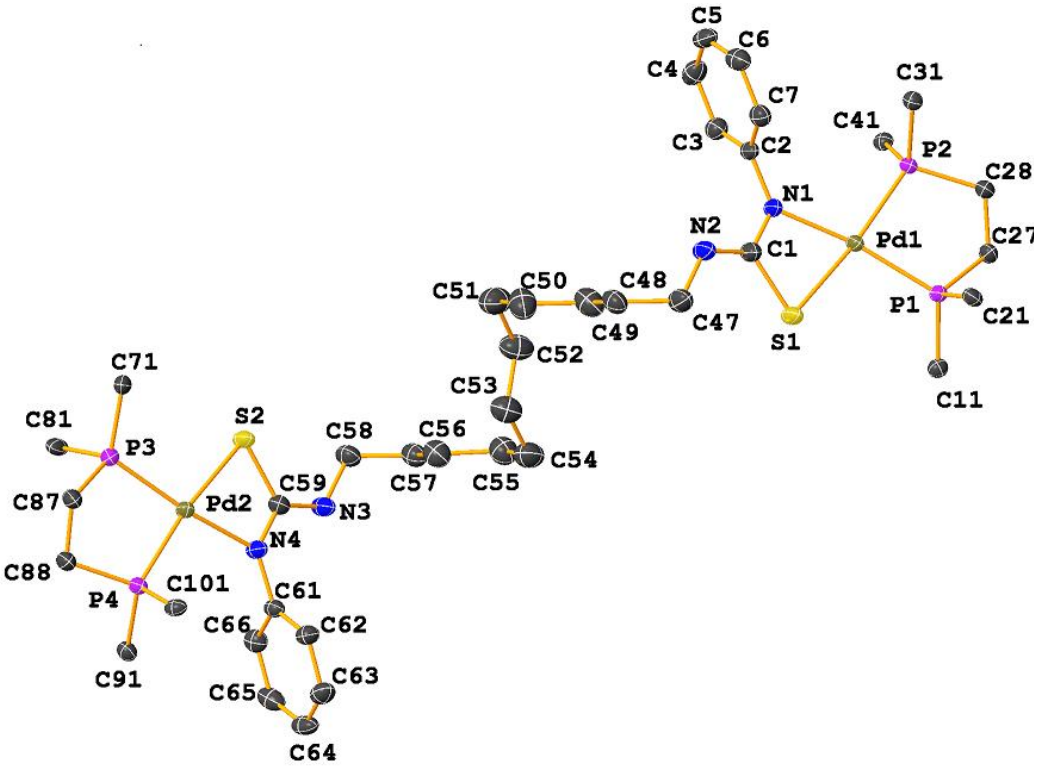

Figure 6.5: Molecular structure of palladium bisthiourea complex $[Pd_2\{SC{=}(NPh)NH\}_2(CH_2)_{12}(dppe)_2]\cdot 2BPh_4$ **6k**. Only ipso carbons of the dppe ligands are shown and BPh_4 anions are omitted for clarity. Ellipsoids are set at 50% probability.

Table 6.5: Table of geometric parameters for palladium bisthiourea complex **6k**

Bond parameters	**6k (a) (Å, º)**	**Bond parameters**	**6k (b) (Å, º)**
Pd(1) – S(1)	2.3518(8)	Pd(2) – S(2)	2.3597(7)
Pd(1) – P(1)	2.2434(7)	Pd(2) – P(3)	2.2407(7)
Pd(1) – P(2)	2.2795(7)	Pd(2) – P(4)	2.2693(7)
Pd(1) – N(1)	2.081(2)	Pd(2) – N(4)	2.067(2)
S(1) – C(1)	1.759(3)	S(2) – C(59)	1.761(3)
N(2) – C(1)	1.325(4)	N(3) – C(59)	1.331(4)
N(2) – C(47)	1.468(4)	N(3) – C(58)	1.475(4)
N(1) – C(2)	1.424(4)	N(4) – C(61)	1.421(4)
N(1) – C(1)	1.327(4)	N(4) – C(59)	1.320(4)
P(1) – Pd(1) – S(1)	100.65(3)	P(3) – Pd(2) – S(2)	102.68(3)
P(2) – Pd(1) – S(1)	173.59(4)	P(4) – Pd(2) – S(2)	172.58(3)
P(2) – Pd(1) – P(1)	85.36(2)	P(4) – Pd(2) – P(3)	84.70(3)
N(1) – Pd(1) – S(1)	70.16(7)	N(4) – Pd(2) – S(2)	70.20(7)
N(1) – Pd(1) – P(1)	170.39(7)	N(4) – Pd(2) – P(3)	172.51(7)
N(1) – Pd(1) – P(2)	103.45(6)	N(4) – Pd(2) – P(4)	102.44(7)
C(1) – S(1) – Pd(1)	77.74(10)	C(59) – S(2) – Pd(2)	77.92(10)
C(1) – N(1) – Pd(1)	98.06(19)	C(59) – N(4) – Pd(2)	99.68(18)
C(1) – N(1) – C(2)	121.8(2)	C(59) – N(4) – C(61)	124.9(2)
C(2) – N(1) – Pd(1)	135.59(18)	C(61) – N(4) – Pd(2)	134.10(18)

*Note (**a**) and (**b**) represent the two inequivalent ends of the bisthiourea complex **6k***

6.2.7 *Crystal structure of nickel bisthiourea complexes*

Crystals of the nickel bisthiourea complexes **6l** and **6m** suitable for X-ray crystallography were isolated from a dichloromethane and diethyl ether solvent mixture by vapour diffusion. The X-ray crystal data of the two complexes show that the compounds crystallised in a monoclinic P21/c crystal system with a half-molecule of the compound each in the asymmetric unit. The molecular structures of the complexes in **Figure 6.7** show dichelated square planar arrangements, where the Ni atom is chelated to the thiolate-S and N donor atoms of the thiourea, with the two remaining positions in the slightly distorted square planes occupied by the two phosphorus atoms of the dppe ligand.

a

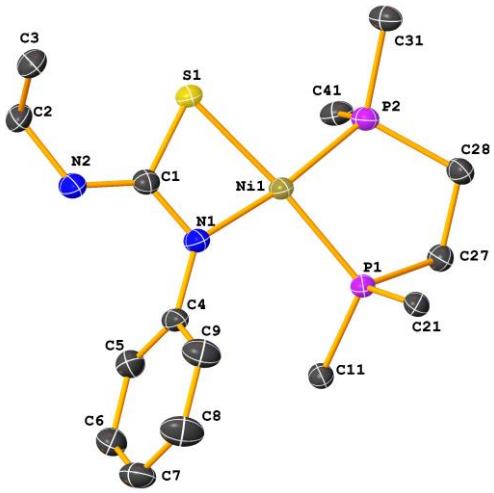

b

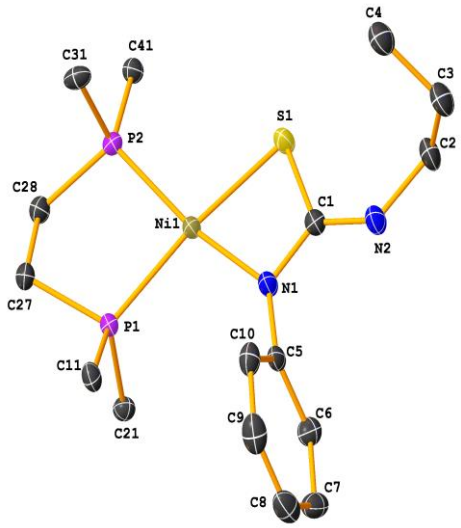

Figure 6.6: Molecular structure of one half of nickel bisthiourea complexes (a) $[Ni_2\{SC=(NPh)NH\}_2(CH_2)_4(dppe)_2]\cdot 2BPh_4$ **6l** and (b) $[Ni_2\{SC=(NPh)NH\}_2(CH_2)_6(dppe)_2]\cdot 2BPh4$ **6m**. Only one half of the complexes and ipso carbons of the PPh_3 ligand are shown for clarity. Ellipsoids are drawn at 50% probability. BPh_4 anions are also omitted for clarity.

The N(1)-P(1)-P(2)-S(1) square planes are slightly puckered and fairly planar respectively, with r.m.s. deviations of 0.108 and 0.027 Å for **6l** and **6m** respectively. These are equivalent to the values reported for the palladium complex analogue of these complexes, $[Pd_2\{SC=(NPh)N\}_2(CH_2)_{12}(dppe)_2]\cdot 2BPh_4$. This *cis*-angles subtended by the S,N chelate-pair in the complexes **6l**, 74.70(5)^o and **6m**, 74.11(4)^o are similar while the angles between the phosphorus donor pair are wider but also similar for both complexes **6l**, 87.31(2) and **6m**, 86.44(7)^o. These angles are similar to the angles reported for a tri-substituted thiourea nickel complex $[Ni\{SC(NMe_2)NPh\}(dppe)]BPh_4$, 74.67(6)^o and 86.38(8)^o [4] and wider than the angles reported for the two square planes in the palladium bisthiourea complex $[Pd_2\{SC=(NPh)N\}_2(CH_2)_{12}(dppe)_2]\cdot 2BPh_4$, **6k**. The *trans*-angles in the complex **6l** are deviated from the ideal 180^o by 6 and 8^o while the deviation of the trans angles in **6m** are approximately 4 and 10^o respectively. The P(1)-Ni(1) and P(2)-Ni(1) bond lengths in the two complexes are different by a value of 0.0127 and 0.0312 Å for **6l** and **6m** respectively. This is an indication of a greater *trans*-influence of the thiolate S–donor atom in **6m** than that in **6l**. The difference in *trans*-influence between thiolate S-donor atoms and N-donor atoms has been reported in several S,N-donor metal complexes containing phosphorus ligands[1-3,15]. The Ni(1)-S(1)-C(1)-N(1) metallacyclic ring in the complex **6l** is slightly puckered with a r.m.s. deviation of 0.019 from planarity, while that in **6m** is planar with r.m.s. deviation of 0.00. The angles on the thiolate S-donor groups of the metallacycle are similar in the two complexes and acute. The more sterically encumbered angles at the N-donor atoms, are however wider, but smaller than the angles involving the N(1) bound phenyl by a factor 36^o in both complexes **6l** and **6m** (**Table 6.6**). Similar values have been reported for other thiourea complexes having four-membered metallacycles with *N*-bound substituents[4,19].

Apart from the difference in planarity of the metallacyclic rings in the two complexes, the only other apparent structural difference between the complexes **6l** and **6m** are the value of the dihedral angles between the chelate ring and the N(1)-bound phenyl and N(2) alkyl substituents in the two complexes. The dihedral angles between the chelate ring and N(1) and N(2) bound substituents in **6l** are 78.22(7) and 67.60(5)^o while those in **6m** are 81.33(4) and 84.90(6)^o. The similarities in the structural arrangement of the square plane and conformational differences in the two structures are depicted in the structural overlay in **Figure 6.7**.

Table 6.6: Table of geometric parameters for nickel bisthiourea complexes **6l** and **6m**

Bond parameters (Å,º)	**6l**	**6m**
Ni(1) – S(1)	2.2308(5)	2.2361(4)
Ni(1) – P(1)	2.1613(5)	2.1840(4)
Ni(1) – P(2)	2.1486(6)	2.1528(4)
Ni(1) – N(1)	1.9047(16)	1.9086(13)
Ni(1) – C(1)	2.4827(18)	2.4910(15)
S(1) – C(1)	1.7538(19)	1.7558(16)
N(2) – C(1)	1.328(2)	1.327(2)
N(2) – C(2)	1.462(2)	1.464(2)
N(1) – C(4)	1.427(3)	1.4268(2)
N(1) – C(1)	1.313(3)	1.315(2)
P(1) – Ni(1) – S(1)	174.20(2)	176.71(19)
P(2) – Ni(1) – S(1)	98.49(2)	96.85(2)
P(1) – Ni(1) – P(2)	87.31(2)	86.447(16)
N(1) – Ni(1) – S(1)	74.70(5)	74.11(4)
N(1) – Ni(1) – P(2)	172.57(5)	170.06(4)
N(1) – Ni(1) – P(1)	99.50(5)	101.62(4)
N(1) – Ni(1) – C(1)	31.47(6)	31.38(5)
C(1) – S(1) – Ni(1)	76.04(6)	76.16(5)
C(1) – N(1) – Ni(1)	99.33(11)	99.54(10)
C(4) – N(1) – Ni(1)	137.16(12)	136.11(12)

*Note C4 in **6l** is the same atom as C5 in **6m***

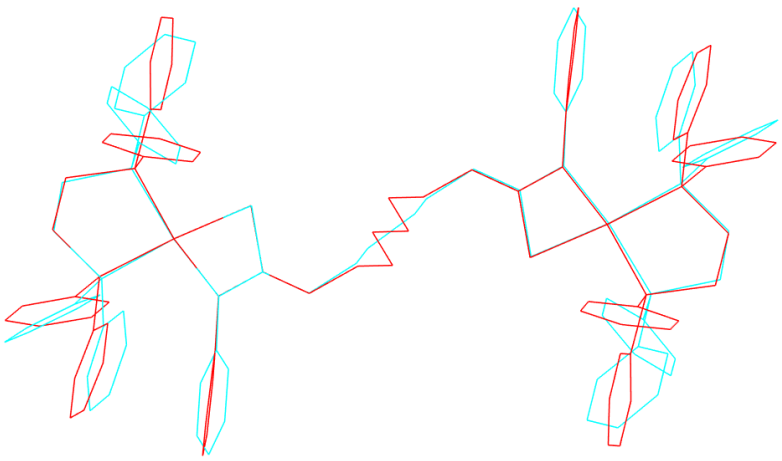

Figure 6.7: Structure overlay of nickel bisthiourea complexes **6l** (cyan) and **6m** (red) showing conformational differences between the two structures. BPh_4 anions are omitted for clarity.

6.3 Conclusions

Platinum, palladium and nickel complexes of alkyl-bridged bifunctional thiourea ligands were synthesised and characterised. The ESI-mass spectra of most of the complexes showed the presence of both the dichelated and monochelated derivatives. The $^{31}P\{^{1}H\}$ NMR data showed the presence of multiplets in the methylene-bridged complexes **6a-6c**, attributed to isomerism of the complexes in $CDCl_3$ solution. The butylene, hexylene, octylene, and dodecylene bridged complexes **6d-6o** did not show any sign of isomerisation. X-ray crystal structures of complexes **6e**, **6l** and **6m** showed that the compounds crystallised with half a molecule each in the asymmetric unit, while **6k** crystallised with a whole molecule. The molecular structures of all the complexes showed consistent adoption of the square planar geometry defined by the NP_2S donor atoms from the monoanionic *N,S*-chelating ligands and the two phosphate ligands. Variation in the metal-P bond lengths in all the complexes was attributed to a variable *trans*-influence of the thiolate S and N-donor groups. There were no significant differences between the geometric parameters of the Pt, Pd and Ni complexes.

6.4 Experimental

4,4′-Diaminophenylmethane, 1,4-diaminobutane, 1,6-diaminohexane, 1,8-diaminooctane and 1,12-diaminododecane were purchased from Sigma Aldrich Chemical Company. Refer to the experimental section of Chapters 2 and 3 for sources of other chemicals, solvents and general experimental procedures.

6.4.1 Synthesis of thiourea ligands

(1p) *$PhNHC(S)NHC_6H_4CH_2C_6H_4NHC(S)NHPh$*

4,4′-Diaminophenylmethane (3.96 g, 0.02 mol) in DMF (70 mL) was added phenyl isothiocyanate (4.78 mL, 0.04 mol) dropwise and stirred overnight. A clear yellow solution was formed. Water (150 mL) was added to the solution to precipitate the white product, which was filtered and washed with water (20 mL) and petroleum spirits (10 mL). Yield: 6.23 g, 66%, M.p 160-165^{o}C. ESI-MS: *m/z* 467.06 (100%) $[M-H]^+$, 933 (23%) $[2M-H]^+$. ^{1}H NMR (DMSO-d_6) δ ppm: 9.72 [d, 4H, NH; J = 2.7 Hz], 7.49 [d, 2H, Ar-H; J = 7.9 Hz], 7.36 [dd, 5H, Ar-H; J = 8.2 Hz, J = 7.2 Hz], 7.22 [d, 2H, Ar-H; J = 8.3 Hz], 7.12 [t, 1H, Ar-H; J = 7.3 Hz], 3.89 [s, 2H, CH_2-Ph]. ^{13}C NMR: 180.04 [s, C=S], 139.97 [s, Ar-C], 138.03 [d, 2C, Ar-C; J = 21.6 Hz], 129.12 [d, 2C, J = 27.5 Hz], 124.82 [d, 2C, J = 24.6 Hz]. FTIR (cm^{-1}):

3469(br), 3299(w) 3200(s), 3028(s), 2914(w), 2847(w), 2086(m), 1595(s), 1543(s), 1522(w), 1449(s), 1417(s), 1337(w), 1315(w), 1238(m), 1108(s), 1068(m), 1022(s), 1003(w), 931(s), 865(s), 816(s), 766(s), 690(s), 615(m), 554(s), 482(m).

(1q) *PhNHC(S)NH(CH_2)$_4$NHC(S)NHPh*

This was synthesised from 1,4-diaminobutane (2.01 mL, 0.02 mol) and phenyl isothiocyanate (4.78 mL, 0.04 mol) using a similar method as **1p**. Yield: 4.01 g, 54%, M.p 160-165^{o}C. ESI-MS: *m/z* 357.08 (100%) $[M-H]^+$. ^{1}H NMR DMSO-d_6 δ ppm: 9.47 [s, 1H, NH], 7.76 [s, 1H, NH], 7.34 [m, 4H, Ar-H], 7.10 [dd, 1H, Ar-H; J = 6.4 Hz, J = 5.2 Hz], 3.49 [t, 2H, CH_2; J = 5.3 Hz], 1.57 [s, 2H, CH_2-C]. ^{13}C NMR: 180.75 [s, C=S], 139.71 [s, Ar-C], 129.07 [s, Ar-C], 124.54 [d, Ar-C; J = 25.5 Hz], 44.07 [s, CH_2N], 26.59 [s, CH_2-C]. FTIR (cm^{-1}): 3449(br), 3259(w), 3165(m), 3009(m), 2943(w), 1592(s), 1543(s), 1493(m), 1449(s), 1400(s), 1308(s), 1256(s), 1179(s), 1072(m), 1027(m), 931(s), 909(w), 811(s), 751(s), 721(s), 694(s), 640(s), 602(s), 558(m), 491(s).

(1r)*. PhNHC(S)NH(CH_2)$_6$NHC(S)NHPh*

This ligand was synthesised using a similar method as (**1p**) from 1,6-diaminohexane (3.48 g, 0.03 mol) and phenyl isothiocyanate (7.17 mL, 0.04 mol). Yield: 7.26 g, 76%, M.p 100-116^{o}C. ESI-MS: *m/z* 385.10 (100%) $[M-H]^+$. ^{1}H NMR DMSO-d_6 δ ppm: 9.43 [s, 1H, NH], 7.73 [s, 1H, NH], 7.40 [d, 2H, Ar-H; J = 7.5 Hz], 7.31 [t, 2H, Ar-H; J = 7.5 Hz], 7.09 [t, 2H, CH_2; J = 7.0 Hz], 3.47 [d, 2H, CH_2; J = 5.2 Hz], 1.56 [t, 2H, CH_2; J = 7.0 Hz], 1.33 [t, 2H, CH_2; J = 5.2 Hz]. ^{13}C NMR: 180.74 [s, C=S], 139.79 [s, Ar-C], 129.03 [s, Ar-C], 124.46 [d, Ar-C; J = 25.5 Hz], 44.27 [s, CH_2N], 26.90 [s, CH_2-C], 26.68 [s, CH_2-C]. FTIR (cm^{-1}): 3462(w), 3332(s), 3059(m), 2926(s), 2852(s), 1601(w), 1555(br), 1495(m), 1450(m), 1350(s), 1206(w), 1106(w), 1073(m), 1026(m), 1003(s), 894(m), 866(m), 795(w), 752(s), 707(s), 614(m), 592(m), 493(w).

*(**1s**). PhNHC(S)NH(CH_2)$_8$NHC(S)NHPh*

This ligand was synthesised using a similar method as (**1p**) from 1,8-diaminooctane (2.88 g, 0.02 mol) and phenyl isothiocyanate (0.04 mol, 4.78 mL). Yield: 6.21 g, 70 %, M.p: 90-96^{o}C. ESI-MS: *m/z* 413.12 (100%) $[M-H]^+$. ^{1}H NMR DMSO-d_6 δ ppm: 9.42 [s, 1H, NH], 7.41 [dd, 2H, Ar-H; J = 1.2, 8.6 Hz], 7.31 [m, 2H, Ar-H], 7.11 [t, 1H, Ar-H; J = 7.4 Hz], 1.54 [t, 2H, CH_2-N], 1.30 [s, 6H, CH_2-C]. ^{13}C NMR: 180.73 [s, C=S], 139.78 [s, Ar-C], 129.07 [s, Ar-C], 124.47 [s, Ar-C], 123.4 [s,Ar-C], 44.29 [s, CH_2N], 28.20 [d, CH_2-C; J = 29 Hz], 26.85 [d, CH_2-C]. FTIR (cm^{-1}): 3480(br), 3233(s), 3048(s), 2923(s), 2949(s), 1603(s), 1555(br), 1496(s), 1451(s), 1351(m), 1322(w), 1266(w), 1232(w), 1199(w), 1111(w), 1071(m), 1028(w), 892(s), 865(s), 751(s), 708(s), 689(s), 614(m), 596(m), 569(w), 492(w).

***(1t)**. PhNHC(S)NH(CH_2)$_{12}$NHC(S)NHPh*

This ligand was synthesised using a similar method as (**1p**) from 1,12-diaminododecane (4.00 g, 0.02 mol) and phenyl isothiocyanate (4.78 mL, 0.04 mol). Yield: 4.01 g, 54 %, M.p: 108-112^{o}C. ESI-MS: *m/z* 469.18(100%) $[M-H]^+$. ^{1}H NMR (DMSO-d_6) δ ppm; 7.76 [s, 1H, NH], 7.40 [t, 2H, Ar-H; J = 7.9 Hz], 7.32 [dd, 1H, Ar-H; J = 7.7, 9.3 Hz], 7.23 [d, 2H, Ar-H; J = 8.3 Hz], 6.02 [s, 1H, NH], 3.64 [dd, 2H, CH_2; J = 7.0, 6.2 Hz], 1.63 [t, 2H, CH_2; J = 6.6 Hz], 1.27 [t, 8H, CH_2; J = 8.2 Hz], 1.33 [t, 2H, CH_2; J = 5.2 Hz]. ^{13}C NMR: 180.74 [s, C=S], 139.79 [s, Ar-C], 129.03 [s, Ar-C], 124.46 [d, Ar-C; J = 25.5 Hz], 44.27 [S, CH_2N], 26.90 [s, CH_2-C], 26.68 [s, CH_2-C]. FTIR (cm^{-1}): 3452(br), 3332(s), 3055(s), 2917(s), 2949(s), 1605(m), 1559(br), 1496(s), 1463(w), 1451(w), 1350(s), 1326(w), 1277(w), 1227(w), 1191(w), 1118(w), 1067(m), 1028(w), 829(s), 865(s), 749(s), 709(s), 689(s), 615(m), 594(s), 570(m), 493(m).

6.4.2 *Synthesis and characterisation of the complexes*

The complexes were synthesised using the same general method previously reported by Henderson and co-workers[19]. 2 : 1 molar quantities of the metal precursors, *cis*-[$PtCl_2(PPh_3)_2$], [$PdCl_2$(dppe)] or [$NiCl_2$(dppe)] and bisthiourea ligands were warmed gently and triethylamine (0.5 mL) was added. The solutions were refluxed for 8 hours and the complexes were isolated by addition of $NaBPh_4$

(3 mol equivalent). The resulting product was filtered, washed with diethyl ether (10 mL) and dried in a desiccator under vacuum.

$[Pt_2\{(SC(NPh)NHC_6H_4)_2CH_2\}(PPh_3)_4]\cdot 2BPh_4$ ***(6a)***

cis-$[PtCl_2(PPh_3)_2]$ (79 mg, 0.2 mmol) and $[(PhNHC(S)NHC_6H_4)_2CH_2]$ (46 mg, 0.1 mmol). Yield: 174 mg, 84 %. Elemental analysis %: calculated for $C_{147}H_{124}B_2N_4P_4Pt_2S_2$; C 69.34, H 4.91, N 2.20, found: C 70.10, H 5.02; N 2.38. ESI-MS: Calculated *m/z*; 952.71 $[M]^{2+}$, experimental *m/z*: CEV 60 V, 952.80 (100%) $[M]^{2+}$, 1904.52 (8%) $[M\text{-}H]^+$. CEV 120-180 V, 718.20 (49%) $[Pt(PPh_2C_6H_4)(PPh_3)]^+$, 952.76 (87%) $[M]^{2+}$, 1187.34 (7%) $[M\text{-}(Ph_3P)_2Pt+H]^+$, 1904.80 (5%) $[M\text{-}H]^+$. $^{31}P\{^1H\}$ NMR δ ppm: 13.68 [$^1J_{(PtP)}$ = 3207 Hz, $^2J_{(PP)}$ = 21 Hz] and δ 9.39 [$^1J_{(PtP)}$ = 3480 Hz, $^2J_{(PP)}$ = 21 Hz]. FTIR (cm^{-1}): 3449(br), 3053(s), 2998(s), 2851(m), 1579(m), 1551(s), 1497(s), 1481(s), 1435(s), 1384(m), 1340(m), 1225(w), 1184(w), 1098(s), 1029(w), 1029(s), 999(m), 929w), 844(m), 744(m), 704(s), 692(s), 612(s), 547(s), 525(s), 499(s).

$[Pd_2\{(SC(NPh)NHC_6H_4)_2CH_2\}(dppe)_2]\cdot 2BPh_4$ ***(6b)***

$[PdCl_2(dppe)]$ (115 mg, 0.2 mmol) and $[(PhNHC(S)NHC_6H_4)_2CH_2]$ (47 mg, 0.1 mmol) Yield: 87 mg, 53 %. Elemental analysis %: calculated for $C_{127}H_{112}B_2N_4P_4PdS_2$; C 72.06, H 5.33, N 2.65, found: C 72.54, H 5.62; N 3.01. ESI-MS: Calculated *m/z*; 737.58 $[M]^{2+}$, experimental *m/z*: CEV 60 V, 737.80 (100%) $[M]^{2+}$, 970.84 (42%) $[M\text{-}(dppeNi+H)]^+$. CEV 120-180 V, 737.80 (100%) $[M]^{2+}$, 970.84 (42%) $[M\text{-}(dppeNi)+H]^+$, 1794.72 (6%) $[MBPh_4]^+$. NMR: $^{31}P\{^1H\}$ NMR δ ppm; isomer 1; 63.29 [$^2J_{(PP)}$ = 32 Hz] and 68.67 [$^2J_{(PP)}$ = 33 Hz], isomer 2; 59.28, [$^2J_{(PP)}$ 14 Hz] and δ 45.75 [$^2J_{(PP)}$ = 12 Hz]. ^1H NMR δ ppm: 2.02 [m, 8H, CH_2, dppe], 2.68 [s, 1H, CH_2, dppe], 3.67 [m, 2H], 6.39-7.90 [m, 57H, Ar-H]. FTIR (cm^{-1}): 3410(br), 3053(s), 3032(w), 2998(s), 2914(w), 1579(s), 1548(s), 1483(s), 1435(s), 1408(w), 1385(w), 1308(s), 1268(w), 1224(m), 1186(m), 1103(s), 1028(s), 998(s), 912(m), 876(m), 843(w), 818(s), 744(s), 704(s), 690(s), 612(s), 531(s), 481(s).

*$[Ni_2\{(SC(NPh)NHC_6H_4)_2CH_2\}(dppe)_2]\cdot 2BPh_4$ (**6c**)*

$[NiCl_2(dppe)]$ (106 mg, 0.2 mmol) and $[(PhNHC(S)NHC_6H_4)_2CH_2]$ (48 mg, 0.1 mmol). Yield: 132 mg, 80%. Elemental analysis %: calculated for $C_{127}H_{112}B_2N_4P_4Pd_2S_2$; C 75.46, H 5.15, N 2.77, found: C 75.52, H 5.82; N 2.80. ESI-MS: Calculated *m/z*; 690.14 $[M]^{2+}$, experimental *m/z*: CEV 60 V, 690.15 (100%) $[M]^{2+}$, 923.24 (12%) $[M\text{-}(Nidppe)+H]^+$. CEV 120-180 V, 690.15 (100%) $[M]^{2+}$, 923.24 (22%) $[M\text{-}(Nidppe)+H]^+$. 1699.40 (13%) $[MBPh_4]^+$. $^{31}P\{^1H\}$ NMR δ ppm: 61.69 [$^2J_{(PP)}$ = 50 Hz] and δ 59.14 [$^2J_{(PP)}$ = 50 Hz]. ^1H NMR δ ppm: 1.87 [m, 8H, CH_2; dppe], 2.58 [s, 1H, CH_2; dppe], 3.64 [m, 2H], 6.18-7.0 [m, 17H, Ar-H], 7.10-7.76 [m, 32H, Ar-H]. FTIR (cm^{-1}): 3267(br) 3054(s), 2923(m), 2850(m), 1593(m), 1548(s), 1497(w), 1324(s), 1266(w), 1184(m), 1101(s), 1069(w), 1029(s), 931(m), 842(m), 816(s), 733(s), 704(s), 654(w), 611(s), 532(s), 481(s).

*$[Pt_2\{SC(NPh)NH\}_2(CH_2)_4(PPh_3)_4]\cdot 2BPh_4$ (**6d**)*

cis-$[PtCl_2(PPh_3)_2]$ (158 mg, 0.2 mmol) and $PhNHC(S)NH(CH_2)_4NHC(S)NHPh$ (35 mg, 0.1 mmol). Yield: 150 mg, 77%. Elemental analysis %: calculated for $C_{138}H_{120}B_2N_4P_4Pt_2S_2$; C 68.09, H 4.97, N 2.30, found; C 68.10, H 5.02; N 2.48. ESI-MS: Calculated *m/z*; 897.71 $[M]^{2+}$, experimental *m/z*: CEV 60 V, 897.47 (100%) $[M]^{2+}$, 1042.03 (42%) $[M\text{-}Pt(PPh_3)_2S]^+$, 1076.03 (15%) $[M\text{-}Pt(PPh_3)_2+H]^+$, 2112.57 (5%) $[MBPh_4]^+$, 120-150 V; 718.20 (52%) $[Pt(PPh_2C_6H_4)(PPh_3)]^+$, 897.47 (100%) $[M]^{2+}$, 1042.03 (47%) $[M\text{-}Pt(PPh_3)_2S]^+$, 1076.03 (19%) $[M\text{-}Pt(PPh_3)_2+H]^+$, 1530 (7%) $[M\text{-}PPh_3]^+$, 2112.57 (5%) $[MBPh_4]^+$, 180 V; 718.20 (18%) $[Pt(PPh_2C_6H_4)(PPh_3)]^+$, 897.47 (100%) $[M]^{2+}$, 1042.03 (32%) $[M\text{-}Pt(PPh_3)_2S]^+$, 1076.03 (12%) $[M\text{-}Pt(PPh_3)_2+H]^+$, 2112.57 (5%) $[MBPh_4]^+$. $^{31}P\{^1H\}$ NMR δ ppm: 13.58 [$^1J_{(PtP)}$ = 3234 Hz, $^2J_{(PP)}$ = 22 Hz] and 9.22 [$^1J_{(PtP)}$ = 3462 Hz, $^2J_{(PP)}$ = 22 Hz]. ^1H NMR δ ppm: 0.6 [s, 2H, CH_2], 0.9 [t, 2H, CH_2; J = 6.9 Hz], 1.06 [t, 2H, CH_2; J = 6.2 Hz], 1.24 [t, 2H, CH_2, J = 6.9 Hz], 2.34 [d, 2H, CH_2; J = 5.8 Hz], 2.56 [dd, 2H, CH_2; J = 7.0, 7.4 Hz], 4.62 [t, 1H, NH; J = 5.8 Hz], 5.37 [m, 1H, NH], 6.61 [t, 3H, Ar-H; J = 8.4 Hz], 6.70 [t, 3H, Ar-H; J = 7.4 Hz], 6.8 [t, 7H, Ar-H; J = 6.9 Hz], 7.0 [t, 12H, Ar-H; J = 7.4 Hz], 7.21 [m, 16H, Ar-H], 7.31-7.50 [m, 25H, Ar-H]. FTIR (cm^{-1}): 3440(br), 3377(w). 3134(s) 3053(s), 2997(w), 2855(w), 1593(m), 1568(s), 1480(s), 1436(s), 1380(m), 1339(m), 1266(w), 1184(m), 1160(w), 1097(s), 1071(w), 1030(s), 999(s), 920(w), 843(m), 811(w), 744(s), 703(s), 612(s), 547(s), 525(s), 497(s).

*$[Pt_2\{SC(NPh)NH\}_2(CH_2)_6(PPh_3)_4]\cdot 2BPh_4$ (**6e**)*

cis-$[PtCl_2(PPh_3)_2]$ (160 mg, 0.2 mmol) and $PhNHC(S)NH(CH_2)_6NHC(S)NHPh$ (39 mg, 0.1 mmol). Yield: 87 mg, 84 %. Elemental analysis %: calculated for $C_{116}H_{104}B_2N_4P_4Pt_2S_2$; C 65.01, H 4.89, N 2.61, found; C 65.10, H 5.02; N 2.58. ESI-MS: Calculated *m/z*; 911.44 $[M]^{2+}$, experimental *m/z*: CEV 60 V, 911.47 (95.8%) $[M]^{2+}$, 2141.90 $[MBPh_4]^+$, 120-180 V, 718.94 (68%) $[Pt(PPh_2C_6H_4)(PPh_3)]^+$, 911.47 (95.8%) $[M]^+$, 2141.98 (7%) $[MBPh_4]^+$. $^{31}P\{^1H\}$ NMR δ ppm: 13.46 [$^1J_{(PtP)}$ = 3241 Hz, $^2J_{(PP)}$ = 21 Hz] and 9.23 [$^1J_{(PtP)}$ = 3461 Hz, $^2J_{(PP)}$ = 21 Hz]. ^1H NMR δ ppm: 0.82 [m, 2H, CH_2], 1.02 [t, 2H, CH_2; J = 6.7 Hz], 2.70 [dd, 2H, CH_2; J = 6.6, 7.1 Hz], 2.88 [s, 1H, NH], 4.73 [t, 1H, NH; J = 6.2 Hz], 6.17 [d, 2H, Ar-H; J = 7.4 Hz], 6.62 [t, 2H, Ar-H; J = 7.4 Hz], 6.75 [t, 1H, Ar-H; J = 7.0 Hz], 6.89 [t, 5H, Ar-H; J = 7.0 Hz], 7.0-7.2 [m, 23H, Ar-H], 7.31 [m, 9H, Ar-H; J = 7.4 Hz], 6.69-7.5 [m,17H, Ar-H]. FTIR (cm^{-1}): 3440(br), 3377(w), 3134(s), 3053(s), 2997(w), 2855(w), 1599(m), 1568(s), 1480(s), 1436(s), 1380(m), 1339(m), 1266(w), 1184(m), 1160(w), 1097(s), 1071(w), 1030(s), 999(s), 920(w), 843(m), 811(w), 744(s), 703(s), 612(s), 547(s), 525(s), 497(s).

*$[Pt_2\{SC(NPh)NH\}_2(CH_2)_8(PPh_3)_4]\cdot 2BPh_4$ (**6f**)*

cis-$[PtCl_2(PPh_3)_2]$ (160 mg, 0.2 mmol) and $PhNHC(S)NH(CH_2)_8NHC(S)NHPh$ (47 mg, 0.1 mmol). Yield: 195 mg, 94 %. Elemental analysis %: calculated for $C_{142}H_{128}B_2N_4P_4Pt_2S_2$; C 68.48, H 5.18, N 2.25, found; C 68.51, H 5.25; N 2.19. ESI-MS: Calculated *m/z*; 925.70 $[M]^{2+}$, experimental *m/z*: CEV 60 V, 925.56 (100%) $[M]^{2+}$, 2170.30 $[MBPh_4]^+$, CEV 120-180 V, 718.00 (42%) $[Pt(PPh_2C_6H_4)(PPh_3)]^+$, 925.58 (95.8%) $[M]^{2+}$, 2170.31 (8%) $[MBPh_4]^+$. $^{31}P\{^1H\}$ NMR δ ppm; 13.42 [$^1J_{(PtP)}$ = 3232 Hz, $^2J_{(PP)}$ = 21 Hz] and 9.23 [$^1J_{(PtP)}$ = 3470 Hz, $^2J_{(PP)}$ = 22 Hz]. ^1H NMR δ ppm: 0.82 [m, 4H, CH_2], 1.17 [t, 2H, CH_2; J = 7.2 Hz], 2.80 [dd, 2H, CH_2; J = 6.5, 7.0 Hz], 4.83 [t, 1H, NH; J = 5.7 Hz], 6.18 [d, 2H, Ar-H; J = 7.6 Hz], 6.63 [t, 2H, Ar-H; J = 7.9 Hz], 6.80 [t, 1H, Ar-H; J = 7.5 Hz], 6.92 [t, 5H, Ar-H; J = 7.4 Hz], 7.01-7.20 [m, 23H, Ar-H], 7.38-7.54 [m, 19H, Ar-H; J = 7.4 Hz], 6.69-7.5 [m, 17H, Ar-H]. FTIR (cm^{-1}): 3440(br), 3377(w), 3134(s), 3053(s), 2997(w), 2855(w), 1599(m), 1568(s), 1480(s), 1436(s), 1380(m), 1339(m), 1266(w), 1184(m), 1160(w), 1097(s), 1071(w), 1030(s), 999(s), 920(w), 843(m), 811(w), 744(s), 703(s), 612(s), 547(s), 525(s), 497(s).

$[Pt_2\{SC(NPh)NH\}_2(CH_2)_{12}(PPh_3)_4]\cdot 2BPh_4$ ***(6g)***

cis-$[PtCl_2(PPh_3)_2]$ (160 mg, 0.2 mmol) and $PhNHC(S)NH(CH_2)_{12}NHC(S)NHPh$ (48 mg, 0.1 mmol). Yield: 109.5 mg, 53 %. Elemental analysis %: Calculated for $C_{146}H_{136}B_2N_4P_4Pt_2S_2$; C 68.86, H 5.38, N 2.20, found; C 68.80, H 5.40; N 2.26. ESI-MS: Calculated *m/z*; 953.41 $[M]^{2+}$, experimental *m/z*: CEV 60 V, 953.50 (100%) $[M]^{2+}$, 2225.99 (3%) $[MBPh_4]^+$; 120-180 V, 718.94 (68%) $[Pt(PPh_2C_6H_4)(PPh_3)]^+$, 953.50 (100%) $[M]^{2+}$, 1188.06 (3%) $[M\text{-}Pt(PPh_3)_2+H]^+$, 2225.99 (3%) $[MBPh_4]^+$. $^{31}P\{^1H\}$ NMR δ ppm: 13.40 [$^1J_{(PtP)}$ = 3241 Hz, $^2J_{(PP)}$ = 21 Hz] and 9.21 [$^1J_{(PtP)}$ = 3461 Hz, $^2J_{(PP)}$ = 21 Hz]. ^1H NMR δ ppm: 1.05-1.15 [m, 4H, CH_2; J = 7.0 Hz], 1.22-1.30 [m, 4H, CH_2, J = 5.6 Hz], 2.90 [dd, 2H, CH_2, J = 7.0 Hz], 4.79 [t, 2H, CH_2; J = 6.0 Hz], 6.19 [d, 2H, NH; J = 7.6 Hz], 6.69-7.5 [m, 17H, Ar-H]. FTIR (cm^{-1}): 3447(br), 3375(w), 3054(s), 2923(s), 2851(m), 1593(m), 1568(s), 1480(s), 1435(s), 1265(m), 1334(m), 1266(w), 1183(w), 1159(m), 1095(s), 1029(s), 998(s), 920(w), 842(m), 732(s), 703(s), 547(s), 611(s), 547(s), 525(s), 476(s).

$[Pd_2\{SC(NPh)NH\}_2(CH_2)_4(dppe)_2]\cdot 2BPh_4$ ***(6h)***

$[PdCl_2(dppe)]$ (115 mg, 0.2 mmol) and $PhNHC(S)N(CH_2)_4NC(S)NHPh$ (36 mg, 0.1 mmol). Yield: 102 mg; 67 %. Elemental analysis %: calculated for $C_{94}H_{88}BN_4P_4PdS_2$; C 66.99, H 5.26, N 3.32, found; C 67.04, H 5.22; N 3.28. ESI-MS: Calculated *m/z*; 683.11 $[M]^{2+}$, experimental *m/z*: CEV 60 V, 682.99 (100%) $[M]^{2+}$, 120-180 V, 682.99 (100%) $[M]^{2+}$, 1684.83 (28%) $[MBPh_4]^+$. $^{31}P\{^1H\}$ NMR δ ppm: 62.55 [$^2J_{(PP)}$ = 28 Hz] and 58.15 [$^2J_{(PP)}$ = 28 Hz]. ^1H NMR δ ppm: 0.98 [m, 2H, CH_2], 2.18 [m, 4H, CH_2 dppe; J = 22, 10.7 Hz], 2.79 [d, 2H, CH_2; J = 5.9 Hz], 5.0 [t, 1H, NH; J = 6.4 Hz], 6.35 [d, 2H, Ar-H; J = 7.9 Hz], 6.75 [t, 5H, Ar-H; J = 7.2 Hz], 7.04 [t, 1H, Ar-H; J = 7.4 Hz], 7.10-7.25 [m, 5H, Ar-H], 7.32 [m, 14H, Ar-H], 7.45-7.65 [m, 14H, Ar-H]. FTIR (cm^{-1}): 3443(br), 3338(w), 3053(s), 2982(w), 1592(m), 1562(s), 1482(s), 1435(s), 1383(m), 1336(m), 1307(m), 1239(w), 1185(w), 1149(w), 1103(s), 1067(w), 1030(s), 997(s), 917(w), 876(w), 818(s), 732(s), 705(s), 689(s), 612(s), 530(s), 481(s).

$[Pd_2\{SC(NPh)NH\}_2(CH_2)_6(dppe)_2]\cdot 2BPh_4$ ***(6i)***

$[PdCl_2(dppe)]$ (115 mg, 0.2 mmol) and $PhNHC(S)NH(CH_2)_6NHC(S)NHPh$ (36 mg, 0.1 mmol). Yield: 102 mg; 67 %. Elemental analysis %: calculated for $C_{96}H_{92}BN_4P_4Pd_2S_2$; C 67.29, H 5.41, N 3.27, found; C 67.24, H 5.42; N 3.28. ESI-MS: Calculated *m/z*; 697.05 $[M]^{2+}$, experimental *m/z*: CEV 60 V, 697.04 (100%) $[M]^{2+}$, 120-180 V, 697.06 (100%) $[M]^{2+}$, 1713.03 (32%) $[MBPh_4]^+$. $^{31}P\{^1H\}$ NMR δ ppm: 62.69 [$^2J_{(PP)}$ = 28 Hz] and 58.34 [$^2J_{(PP)}$ = 28 Hz]. ^1H NMR δ ppm: 1.05 [m, 2H, CH_2], 1.13 [t, 2H, CH_2; J = 7.1 Hz], 2.07 [m, 4H, CH_2 dppe; J = 23, 10.5 Hz], 2.69 [d, H, NH; J = 6.9 Hz], 3.02 [dd, 2H, CH_2; J = 6.0, 6.9 Hz], 5.06 [t, 2H, CH_2, J = 6.3 Hz], 6.37 [d, 2H, Ar-H; J = 7.7 Hz], 6.73-6.96 [m, 16H, Ar-H], 7.0-7.25 [m, 7H, Ar-H], 7.33 [m, 13H, Ar-H], 7.44-7.66 [m, 13H, Ar-H]. FTIR (cm^{-1}): 3435(br), 3378(w). 3134(s) 3053(s), 2999(w), 2855(w), 1592(m), 1562(s), 1479(s), 1435(s), 1384(m), 1334(m), 1266(w), 1181(w), 1149(m), 1103(s), 1065(s), 1031(s), 997(m), 914(w), 841(m), 817(m), 741(s), 705(s), 612(s), 604(s), 530(s), 479(s).

$[Pd_2\{SC(NPh)NH\}_2(CH_2)_8(dppe)_2]\cdot 2BPh_4$ ***(6j)***

$[PdCl_2(dppe)]$ (115 mg, 0.2 mmol) and $PhNHC(S)NH(CH_2)_8NHC(S)NHPh$ (36 mg, 0.1 mmol). Yield: 126 mg; 87 %. Elemental analysis %: calculated for $C_{122}H_{116}B_2N_4P_4Pd_2S_2$: C 71.11, H 5.67, N 2.72, found; C 70.94, H 5.82; N 2.83. ESI-MS: Calculated *m/z*; 910.95 $[M]^{2+}$, experimental *m/z*: CEV 60 V, 710.99 (100%) $[M]^{2+}$, 120-180 V, 710.99 (100%) $[M]^{2+}$, 1221.18 (7%) $[M\text{-}(dppePdS)]^+$, 1742.18 (5%) $[MBPh_4]^+$. $^{31}P\{^1H\}$ NMR δ ppm; 62.78 [$^2J_{(PP)}$ = 27 Hz] and 58.43 [$^2J_{(PP)}$ = 27 Hz]. ^1H NMR δ ppm: 0.95 [m, 2H, CH_2], 1.13 [t, 2H, CH_2; J = 7.1 Hz], 2.09 [m, 4H, CH_2 dppe; J = 21, 11 Hz], 2.34 [d, H, NH; J = 5.9 Hz], 3.11 [dd, 2H, CH_2; J = 6.9, 7.2 Hz], 5.13 [t, 2H, CH_2, J = 6.3 Hz], 5.32 [d, 1H, NH, J = 3.2 Hz], 6.35 [d, 2H, Ar-H; J = 7.7 Hz], 6.79 [t, 5H, Ar-H; J = 6.9 Hz], 7.0-7.25 [m, 16H, Ar-H], 7.30-7.4 [m, 12H, Ar-H], 7.45-7.65 [m, 13H, Ar-H]. FTIR (cm^{-1}): 3435(br), 3378(w), 3134(s) 3053(s), 2999(w), 2855(w), 1592(m), 1562(s), 1479(s), 1435(s), 1384(m), 1334(m), 1266(w), 1181(w), 1149(m), 1103(s), 1065(s), 1031(s), 997(m), 914(w), 841(m), 817(m), 741(s), 705(s), 612(s), 604(s), 530(s), 479(s).

*[Pd_2{SC(NPh)NH}$_2(CH_2)_{12}(dppe)_2$]·2BPh_4 (**6k**)*

[$PdCl_2$(dppe)] (115 mg, 0.2 mmol) and PhNHC(S)NH$(CH_2)_{12}$NHC(S)NHPh (48 mg, 0.1 mmol). Yield: 132 mg, 80 %. Elemental analysis %: calculated for $C_{126}H_{124}B_2N_4P_4Pd_2S_2$; C 71.47, H 5.90, N 2.65, found: C 71.49, H 5.87; N 2.62. ESI-MS: Calculated *m/z*; 739.01 $[M]^{2+}$, experimental *m/z*: CEV 60 V; 738.94 (100%) $[M]^{2+}$, 973.00 (12%) $[M\text{-}Pd(dppe)+H]^+$, 1795.98 (5%) $[MBPh_4]^+$, 120-180 V; 738.96 (100%) $[M]^{2+}$, 973.00 (12%) $[M\text{-}Pd(dppe)+H]^+$, 1795.98 (22%) $[MBPh_4]^+$. $^{31}P\{^1H\}$ NMR δ ppm: 62.84 [$^2J_{(PP)}$ = 28 Hz] and 58.47 [$^2J_{(PP)}$ = 28 Hz]. ^1H NMR δ ppm: 1.19 [m, 4H, CH_2], 1.94-2.05 [m, 4H, CH_2 dppe, J = 22 Hz, J = 2.58 Hz], 2.58 [dd, 2H, CH_2; J = 7.6, 6.2 Hz], 3.16 [dd, 2H, CH_2; J = 7.9, 5.2 Hz]. 5.14 [t, 2H, CH_2; J = 5.7 Hz], 6.39 [d, 2H, NH; J = 7.6 Hz], 6.79 [m, 39H, Ar-H]. FTIR (cm^{-1}): 3448(br), 3332(w), 3134(s) 3054(s), 2922(s), 2851(m), 1592(m), 1566(s), 1479(s), 1435(s), 1385(m), 1334(m), 1266(w), 1180(w), 1149(m), 1103(s), 1065(s), 1031(s), 997(m), 915(w), 841(m), 818(m), 742(s), 705(s), 613(s), 604(s), 531(s), 479(s).

*[Ni_2{SC(NPh)NH}$_2(CH_2)_4(dppe)_2$]·2BPh_4 (**6l**)*

[$NiCl_2$(dppe)] (106 mg, 0.2 mmol) and PhNHC(S)NH$(CH_2)_4$NHC(S)NHPh (47 mg, 0.1 mmol). Yield: 115 mg, 73 %. Elemental analysis %: calculated for $C_{94}H_{88}BN_4P_4Ni_2S_2$; C 71.01, H 5.58, N 3.52, found; C 69.92, H 5.62; N 3.50. ESI-MS: Calculated *m/z*; 635.01 $[M]^{2+}$, experimental *m/z*: CEV 60 V; 634.96 (100%) $[M]^{2+}$, 812.99 (85%) $[M\text{-}Ni(dppe)+H]^+$, 120-180 V; 634.96 (94%) $[M]^{2+}$, 812.99 (100%) $[M\text{-}Ni(dppe)+H]^+$, 1589.11(26%) $[MBPh_4]^+$, 240 V; 812.99(100%) $[M\text{-}Ni(dppe)+H]^+$, 1589.11(32%) $[MBPh_4]^+$. $^{31}P\{^1H\}$ NMR δ ppm: 61.52 [$^2J_{(PP)}$ = 50 Hz] and 59.06 [$^2J_{(PP)}$ = 51 Hz]. ^1H NMR δ ppm; 0.73 [m, 2H, CH_2], 1.96 [m, 4H, CH_2, dppe], 2.57 [m, 2H, CH_2], 4.76 [t, 4H, 1H; J = 5.9 Hz], 6.20-6.40 [m, 3H, CH_2], 6.70-6.90 [m, 18H, Ar-H], 7.12-7.80 [m, 39H, Ar-H]. FTIR (cm^{-1}): 3343(br), 3054(s), 3033(w), 2998(w), 2926(w), 1593(m), 1567(s), 1483(w), 1436(s), 1406(w), 1382(w), 1338(m), 1267(w), 1185(w), 1103(s), 1069(m), 1031(m), 998(m), 919(w), 843(w), 817(m), 733(s), 704(s), 690(m), 612(s), 532(s), 482(m).

[Ni_2{SC(NPh)NH}$_2(CH_2)_6(dppe)_2$]·2BPh_4 ***(6m)***

[$NiCl_2$(dppe)] (106 mg, 0.2 mmol) and PhNHC(S)NH$(CH_2)_6$NHC(S)NHPh (48 mg, 0.1 mmol). Yield: 112 mg, 75 %. Elemental analysis %: calculated for $C_{96}H_{92}BN_4Ni_2P_2S_2$; C 71.26, H 5.73, N 3.46, found; C 69.98, H 5.82, N 3.22. ESI-MS: Calculated *m/z*; 649.01 $[M]^{2+}$, experimental *m/z*: CEV 60 V, 648.97 (100%) $[M]^{2+}$ 841.02 (46%) [M-Ni(dppe)+H]$^+$. 120-180 V; 648.97 (100%) $[M]^{2+}$, 841.02 (46%) [M-Ni(dppe)+H]$^+$, 1617.12 (23%) $[MBPh_4]^+$, 240 V; 648.95 (35%) $[M]^{2+}$, 841.03 (100%) [M-Ni(dppe)+H]$^+$, 1617.13 (25%) $[M]^+BPh_4^-$. $^{31}P\{^1H\}$ NMR δ ppm: 61.55 [$^2J_{(PP)}$ = 50 Hz] and 59.17 [$^2J_{(PP)}$ = 50 Hz]. ^1H NMR δ ppm: 1.07 [d, 2H, CH_2; J = 6.7 Hz], 1.84-1.98 [m, 8H, CH_2 dppe], 2.83 [dd, 2H, CH_2; J = 6.6 Hz], 4.80 [t, 2H, NH; J = 11.2 Hz], 6.27 [d, 2H, CH_2; J = 8.0 Hz], 6.70-7.72 [m, 48H, Ar-H]. FTIR (cm^{-1}): 3338(br), 3053(s), 3003(w), 2982(w), 2964(w), 2854(w), 1593(m), 1567(s), 1482(s), 1436(s), 1406(w), 1337(s), 1307(w), 1265(w), 1185(w), 1103(s), 1069(w), 1031(s), 998(s), 919(w), 875(w), 816(s), 733(s), 704(s), 690(s), 612(s), 531(s), 483(s).

[Ni_2{SC(NPh)NH}$_2(CH_2)_8(dppe)_2$]·2BPh_4 ***(6n)***

[$NiCl_2$(dppe)] (106 mg, 0.2 mmol) and PhNHCSNH$(CH_2)_8$NHC(S)NHPh (41 mg, 0.1 mmol). Yield: 122 mg, 83 %. Elemental analysis %: calculated for $C_{122}H_{116}B_2N_4Ni_2P_2S_2$; C 74.56, H 5.95, N 2.85, found; C 75.18, H 5.82; N 2.22. ESI-MS: Calculated *m/z*; 663.02 $[M]^{2+}$, experimental *m/z*: CEV 60 V; 662.99 (100%) $[M]^{2+}$ 869.06 (14%) [M-Ni(dppe)+H]$^+$, 150-180 V; 662.99 (70%) $[M]^{2+}$, 869.08 (100%) [M-Ni(dppe)+H]$^+$, 1645.10 (3%) $[M]^+BPh_4$, 240 V; 662.99 (68%) $[M]^{2+}$, 869.06 (100%) [M-(dppeNi)+H]$^+$, 1645.11 (8%) $[M]^+BPh_4$. $^{31}P\{^1H\}$ NMR δ ppm: 61.54 [$^2J_{(PP)}$ = 50 Hz] and 59.18 [$^2J_{(PP)}$ = 50 Hz]. ^1H NMR δ ppm: 1.20 [s, 2H, CH_2; J = 5.7 Hz], 1.88 [m, 8H, CH_2 dppe], 2.94 [dd, 2H, CH_2; J = 6.0 Hz], 4.94 [t, 2H, CH_2; J = 7.5 Hz], 6.28 [d, 2H, NH; J = 8.2 Hz], 6.70-7.76 [m, 48H, Ar-H]. FTIR (cm^{-1}): 3364(br), 3053(w), 2999(s), 2926(s), 2854(w), 1594(s), 1569(s), 1483(s), 1436(s), 1403(w), 1374(w), 1330(s), 1308(w), 1254(m), 1186(w), 1103(s), 1070(w), 1030(s), 998(s), 824(m), 734(s), 704(s), 690(s), 612(s), 533(s), 482(s).

[Ni_2{SC(NPh)NH}$_2(CH_2)_{12}(dppe)_2$]·2BPh_4 ***(6o)***

[$NiCl_2$(dppe)] (106 mg, 0.2 mmol) and PhNHC(S)N$(CH_2)_{12}$NC(S)NHPh (0.1 mmol, 48 mg). Yield: 132 mg, 86 %. Elemental analysis %: calculated for

$C_{126}H_{124}B_2N_4P_4Ni_2S_2$; C 74.87, H 6.18, N 2.77, found; C 75.01, H 6.10; N 2.80; ESI-MS: Calculated *m/z*; 691.01 $[M]^{2+}$ experimental *m/z*: CEV 60 V; 691.02 (100%) $[M]^{2+}$, 925.12 (20%) $[M\text{-}Ni(dppe)+H]^+$, 1701.11 (3%) $[MBPh_4]^+$, 120-180 V; 691.02 (100%) $[M]^{2+}$, 925.12 (12%) $[M\text{-}Ni(dppe)+H]^+$, 1701.11 (63%) $[MBPh_4]^+$. $^{31}P\{^1H\}$ NMR δ ppm: 61.56 [$^2J_{(PP)}$ = 50 Hz] and 59.20 [$^2J_{(PP)}$ = 50 Hz]. ^1H NMR δ ppm: 1.16 [d, 4H, CH_2; J = 6.9 Hz], 1.81-1.95 [m, 8H, CH_2 dppe], 3.02 [dd, 4H, CH_2; J = 7.1 Hz, 8.2 Hz], 4.97 [t, 4H, CH_2; J = 5.9 Hz], 6.39 [d, 2H, NH; J = 7.7 Hz], 6.79-7.78 [m, 49H, Ar-H]. FTIR (cm^{-1}): 3370(br), 3055(s), 2924(s), 2853(s), 1595(m), 1571(s), 1485(w), 1436(s), 1410(w), 1338(w), 1309(w), 1282(w), 1188(w), 1083(w), 1056(s), 997(s), 921(w), 876(s), 817(s), 748(s), 717(m), 691(s), 659(w), 625(w), 531(s), 483(s).

6.4.3 *Single crystal X-ray structure determinations*

Crystal data and refinement details for the investigated complexes are included in **Table 6.7**. The intensity was measured at T = 100 K on a SuperNova Dual AtlasS2 diffractometer fitted with Cu Kα radiation (λ = 1.54184). Data reduction, including absorption correction, was accomplished with CrysAlisPro[20]. The structures were solved by intrinsic phasing method on ShelXT[21] and refined (with anisotropic displacement parameters and C-bound H atoms in the riding model approximation) on F^2 [22]. Some residual electron density peaks in **6e**, evident after the complex molecule was refined, was modelled as H_2O molecule and CH_2Cl_2 solvents of crystallisation. Structures (**6e**) and (**6k)** featured large residual electron density peaks with the maximum of these always located near the Pt atom and Pd atoms. The molecular structure diagrams were generated with Olex11 Draw [23] with 50% displacement ellipsoids.

Table 6.7: Crystallographic refinement parameters for complexes, **6e**, **6k**, **6l** and **6m**

Complexes	**6e**	**6k**	**6l**	**6m**
Formula	$C_{71}H_{66}BCl_2N_2OP_2PtS$	$C_{126}H_{124}B_2N_4P_4Pd_2S_2$	$C_{59}H_{54}BN_2NiP_2S$	$C_{60}H_{59}BN_2NiP_2S$
Formula weight (g/mol)	1334.05	2116.70	954.56	968.58
Temperature /K	99.97(12)	100.01(10)	100.00(10)	100.01(10)
Crystal System	monoclinic	triclinic	monoclinic	Monoclinic
Space group	$P2_1/n$	P-1	$P2_1/c$	P21/c
a/Å	9.6550(2)	17.3367(5)	14.8861(2)	10.7617(10)
b/Å	35.0030(5)	18.5561(6)	9.6453(10)	19.9757(2)
c/Å	18.1716(2)	20.0242(5)	34.6767(10)	23.8797(3)
α/°	90	105.841(2)	90	90
β/°	104.965(2)	100.944(2)	94.5250(10)	98.1270(10)
γ/°	90	114.611(2)	90	90
Volume/$Å^3$)	5932.88(17)	5284.0(3)	4956.72(18)	5081.92(10)
Z	4	2	4	4
ρ_{calc} g/cm^3	1.494	1.330	1.279	1.266
μ/mm^{-1}	6.454	5.784	1.874	1.835
F (000)	2708.0	2204.0	2000.0	2036.0
Crystal Size/mm^2	0.173x0.12x0.057	0.141x0.10x0.07	0.18x0.14x0.13	0.23x0.21x0.16
2Θ(°)	7.132 to 147.654	7.53 to 148.128	7.546 to 148.074	7.480 to 147.926
Goof	1.092	1.025	1.176	1.156
R-Factor (%)	4.40	3.75	4.03	3.62
Reflections used	11362	20754	9907	10176
Independent reflections	30093	60159	47296	48181
Abs correction	multiscan	gaussian	multiscan	multiscan

6.5 References

1. Henderson, W.; Nicholson, B. K.; Rickard, C. E. F. *Inorg. Chim. Acta* **2001**, *320*, 101-109.

2. Okeya, S.; Fujiwara, Y.; Kawashima, S.; Hayashi, Y.; Isobe, K.; Nakamura, Y.; Shimomura, H.; Kushi, Y. *Chem. Lett.* **1992**, 1823-1826.

3. Okeya, S.; Kameda, H.; Kawashima, H.; Shimomura, H.; Nishioka, T.; Isobe, K. *Chem. Lett.* **1995**, *24*, 501-502.

4. Yuen, H. Y.; Henderson, W.; Oliver, A. G. *Inorg. Chim. Acta* **2011**, *368*, 1-5.

5. Robinson, S. D.; Sahajpal, A.; Steed, J. W. *Inorg. Chim. Acta* **2000**, *306*, 205-210.

6. Bolaño, S.; Plaza, M.; Bravo, J.; Castro, J.; Peruzzini, M.; Gonsalvi, L.; Ciancaleoni, G.; Macchioni, A. *Inorg. Chim. Acta* **2010**, *363*, 509-516.

7. Dinger, M. B.; Henderson, W.; Nicholson, B. K.; Robinson, W. *J. Organomet. Chem.* **1998**, *560*, 169-181.

8. Tarantelli, T. *J. Chem. Soc., Dalton Trans.* **1974**, 837-841.

9. Cauzzi, D.; Costa, M.; Cucci, N.; Graiff, C.; Grandi, F.; Predieri, G.; Tiripicchio, A.; Zanoni, R. *J. Organomet. Chem.* **2000**, *593*, 431-444.

10. Bierbach, U.; Hambley, T. W.; Farrell, N. *Inorg. Chem.* **1998**, *37*, 708-716.

11. Lee, K.; Fesus, L.; Yancey, S.; Girard, J.; Chung, S. *J. Biol. Chem.* **1985**, *260*, 14689-14694.

12 Pansuriya, P.; Friedrich, H. B.; Maguire, G. E. *"Acta Crystallogr., Sect. E: Struct. Rep. Online "* **2011**, *67*, 2380-2380.

13. Pansuriya, P. B.; Parekh, H. M.; Friedrich, H. B.; Maguire, G. E. *J. Therm. Anal. Calorim.* **2013**, *111*, 597-603.

14. Burrows, A. D.; Coleman, M. D.; Mahon, M. F. *Polyhedron* **1999**, *18*, 2665-2671.

15. Henderson, W.; Nicholson, B. K.; Dinger, M. B.; Bennett, R. L. *Inorg. Chim. Acta* **2002**, *338*, 210-218.

16. Henderson, W.; Rickard, C. E. F. *Inorg. Chim. Acta* **2003**, *343*, 74-78.

17. Pansuriya, P. B.; Friedrich, H. B.; Maguire, G. E. *"Acta Crystallogr., Sect. E: Struct. Rep. Online "* **2011**, *67*, 2819-2819.

18. Henderson, W.; Kemmitt, R. D. W.; Mason, S.; Moore, M. R.; Fawcett, J.; Russell, D. R. *J. Chem. Soc., Dalton Trans.* **1992**, 59-66.

19. Spenceley, J. E.; Henderson, W.; Lane, J. R.; Saunders, G. C. *Inorg. Chim. Acta* **2015**, *425*, 83-91.

20. Rigaku Oxford Diffraction CrysAlisPro Software System, version 1.171. 38.41 l, Rigaku Coorporation. Oxford, UK, (2015).

21. Sheldrick, G. M. *Acta Crystallogr., Sect. A: Found. Adv* **2015**, *71*, 3-8.

22. Sheldrick, G. M. *Acta Crystallogr., Sect. C: Struct. Chem.* **2015**, *71*, 3-8.

23. Dolomanov, O. V.; Bourhis, L. J.; Gildea, R. J.; Howard, J. A. K.; Puschmann, H. *J. Appl. Crystallogr.* **2009**, *42*, 339-341

Chapter 7

General summary and recommendations

7.1 Summary

A range of asymmetrically substituted thiourea dianion and monoanion ligands containing various functional groups including, pyridyl, methylenepyridyl, ethylenepyridyl, phenyl, *p*-nitropheny, and *p*-methoxyphenyl functional groups were synthesised and characterised. Platinum complexes of the type $[Pt\{SC(=NR^1)NR^2\}(PPh_3)_2]$ and $[Pt\{SC(=NR^1)NH(CH_2)Py\}(PPh_3)_2]^+$ were successfully synthesised and characterised by ESI-MS, NMR and single-crystal X-ray crystallography. Theoretical Gibbs free energy calculations and NMR investigations revealed the initial formation of a kinetically stable proximal isomer which isomerised into the thermodynamically favoured distal isomer or a stable mixture of both at equilibrium for the thiourea dianion complexes. The monoanion complex, on the other hand, showed an initial distal isomeric configuration which subsequently isomerised into a stable mixture of the proximal and distal isomer. The pyridyl-substituted thiourea dianion complexes $[Pt\{SC(=NPy)NPh\}(PPh_3)_2]$ (**2a**) and $[Pt\{SC(=NC_6H_4OMe)NPy\}(PPh_3)_2]$ (**2b**) showed evidence of *E/Z* isomerism when the pyridyl functional group was attached to the nitrogen remote to the platinum metal centre.

X-ray crystallography on **2a**, **2b** and **2d**-**2h** established the consistent adoption of square-planar geometries defined by NP_2S donor set provided by di-anionic, *N,S*-chelating ligands and two phosphane ligands. Systematic variations in Pt–P bond lengths are ascribed to a *trans*-influence by the S- and N-donors. In the salt **2i**, protonation at the imine-nitrogen was proven to generate a mono-anionic ligand that provided similar coordination and anticipated variations in geometric parameters.

Palladium and nickel complexes of these asymmetrically substituted thioureas were also synthesised and characterised. ESI-MS data for the complexes showed molecular ion fragments for loss of the bulky PPh_3 ligand at CEV above 120 V, for the PPh_3 substituted palladium complexes. $^{31}P\{^1H\}$ NMR of the pyridyl and phenyl substituted complex **3a** indicated the possibility of *E/Z* isomerism. The

crystal structure of the complexes showed a six-membered boat-like conformation for the palladium complex **3a**, with the pyridyl nitrogen coordinated to the palladium centre. while the other palladium **3c-e** and nickel complexes **3j** and **3l** showed the four-membered square planar geometry, similar to the platinum complexes (**2a-2i**). Introduction of an alkyl spacer between the pyridyl and thiourea functional groups of the ligand resulted in juxtaposition of the pyridyl functional group from the proximal position in **3a** and **3e** to the distal position in **3d-e**, **3j** and **3l** giving rise to both intermolecular and intramolecular hydrogen bonding interactions between the thiourea N-H and pyridyl nitrogen of the alkyl pyridyl functional group.

Ruthenium arene, Cp* rhodium and iridium complexes of these ligands formed both neutral and cationic mononuclear complexes. Substitution of the chloride ion in the complexes with a bulkier PPh_3 ligand resulted in changes in the geometric parameters around the metal coordination sphere, while substitution of the pyridyl functional group with a methylene pyridyl and ethylene pyridyl groups resulted in an eight-membered bidentate chelate ring in **4c** or juxtaposition of the pyridyl functionality from the proximal to the distal position and formation of a four-membered chelate ring.

Thioureas containing phosphonate-, hydroxyethyl-, and silatrane-functional groups were also synthesised and characterised. The X-ray crystal structure of the phosphonate substituted thioureas showed the formation of unusual hydrogen-bond motifs, resulting from noncovalent interactions in competing functional groups. were synthesised and characterised. $^{31}P\{^{1}H\}$ NMR spectra of the platinum and palladium complexes of the phosphonate and hydroxyethyl-substituted complexes showed the presence of two isomers of the complex in $CDCl_3$ solution, while the bis(hydroxyethyl) and silatrane-substituted complexes showed only a single isomer. The X-ray crystal structures of the hydroxyethyl, bis(hydroxyethyl) and silatrane-substituted platinum thiourea complexes **5c**, **5d** and **5e** showed the regular NP_2S square planar geometry with a protonated imine nitrogen at the remote position to give BF_4 salts of the complexes.

Finally, platinum, palladium and nickel complexes of some alkyl-bridged bifunctional thiourea ligands were synthesised and characterised. Coordination of both thiourea functional groups was found to be dependent on the amount of reactants as well as the reaction time. Increase in the length of the alkyl spacer

between the two thiourea functionalities resulted in loss of isomerism in the complexes. X-ray crystal structures of complexes **6e**, **6l** and **6m** showed that the compounds crystallised with half a molecule each in the asymmetric unit, while **6k** crystallised as a whole molecule. The molecular structures of all the complexes showed consistent adoption of the square planar geometry defined by the NP_2S donor atoms from the monoanionic *N,S*-chelating ligands and the two phosphate ligands. There were no significant differences between the geometric parameters of the Pt, Pd and Ni complexes.

7.2 Recommendations

Due to the structural and geometric variations in the thioureas and their metal complexes reported in this thesis, it would have been interesting to look at the biological properties of these complexes. Owing to insufficient funding and time, the study could not be carried out as part of this thesis. We have however recently collaborated with other scientists at the Bulent Ecevit University in Turkey to explore the biological properties of these thioureas and their complexes. Apart from that, the versatility of the thioureas provides for the presence of protonated imines of functional groups lone pairs in their complexes and this can be explored to study the solubility properties of these compounds and possibly the anion binding properties of these complexes[1].

7.3 References

1. Singh, G.; Saroa, A.; Rani, S.; Choquesillo-Lazarte, D.; Sahoo, S. *Arabian J. Chem.* **2017**, *10*, 523-531.

Appendices

Appendix 1: General Experimental Procedures

A.1 General experimental techniques

All compounds used or prepared in this study are not oxygen or moisture sensitive and do not require reactions to be carried out under an inert atmosphere. All the reactions were carried out under normal laboratory conditions. Reactions involving foul-smelling compounds like COD were carried out in a fume hood.

A.2 Melting point and elemental analysis

Melting point determinations were undertaken on a Reichert–Jung Thermovar Melting point instrument as solid samples on glass slides and are uncorrected. Carbon, hydrogen and nitrogen microelemental analysis was undertaken on the vacuum at Campbell Microanalytical Laboratory, University of Otago.

A.3 Mass spectrometry

Electrospray ionisation mass spectra were obtained on a Bruker Microtof instrument. The characterisation of synthesised thiourea ligands was carried out capillary exit voltage of 150 V in the negative-ion mode while the isolated complexes were analysed at a range of capillary exit voltages; 60, 120, 150 and 180 V to study the fragmentation pattern of the complexes. In all cases, the practical isotope patterns generated were on the ESI-MS platform was compared with theoretical isotope patterns generated using an internet-based programme mMass. Methanol was used as the solvents and in some cases where the compound is not soluble in methanol, the sample was dissolved in a small amount of dichloromethane or dimethylsulfoxide before diluting with methanol. Approximately 1 mg of the solid sample or 1 drop of the reaction solution was dissolved in 1 mL of methanol in an Eppendorf vial, and after centrifuging to isolate any suspended solid matter is then immediately injected into the ESI-MS.

A.4 Infrared spectroscopy

Infrared spectra were recorded out on a Perkin Elmer Spectrum 100, FT-IR spectrometer. The spectra were obtained on a disc of 1: 10 ratio of the compound and KBr. Observations were made of the appropriate bands.

A.5 Nuclear magnetic resonance (NMR) spectroscopy

NMR spectroscopy was performed using a Bruker Avance (III) 400 MHz instruments (^{1}H 400.13 MHz, ^{13}C 100.16 MHz, ^{31}P 161.9 MHz) at 300 K and processed with Topspin 3.0 NMR software. Deuterated solvents used for the NMR include $CDCl_3$, DMSO-d_6, D_2O with ^{1}H and ^{13}C referenced to TMS (Me_4Si) and ^{31}P spectra referenced to 85% H_3PO_4. Coupling constants (J) are measured in Hertz.

Appendix 2: Noncovalent interaction pictures

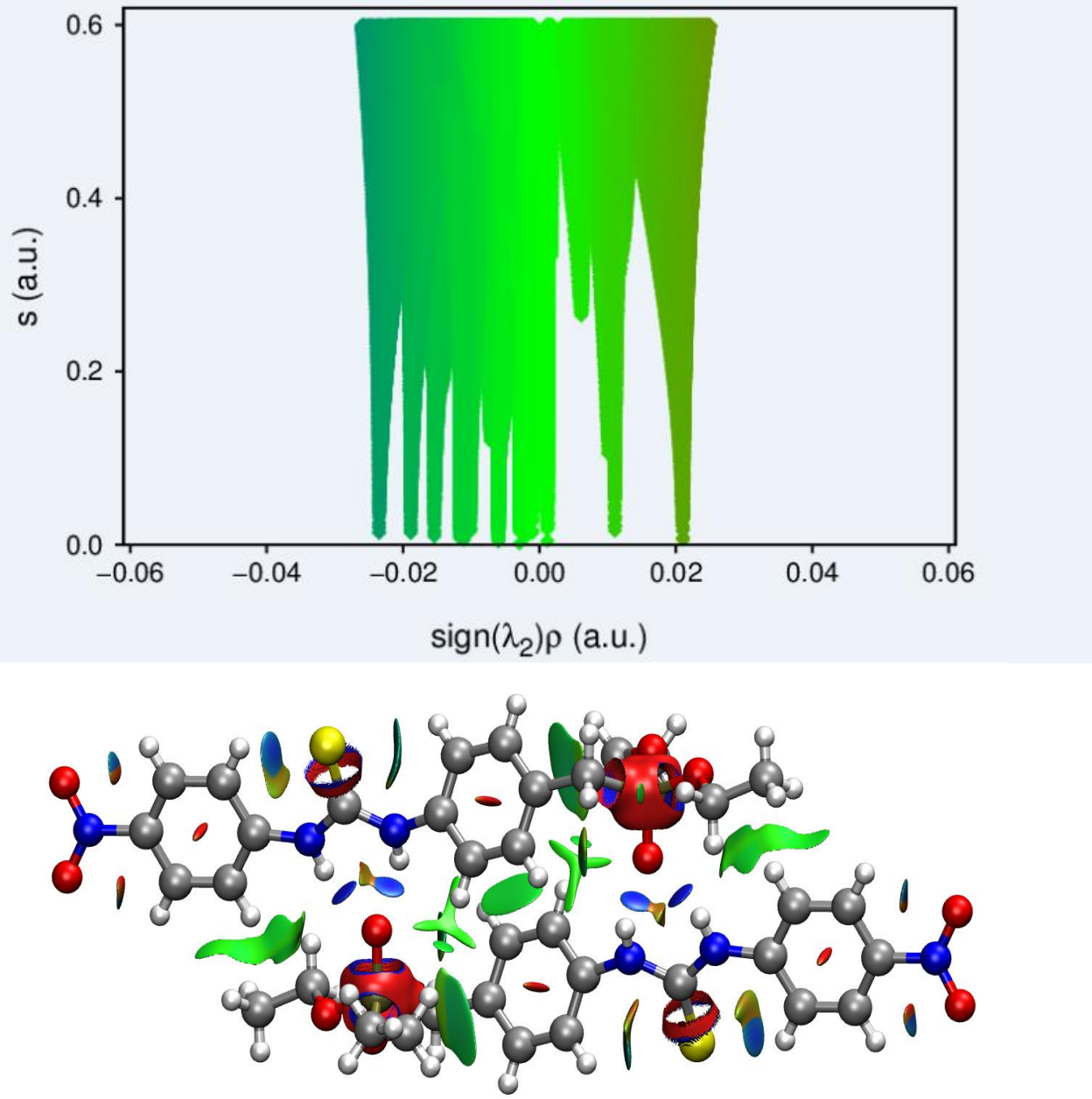

Figure B1: 2D bonder plots (top) and 3D isosurface interactions in the bifurcated hydrogen-bonded dimer of the *p*-nitrophenyl-substituted phosphonate thiourea (s = 0.5au).

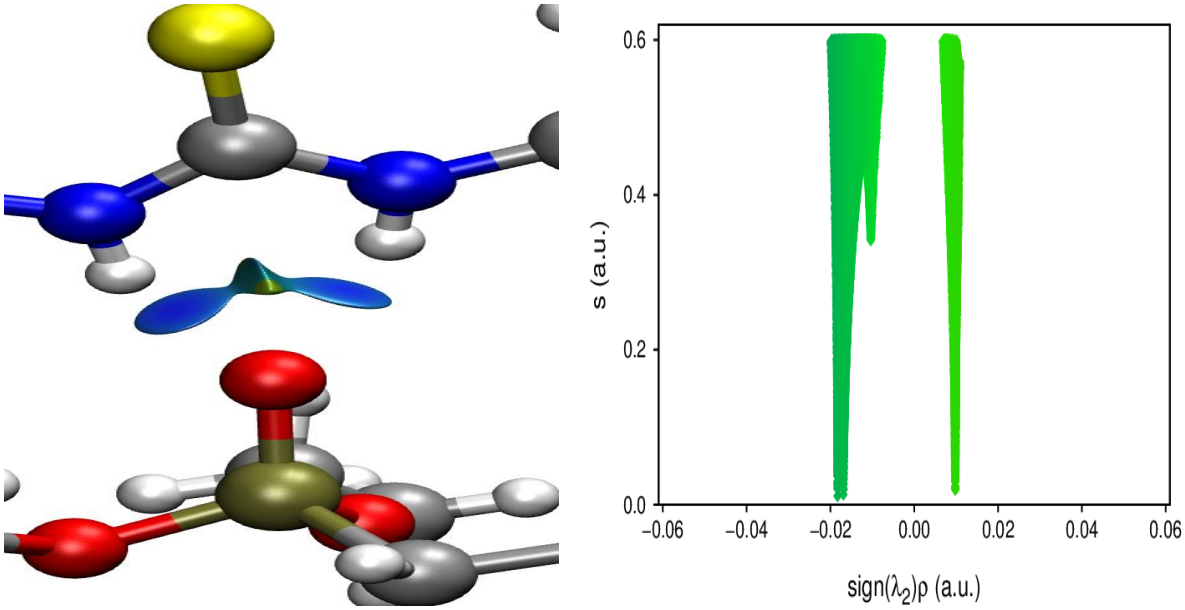

Figure B2. (a) 3D individual isosurface representation b.; 2D bonder plot for inter-molecular hydrogen bonding interaction btw N-H and P = O groups on **1i** (s = 0.5au, -0.05 < λ_2 > 0.05)

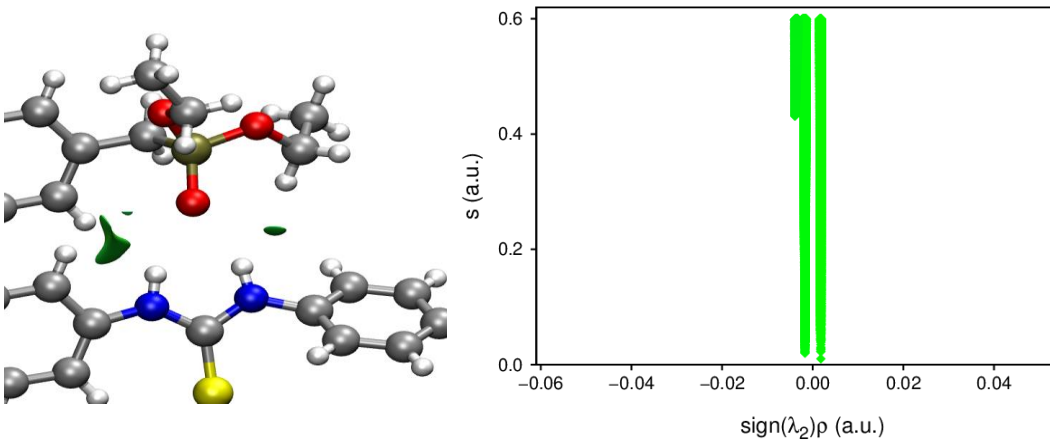

Figure B3: Isorsuface representation and 2D bonder plots for weak intermolecular NH…C interactions (s = 0.5au; -0.05au >Sign λ_2<+0.05au)

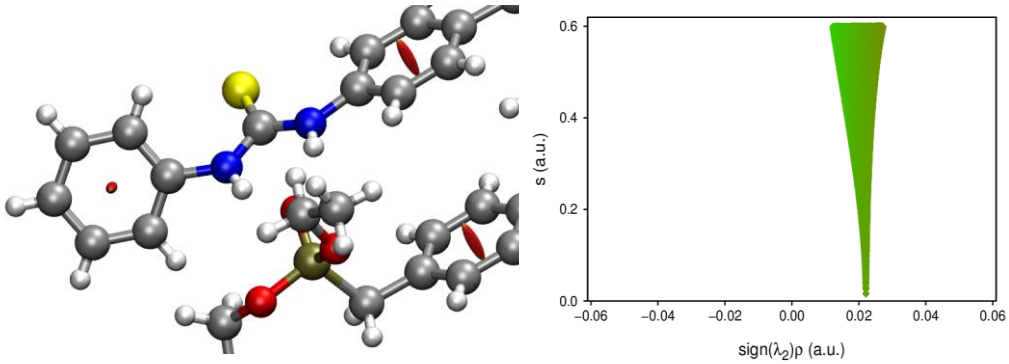

Figure B4 : 3D isosurface representations and 2D bonder plots for ring strain / steric interactions in the benzene rings of the phosphonate thiourea. (s = 0.5au; Sign λ_2 = +0.22au

Appendix 3: List of Publications

Expected publications from the thesis.

1. O.C. Okpareke, W. Henderson, J. R. Lane and E.R.T Tienkink. Isomerism in platinum complexes containing pyridyl-substituted thiourea dianion and monoanion ligands: Synthesis, structure and theoretical investigations. *Proposed for Inorganic Chemistry(ACS).*

2. O.C. Okpareke, W Henderson, J. R. Lane and B. Coban, Platinum and palladium and nickel complexes of bisthiourea ligands; Synthesis structure, DNA cleavage and anticancer studies. *Proposed for European Journal of Inorganic Chemistry.*

3. O.C. Okpareke, W. Henderson and J. R. Lane, Palladium and nickel complexes of pyridyl-substituted thiourea dianion and monoanion complexes. Synthesis, structure and noncovalent interaction studies. *Proposed for Journal of the Chemical Society, Dalton Transactions.*

4. O.C. Okpareke, W. Henderson and J R. Lane; Organo-phosphorus ruthenium complexes of some pyridyl-substituted thiourea complexes; Synthesis, structure and biological activity studies. *Proposed for Applied Organometallic Chemistry.*

5. O.C. Okpareke, W. Henderson and J. R. Lane; Rhodium and Iridium complexes of some pyridyl-substituted thiourea dianion and monoanion complexes; Synthesis, structure and Mass-Spectrometric determinations. *Proposed for European Journal of Inorganic Chemistry*.

6. O.C. Okpareke, W. Henderson, J. R. Lane and E.R.T Tienkink. Platinum and palladium complexes of phosphonate-, silatrane- and carboxyl-substituted thiourea complexes. Synthesis, structure and non-covalent interaction studies. *Proposed for Polyhedron*

Others papers published during the PhD research:

1. O.C. Okpareke, W. Henderson, J. R. Lane and S.N. Okafor; Synthesis, structure computational and molecular docking studies of asymmetrically di-substituted ureas containing carboxyl and phosphoryl hydrogen bond. *Journal of Molecular Structure*, 2020, 1203, 127360.

2. W. Henderson, J. C. Thomas, O.C. Okpareke, E. R. T. Tienkink. Synthesis ,structural and mass spectrometric investigations of pyridinium bis(thiosalicylato) mecurate(II); *Inorganica Chimica Acta*, 2019 490, 104-111

3. W Henderson, O.C. Okpareke, A.H.S Azizan, E. R. T. Tienkink. Dicyclohexyl (Sulfanylidene)-ʎ-5-phosphanyl] methanol, *Molbank* 2019-mdpi.com.

4. F.F. Bobinihi, D.C. Onwudiwe, A.C. Ekennia, O.C. Okpareke, C. Arderne, J.R. Lane; Group 10 metal complexes of dithiocarbamates derived from

primary anilines: Synthesis, characterisation, computational and antimicrobial studies, *Polyhedron*, 2019,158, 296-310.

5. A.C. Ekennia, D. C. Onwudiwe, A.A. Osowole O.C. Okpareke, J.R. Lane, O.O Olubiyi, T.E. Olalekan; Coordination compounds of heterocyclic bases; synthesis characterisation, computational and biological studies, *Research on Chemical Intermediates*, 2019, 45, 1169-1205.

6. E.E. Oyeka, J.N. Asegbeloyin, I. Babahan, B. Eboma, O.C. Okpareke, J. R. Lane, A Ibezim, H.H Biyik, B. Torun, D.C. Izuogu, Synthesis, crystal structure, computational analysis and biological properties of 1-(4-chlorobenzoyl)-3-[2-(2-{2-[3-(4-chlorobenzoyl)-thioureido]-ethoxy}ethoxy)ethyl]-thiourea and its Ni(II) and Cu(II) complexes, *Journal of Molecular Structure 2018,* 1168, 153-164.